872
2-20-80

October 1979

DR-711

SERI/TP-31-248

Reliability of Materials for Solar Energy

December 18-20, 1978

Workshop Proceedings

MASTER

Volume II
Part I
Workshop Proceedings

Sponsored by



SERI

Solar Energy Research Institute

1617 Cole Boulevard
Golden, Colorado 80401

Operated for the
U.S. Department of Energy
under Contract No. EG-77-C-01-4042
by Midwest Research Institute

and the
U.S. Department of Energy

DISTRIBUTION OF THIS DOCUMENT IS UNLIMITED

DISCLAIMER

This report was prepared as an account of work sponsored by an agency of the United States Government. Neither the United States Government nor any agency Thereof, nor any of their employees, makes any warranty, express or implied, or assumes any legal liability or responsibility for the accuracy, completeness, or usefulness of any information, apparatus, product, or process disclosed, or represents that its use would not infringe privately owned rights. Reference herein to any specific commercial product, process, or service by trade name, trademark, manufacturer, or otherwise does not necessarily constitute or imply its endorsement, recommendation, or favoring by the United States Government or any agency thereof. The views and opinions of authors expressed herein do not necessarily state or reflect those of the United States Government or any agency thereof.

DISCLAIMER

Portions of this document may be illegible in electronic image products. Images are produced from the best available original document.

NOTICE

This report was prepared as an account of the meeting sponsored by the United States Government. Neither the United States nor the United States Department of Energy, nor any of their employees, nor any of their contractors, subcontractors, or their employees, makes any warranty, express or implied, or assumes any legal liability or responsibility for the accuracy, completeness or usefulness of any information, apparatus, product or process disclosed, or represents that its use would not infringe privately owned rights.

This report has been reproduced directly from the best available copy.

SERI/TP-31-248

DISTRIBUTION CATEGORY UC 59-64
CONFERENCE 781228

RELIABILITY OF MATERIALS FOR SOLAR ENERGY

WORKSHOP PROCEEDINGS

VOLUME II

PART 1

SPONSORED BY:

SOLAR ENERGY RESEARCH INSTITUTE

AND

U. S. DEPARTMENT OF ENERGY

DISCLAIMER

This book was prepared as an account of work sponsored by an agency of the United States Government. Neither the United States Government nor any agency thereof, nor any of their employees, makes any warranty, express or implied, or assumes any legal liability or responsibility for the accuracy, completeness, or usefulness of any information, apparatus, product, or process disclosed, or represents that its use would not infringe privately owned rights. Reference herein to any specific commercial product, process, or service by trade name, trademark, manufacturer, or otherwise, does not necessarily constitute or imply its endorsement, recommendation, or favoring by the United States Government or any agency thereof. The views and opinions of authors expressed herein do not necessarily state or reflect those of the United States Government or any agency thereof.

DECEMBER 18-20, 1978

DENVER, COLORADO

DISTRIBUTION OF THIS DOCUMENT IS UNLIMITED

THIS PAGE

WAS INTENTIONALLY

LEFT BLANK

TABLE OF CONTENTS

	Page
Introduction, S. L. Pohlman.	1
Introduction	
SERI's Research and Development Program, C. Grosskreutz	3
Overview of Solar Technology, B. Butler	13
Effect of Materials on the Reliability of Large Engineering Systems, R. Staehle	23
Thermal Conversion - Gas Coolant	
1 MW_{th} Gas Cooled Solar Receiver Design, D. Bartlett.	83
Solar Thermal Conversion Test Systems Design, R. Mar.	121
Black and Veatch Receiver Design, E. McBride.	133
Design of Structural Ceramic Components for Solar High Temperature Thermal Conversion with a Gas Coolant, D. Kotchick. .	143
High Temperature Diffusion/Materials Stability, J. Manning. . . .	149
High Temperature Oxidation of Metals and Alloys, C. Birchenall. .	159
The High Temperature Oxidation of Materials in Solar Thermal Conversion Systems Utilizing a Gas Coolant, J. Stringer	171
Thermal Conversion - Liquid Metal/Molten Salt Coolant	
Conceptual Design of Advanced Central Receiver Power Systems, R. Salemme	187
Advanced Sodium Cooled Central Receiver Power Plant, T. Springer.	221
Alternative Central Receiver Power System Using Molten Salt as the Heat Transfer and Storage Medium, T. Tracey	235
Molten Salt Compatibility, J. DeVan	267
Role of Material Variables in the Thermal Stress Fracture of Brittle Materials, D. Hasselman	277

Page

Liquid Metal Heated Steam Generators Effects of Corrosion on Performance, C. Spalaris 321

Effects of Liquid Metals on Structural Alloys, N. Stoloff 345

Materials Considerations in the Design of a Sodium Cooled Central Receiver Solar Thermal Power Plant, G. Whitlow. 391

Thermal Conversion - Aqueous/Steam Coolant

External Single Pass to Superheat Receiver, G. Coleman. 403

Material Problems Related to High Temperature Structural Design of Water/Steam Solar Receivers, A. Gangadharan. 415

A Central Receiver Using Natural Circulation Steam Generation for High Temperature Solar Thermal Conversion, D. Gorman. 423

Characteristics of Hot Water as a Chemical Solvent, J. Cobble . . 445

Possible Environmentally-Enhanced Cracking Problems in Solar-Powered Steam Generators, F. Ford 455

Water Chemistry and High Temperature Thermal Conversion with Aqueous/Steam Coolant, W. Lindsay, Jr. 461

Hydrogen Embrittlement in High Pressure Steam, J. Lux 471

Thermal Conversion - Aqueous/Oil Coolant

Design Considerations for Parabolic-Cylindrical Solar Collectors, G. Treadwell. 473

Corrosion Problems in Medium Temperature Thermal Conversion Systems with Aqueous/Oil Coolants, J. Kruger. 509

Absorber Coatings, P. Call. 517

Anhydrous Organic Heat Transfer Fluids in Medium Temperature Solar Conversion, D. Miller 519

A Survey of Organic Coolant Experience in Nuclear Reactors, H. Pearlman 539

Flat-Plate Collector

Low Temperature Flat-Plate Collector Space/Water Heating, S. Moore. 551

Fluid Corrosivity Sensor for Solar Systems, R. Baboian. 585

Page

Preliminary Materials Assessment in Solar Demonstration Systems, C. Cheng 591

Electrochemical Measurements of Time-of-Wetness and Atmospheric Corrosion Rates, F. Mansfeld. 621

Results of Thirty Months Atmospheric Corrosion Testing in St. Louis, MO, USA, F. Mansfeld 627

Inhibitors for Low Temperature Flat-Plate Solar Collectors in Space/Water Heating, C. Nathan. 659

Aluminum Alloys, E. Verink. 671

VOLUME II

Part 1

Presentations and Papers

from the workshop on

RELIABILITY OF MATERIALS

FOR

SOLAR ENERGY SYSTEMS

December 18 - 20, 1978

Sponsored by:

The Solar Energy Research Institute

Workshop Co-chairmen:

Dean Roger Staehle
Institute of Technology
University of Minnesota
Minneapolis, Minnesota

Dr. Steven Pohlman
Materials Branch
Solar Energy Research Institute
Golden, Colorado

INTRODUCTION

VOLUME II

Steven L. Pohlman

Solar Energy Research Institute

Recommendations and conclusions of the Reliability of Materials workshop for solar energy are presented in Volume I. Volume II contains the papers presented during the workshop including the introductory papers.

Following the introductory talks the attendees were divided into working groups. Design presentations were given in each working group describing their respective solar technology. The design speakers were asked to describe their particular system, identify important parameters such as operating temperatures, pressures, etc., and discuss material choices that had been contemplated by the design community. The design presentations were followed by discussions of limitations of materials. The materials presentations were directed toward describing the potential effect of specific degradation mechanisms on the respective solar technology. Following these opening presentations each working group was engaged in open discussion to develop recommendations.

Most of the papers contained in Volume II are copies of the original viewgraphs or transcripts presented during the workshop. Authors were given the opportunity to review and revise their manuscripts following the workshop.

As a compilation of design and material pertinent to solar energy technologies, Volume II serves as a useful source of information for both design and materials.

THIS PAGE

WAS INTENTIONALLY

LEFT BLANK

Introductory Paper

SERI'S RESEARCH AND DEVELOPMENT PROGRAM

by

C. Grosskreutz

Director for Technology Development

Solar Energy Research Institute

Golden, Colorado

OVERVIEW OF SOLAR ENERGY TECHNOLOGY

Solar energy conversion can be categorized by the processes of the physical interaction of solar radiation with matter.* Figure 1 is a schematic representation of the two major absorption processes: the production of heat and quantum interactions. Both processes, by means of suitable conversion mechanisms, can lead to useful energy products. These two general conversion processes or paths are referred to as Thermoconversion and Photoconversion. Given today's knowledge, they are the only two paths currently available. The most common conversion technologies today that use the two primary interactions are flat-plate collectors which convert the heat produced by thermoconversion to hot water or air, and photovoltaic cells which convert to an electric current the electron-hole pairs created in semiconductors by photoconversion.

A more detailed view of the multiple conversion pathway with thermoconversion and photoconversion is shown in Figures 2 and 3. These figures are arranged so that from bottom to top one moves from already or nearly commercialized technologies to those which are not yet out of the basic research stage. Similarly, the photoconversion paths may be placed above the thermoconversion paths so that the same vertical axis takes one from relatively simple mechanical and structural systems in thermoconversion to highly sophisticated, solid-state biological and chemical systems in photoconversion.

Another way of viewing the phenomenological framework shown in Figures 2 and 3 is to use the horizontal axis to designate how far a particular conversion mechanism has progressed along the RD&D sequence. The wavy shaded line denotes that (fuzzy) boundary between what is already known, understood or developed (the area to the left), and the region where research is still required to advance the technology (the area to the right of the shaded line). Clearly, lowhead hydro and wind turbine technology are in various stages of engineering development, while photobiological and photochemical conversion still require research in the mechanisms of primary product formation. Photovoltaic research is now concentrating on conversion mechanisms and device technology, with single crystal silicon much further advanced than other materials such as gallium arsenide or amorphous silicon.

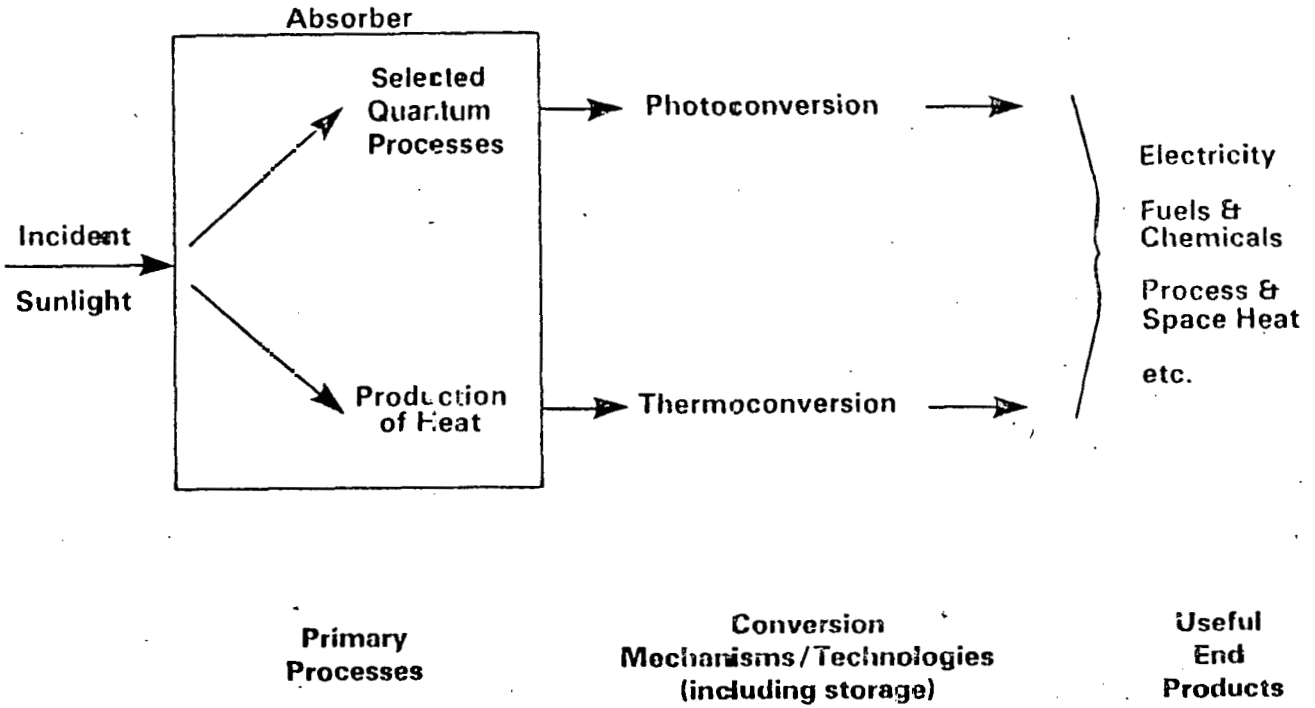
Any new conversion technology must fit into this overall scheme, either deriving from primary quantum processes, or from the heat produced in some absorber. Note, too, that storage of the energy produced along any of these paths can occur at any point along the horizontal axis, e.g., storage of the final electricity product in batteries, or of the primary excited photochemical states in a suitably stable chemical compound.

---

* SERI/MR-12-207, Institutional Plan for the Solar Energy Research Institute, Fiscal Year 1980-1985, April 1979.

Furthermore, the horizontal axis is a continuum in mission-oriented research. Domains of fundamental research occur near the left-hand side. These evolve into mission-oriented research as one proceeds to the right and begins engineering research and development, market and policy analysis, and the commercialization activities required for the marketplace to accept the technology. The position of the wavy shaded line expresses qualitatively the kind of research still required and distinguishes the near-term technologies from those far removed from application.

Solar Radiation Processes and Conversion Paths



SERI

FIGURE I

Detailed Framework for Solar Thermoconversion Paths

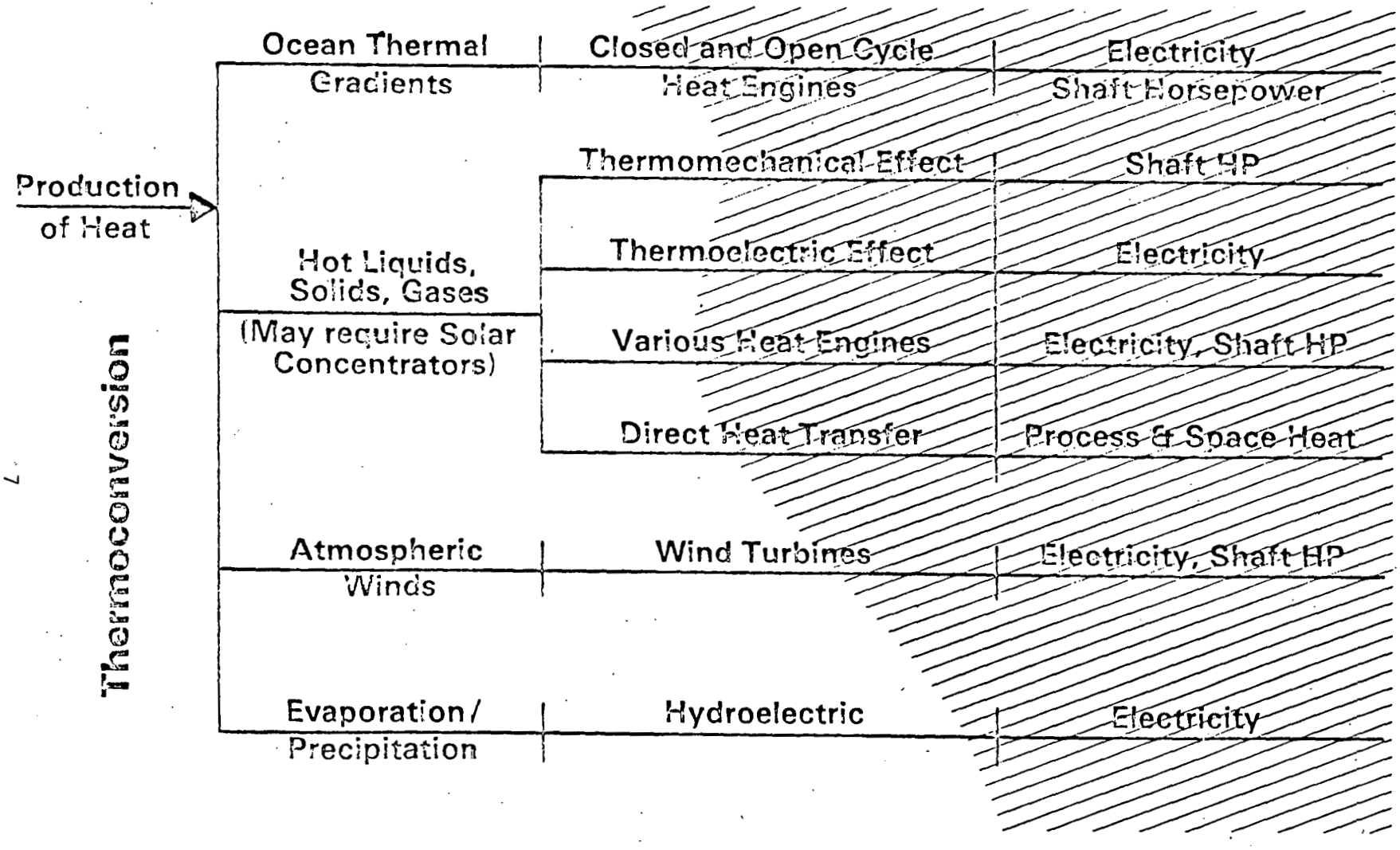


FIGURE 2

Detailed Framework for Solar Photoconversion Paths

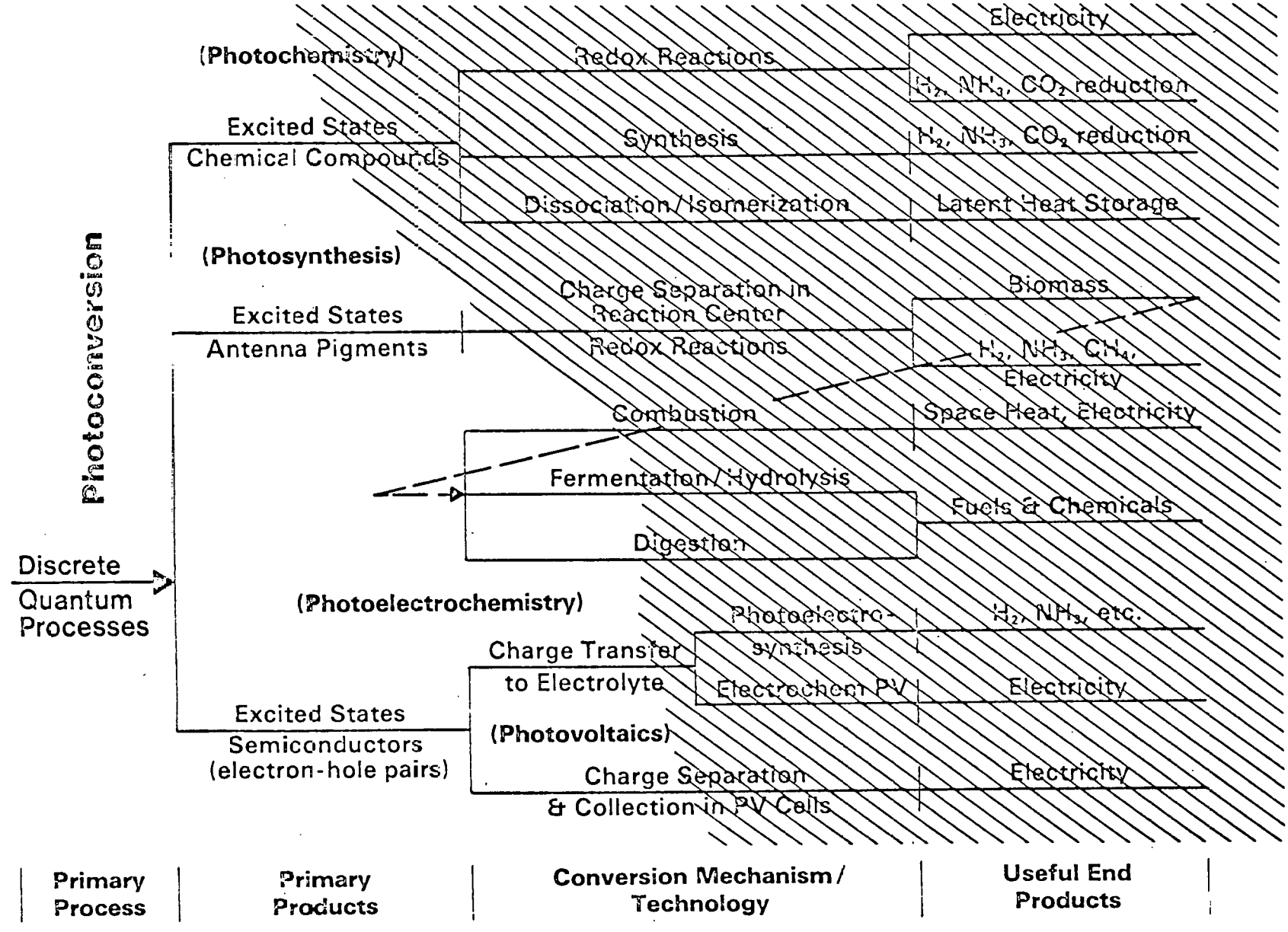
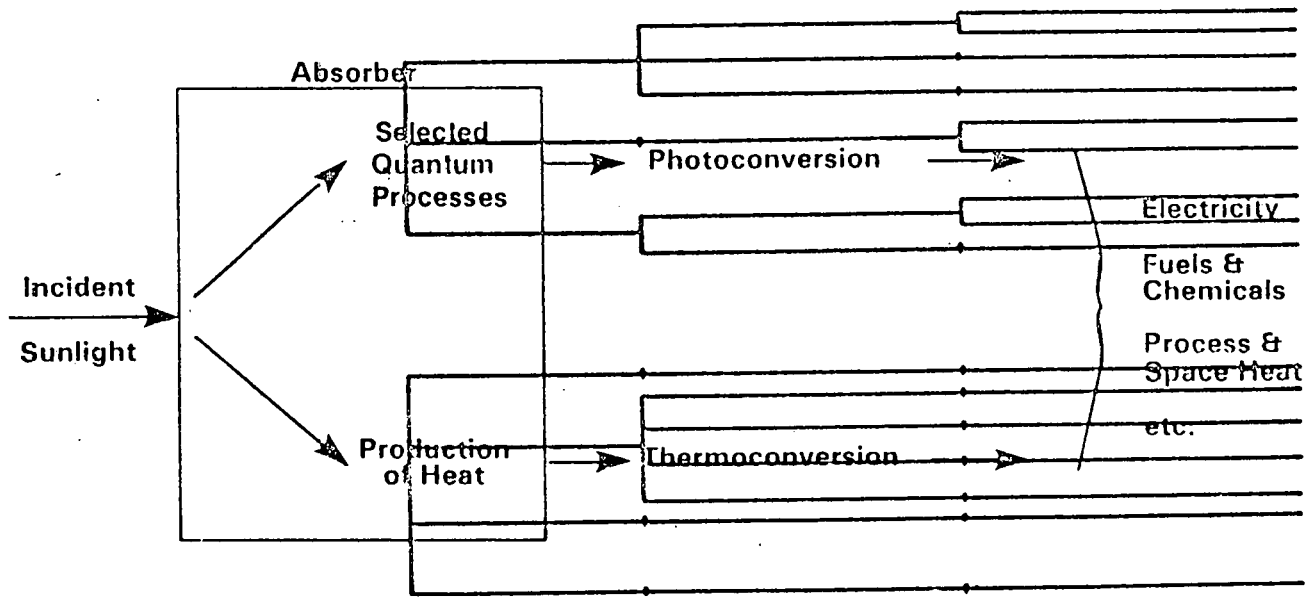


FIGURE 3

SERI

Solar Radiation Processes and Conversion Paths



Primary Processes

Conversion Mechanisms / Technologies (including storage)

Useful End Products

SERI

FIGURE 4

Detailed Framework for Solar Photoconversion Paths

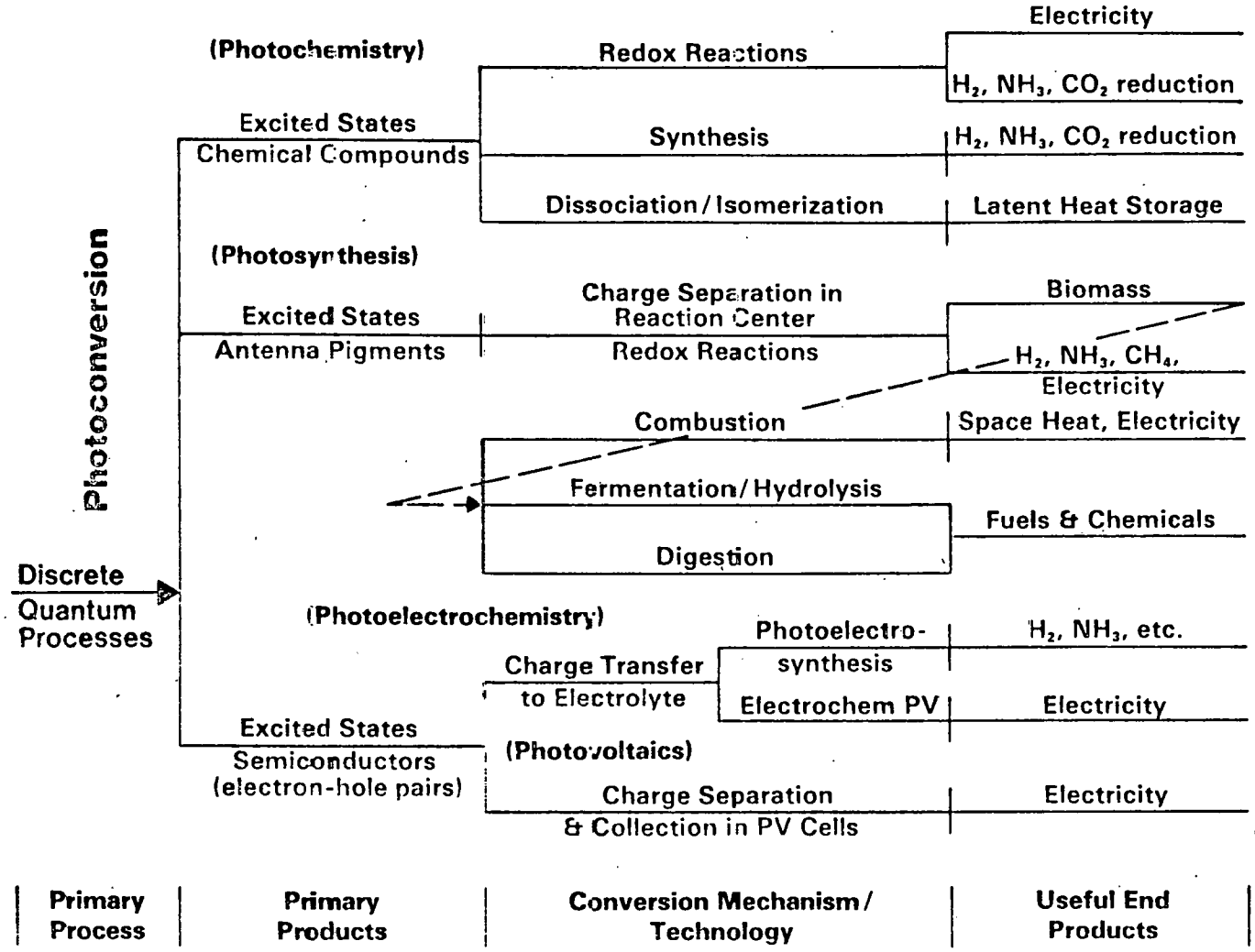


FIGURE 5

Detailed Framework for Solar Thermoconversion Paths

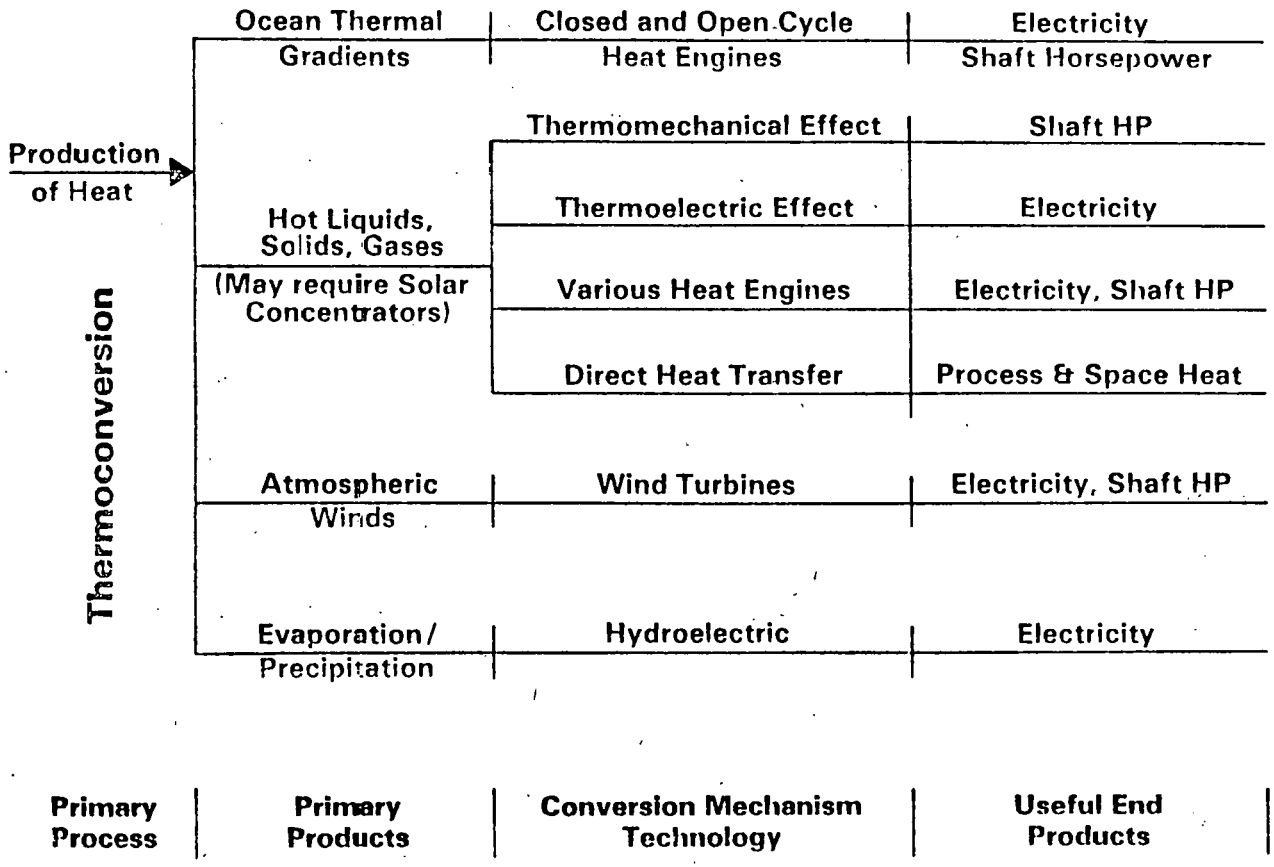


FIGURE 6

THIS PAGE

WAS INTENTIONALLY

LEFT BLANK

Introductory Paper

SOLAR MATERIALS R&D OVERVIEW EMPHASIZING SOLAR THERMAL POWER SYSTEMS

by

B. L. Butler

Branch Chief--Materials Research Division

Solar Energy Research Institute

Golden, Colorado

Abstract

A brief discussion is presented about the major thrusts of the DOE/SERI materials program. The more significant problem areas are identified as are the planned elements of a materials program which address those problems. Relevant research areas are outlined.

Introduction

The long-range goal of the materials research program is to lower the life-cycle costs of solar thermal systems. This goal can be achieved by improving performance, lowering cost and increasing useful life or by combinations of the above. The program has been designed to support three major areas. They are: receiver technology; optical concentrator technology; and performance and reliability of materials. In each of these areas limitations have been identified by the major hardware demonstration projects sponsored by DOE,[1-3] whereas basic research needs have been identified by the Office of Energy Research.[4-5] The activities in each of these technologies are shown in Table I.

The solar technologies are related to materials research and development by the functions which the materials are asked to perform. The relation of solar components to materials disciplines is given in Figure 1. Most solar systems require an optical window or concentrator, an energy receiver/converter, an energy transfer system and supporting structures. The two major exceptions are wind and ocean thermal energy systems which use the atmosphere and ocean surface to replace the optical window or concentrator. The components of solar systems require materials to perform the optical, energy transfer and storage and structural functions outlined in Figure 1. In addition to the primary function the materials must also provide long stable lives for components while maintaining low capital and maintenance costs. Aggressive terrestrial and component environments make selection of low cost stable components difficult.

Disciplinary materials research to provide materials options to solar component designers must consider the component requirements and the materials functions. If materials can not be adapted or developed for the perceived needs, the designer must redesign the component or modify the specifications or the operating environments. The materials research activities must support the system and component design community.

Materials research is divided into Basic Fundamental research, Applied research and Performance research. The basic materials research funded by DOE/Office of Energy Research deals with generic material, properties and behavior. This research provides the basis for the Applied research, which uses specific materials in simulated solar environments to determine the practical applications of materials. Applied materials research is funded by DOE/Energy Technology. The performance research is used to document how real materials perform in real environments so handbooks can be developed. This phase of the research has been sponsored by DOE/Conservation and Solar Applications. Each of these entities at DOE supported solar materials research in FY79, with ET supporting the major share.

Receiver Technology

The major material problems associated with solar thermal receivers are: (a) thermal stress; (b) fatigue; (c) corrosion; (d) compatibility of receiver/heat exchangers with heat transfer fluids; (e) properties and stability of absorber surfaces. The high temperature (1100^{0}C) and high concentration (1000X) applications have stimulated work on metallic super-alloys and on high temperature ceramics such as silicon carbide. Heat transfer fluids, such as liquid sodium, molten salts, high pressure steam, and high temperature gasses such as He and air, exacerbate the thermal environment. Metallurgical research is aimed at understanding how metals respond to the thermal, thermal-mechanical and environmental stresses produced by heat receiver operation. The effects of alloying elements, heat transfer fluids and thermal transients on metals must be known in order to design long-life receivers. Ceramic research activities are focused on receiver designs that use brittle ceramics such as silicon-carbide. Ceramics, thermal shock and fracture

toughness must be related to their microstructure and processing history. R&D efforts should yield tailored ceramics and metals for solar applications. Environmental and thermal stabilities of solar thermal absorber coatings are important because they affect receiver performance and life. High absorptance coatings are being studied for high temperature, high concentration systems. High absorptance, low emittance "selective" coatings are being studied for the 400^{0}C temperature range and improved low temperature selective coatings are being evaluated for process heat applications. Chemical changes resulting from high temperature diffusion and reaction with both the atmosphere and substrates at present limit operating temperatures. Research to understand and mitigate these effects is the thrust of the absorber program.

Optical Concentrator Technology

Development of cost-effective solar concentrators will depend on the availability of improved transmitting and reflecting materials which not only cost less but do not sacrifice performance or life. Many materials have been used for solar concentrators, but their use has not been optimized. The durability and stability of anodized aluminum and of composite stacks of silver on glass and silver on plastic films are being investigated. The mechanisms of silver and aluminum corrosion are being studied to determine how to protect these metals in outdoor environments. The optical and mechanical properties of transmitting plastics and structures to support and shape mirror surfaces are also being optimized.

Performance and Reliability or Materials

Long-term performance and reliability of materials have had the least emphasis in the past, but are now receiving more attention. The performance of a given solar system depends on the optical properties and geometry of the components. The appropriate optical properties must be measured to allow systems designers to calculate expected performance. Optical property standards and measurement procedures are being developed by the National Bureau of Standards, the American Society for Testing Materials and the National Laboratories. Mechanical characterizations are already available

for most structural materials but not for high temperature receiver materials.

Changes in optical and mechanical properties can cause scattering and absorption. Dust can have similar effects. How and why these changes take place are the subjects of many investigations. Polymers and glasses are being studied most widely. Corrosion often limits the component life; so quantitative corrosion monitoring techniques are being developed to allow life prediction and study techniques to inhibit corrosion.

The area of appropriate life testing is being studied intensively. Ways to certify both performance and life have been pioneered by the auto industry. Their technology and methods will serve as a guide to the solar program. Accelerated life testing will be performed in laboratories and at the solar thermal component test facilities at Georgia Institute of Technology, Sandia, SERI and Jet Propulsion Lab. Specification of the operating environments will be a primary thrust of this program.

Conclusion

The solar materials program is focussed on obtaining appropriate data on material performance, on developing methods to study performance as a function of time, and on optimization of materials for solar applications to reduce amounts and costs of materials required. The materials program has evolved over the past four years through problems encountered in design construction and operation of solar collector systems both within and outside the Department of Energy.

FIGURE 1 RELATION OF SOLAR COMPONENTS TO MATERIALS RESEARCH

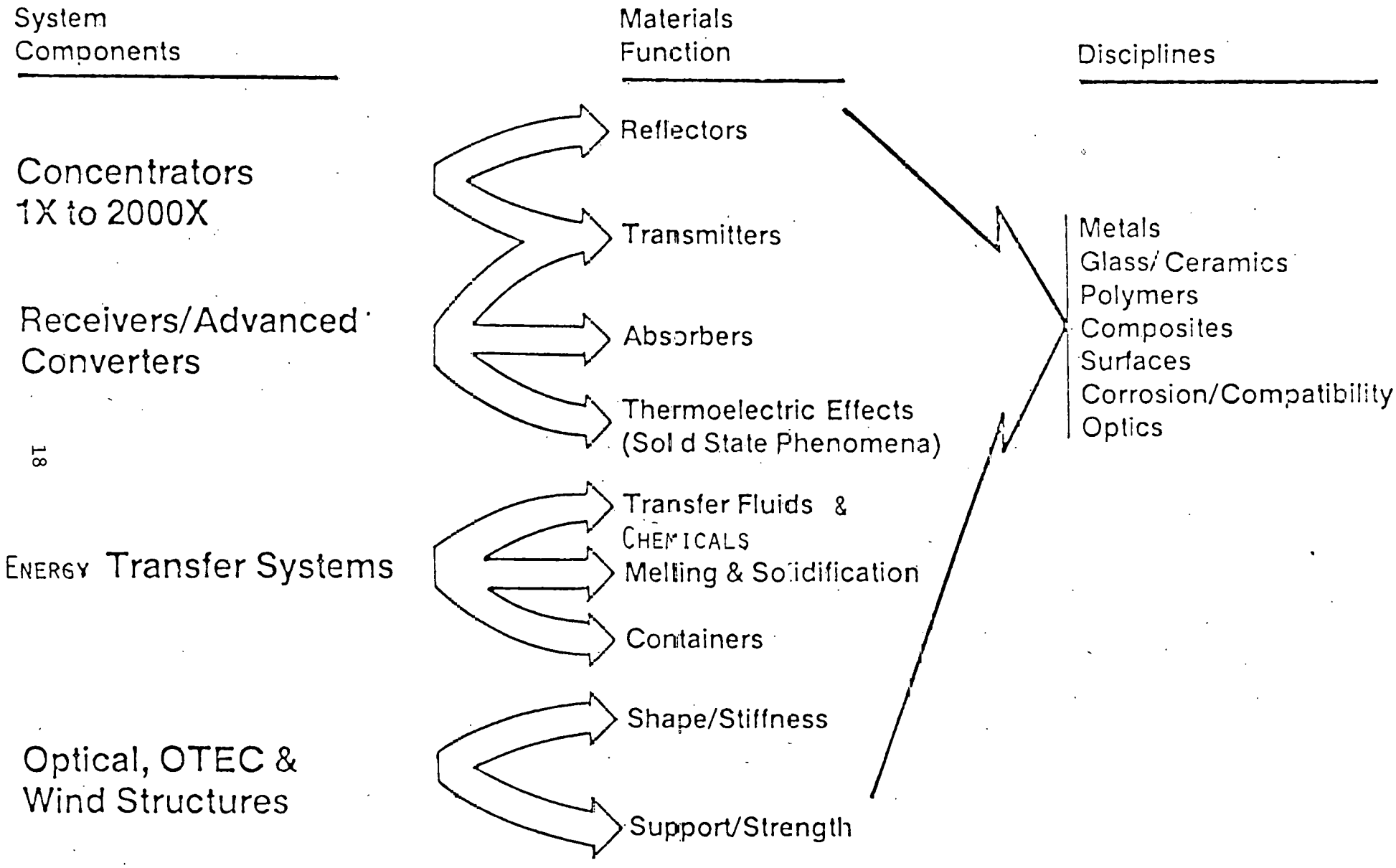


TABLE I

Solar Thermal Materials Program

I. Receiver Technology
   A. Ceramics
      1. Thermochemical receivers
      2. Porous ceramic thermal receivers (SiC, cellular glass)
      3. High temperature receiver tube development
   B. Metals
      1. Receiver materials characterization (9Cr-1Mo, Inconel 617)
      2. Heat transfer fluid compatibility and stability
   C. Absorber Surfaces
      1. High temperature absorbers
      2. Intermediate temperature selective absorbers (black cobalt, organometallic solutions, cermets)
      3. Low temperature selective absorbers (black chrome, alumina-molybdenum-alumina)

II. Optical Concentrator Technology
   A. Transmitters
      1. Glazing characterization
   B. Reflectors
      1. Silver alloy research for polymer reflectors
      2. Thin and ultrathin glass research
      3. Polymer coatings for silver mirrors
      4. Thin aluminum reflectors
      5. Reflectance measurement standard development
      6. Mirror corrosion (silver)
   C. Structures
      1. Cellular glass research
      2. Advanced lightweight structures, and designs to utilize them

III. Performance and Reliability Technology
   A. Characterization
      1. Optical characterization of reflectors and transmitters
      2. Absorber characterization
      3. Mechanical characterization

B. Degradation
   1. Optical polymers
   2. Glass
   3. Dust accumulation and cleaning
C. Corrosion
   1. Monitoring of solar systems
   2. Failure analysis
D. Thermal/Mechanical Fatigue and Shock
   1. Metals
   2. Ceramics
E. Life Testing
   1. Accelerated
   2. Real time

References

1. Report of the Office of Science and Technology Policy Working Group on Basic Research in the Department of Energy, edited by Dr. S. J. Buchsbaum, June 1978.

2. Solar Thermal Power Systems Program, DOE/ET-0018/1, January 1978.

3. The Solar Heating and Cooling Research and Development Project Summaries, DOE/CS-0010, May 1978.

4. Materials Sciences Programs Fiscal Year 1978, Office of Basic Energy Sciences, DOE/ER-0013, September 1978.

5. Research Projects in the Physical Sciences, DOE/ER-0003 (78), April 1978.

THIS PAGE

WAS INTENTIONALLY

LEFT BLANK

Introductory Paper

EFFECT OF MATERIALS ON THE RELIABILITY OF LARGE ENGINEERING SYSTEMS

by

Dean Roger W. Staehle

Institute of Technology

Minneapolis, Minnesota

REASONS FOR RAISING QUESTIONS ON

RELIABILITY OF SOLAR SYSTEMS

- FEW COMMON THREADS AMONG SOLAR DEVICES--
  EXCEPT VERY GENERALLY

- BIG DEVICES HAVE SAME ONUS AS LARGE PLANTS
  ANYWHERE

- SMALL DEVICES (ALMOST MAJOR SERI EFFORT) MUST
  BE AFFORDABLE BUT RELIABLE FOR LONG TIME

- CREDIBILITY FOR SOLAR PROGRAM

products, developments, and applications in corrosion engineering

Skylab 3 Launch Delayed by Stress Corrosion

Engine Gremlins Delay Maiden Voyage of Space Shuttle

26

It informed us that vast numbers of books in the great libraries of the land are quite literally turning to dust. The reason, according to the *Times* report, is that paper is now made from wood pulp that has been treated with alum-rosin compounds, which give off sulphuric acid, so that the books actually consume themselves, with the help of "rough handling, humidity, heat, mold, and cockroaches."

PUBLIC IMAGE

"...STUDIES OF STRESS CORROSION CRACKING OF NUCLEAR REACTORS ARE NOT NECESSARY SINCE SUCH PROBLEMS WILL BE HANDLED BY SPECIFICATIONS..."

GLENN SEABORG
CHAIRMAN, USAEC (1971)

"...A POSSIBLE ARTICLE ON CORROSION COST IN SCIENTIFIC AMERICAN DOES NOT HAVE BROAD ENOUGH APPEAL..."

EDITOR
SCIENTIFIC AMERICAN (1978)

WHY HAVE CORROSION STUDIES NOT BEEN EMPHASIZED

- o "BLACK MAGIC"
- o "NON-SCIENTIFIC"
- o "NO PROBLEM"
- o DESIGN DOMINATED - NOT LIFE CYCLE DOMINATED
- o INCREDIBILITY: BREACH OF STAINLESS
- o "WORK ALREADY DONE"
- o HARD TO SEE CAUSE AND EFFECT
- o COMPLICATED: STRESS, MATERIAL, ENVIRONMENT

WHY CORROSION IS NOW MORE IMPORTANT

- o Big Machines for Efficiency
  - still weak link problem
- o Small Electronic Devices
  - atomic migration
- o Light Weight Machines
  - Light, Metallic Materials are Reactive
  - High Strength is Unstable
- o Conservation/Resource Availability
- o Lifecycle Emphasis
- o Inflation
- o Political/International Pressures
- o Safety

APPROACHING THE IDENTIFICATION OF ISSUES IN THE RELIABILITY OF MATERIALS FOR SOLAR ENERGY SYSTEMS OBJECTIVES

- DEFINE SPECIFIC ISSUES (CIRCUMSTANCES, CONDITIONS, REGIMES, MATERIALS, DESIGN, STRESS, ENVIRONMENT) WHICH MIGHT (POSSIBLY) REASONABLY (CERTAINLY) CAUSE PREMATURE FAILURE AT TIMES SIGNIFICANTLY SHORTER THAN INTENDED LIFE.

- DEFINE WHAT NEEDS DOING (MATERIALS DEVELOPMENT, DESIGN, ENVIRONMENTAL MODIFICATION, FABRICATION, MONITORING, QUALITY CONTROL, MODEL TESTING, IN-SITU MONITORING, CORRELATION EQUATIONS) TO PREVENT FAILURE.

SET OF DEGRADATION PHENOMENA

- o CORROSION
  - CHEMICAL
  - BIOLOGICAL
  - CHEMICAL-MECHANICAL
- o MECHANICAL
  - FRACTURE
  - FATIGUE
- o RELATIVE MOTION
  - WEAR
  - FRICTION
  - EROSION
  - FLOW
- o EMBRITTLEMENT
  - UV
  - NEUTRON
  - AGING
- o ANIMAL
  - INSECT
  - RODENTS
  - BACTERIAL

TABLE 2 – Mechanical Failures in Metallic Piping and Equipment–1971

Type of Mechanical Failure	% Occurrence 1968	1969	1970	1971	Cumulative*
Abrasion, Erosion or Wear	2.0	6.2	6.8	4.7	5.4
Blisters, Plating			0.5	0.0	0.1
Brinelling			0.5	0.0	0.1
Brittle Fracture	2.0	1.0	1.8	0.0	1.2
Cracking, Heat Treatment	1.0	3.3	1.8	0.7	1.9
Cracking, Liquid Metal Pen.	1.0	0.0	0.0	0.0	0.1
Cracking, Plating	1.0	0.5	0.0	1.3	0.6
Cracking, Thermal	7.1	2.3	2.2	2.7	3.1
Cracking, Weld	0.0	1.0	0.0	1.3	0.6
Creep or Stress-Rupture	4.1	1.9	1.8	0.7	1.9
Defective Material	0.0	1.0	2.2	2.7	1.6
Embrittlement, Sigma	0.0	1.0	0.0	0.0	0.3
Embrittlement, Strain Age	1.0	0.0	0.5	0.7	0.4
Fatigue	11.1	12.9	17.8	16.3	*14.8*
Galling	1.0	0.0	0.0	0.0	0.1
Impact	0.0	0.0	0.0	0.7	0.1
Leaking Through Defects	0.0	1.4	0.0	0.0	0.4
Overheating	0.0	1.9	2.2	2.7	1.9
Overload	4.1	4.8	7.2	4.7	5.4
Poor Welds	4.1	4.3	1.3	6.0	4.4
Warpage			1.3	0.0	0.4
Total	39.5	43.5	47.9	45.2	44.8

*685 cases.

Estimated cost of fatigue failures is $4.7 MM/year.

TABLE 1 – Corrosion Failures in Metallic Piping and Equipment–1971

Type of Corrosion Failure	% Occurrence 1968	1969	1970	1971	Cumulative*
Cavitation	1.0	0.5	0.0	0.0	0.3
Cold Wall	1.0	1.0	0.0	0.0	0.4
Cracking, Corrosion Fatigue	0.0	1.4	2.7	0.7	1.5
Cracking, Stress Corrosion	13.1	11.5	11.5	15.5	*13.1*
Crevice	1.0	1.0	0.9	0.7	0.9
De(metal)ification	0.0	1.0	0.5	0.7	0.6
End Grain	1.0	0.5	0.0	0.7	0.4
Erosion-Corrosion	6.1	3.3	3.2	4.2	3.8
Fretting	1.0	0.0	0.5	0.0	0.3
Galvanic	0.0	0.0	1.4	0.0	0.4
General	18.1	18.1	15.2	9.2	*15.2*
Graphitization				0.7	0.1
High Temperature	0.0	1.9	1.4	1.3	1.3
Hot Wall	1.0	0.0	0.0	0.0	0.1
Hydrogen Blistering			0.5	0.0	0.1
Hydrogen Embrittlement	0.0	0.5	0.5	0.7	0.4
Hydrogen Grooving			0.5	0.7	0.3
Intergranular	7.1	5.3	2.7	9.2	*5.6*
Pitting	10.1	8.6	8.8	4.2	*7.9*
Weld Corrosion	0.0	1.9	1.8	6.3	2.5
Total	60.5	56.5	52.1	54.8	55.2

*685 cases.

TYPES OF ENVIRONMENTS (AGENTS)

- o LIQUID
  - AQUEOUS
  - LIQUID METALS
  - MOLTEN SALTS
- o GAS
  - POLLUTED AIR
  - HIGH TEMPERATURE
- o SOLID
  - EROSIVE PARTICLES
- o VACUUM (SPACE)
  - EVAPORATION
- o ULTRAVIOLET
  - EMBRITTLEMENT
- o NEUTRON
- o ELECTRIC FIELDS (WHISKER FORMATION)
- o BACTERIAL
- o INSECT/ANIMAL

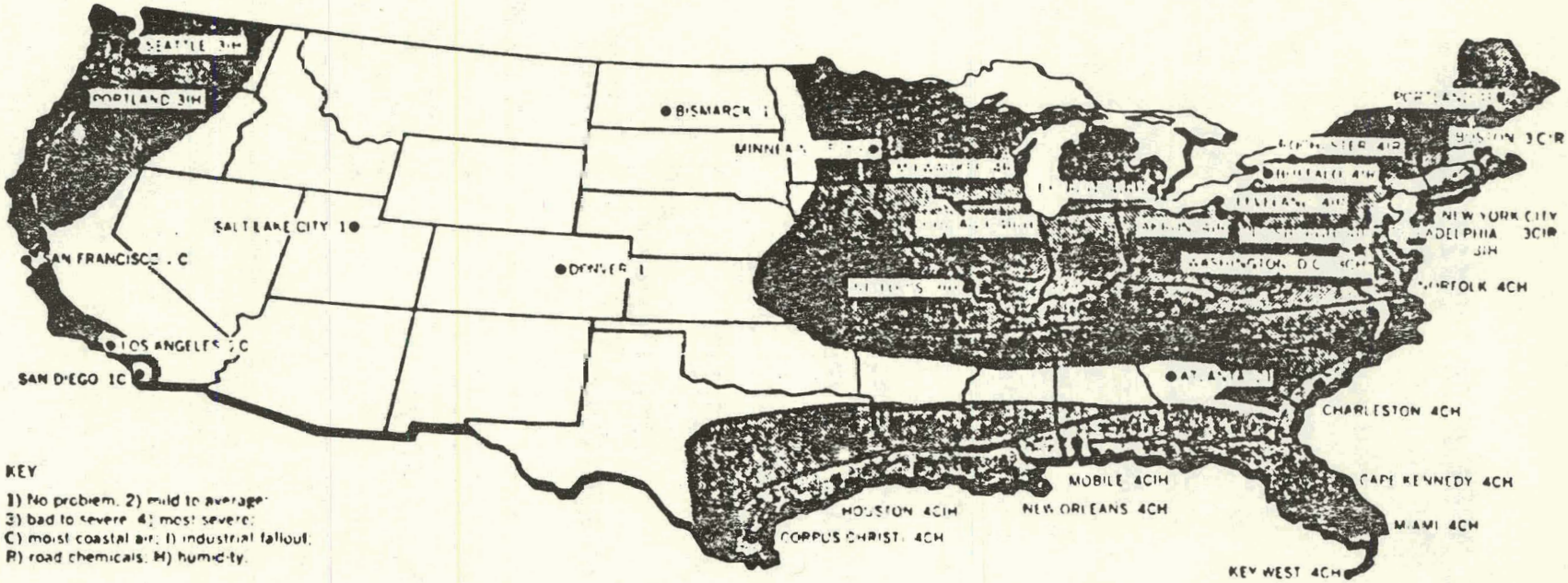
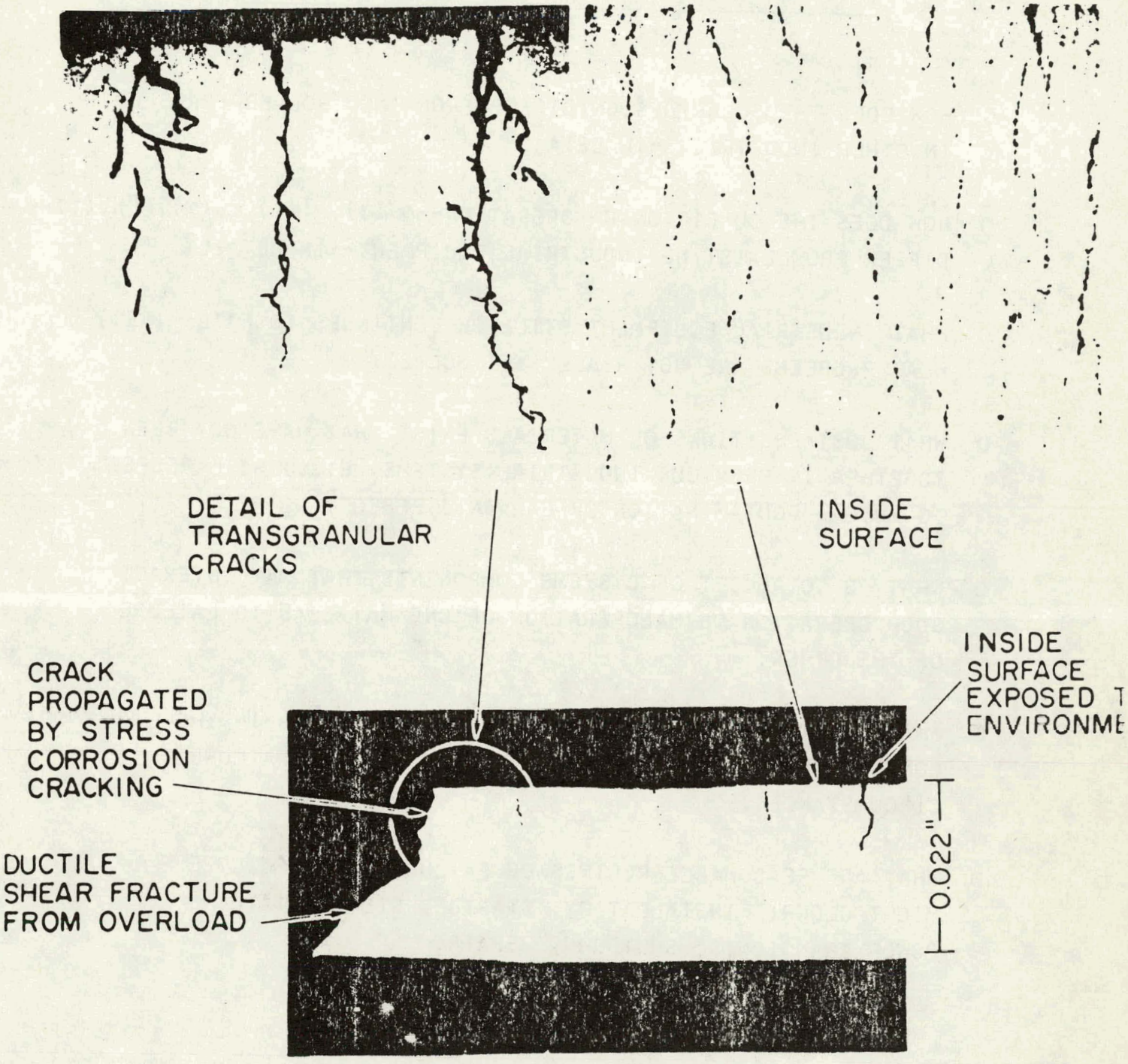


Figure 2—Wherever water and/or industrial fallout exists, rust also exists. Index to rust hazards is supplied by map, Keyed by area and community to the best, through the worst, conditions of sea air, humidity, winter salting, and industrial fallout. (Courtesy of Popular Science Monthly)



Composite showing interaction of stress corrosion cracking and subsequent ductile overload. Example taken from a Ti-6Al-4V alloy exposed to N_2O_4. Specimen taken from a bottle fabricated from this alloy approximately 30 cm by 40 cm in overall dimension. Wall thickness is 0.28 mm.

POINTS OF VIEW FOR IDENTIFICATION OF ISSUES

- HOW DOES THE SOLAR DESIGN DIFFER FROM THE "SOLVED" PROBLEMS IN OTHER INDUSTRIES--IN DETAIL?

- HOW DOES THE CONDITION OF OPERATION--$Q''(\tau)$, $T(\tau)$, $\sigma(\tau)$, $ENV(\tau)$--DIFFER FROM EXISTING INDUSTRIAL EQUIPMENT--IN DETAIL?

- WHAT INDUSTRIAL EQUIPMENT STILL OR CONTINUES TO FAIL, I.E., WHAT PROBLEMS ARE NOT REALLY YET SOLVED?

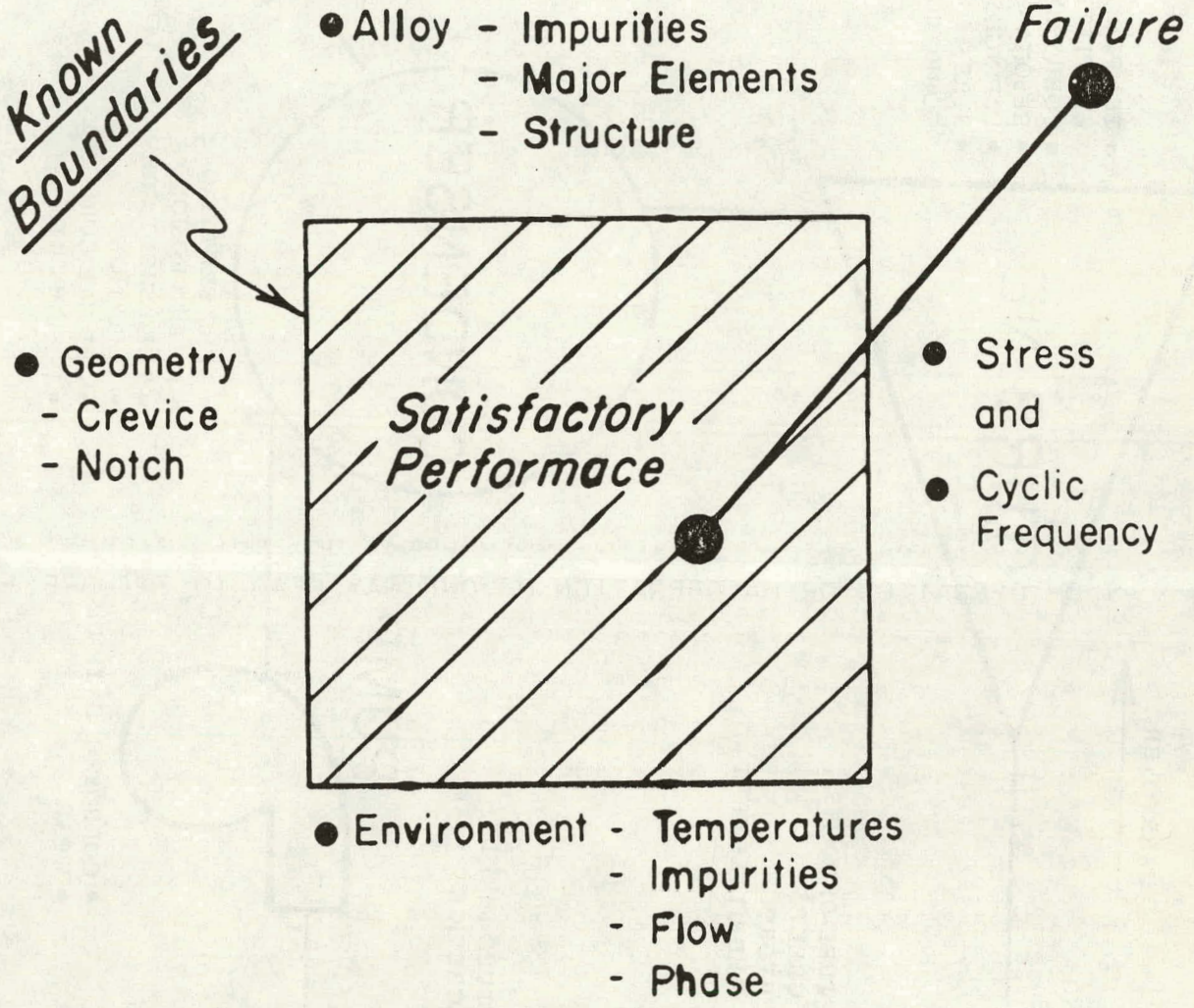
- WHAT JUSTAPOSITIONS OF MATERIALS EXIST THAT HAVE NOT BEEN TOGETHER IN PREVIOUS INDUSTRIAL SYSTEMS, E.G., WITH RESPECT TO MUTUAL CONTAMINATION OR GALVANIC EFFECT?

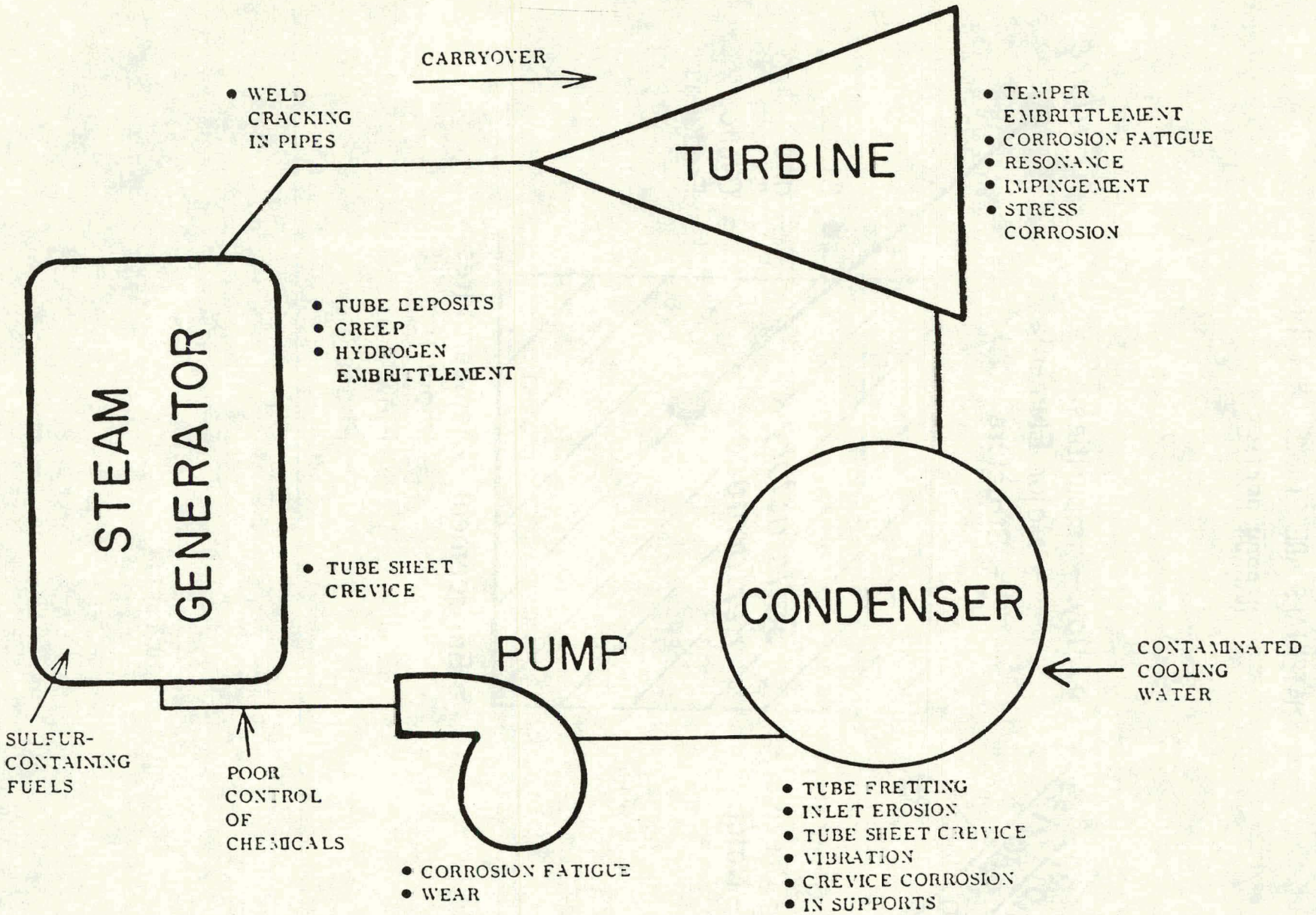
- WHAT IS TOTAL SET OF SYSTEMS COMPONENTS THAT MAY INTERACT SUCH OPERATION OR MALOPERATION OF ONE MAY LEAD TO FAILURE OF THE OTHER?

- WHAT ARE THE REASONABLE ADVENTITIOUS PROCESSES IN THE COMPONENTS--INSIDE OR OUTSIDE--WHICH PRODUCE FAILURE CIRCUMSTANCES?

- WHAT ARE REASONABLE REGIMES OF FAILURE WHERE FAILURE MIGHT OCCUR: INSTALLATION, STARTUP, STEADY STATE, POWER TRANSIENTS, SHUTDOWN, REPAIR.

MATERIALS ARE STABLE ONLY IN NARROW REGIMES



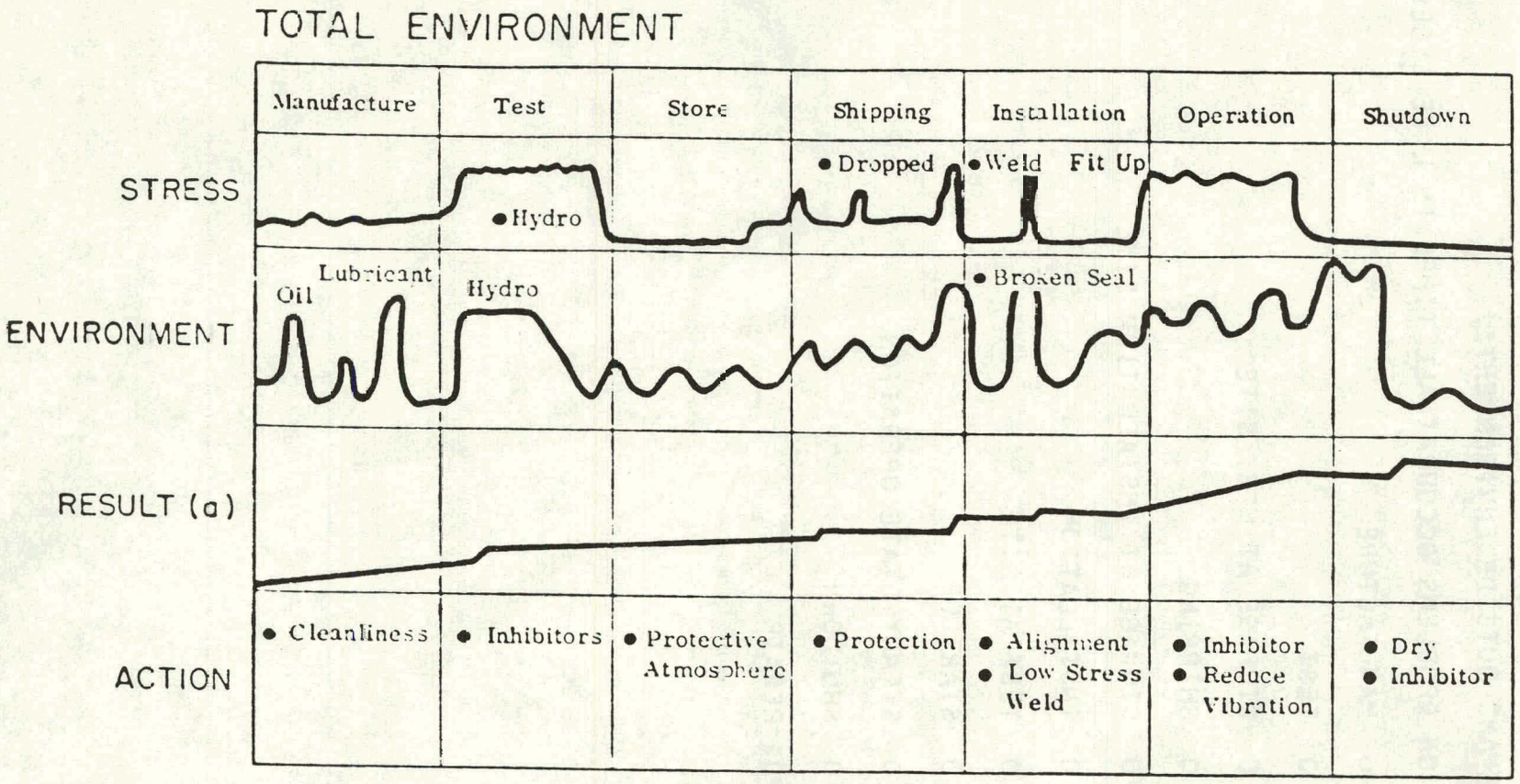

CARRYOVER
• WELD CRACKING IN PIPES
TURBINE
• TEMPER EMBRITTLEMENT
• CORROSION FATIGUE
• RESONANCE
• IMPINGEMENT
• STRESS CORROSION
STEAM GENERATOR
• TUBE DEPOSITS
• CREEP
• HYDROGEN EMBRITTLEMENT
• TUBE SHEET CREVICE
CONDENSER
PUMP
CONTAMINATED COOLING WATER
SULFUR-CONTAINING FUELS
POOR CONTROL OF CHEMICALS
• CORROSION FATIGUE
• WEAR
• TUBE FRETTING
• INLET EROSION
• TUBE SHEET CREVICE
• VIBRATION
• CREVICE CORROSION
• IN SUPPORTS

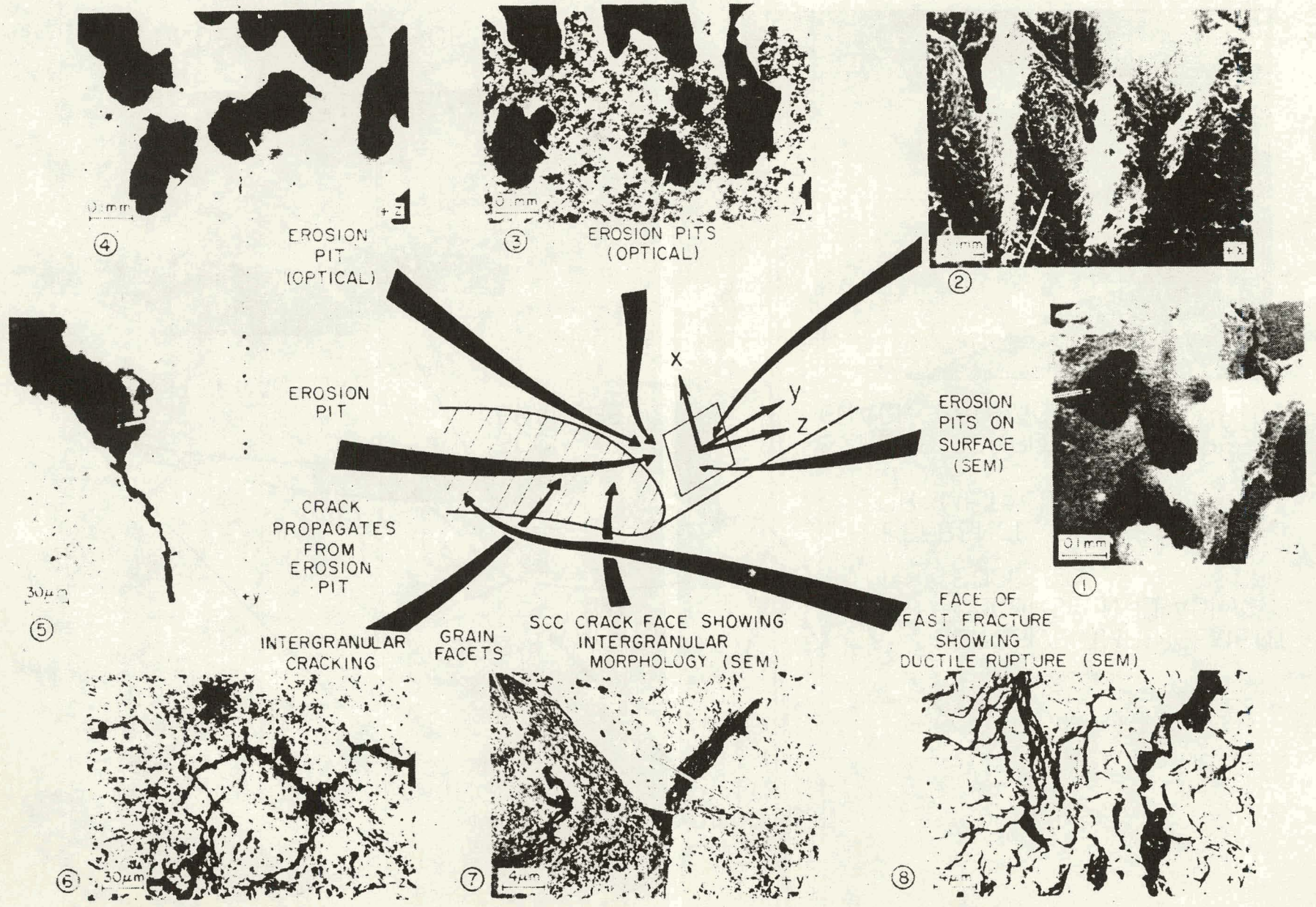
TOTAL ENVIRONMENT

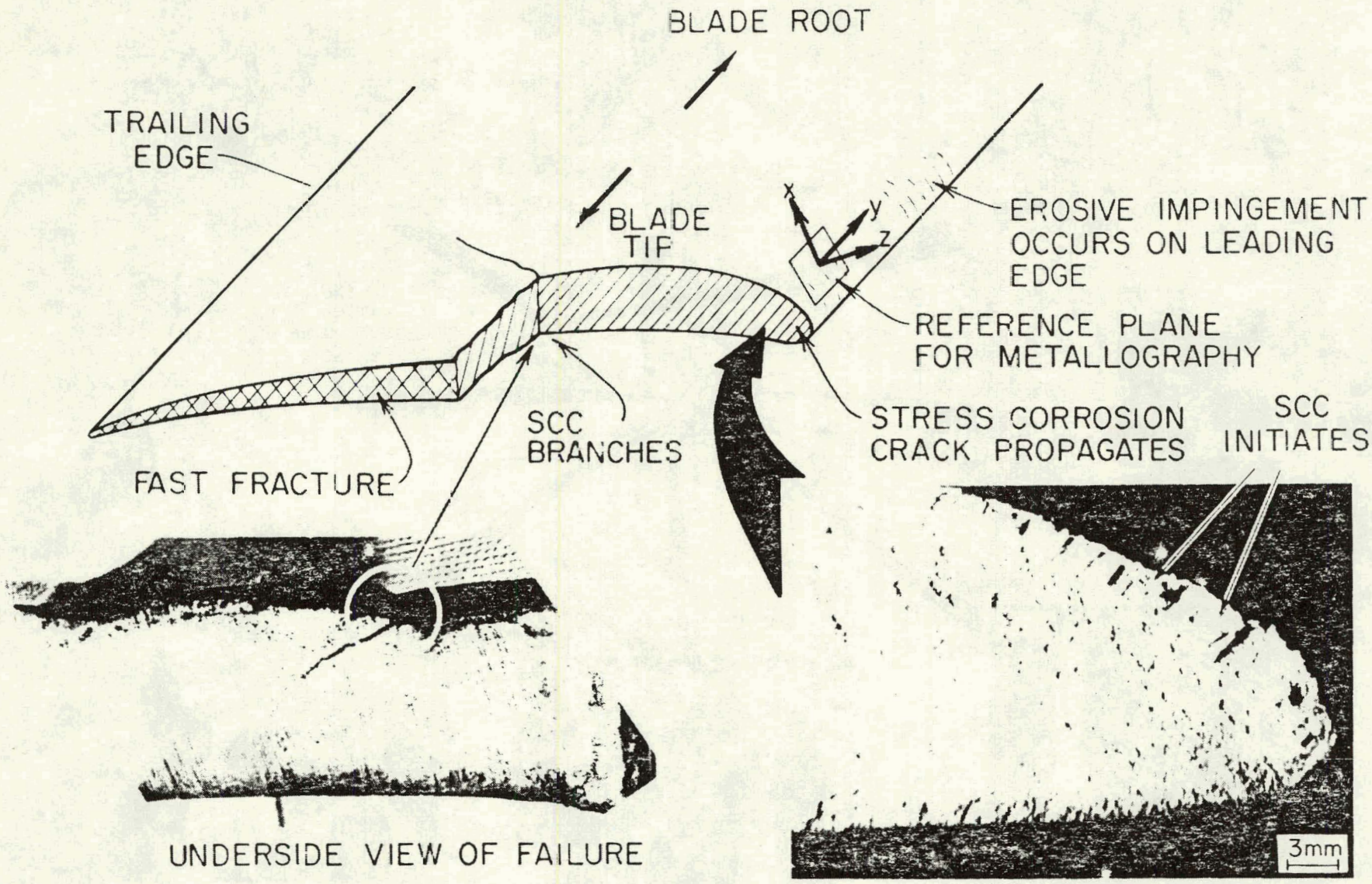
(INSIDE AND OUTSIDE ENVIRONMENTS)

CORROSION PROBLEMS OCCUR AT ALL TIMES IN LIFE CYCLE

- MANUFACTURE
- TEST
- STORAGE AT MFG. SITE
- SHIPPING
- STORAGE AT INSTALLATION SITE
- INSTALLATION
- TEST AT SITE
- START UP
- STEADY STATE OPERATION
- SHUTDOWN
- REPAIR


TOTAL ENVIRONMENT
Manufacture
Test
Store
Shipping
Installation
Operation
Shutdown
STRESS
• Dropped
• Weld
Fit Up
• Hydro
ENVIRONMENT
Oil
Lubricant
Hydro
• Broken Seal
RESULT (a)
ACTION
• Cleanliness
• Inhibitors
• Protective Atmosphere
• Protection
• Alignment
• Low Stress Weld
• Inhibitor
• Reduce Vibration
• Dry
• Inhibitor


EROSION PIT (OPTICAL)
EROSION PITS (OPTICAL)
EROSION PIT
CRACK PROPAGATES FROM EROSION PIT
EROSION PITS ON SURFACE (SEM)
INTERGRANULAR CRACKING
GRAIN FACETS
SCC CRACK FACE SHOWING INTERGRANULAR MORPHOLOGY (SEM)
FACE OF FAST FRACTURE SHOWING DUCTILE RUPTURE (SEM)
x
y
z
0.1 mm
30μm
4μm
+x
+y
+z
-z
1
2
3
4
5
6
7
8


BLADE ROOT
TRAILING EDGE
BLADE TIP
EROSIVE IMPINGEMENT OCCURS ON LEADING EDGE
REFERENCE PLANE FOR METALLOGRAPHY
STRESS CORROSION CRACK PROPAGATES
SCC INITIATES
SCC BRANCHES
FAST FRACTURE
UNDERSIDE VIEW OF FAILURE
3mm

The Saving Of Flight 1080

Why had it stuck? Water from from rain, fog and mist had dripped down a structure in the tail onto a bearing. As the plane had repeatedly ascended and descended during the many flights, changes in pressure had sucked the water into the bearing. The bearing corroded and broke. When Capt. McMahan maneuvered his flight controls just before takeoff, the elevator, linked to the broken bearing, jammed.

APPROACHES TO

UNDERSTANDING AND PREVENTING FAILURES

- MATERIALS ARE CHEMICALS AND MOST ARE UNSTABLE IN ENGINEERING ENVIRONMENTS.
  - QUESTION: NOT WHY DO THEY FAIL, BUT WHY THEY DO NOT FAIL?
- FAILURE IS A MULTIPLICATIVE FUNCTION OF:

  (MATERIALS) (ENVIRONMENT) (STRESS)
- MOST FAILURES FOLLOW PATTERNS OF "CONNECTED CAUSE." CONCEPTS OF MONOTONIC DAMAGE ACCUMULATION NOT USUALLY USEFUL.

EXAMPLE OF BAD ASSUMPTION

- PURE ENVIRONMENTS (H_2O) ARE NOT CORROSIVE
- PURE METALS DO NOT STRESS CORROSION CRACK
- HIGH STRENGTH MATERIALS HAVE STRENGTHS
- TOUGH MATERIALS ARE TOUGH
- CRACKS NEED PRECRACKS TO INITIATE
- FAILURE IS MONOTONIC
- STAINLESS STEEL IS STAINLESS
- THE ONLY STRESSES ARE DESIGN STRESSES
- LOW INITIAL COST PRODUCES ECONOMICAL PLANTS
- "OFF THE SHELF" EXISTS

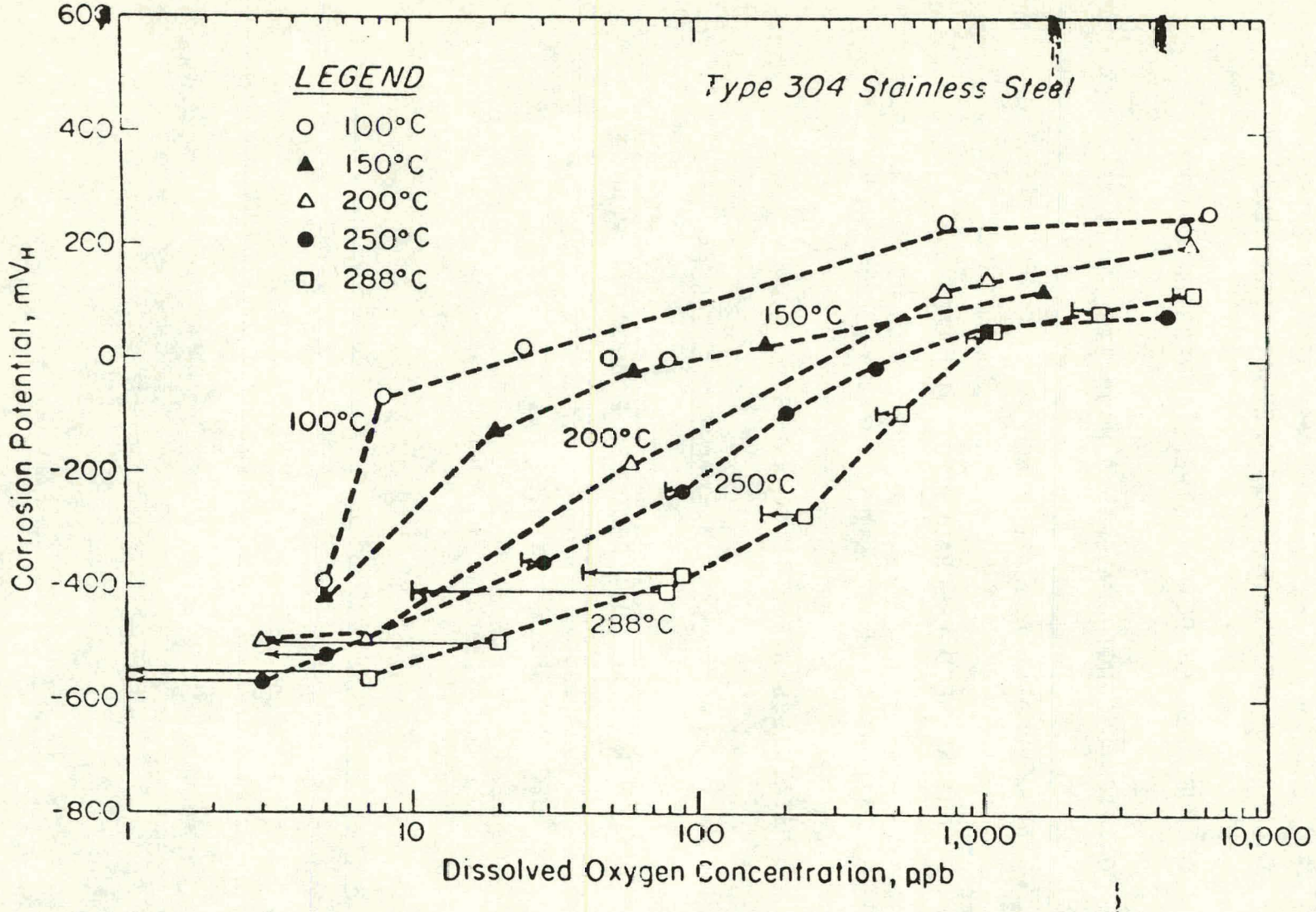


Figure 2.3.1. Corrosion potentials of Type 304 stainless steel as a function of oxygen concentration at 100, 150, 200, 250, and 288°C in high purity water.

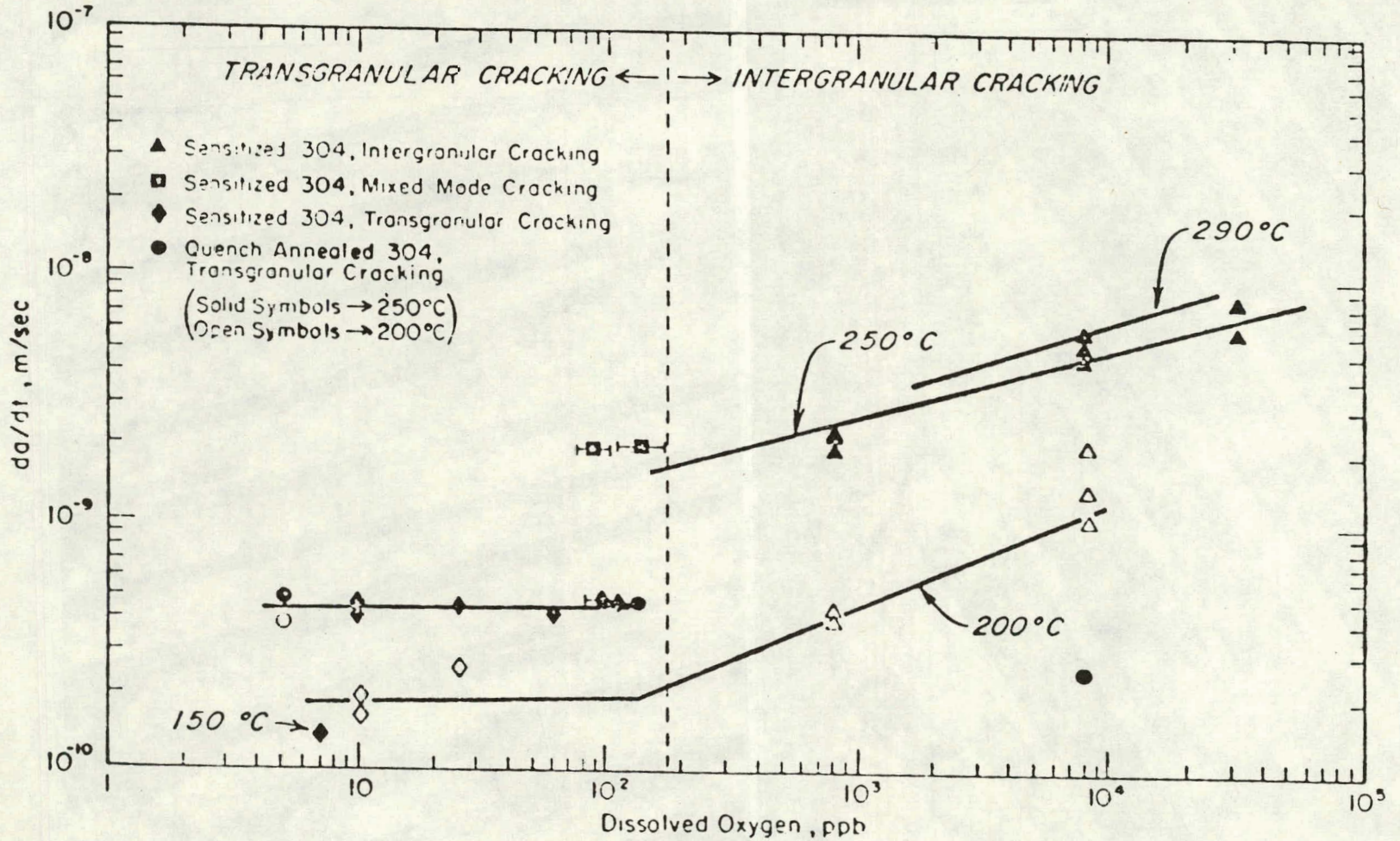
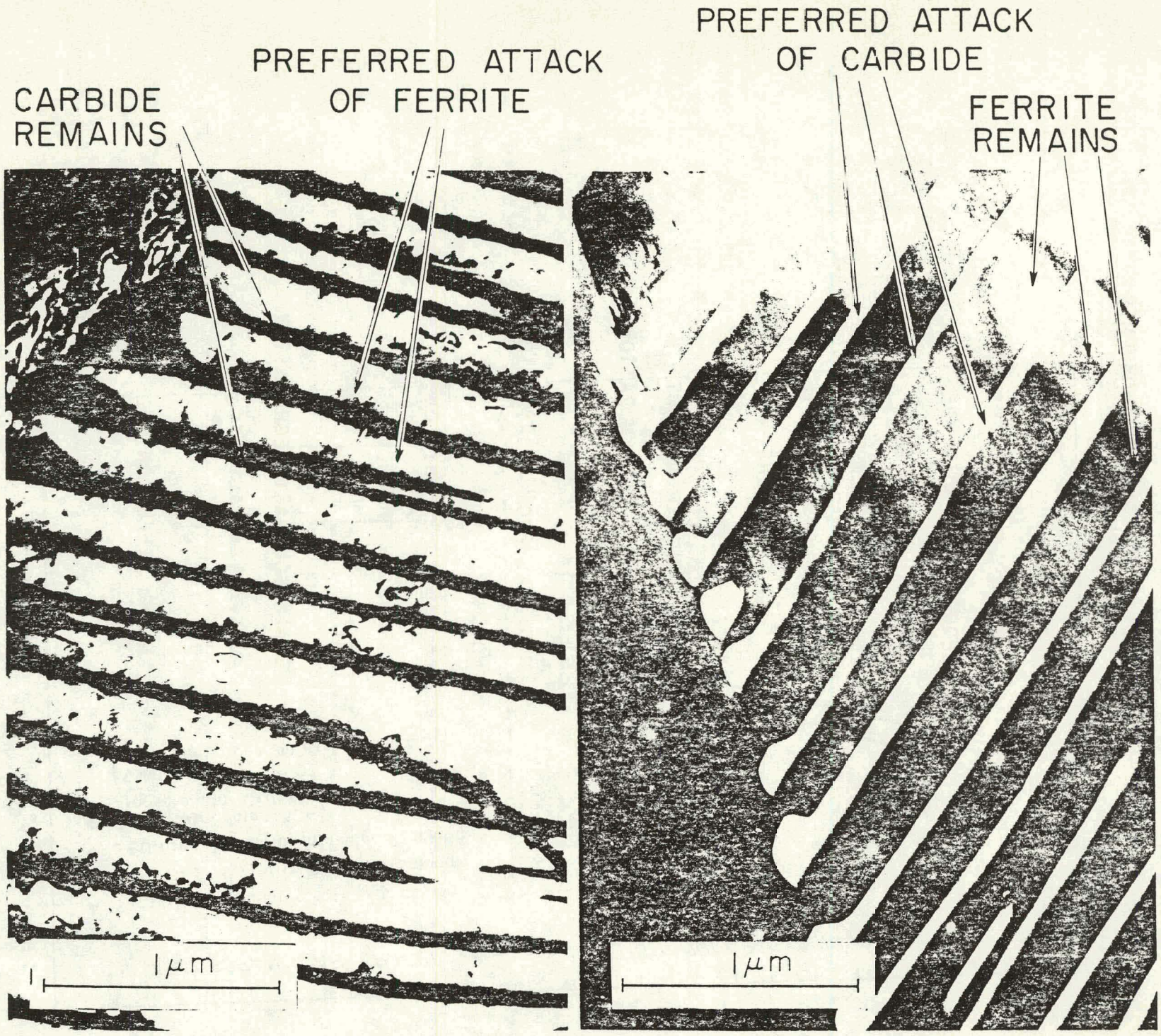


Figure 2.4.3. Estimated stress corrosion crack growth rates of Type 304 stainless steel in high temperature water as a function of oxygen concentration.


CARBIDE
REMAINS
PREFERRED ATTACK
OF FERRITE
1 μm
(a)
PREFERRED ATTACK
OF CARBIDE
FERRITE
REMAINS
1 μm
(b)

ADVENTITIOUS & EXACERBATING ENVIRONMENTS

- o CHEMICAL
  - WET AND DRY (CONCENTRATE)
  - SEQUESTERED MOISTURE
  - OXIDIZING SPECIES
  - LEACHED CHEMICALS
  - CREVICES AND DEPOSITS
  - CATHODIC POISONS
  - BACTERIA
  - HEAT TRANSFER DRY OUT
  - SUPERNATANT CONCENTRATION
- o STRESS
  - RESIDUAL FROM FABRICATION
  - NOTCHES
  - CYCLIC SUPERPOSITION
  - CORROSION PRODUCTS
- o MATERIAL
  - GRAIN BOUNDARY SEGREGATION
  - AGING/METASTABILITY
  - LEACHING
  - INWARD DIFFUSION

EXAMPLES OF ADVENTITIOUS ENVIRONMENT

- ATMOSPHERIC IMPURITIES CONCENTRATED IN COOLING TOWER VAPORS
- SODIUM THROW FROM DEIONIZERS DEPOSITS IN TURBINES
- LEAKING CONDENSERS PRODUCES IMPURITIES IN STEAM GENERATORS
- WET INSULATION LEACHES CHLORIDE
- HEATED PVC PRODUCES HCL
- RETROGRADE SOLUBILITY PRODUCES DEPOSITS
- DISSOLVED OXYGEN AT STARTUP PERSISTS

CONTAMINATED ENVIRONMENTS

AIR

$SO_2 \rightarrow H_2SO_4$	Acid
$CO_2 \rightarrow H_2SO_3$	Acid
$NO_x \rightarrow HNO_3$	SCC, Acid
$NH_3 \rightarrow Cu(NH_4)_x$	SCC
O_3	SCC of Rubber

WATER

Cd^-

F^-

Pesticide (As, Sb)

S^2

Microbes ($SO_4 \rightarrow S^=$)

CO_3

O_2

N_2H_4

TIME DEPENDENCE

- O AGING
- O CREEP
- O PITTING INITIATES FATIGUE
- O LEACHING

CHARACTERISTICS

- O NON MONOTONIC
- O CONNECTED SEQUENTIAL CAUSE

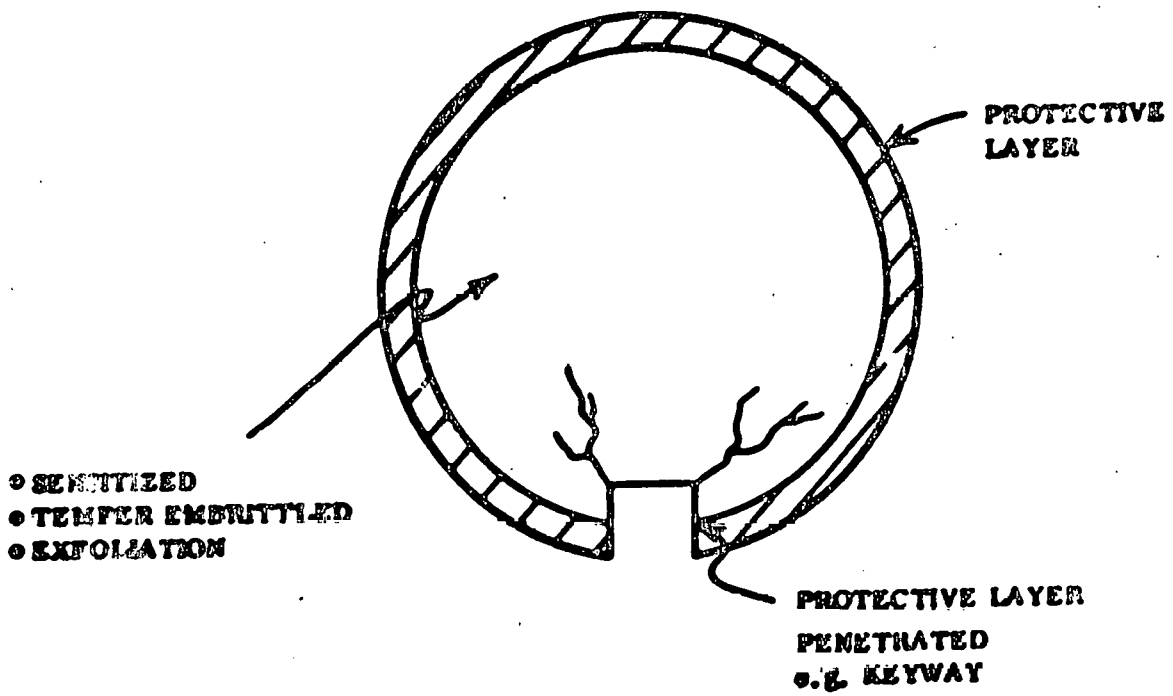
SOURCES OF STRESS

USUAL

- Pressure
- Centrifugal
- Thermal
- Loads
- Stress Concentration

UNUSUAL

- Residual
  - Cold work
  - Welding
  - Identifying
  - "Smoked Tubes"
  - Spatial "Adjustment"
- Corrosion Product Wedging
- Thermal Shock


PROTECTIVE LAYER
• SENSITIZED
• TEMPER EMBRITTLED
• EXFOLIATION
PROTECTIVE LAYER PENETRATED e.g. KEYWAY

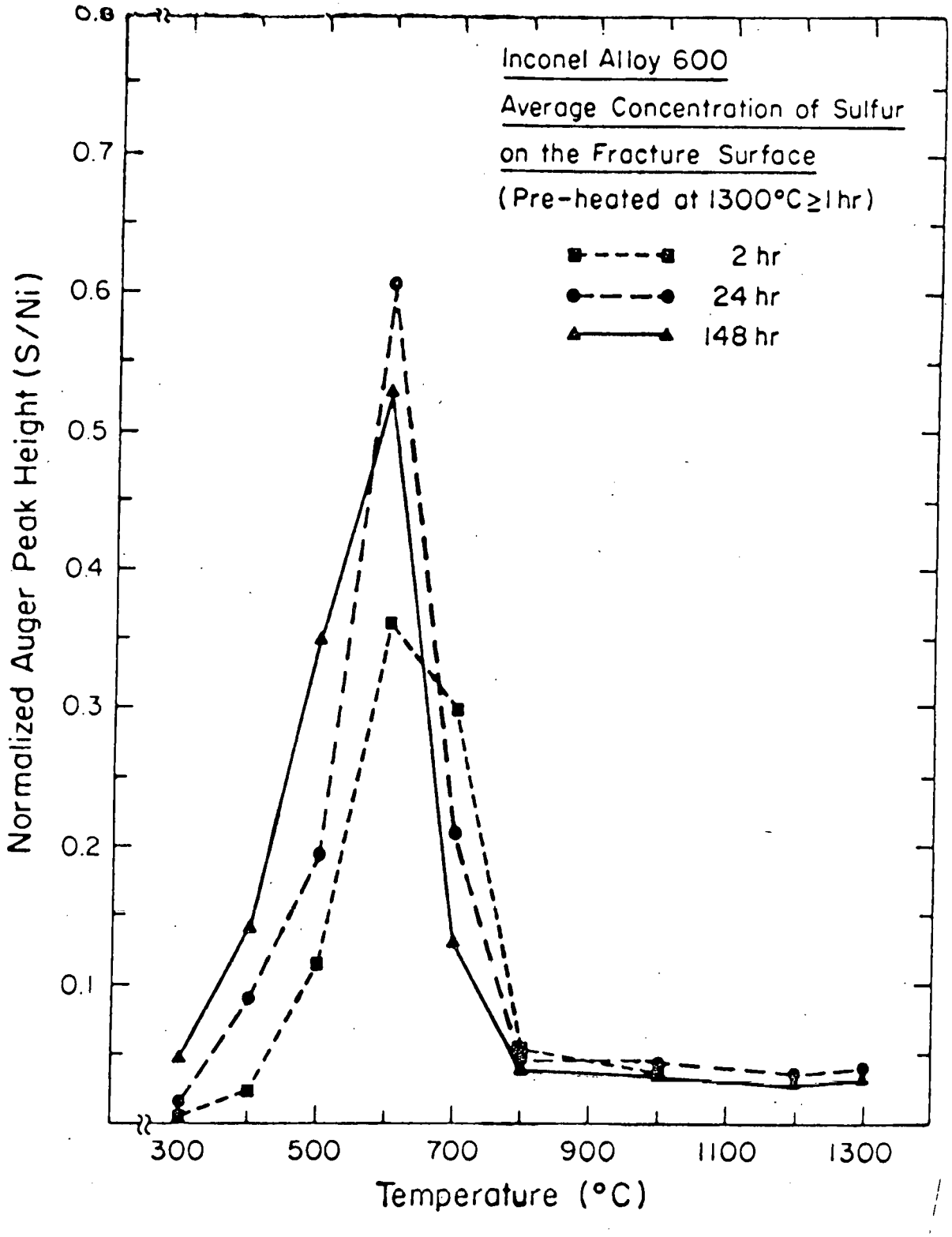


Figure 1.5.3. The changes in average surface concentration on the fracture surface of Inconel 600 as a function of temperature and time.

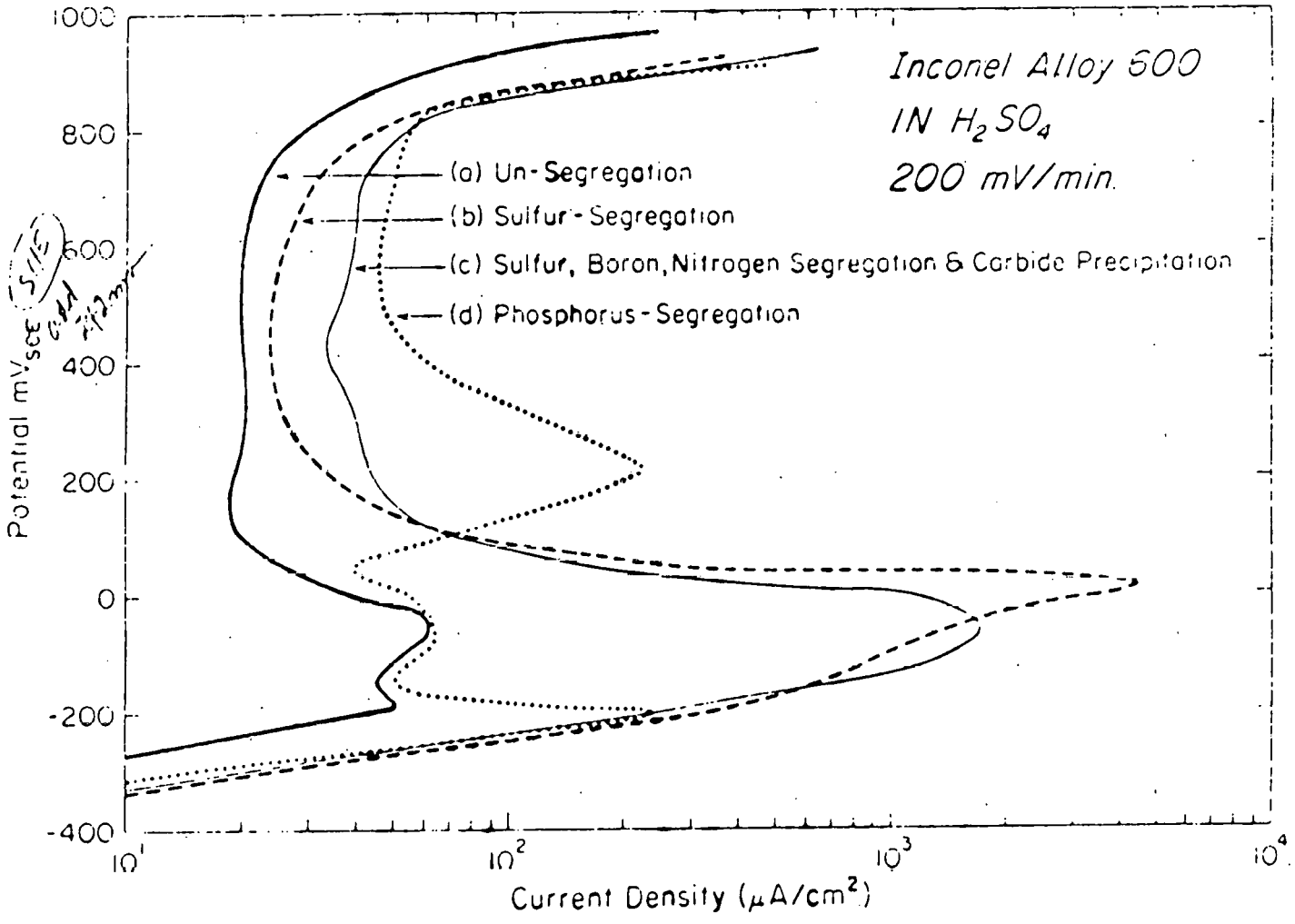


Figure 1.6.2. Polarization ~~behavior~~ of Inconel 600 in 1N H_2SO_4 solutions showing segregation effect.

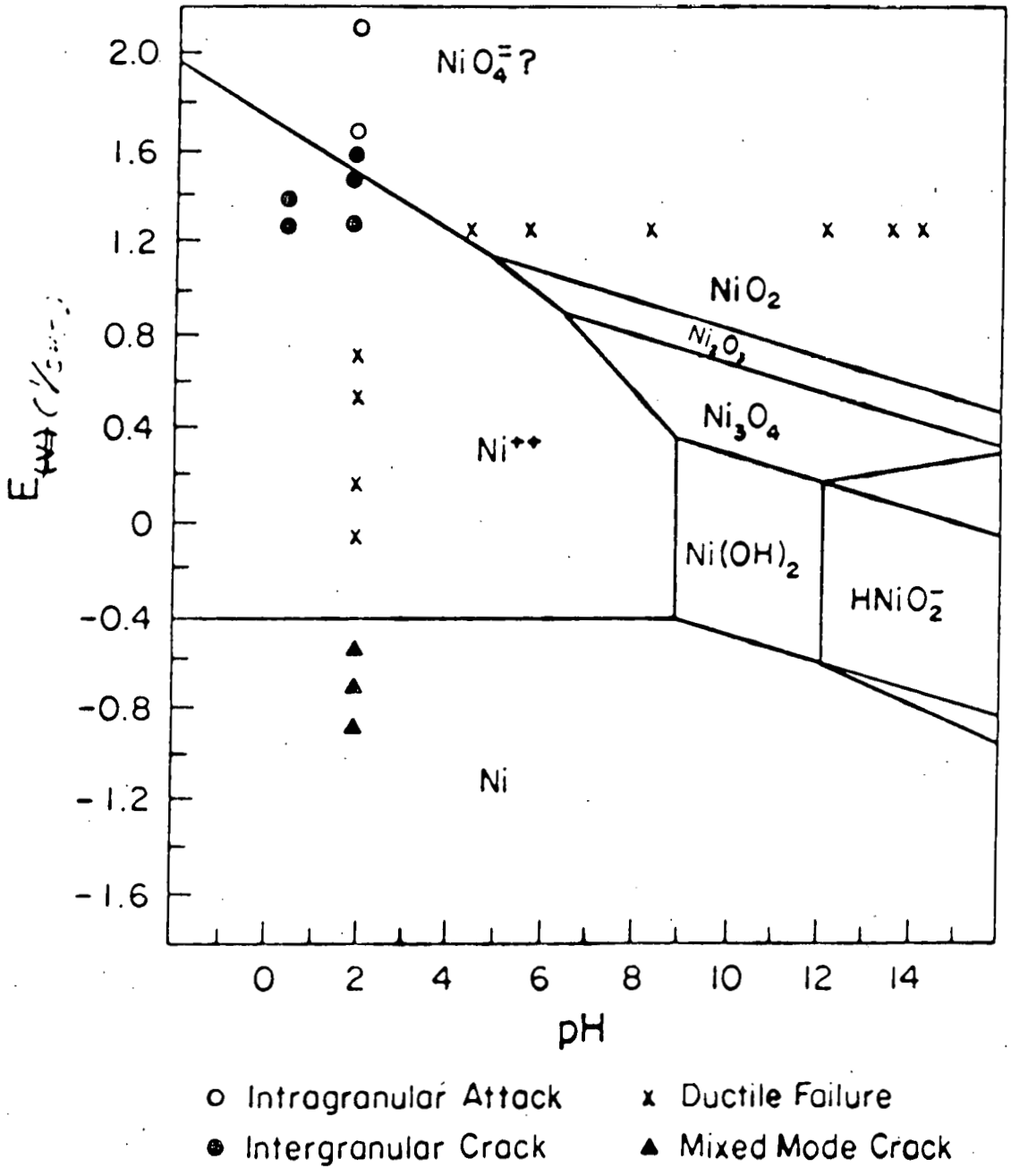


Figure 1.3.7. Slow strain rate failure morphology of Ni tested in H_2SO_4 at various pH levels and applied potentials.

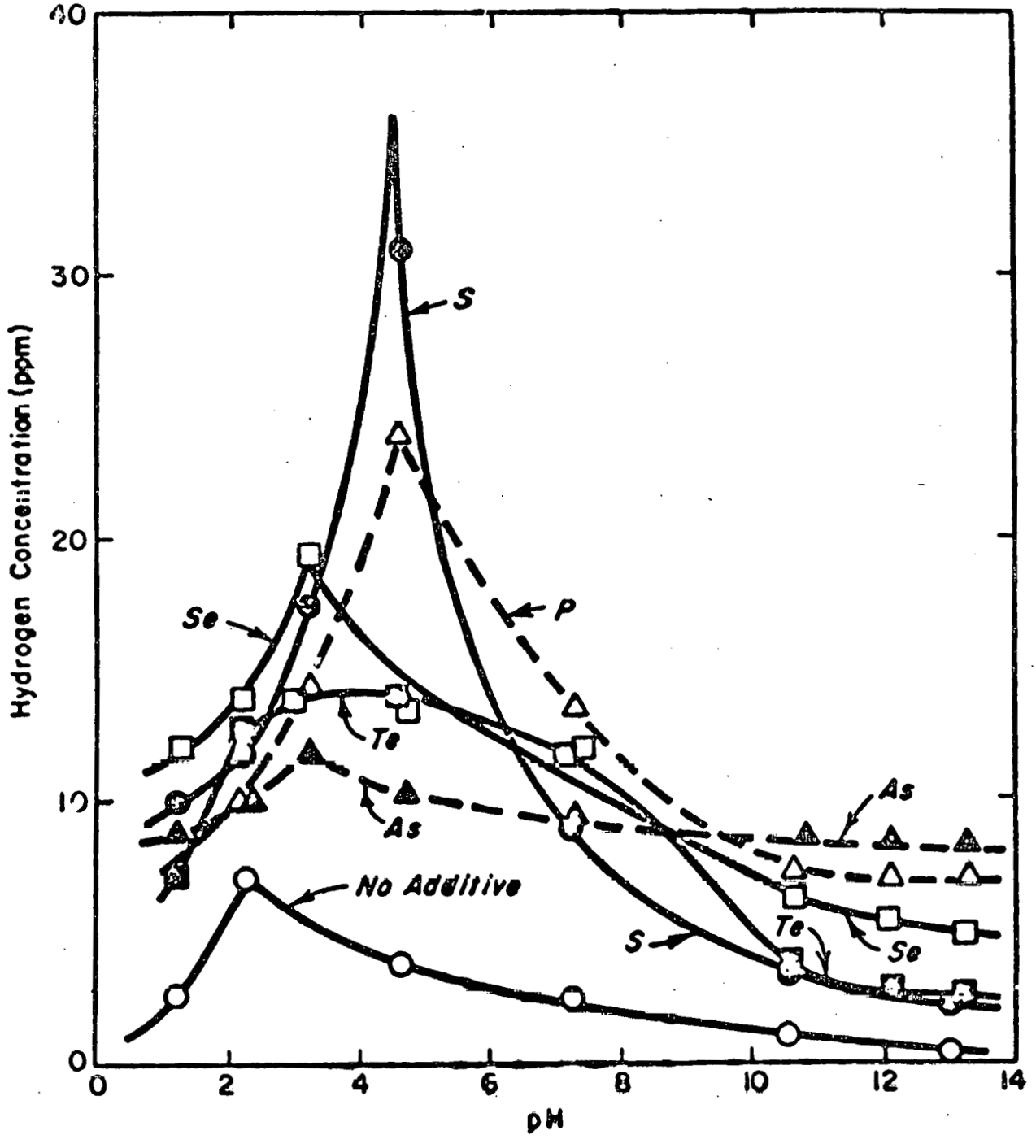


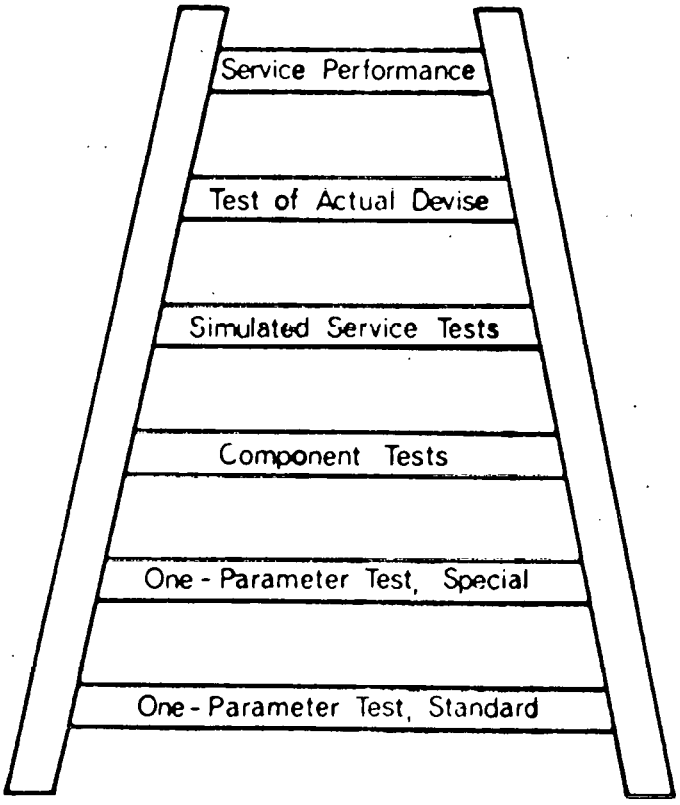
Figure 4.6.2.1

Effect of pH on the efficacy of various promoter elements in the hydrogenation of iron specimens. (From the work of Newman and Shreir) (54).

ERRORS IN EARLY DEVELOPMENT

- PROTOTYPE TESTING DOES NOT MODEL RELIABILITY ISSUES:
  - STRESS
  - MATERIALS
  - HEAT FLUX
  - ADVENTITIOUS
  - ENVIRONMENT
  - FABRICATION
  - CONNECTEDNESS TO COMPONENTS
- PREDICTIVE CAPACITY DOES NOT INCLUDE FULL SET OF REASONABLE MATERIALS, ENVIRONMENTS, STRESS PARAMETERS
- MONITORING AND IN-SERVICE INSPECTION NOT DEVELOPED
- DESIGN FUNCTION DOMINATES
- MATERIALS FUNCTION NOT CONSIDERED
- MOST FAILURES OCCUR FOR REASONS THE FACTS OF WHICH ARE ALREADY WELL KNOWN

Predictive Testing: Degree of Complexity



expensive
time consuming
convincing
limited applicability

more

generally applicable
useful for predictive correlation equation
wide range of parameters
cheap, fast

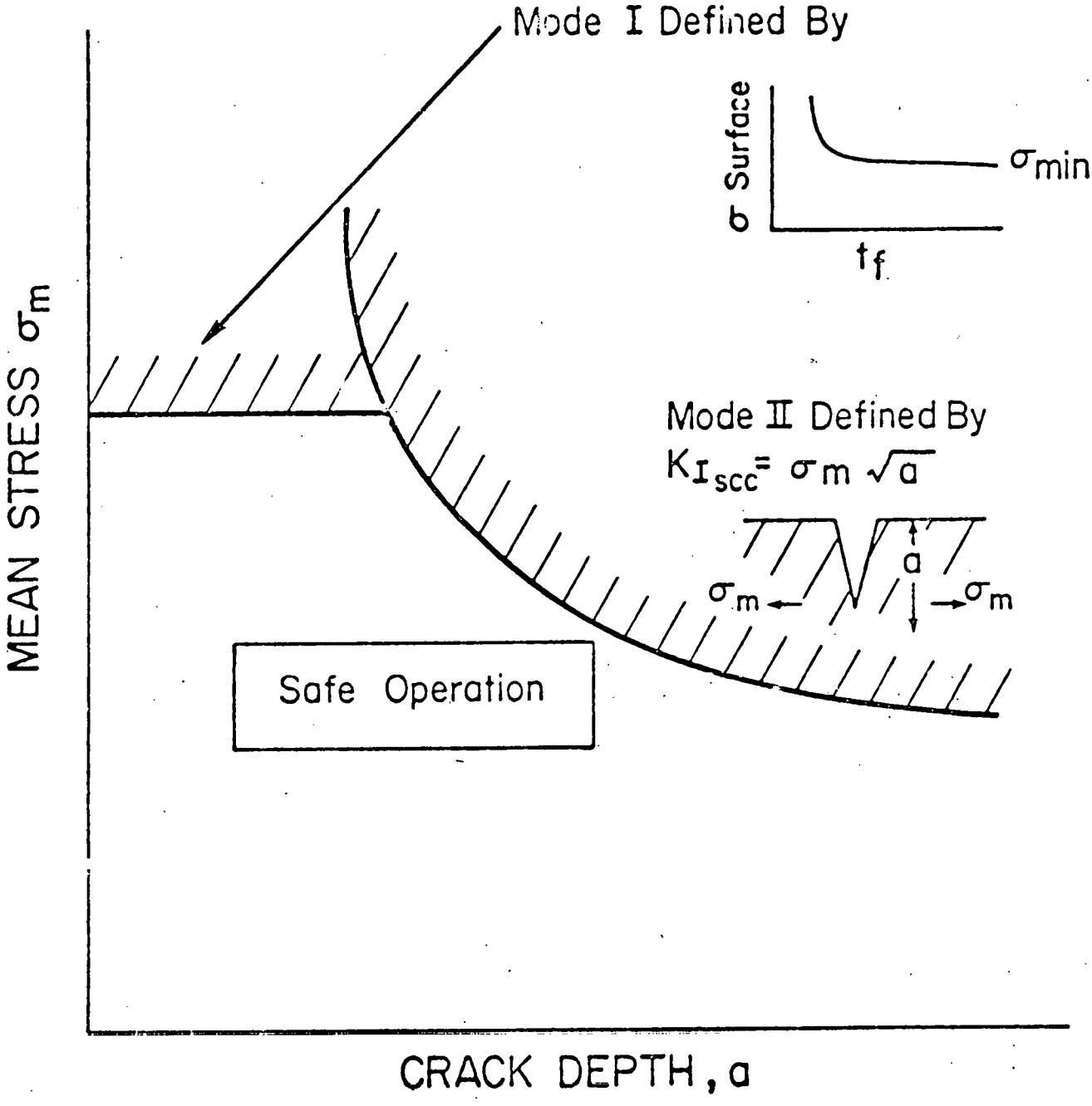


Figure 13 Schematic illustration in the relationship between fracture stress, crack size and fracture mode.

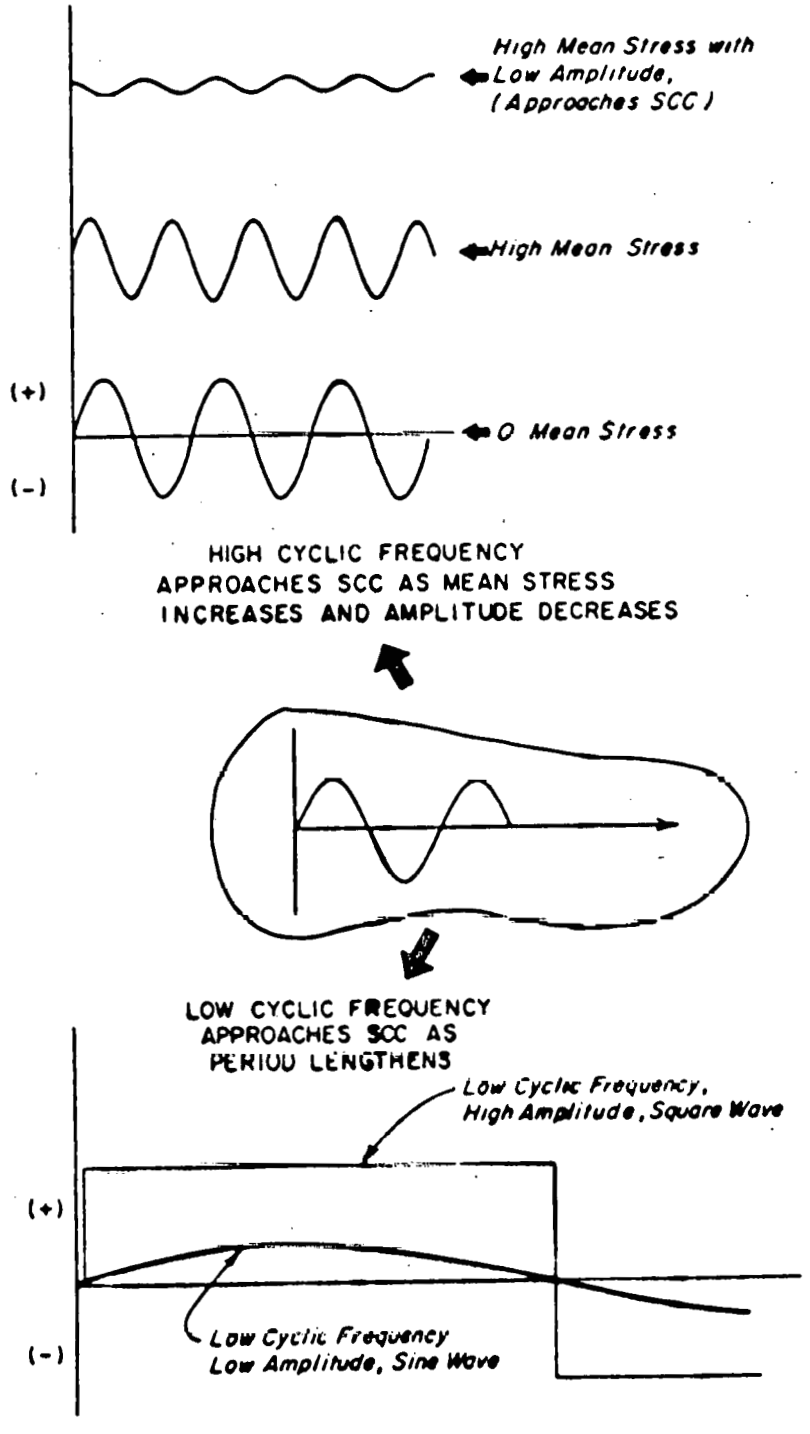
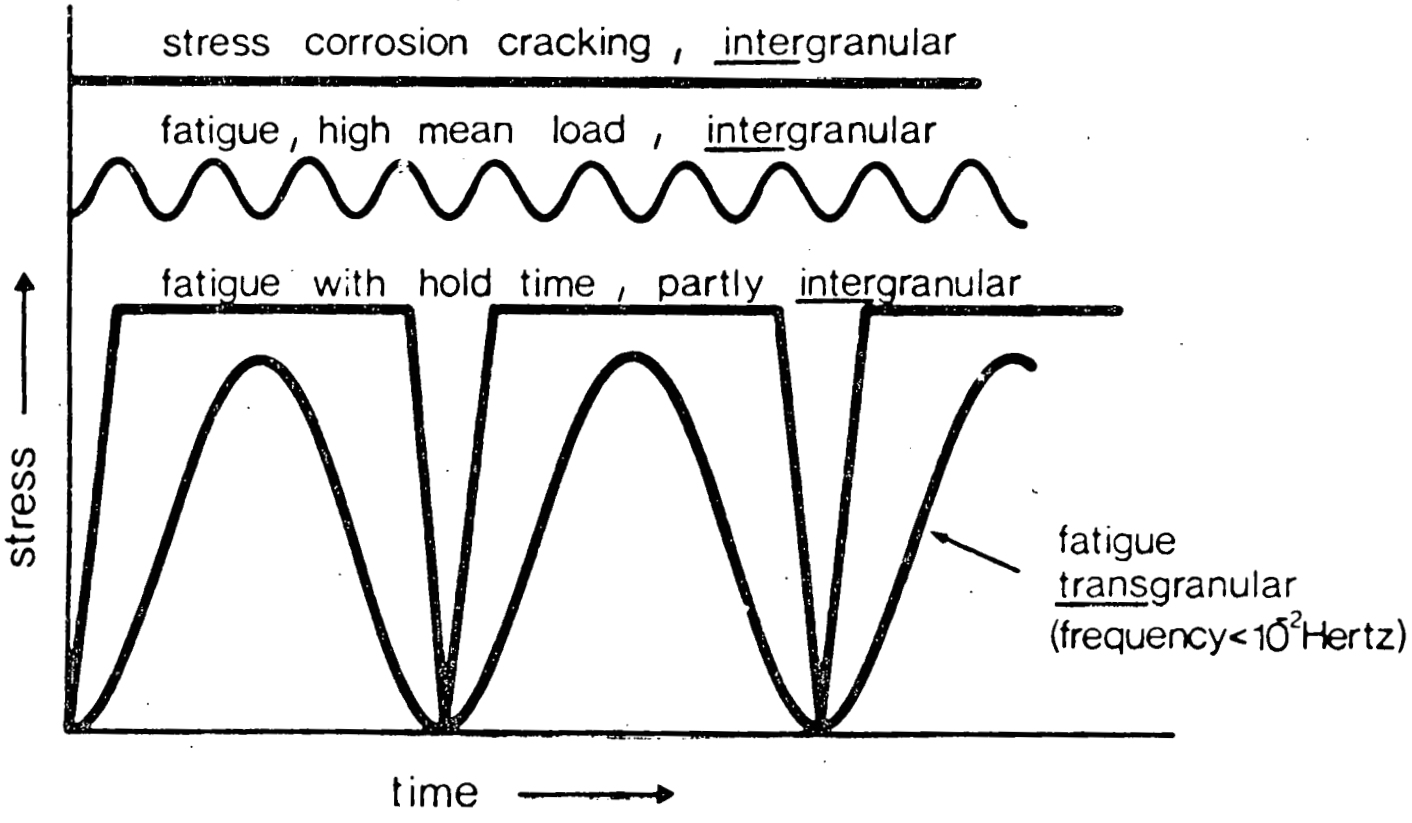
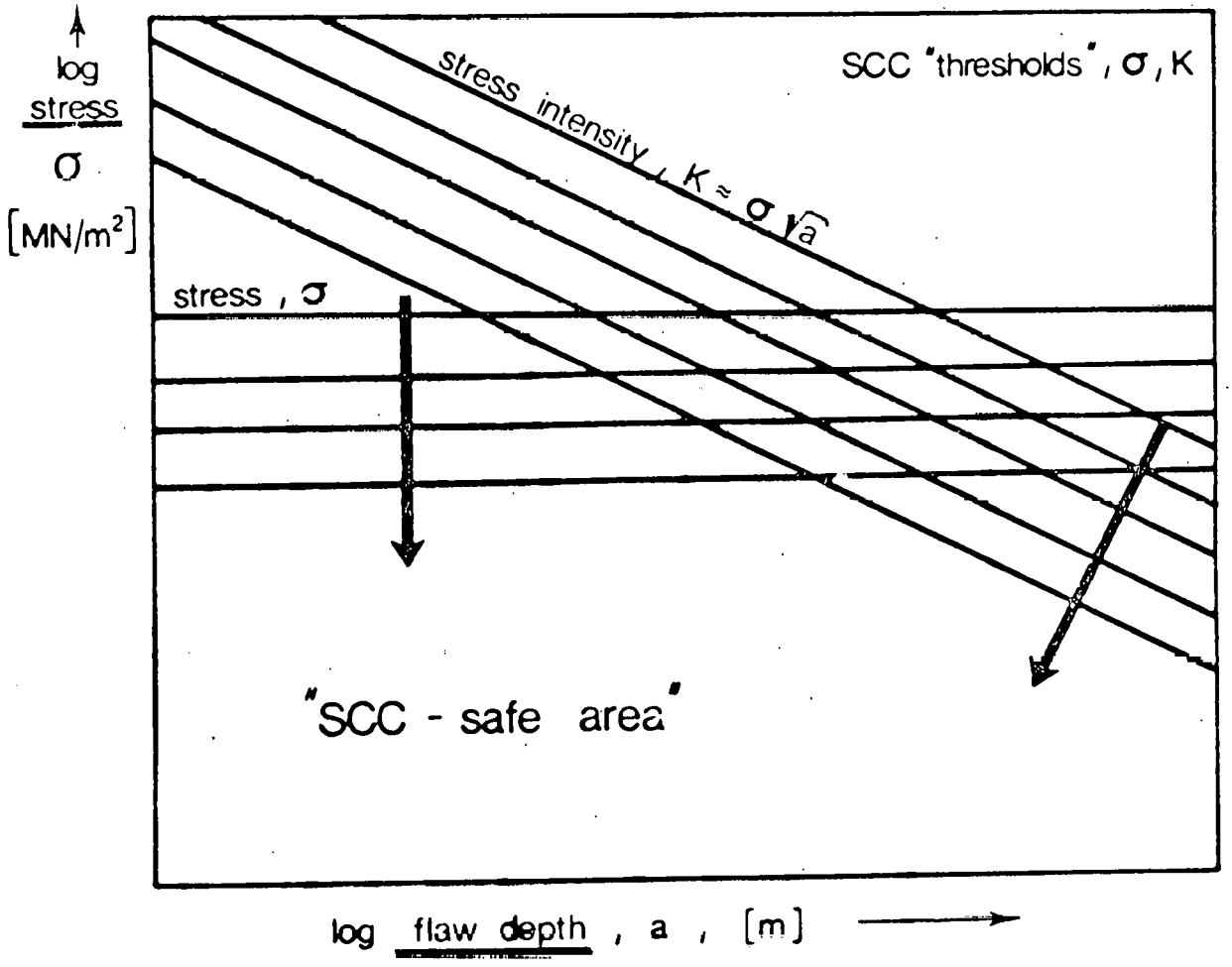
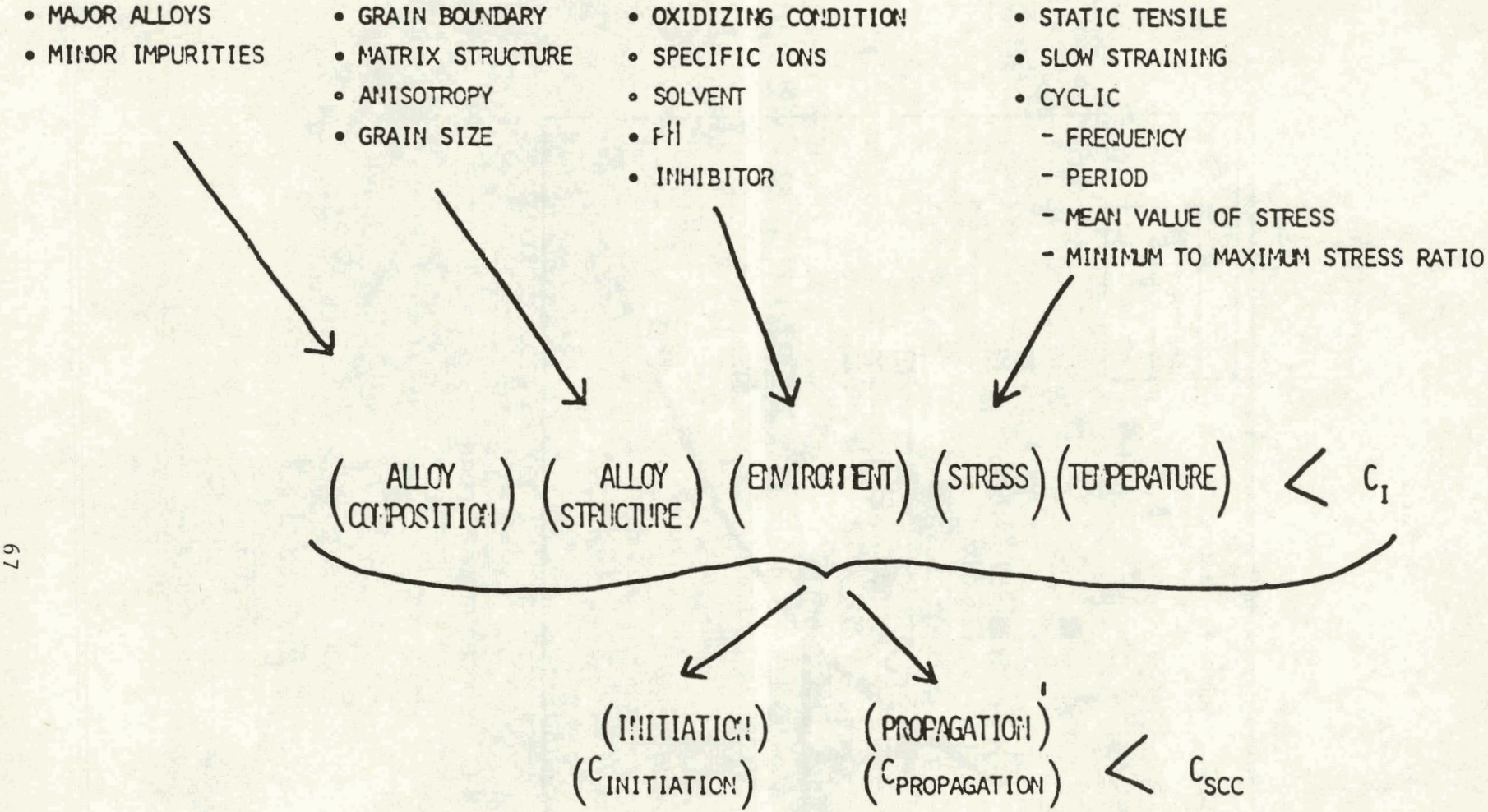

High Mean Stress with
Low Amplitude,
(Approaches SCC)
High Mean Stress
(+)
(-)
0 Mean Stress
HIGH CYCLIC FREQUENCY
APPROACHES SCC AS MEAN STRESS
INCREASES AND AMPLITUDE DECREASES
LOW CYCLIC FREQUENCY
APPROACHES SCC AS
PERIOD LENGTHENS
Low Cyclic Frequency,
High Amplitude, Square Wave
(+)
(-)
Low Cyclic Frequency
Low Amplitude, Sine Wave

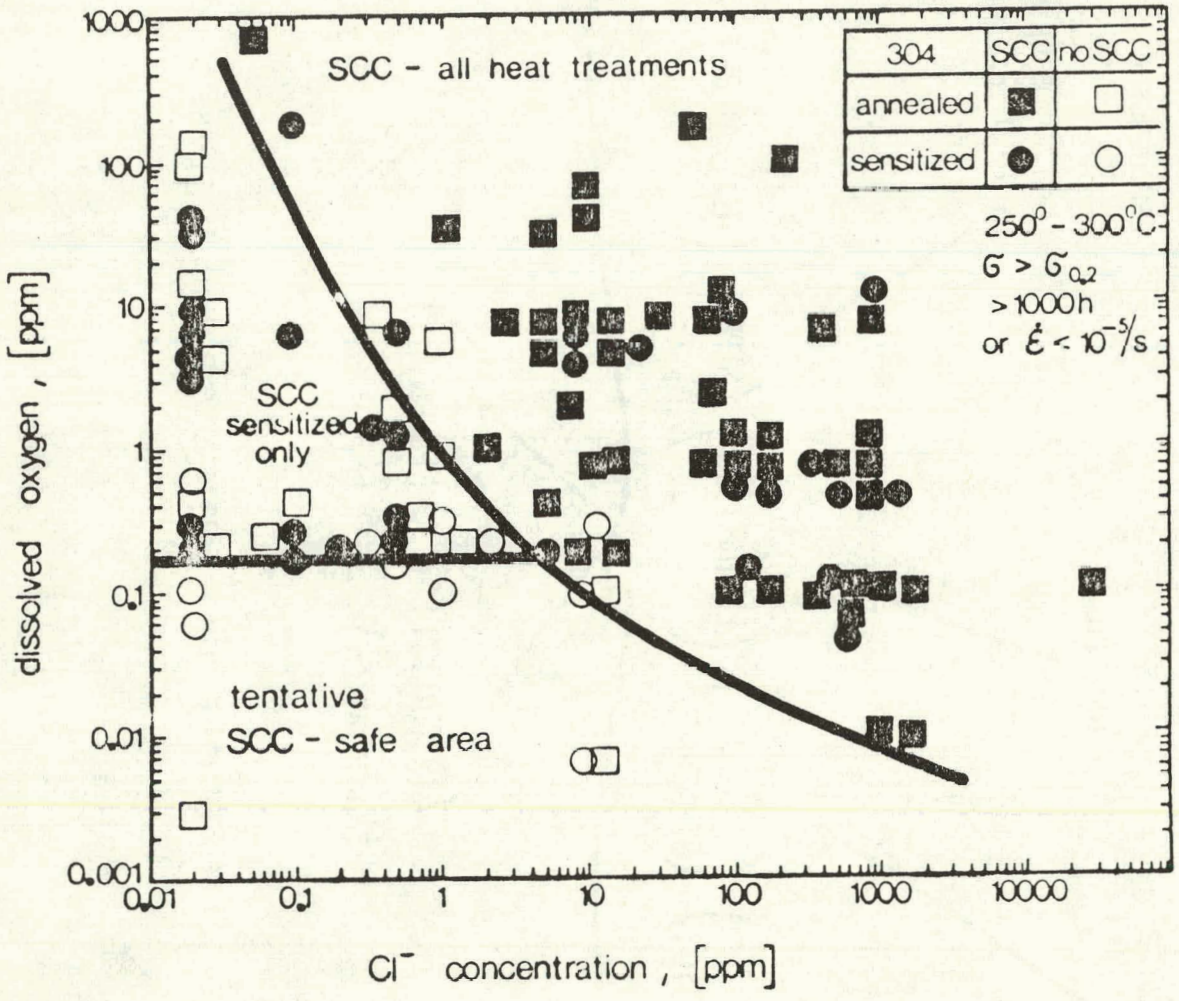
FIGURE 2.17

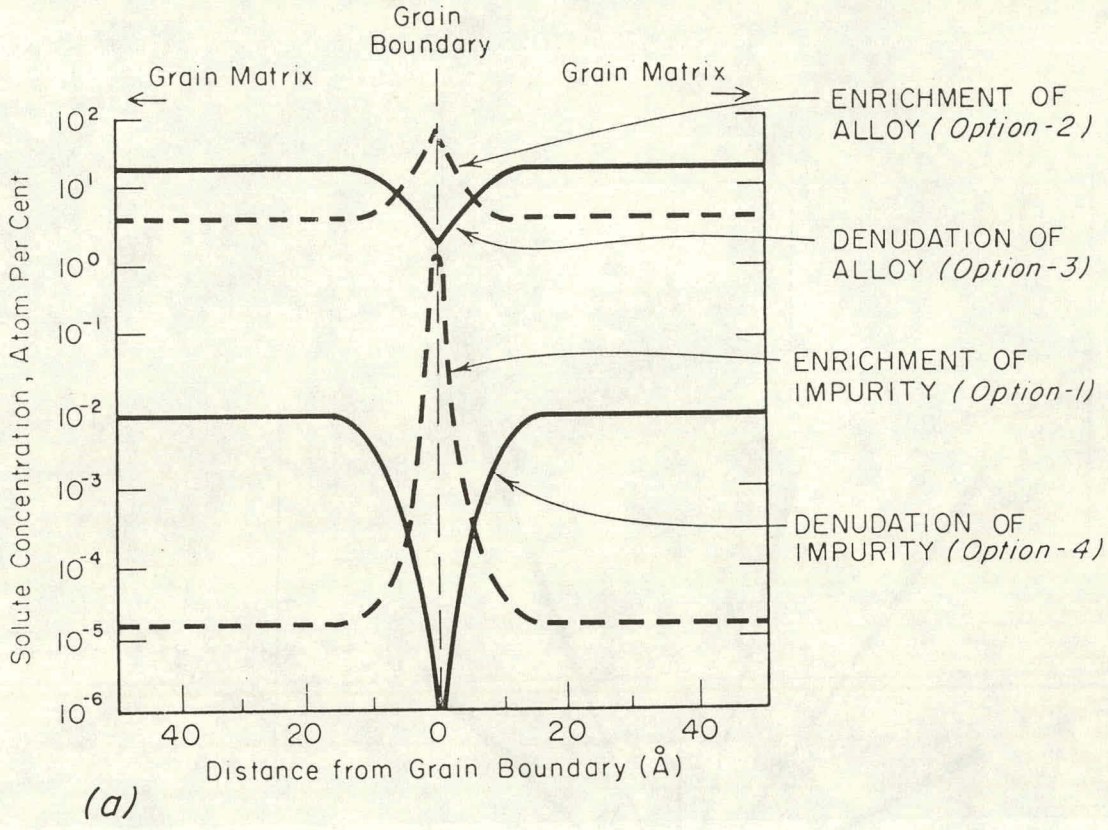

stress corrosion cracking , intergranular
fatigue , high mean load , intergranular
fatigue with hold time , partly intergranular
fatigue
transgranular
(frequency< 10^2 Hertz)
stress
time


log
stress
σ
[MN/m²]
SCC "thresholds", σ, K
stress intensity, K ≈ σ √a
stress, σ
"SCC - safe area"
log flaw depth, a, [m]

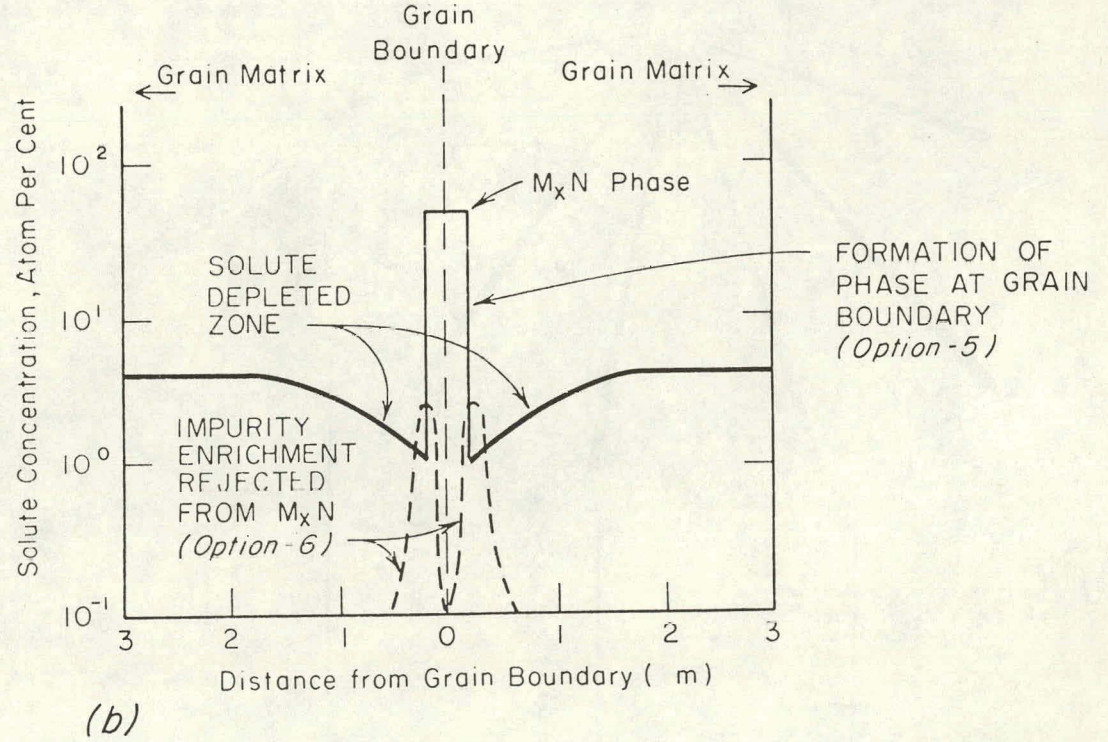


FIVE FACTOR RELATIONSHIP GIVING CRITICAL COMPONENTS IN STRESS CORROSION CRACKING.

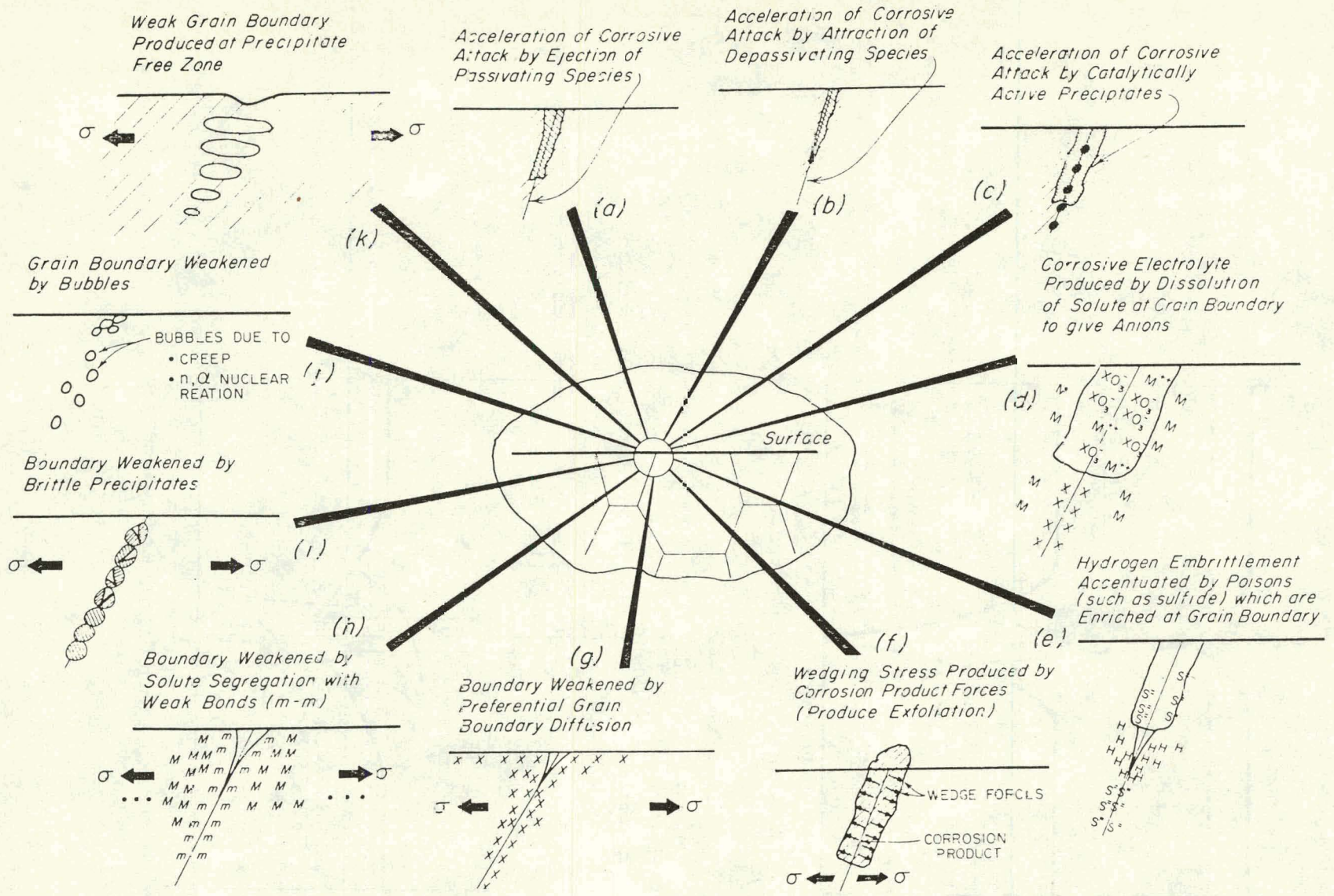

SCC - all heat treatments
304 | SCC | no SCC
annealed
sensitized
250° - 300°C
σ > σ0.2
> 1000 h
or ε̇ < 10⁻⁵/s
SCC sensitized only
tentative
SCC - safe area
dissolved oxygen, [ppm]
Cl⁻ concentration, [ppm]
1000
100
10
1
0.1
0.01
0.001
0.01
0.1
1
10
100
1000
10000


Grain Boundary
Grain Matrix
Grain Matrix
ENRICHMENT OF ALLOY (Option-2)
DENUDATION OF ALLOY (Option-3)
ENRICHMENT OF IMPURITY (Option-1)
DENUDATION OF IMPURITY (Option-4)
Solute Concentration, Atom Per Cent
10^{2}
10^{1}
10^{0}
10^{-1}
10^{-2}
10^{-3}
10^{-4}
10^{-5}
10^{-6}
40
20
0
20
40
Distance from Grain Boundary (Å)

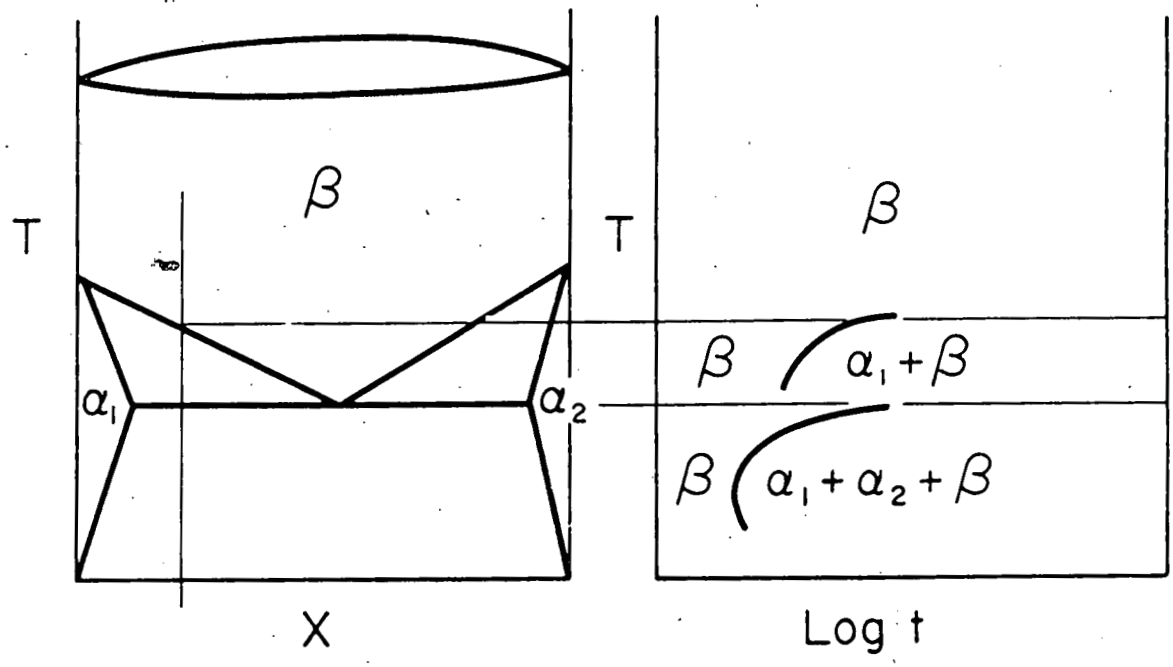
(a)

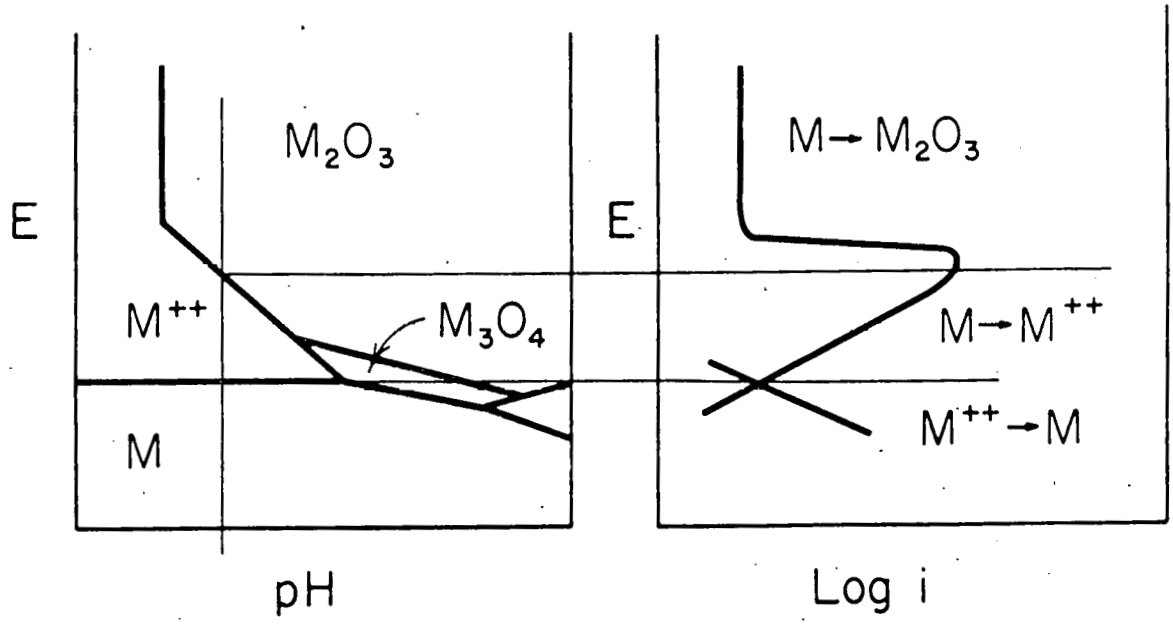

Grain Boundary
Grain Matrix
Grain Matrix
M_xN Phase
FORMATION OF PHASE AT GRAIN BOUNDARY (Option-5)
SOLUTE DEPLETED ZONE
IMPURITY ENRICHMENT REJECTED FROM M_xN (Option-6)
Solute Concentration, Atom Per Cent
10^{2}
10^{1}
10^{0}
10^{-1}
3
2
1
0
1
2
3
Distance from Grain Boundary (m)

(b)


Weak Grain Boundary Produced at Precipitate Free Zone
Acceleration of Corrosive Attack by Ejection of Passivating Species
Acceleration of Corrosive Attack by Attraction of Depassivating Species
Acceleration of Corrosive Attack by Catalytically Active Precipitates
Grain Boundary Weakened by Bubbles
BUBBLES DUE TO
• CREEP
• n,α NUCLEAR REATION
Corrosive Electrolyte Produced by Dissolution of Solute at Grain Boundary to give Anions
Surface
Boundary Weakened by Brittle Precipitates
Hydrogen Embrittlement Accentuated by Poisons (such as sulfide) which are Enriched at Grain Boundary
Boundary Weakened by Solute Segregation with Weak Bonds (m-m)
Boundary Weakened by Preferential Grain Boundary Diffusion
Wedging Stress Produced by Corrosion Product Forces (Produce Exfoliation)
WEDGE FORCES
CORROSION PRODUCT
(a)
(b)
(c)
(d)
(e)
(f)
(g)
(h)
(i)
(k)

THERMODYNAMICS → KINETICS





Sulfide Kinetics

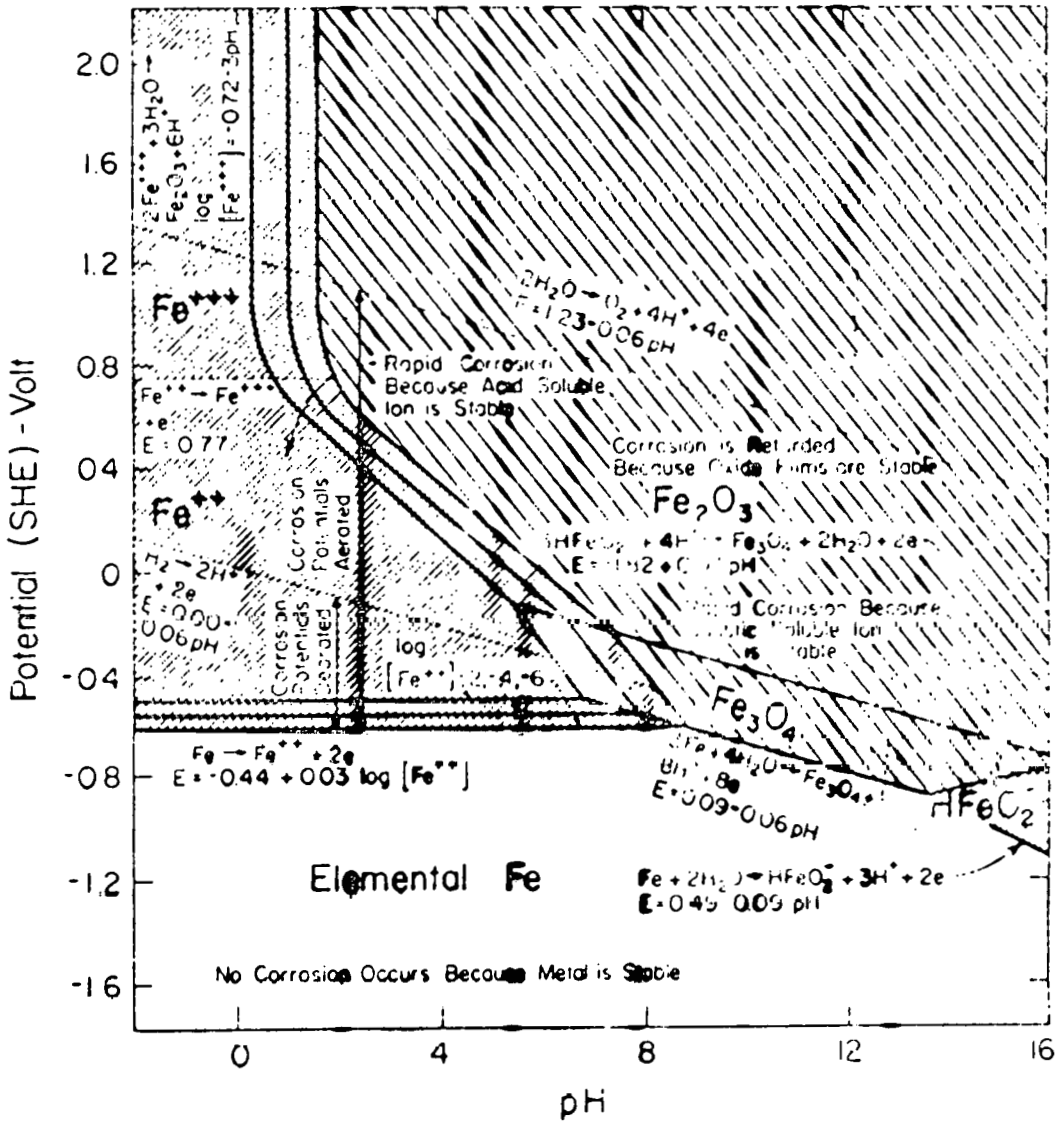

Potential (SHE) - Volt
2.0
1.6
1.2
0.8
0.4
0
-0.4
-0.8
-1.2
-1.6
0
4
8
12
16
pH
Fe+++
Fe++
Fe2O3
Fe3O4
HFeO2
Elemental Fe
Rapid Corrosion Because Acid Soluble Ion is Stable
Corrosion is Retarded Because Oxide Films are Stable
Corrosion Potentials Deaerated
Corrosion Potentials Aerated
Fe → Fe++ + 2e
E = -0.44 + 0.03 log [Fe++]
2H2O → O2 + 4H+ + 4e
E = 1.23 - 0.06 pH
Fe + 2H2O → HFeO2- + 3H+ + 2e
E = 0.45 - 0.09 pH
No Corrosion Occurs Because Metal is Stable

FIGURE 2.5

WHAT IS FAILURE

- DOES NOT PERFORM ACCORDING TO EXPECTATIONS
- ARE WE LIMITED BY:
  - A. IGNORANCE OF EXISTING INFO
  - B. LACK OF INFO
  - C. SURPRISE OCCURENCE

REPORT OF THE NASA AD HOC COMMITTEE ON FAILURE OF HIGH STRENGTH STRUCTURAL MATERIALS

Most of the failures involved ground equipment, development hardware, or the ground testing of flight hardware. A major conclusion of the Committee is that very few structural failures could be attributed to deficiencies in the technology of high strength materials and structural analysis. However, these few were very serious and had a large impact on both program cost and schedule. The great majority of failures were traceable to inadequate dissemination or utilization of available information, and to the unrealistic assessments of technology, cost, and schedule that too often characterize the initial planning stages of aerospace programs.

PSYCHOLOGICAL PROBLEMS

FALSE CAPACITY

- STAINLESS
- HIGH STRENGTH
- SPACE AGE

SMALL AMOUNTS OF IMPURITIES

- ALLOY
- ENVIRONMENT

EXPECTATIONS

PURE WATER

COMPLICATING FACTORS

- MULTIPLE DISCIPLINES
- SPATIAL. (OPERATION NOT NEAR MANUFACTURER)
- CHANGE OF PEOPLE.
- DEFICIENCIES IN TRAINING
- MULTIPLE PARTS IN SYSTEM, I.E. "WEAR LINK"

PREVENT FAILURES

- INCREASE CAPITAL COST FOR BETTER MATERIALS
- EDUCATE OPERATORS, DESIGNERS, BUILDER
- MODEL TEST AHEAD
- ENVIRONMENT INVENTORY
- REDUNDANCY
- SPARE PART
- PROOF TEST
- SYSTEM ANALYSIS
- PROCESS SPECIFICATIONS
- PRODUCT SPECIFICATION
- NDE
- MAINTENANCE
- INTERDISCIPLINARY CHECK OFF

DEVELOPMENT OF PRINCIPAL ISSUES

- FOCUS ON SPECIFIC PROBLEM
- ESTABLISH IMPORTANCE
- IDENTIFY EXISTING KNOWLEDGE
- RECOMMEND WORK REQUIRED

FOCUS

- DESCRIBE SPECIFIC PROBLEM
- IDENTIFY PARAMETERS
- EXAMPLE

  CORRECT:

  CORROSION FATIQUE OF RECEIVER TUBES /THERMAL CYCLING--
  WORKING ENVIRONMENT

  TOO SPECIFIC:

  CORROSION FATIGUE OF INCOLLOY 800

  TOO GENERAL:

  CORROSION FATIGUE

IMPORTANCE

- SEVERITY OF PROBLEM--RAMIFICATIONS
- EXAMPLES IN RELATED INDUSTRY
- SPECIFIC DETAILS (E.G. CORROSION FATIGUE OF INCOLLOY 800)
- CONDITIONS
- RAPIDITY

STATE OF ART

- IDENTIFY RELATED INDUSTRY
- DEGREE OF EXPERTISE
- LACK OF KNOWLEDGE

WORK REQUIRED

- MATERIAL DEVELOPMENT
- CODE QUALIFICATION
- THEORETICAL STUDY
- APPLIED RESEARCH
- FIELD SURVEY
- COMPLETE RESEARCH PROGRAM
- TYPE AND/OR EXTENT OF TESTING

Thermal Conversion - Gas Coolant

1 MW_{th} GAS COOLED SOLAR RECEIVER DESIGN

by

John Gintz, Don Bartlett and Ron Zentner

Boeing Engineering and Construction Company

Seattle, Washington

Since December, 1976, The Electric Power Research Institute (EPRI) has contracted Boeing Engineering and Construction Company (BEC) to examine the technical feasibility of a cavity type, high temperature gas cooled central receiver in a solar plant employing a closed Brayton cycle power conversion system. The concept is attractive because: (1) Studies have shown the central receiver system to be the most economical approach; (2) The Brayton gas cycle precludes the two-phase flow problems of water/steam Rankine cycles while promising the highest power conversion efficiencies and (3) The minimal cooling water requirements facilitate plant siting.

The program was extended, in July 1976, to achieve the design, fabrication, and testing of a 1 MW_{th} Bench Model Solar Receiver (BMSR). The BMSR was designed to simulate the performance of a conceptual commercial plant receiver and to model closed cycle characteristics with an open cycle test system. The primary test objective is to evaluate thermal performance of the BMSR in the DOE Central Receiver Test Facility (CRTF).

The BMSR is of welded-steel-frame construction and is lined with a composite insulation. An eight-sided configuration with a truncated conical base section ahs been adopted. The BMSR has a 43 inch diameter aperture, inclined 32^0 below the horizontal, to best utilize the 1 MW_{th} north field of the CRTF. The cavity is configured to allow solar flux from the heliostat field to impinge mainly on the truncated cone portion of the insulated cavity walls, not the heat exchanger tubes. The flux is thus reflected and reradiated to provide a diffuse, evenly distributed thermal enviornment for the heat exchangers. The overall dimensions of the BMSR are 13 ft. high by 10 ft. wide and the weight is approximately 10,000 lbs.

The framework is constructed of ASTM A36 steel and features eight leaf

springs of ASTM A588 steel (50,000 psi yield) which support the entire heat exchanger system. The springs accommodate thermal growth of heat exchanger manifolds. The cavity insulation is a composite of three-inch-thick mineral wool block, two one-inch-thick layers of Kaowool blanket (aluminum-Silica fiber) and one one-inch-thick layer of Saffil blanket (alumina fiber). The lower cost mineral wool block is located against the framework's steel shell and the entire composite is impaled on Inconel 601 studs welded to the shell. Metallic and ceramic anchors hold the composite in place on the studs, the ceramic being used in areas of high solar flux impingement. Initial estimates of insulation surface temperatures were made using vendor supplied spectral properties for similar materials. Laboratory tests with a simulated solar source proved the initial insulation design concept (Kaowool inner layer) was inadequate for the intended use. Laboratory tests were then performed with the Saffil and Kaowool products, to obtain spectral properties. New temperature predictions were made with these properties and the solar source tests repeated. Reasonably good correlation was obtained and it was concluded a Saffil blanket was necessary to survive the thermal environment of the inner cavity wall in areas of direct flux impingement.

The aperture rim is shielded with alumina board insulation. Further protection from misdirected solar flux is provided by a layer of one half-inch-thick Zirconia board bonded to the alumina board with an alumina cement. The original BMSR design employed alumina board insulation two feet wide in an annular configuration around the aperture. Subsequent analysis revealed the possibility of misaligned heliostats which could produce up to 1800 KW/m^2 incident flux on the aperture rim. Tests were conducted at White Sands with both the alumina board and the alumina/Zirconia laminate. Survival limits were, respectively; 800 KW/m^2 and > 3000 KW/m^2. The tests proved the original design adequate for its intended use but when potential facility malfunctions were considered it was deemed advisable to protect the entire BMSR aperture face with the alumina/Zirconia board laminate.

The heat exchanger system comprises elements inside and outside of the cavity. The external elements consist of 4 inch diameter stainless steel (304) inlet and outlet manifolds which encircle the BMSR. There are eight

flanges welded to each manifold which serve as the connection to the heat exchanger panels. Within the cavity are eight heat exchanger panels each consisting of an inlet and outlet header and 54 two-pass tubes. A flanged connector pipe is welded to each header and these protrude through the cavity wall to the outside where they are bolted to the manifolds. The entire panel assembly is of welded construction and the material selected for this application is Inconel 617. The selection was based on thermal cycling/fatigue tests at service temperatures, and on fabrication characteristics. The headers and connector pipes are 2 inch diameter and have 1/4 inch-thick walls. The heat exchanger tubes are 0.20 inch inside diameter and have 0.038" thick walls. The heated length within the cavity is 50.5 inches. Considerable effort was directed to development of an acceptable tube-to-header weld joint.

The coolant gas used in the BMSR tests is air. Gas flow in the heat exchanger system is controlled by valves located at the inlet headers of each panel. The valves are controlled by a signal from a thermocouple located in the outlet gas stream and maintain a setpoint outlet temperature by throttling the gas flow. The gas is introduced into the panel at 1000^0F. This temperature environment allows use of off-the-shelf valves. Within the cavity, sufficient solar energy is applied to the gas to raise the temperature to 1500^0F. In a commercial plant this 1500^0F gas would be used to drive a turbine/generator set; however, in the BMSR test the gas is discharged through a tube-shell heat exchanger to preheat incoming gas to 1000^0F. Gas flow rates up to 6 lb/sec at 130 psia are used to cool the heat exchangers. The system back-pressure is controlled to 75 psia by means of a valve downstream of the BMSR outlet.

At this time, the BMSR is in test at CRTF. Initial checkout and system verification tests with solar-heating have been completed. Temperatures to 1300^0F have been achieved in the outlet gas stream and solar input levels have reached over 700 KW_{th}. Testing is expected to be completed in February 1979.

In summary, material data of a general nature was available for most products,

however specific information regarding performance in a high solar flux environment was lacking for design of the BMSR. It was necessary to perform supporting tests in conjunction with design development in order to verify the concept. In addition, extrapolation to the 30 year life expectancy postulated for solar power plants will require substantially greater knowledge of the survivability of heat exchanger and insulation materials in the service environment. Some of the data requirements are; stress-rupture, creep and thermal cyclic fatigue of heat exchanger alloys; thermal cyclic behavior of cavity and aperture rim insulation and; effects of prolonged exposure on insulation spectral properties.

1 MW_{th} GAS COOLED SOLAR RECEIVER DESIGN

Viewgraphs Presented

by

Don Bartlett

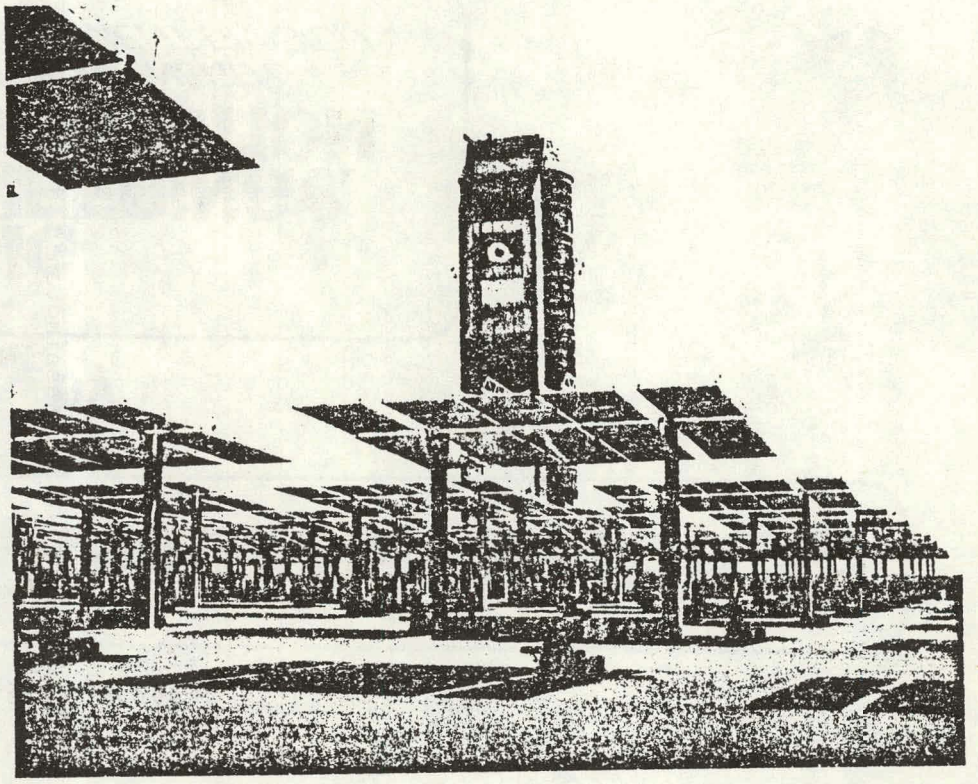
Boeing Engineering and Construction Company

Seattle, Washington

1 MW Gas Cooled Solar Receiver Design

SERI MATERIALS FOR SOLAR ENERGY SYSTEMS WORKSHOP

Denver, Colorado
December 18, 1978



RP 377-2
1 MW_{th} Bench Model Solar Receiver

Designed and Fabricated for

Electric Power Research Institute

by

BOEING ENGINEERING & CONSTRUCTION
THE BOEING ENERGY AND ENVIRONMENT DIVISION

Subcontractors:

STEEL-FAB INC.

EMFCO

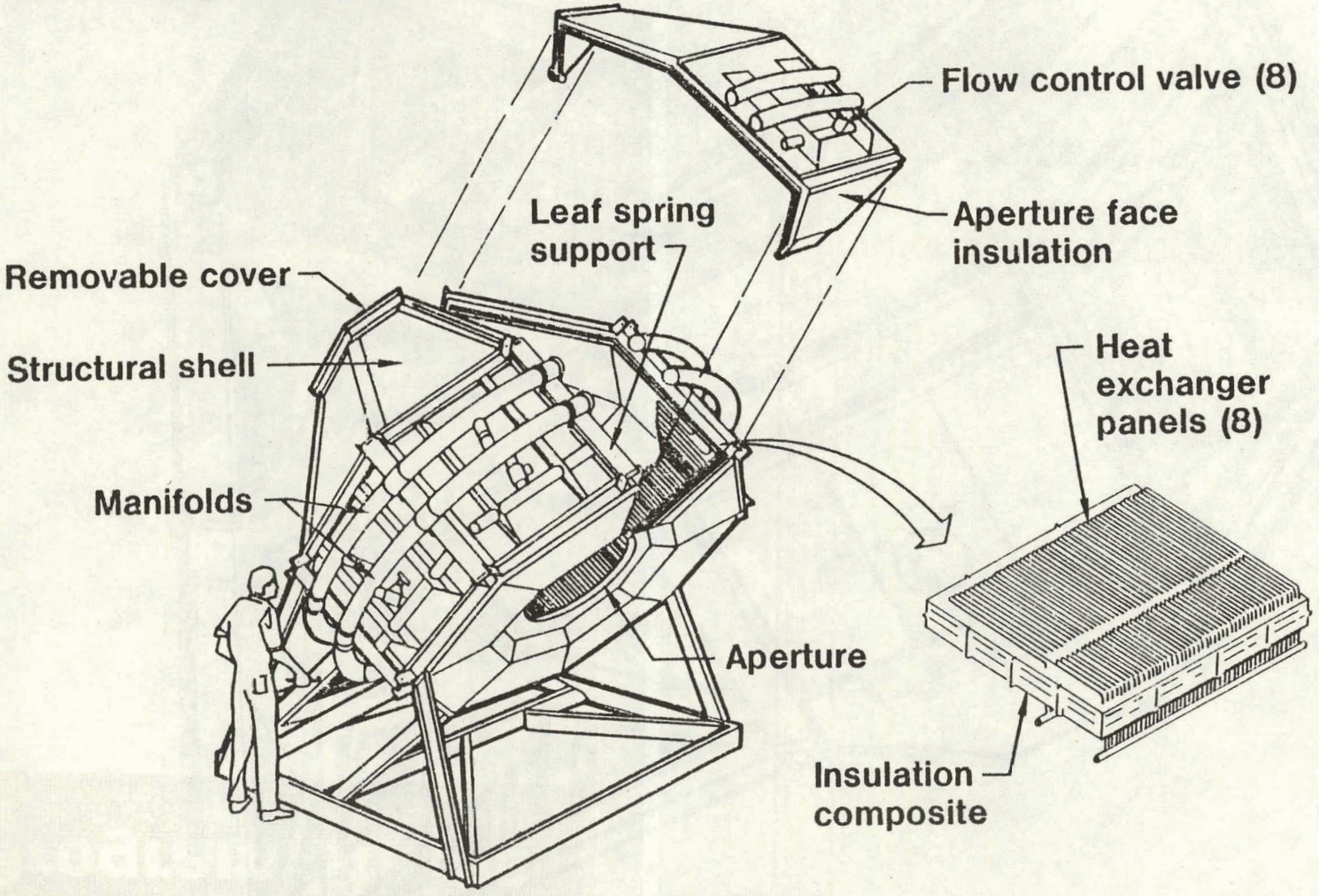
1-MWth Bench Model Receiver Program

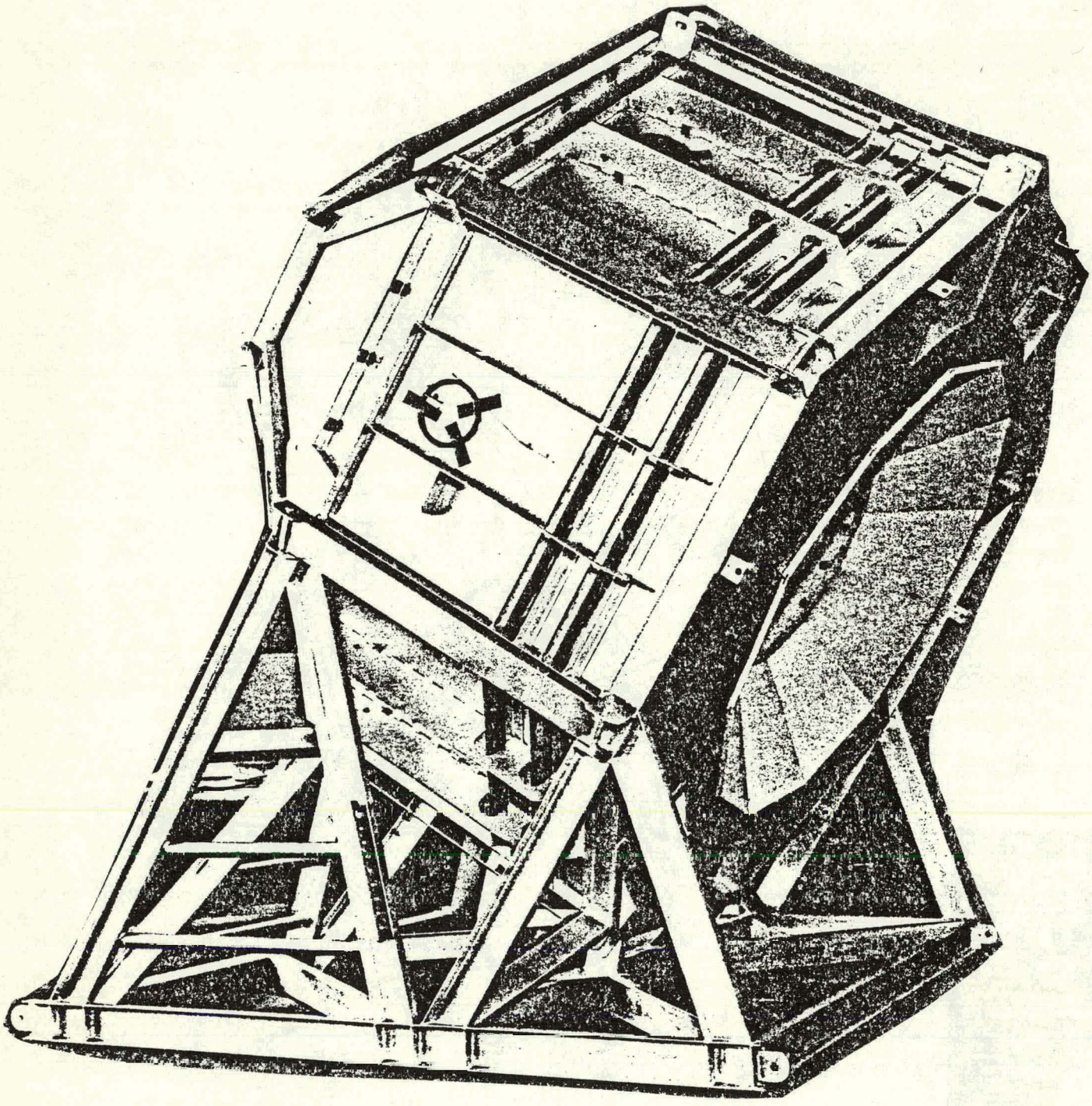
- Configured for DOE-STTF, Albuquerque, N. Mex.
- Simulate 300 MW_{th} commercial receiver.
- Extend RP377-1 gas-cooled receiver technology to working model.
- Gain operational experience:
  - Materials
  - Design concept
  - Heat transfer
  - Flow control
- Evaluate solar-energy conversion efficiency.

Program Status

- Program initiation in July 1976
- Design and fabrication completed
- Hot-flow checkout testing completed
- BMSR installed in DOE-STTF facility at 140-ft level
- Flow checkout and systems verification tests completed
- Equilibrium heat-balance testing in progress
  - Thermal input 750 kW

Bench Model
Construction Features

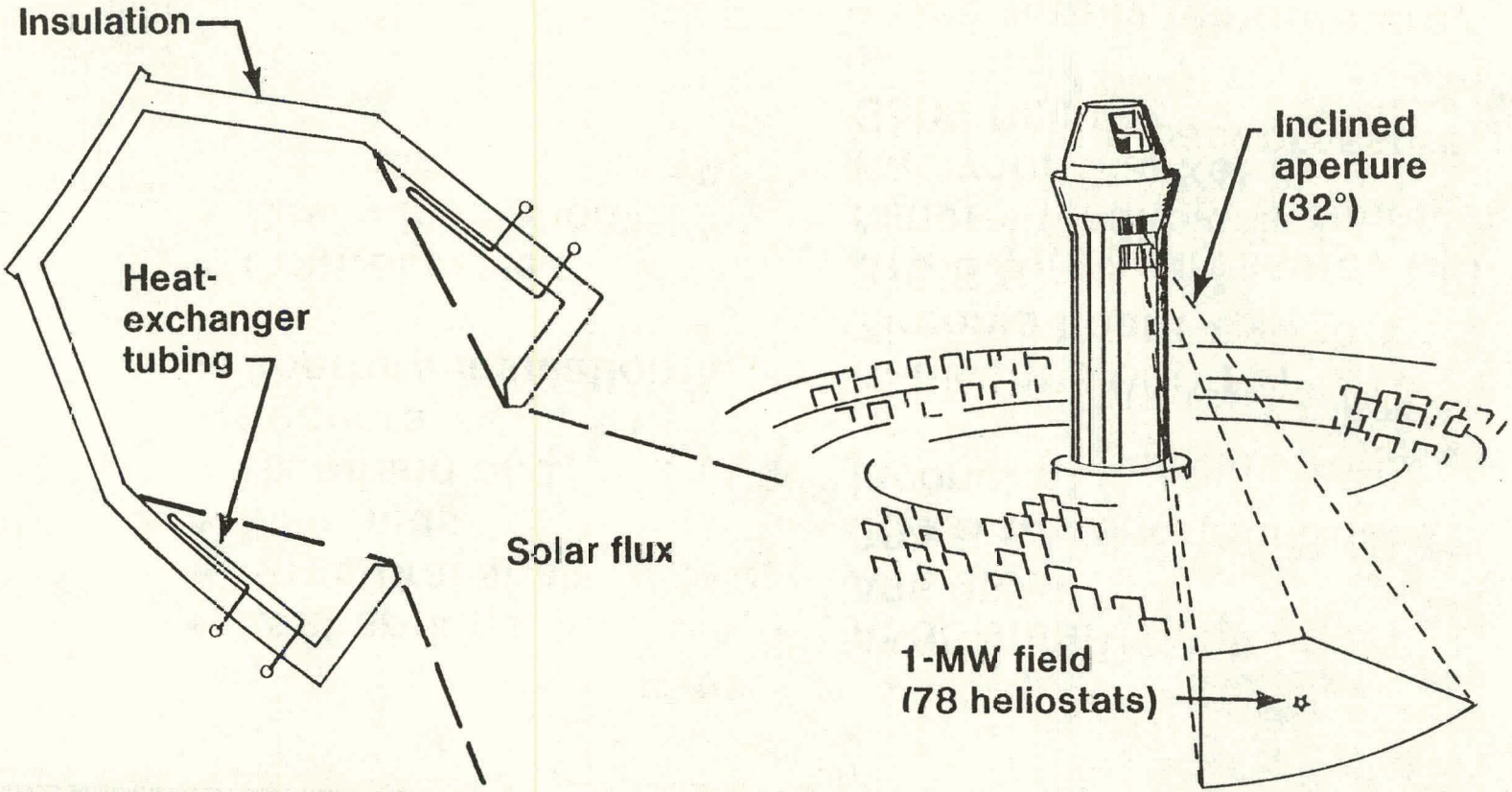




Construction Materials

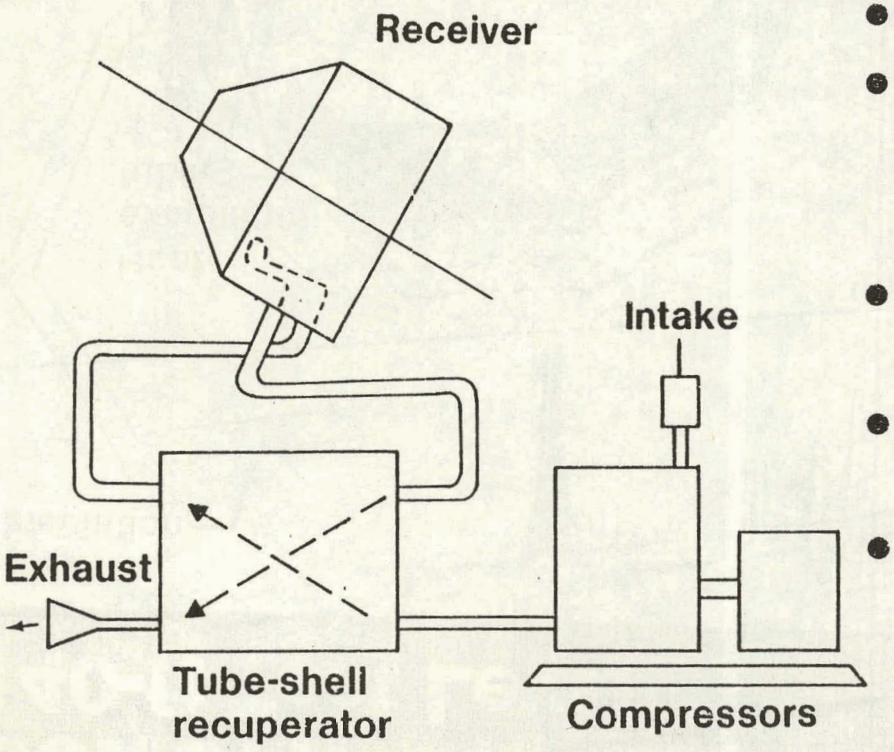
• Leaf springs	A588 steel
• Structural shell	A36 steel
• Manifolds	304 S.S.
• Hx tubing and headers	Inconel 617
• Aperture insulation	Kaowool 3,000°F + Zirconia board
• Control valve	316 S.S.
• Cavity insulation	Mineral wool block + Kaowool Blanket + Saffil Blanket

DOE-STTF Bench Model Installation–140-ft Test Level



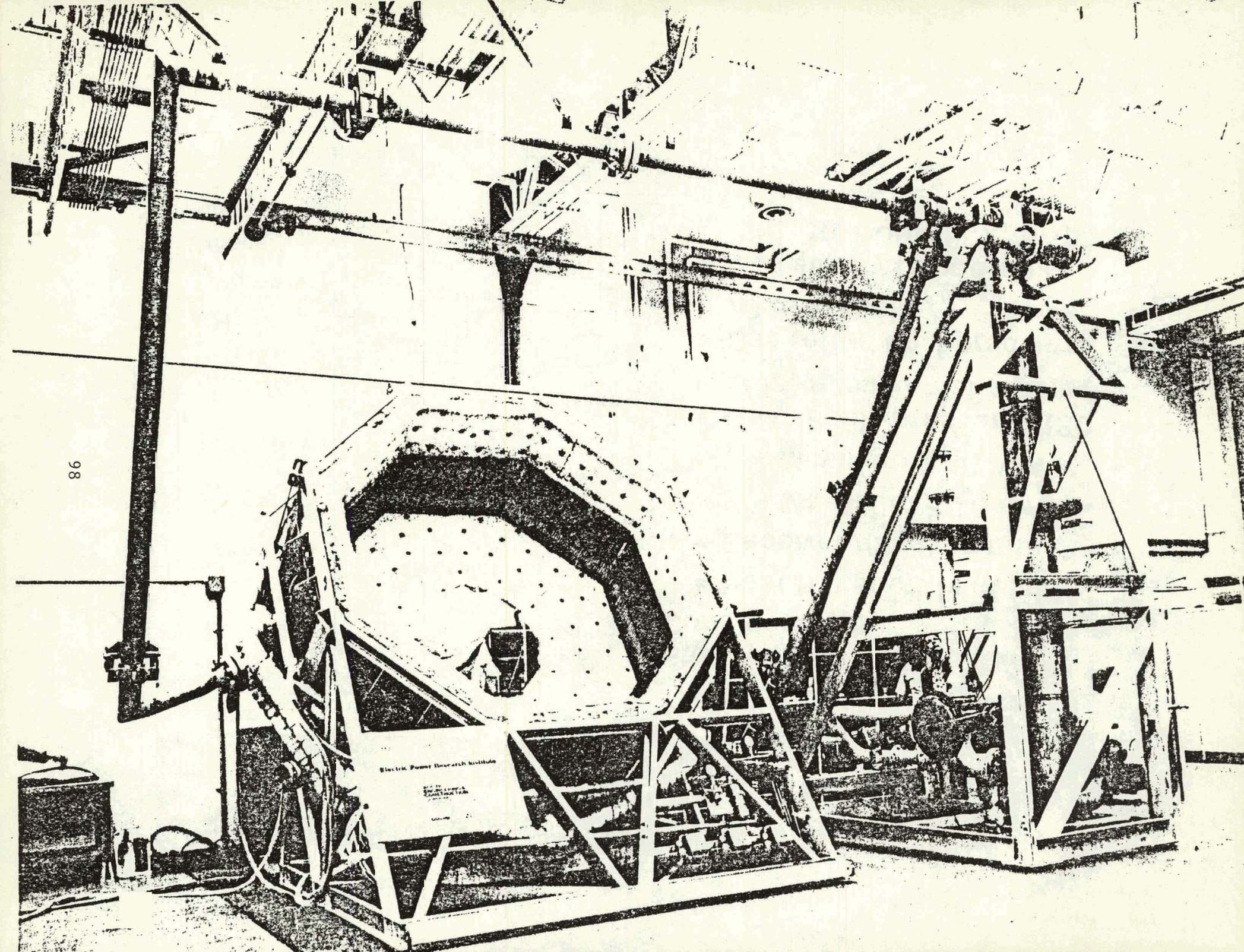
Bench model section view

Test Gas Flow System

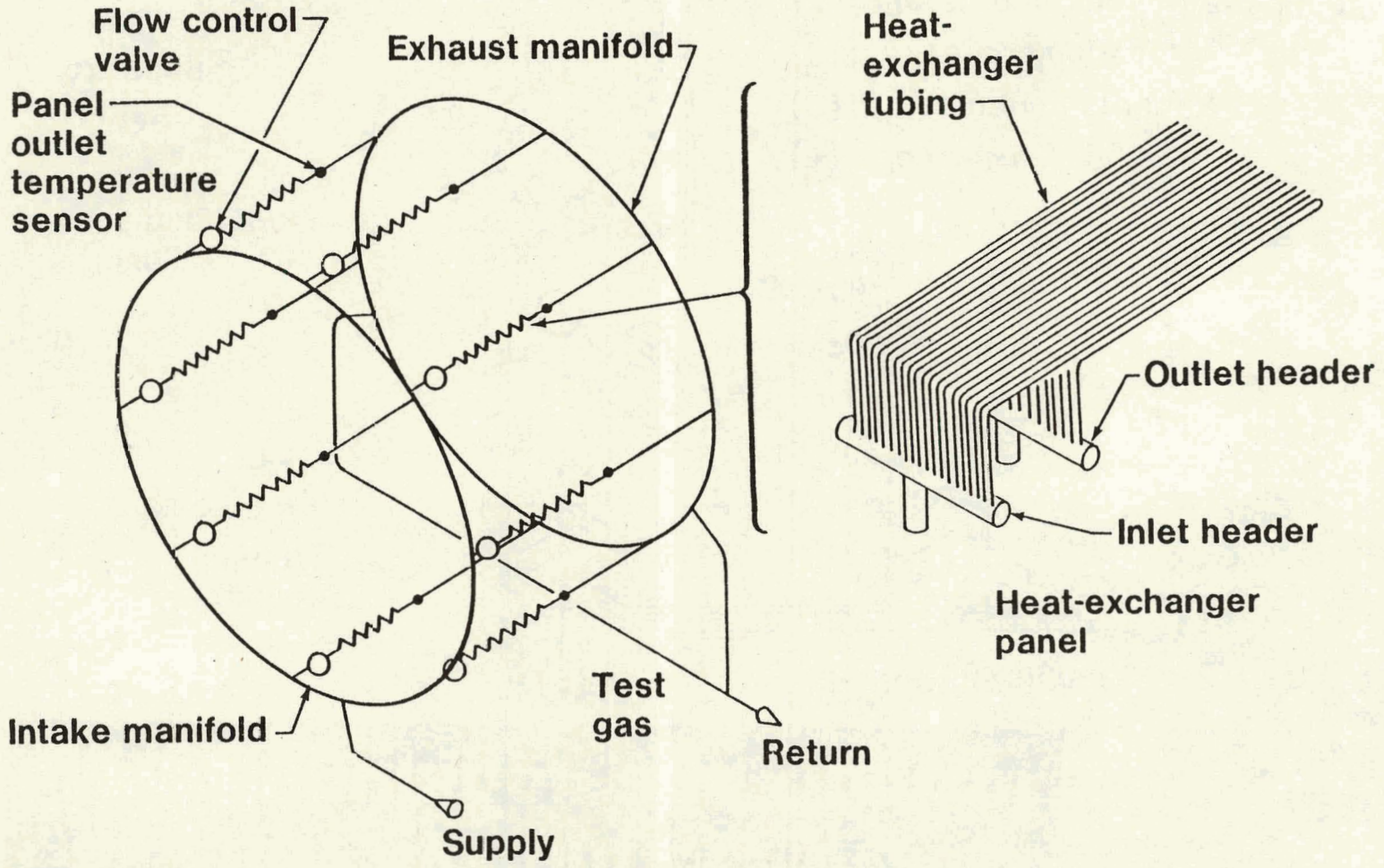


Steady-State Design Conditions

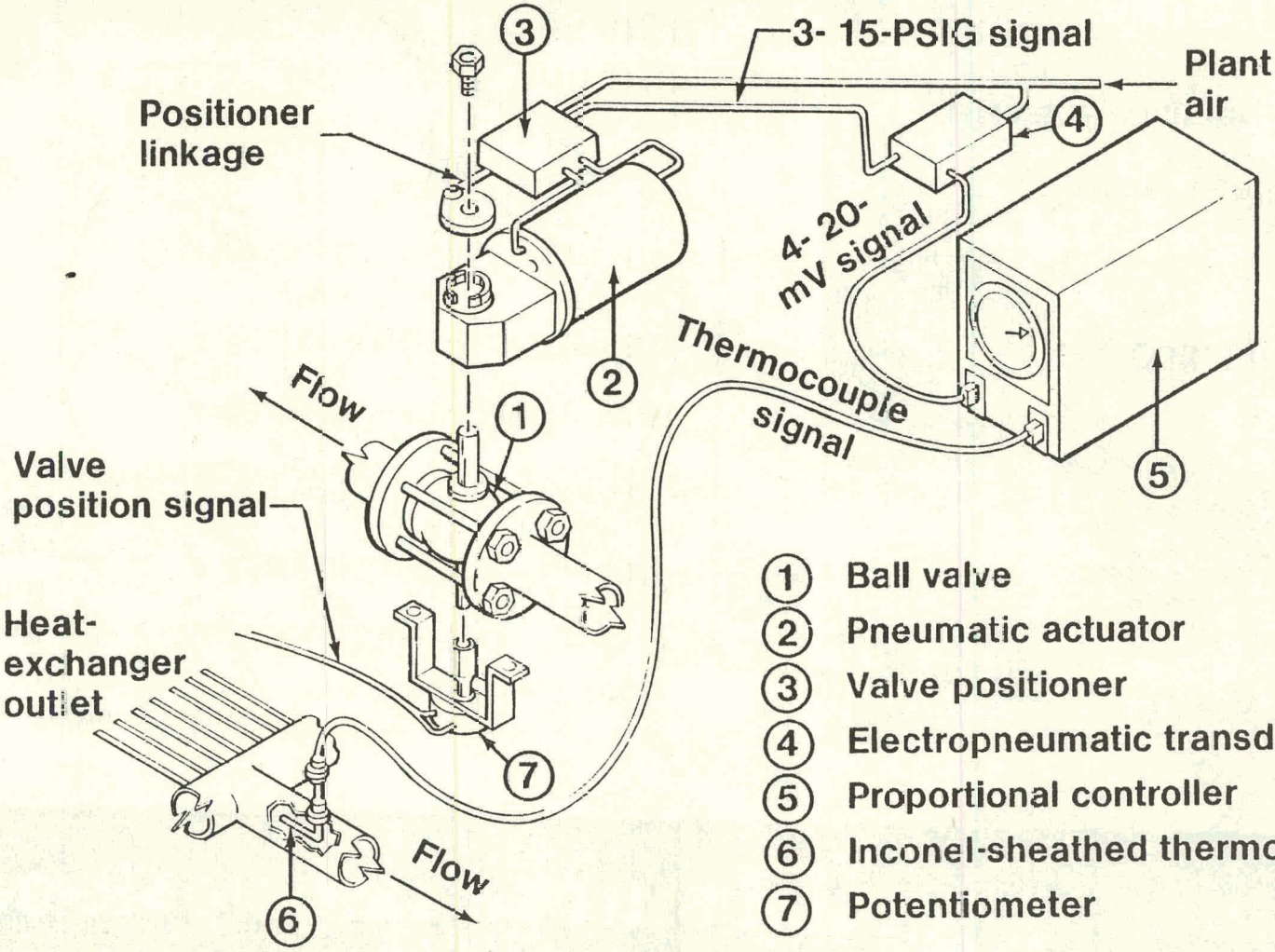
- Heat transport fluid (air)
- Receiver gas flow rates
  - Maximum 5.76 lb/s
  - Minimum 1.40 lb/s
- Gas supply pressure, 130 psia, minimum at receiver
- Gas return backpressure, 70 to 80 psia
- Gas supply temperature, 750° to 1,000°F



Receiver Gas Flow System Schematic



Gas Flow System
Flow Regulation and Control



1. Ball valve
2. Pneumatic actuator
3. Valve positioner
4. Electropneumatic transducer
5. Proportional controller
6. Inconel-sheathed thermocouple
7. Potentiometer

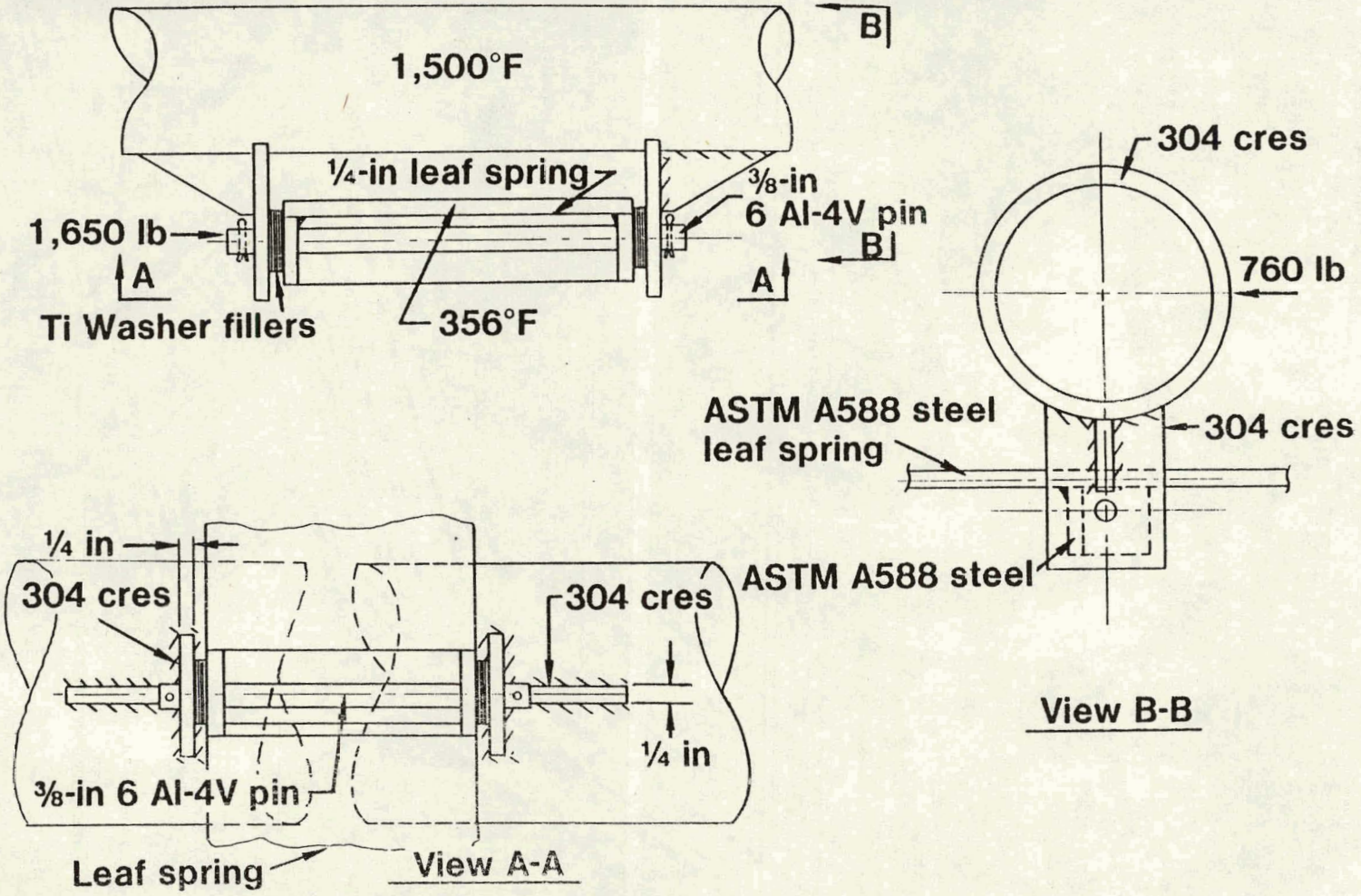
Design Requirements

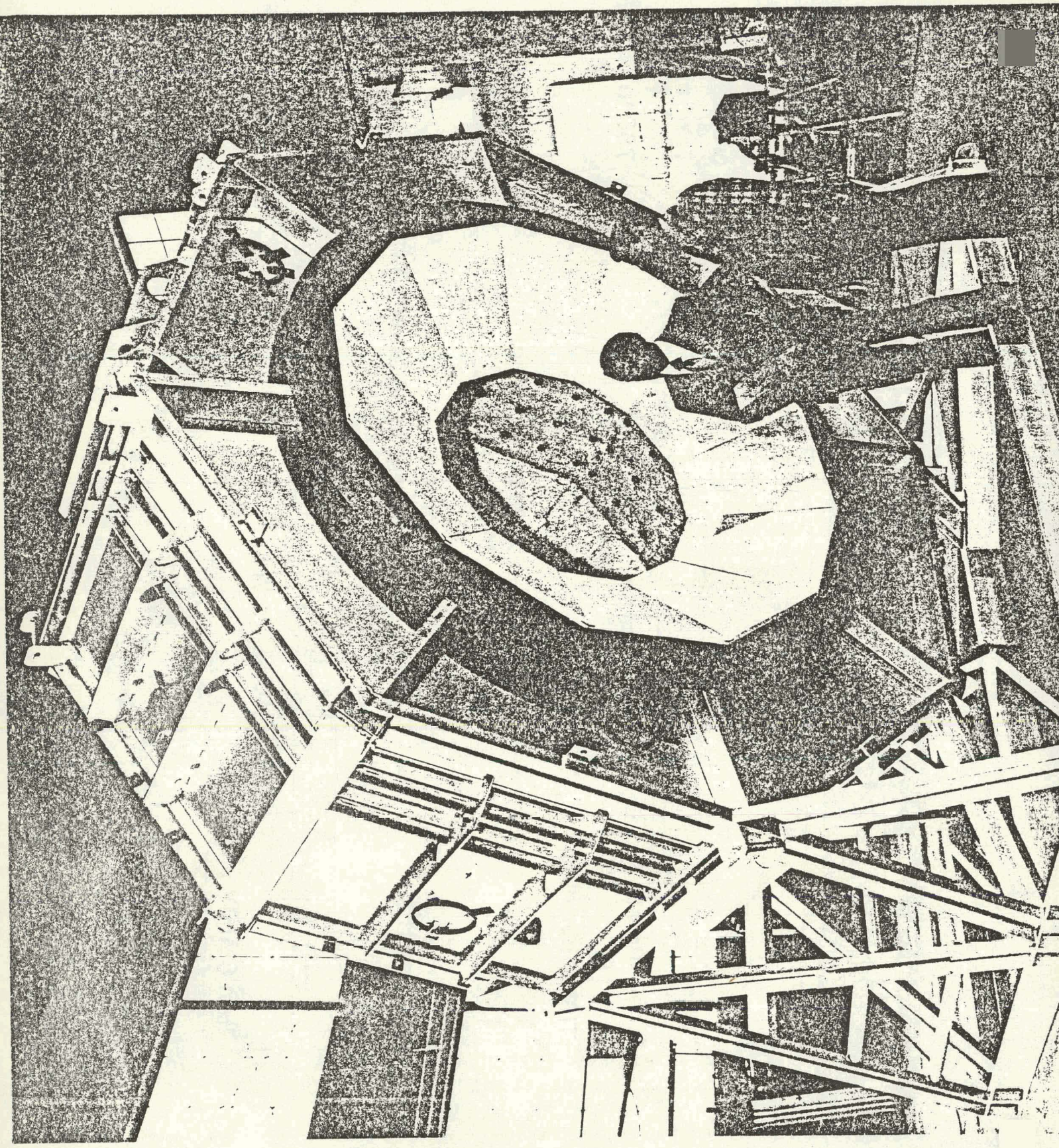
- 1,000-hr life
- 750-1,000°F gas inlet; 1,500°F outlet
  - Maximum Hx tubing temperature = 1,600°F
- Use DOE-STTF 1-MW_{th} collector field
  - Maximum cavity wall flux = 425 kW/m^2
  - Maximum aperture rim flux = 1,800 kW/m^2
- Sandia seismic response spectrum at 140-ft level
- Wind
- Standard codes and practices where applicable (ASME, ANSI, AWS, AISC, ASTM)
- Transportation and handling loads

Design Features

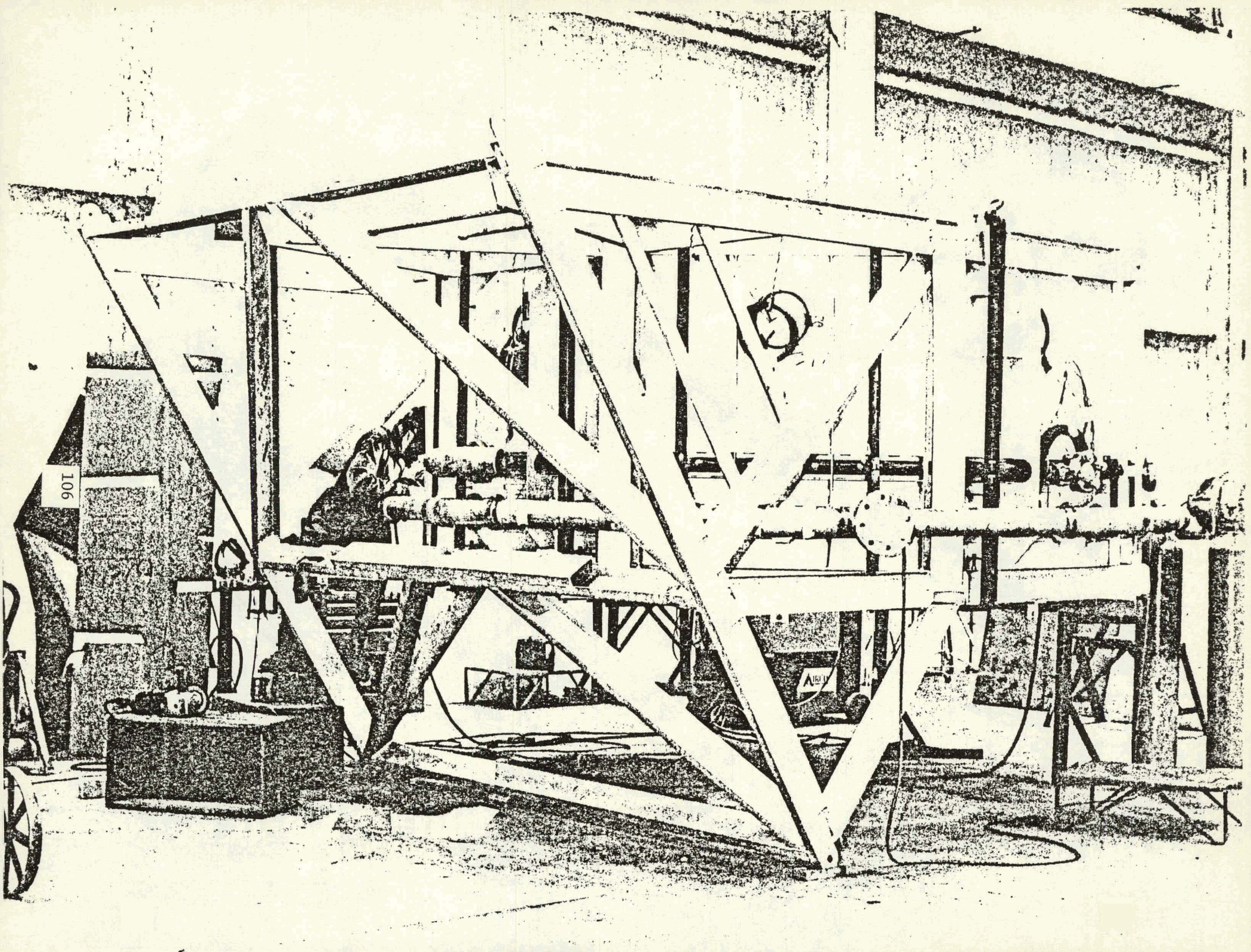
- Heat-exchanger system support
- Heat-exchanger system
- Cavity insulation
- Aperture thermal protection

Manifold: Leaf-Spring Attachment





X-RAY C/N 2487


106

Heat-Exchanger Materials Assessment

	Inconel 617	HS 188
Supplier stress-rupture (1,000 hr at 1,600°F)	10,000 lb/in^2	9,600 lb/in^2
Boeing tests	30-yr diurnal cycling; thermal cycling to rupture	
Weld-drawn tubing	Special order (Superior Tube)	Special order (Cabot Corp)
Lead time	8 weeks	30 weeks
Cost (0.20 x 0.035-in tube)	$46.90/lb	$50.40/lb
Weldability	Good	Good (limited experience)
Inspection	Conventional techniques • X-ray • Penetrant	Special practice X-ray

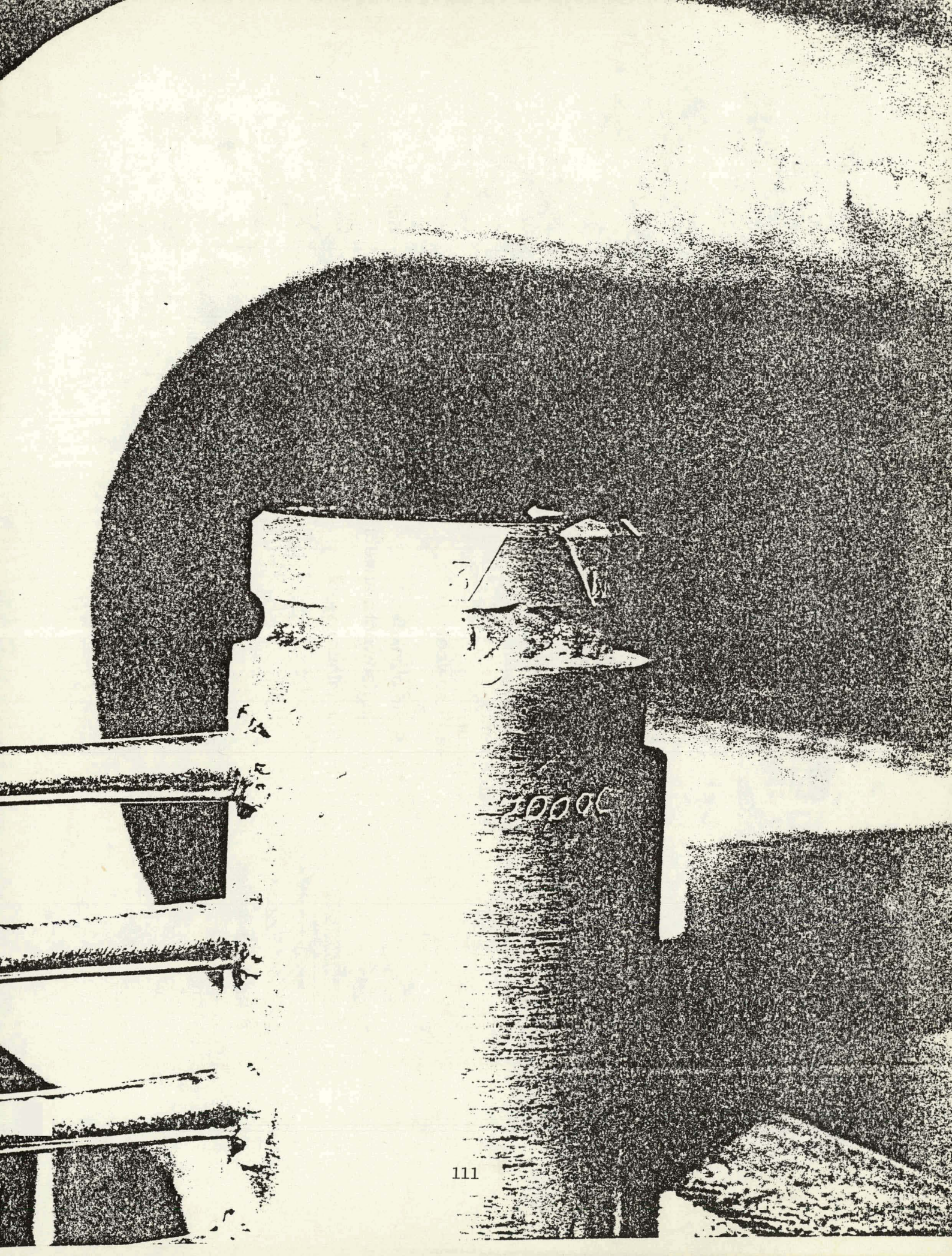
Heat-Exchanger Design

Inconel 617 elements

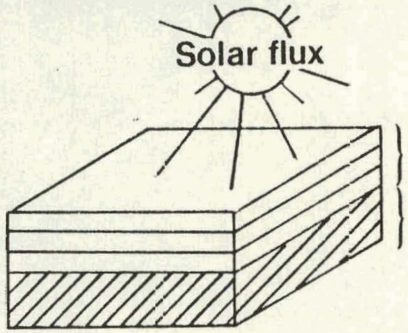
- Design approach
  - 1,000-hr life at 1,600°F, stress rupture = 6,900 psi
  - Allowable primary membrane stress (pressure)
    S_m = ¼ x 6,900 psi = 1,725 psi
  - Allowable primary plus secondary stress (pressure + thermal + gravity)
    3 S_m = 5,175 psi
  - Allowable primary stress (membrane + bending)
    1.5 S_m = 2,588 psi
    Design pressure = 300 psi

304 cres manifolds

- Design approach
  - ASME code, section 1, "Power Boilers"
  - Stress = $\frac{P}{2}\left[\frac{D}{t - 0.005D} - 1\right]$
  - Allowable primary stress, seam-welded pipe (ASTM SA312)
    S_m = 1,200 psi at 1,500°F
  - Design pressure = 150 psi



Cavity Insulation Design

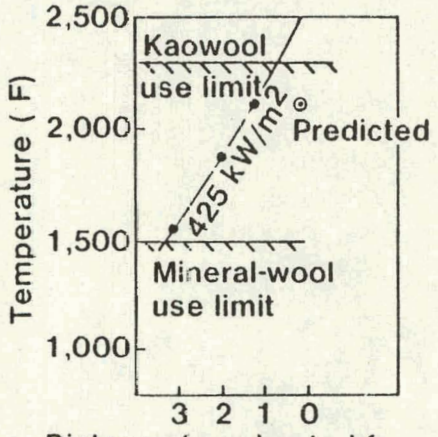


Three 1-in Kaowool blankets

One 3-in mineral-wool block

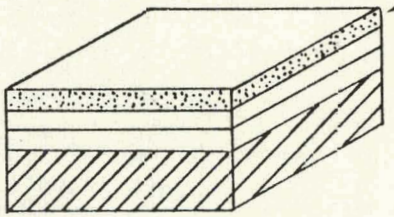
Initial concept

Test



Spectral properties measurements

- Kaowool
- Exposed Kaowool
- Saffil



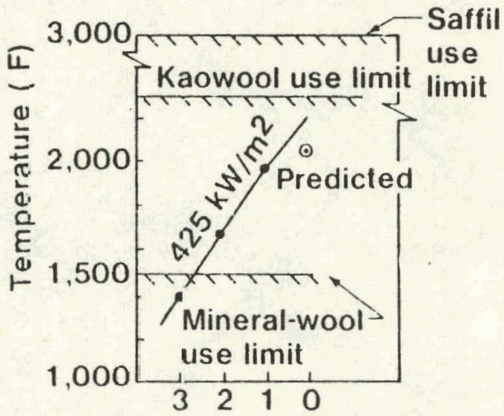
1-in Saffil blanket

Two 1-in Kaowool blankets

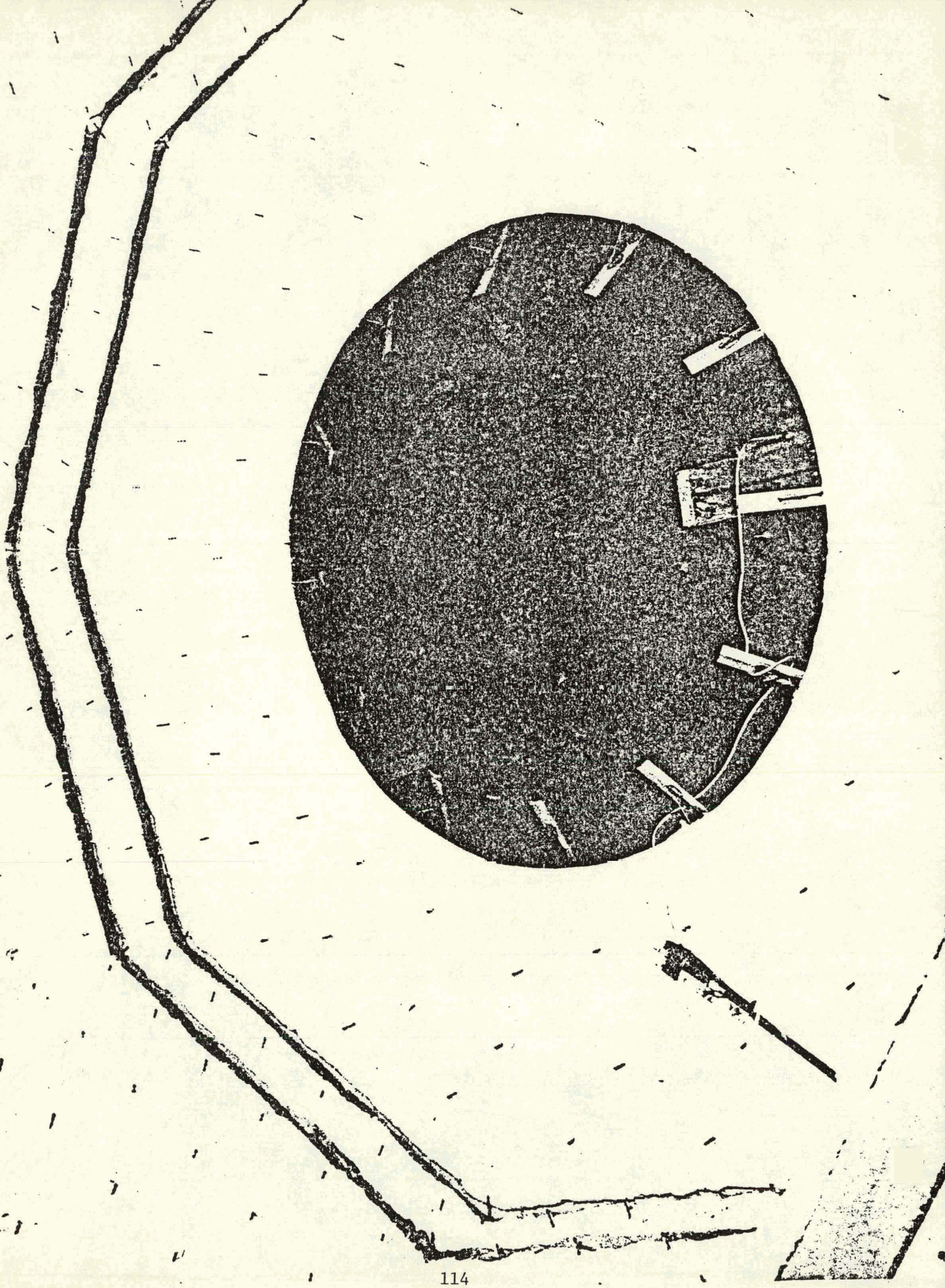
One 3-in mineral-wool block

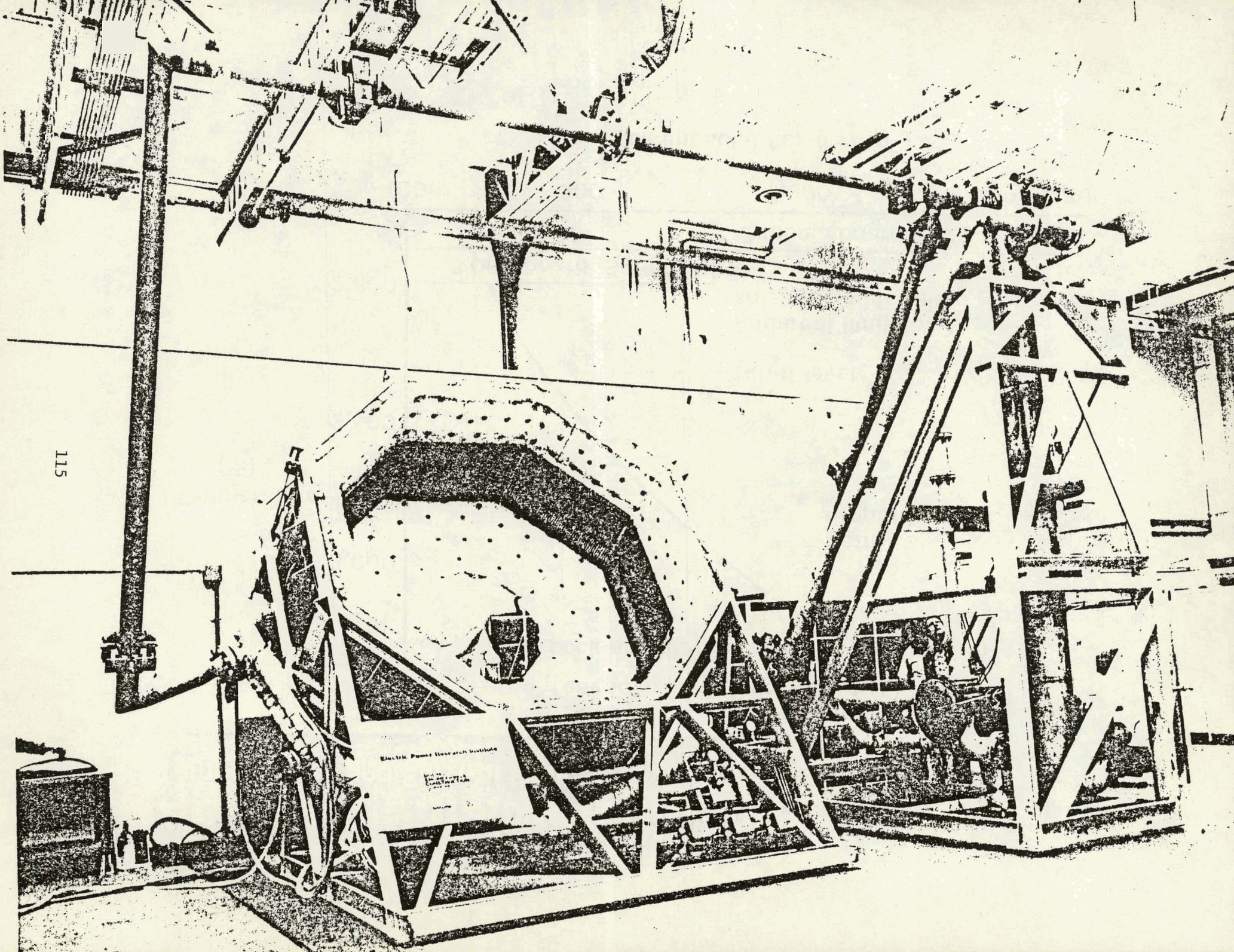
Revised design

Test

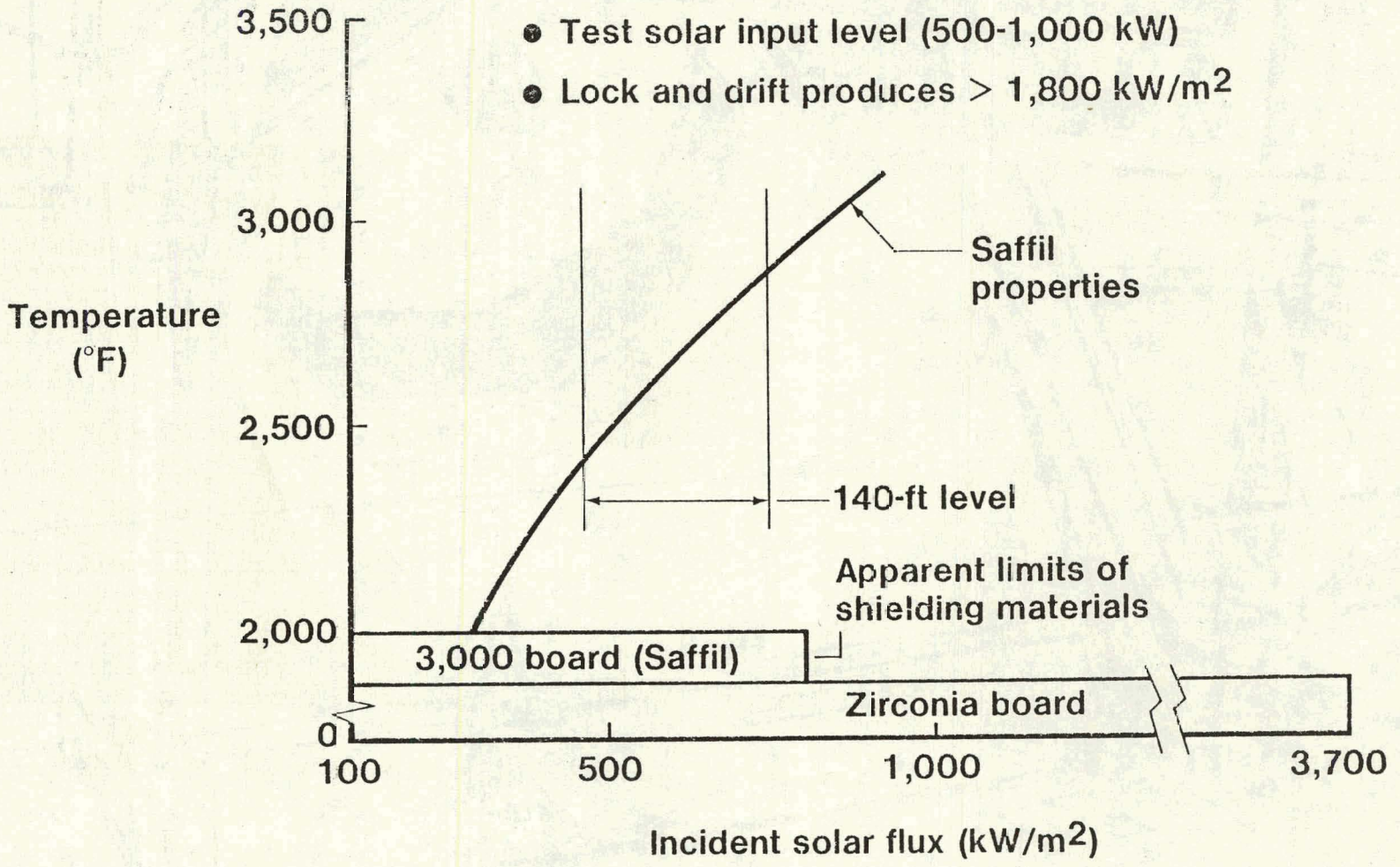


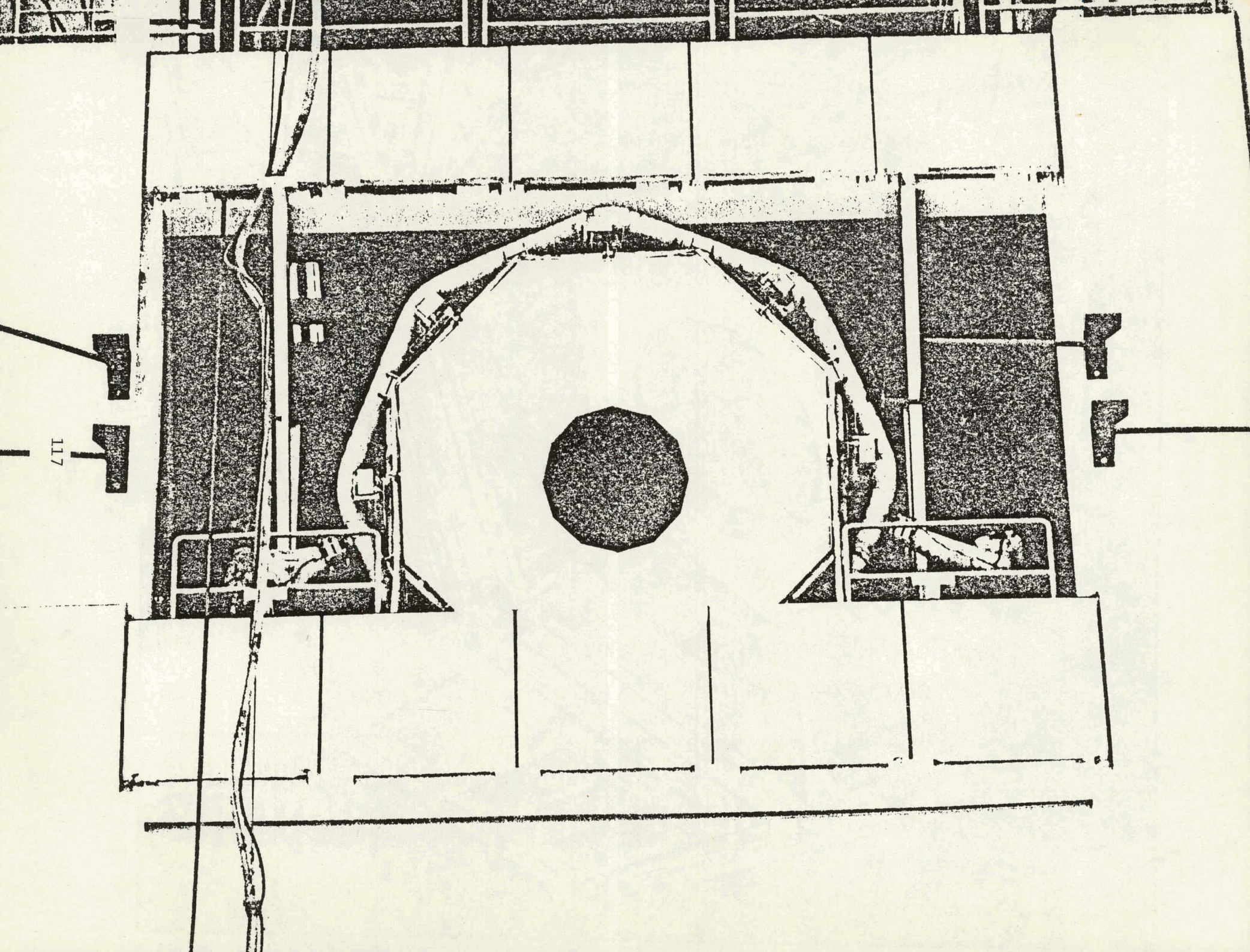
113

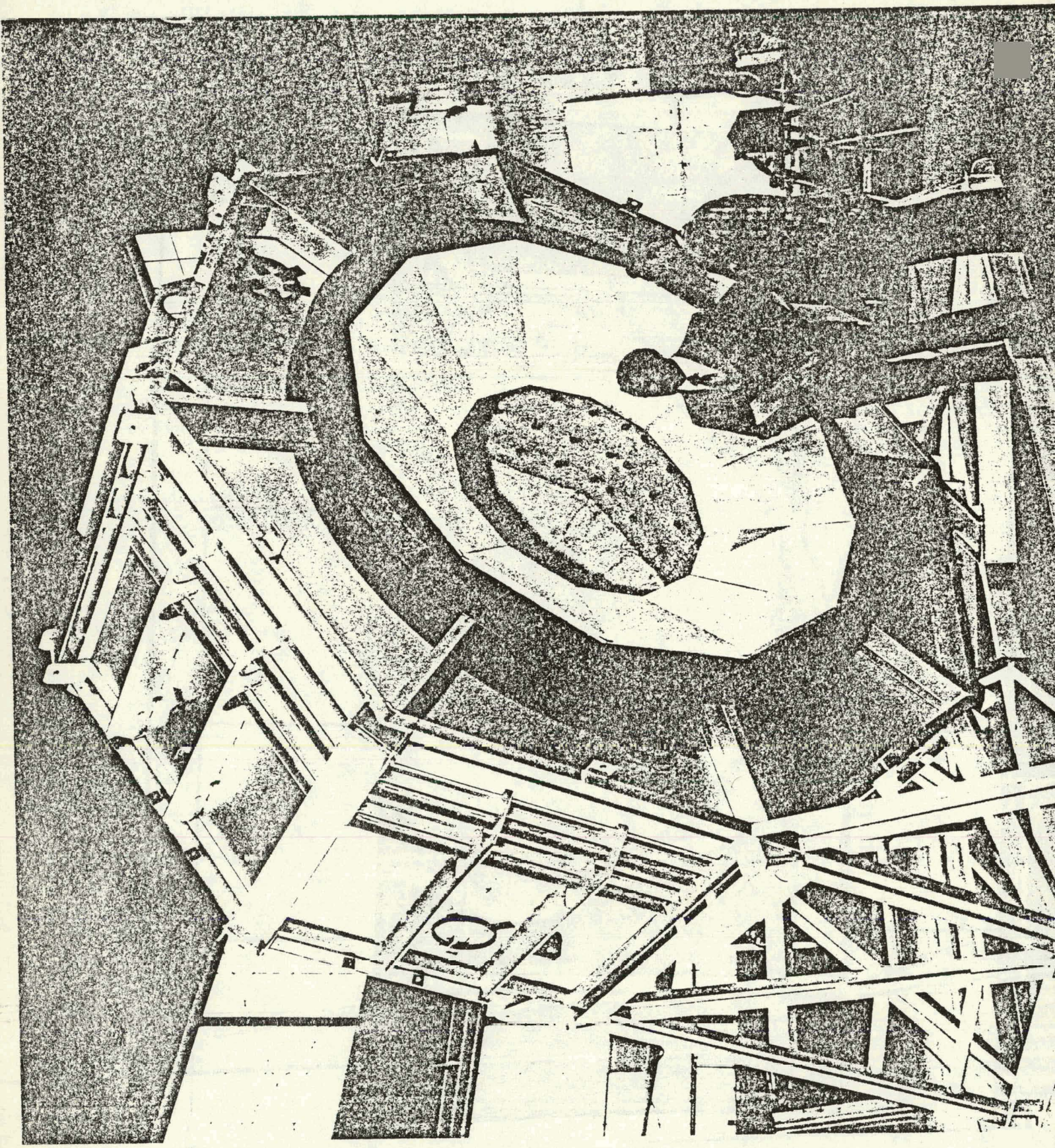



Electric Power Research Institute

Aperture Shield Insulation
Temperatures and Survival Limits







Summary

- BMSR designed with limited heat-exchanger and insulation material data
- Vendor data generally not applicable for solar environment
- Laboratory tests needed to supplement development of a major SRE
- Design for 30-year life requires:
  - Hx stress-rupture and creep—1,000-10,000 hrs
  - Hx thermal cyclic fatigue
  - Cavity and aperture insulation thermal cyclic behavior
  - Effects of solar exposure on insulation spectral properties

THIS PAGE
WAS INTENTIONALLY
LEFT BLANK

SOLAR THERMAL CONVERSION

TEST SYSTEMS DESIGN

Viewgraphs Presented

by

Raymond Mar

Sandia Laboratories

Livermore, California

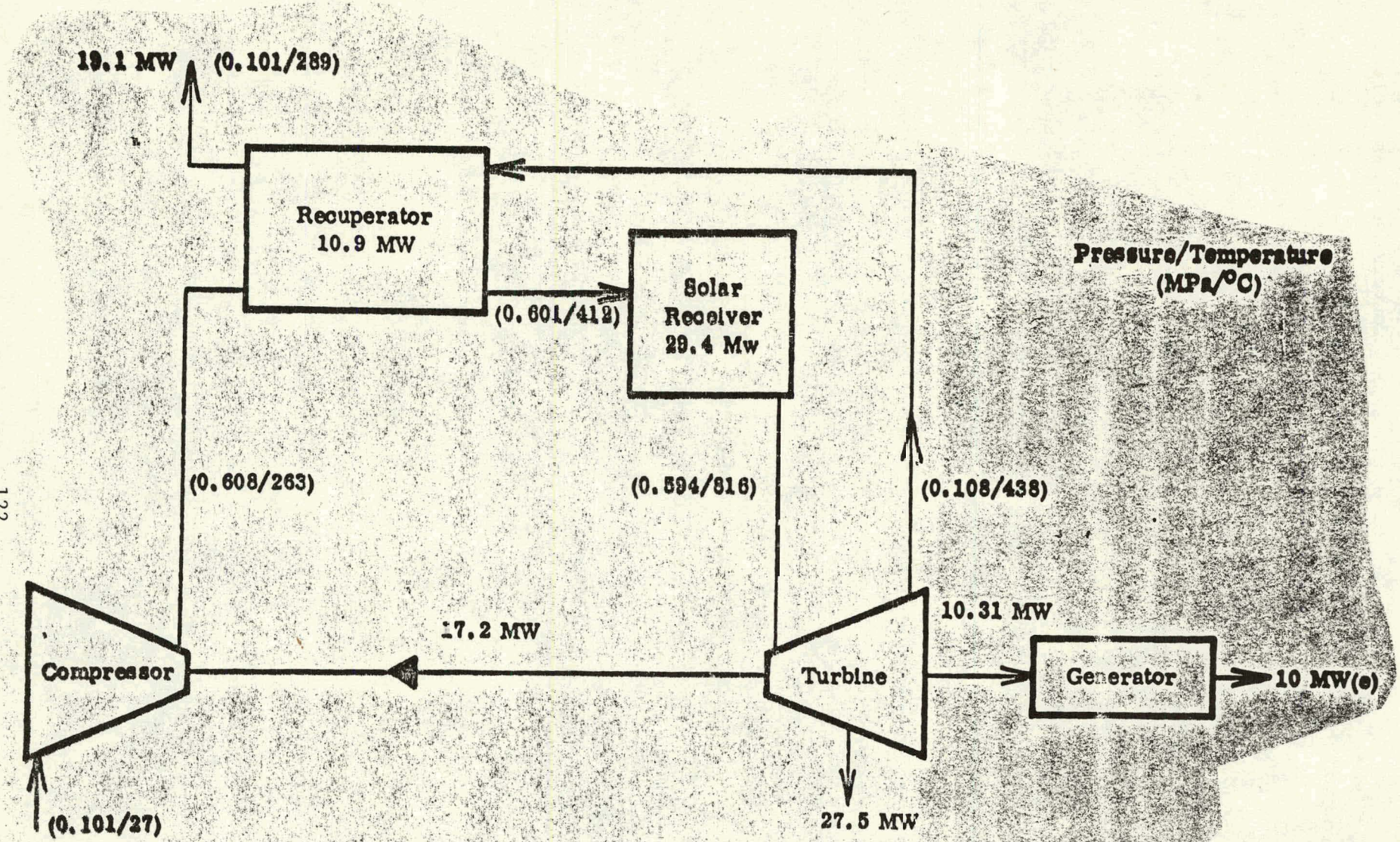
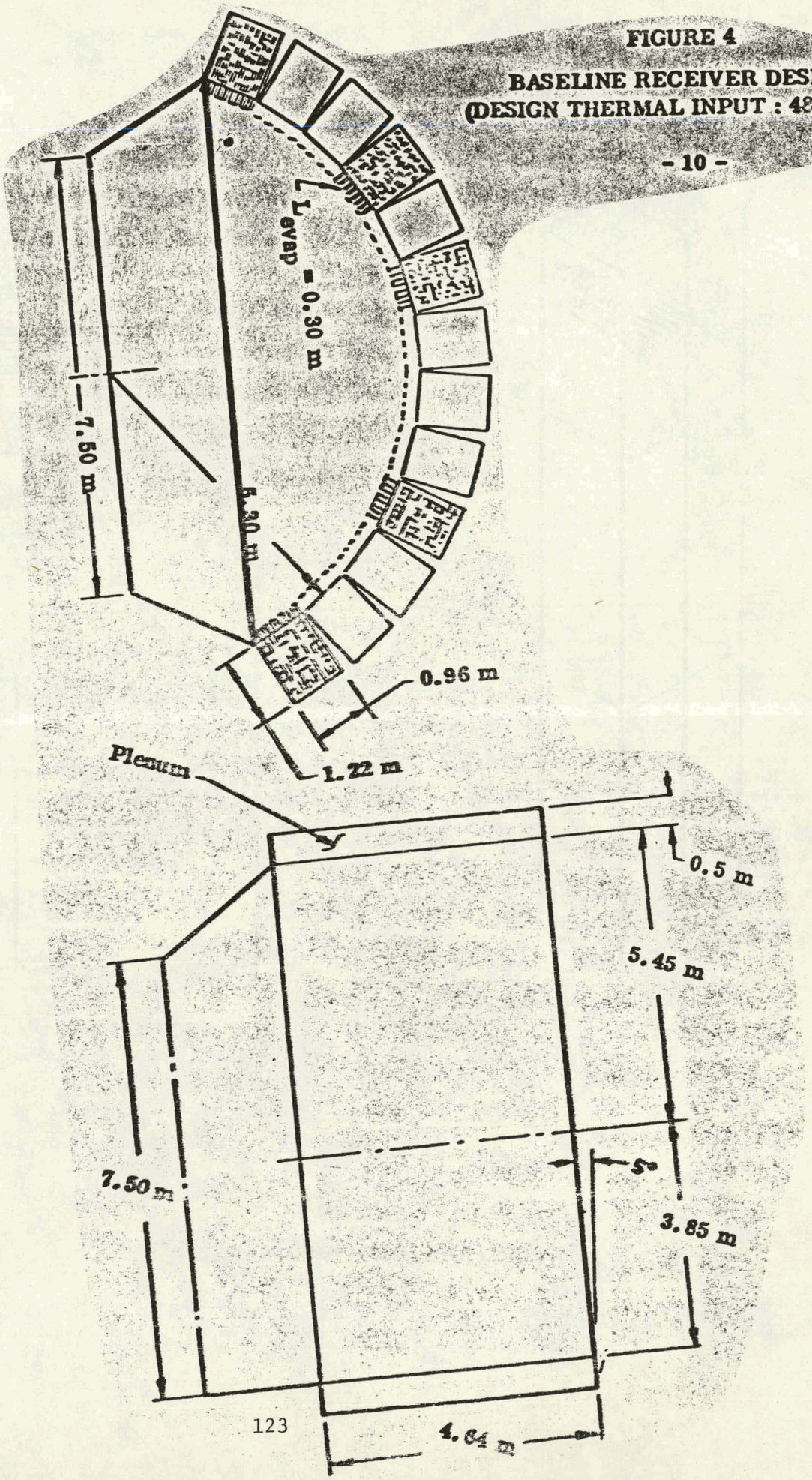


FIGURE 1

FLOW SHEET OF RECUPERATIVE OPEN GAS CYCLE ($\eta = 0.35$)

FIGURE 4

BASELINE RECEIVER DESIGN
(DESIGN THERMAL INPUT : 48.8 MW)



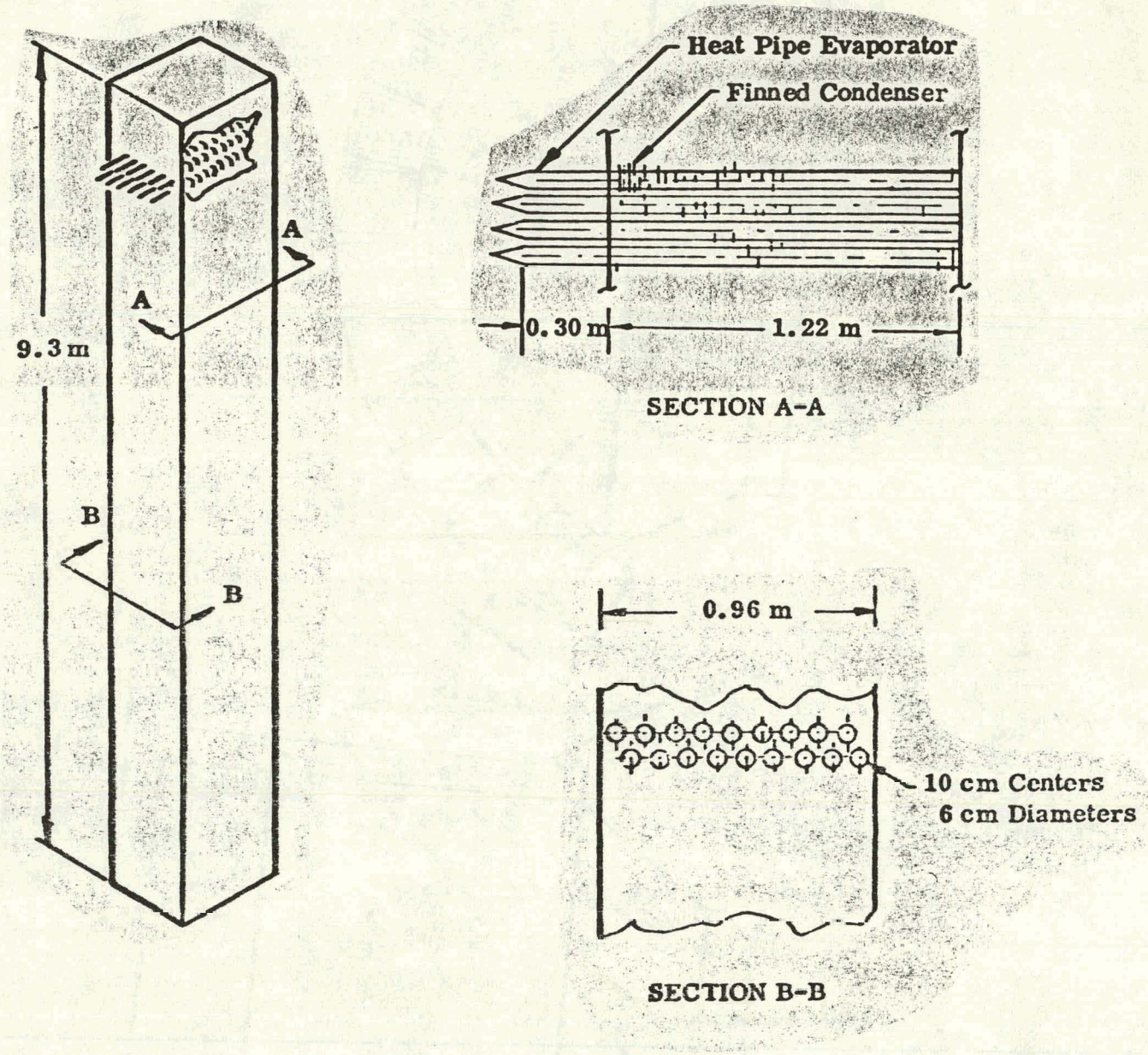
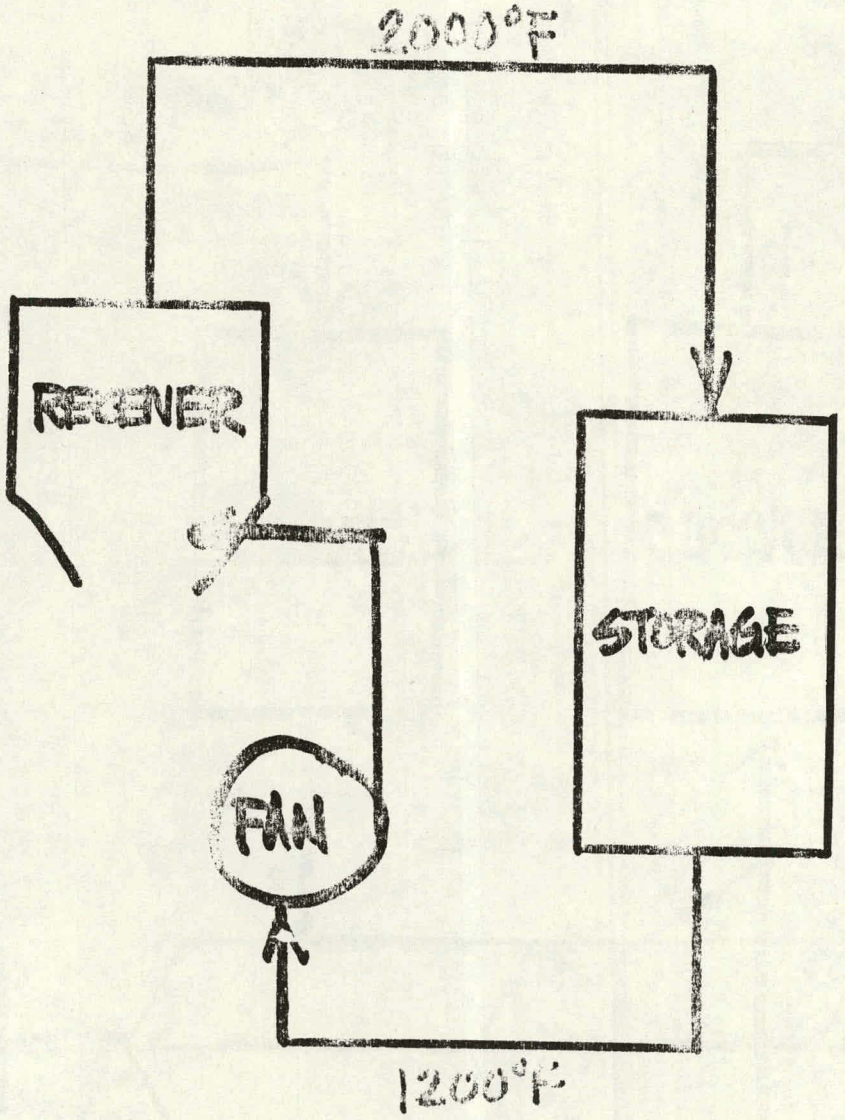
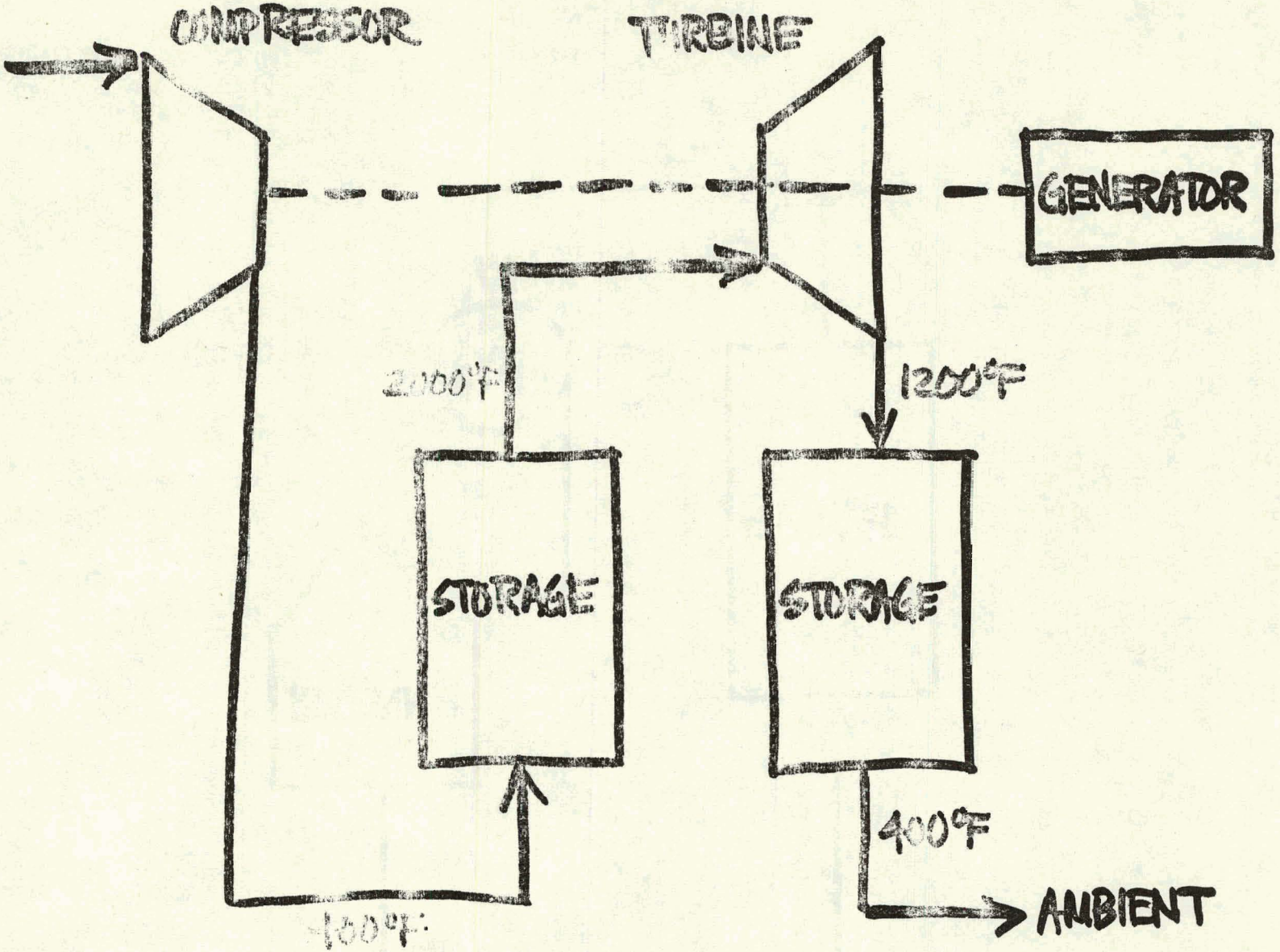


FIGURE 5

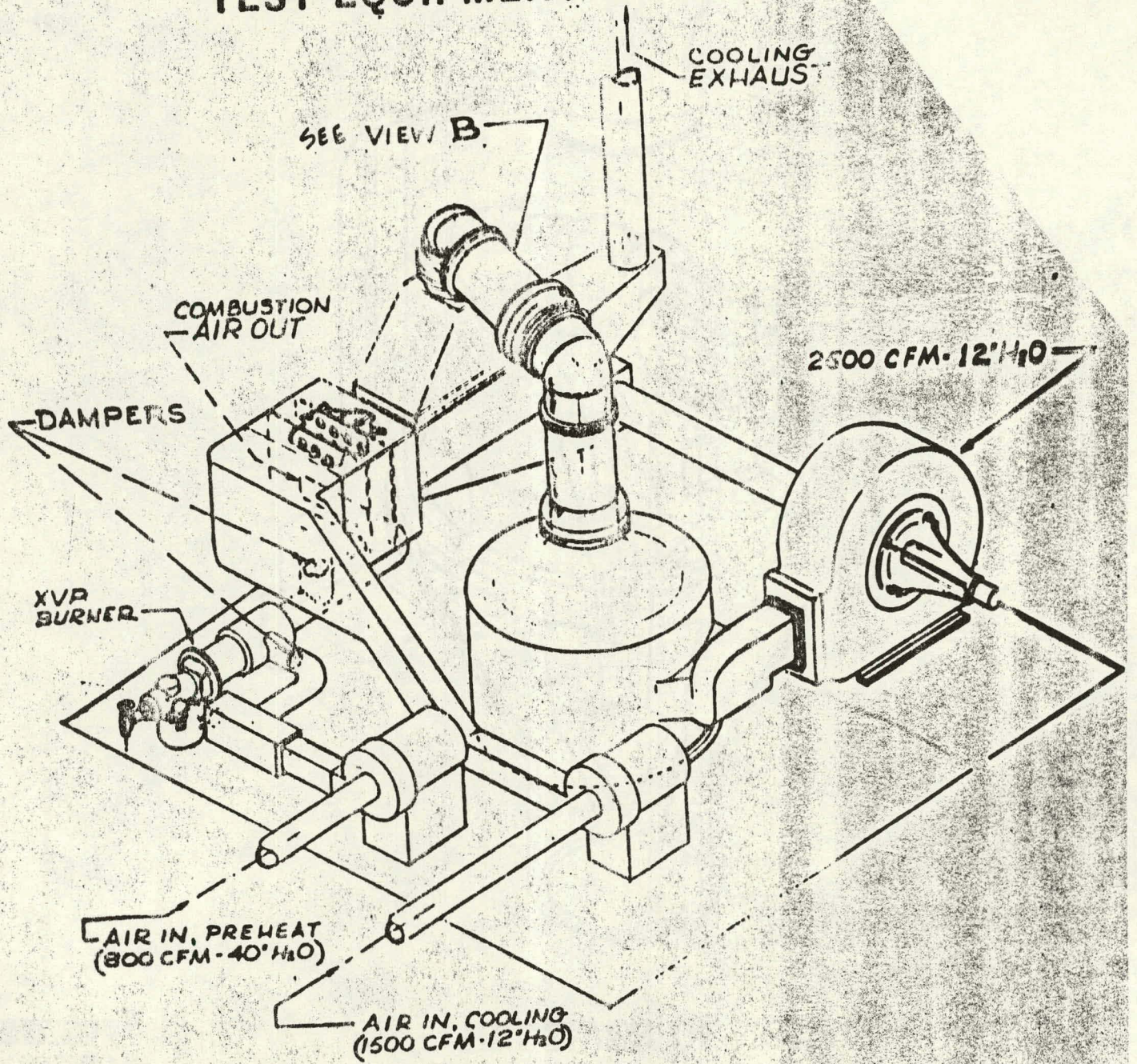
TYPICAL RECEIVER PANEL


2000°F
REGENER.
STORAGE
FAN
1200°F


COMPRESSOR
TURBINE
GENERATOR
1200°F
1200°F
STORAGE
STORAGE
400°F
AMBIENT

BUILDERS ASSOCIATES, INC.

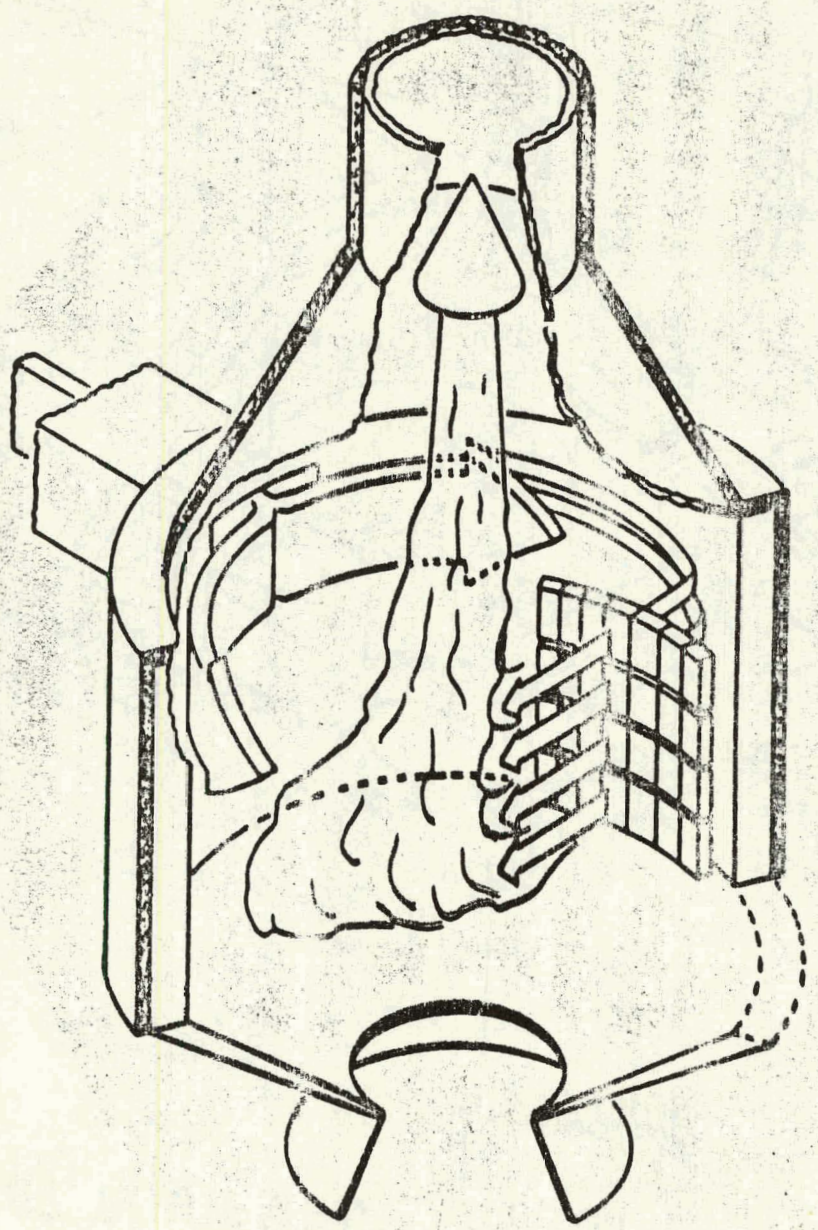
TEST EQUIPMENT LAYOUT



12207-11

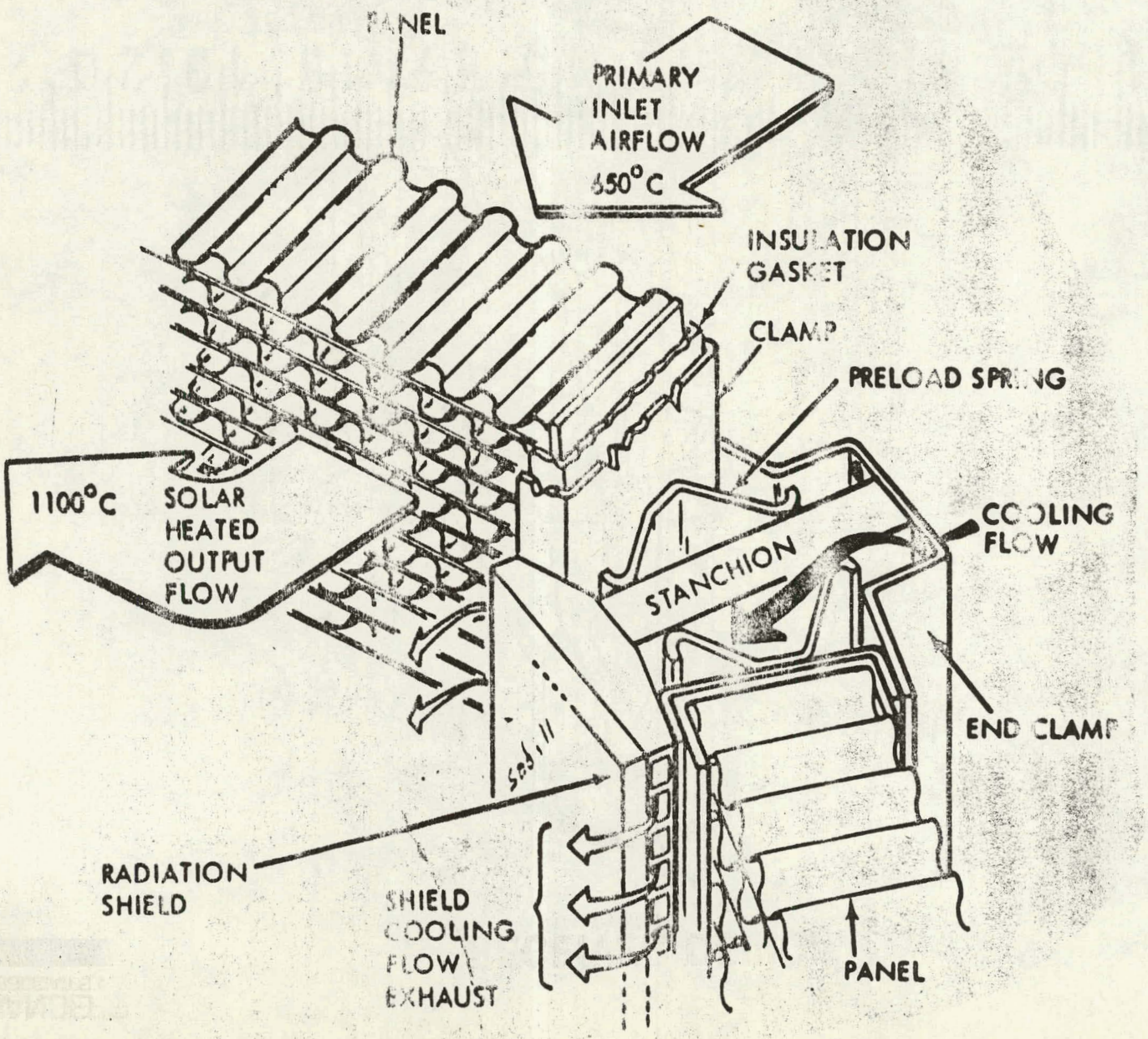
SANDERS ASSOCIATES, INC.
DEFENSIVE SYSTEMS DIVISION

RECEIVER DESIGN



SANDERS ASSOCIATES INC

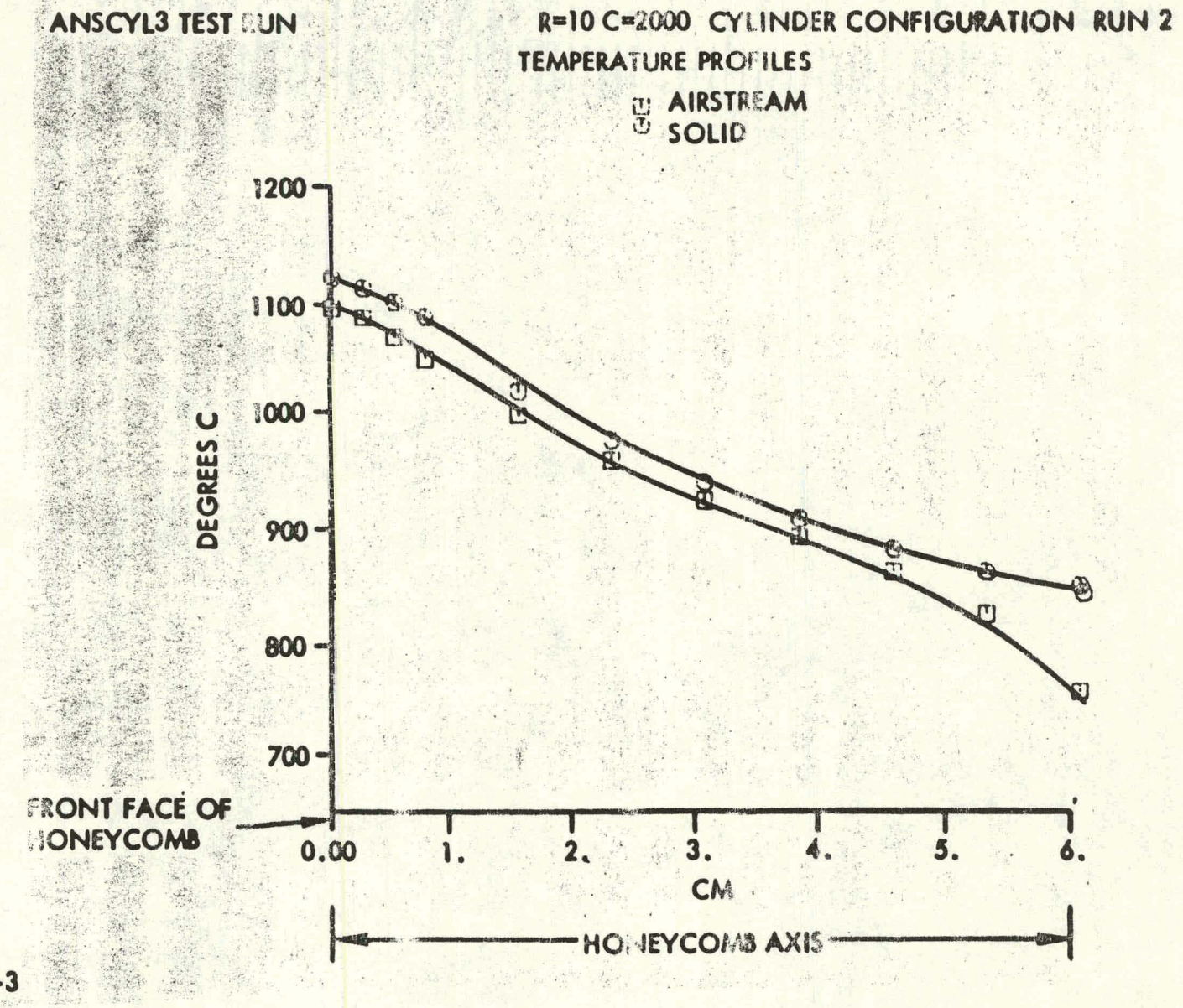
DETAIL OF HEAT EXCHANGER PANEL SUPPORT AND AIRFLOWS



06268-47

SANDERS ASSOCIATES, INC
DEFENSIVE SYSTEMS DIVISION

ANSCYL TEMPERATURE RUN



BLACK AND VEATCH RECEIVER DESIGN

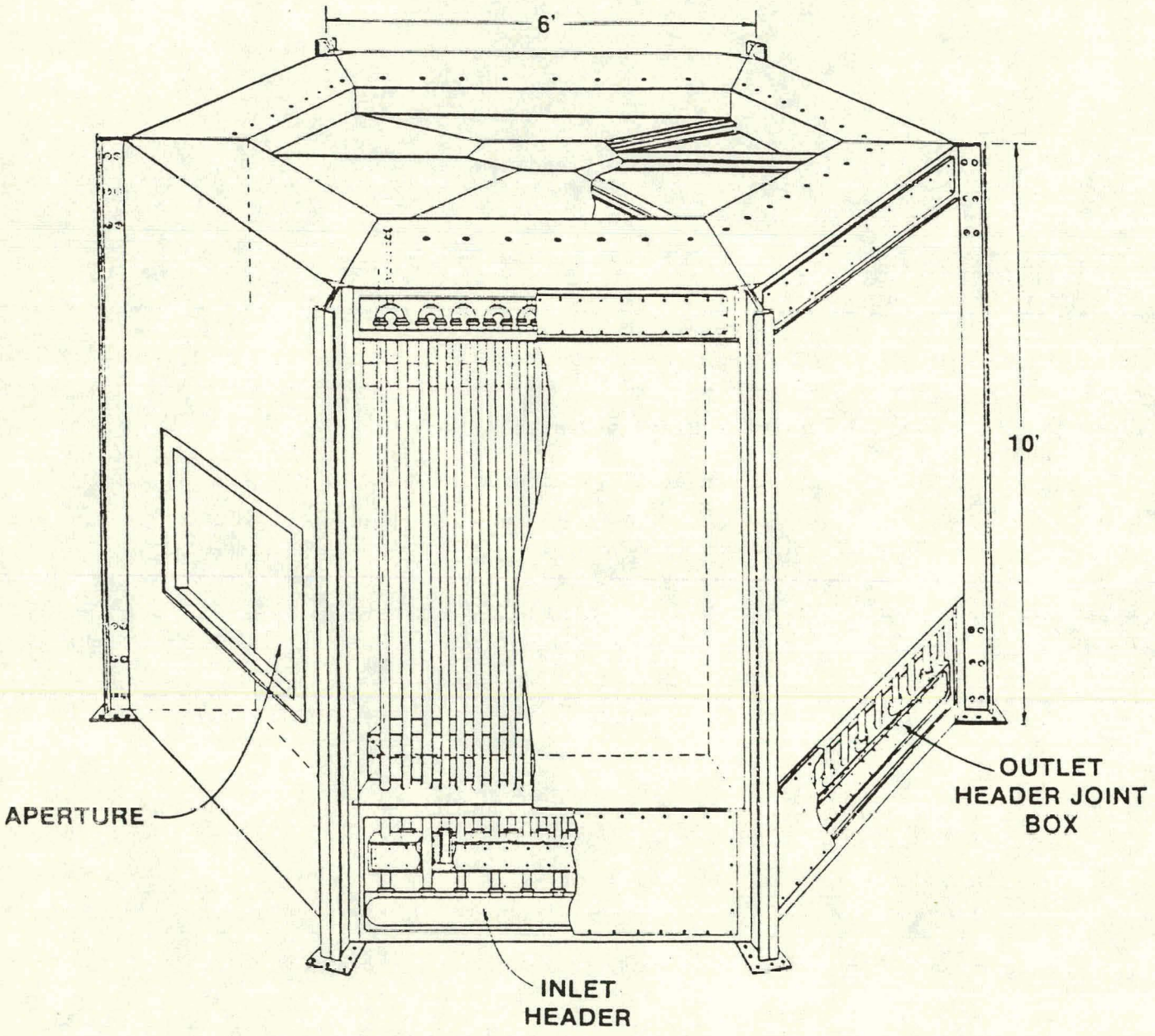
Viewgraphs Presented

by

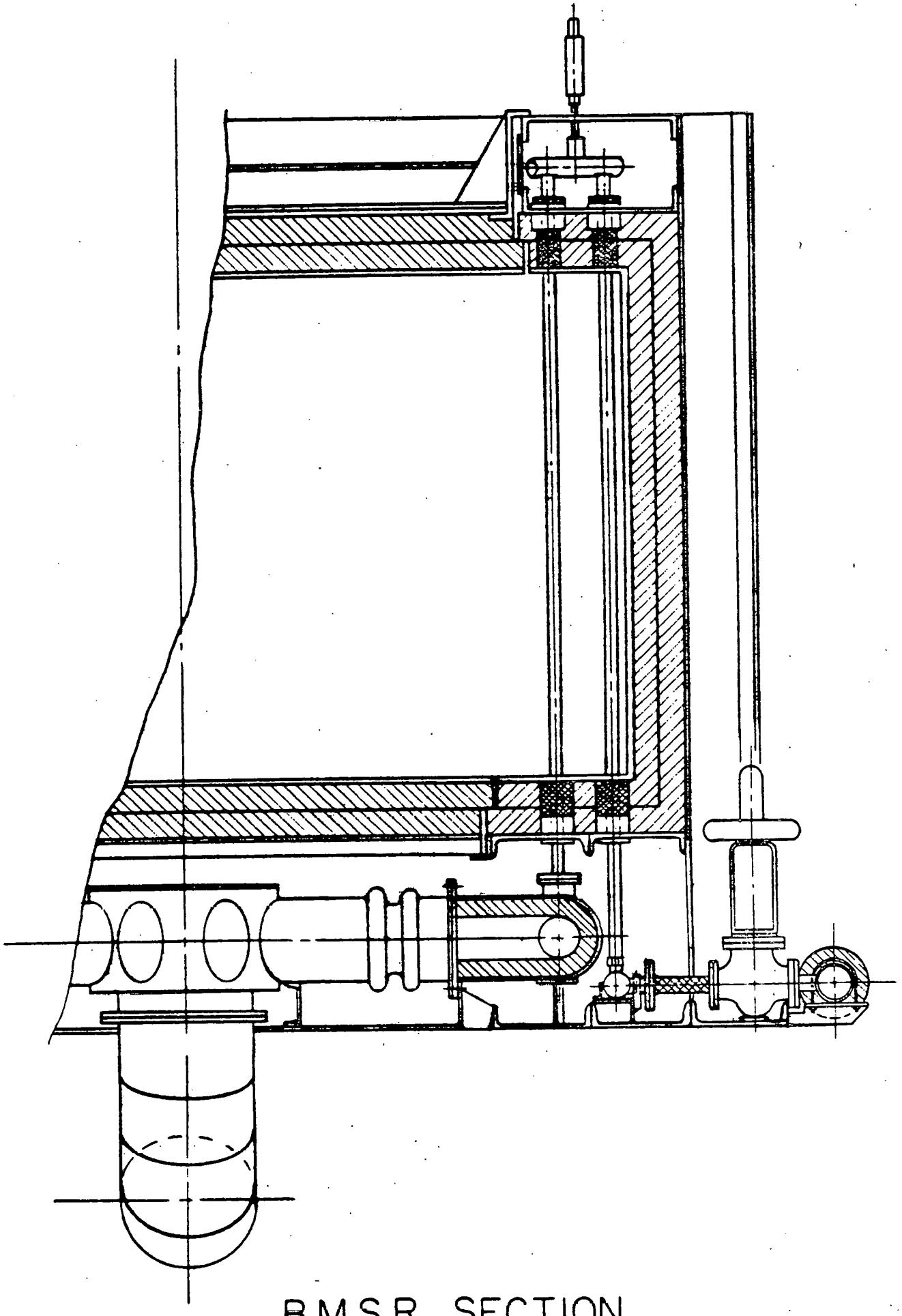
Edward McBride

Black & Veatch

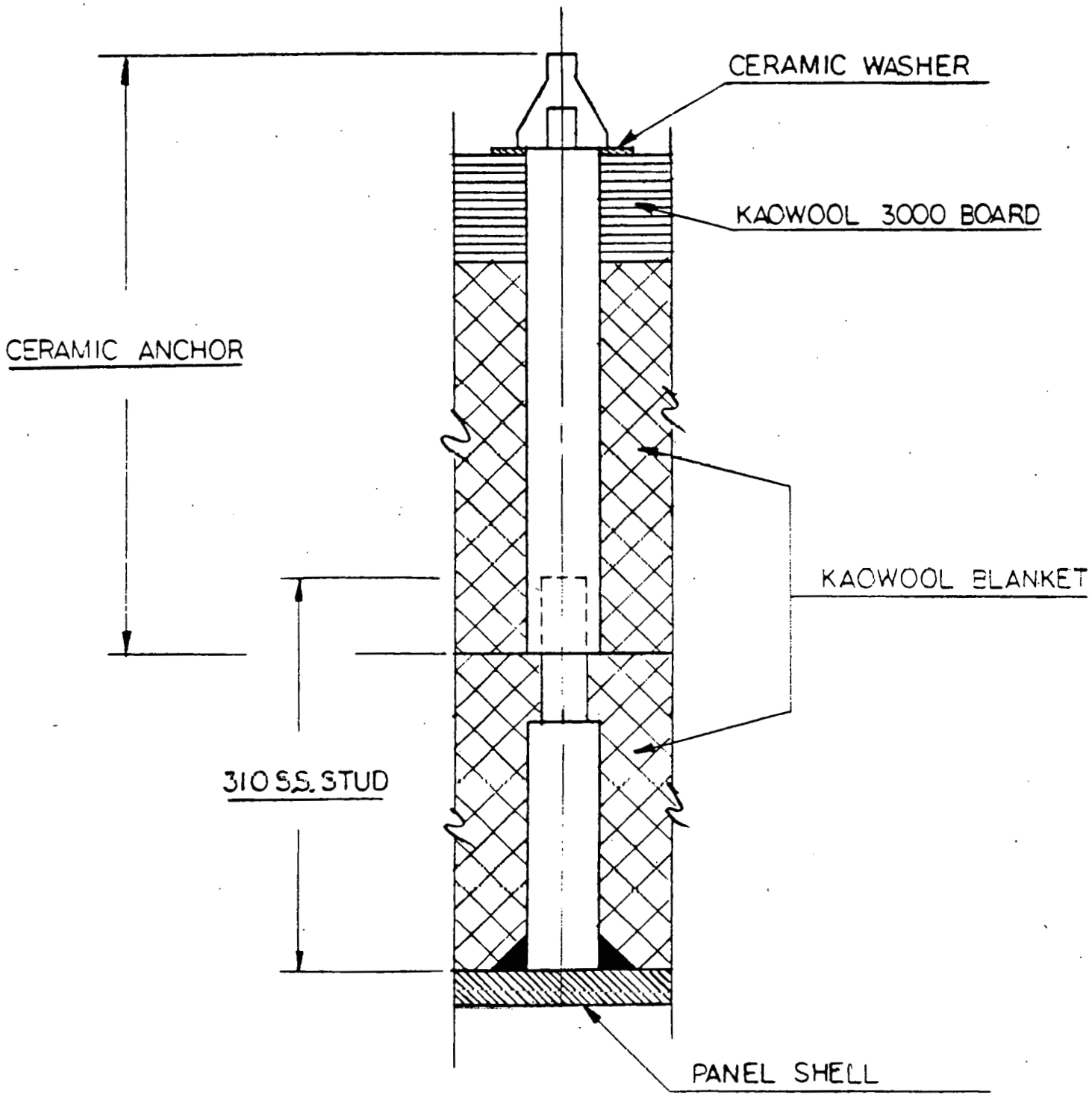
Kansas City, Missouri



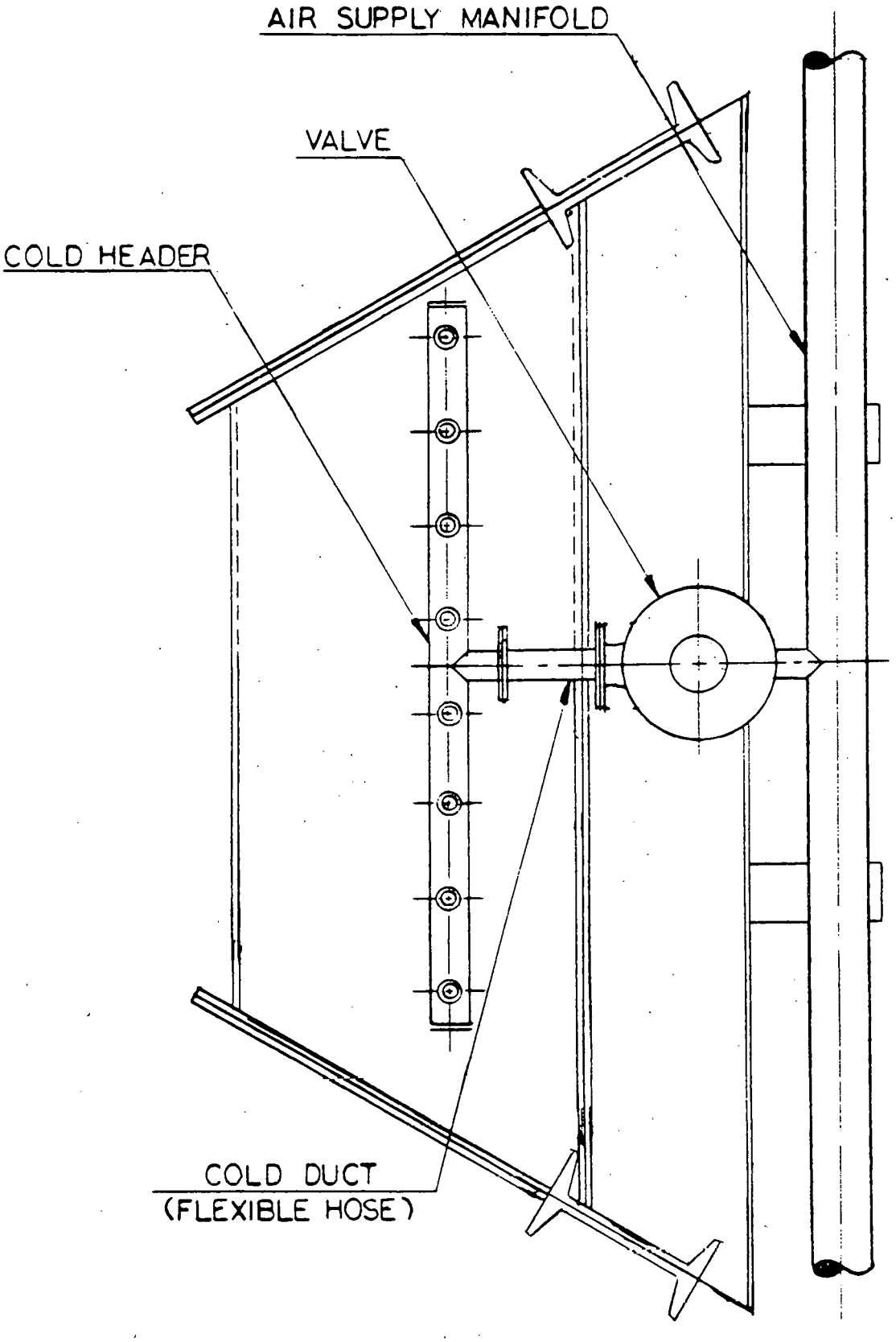
PERSPECTIVE OF 1 MWt
BENCH MODEL RECEIVER



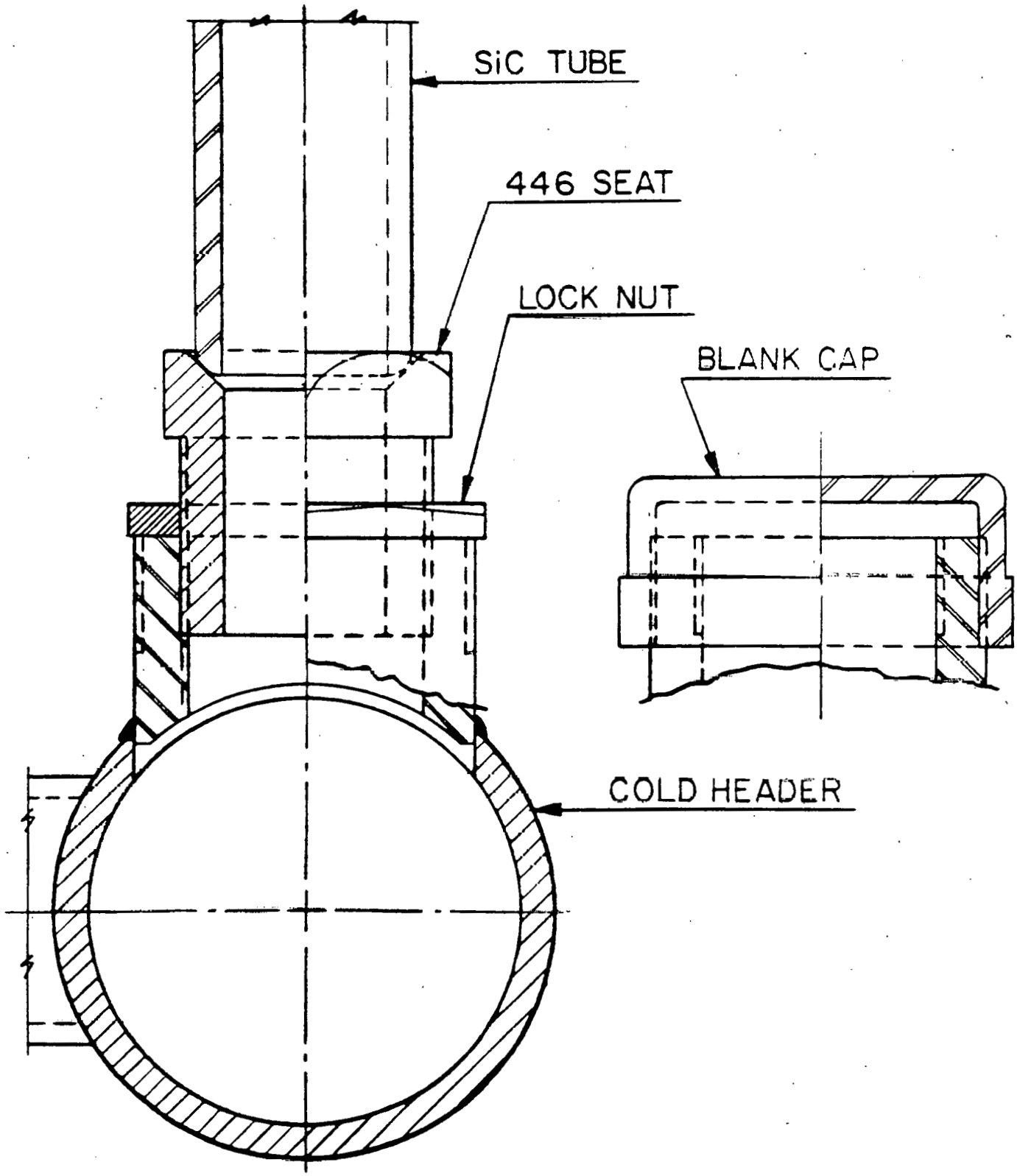
B.M.S.R. SECTION



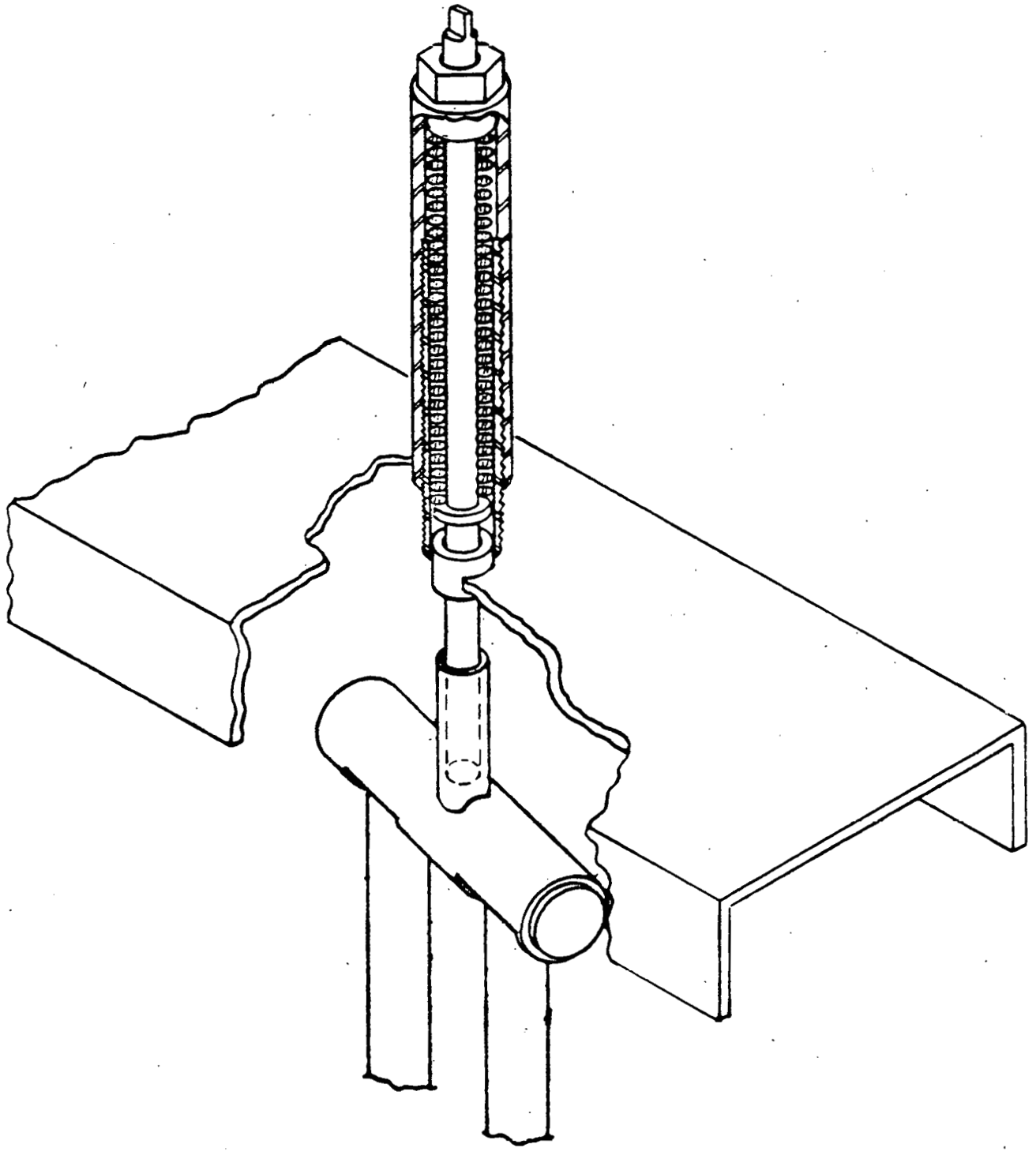
INSULATION ANCHOR PIN



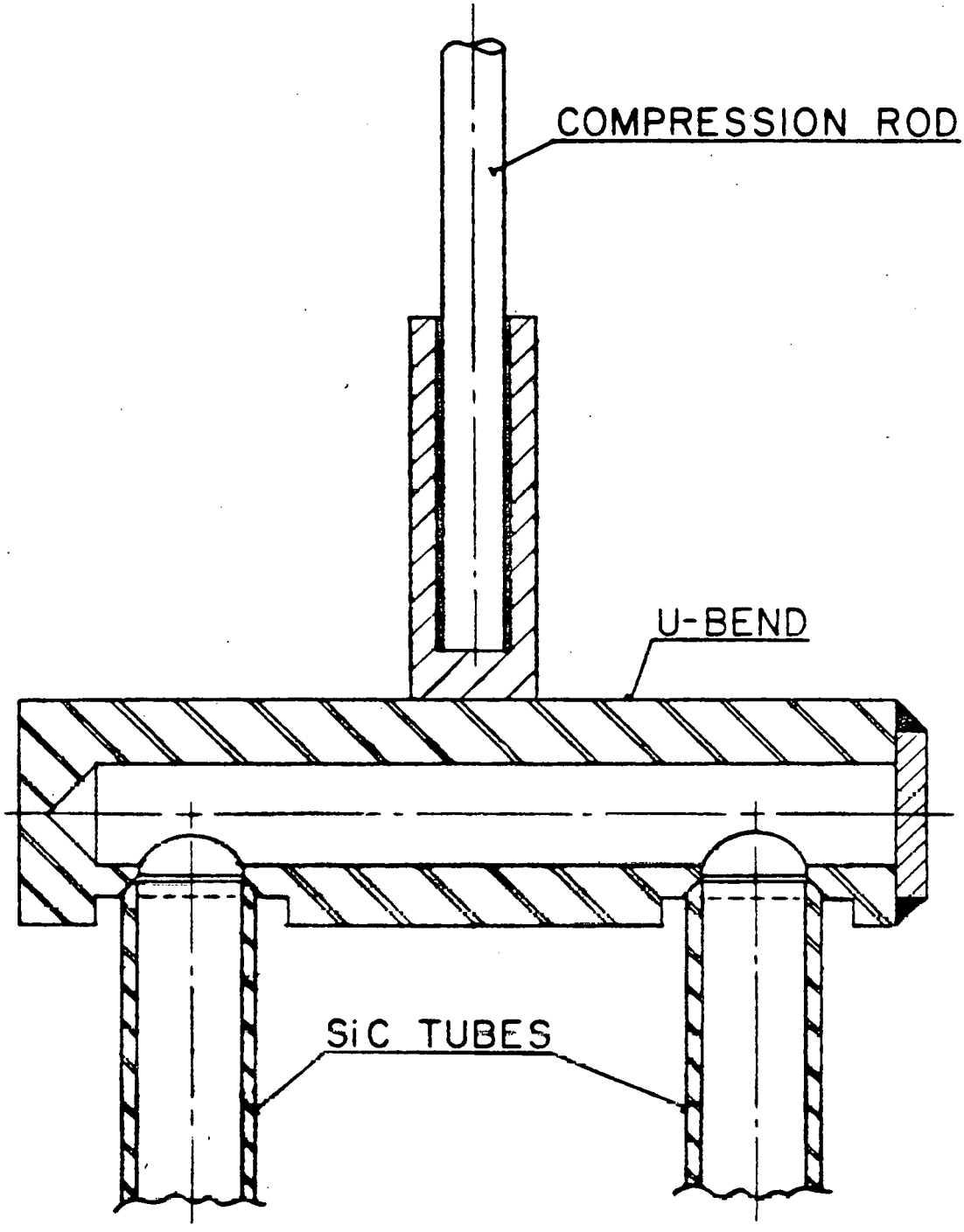
AIR INLET ARRANGEMENT



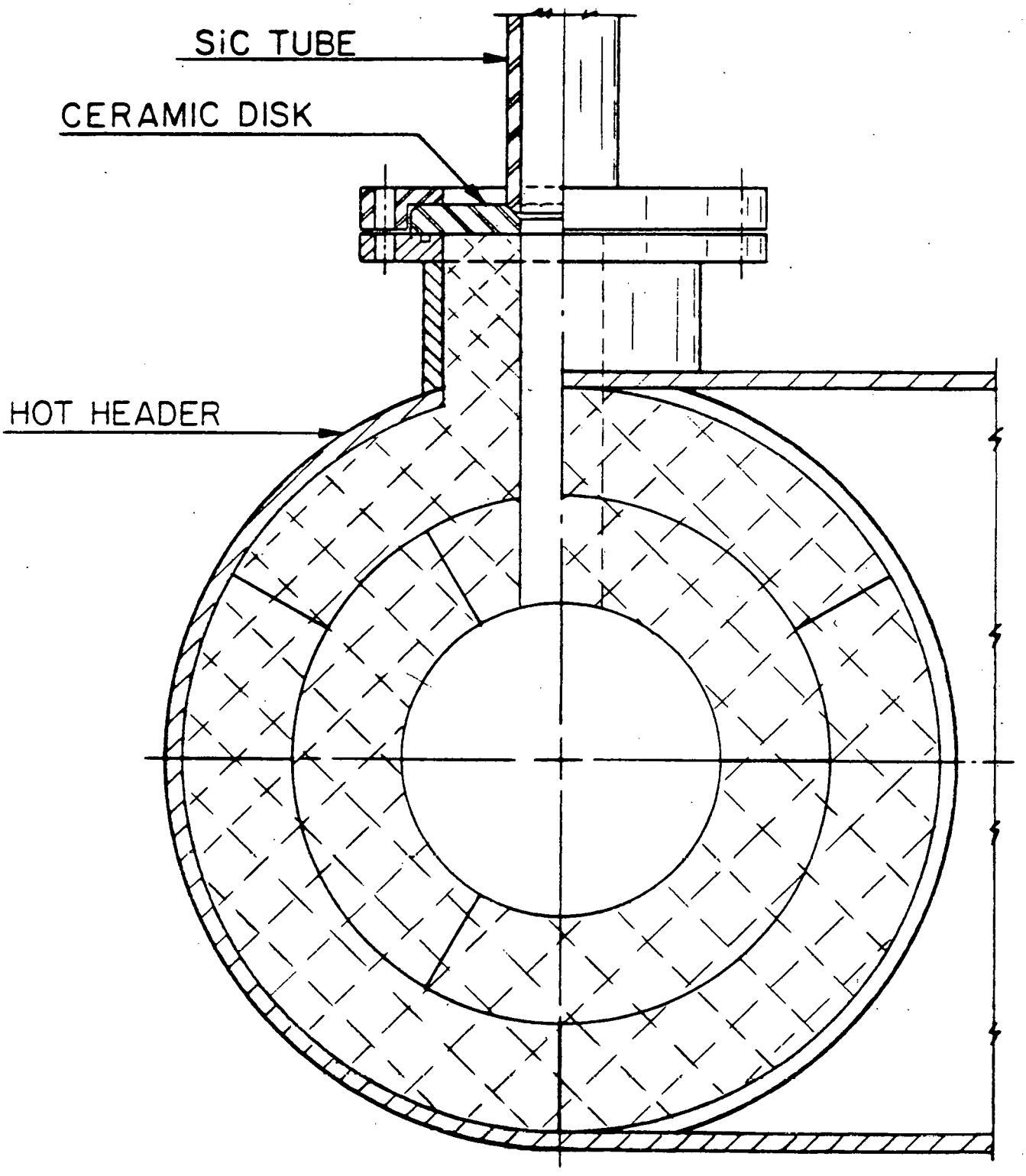
COLD HEADER JOINT



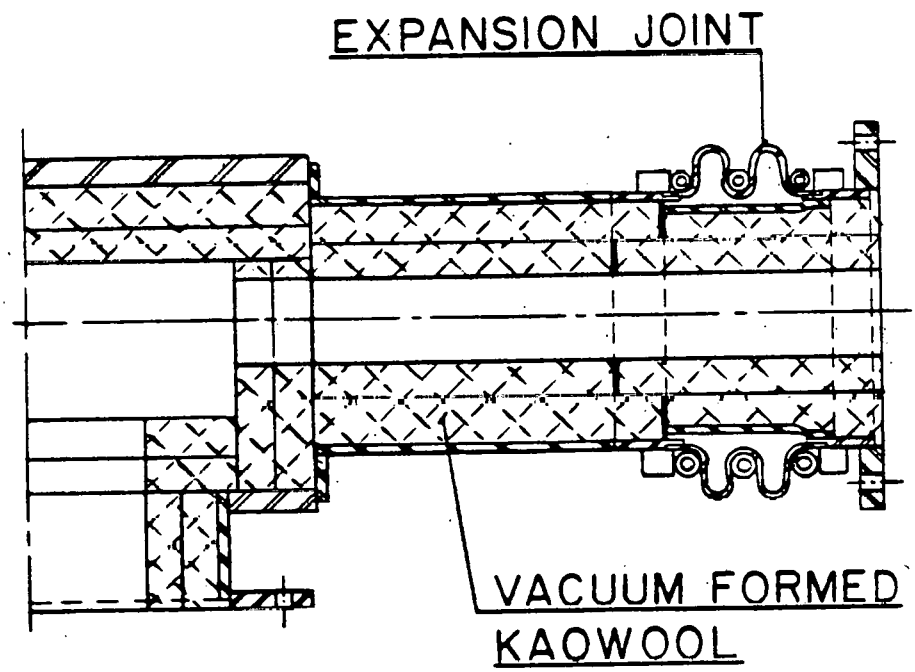
SPRING and U-BEND ARRANGEMENT



U-BEND



HOT HEADER JOINT



HOT AIR DUCT

DESIGN OF STRUCTURAL CERAMIC COMPONENTS

FOR

SOLAR HIGH TEMPERATURE THERMAL CONVERSION WITH A GAS COOLANT

by

Dr. David M. Kotchick

Garrett AiResearch Mfg. of California

Torrance, California

DESIGN OF STRUCTURAL CERAMIC COMPONENTS FOR SOLAR HIGH TEMPERATURE THERMAL CONVERSION WITH A GAS COOLANT

Ceramic components are currently under development for use in high temperature solar energy thermal power conversion systems. Studies by EPRI (The Electric Power Research Institute) and DOE (The Department of Energy) have shown that the closed and open Brayton cycle engines are attractive solar power conversion systems due to their high conversion efficiency, high heat rejection temperature and the simplicity of single phase working fluid. Figure I illustrates the maximum cycle efficiency and approximate material temperatures as a function of turbine inlet temperature for closed-cycle gas turbines. For each of the five components identified on the left side of the figure, the material choices are identified. For example, super alloys are required when fabricating turbine rotors exposed to, turbine inlet temperatures up to 1800°F; from 1800° to 2300°F, refractories can be considered (with an inert gas); above 2300°F, ceramic materials are indicated. For the primary heater system, ceramic materials are indicated at turbine inlet temperatures of 1600°F and above--a temperature much lower than is generally associated with the use of ceramic materials. This is because the primary heater material (in this case the solar receiver) operates at a temperature significantly higher than the turbine inlet temperature.

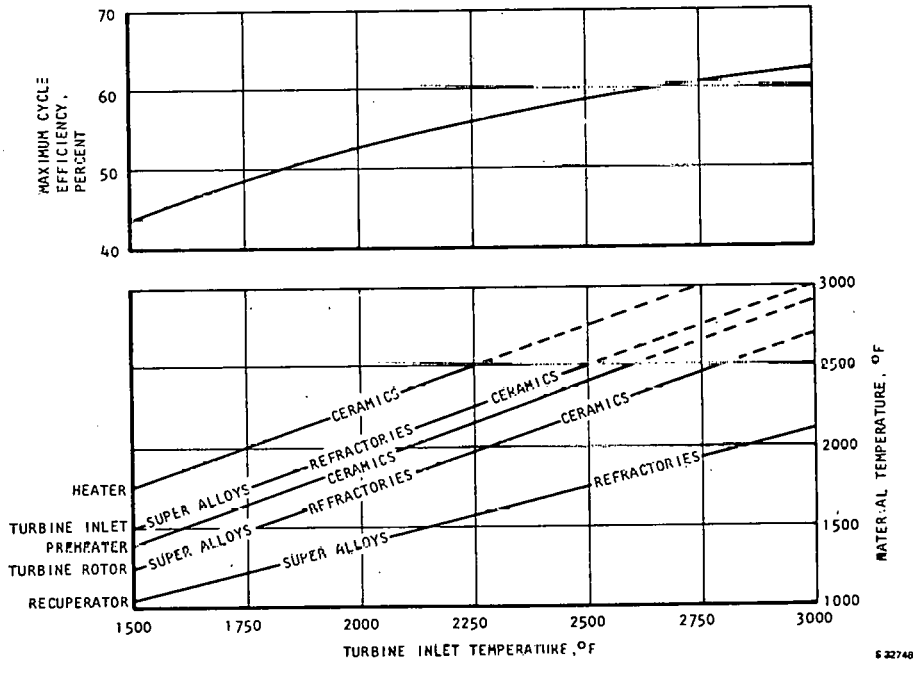


Figure 1. Closed Brayton Engine

Depending on the turbine inlet temperature (TIT) ceramic components may be desirable in several areas of the power conversion system. A logical development would parallel increasing TIT through the ceramic heat exchanger, ceramic ducting, and first stage ceramic turbine components.

Ceramic candidate materials must withstand severe operating conditions. They must be strong and relatively inert in high temperature oxidizing environments. Candidate materials should also have high thermal conductivity at operating temperatures, for example, silicon carbide which has a thermal conductivity greater than stainless steel above 1600°F. Ceramic materials with high thermal conductivity (SiC and Si_3N_4) are desirable to eliminate severe local thermal gradients in the material (> 400°C) which would cause thermal shock cracks to develop.

High performance structural ceramic materials are relatively new. In an effort to provide the best possible materials, producers have been constantly refining the composition and processing of their products. Unfortunately, data in the literature only a few months may not be as accurate as desired. A system of material specifications and accurate designations to reflect processing and compositional changes should be worked out with the suppliers. Only the most up to date information should be gleened from the literature. Since processing can make a difference in material properties, all component designs should be fabricable within the normal processing capabilities of the suppliers. New processing techniques are being rapidly developed. One notable example is the development of advanced slip casting technology and permanent ceramic joints by Norton Company to make intricate ceramic components of siliconized silicon carbide. Figure 2 shows a finned tube heat exchanger module made under EPRI contract for Garrett AiResearch.

Many important material properties have not been accurately determined over the range of temperatures and environmental conditions necessary to design for the operational lifetime. These include stressed lifetime under static and cyclic loading conditions.

Finally mechanical joining and compatability problems have not been solved. These include the development of pressure tight ceramic to ceramic and ceramic to metal seals.

To understand the potential failure modes of ceramics and the techniques used for the design of ceramic components it is necessary to recognize several important ceramic properties. Ceramic materials are brittle. Geometric irregularities either small (surface or volume flaws) or large (sharp corners) act as stress concentrators when the component is mechanically or thermally stressed. Since ceramics do not deform plastically (except very near their melting points) this stress concentration can cause a crack to develop or extend to a critical length where spontaneous crack propagation causes catastrophic failure. The strength of ceramics is generally controlled by sharp, tensile stressed surface flaws. Compressively stressed volumes are relatively much stronger since crack growth is not favored. Because the strength of a uniformly stressed ceramic components is controlled by the severity and distribution of flaws, the characteristic material strength has a relatively large standard deviation and can not be accurately described by one number as the strength of metal is described. Instead, a statistical description must be employed which reflects the population of strength limiting flaws and designates safe design stresses as a function of reliability.

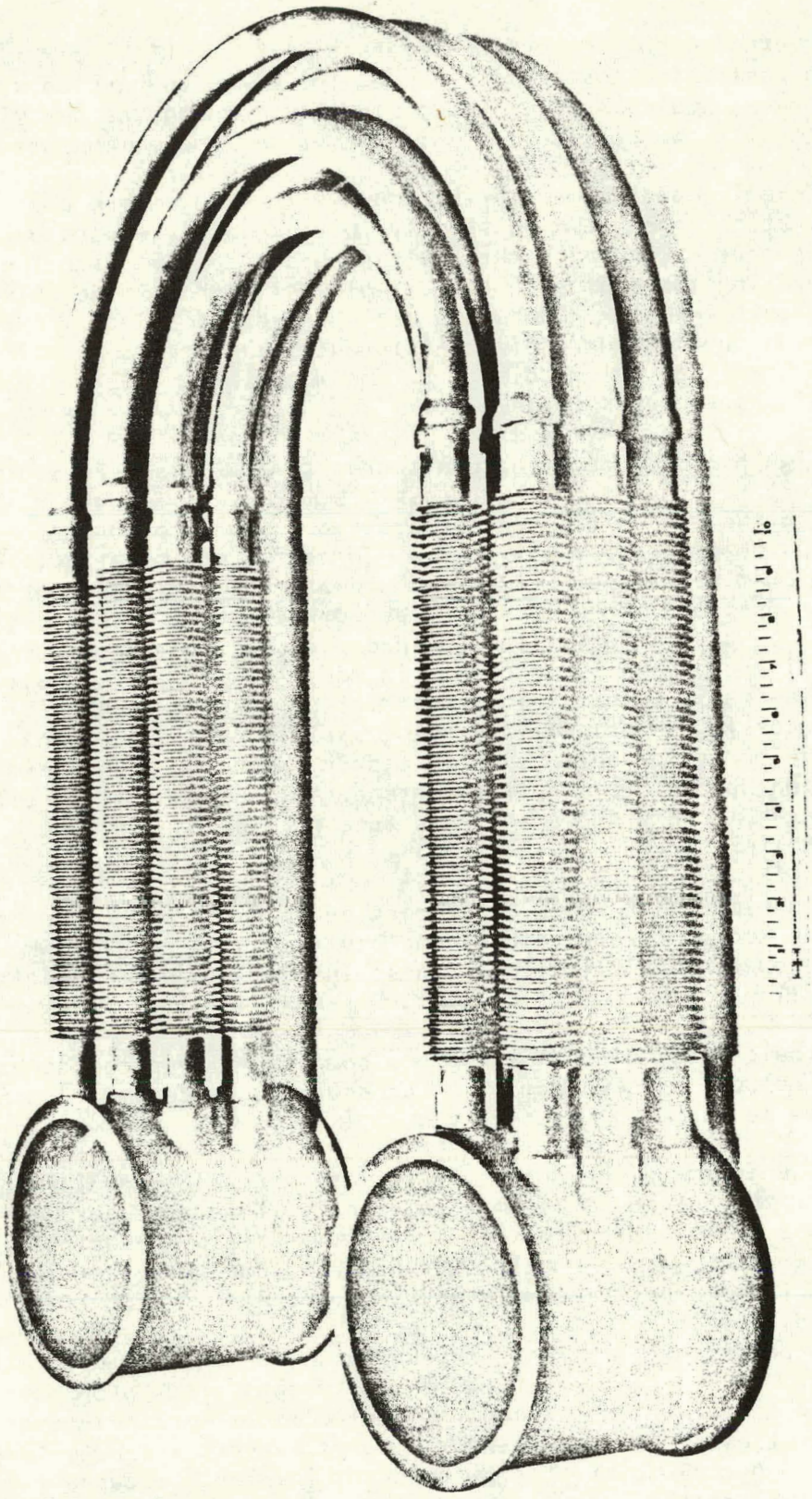


Figure 2. Finned Tube Heat Exchanger Module

Any large number of natural events that are random in time (such as traffic flow or agricultural and ecological events) often can be described by the compound Poisson process. The "weakest link" or weakest flaw theory, originally developed by Weibull to statistically describe the strength of materials, is a subcase of the Poisson process used to describe a fracture that occurs randomly. The parameters of the Weibull distribution (which must be experimentally determined) are a function of the type of material and its surface and volume condition.

The Weibull distribution function allows the comparison of strength distribution parameters with calculated stress fields. Since the Weibull parameters are not material constants, they must be determined as a function of the use environment and surface condition. The Weibull function can be written as:

$$S = 1 - e^{\left[-V\left(\frac{\sigma}{\sigma_o}\right)^m\right]} \qquad (1)$$

where S = probability of failure

σ = operating stress

σ_o = characteristic strength (median strength)

m = Weibull slope (Weibull modulus)

V = stressed volume or surface area

The fracture strengths of a group of samples can be used to estimate m and σ_o when Equation (1) is rewritten as

$$\ln \ln \frac{1}{1-S} = \left\{\ln V - m \ln \sigma_o\right\} + m \ln (\sigma_f) \qquad (2)$$

The value of S can be estimated from $S = s/n + 1$ where N is the total number of samples in a test and s is the number of the sample when the group is arranged in increasing order of fracture stress. When $\ln \ln(1/1-s)$ is plotted versus $\ln \sigma_f$, m is the slope and σ_o can be taken as the value that will make the data best fit a straight line. Figure 2 shows a computer-drawn plot and calculated Weibull m for a group of SiC strength data. It is important that this data be collected on samples with surfaces processed exactly as components and tested in the appropriate environment.

Fracture mechanics theory can be used to generate stress-time-probability curves (STP) for long times (> 100 hours) from relatively short time dynamic loading tests but the extrapolation may not simulate time related changes in the material. Static fatigue or stress rupture testing is more expensive and time consuming but the results are probably a more accurate representation of the material stressed lifetime when extrapolated to longer lifetimes.

The final design of ceramic components should be refined by finite element computer modeling. Design criteria embodying aspects of a deterministic approach, and utilizing a probabilistic basis built into the analytical tools on an individual finite-element volume and surface area basis, are felt to provide the best approach to effective design with ceramics. In the presence of adequate materials and component test data, this approach is valid. Even with a lower level of materials data, it provides a realistic method of comparing designs.

Figure 3 shows a finite-element model constructed for a ceramic transition duct as part of an EPRI funded program to develop a high temperature ceramic heat exchanger at Garrett AiResearch Mfg. of California.

Finally, proof testing of ceramic components can be performed as an additional safety measure if the proof test can simulate the operating conditions. Over pressurization of tubes or ducts could be used as a good proof test but it would be difficult to simulate the thermal and mechanical stresses imposed on a turbine blade. Many elaborate non-destructive evaluation techniques are currently under development to detect the strength limiting flaws. These flaws are generally very small (< 10 microns) for high performance ceramics and therefore are hard to differentiate from the normal surface topography.

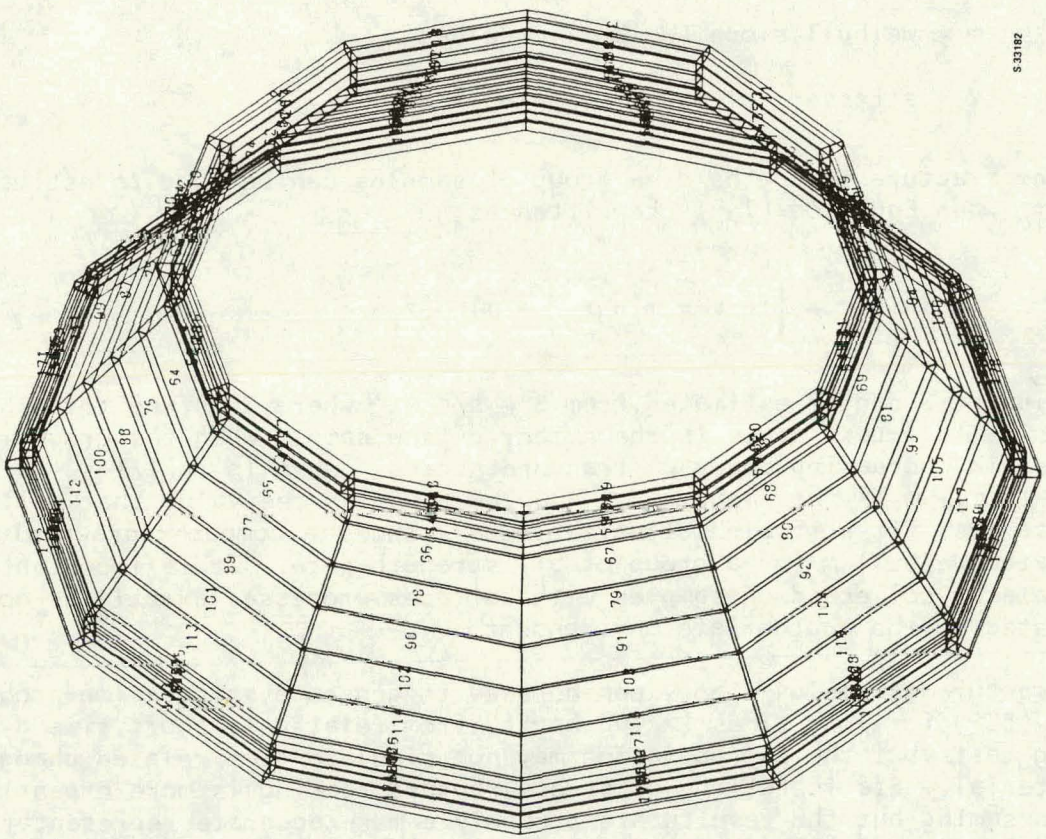


Figure 3. Model for Ceramic Transition Duct

HIGH TEMPERATURE DIFFUSION/MATERIALS STABILITY

Viewgraphs Presented

by

John R. Manning

National Bureau of Standards

Washington, D.C.

CLASSES OF HIGH TEMPERATURE STABILITY PROBLEMS

A. STRESSES CREATED BY THERMAL EXPANSION MISMATCH DURING CYCLING

B. INTERDIFFUSION IN THIN FILM COATINGS

C. CHEMICAL REACTIONS AND CORROSION

DESIGN OF STRUCTURAL CERAMIC COMPONENTS FOR SOLAR HIGH TEMPERATURE THERMAL CONVERSION WITH A GAS COOLANT

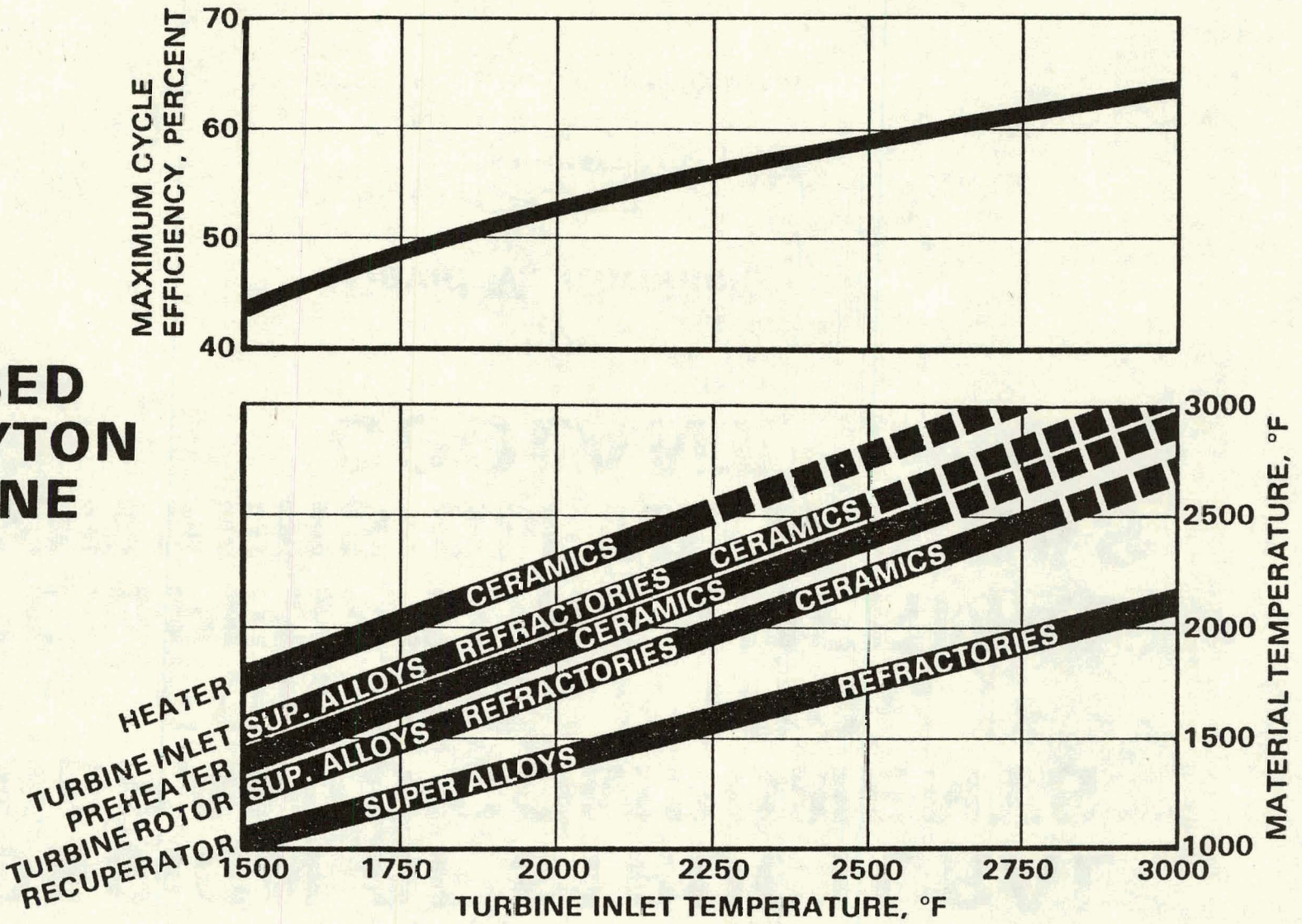
by
David M. Kotchick

GARRETT

AIRESEARCH MANUFACTURING COMPANY
OF CALIFORNIA

S-33467

CLOSED BRAYTON ENGINE



S-33475



DESIRABLE CANDIDATE MATERIAL PROPERTIES

- HIGH STRENGTH
- INERT TO HIGH TEMPERATURE OXIDIZING ENVIRONMENTS
- HIGH THERMAL CONDUCTIVITY



MATERIAL PROCESSING LIMITATIONS

- CONSTANT REFINEMENT OF PROPERTIES NEGATES OLD DESIGN DATA
- CHANGES IN SHAPE PROCESSING CHANGES PROPERTIES.
- NEW PROCESSING TECHNIQUES ARE RAPIDLY DEVELOPING

S-33463

DESIGN PROPERTIES TO BE DETERMINED

- STRESSED LIFETIME UNDER STATIC AND CYCLIC LOADING CONDITIONS
- EFFECT OF LONG TERM OXIDATION
- STRENGTH AS A FUNCTION OF COMPONENT VOLUME (SURFACE AREA) AND PROCESSING

S-33464



COMPATABILITY PROBLEMS

- COMPATABILITY WITH METAL COMPONENTS AT HIGH TEMPERATURE
- CERAMIC TO CERAMIC SEALS FOR HIGH TEMPERATURE
- CERAMIC TO METAL SEALS

S-33466

DESIGN REQUIREMENTS FOR CERAMIC COMPONENTS

- STATISTICAL APPROACH TO DESIGN RELIABILITY AND DATA COLLECTION
- DESIGN REQUIREMENT USING FINITE ELEMENT COMPUTER MODELING USING A PROBABILISTIC BASIS
- PROOF TESTING WHERE POSSIBLE

S-33465

THIS PAGE

WAS INTENTIONALLY

LEFT BLANK

HIGH TEMPERATURE OXIDATION OF METALS AND ALLOYS

Viewgraph Presented
by

C. E. Birchenall

University of Delaware

Newark, Delaware

Driving Force is Thermodynamic

$$\frac{2X}{y}\ M + O_2 = \frac{2}{y}\ M_x\ O_y$$

$$K\ \frac{a_{M_x O_y}^{2/y}}{a_M^{2x/y}\ P_{O_2}}$$

$$2_{M_x\ O_y} = 1 \quad ; \quad a_m = 1$$

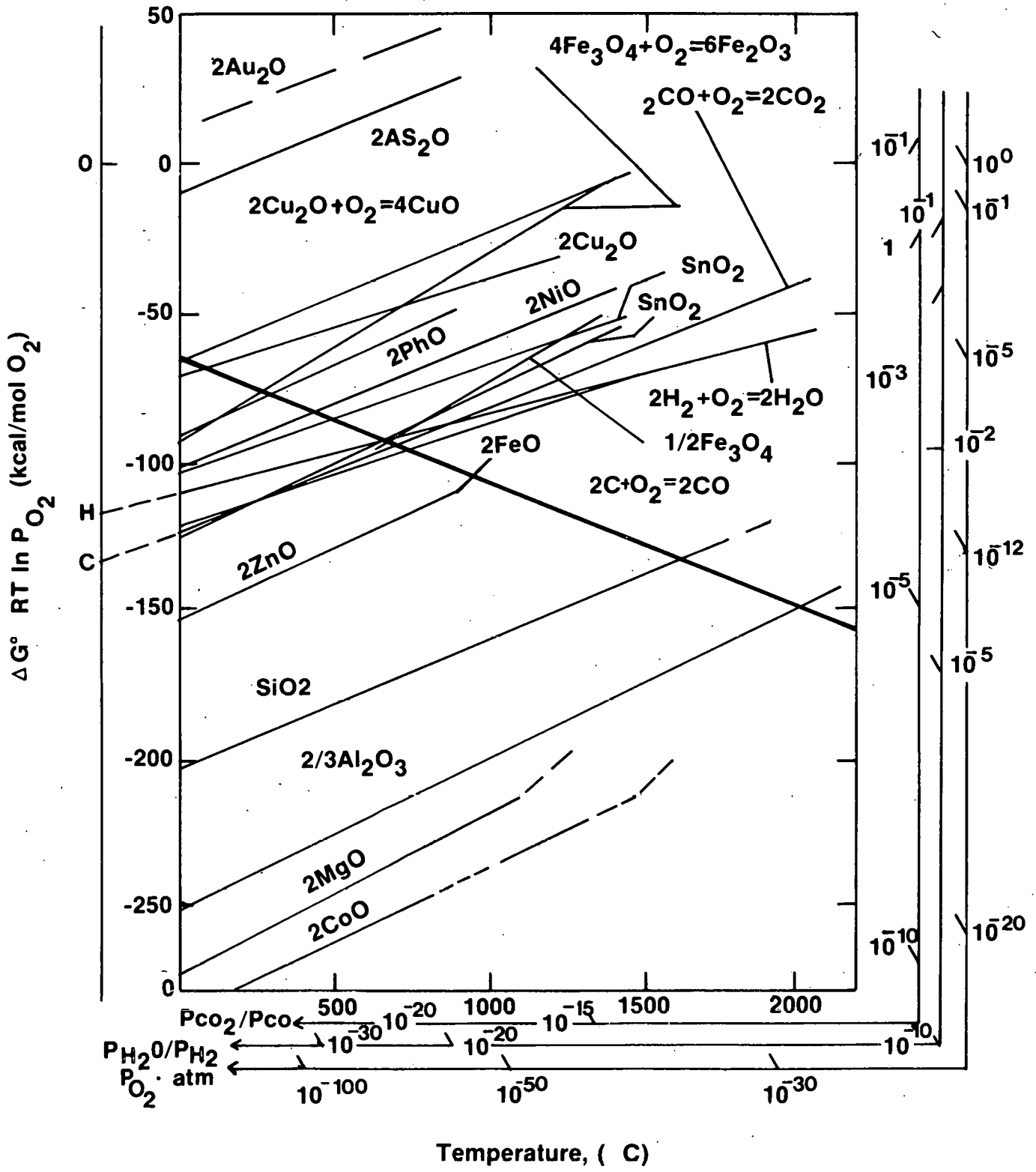
$$\Delta G^\circ = -\ RT\ \ln K = RT\ \ln P_{O_2}$$

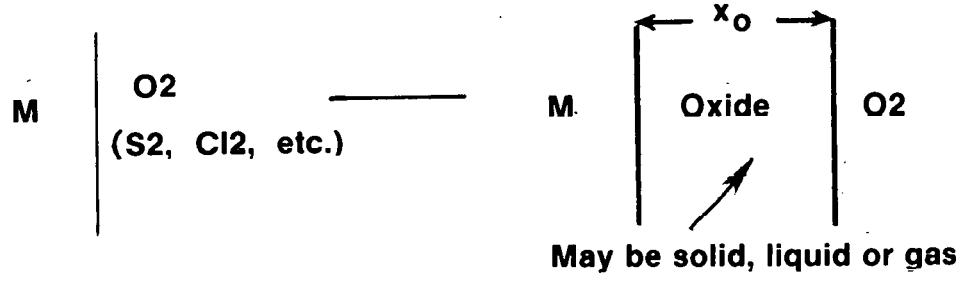
$$P_{O_2} = K_H^{-1} \left(\frac{P_{H_2O}}{P_{H_2}}\right)$$

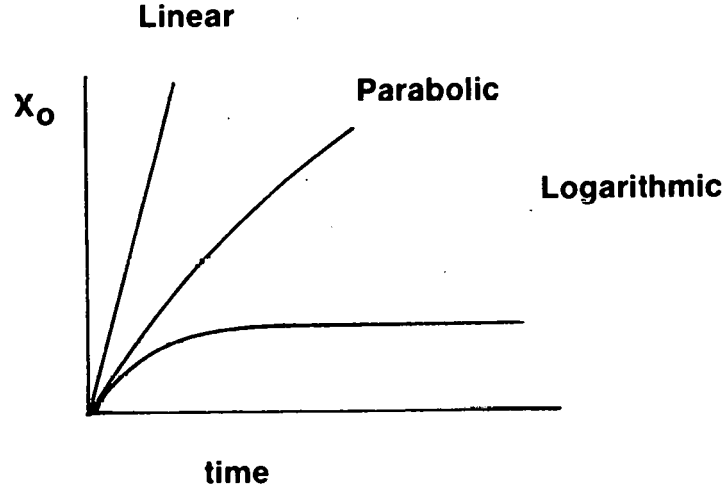
$$P_{O_2} = K_{Cl}^{-1} \left(\frac{P_{CO_2}}{P_{CO}}\right)$$

$$P_{O_2} = \frac{K_{C_2}^{-1}}{a_C^2}\ P_{CO}^2$$

Ellingham Diagram







$x_o = lt + C_1$ } Fluid or discontinuous oxide

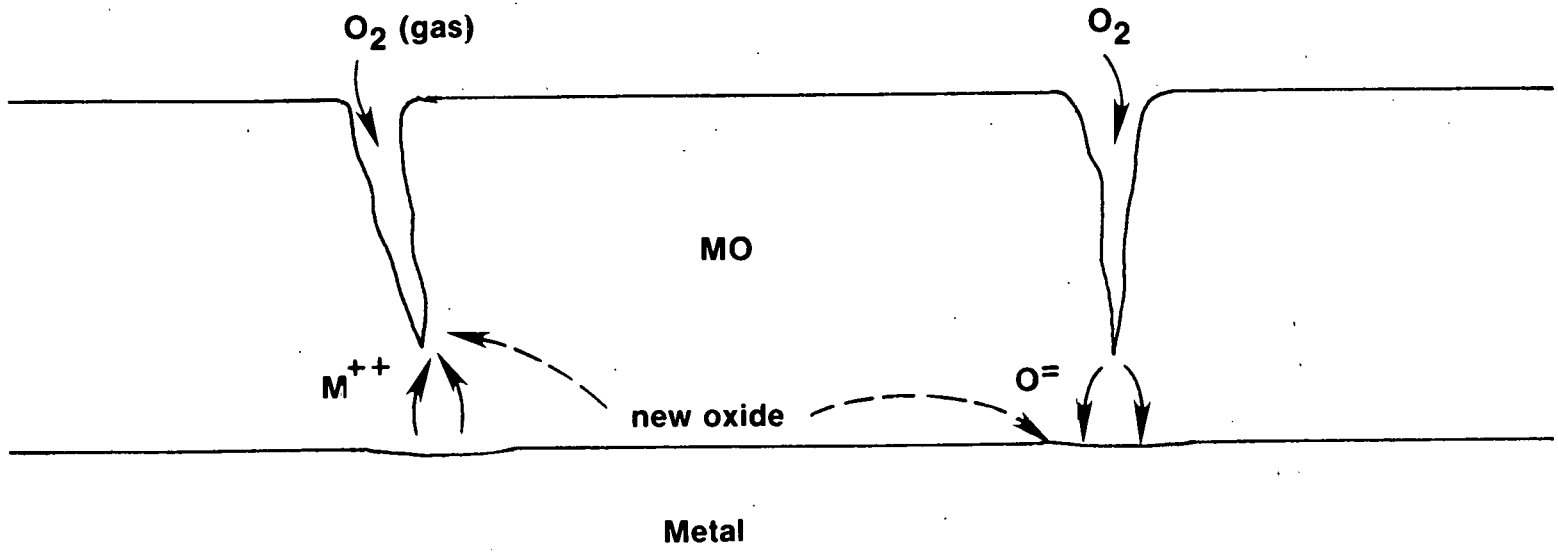
$x_o^2 = kt + C_2$ Continuous oxide at high enough temp. for ion diffusion

$x = K_3 \log t + C_3$ Continuous oxide, temp. too low for ions to diffuse without assistance from electrical field.

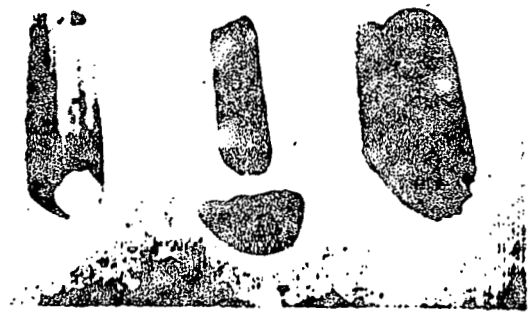
THIS PAGE

WAS INTENTIONALLY

LEFT BLANK



Wagner Cracking Model

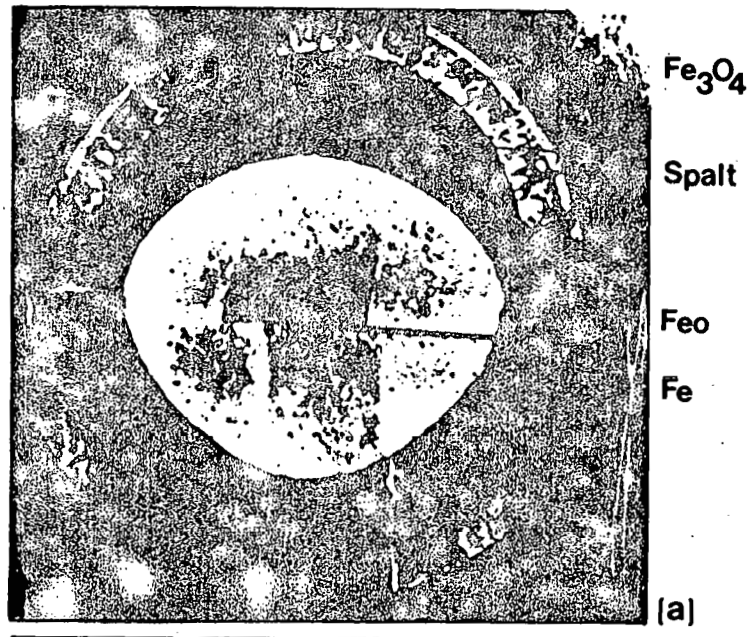


(a)



(b)

Cavity formation during oxidation of iron.

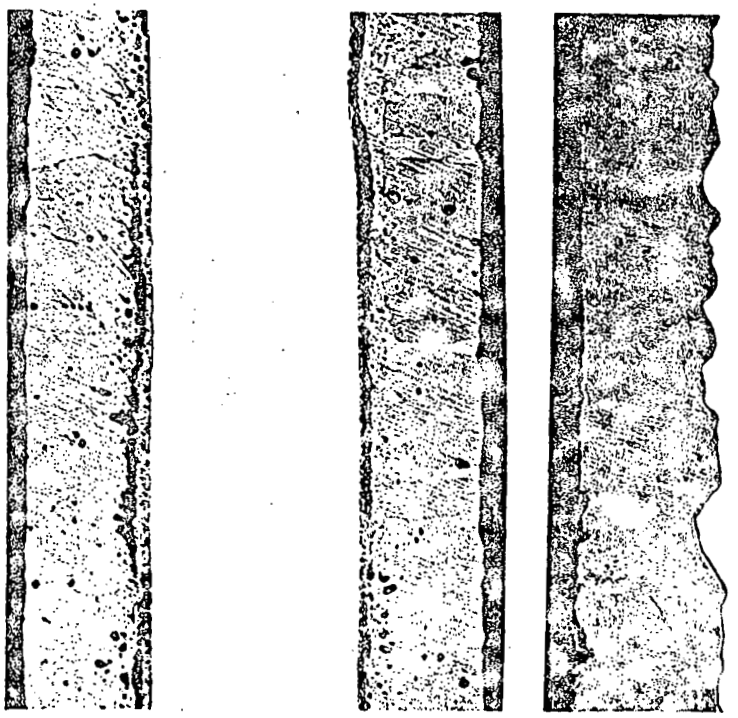




(b)

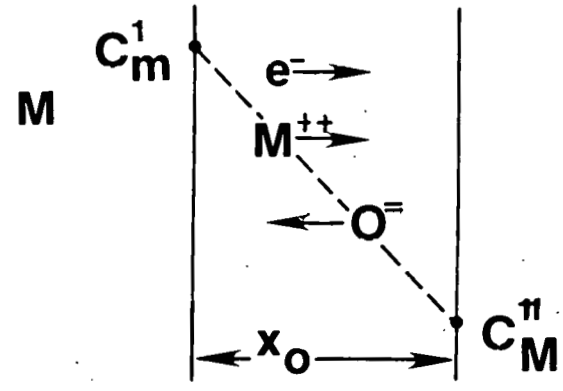
Effect of lateral compressive stresses on oxide film behavior.

(a) Blistering in FeO film due to weak adhesion. After Engell and Wever.
(b) Shear cracking in NiO film due to strong adhesion.



Structure of NiO films on Ni. (a) "Low-temperature" duplex film. (b) "High-temperature" single-layer film.

Diffusion model for parabolic growth:



$$\frac{dx_o}{dt} \sim J\Omega = -D \left(\frac{dc}{dx}\right)_{x_o}$$

$$\frac{dc}{dx} \approx -\left|\frac{\Delta C}{x_o}\right|$$

$$\frac{dx_o}{dt} = \frac{k}{2X_o}$$

$k = 2D\Omega\,\Delta c$

parabolic law: $x_o^2 = kt + \text{const.}$

D and Δc depend on T and defect character of the oxide

Wagner model: $M \rightarrow M^{3+} + 3e^-$

$$\tfrac{3}{4}\, O_2 + ze^- \rightarrow \tfrac{z}{2}\, O^=$$

$$J_i = -D_i \frac{dc_i}{dx} + z_i e \frac{d\Phi}{dx}$$

flux eqs. i = electron, cations, anions

$J_M - J_e - J_O = o$ electroneutrality

$$\frac{dx}{dt} \left| J_M \right| \Omega_M + \left| J_o \right| \Omega_o$$

$$K = \int_{P_{O_2}^1}^{P_{O_2}^{11}} c_o \left(D_M \Omega_M - D_o \Omega_o\right) d \ln P_{O_2}$$

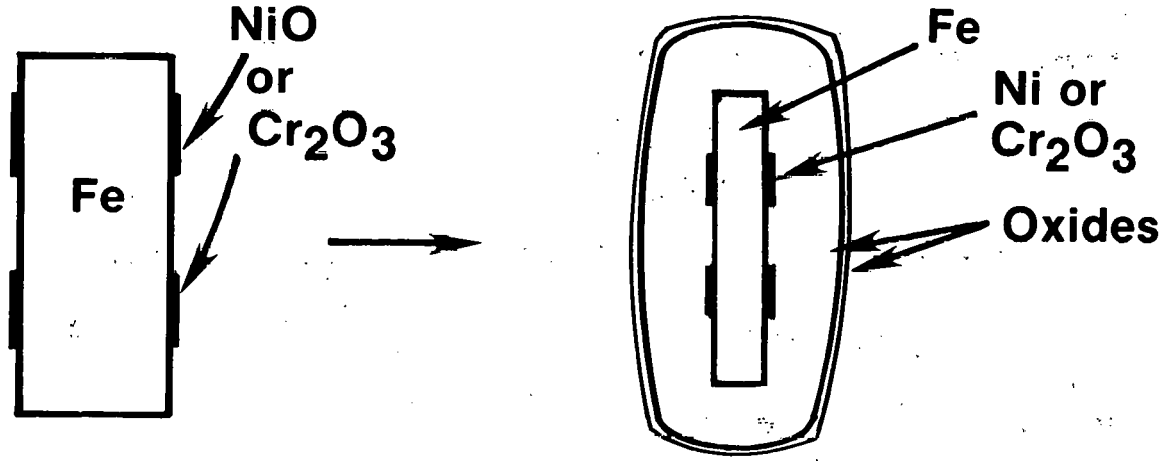
Wagner's model based on independent migration of ions was verified for Ag_2S (1933) by electrical conductivity measurements that showed $D_{Ag} >> D_S$.

Also in 1940's and 1950's for Cu_2O using self-diffusion of Cu , FeO and Fe_3O_4 using self-diffusion of Fe , and Fe S using Fe and S , showing that $D_{Fe} >> D_S$.

Iron oxidation as example.

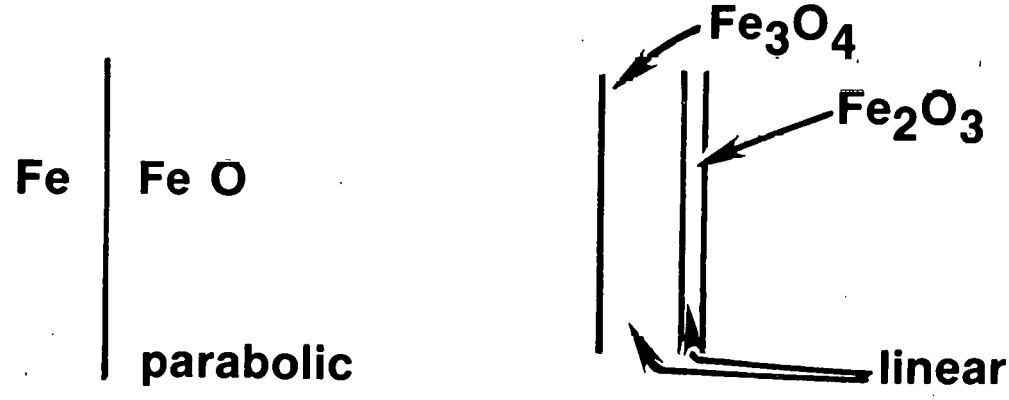
Oxidation of Iron

Pfeil (1929) - first market studies



Conclusion: $D_{Fe} >> D_O$

Bénard and Coquelle (1946)



total thickness $\alpha \sqrt{t}$
T>570°C $Fe_{1-S}O$ up to 95% of thickness

Jette & Foote (1936)

Comparison of densities and lattice parameters for $Fe_{1-\delta}$ O (NaCl structure) versus δ demonstrated Fe vacancies in 5 to 12% of sites. So concentrated that there is little effect of doping by foreign ions on the diffusion processes in this oxide.

Valensi (1948)

Application of L^1 Hospital's theorem

If $X_O(t)$ and $\frac{dx_o}{dt}$ are continuous from t = o until t = t and all x_o's are equal at t = o, etc...

$$X_1^2 = k, t;\ X_2^2 = k_2 t;\ X_3^2 = K_3 t$$

$$(X_1 + X_2 + X_3)^2 = K_4 t$$

Verified for CuO & Cu_2O on Cu

1948 D,S & B

$Fe_{1-\delta}O$, Fe_3O_4, Fe_2O_3 all parabolic

1952 H,M & B

Measured D^*_{Fe} 's in all three oxides and calculated growth rates of $Fe_{1-\delta}O$ and Fe_3O_4 from Wagner's Eq.

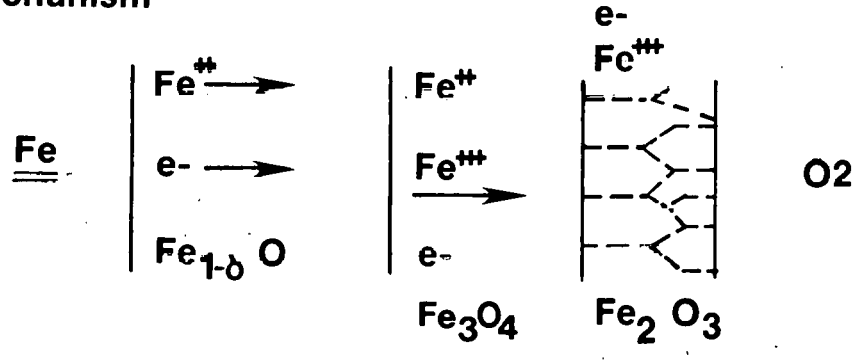
D_{Fe} too slow to account for Fe_2O_3 growth.

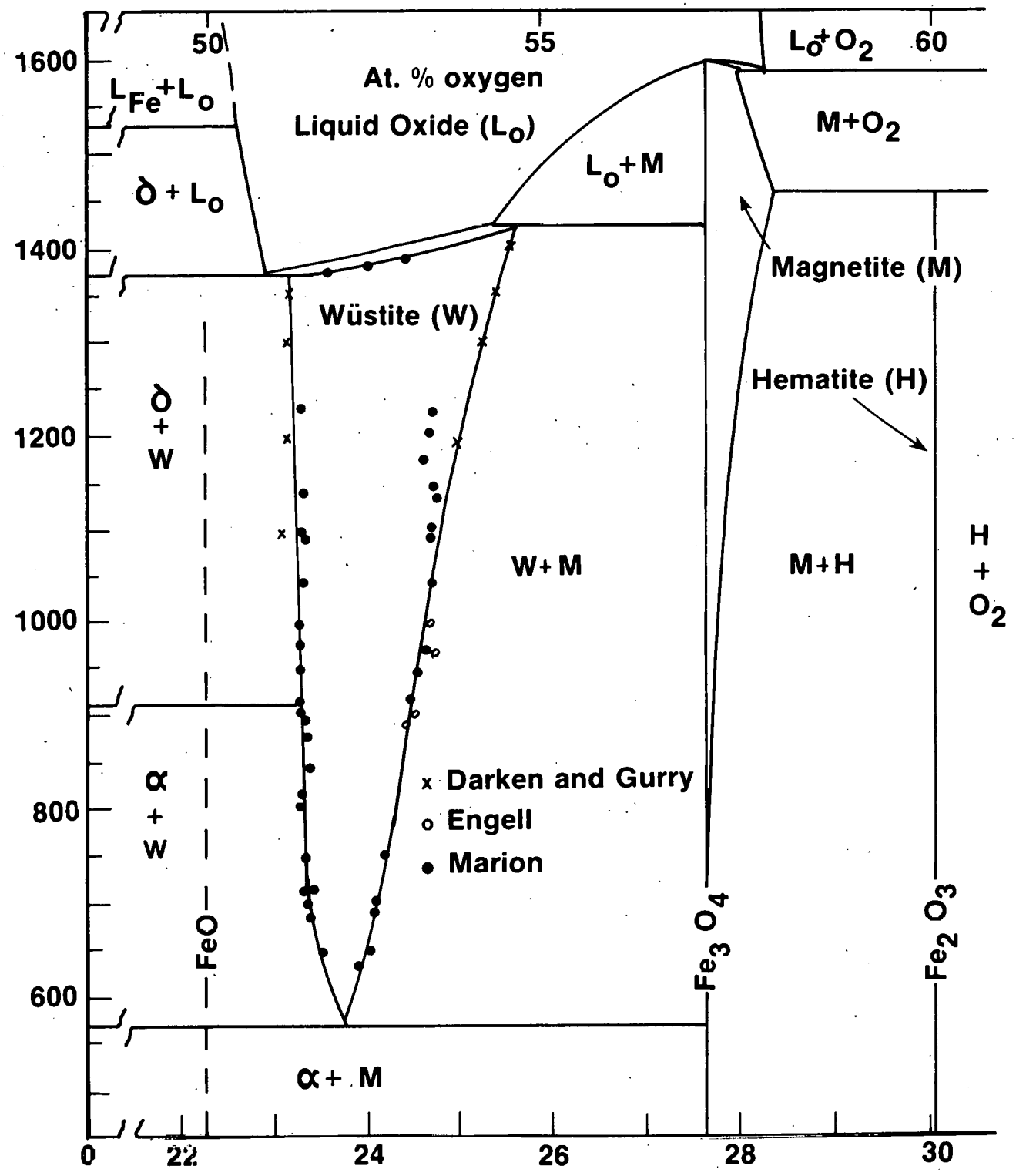
1967 Himmel, Condit, Holt

$D_{Fe} >> D_O$ in polycrystalline Fe_2O_3

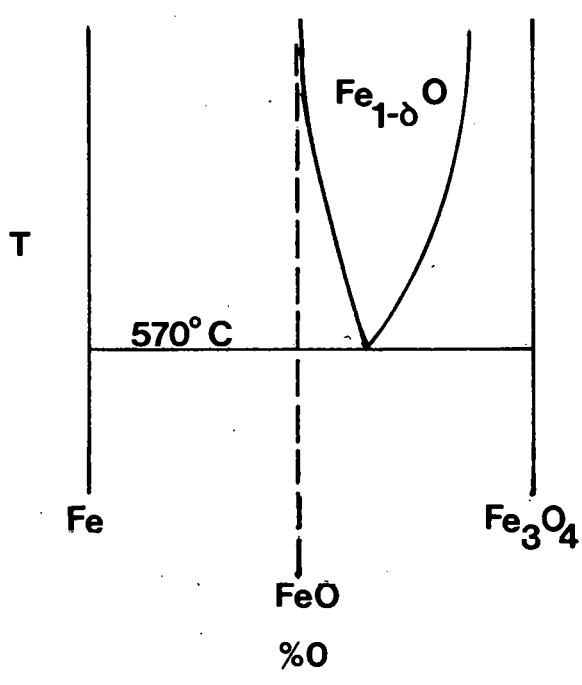
Grain boundary diffusion controls growth of Fe_2O_3

Mechanism




50
55
60
1600
1400
1200
1000
800
600
0
22
24
26
28
30
At. % oxygen
Liquid Oxide (L_o)
$L_{Fe}+L_o$
$\delta + L_o$
L_o+M
L_o+O_2
$M+O_2$
Magnetite (M)
Hematite (H)
Wüstite (W)
δ + W
W+M
M+H
H + O_2
α + W
α + M
x Darken and Gurry
o Engell
• Marion
FeO
Fe_3O_4
Fe_2O_3

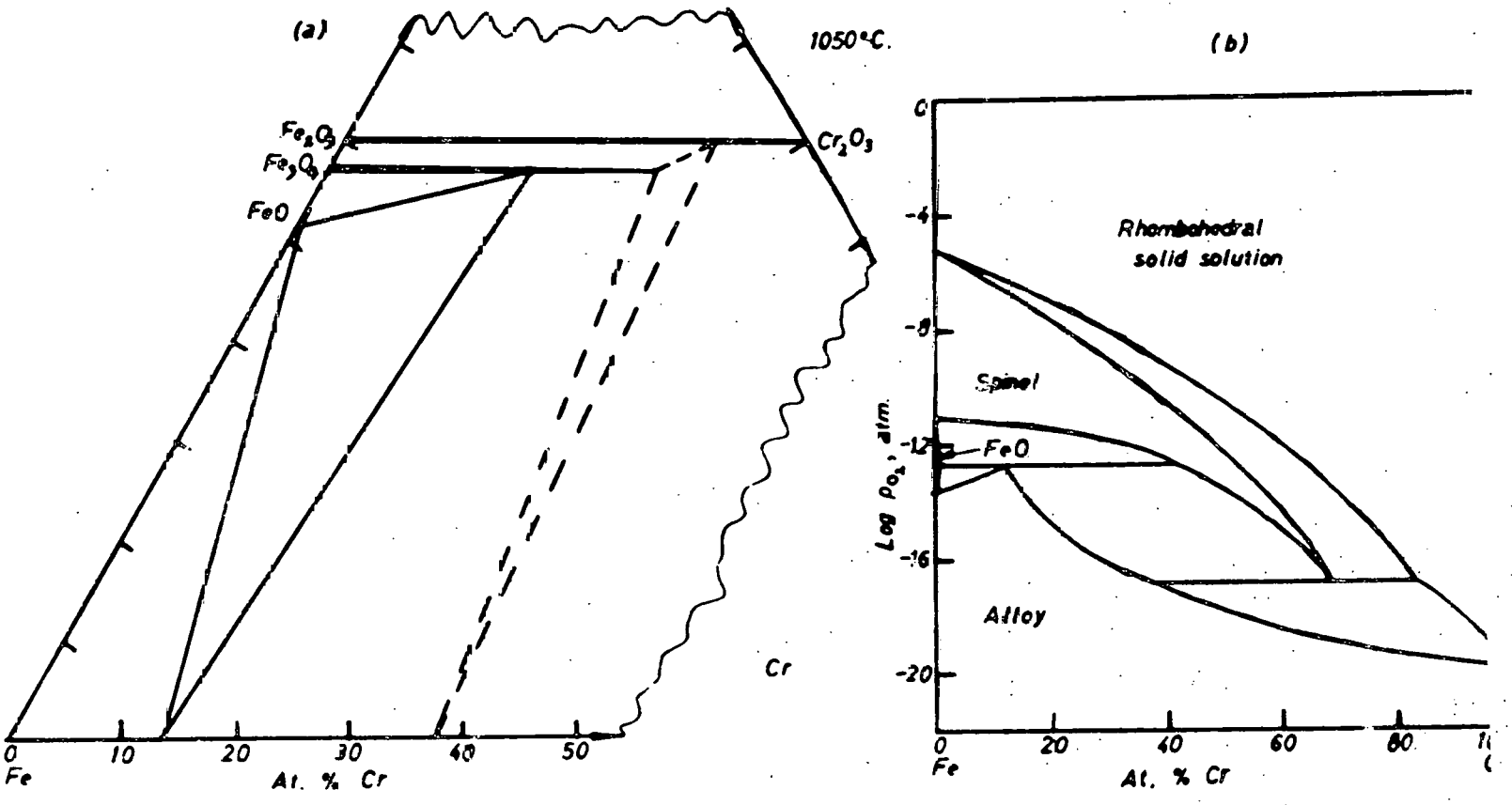
Alloying iron for oxidation resistance
Slow growth of fastest oxide
Narrow stagle range or $Fe_{1-\delta}O$,
or eliminate it completely.



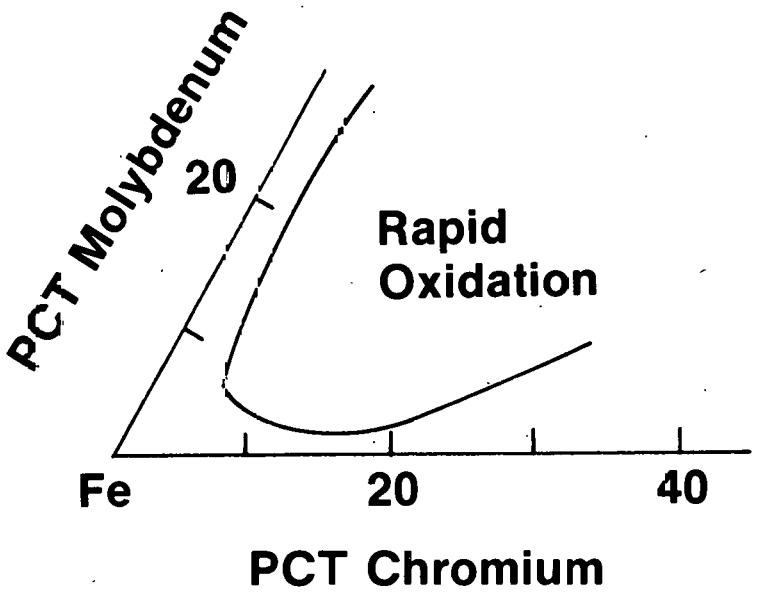
Some elements raise eatectoid temperature. They dissolve in alloy and spinel (replace Fe in Fe_3O_4) to Stabilize relative to $Fe_{1-\delta}O$ in which they do not dissolve.

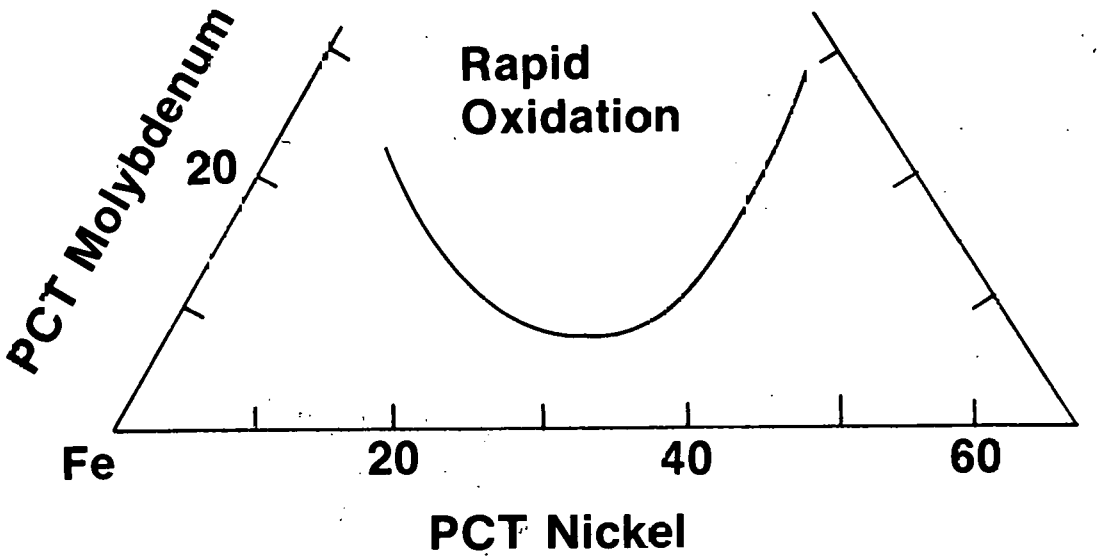
Ni goes preferentially into alloy
Cr & Al go preferentially into oxides (spinel & M_2O_3)

Ions substituting for Fe in $Fe_3 O_4$ greatly diminish D_{Fe} , slow spinel growth. Enough Ni, Cr or Al or combination eliminates $Fe_{1-\delta} O$, slows Spinel growth, but increase cost and affect mechanical properties. Moderate amounts of Cr and/or Al eliminate spinel by stabilizing the slowest growing rhombohedral sesquioxides $M_2 O_3$, but also make alloys more brittle. Therefore, often are applied as surface enrichment or coating. Growth rates: $Al_2 O_3 < Cr_2 O_3 < Fe_2 O_3$
High Temperature alloys of Ni or Co (instead of Fe) with Cr and/or Al have exceptional resistance to oxidation (Superalloys). Next step up likely to be ceramics.


(a)
1050°C.
Fe_2O_3
Fe_3O_4
FeO
Cr_2O_3
Cr
0
10
20
30
40
50
Fe
At. % Cr
(b)
C
-4
-8
-12
-16
-20
Rhombohedral
solid solution
Spinel
FeO
Alloy
Log p_{O_2}, atm.
0
20
40
60
80
Fe
At. % Cr

(a)
Fe2 O3
Fe, O4
FeO
1050 C
Cr2 O3 (b)
0 10 20 30 40 50 Fe At. % Cr
Cr 0 -4 -8 -12 -16 -20 0 20 40 60 80 100
At. % Cr Log Po2 atm.
Spinel FeO Alloy
Rhombohedral
Solid solution


PCT Molybdenum
20
Rapid
Oxidation
Fe
20
40
PCT Chromium


PCT Molybdenum
20
Rapid
Oxidation
Fe
20
40
60
PCT Nickel

THE HIGH TEMPERATURE OXIDATION OF MATERIALS IN SOLAR THERMAL CONVERSION SYSTEMS UTILIZING A GAS COOLANT

by

John Stringer

EPRI

Palo Alto, California

*Prepared for, but not presented at this workshop.

THE HIGH TEMPERATURE OXIDATION OF MATERIALS IN SOLAR THERMAL CONVERSION SYSTEMS UTILIZING A GAS COOLANT

John Stringer
EPRI

Synopsis

Solar thermal conversion systems utilizing a gas coolant may employ either air or helium as the coolant; the heat exchanger may be either metallic or ceramic. In most schemes the enthalpy is extracted from the heated gas by a gas turbine. In general, it appears that mechanical properties are a more important limitation than the oxidation resistance on the maximum gas temperature attainable. A brief outline of the important aspects of the oxidation of materials is presented.

Introduction

An important class of solar thermal conversion systems focus the suns rays on a heat exchanger, heating a gas. In most systems, the heat exchanger is of the tube and manifold type, with the working fluid on the inside of the tubes; however, alternative schemes have been outlined by Jarvinen[1] who proposes a ceramic dome heat exchanger, and by Bienert,[2] who proposes a liquid-metal heat-pipe exchanger. In the majority of cases the enthalpy is recovered in a gas turbine; a variety of detailed cycles have been considered. The coolant gas is usually either air or helium.

From the materials point of view, the systems can be divided into two classes: those utilizing a metallic heat exchanger, and those utilizing a ceramic heat exchanger. The advantages of a metallic heat exchanger are that the engineering characteristics are well understood; fabrication is relatively straightforward, and in-situ repair of failed components is usually simple. The disadvantages are that the limited creep resistance and oxidation resistance of metallic materials restrict the maximum gas temperature attainable and hence the overall cycle efficiency. In addition, metals are sensitive to upward temperature fluctuations which might possibly occur in solar systems due to over-focussing or loss of coolant. Ceramic heat exchangers are at a relatively early stage of development;

fabrication is difficult, and an on-site repair capability would predicate modular construction.

A system using a metallic heat exchanger with a helium coolant has been designed for EPRI by Boeing Engineering and Construction[3]. The maximum helium temperature was chosen to be 1500F (816C) at a pressure of 500 psi (3.45 MPa), these conditions being determined by the metallic tube limits. The design consisted of two banks of tubes, 0.5 inch (12.7 mm) bore with a wall thickness of 0.050 inch (1.27 mm) close to the walls of a cavity boiler. Typically, the effective cavity temperature was 2075F (1138C), and the maximum metal temperature was calculated to be approximately 1565F (852C).

Two alloys were selected for detailed study: Haynes 188 (Co-22Ni-22Cr-14W-3Fe-0.15C-0.1La) and Inconel 617 (Ni-12.5Co-22Cr-9Mo-1Al-0.07C). Thermal cycling tests simulating 30 year lifetimes were conducted; both alloys performed satisfactorily. The oxidation loss in these tests was described as "insignificant" in both helium and air; the tests consisted of up to 10,000 cycles each of 6-7.5 minutes duration; the alloy was at peak temperature for approximately 2 minutes each cycle, so the total time at temperature was about 330 hours. This is not in fact a very long test for these materials at this temperature, although the rapid cycling would increase the severity somewhat. Nevertheless, these alloys should be capable of long oxidation lives under these conditions. It was possible to heat the alloys to 1900 to 2000F (1037-1092C) at 500 psi before rupture occurred.

In connection with this project, Nix and Fuchs[4] reviewed the effect of the gaseous environment on the creep and creep-rupture properties of several heat-resisting alloys. They concluded that "Although a large number of reports about the potential deleterious effects of helium on the creep properties of alloys have been written, the evidence to support these claims is very weak. At present we must conclude that no important effects have yet been found".

Oxidation occurs in helium because of the impurities present. Most attention has been payed to the impure helium in high temperature gas cooled reactors. The principle introduced impurity is water vapor, but this reacts with the graphite in the core to give a significant carbon potential and a relatively low oxygen

potential. Typically, the H_2/CH_4 ratio is quoted as of the order of 10 to 1, and the H_2/H_2O ratio is given as 10^4 to 1. The helium used in solar systems will presumably have a much lower carbon activity and a higher oxygen activity. Some studies have indicated that intergranular corrosion products can be formed in reactor-grade helium, and it has been suggested that this is potentially dangerous because of the consequent effect on the mechanical properties; however, as Nix and Fuchs point out. there is no evidence for this.

Black and Veatch[5] designed for EPRI an alternative system utilizing a ceramic heat exchanger with air as the working fluid. The overall design was based on a General Electric MS 7001R gas turbine, with an inlet gas temperature of 1800-1950F (982-1066C); and it was concluded that these gas temperatures precluded the use of any available metal for the heat exchanger. Indeed, in contrast to the results of Boeing, Black and Veatch considered that the maximum gas temperature consistent with a 100,000 hour lifetime at a pressure of 135 psi (0.931 M Pa) for a metallic heat exchanger would be only 1350F (732C). In common with the majority of similar designs, silicon carbide was selected as the material for the ceramic heat exchanger. Neither the high temperature mechanical properties nor the high temperature oxidation resistance appeared to be limitations on the applicability of this material.

The High Temperature Oxidation of Metals and Alloys

In general, an alloy for use at high temperatures must combine good oxidation resistance with adequate mechanical strength and ductility. All practical heat-resisting alloys are based on iron, nickel or cobalt; the refractory metals (niobium, tantalum, molybdenum and tungsten) have good high temperature strength, but poor oxidation resistance in high oxygen-activity atmospheres. The inherent oxidation resistance of iron, nickel and cobalt is inadequate for acceptable lifetimes at elevated temperatures, and thus the aim of alloying for oxidation resistance is to develop a protective layer of another oxide on the metal surface. This protective oxide has to grow slowly, which implies slow transport rates through it of all the metallic constituents of the alloy and the various oxidants in the environment. It must also adhere well to the metal surface, resisting spallation due to differential thermal expansion on thermal cycling, and also resisting mechanical damage. The number of oxides capable of satisfying these conditions is quite

limited. Among the simple oxides, Cr_2O_3, Al_2O_3 and SiO_2 appear to be possible; because of the adverse effect that silicon has on the mechanical properties of the alloys relatively few structural alloys have been developed which develop protective SiO_2 layers, although recently a way around this problem has been developed[6]. Several compound oxides, such as the spinels, of which $FeO.Cr_2O_3$ is an example, appear to be potentially protective; but the conditions that have to be satisfied to form a continuous protective layer of a compound oxide are very restrictive.

For practical purposes then, heat-resisting alloys may be divided into those which form a Cr_2O_3 protective scale, and those which form Al_2O_3. What is the minimum amount of the alloy element (Cr or Al) which must be added to ensure the formation of a protective scale? There are four criteria which must be met.

1. The thermodynamic criterion. The desired oxide must be thermodynamically the most stable phase.

2. The metal flux criterion. It must be possible for the metallic element (Cr or Al) to diffuse out from the alloy sufficiently quickly to match the flux required by the rate of growth of the oxide.

3. The internal oxidation/external oxidation criterion. If oxygen can diffuse into the alloy faster than the metal can diffuse out, the oxide will form as particles <u>within</u> the alloy, rather than as a protective scale on the outside. Note that reducing the oxygen activity in the atmosphere encourages the formation of an external scale.

4. The mechanical disruption criterion. When oxygen is admitted to a clean alloy surface, all the possible oxides form. If the lateral growth of the protective oxide over the metal surface is not rapid enough, the faster-growing less stable oxides may mechanically disrupt it, preventing the establishment of a continuous protective layer.

For chromia-formers, the third and fourth criteria do not appear to differ very much; but for Al_2O_3 formers the fourth criterion seems dominant, certainly for

Ni and Co base alloys. As a result, large amounts of Al are required in the binary alloys. However, the presence of chromium as a ternary component in the alloy reduces greatly the amount of aluminum required to develop a protective Al_2O_3 scale. Several theories exist to explain this phenomenon, but no one is wholly satisfactory.

As a general indication, the amount of chromium required to establish a protective Cr_2O_3 scale on binary alloys is: Co-30Cr, Ni-20Cr, Fe-18Cr. Approximately 5 wt % (10 at %) Al is required to form Al_2O_3, provided the alloy also contains at least 10 wt % Cr.

The adherence of the protective scales is not very good under thermal cycling conditions for the simple alloys. However, it was discovered by chance in the late 1930's that small additions of reactive metals, particularly the rare earths and yttrium, improved the resistance of the alloys to thermal cycling. Recently, considerable improvements in our understanding of the mechanism of this effect have been made, and it is now possible to design adequate scale adhesion into a heat resisting alloy (this is the role of the lanthanum in Haynes 188).

Finally, if the inherent oxidation resistance of the alloy is inadequate, a protective coating or cladding may be applied to the surface of the component. The earliest of these was an aluminum diffusion layer, forming an aluminide of the base metal, which resulted in the development of a protective alumina scale. More recently, PVD or plasma-sprayed coatings of the general composition MCrAlY, where M is Fe, Co or Ni, have been developed.

Systems of this sort, involving either oxidation-resistant alloys or protective coatings can give excellent protection for times of at least 20,000 hours at 1750F (954C) under thermal cycling conditions.

The High Temperature Oxidation of Ceramics

The silicon carbide and silicon nitride ceramics develop thin protective layers of SiO_2 in high temperature oxidation. In general, high density material of good

purity will have excellent oxidation resistance up to 2150F (1177C) in air. There is a remote possibility of a rapid form of oxidation, called "pest" in low oxygen pressures. At very low oxygen activities, silicon oxidizes to form the gaseous oxide SiO. As the oxygen pressure is raised, the SiO oxidizes in the gas phase a little away from the metal surface to form a dispersed "smoke" of SiO_2 particles, which do not form a protective layer: the oxygen pressure can be quite high before this reaction is suppressed and a continuous layer of SiO_2 develops on the metal surface. Pest is also possible on silicon carbide, although the fact that CO is also produced disrupts the boundary layer with the result that the reaction is quenched at much lower pressures. The presence of an inert gas should also reduce the risk of pest. Although it has be considered as a possibility therefore, its incidence in solar conversion systems seems to be very unlikely.

SiO_2 scales are also sensitive to the presence of water vapor: silicon-containing vapor phases are formed and SiO_2 is redeposited in the cooler parts of the system. Again, this should not be a serious problem.

The Effect of Impurities

Small amounts of certain impurities in the atmosphere or on the material surface can have a profound effect on oxidation behavior. Salt, for example, in relatively small amounts can result in a rapid oxidation of heat-resisting alloys called hot corrosion. This attack has been induced by wind-borne alkali salts in desert regions in gas turbine hot components. The possibility of wind-borne salts entering a solar cavity boiler and producing accelerated corrosion of the hot components may have to be considered in certain locations.

Summary

In summary therefore there are many materials and materials systems which have been developed to give excellent oxidation resistance in combustion atmospheres of various kinds, so that the temperature limit imposed by the oxidation performance is not usually appreciably lower than that imposed by the limitations in the high temperature mechanical properties. The environments encountered in solar thermal systems would appear to be much more benign, and it would seem that none of the proposed systems should find high temperature oxidation a limiting condition on their development.

References

1. P.O. Jarvinen, "Solar Heated Air Cavity Receiver Development (SHARE)" presented at the Focus on Solar Technology - A Review of Advanced Solar Thermal Power Systems Meeting, Denver, Colorado, 15-17 November 1978.

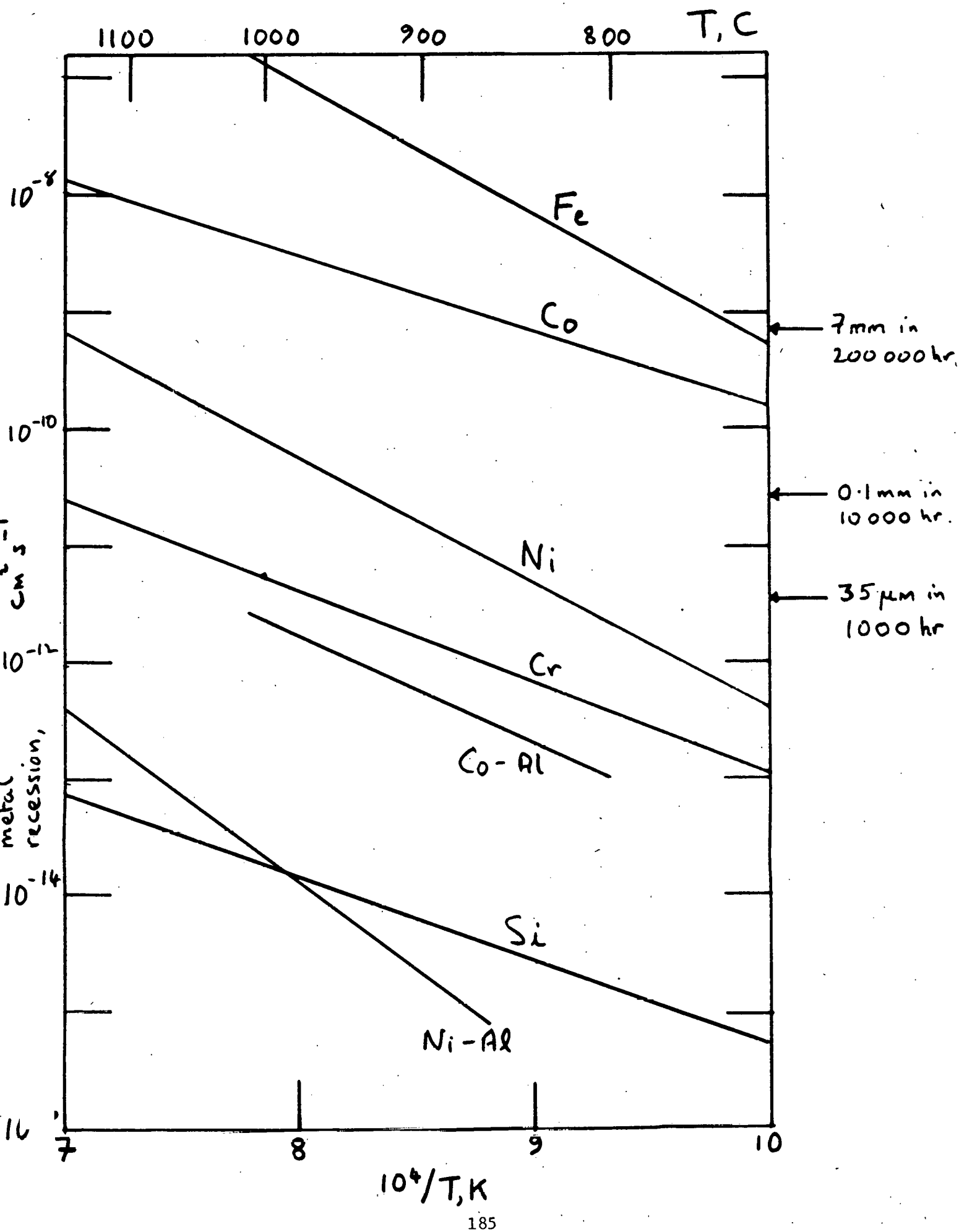
2. W. Bienert, "Heat Pipe Central Solar Receiver" paper sent with advance material for Reliability of Materials for Solar Energy Systems Workshop, Denver, Colorado, 17-20 December 1978.

3. J. R. Gintz, "Closed Cycle, High Temperature Central Receiver Concept for Solar Electric Power",Final Report by Boeing Engineering and Construction to the Electric Power Research Institute on Project 377-1; EPRI ER-629 (January 1978).

4. W. D. Nix and M. P. Fuchs, "The Effects of Gaseous Environments in Gas-Cooled Reactors and Solar Thermal Heat Exchangers on the Creep and Creep-Rupture Properties of Heat-Resisting Metals and Alloys",Final Report by Stanford University to the Electric Power Research Institute on Technical Planning Study TPS76-622; EPRI ER-415 (February 1977).

5. J. C. Grosskreutz, "Solar Thermal Conversion to Electricity Utilizing a Central Receiver, Open-Cycle Gas Turbine Design" Final Report by Black and Veatch Consulting Engineers to the Electric Power Research Institute on Project 475-1; EPRI ER-652 (March 1978).

6. J. Stringer, I. G. Wright and D. P. Whittle, "A Method of Designing Alloys to Develop Protective SiO_2 Scales Without Loss of Strength", to be published.


1100
1000
900
800
T, C
10^{-8}
10^{-10}
10^{-12}
10^{-14}
metal recession, cm s^{-1}
Fe
Co
Ni
Cr
Co-Al
Si
Ni-Al
7mm in 200 000 hr
0·1mm in 10 000 hr.
35 μm in 1000 hr
7
8
9
10
$10^4/T$, K

THIS PAGE

WAS INTENTIONALLY

LEFT BLANK

Thermal Conversion - Liquid Metal/Molten Salt Coolant

CONCEPTUAL DESIGN OF ADVANCED CENTRAL RECEIVER POWER SYSTEMS

by

Robert M. Salemme

General Electric Company

Schenectady, New York

INTRODUCTION

Solar central receiver power systems represent a promising approach to generating electricity that may result in significant savings of petroleum fuels in the future. First generation plants in which superheated steam is generated directly in the receiver have been designed, and a 10 MWe pilot plant is being constructed at Barstow, California, to demonstrate this technology.

The General Electric Company is conducting a conceptual design study of an advanced solar central receiver power plant in which liquid sodium serves as the receiver coolant and heat transfer medium. This concept offers promise for improved plant performance and reduced capital cost with respect to the first generation systems.

The power plant design concept is based upon a steam cycle which receives thermal energy from a liquid sodium cooled receiver. Liquid sodium was selected as the receiver coolant and heat transfer medium because of its very favorable high-temperature heat transfer characteristics. The high heat transfer coefficients associated with the use of liquid sodium as the coolant compared to those that result when water/steam or a gas is used as the receiver coolant permit higher solar fluxes at the receiver surface. Consequently, the size of the receiver may be reduced which will decrease receiver thermal losses and capital cost.

The use of liquid sodium as the heat transfer medium also permits the design of a more efficient reheat steam cycle because the steam generators are located at the base of the tower. A reheat cycle would not be practical in a system employing a water/steam cooled receiver because steam would have to be piped from the high pressure turbine exhaust to the receiver to be reheated.

The design includes a liquid metal thermal storage subsystem which will permit operation of the plant for a period of three hours. With this storage concept, steam can be generated at full throttle inlet conditions during the entire storage discharge cycle. Consequently, the steam turbine need not be derated during operation from storage as is the case with systems employing a water/steam cooled receiver, but will continue to produce full power during this mode of operation.

The collector subsystem employs an advanced low-cost heliostat design of the type anticipated to be forthcoming from the current Department of Energy Advanced Heliostat Design Program.

Reference System

The reference advance central receiver power system which formed the basis of the initial plant design concept is shown schematically in Figure 1. The collector subsystem provides a high flux of solar energy averaging 2 megawatts per square meter to the receiver absorber panels. In passing through the absorber panels, sodium is heated from approximately 700° to 1300°F. The receiver is constructed of a number of individual absorber panels to permit factory fabrication of the individual panels, and to expedite installation and maintenance operations. The flow of sodium is accurately controlled through each absorber panel by a separate EM pump associated with each panel. This ensures accurate panel cooling flow and control of the sodium outlet temperature.

An intermediate heat exchanger located at the base of the tower is used to isolate the high hydrostatic pressure of the primary sodium loop from the balance of the liquid sodium circuit. This permits the components of the secondary sodium loop to be designed for lower pressure and was anticipated to result in lower system cost. The secondary loop contains the steam generator and thermal energy storage subsystem. During the operation of the plant directly from the receiver, hot sodium passes into the superheater and reheater and/or the thermal energy storage subsystem as appropriate. Sodium exiting from the superheater and reheater then passes into the evaporator section of the steam generator and leaves the evaporator at a temperature of approximately 630°F, from which it returns to the intermediate heat exchanger. On the steam side of the system, steam from the superheater expands through the high pressure stages of the steam turbine and is then reheated prior to being expanded down to exhaust conditions. Regenerative feedwater heating to increase the efficiency of the steam cycle is employed in this reference power plant concept.

Parametric Analysis

The design of the power plant began with a parametric analysis to identify the preferred plant configuration. This parametric analysis included the subsystem or component options which are summarized in Table 1. Two advanced heliostat designs,

a General Electric enclosed plastic heliostat, and a glass heliostat were considered. These heliostats were optimally arranged in both 360° and north field configurations. Cylindrical and flat receiver geometries corresponding to the respective collector subsystem geometries were investigated, and a trade-off study comparing an external versus a cavity receiver configuration was conducted. In addition, two peak sodium temperature levels of 1100 and 1300°F were considered. Sodium loop configurations consisting of two loops separated by an intermediate heat exchanger to reduce the hydrostatic pressure in the second loop and a single loop configuration which employed flow throttling to reduce the pressure in the sodium circuit at the base of the tower were investigated. A number of thermal storage subsystem configurations were also investigated as part of the parametric analysis. These configurations included thermal energy storage using hot sodium, sodium plus iron to improve the volumetric thermal storage capacity and reduce the size of the storage vessels, and hot molten salt. Two storage temperatures corresponding to the 1100°F and 1300°F peak receiver temperatures were considered. The thermal storage vessel fabrication technique was also considered to be an important factor in controlling the cost of this system, and both factory and field assembly of these vessels was investigated. In addition, a large number of storage vessel configurations and control strategies were considered. The parameters studied within the electrical power generation subsystem included throttle pressure and temperature, and the optimum feedwater heating strategy.

The materials of construction selected during the parametric analysis stage of the program are shown in Table 2. This materials selection list was modified during subsequent stages of the program as more detailed specifications were developed.

A set of criteria used for evaluating the results of the parametric analysis study and selecting the configuration for the commercial plant design is presented in Table 3. These criteria considered capital cost, operational characteristics, availability of technology, safety, and environmental considerations.

Commercial Plant Conceptual Design

The results of the parametric study led to the selection of the commercial plant configuration described in Table 4 and shown schematically in Figure 2. In this configuration, a 360° heliostat field focuses sunlight onto a cylindrical receiver located on a 190-meter tower. The hot sodium exiting from the absorber flows to the base of the tower into the hot storage vessels. From the storage vessels, hot sodium is pumped to the steam generators where superheated steam at 2400 psi and 1000F is produced for a reheat steam turbine. The cool sodium leaving the evaporator is returned to a bank of cold storage vessels from which is is pumped back up the tower to be heated in the receiver.

Figure 3 shows the advanced receiver concept developed during the program. The receiver is 16 meters in diameter and 16 meters high; it is comprised of 24 individual absorber panels, each 2 meters wide and 16 meters long. The absorber panels are cooled with sodium that enters through a tube header at the vertical midpoint of the panels and flows upward and downward, thereby cooling the panels. Cold sodium entering the panel at the midpoint provides maximum cooling capacity at the location of highest solar flux. The flow to each panel is controlled by an individual electromagnetic (EM) pump, ensuring precise sodium flow control and, therefore, good absorber panel temperature control. The hot sodium exits each absorber panel through upper and lower exit manifolds at 1100F and is mixed at the inlet to the downcomer, which conducts the hot sodium to the base of the tower.

An insulating curtain is used to reduce thermal losses from the receiver during shutdown periods. When the receiver is in operation, the curtain is maintained in a stowed position around the base of the receiver and serves as a shield to protect the upper portion of the tower and receiver/tower structure from radiant flux spillage.

The hot sodium at the base of the tower is throttled through valves to reduce its pressure from 225 to 35 psia. This is done to permit design of the piping and storage vessels for low pressure, resulting in substantial cost savings.

The storage subsystem consists of three hot and three cold storage vessels, each 60 feet in diameter. The hot, low pressure sodium flows to the hot storage vessels and is then pumped to the steam generator as required to supply the steam demand for the turbine. In this arrangement, the hot storage vessels isolate the sodium flow to the steam generator from the sodium flow in the tower, simplifying the operational and control characteristics of the system.

The steam generator section of the plant consists of three separate components: an evaporator, a superheater, and a reheater. Sodium at 1100F enters the hot side of the superheater and reheater, providing steam at 1000F. The flow to each of these components is controlled to satisfy the dynamic heat balance. At the exit of each of these components, the sodium streams are joined and fed to the evaporator where water from the feedwater train is heated and evaporated. The sodium exits the evaporator at 610F and flows to the cold leg storage vessels from which it is pumped up the riser to the receiver EM trim pumps for distribution in the receiver.

On the steam side of the plant, water from the condenser is pumped through a series of feedwater heaters, through a deaerator, and then through additional feedwater heaters to the steam generators. The steam generator design used in this study which is shown in Figure 4 is based on the hockey-stick design developed in the Clinch River Breeder Reactor Program. The feedwater enters the evaporator and passes into a steam drum and moisture separator. Steam then passes to the superheater where it is heated to 1000F, the turbine throttle inlet temperature. The steam is expanded through the high pressure turbine from inlet conditions of 2400 psi and 1000F to 417 psi and 570F. This steam is then passed through the reheater where its temperature is again raised to 1000F for introduction to the reheat turbine. The exhaust from the reheat turbine flows to the low pressure turbine where it expands down to the condenser backpressure of two inches of mercury.

Materials Selection

The selection of materials for the plant conceptual design was governed by the following criteria:

- Alloys must possess documented mechanical properties which form a sound basis for

design. Materials covered by the ASME code or cases within the code are regarded as preferred candidates. Materials which lack a widespread data base may be considered as candidates for a future cost improvement program, but will not be selected for the first commercial plant.

- Alloys must be compatible with each other and with system working fluids.

- Alloys selected must be readily available and not overly difficult to fabricate. Preference will be given to metals which are frequently used in industry, and (or) which are available in a wide variety of product forms.

Applying these criteria and the plant operating conditions limited the peak sodium temperature of the plant to 1100°F and resulted in selection of the materials listed in Table 5. This list differs from that initially selected (for 1100°F peak sodium temperature) in that carbon steel has been identified for cold leg piping and cold storage vessels in order to reduce costs. The initial selection of 2 1/4 Cr - 1 Mo was based on matching the piping and the tanks to the evaporator tube material, where 2 1/4 Cr - 1 Mo was used to achieve low steam-side corrosion. However, this is an expensive approach, and it is unnecessary because carbon steel is qualified for low temperature sodium service.

The limitation of peak sodium temperature to 1100°F was dictated by materials constraints and resulted in a plant performance penalty with respect to the higher efficiencies anticipated at a peak temperature of 1300°F. The higher temperature level had to be abandoned because a qualified material could not be identified for the superheater and reheater. Type 316H stainless steel is compatible with sodium at 1300 F, but it is subject to stress corrosion on the steam side. Inconel 617 may be a candidate for this service, but the available data are incomplete.

FIGURE 1

GENERAL ELECTRIC

REFERENCE ADVANCED CENTRAL RECEIVER POWER SYSTEM

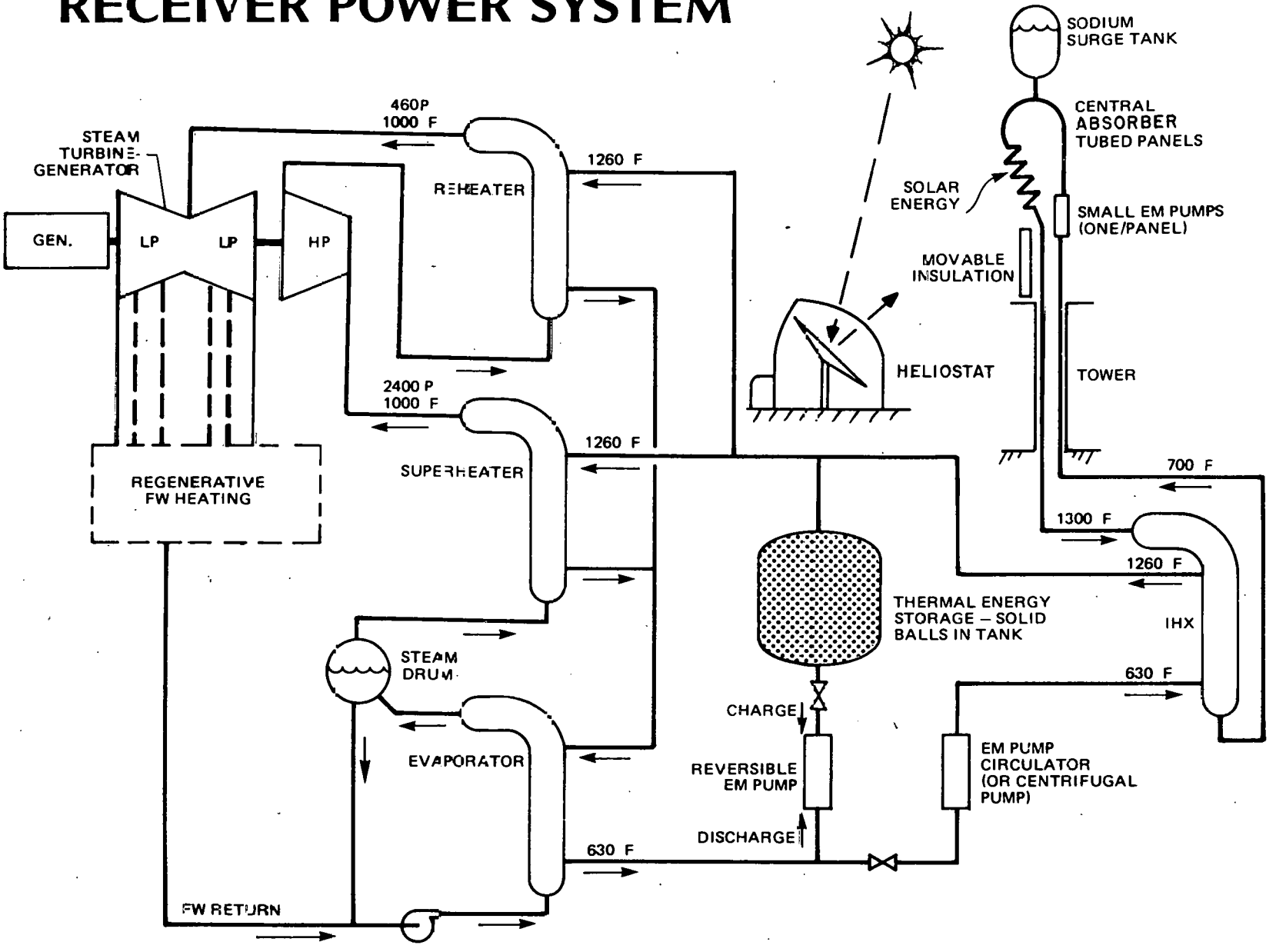


FIGURE 2

ADVANCED CENTRAL RECEIVER POWER SYSTEM COMMERCIAL PLANT CONFIGURATION

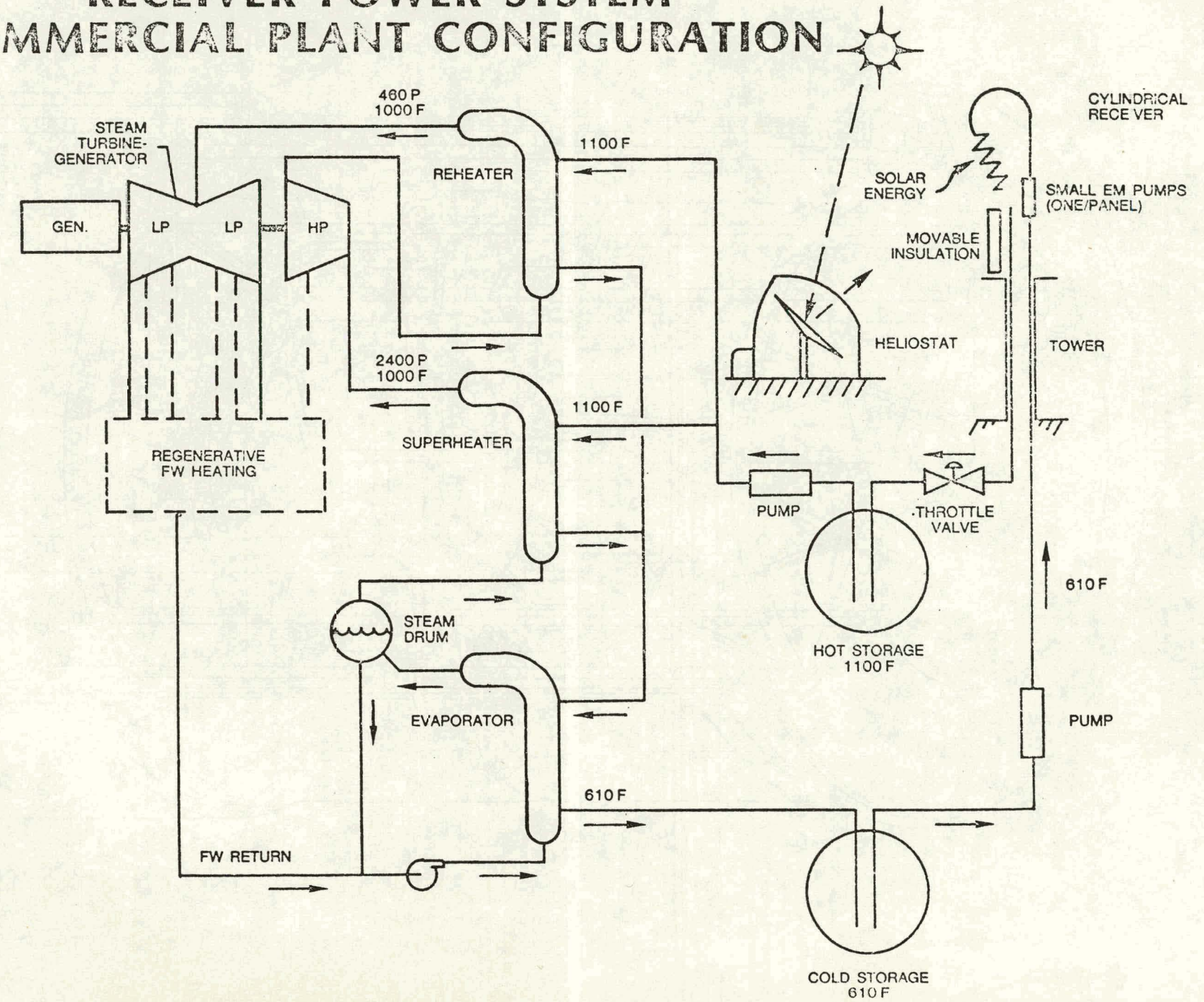
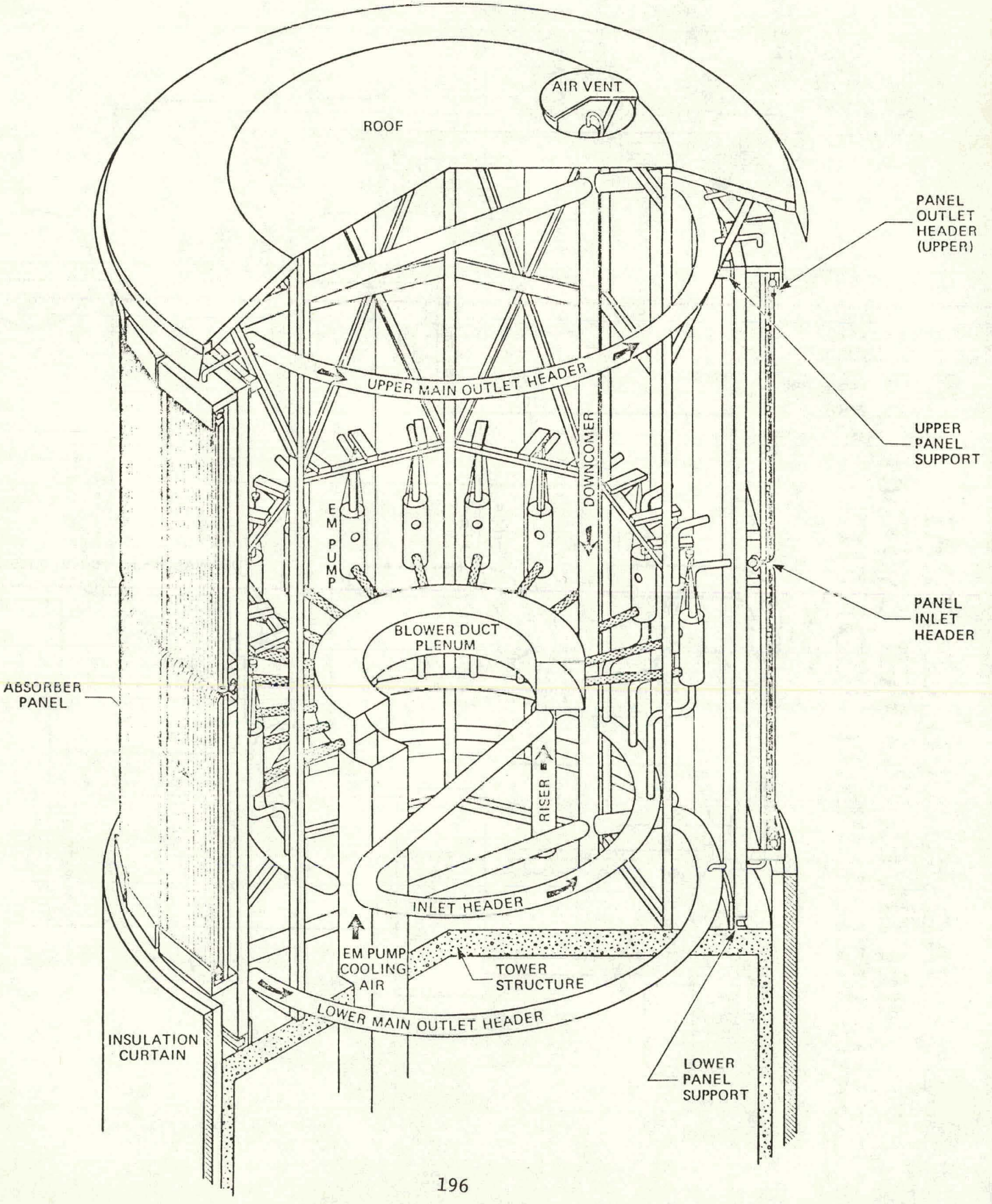
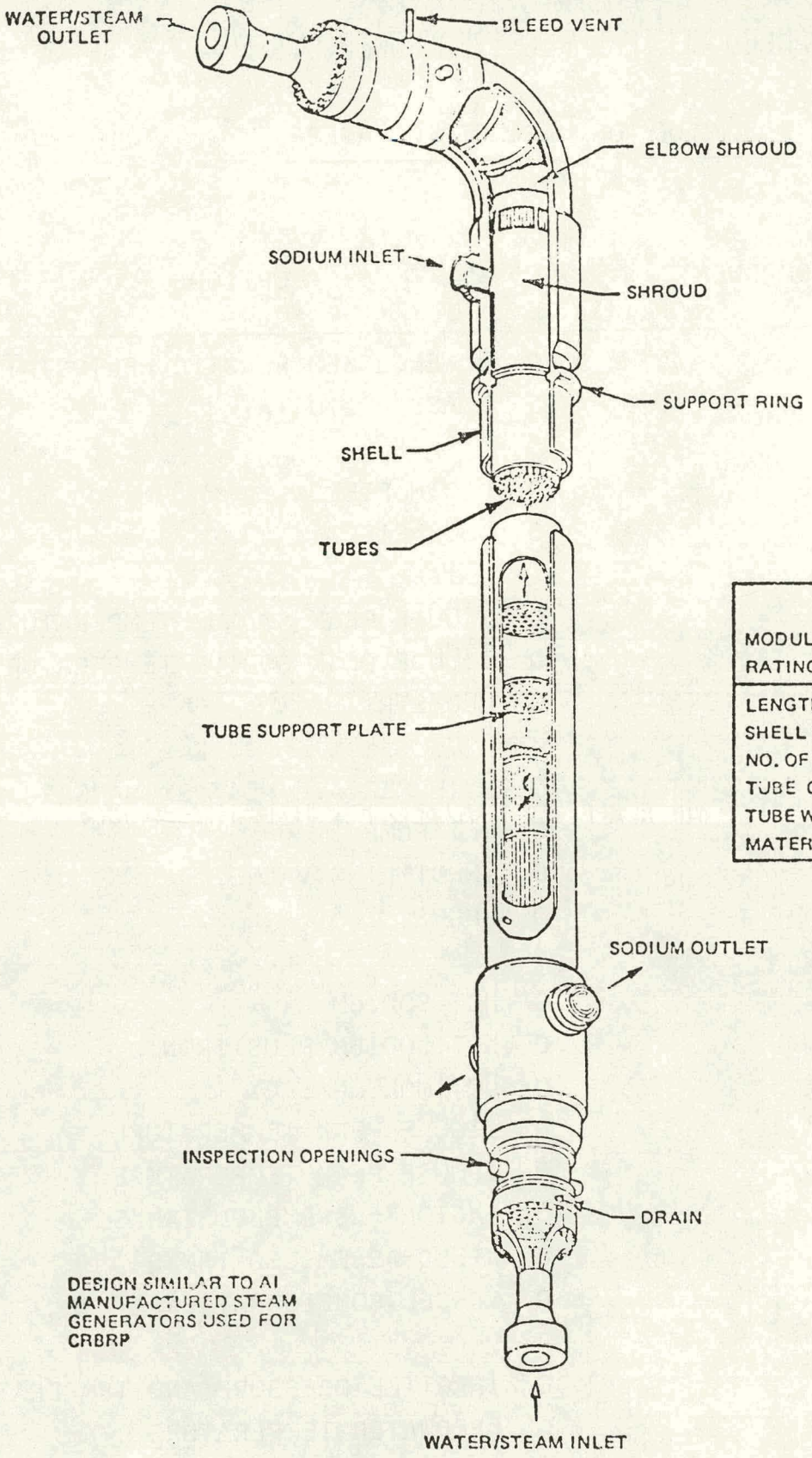


FIGURE 3

SODIUM COOLED RECEIVER CONCEPTUAL DESIGN





MODULE RATING (MWt)	EV 127	SH 81	RH 41
LENGTH (ft)	97	54	54
SHELL DIA. (ft)	4.43	4.08	4.56
NO. OF TUBES	740	572	286
TUBE O.D. (in.)	0.625	0.625	1.05
TUBE WALL (in.)	0.109	0.109	0.05
MATERIAL	2¼Cr	1800	1800

FIGURE 4
STEAM GENERATOR MODULE

TABLE 1

PARAMETRIC STUDY OF
ADVANCED CENTRAL RECEIVER POWER SYSTEM

SUMMARY OF PARAMETRIC CASES

SUBSYSTEM OR COMPONENT	OPTIONS
HELIOSTAT	o GE ENCLOSED PLASTIC HELIOSTAT o GLASS HELIOSTAT
HELIOSTAT FIELD	o NORTH FIELD o 360° FIELD
RECEIVER	o 1100 F PEAK SODIUM TEMPERATURE o 1300 F PEAK SODIUM TEMPERATURE o GEOMETRY
SODIUM LOOP	o INTERMEDIATE HEAT EXCHANGER o JET PUMP o THROTTLING VALVE o PUMPS
THERMAL STORAGE	o HOT SODIUM o HOT SODIUM PLUS IRON o HOT MOLTEN SALT o 1100 F PEAK TEMPERATURE o 1300 F PEAK TEMPERATURE o FACTORY-ASSEMBLED TANKS o FIELD-ASSEMBLED TANKS o VESSEL CONFIGURATION
STEAM CYCLE	o THROTTLE PRESSURE AND TEMPERATURE o FEEDWATER TEMPERATURE

TABLE 2

MATERIALS SELECTION
PARAMETRIC ANALYSIS

Component	Peak Sodium Temperature	
	1100 F	1300 F
Cold Leg Piping	2-1/4 Cr - 1 Mo	2-1/4 Cr - 1 Mo
Hot Leg Piping	316SS	Inconel 625
Absorber Panels	316SS	Inconel 625
Storage Tanks (Hot)	316SS	Inconel 625
Storage Tanks (Cold)	2-1/4 Cr - 1 Mo	2-1/4 Cr - 1 Mo
IHX	316SS	Inconel 625
Evaporator	2-1/4 Cr - 1 Mo	2-1/4 Cr - 1 Mo
Superheater	Incoloy 800	Inconel 625
Reheater	Incoloy 800	Inconel 625

TABLE 3

SELECTION CRITERIA FOR COMMERCIAL PLANT DESIGN

- Capital Cost
- Control Characteristics
- Forced Outage Rate
- Hardware and Materials Availability
- R&D Required
- Industrial Manufacturing Capability
- Plant Safety
- Environmental Intrusion
- Land Requirements

TABLE 4

SUMMARY OF SELECTED SYSTEM CONFIGURATION BASED UPON PARAMETRIC STUDY RESULTS

Receiver/Collector Subsystems	-GE-Enclosed Heliostat 360° Field Configuration Single Sodium Loop 1100°F
Storage Subsystem	-Low Pressure Field Assembled Vessels Hot and Cold Storage Vessels
Electrical Power Generation Subsystem	-Steam Conditions 2400 psi/1000°F/1000°F HARP

TABLE 5

SUMMARY OF CONCEPTUAL DESIGN MATERIALS SELECTION

COMPONENT	MATERIAL
COLD LEG PIPING	CARBON STEEL
HOT LEG PIPING	STAINLESS STEEL 316H
ABSORBER PANELS	INCOLOY 800H
STORAGE TANKS(HOT)	STAINLESS STEEL 316H
STORAGE TANKS(COLD)	CARBON STEEL
SUPERHEATER & REHEATER	INCOLOY 800H
EVAPORATOR	2¼ CR-1Mo

CONCEPTUAL DESIGN OF ADVANCED CENTRAL RECEIVER POWER SYSTEMS

Viewgraphs Presented

by

Robert M. Salemme

General Electric Company

Schenectady, New York

CONCEPTUAL DESIGN OF

ADVANCED CENTRAL RECEIVER POWER SYSTEMS

CONTRACT NO. EM-78-C-03-1725
U. S. DEPARTMENT OF ENERGY

PRESENTED BY
GENERAL ELECTRIC COMPANY

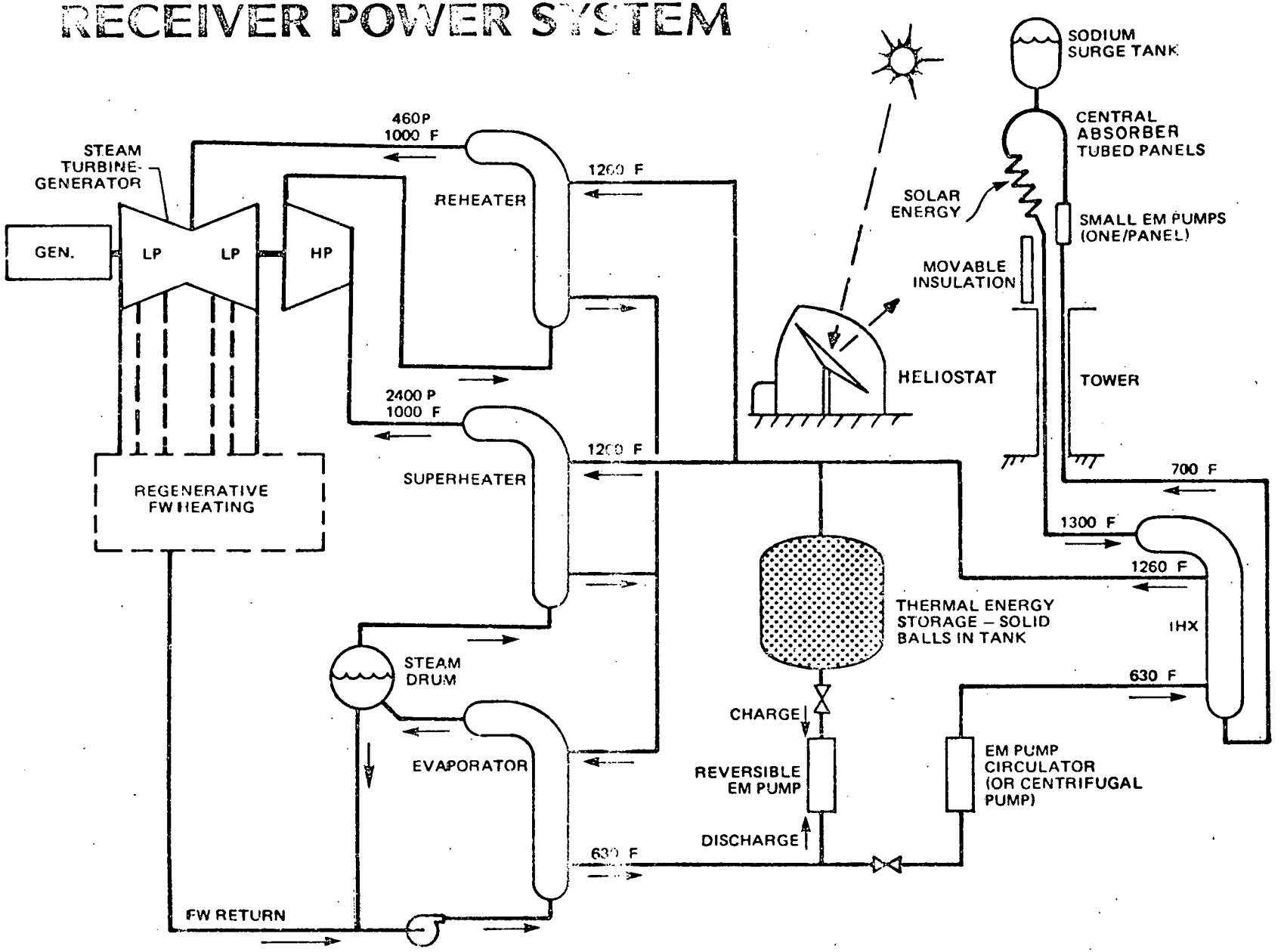
CONTRACT OBJECTIVE

DEMONSTRATE THE POTENTIAL FOR REDUCING THE COST OF ELECTRICITY FROM A SOLAR CENTRAL RECEIVER POWER PLANT THROUGH THE APPLICATION OF ADVANCED TECHNOLOGY.

POWER PLANT DESIGN CONCEPT

Electrical Power Generation Subsystem:	**Steam Turbine-Generator**
Receiver Subsystem:	**Liquid Metal Cooled Tubed Panels**
Storage Subsystem:	**Sensible Heat**
Collector Subsystem:	**High Flux Focusing**

REFERENCE ADVANCED CENTRAL RECEIVER POWER SYSTEM



PARAMETRIC STUDY OF
ADVANCED CENTRAL RECEIVER POWER SYSTEM

SUMMARY OF PARAMETRIC CASES

SUBSYSTEM OR COMPONENT	OPTIONS
HELIOSTAT	o GE ENCLOSED PLASTIC HELIOSTAT o GLASS HELIOSTAT
HELIOSTAT FIELD	o NORTH FIELD o 360° FIELD
RECEIVER	o 1100 F PEAK SODIUM TEMPERATURE o 1300 F PEAK SODIUM TEMPERATURE o GEOMETRY
SODIUM LOOP	o INTERMEDIATE HEAT EXCHANGER o JET PUMP o THROTTLING VALVE o PUMPS
THERMAL STORAGE	o HOT SODIUM o HOT SODIUM PLUS IRON o HOT MOLTEN SALT o 1100 F PEAK TEMPERATURE o 1300 F PEAK TEMPERATURE o FACTORY-ASSEMBLED TANKS o FIELD-ASSEMBLED TANKS o VESSEL CONFIGURATION
STEAM CYCLE	o THROTTLE PRESSURE AND TEMPERATURE o FEEDWATER TEMPERATURE

MATERIALS SELECTION
PARAMETRIC ANALYSIS

Component	Peak Sodium Temperature 1100 F	1300 F
Cold Leg Piping	2-1/4 Cr - 1 Mo	2-1/4 Cr - 1 Mo
Hot Leg Piping	316SS	Inconel 625
Absorber Panels	316SS	Inconel 625
Storage Tanks (Hot)	316SS	Inconel 625
Storage Tanks (Cold)	2-1/4 Cr - 1 Mo	2-1/4 Cr - 1 Mo
IHX	316SS	Inconel 625
Evaporator	2-1/4 Cr - 1 Mo	2-1/4 Cr - 1 Mo
Superheater	Incoloy 800	Inconel 625
Reheater	Incoloy 800	Inconel 625

SELECTION CRITERIA

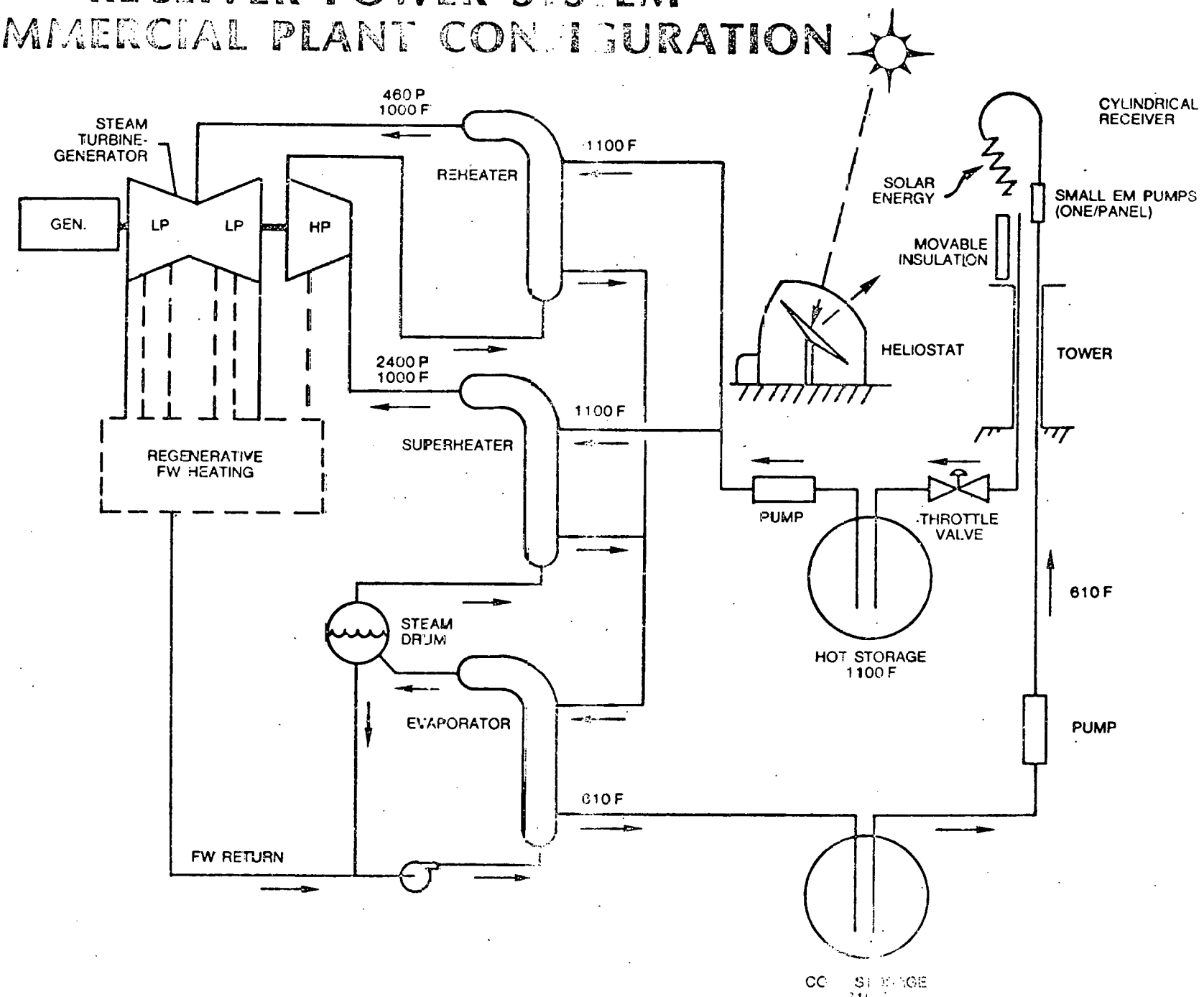
A. CAPITAL COST
B. O & M REQUIREMENTS
C. CONTROL CHARACTERISTICS
D. FORCED OUTAGE RATE
E. STARTUP POWER REQUIREMENTS
F. POTENTIAL FOR IMPROVEMENTS IN COST AND PERFORMANCE
G. ENVIRONMENTAL INTRUSION
H. LAND REQUIREMENTS
I. HARDWARE MATERIALS AVAILABILITY
J. R & D REQUIRED
K. INDUSTRIAL CAPABILITY OF MANUFACTURE
L. PLANT SAFETY

SUMMARY OF SELECTED SYSTEM CONFIGURATION

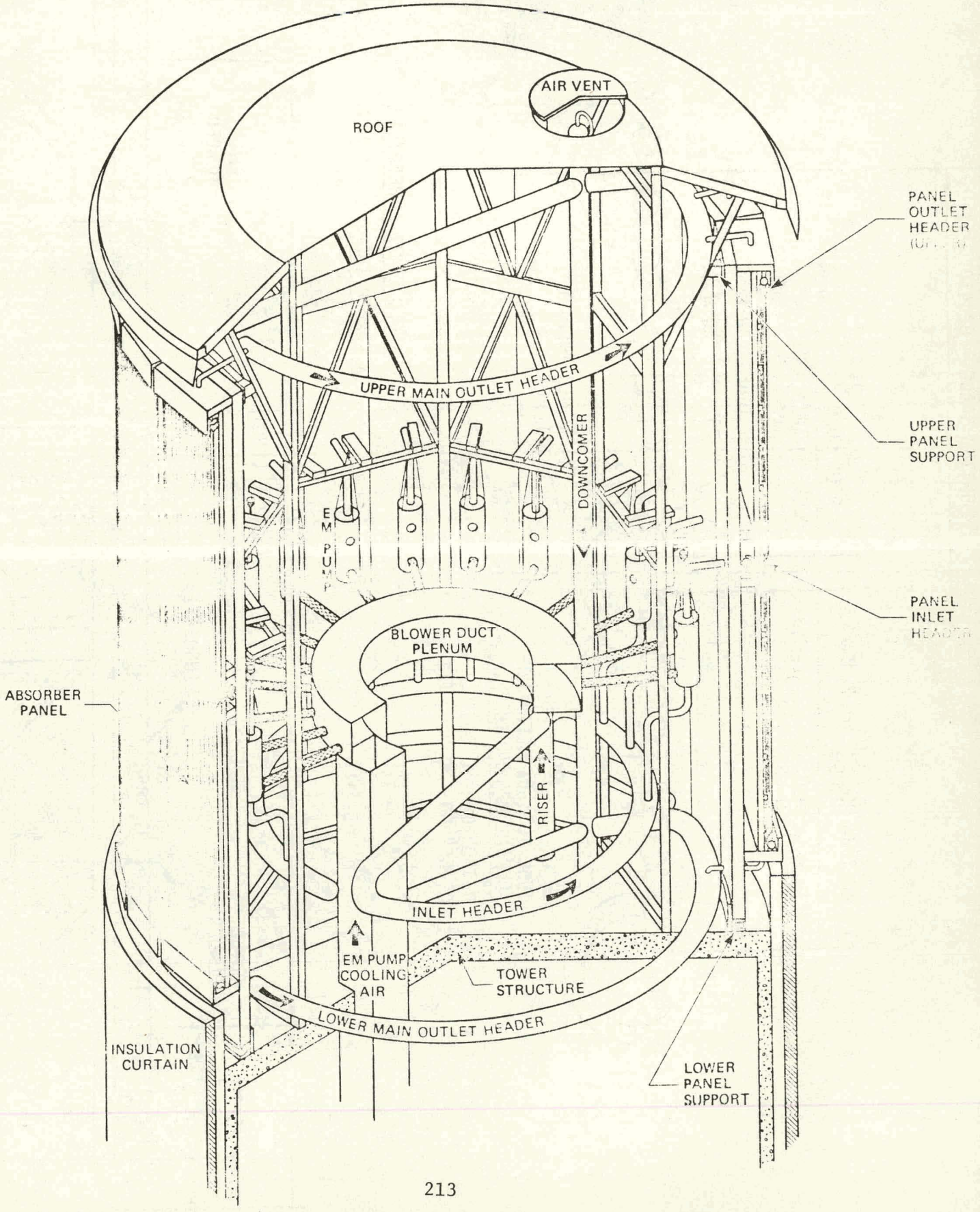
BASED UPON PARAMETRIC STUDY RESULTS

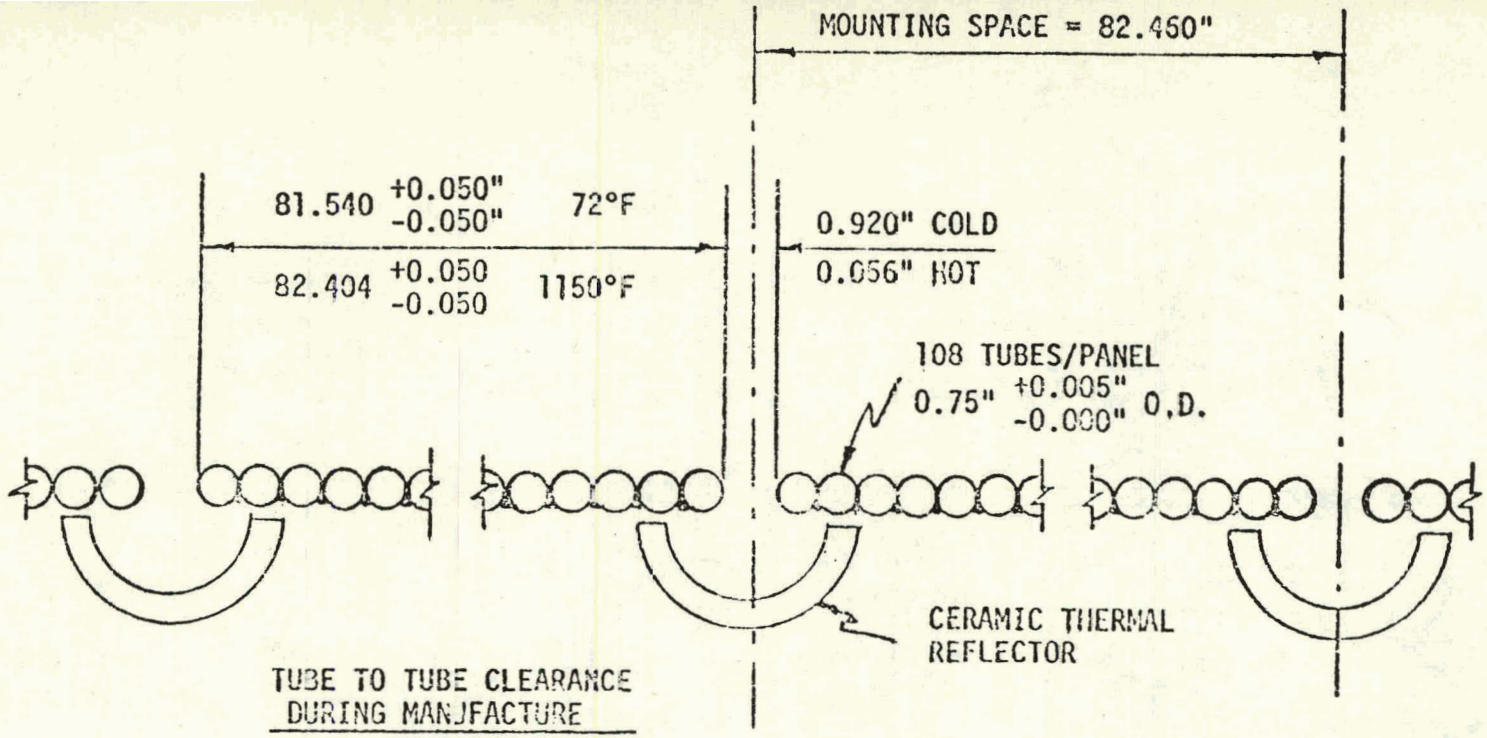
RECEIVER/COLLECTOR SUBSYSTEMS	- GE ENCLOSED PLASTIC HELIOSTAT 360° FIELD CONFIGURATION SINGLE SODIUM LOOP 1100°F
STORAGE SUBSYSTEM	- LOW PRESSURE FIELD ASSEMBLED VESSELS HOT AND COLD STORAGE VESSELS
ELECTRICAL POWER GENERATION SUBSYSTEM	- STEAM CONDITIONS 2400PSI/1000°F/1000°F HARP

ADVANCED CENTRAL RECEIVER POWER SYSTEM COMMERCIAL PLANT CONFIGURATION



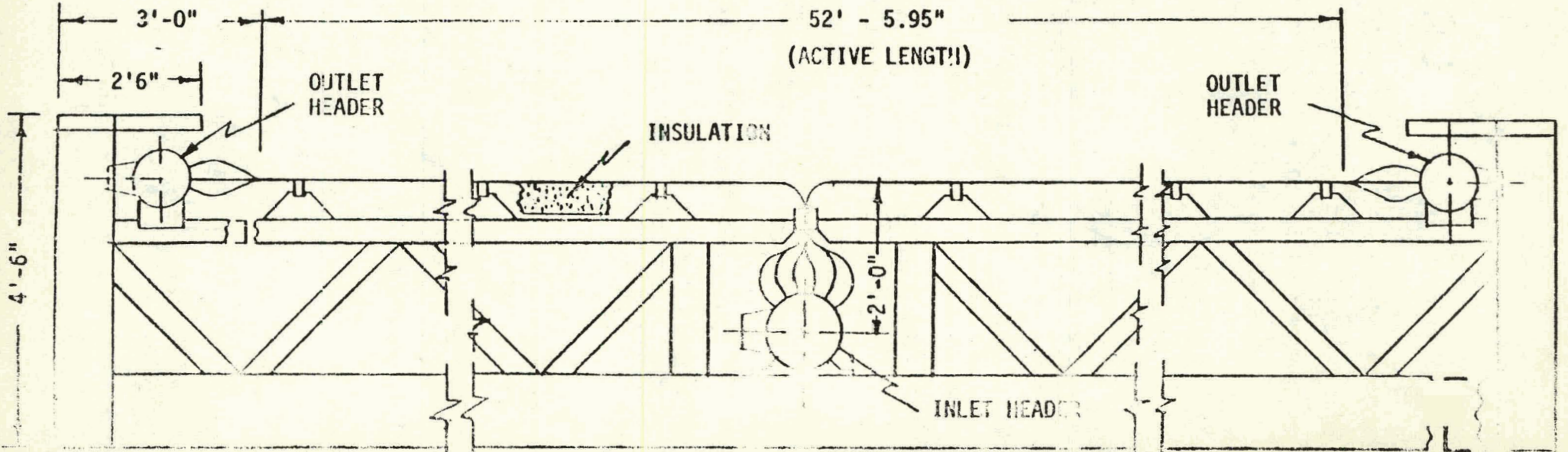
SODIUM COOLED RECEIVER
CONCEPTUAL DESIGN

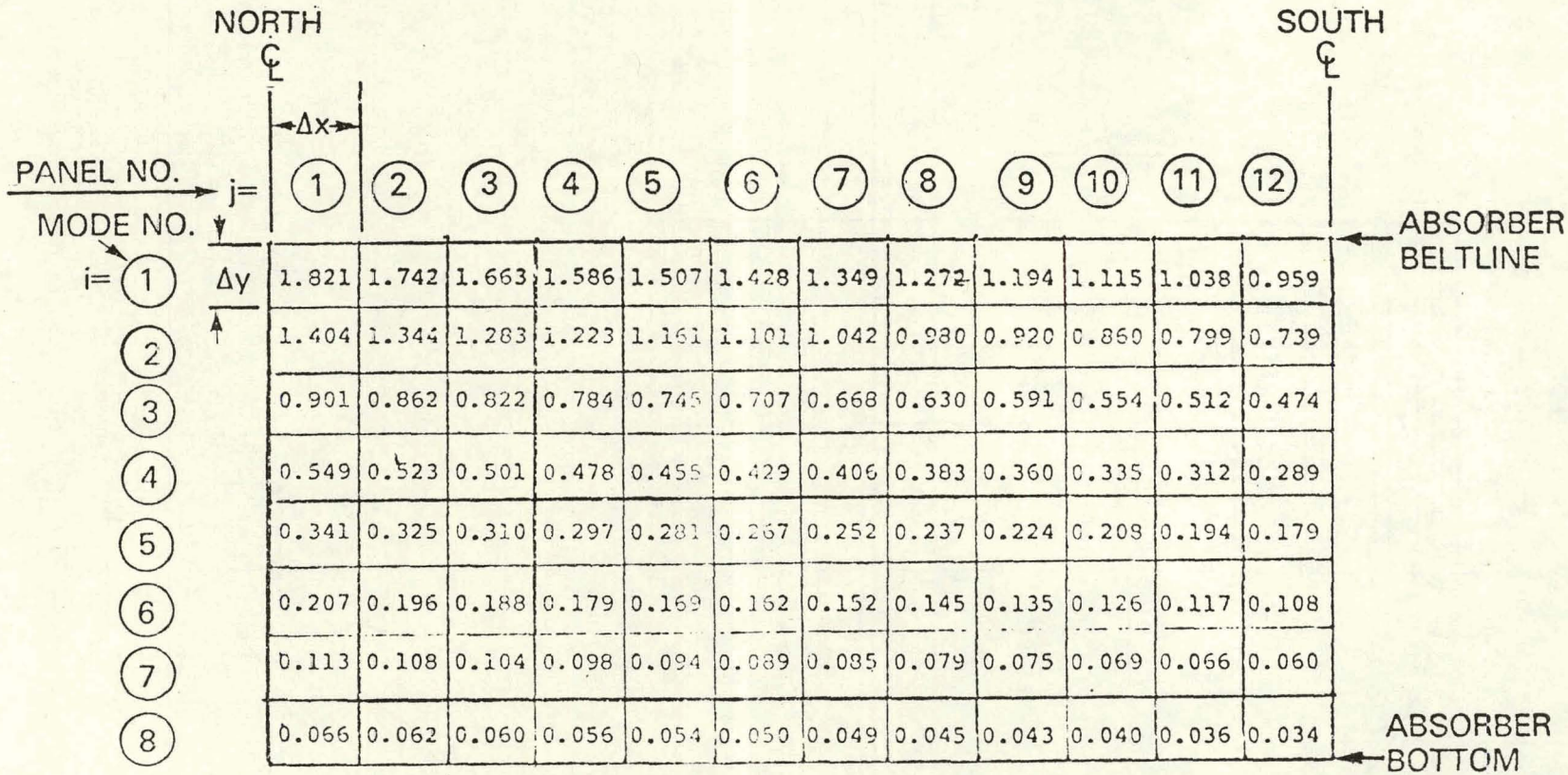




ADVANCED CENTRAL RECEIVER

ABSORBER TUBES & PANEL

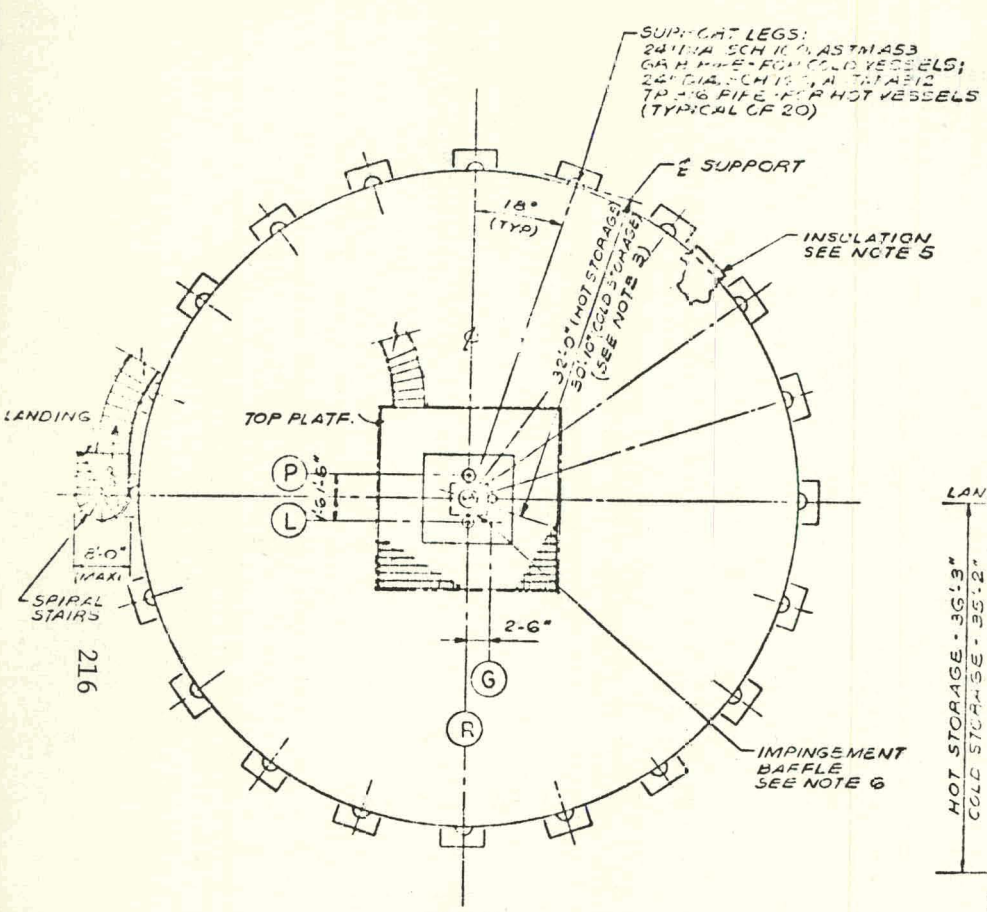




i \ j	1	2	3	4	5	6	7	8	9	10	11	12
1	1.821	1.742	1.663	1.586	1.507	1.428	1.349	1.272	1.194	1.115	1.038	0.959
2	1.404	1.344	1.283	1.223	1.161	1.101	1.042	0.980	0.920	0.860	0.799	0.739
3	0.901	0.862	0.822	0.784	0.745	0.707	0.668	0.630	0.591	0.554	0.512	0.474
4	0.549	0.523	0.501	0.478	0.455	0.429	0.406	0.383	0.360	0.335	0.312	0.289
5	0.341	0.325	0.310	0.297	0.281	0.267	0.252	0.237	0.224	0.208	0.194	0.179
6	0.207	0.196	0.188	0.179	0.169	0.162	0.152	0.145	0.135	0.126	0.117	0.108
7	0.113	0.108	0.104	0.098	0.094	0.089	0.085	0.079	0.075	0.069	0.066	0.060
8	0.066	0.062	0.060	0.056	0.054	0.050	0.049	0.045	0.043	0.040	0.036	0.034

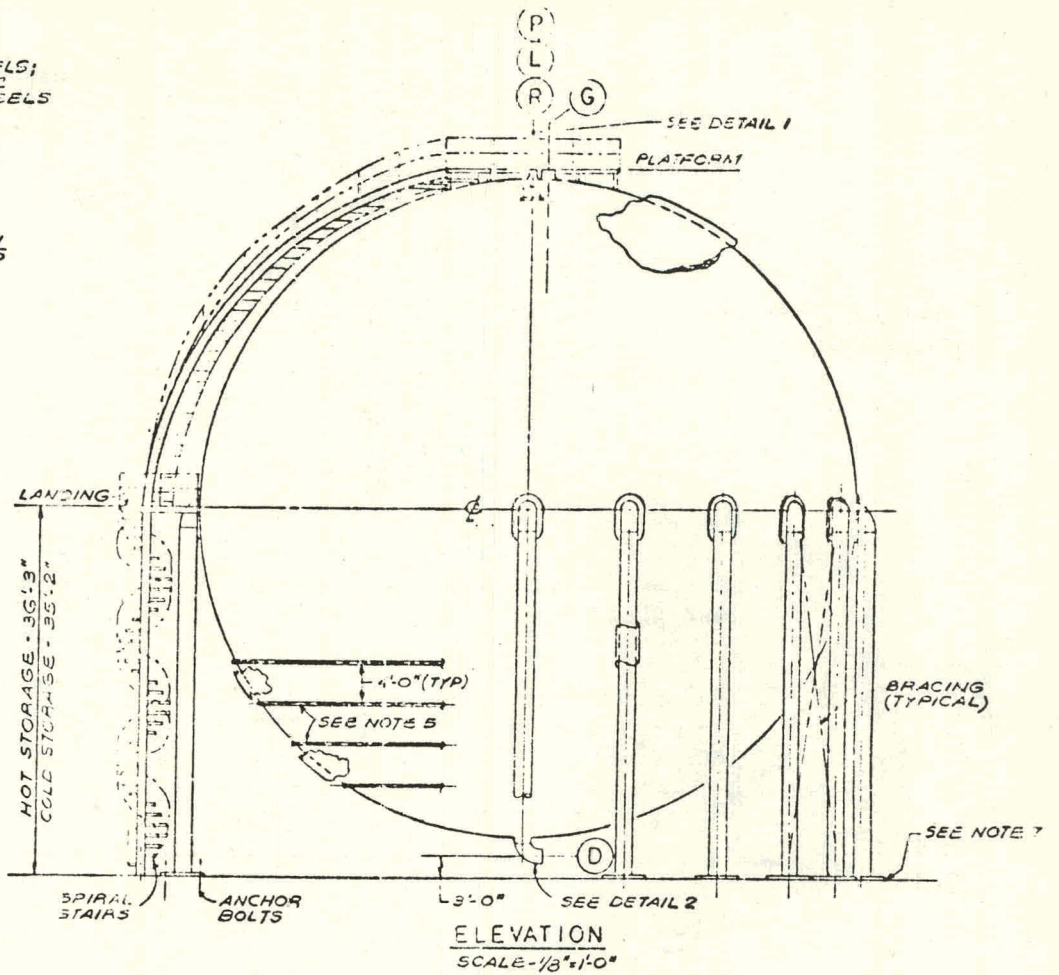
$\Delta x = 2.0944$ m
$\Delta y = 1.0000$ m

Incident Solar Flux (q_{Sij}) in MW/m^2 at Design Point



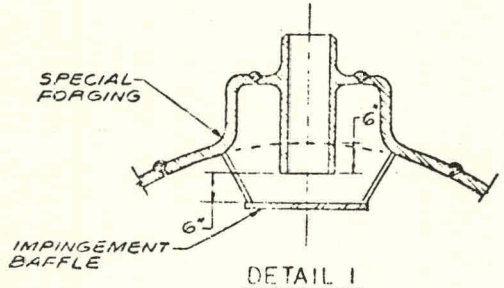
PLAN

SCALE - 1/8" = 1'-0"



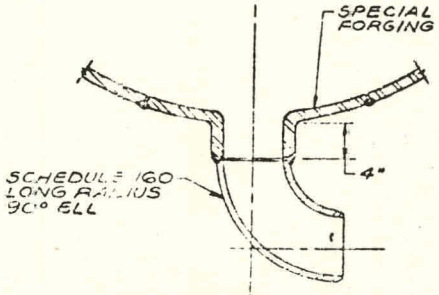
ELEVATION

SCALE - 1/8" = 1'-0"



DETAIL 1

THERMAL SLEEVE



DETAIL 2

(NOTE 4)

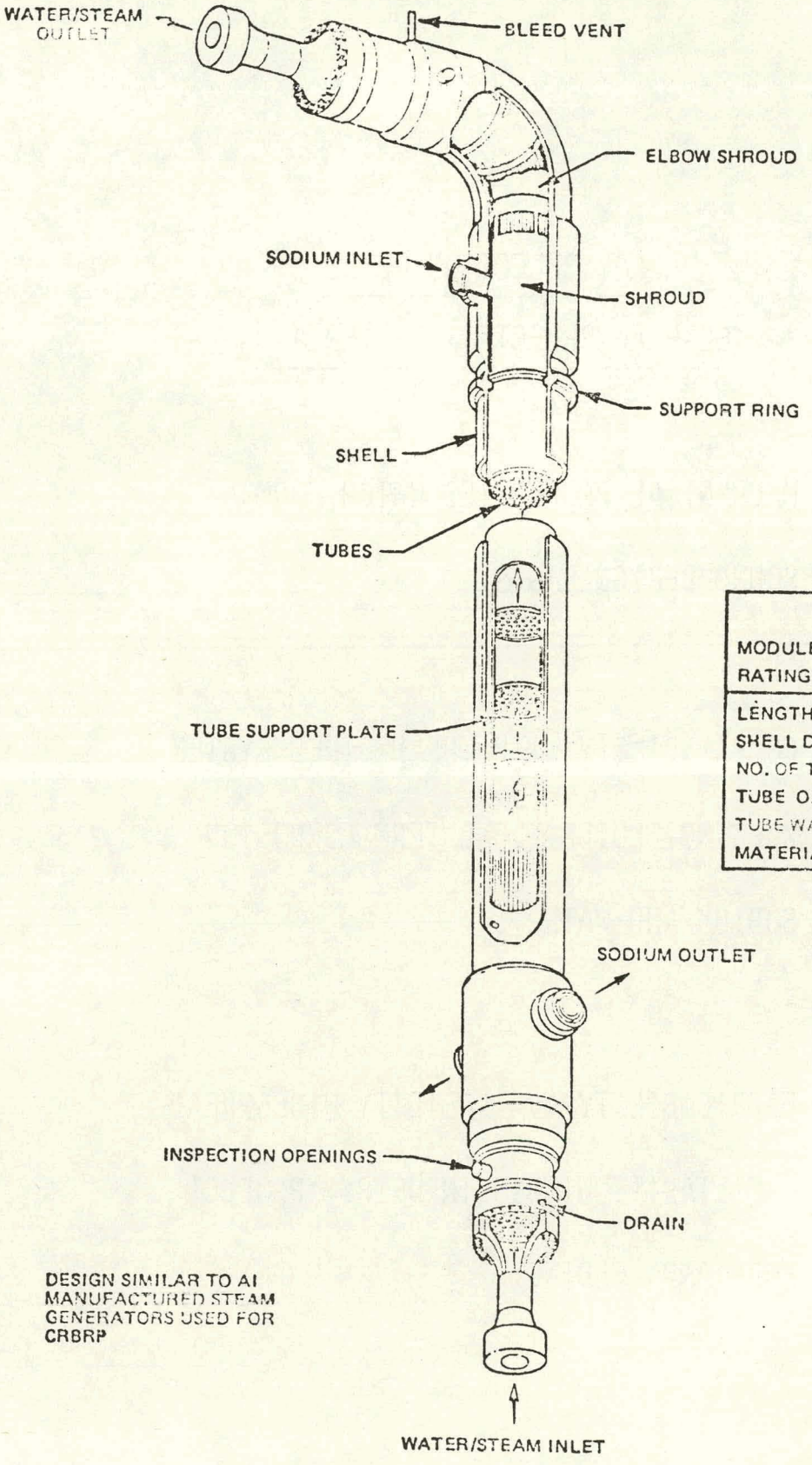
KAISER ENGINEERS

KAISER ENGINEERS, INC.
300 LAKESIDE DRIVE
P.O. BOX 23210
OAKLAND, CALIFORNIA 94623

GE/ACRS SOLAR STUDY

THERMAL ENERGY
STORAGE VESSELS

JOB NO. 5023 | DWG. No. P-01



MODULE RATING (MWt)	EV 127	SH 81	RH 41
LENGTH (ft)	97	54	54
SHELL DIA. (ft)	4.43	4.08	4.56
NO. OF TUBES	740	572	372
TUBE O.D. (in.)	0.625	0.625	1.05
TUBE WALL (in.)	0.109	0.109	0.083
MATERIAL	2¼Cr	1800	1800

DESIGN SIMILAR TO AI MANUFACTURED STEAM GENERATORS USED FOR CRBRP

Stesm Generator Module

ALLOY SELECTION GUIDE

GENERAL SELECTION CRITERIA

- MECHANICAL PROPERTIES WHICH FORM A SOUND DESIGN BASIS.

- COMPATIBILITY WITH THE DESIRED SYSTEM WORKING FLUIDS (LONG TERM CORROSION SODIUM AND WATER).

- FABRICABILITY/AVAILABILITY WIDESPREAD FAMILIARITY WITHIN INDUSTRY. PRODUCT FORM AND WELDING.

SUMMARY OF CONCEPTUAL DESIGN MATERIALS SELECTION

COMPONENT	MATERIAL
COLD LEG PIPING	CARBON STEEL
HOT LEG PIPING	STAINLESS STEEL 316H
ABSORBER PANELS	INCOLOY 800H
STORAGE TANKS(HOT)	STAINLESS STEEL 316H
STORAGE TANKS(COLD)	CARBON STEEL
SUPERHEATER & REHEATER	INCOLOY 800H
EVAPORATOR	2¼ CR-1Mo

REASONS FOR REFERENCE TEMPERATURE AT 1100°F

1. HIGH STRENGTH MATERIALS WITH "REASONABLE" DATA BASE (INCONEL 625) HAVE BEEN FOUND INADEQUATE. (PROJECTED HIGH SODIUM CORROSION, LOSS OF DUCTILITY.)

2. TYPE INCONEL 617 POTENTIAL CANDIDATE TO OVERCOME LOSS OF DUCTILITY AND RAPID CORROSION PROBLEMS.
   - LACK OF DATA BASE

3. TYPE 316 WHICH CAN BE MADE TO WORK AT 1300°F IN SODIUM HAS DRAWBACKS IN WATER (STRESS CORROSION).

4. CORROSION IN SODIUM AND WATER CAN BE ACCOMMODATED AT 1100°F. (INCOLOY 800)

5. DATA BASE IN AIR FOR SUGGESTED REFERENCE MATERIALS EXTENSIVE. (ASME CODE AND MORE) (INCOLOY 880, TYPE 316, 2-1/4Cr-1Mo)

ADVANCED SODIUM COOLED CENTRAL RECEIVER POWER PLANT

by

Thomas Springer

Rockwell International

Canoga Park, California

1. INTRODUCTION

The conceptual design of a 100 MWe Advanced Central Receiver System using liquid sodium as a heat transport medium has been completed by a team consisting of Rockwell International Energy Systems Group (prime contractor), McDonnell-Douglas, Stearns-Roger, The University of Houston, and Salt River Project. The purpose of this study was to determine the technical and economic advantages of this concept for commercial-scale power plants. The concept is similar to that being studied on the water/steam programs, except that liquid sodium cools the receiver instead of water.

The materials problems in this concept are associated with the containment of sodium at elevated temperatures (593°C (1100°F)) in the stainless steel receiver tubes and around the stainless steel or 2-1/4 Cr - 1 Mo sodium steam generator tubes.

There are several advantages to the sodium-cooled system. One of these is that the heat transport fluid remains in the liquid state at all times; therefore, the control of the system is simpler, and there is not a large density change between receiver inlet and outlet. A second advantage is that liquid sodium is a very good heat transfer material; consequently, the receiver can be made smaller and the heat flux can be substantially higher. A third advantage is that the heat transport fluid can also serve as the heat storage material, and operation from storage can be accomplished under the same thermodynamic conditions as would exist when operating directly from the receiver. In addition, the receiver, which is subject to varying heat input, can be totally decoupled from the power cycle. Finally, the sodium system is capable of providing steam to a turbine at temperatures and pressures commensurate with or exceeding modern steam plant requirements and can conveniently incorporate a reheat cycle. These advantages are offset, to some extent, by the need for some additional pieces of equipment not necessarily required by a water/steam system. However, the cost of these additional items is more than compensated by the substantial increase in system efficiency.

One of the advantages of this concept is that there are materials available to achieve the performance listed herein at a reasonable level of confidence and cost.

2. SYSTEM CONCEPTUAL DESIGN

The baseline 100 MWe advanced central receiver configuration is shown in Figure 1 with the performance characteristics summarized on the system Design Data Sheets of Table 1. The system incorporates an external cylindrical receiver concept on a single tower (174 m (571 ft) to the receiver centerline) and an all-sodium, two tank thermal storage system. The collector field, consisting of 14,106 heliostats, surrounds the tower with the tower located to the south of the field center (north biased field). Based on insolation of 950 w/m^2, the collector field mirror area is 692,000 m^2 (6.95 x 10^6 ft^2).

Liquid sodium from the cold storage tank at 288°C (550°F) is pumped by the receiver feed pump through the receiver where the sodium is heated to 593°C (1100°F). The sodium flows from the receiver down the tower through a pressure reducing valve to the hot storage tank. The pressure reducing device reduces the tower static head so that the storage tank operates at atmospheric pressure with an inert cover gas such as argon. The sodium in the hot storage tank is pumped by the steam generator supply pump to the steam generator units where steam at 538°C (1000°F) and 12.4 Mn/m^2 (1800 psig) turbine inlet pressure is produced. The steam generator units consist of an evaporator, a superheater, and reheater units. Sodium from the evaporator returns to the cold storage tank, completing the circuit.

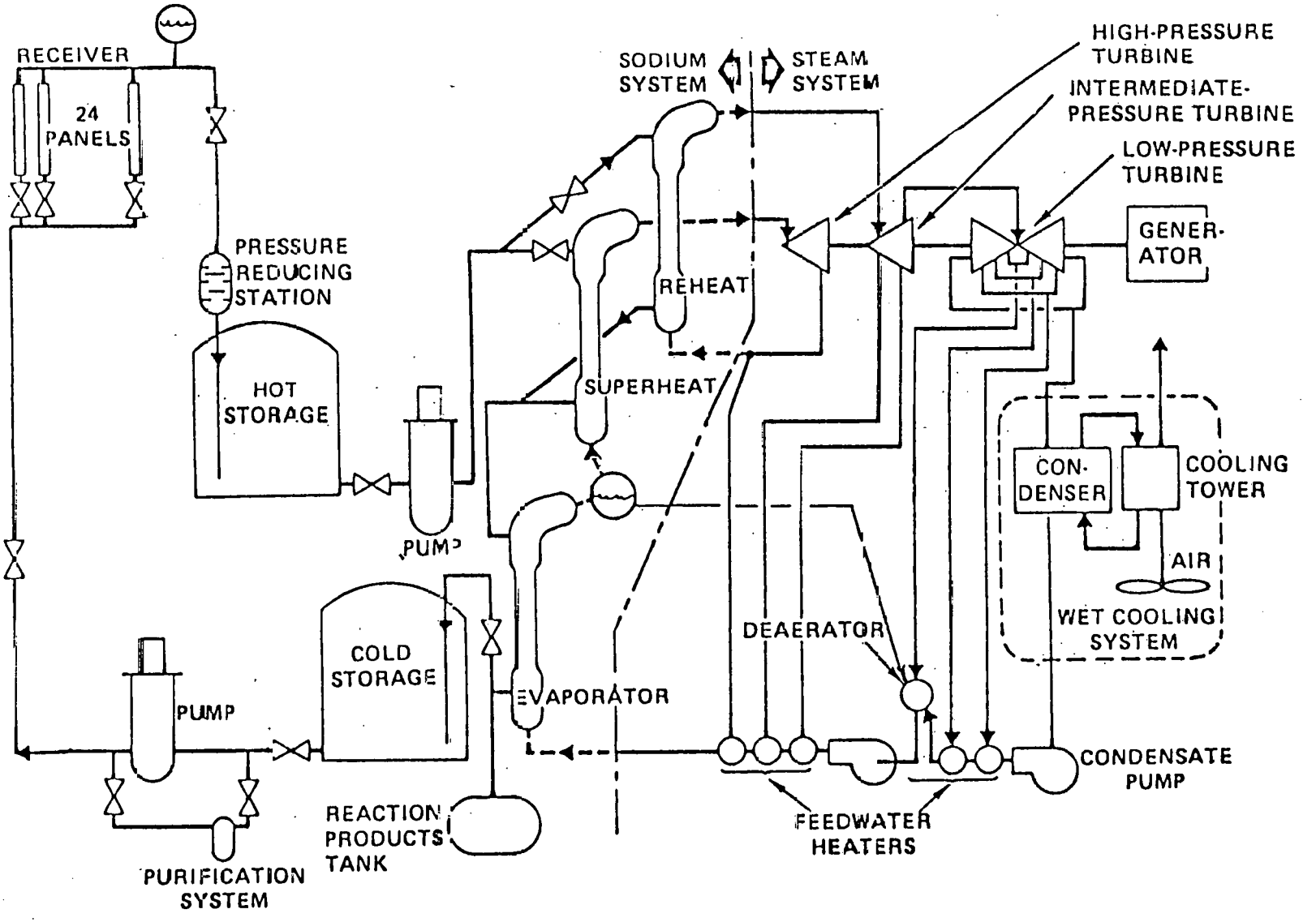


Figure 1 Sodium Cooled Advanced Centra Receiver System

42400-1096C

TABLE I

ADVANCED CENTRAL RECEIVER
SYSTEM SUMMARY DATA
(Sheet 1 of 2)

New Electrical Power MWe)	100
Parasitic Power (MWe)	
Daytime	12
Nighttime	6
Insolation (W/m^2)	950
Maximum Solar Power Absorbed (MWt)	390
Nominal Solar Power Absorbed for Direct Operating (MWt)	260
Plant Net Efficiency (%)	24.5
Collector Field Configuration	Single 360^o, North Biased
Solar Multiple, Equinox Noon	1.5
Number of Heliostats	14,106
Heliostat Shape and Size [m (ft)]	Square, 6.5 x 6.5 (21.3 x 21.3)
Number of Towers/Receivers	1
Receiver Mid-Point Elevation [m (ft)]	174 (571)
Receiver Configuration	External Cylinder
Number of Receiver Panels	24
Receiver Height and Diameter [m (ft)]	16.1 x 16.1 (52.8 x 52.8)
Receiver Maximum Heat Flux (MW/m^2)	1.53
Sodium Temperatures [^oC (^oF)]	288/593 (550/1100)
Receiver Sodium Flow Rate [kg/hr (lb/hr)]	3.66×10^6 (8.07×10^6)
Steam Generator Sodium Flow Rate (Direct Operation) [kg/hr (lb/hr)]	2.45×10^6 (5.36×10^6)

TABLE I

ADVANCED CENTRAL RECEIVER
SYSTEM SUMMARY DATA
(Sheet 2 of 2)

Thermal Storage Capacity (MWth)	805
Total Sodium Inventory kg (lb)	7.6×10^6 (16.8×10^6)
Steam Generator and Reheater Type	Modular Steam Generator
Steam Conditions [MN/m^2, ^oC (psia, ^oF)]	
Initial	12.51, 538 (1815, 1000)
Reheated	2.72, 538 (394, 1000)
Steam Flow Rate [kg/hr (lb/hr)]	
Daytime	3.32×10^5 (7.32×10^5)
Nighttime	3.15×10^5 (6.95×10^5)
TSS Sodium Flow Rate [kg/hr (lb/hr)]	2.31×10^6 (5.09×10^6)
Feedwater Temperature [^oC (^oF)]	234 (453)
Turbine Back Pressure [MN/m^2 (in. Hg)]	0.007 (2.0)
Heat Rejection [MW (Btu/hr)]	
Daytime	158 (540×10^6)
Nighttime	150 (511×10^6)

3. RECEIVER SYSTEM

The receiver system can be considered to operate as two independent loops. The first loop transfers sodium from the cold storage tank, T-1, at about 288°C (550°F) through the receiver which heats it to approximately 593°C (1100°F). The sodium then flows by gravity through the drag valve to the hot storage tank, T-2. Nominal maximum flow rates are about 1.3 M^3/sec (20,000) gpm. The second loop transports sodium from the hot storage tank through the sodium heated superheater and reheater, through the evaporator and then to the cold storage tank, T-1. The maximum nominal flow is about 1.0 m^3/sec (15,000) gpm range.

Sodium circulation is provided by means of the P-1 and P-2 pumps. These are free surface "Fermi" type centrifugal pumps. The P-1 pump is a high-head (approximately 300 m (1000 ft) TDH) two-speed (full speed and 25% speed), single-stage centrifugal pump. The lower speed is only used at plant startup. The free surface level is maintained by pressurizing the pump ullage with argon. The P-2 pump is a variable speed, single-stage pump of the same type as the P-1 pump.

Sodium flow through the receiver is modulated by the control valves on each panel to maintain the panel outlet at a constant temperature. The surge tank permits these fast acting valves to operate independently of the drag valve. The drag valve reduces the sodium pressure to near atmospheric pressure to match the pressure requirements of the storage tank. The flow in the downcomer line is modulated to maintain the sodium level in the surge tank fixed.

The anti-siphon system and the surge tank operate to prevent the draining of the sodium from the receiver on loss of pump power. The anti-siphon device also prevents backflow in this event which would draw hot sodium into the cold header and riser.

4. RECEIVER DESIGN

Figure 2 shows some of the structural details of the receiver. The panel and panel structure are supported by the main structure. Sodium piping with bends to allow for thermal expansion connects the panels and acts as a standpipe to provide sodium to the panels in case of pump and/or check valve failure. The sodium expansion tank is toroidal in shape and is located near the top of the receiver.

The baseline receiver is of the external type, and it is 16.1 m (52.8 ft) in diameter and 16.1 m in height. It consists of 24 separate vertical panels - each panel being constructed of 110 stainless steel tubes. Each tube has a diameter of 1.91 cm (0.75 in.) and a wall thickness of 0.124 cm (0.049 in.). See Figure 2.

The panel tubes are placed tangent to one another forming a flat panel 209.6 cm (82.5 in.) wide. The tubes are held mechanically in this position, being neither welded nor brazed. The tubes are anchored to the support structure at the panel base and are permitted to grow vertically - the maximum growth being in the neighborhood of 18 cm (7 in.). The tubes are supported every 1.2 m (4.0 ft) by a pin and bracket arrangement which firmly mounts the tubes to the support structure while permitting thermal expansion.

The tubes enter manifolds at the top and bottom of the panels. The manifolds are constructed of 20 cm (8 in.) pipe with a 0.277 cm (0.109 in.) wall, and are the width of the panel. The manifold at the bottom is connected to the main sodium riser pipe by means of a circuitous 20 cm (8 in.) pipe. The analogous pipe at the upper manifold doubles back parallel to the panel and for about 2/3 of the panel length. Thus, the growth of the panel is compensated by the reverse growth of this pipe, minimizing the pipe stress.

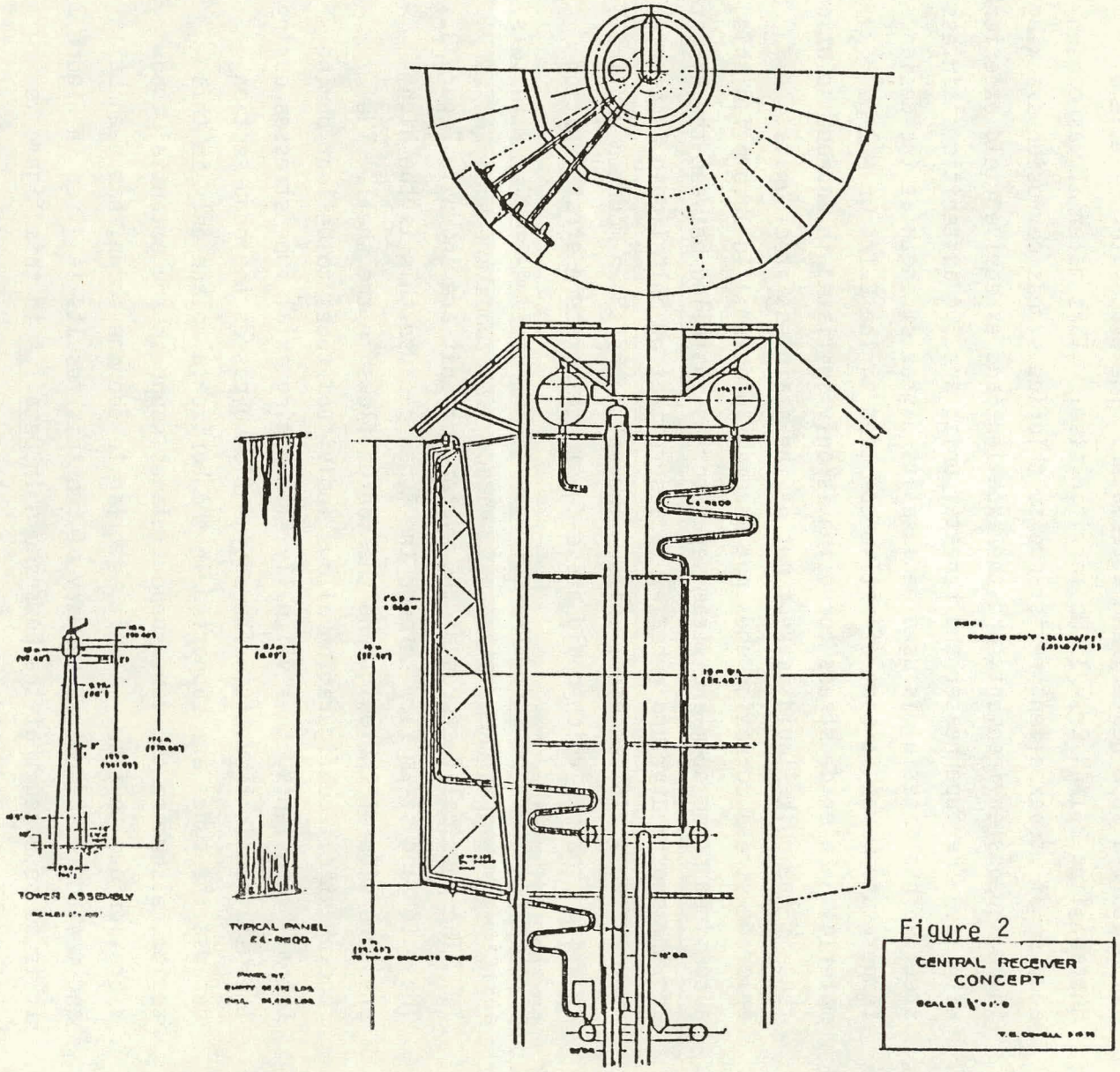


Figure 2

CENTRAL RECEIVER CONCEPT

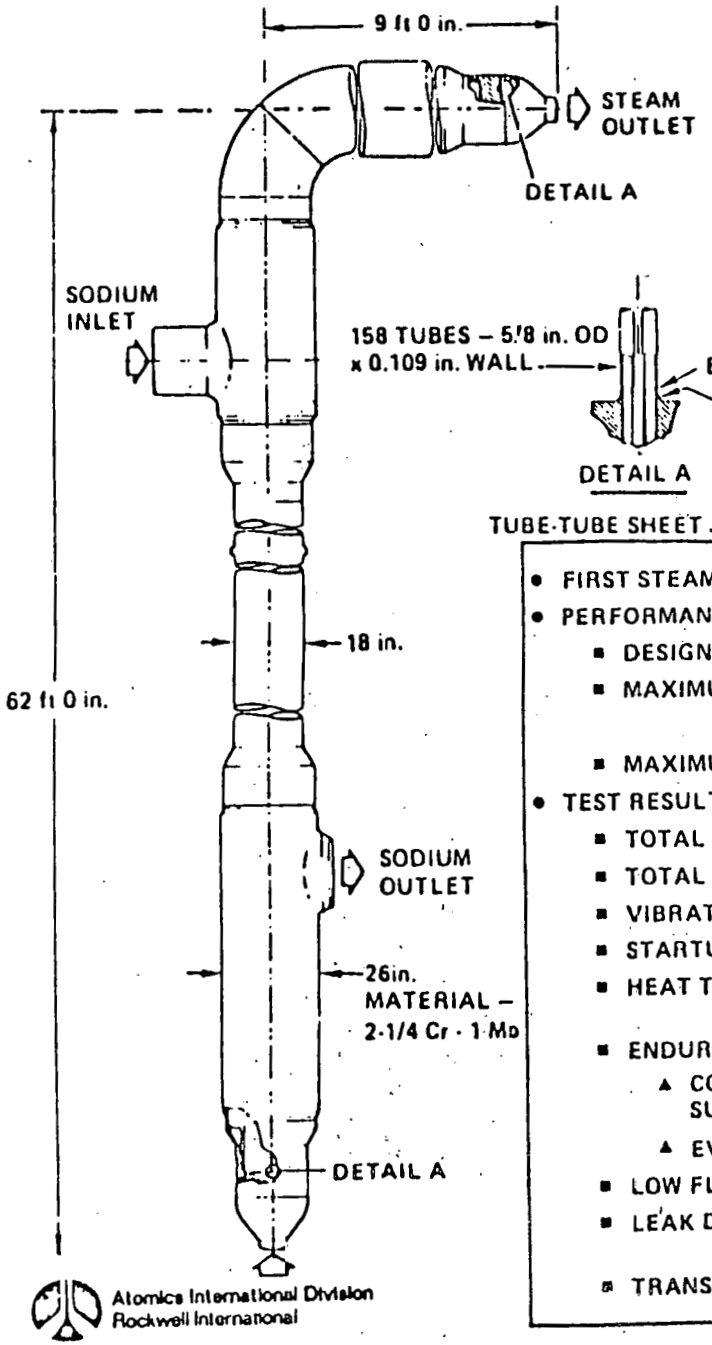
5. STEAM GENERATOR

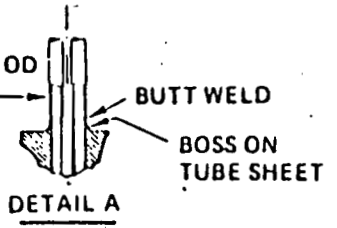
The reference design utilizes three steam generator units; an evaporator, a superheater, and a reheater. The evaporator is made of unstabilized 2-1/4% Cr - 1% Mo ferritic steel. This material was chosen because of its excellent resistance to chloride stress corrosion cracking in an aqueous environment, and the excellent and extensive field experience with it. The superheater and reheater units are 304 austenitic stainless steel. This material is used because its higher strength at the design temperature makes it cost effective compared to the 2-1/4 Cr - 1 Mo material. Chloride stress corrosion is only initiated in aqueous solution, thus if the bulk liquid is kept out of the stainless steel units chloride stress corrosion does not become a problem. To accomplish this, a combined steam drum and steam separator is installed between the evaporator and the superheater and reheater to assure that no bulk liquid is carried over to the stainless steel units. The units are shown mounted vertically to avoid problems which could arise due to temperature stratification on the sodium side.

The physical features of the evaporator unit are shown in Figure 3. The water and steam flow through the tubes because this is the high pressure side of the unit, and the sodium flows in the shell. The "hockey stick" configuration allows individual tubes to deflect during thermal transients, thus virtually eliminating axial tube stresses during thermal transient events. The sodium flow bypasses the bend section because the tubes are supported in the horizontal plane only in this region, elsewhere the tube support plates suppress any potential tube vibration due to flow. A unit, similar to the one shown, has been built and tested in sodium. A summary of the test results is given in Figure 3. It is to be noted that the boss shown in Detail A in this figure is milled out of the solid tubesheet forging, thus the autogeneous butt weld provides a tube-to-tubesheet weld that can be 100% x-rayed. The performance characteristics of these units correlate well with the engineering predictions.

HIGHLIGHTS OF

LMEC/SCTI TEST OF AI MSG





TUBE-TUBE SHEET JOINT

• FIRST STEAM PRODUCED	7-9-72
• PERFORMANCE	
▪ DESIGN POWER	28.4 Mwt
▪ MAXIMUM POWER AT 100% FLOW	32.1 Mwt (FOR 2400 psig STEAM)
	33.8 Mwt (FOR 1450 psig STEAM)
▪ MAXIMUM STEAM CONDITIONS	2430 psig/930°F
• TEST RESULTS	
▪ TOTAL (MAIN LINE) STEAMING TIME	4015 hr
▪ TOTAL SODIUM OPERATING TIME	9305 hr
▪ VIBRATION	LEVELS LOW, SAFE
▪ STARTUP/SHUTDOWN	37 CYCLES, STABLE
▪ HEAT TRANSFER PERFORMANCE	PARAMETRIC DATA OBTAINED FROM 1450 TO 2450 psig
▪ ENDURANCE	
▲ COMBINED EVAPORATOR/ SUPERHEATER MODE	500 hr
▲ EVAPORATOR MODE	500 hr
▪ LOW FLOW STABILITY	STABLE, ALL CONDITIONS OF INTEREST
▪ LEAK DETECTION	DETECTABILITY OF 10^{-6} lb/sec H_2O DEMONSTRATION
▪ TRANSIENTS	INTEGRITY MAINTAINED

FIGURE 3

6. THERMAL STORAGE SUBSYSTEM

The thermal storage subsystem contains the hot and cold storage liquid sodium tanks, the P-2 pump, a pressure-reducing device, and interconnecting pipe. Liquid sodium from the receiver subsystem is stored in the hot storage tank at energy rates up to 390 MWt, which corresponds to a flow rate of 3.66×10^6 kg/h (8.07×10^6 lb/h). Sodium is drawn from the hot storage tank at energy rates of up to 250 MWt 2.34×10^6 kg/h (5.29×10^6 lb/h) to generate steam for the Electric Power Generating Subsystem. Sodium from the steam generator units flows to the cold storage tank. During the day, hot sodium is accumulated by the hot tank in a sufficient quantity to store up to 3.25 hrs of operation at 100% rated power. With this storage arrangement, plant operation is always from storage. The steam conditions provided are the same regardless of whether the receiver loop is operating or not.

The storage tanks are 30.5 m (100 ft) in diameter with a height of 13.6 m (45 ft) for the hot storage tank and 12.3 m (41 ft) for the cold. The hot tank operating at 593°C (1100°F) is made of stainless steel; the cold tank at 288°C (550°F) is made of carbon steel. The tanks operate at ambient pressures in order to minimize cost. This requires a pressure-reducing device to dissipate the tower static head.

The pressure-reducing device for the baseline configuration consists of a nominal 18 in. drag valve. A steam generator pump in this system moves the hot sodium through the steam generator units to the cold storage tank. The receiver pump identified in the Receiver Subsystem description charges the hot storage tank. The steam generator pump is similar to the FFTF pump with approximately the same head and flow requirements. The developed head for this pump is 76 m (250 ft) at 0.95 m^3/s (15,000 gpm).

7. MATERIALS

The materials used in this concept are available and permit the achievement of the performance goals. Of course, if certain improvements are made in the materials, then the performance could be markedly improved and the plant costs could be lowered. In the receiver tubes, for example, any of the following improvements would be most useful.

1) Increase allowable stresses
2) Increase thermal conductivity
3) Decrease allowable wall thicknesses

Table 2 lists the chief materials in the heat transport portion of this power plant and the maximum temperature expected in them.

TABLE 2
POWER PLANT MAJOR MATERIALS

Material Function	Material	Maximum Temperature
		^{o}C (^{o}F)
Heat transport fluid	Sodium	593 (1100)
Storage medium	Sodium	593 (1100)
High temperature sodium containment	304 SS	704 (1300)
Low temperature sodium containment	Carbon Steel	288 (550)
Evaporator	2-1/4 Cr - 1 Mo	396 (746)
Superheater	304 SS	593 (1100)
Reheater	304 SS	593 (1100)

714-F.93/hgw

THIS PAGE

WAS INTENTIONALLY

LEFT BLANK

ALTERNATIVE CENTRAL RECEIVER POWER SYSTEM USING MOLTEN SALT AS THE HEAT TRANSFER AND STORAGE MEDIUM

by

Tom Tracey

Martin Marietta Corporation

Denver, Colorado

I. INTRODUCTION

The primary objective of the program is to develop a solar power plant to reduce the cost of electricity significantly below that of the first-generation plants. Other desirable benefits are higher capacity displacement, greater national market penetration, increased potential for subsequent performance improvement, and reduced environmental impact. We believe our recommended system achieves the objectives and does so with low technical risk.

Table I-1 gives the cost of electricity for the recommended system. We believe the proposed alternative molten salt system has potential to reduce the cost of electricity well over a factor of two relative to the first generation. Because solar energy is available only on an intermittent basis, the cost of storage is important to the future success of solar power. The attractive cost of the molten salt storage system is quite competitive with existing pumped storage systems in use today. The low storage cost will undoubtedly result in a significant improvement in capacity displacement. In fact, we believe that the proposed system will meet utility requirements for an intermediate plant. The requirements are as follows:

1) Must be operated at least 4000 hours per year;
2) Must be available most of the time during the utility's peak period.

The primary factor affecting market penetration is cost; therefore, the recommended system will be able to provide larger market penetration than the first-generation plants. Also, the attractive cost of storage will undoubtedly add to wider acceptance of solar power. The primary factor in environmental impact is land use. The recommended system is approximately 20 percent more efficient than the first-generation plants when operating from the receiver and is 70 percent more efficient when operating from storage; therefore, the percentage of improvement in performance

Table I-1 Cost of Electricity ($\overline{BBEC}$) and Storage

	Recommend Alternative Molten Salt System
Cost of Electricity (mills/kWhe) - with Economic Ground Rules Used in First Generation (Cost of Money 7.5%)	28.0
- Present Economic Ground Rules (Cost of Money 11%)	38.4
Cost of Storage - Thermal ($/kWht)	3.40
- Electrical ($/kWhe)	8.20

depends on the amount of storage used. For the recommended plant, the overall average performance is at least 30 percent better than the first generation. As a result it will require about 30 percent fewer heliostats and less land per unit output.

Another important advantage of a molten salt system is safety. The salt does not react with water or air. It is commonly used in open baths in industry and has an excellent safety record. On the other hand, sodium reacts spontaneously with air and violently with water.

Major program tasks will be summarized; they are titled as follows:

1) Recommended Commercial Plant Conceptual Design and Performance
2) Development Schedule
3) Recommended Materials Development and Test

II. RECOMMENDED COMMERCIAL PLANT CONCEPTUAL DESIGN AND PERFORMANCE

A. SYSTEM DESCRIPTION

The system has a net electrical output of 300 MWe and has sufficient heliostats and storage capacity to provide full load operation 24 hours per day at summer solstice. The system consists of nine heliostat fields with 7711 heliostats in each (Fig. II-1). The heliostats track the sun and direct the solar energy incident on them to one of four cavity apertures located at the top of a 155-meter (510 ft) tower. The system is shown schematically in Figure II-2. Inside the cavity the flux is absorbed on panels. The panels are cooled by molten salt that enters the receiver at 561 K (550°F) and leaves the receiver at 838 K (1050°F). Salt flowrate is controlled to maintain a

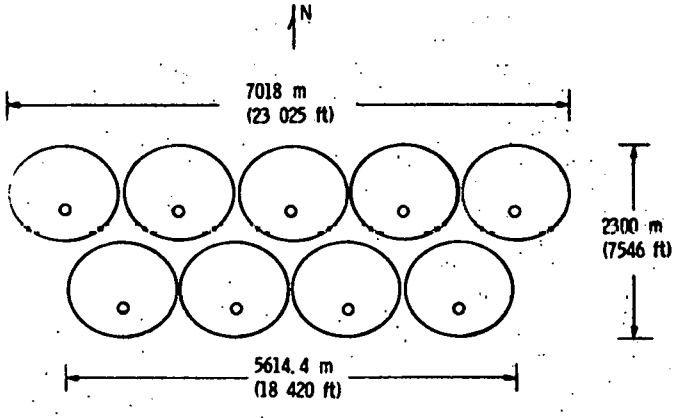


Figure II-1 300 MWe Module Layout

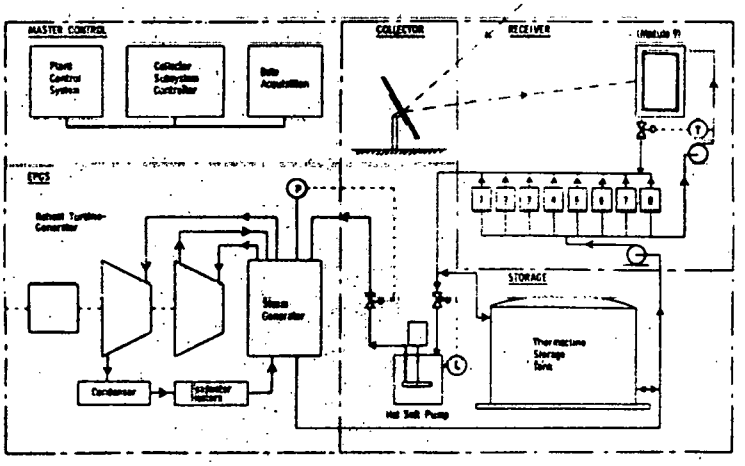
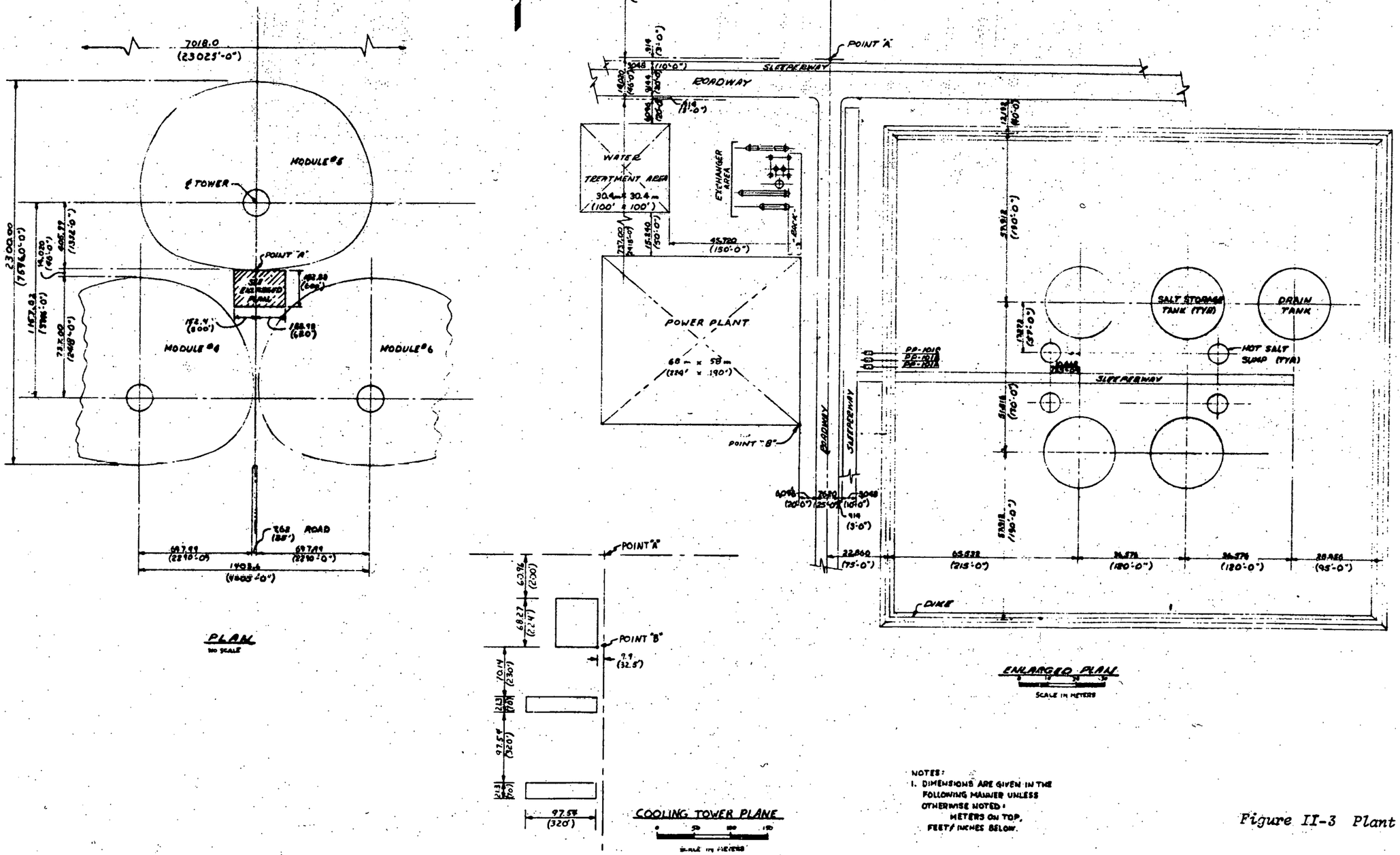


Figure II-2 System Schematic

constant salt exit temperature at the receiver outlet. The hot salt is pumped to the steam generator and/or the storage system. Hot salt pumped to the storage system is stored for later use by the steam generator. The hot salt pumped to the steam generating system is used by the steam generator to heat boiler feedwater and make 783 K (950°F), 16.5 MPa (2400 psig) superheated steam for the steam turbine/generator. During the process the hot salt is cooled to 561 K (550°F). The cold salt is pumped to the bottom of the thermal storage tank and/or back to the receivers. During periods when solar insolation is insufficient for rated operation, energy is extracted from the storage system and used to supply heat to the steam generator. The master control system is computerized and provides operator over-rides that serve as overall plant control. It also provides data display and storage.

The electrical power generating plant and the storage facility are located between the middle three module fields (Fig. II-1). The location was selected to minimize salt piping runs to the field. The plant layout consists of four areas (Fig. II-3). The electric power generation subsystem (EPGS) building houses EPGS equipment with the turbine on the upper, or operating floor, and the condenser and condensate/feedwater pumps on the lower floor. The building also houses the master control system and the collector control system on a mezzanine floor. The steam generator (heat exchanger) area is located as near as possible to the turbine to minimize piping runs. The thermal storage tanks are across the road. The area is diked to contain the molten salt in case of a tank rupture. The EPGS water treatment area is similar to conventional plants. An artist's concept of the system is shown in Figure II-3a.



NOTES:
1. DIMENSIONS ARE GIVEN IN THE FOLLOWING MANNER UNLESS OTHERWISE NOTED: METERS ON TOP, FEET/ INCHES BELOW.

Figure II-3 Plant Layout

240

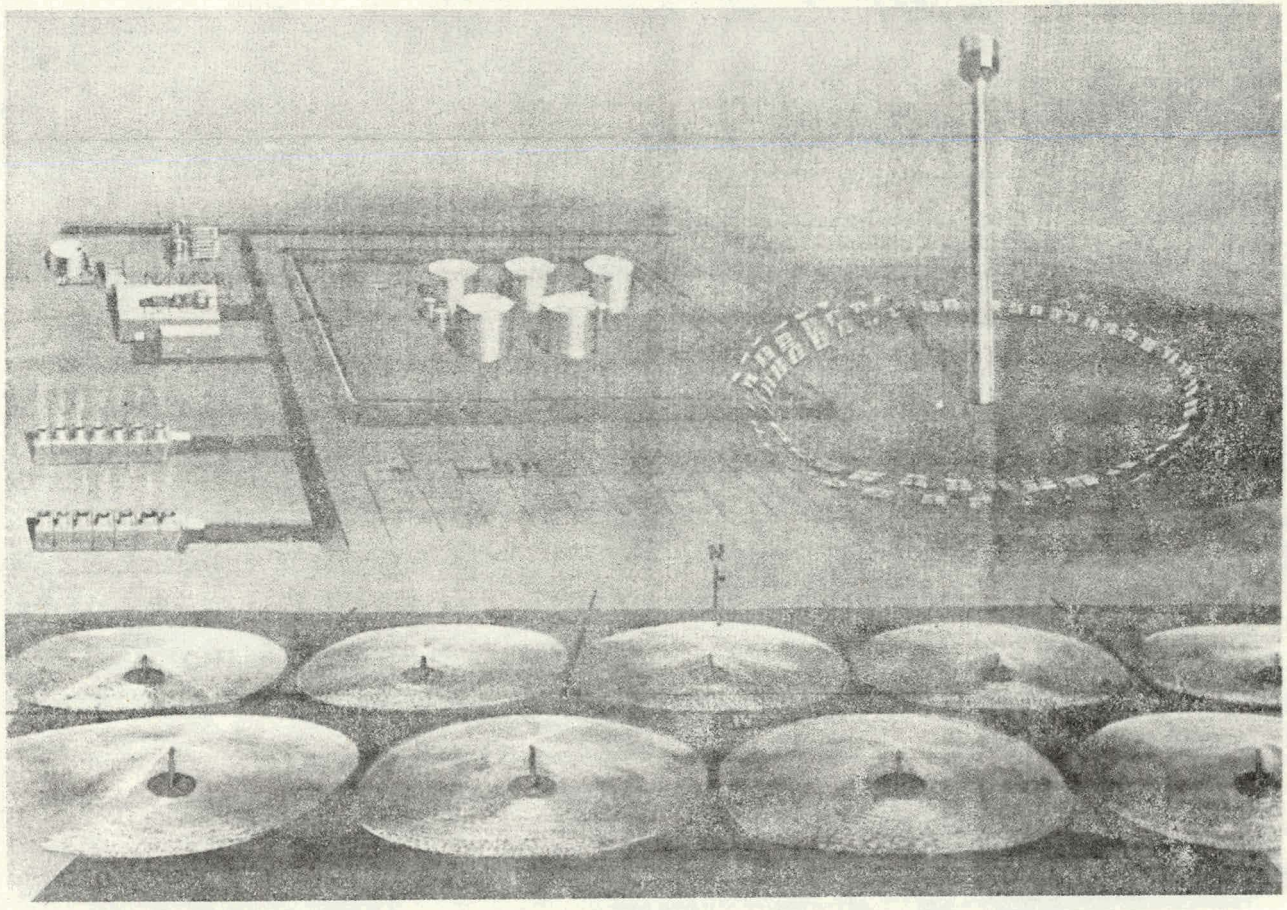


Figure II-3a Artist's Concept of Advanced Central Receiver Power System

B. SUBSYSTEM DESCRIPTION

The system is comprised of a collector, a tower, an electric power generation subsystem (EPGS), molten-salt components that include receivers, tanks, heat exchangers, pumps, associated piping, thermal storage, and master control.

1. Collector

The module configuration shown in Figure II-1 consists of nine modules, five in an east-west row with another four modules in a row just to the south of the first row; both rows are symmetrically aligned on the same north-south line. This layout was selected to minimize salt piping runs and expansion joints in the piping.

The heliostats in the field are positioned along radial lines with the receiver tower at the center. The rows of heliostats are spaced to minimize shadowing or blocking along the north-south line at the design point (21 June). An aiming strategy was developed to minimize spillage and produce an acceptable receiver heat flux.

The heliostat requirements for the conceptual design are given in Table II-1. It is emphasized that the system could use various heliostat designs and is not limited to the ones that meet the requirements of Table II-1. In fact, as discussed in

Table II-1 Heliostat Requirements

Size	39.95 m^2 (430 ft^2)
Reflectivity (clear)	0.91
Focal Length*	712.3 m (2338 ft)
Tolerances (Mirror Normal 1σ) - Aiming (Elevation and Azimuth) - Image Quality	 0.75 m rad. 0.70 m rad
* Facets focused and canted	

Task 5, there is potential for reducing system cost by reducing heliostat requirements.

2. Tower

The selected tower design is shown in Figure II-3b. It is a reinforced concrete tower of 12.9 m (40 ft) diameter at the base and 7.63 m (25 ft) diameter at an elevation of 155.45 m (510 ft).

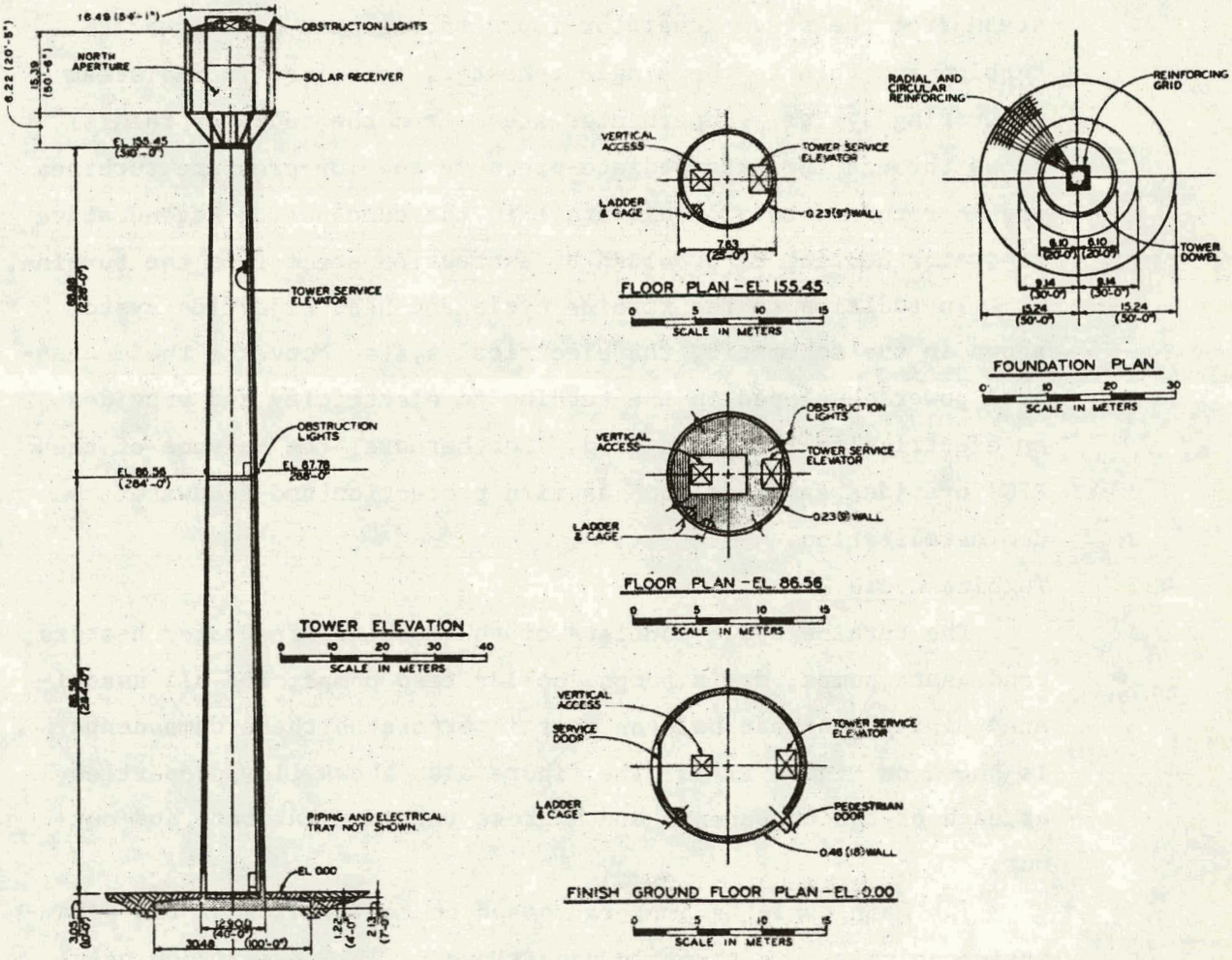


Figure II-3b Receiver Tower and Foundation

3. Electric Power Generation System (EPGS)

In overall design, the EPGS is similar to the EPGS of a conventional fossil-fired 300 MWe plant. The interface between the EPGS and the other subsystems of the plant are the main steam line, the cold and hot reheat steam lines, the feedwater line, auxiliary electrical power, the control system, and the net electrical output of the plant. The functional relationships of major EPGS components are shown on Figure II-4. Superheated steam from the steam generator flows through the high-pressure turbine and then to the single reheater, contained in the steam generating system. Superheated steam from the reheater then flows through the intermediate-pressure and low-pressure turbines and is returned to a liquid state in the condenser. Regenerative feedwater heating is provided by extraction steam from the turbine.

In addition to the turbine cycle and heat rejection system shown in the schematic, the electrical system converts the mechanical power developed in the turbine to electricity and provides an electrical path to the grid. Furthermore, the balance of the EPGS provides services such as fire protection and feedwater demineralization.

4. Turbine Cycle

The turbine cycle consists of the turbine, feedwater heaters, condensate pumps, drain pumps, boiler feed pumps, and all associated piping. A heat balance that incorporates these components is shown on Figure II-5. The figure also shows flow properties at each of the components and a gross turbine heat rate and output.

The main cycle parameters, based on the results of the parametric analysis, are throttle conditions of 16.5 MPag (2400 psig) and 783K (950°F) with reheating to 783 K (950°F) and a turbine backpressure of 8.5 kPa (2.5 inches Hg absolute). After an allowance for auxiliary loads of approximately 35 MWe, the unit

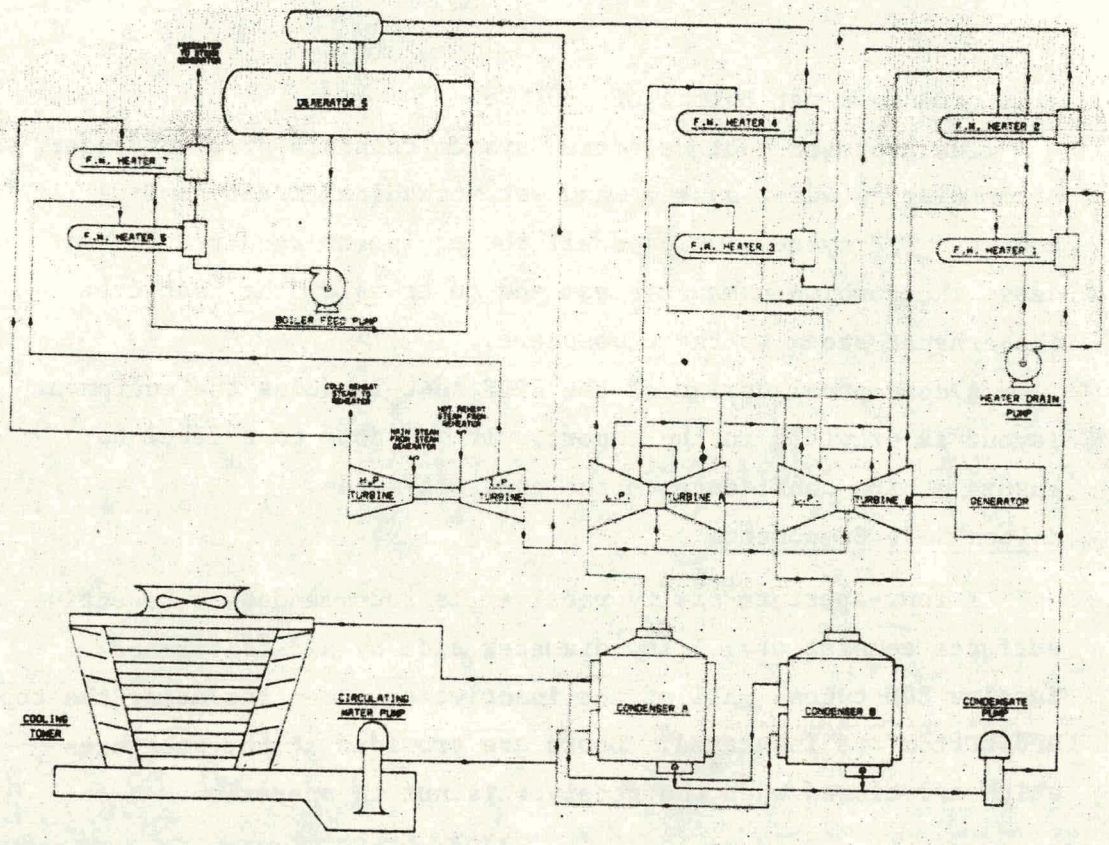


Figure II-4 Electric Power Generation Subsystem System Schematic

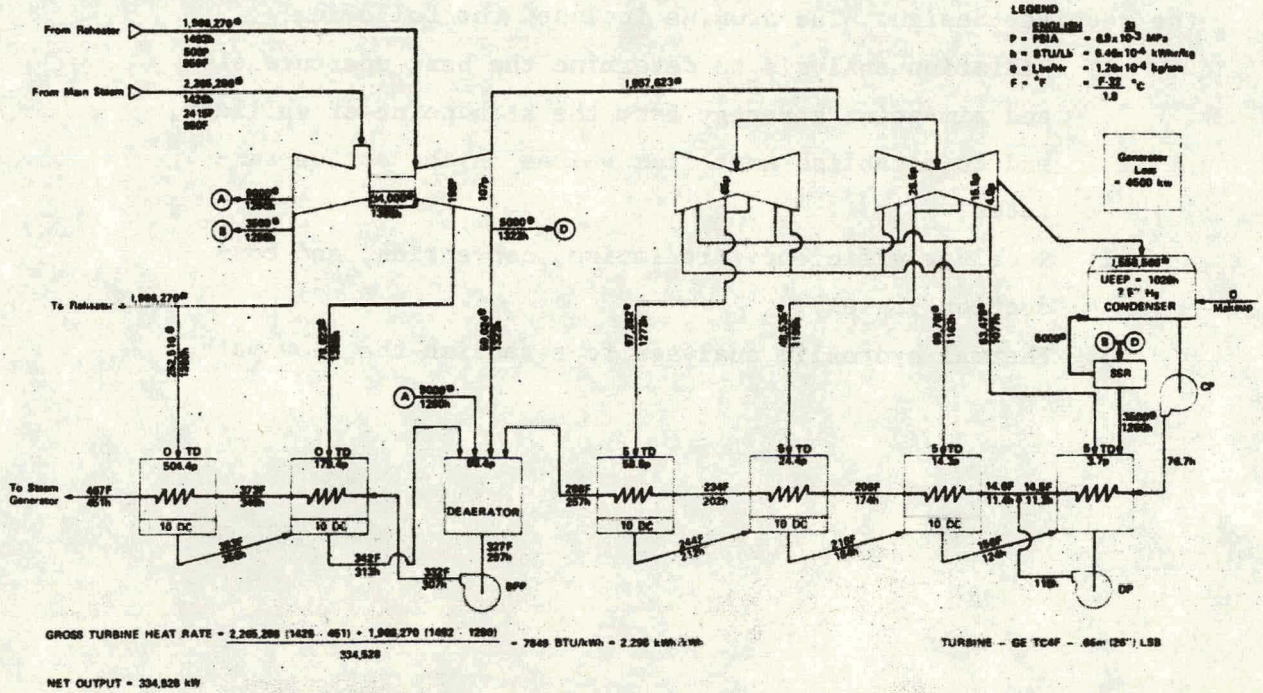


Figure II-5 Heat Balance for 300-MWe EPGS

will produce a net output of 300 MWe.

The proposed heat rejection system consists of a condenser, a circulating water system, and wet mechanical draft cooling towers. The system includes all the equipment required to condense the turbine exhaust steam and to transfer the heat from the exhaust steam to the atmosphere.

A conceptual design of the EPGS that includes the equipment layout is provided in the report. It was done to a level to ensure a high confidence in the cost estimates.

5. Molten-Salt Components

A four-aperture cavity receiver is recommended. The active surfaces consist of 1.5 in. diameter side by side blackened Incoloy 800 tubes. All of the inactive surfaces including the top and bottom are insulated. Doors are provided at the apertures which are closed when the receiver is not in operation.

A series of parametric studies were conducted to quantify the receiver design. The studies included the following:

1) Radiation analysis to determine the best aperture size and aim-point strategy from the standpoint of spillage, and to establish heat flux values on the active surfaces;
2) Receiver efficiency (radiation, convection, and conduction losses);
3) Thermal hydraulic analyses to establish the flow path,

pressure drop, heat transfer coefficients, and tube metal temperatures;

4) Receiver tube thermal stress analyses to determine tube life;

5) Mechanical design studies to establish the active surface configuration and method of support, enclosure configuration, and structure configuration.

6. Heat Exchangers

Heat exchangers required to transfer the heat from the molten salt to the water stream are shown schematically in Figure II-8. The exchangers consist of a superheater, reheater, two boilers, and two preheaters. The relatively low-pressure molten salt is on the shell side of the exchangers and the high-pressure water/steam is on the tube side. The hot molten salt at 836 K (1045°F) flows through the superheater and reheater in parallel and then through the two boilers in parallel followed by the two preheaters in series. Steam is produced out of the superheater at 16.5 MPag (2400 psig), 783 K (950°F), and at 3.45 MPag (500 psig), 783 K (950°F) from the reheater.

7. Pumps

The pumps that pump molten salt from the storage area to the base of the towers (circulating pumps) and the pumps that pump the salt up the towers (booster pumps) are conventional single-stage centrifugal pumps with mechanical seals. The pumps operate at 561 K (550°F). The hot molten salt pumps that operate at 838 K (1050°F) are conventional single-stage vertical cantilevered centrifugal pumps. No bearings or seals are exposed to the hot salt.

8. Piping

The recommended piping system uses a basic plant layout that allows thermal expansion of the piping within allowable stresses

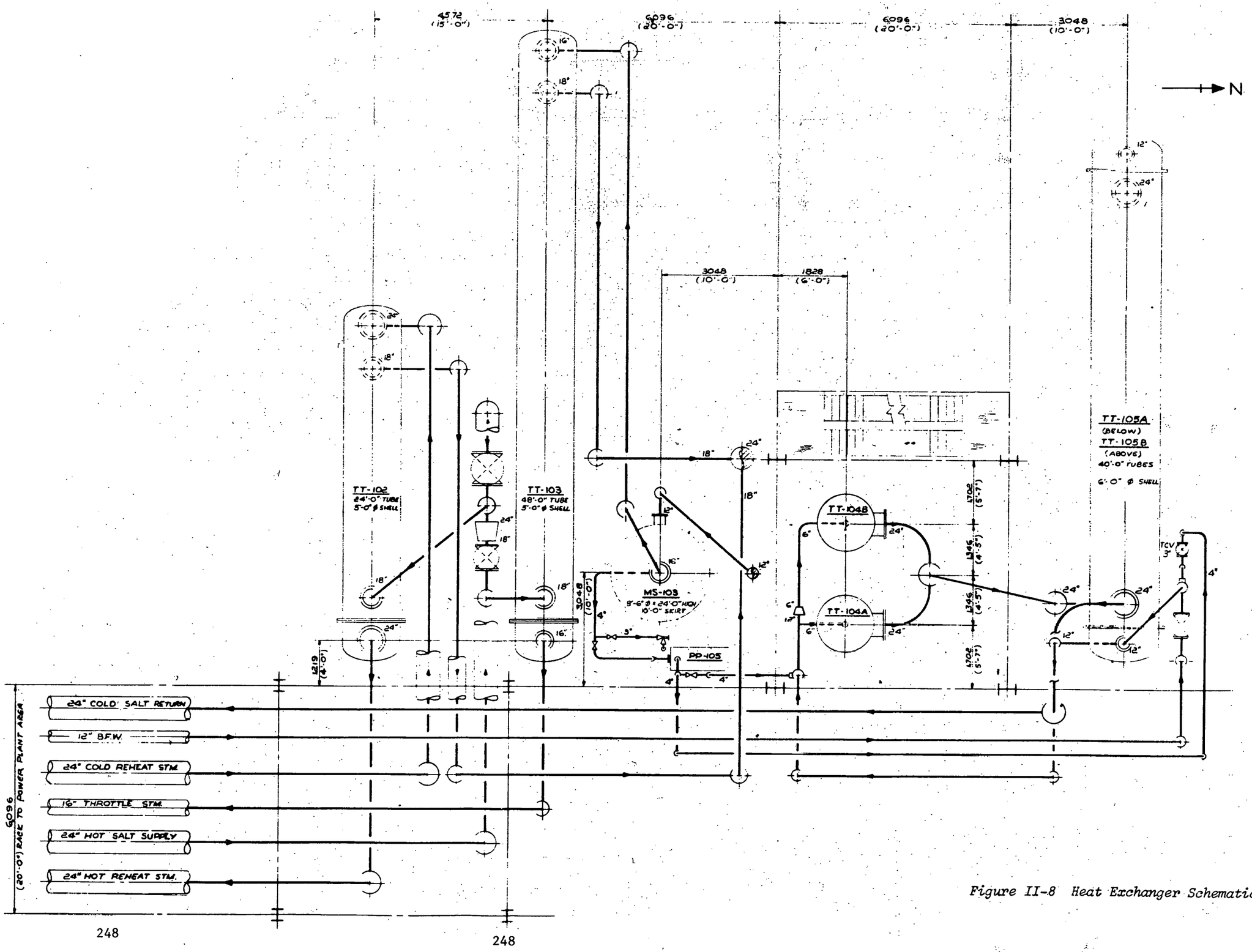


Figure II-8 Heat Exchanger Schematic

248

and a minimum number of expansion joints to minimize cost. Pipe sizes vary from 12- to 30-inch diameter. Incoloy 800 is used on the hot lines and carbon steel is used on the cold side. A detailed flow and stress analysis of the piping was done to prove feasibility of the concept.

9. Thermal Storage

Thermal energy is stored as sensible heat in four cylindrical flat-bottomed tanks, each of which is designed to operate as a thermocline. The tanks are 23.8 m (78 ft) in diameter and 26.8 m (88 ft) high. The API tanks are specially insulated on the inside to allow use of carbon steel and to minimize heat loss. Each storage tank is complete with its own cantilever type hot salt pump and sump. The storage tanks area is completely enclosed by a dike, designed to contain the total volume of working media in the event of an emergency.

Except for the concept of the internal insulation in the tanks, all the components of the storage subsystem use concepts and/or hardware consistent with existing and proven technology.

III. DEVELOPMENT SCHEDULE

The development schedule recommended for the program is given on Figure III-1. The Preliminary Design and SRE phase consists of the four SREs listed, a preliminary design of the critical module, and updating of the commercial plant. The phase is approximately 15-months long. It is assumed that the thermocline tank testing program will start at the beginning of FY 1979 because the tank's development data is needed to complete the preliminary design of the storage tanks. The long-term loop extends beyond the preliminary design phase. Because the data from this test is primarily long-life verification, it is not necessary to complete the testing before completion of the preliminary design. The Critical Module program would start in midfiscal 1980 and continue for a three-year period that includes a six-month engineering test period. The build of the Barstow heliostats is shown for reference.

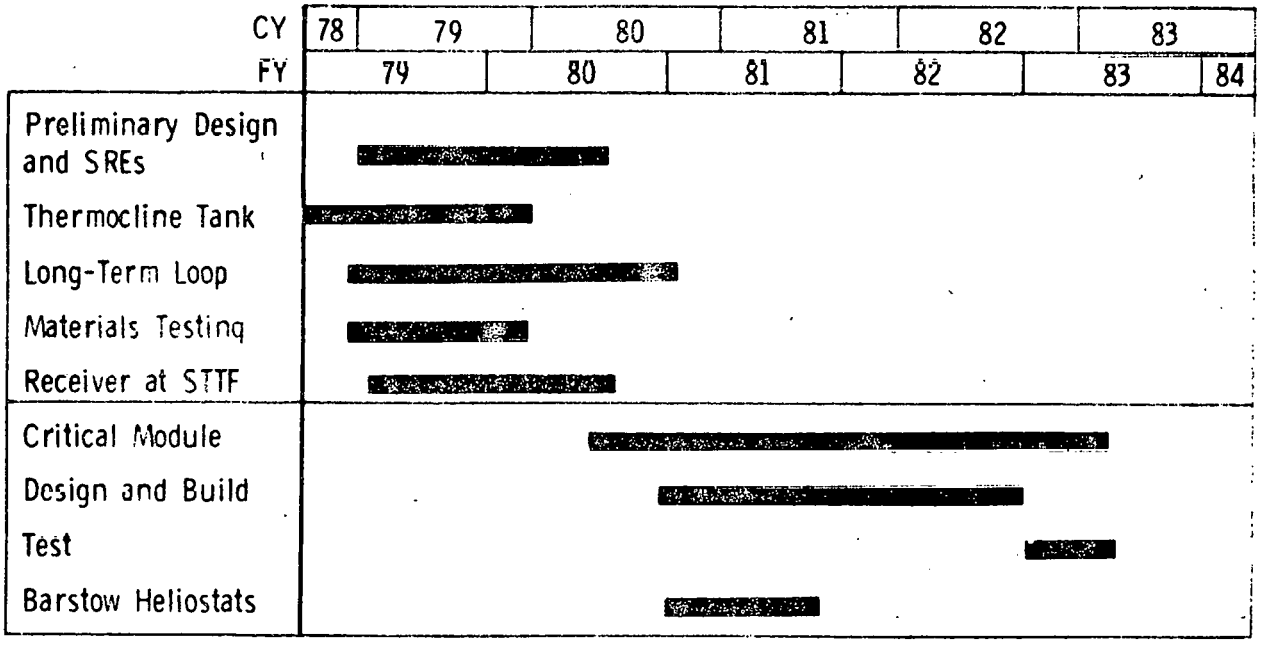


Figure III-1 *Critical Module Development Schedule*

IV. RECOMMENDED MATERIALS TEST AND DEVELOPMENT

The following materials test and development is recommended in support of the program:

1) Determine the thermophysical properties of the salt over the complete range of operating conditions. The properties required include:
   a) Thermal conductivity (both liquid and solid),
   b) Viscosity vs temperature,
   c) Density vs temperature,
   d) Specific heat.

   We have reasonably good estimates of the properties from the literature and testing done at Martin Marietta. However, this is the first application of this fluid to a closed loop heat transfer system. Therefore, it is important to know the thermophysical properties accurately with a high degree of confidence.

2) Determine the thermochemical properties of the molten salt.
   a) Determine the equilibrium constants of the molten salt as a function of temperature,
   b) Determine the "stability" as a function of temperature,
   c) Investigate the effects of trace impurities on the chemical behavior of the molten salt.

   Work done at Martin Marietta shows that the salt is stable up to at least 1100°F. However, a more detailed understanding of the chemistry is important to the long term successful operation of the system.

3) Long term material compatibility testing.
   a) Long term material compatibility testing of Incoloy 800 and 316 and 316L should be done with controlled amounts of trace impurities at temperatures up to 1150°F. Stress corrosion tests should be conducted. Weld samples including the use of fillers should also be tested.

b) Carbon steel should be tested up to at least 750°F including the tests indicated in (a) above.

Preliminary feasibility testing done at Martin Marietta show a high probability of success for the materials tests suggested. Also, additional work will be done in Phase II if the molten salt system is selected. Therefore, materials compatibility test work should be coordinated with Martin Marietta and Sandia Labs.

4) Internal Insulation

Internal insulation has the potential to substantially reduce the cost of thermal storage because relatively thin-walled carbon steel tanks can be used instead of thick-walled stainless tanks. The potential material problems are:

a) Long term high temperature (1100°F) compatibility with molten salt,

b) Thermal performance of the insulation in molten salt. Particularly the effects of natural convection in the insulation.

This work is presently being pursued by Martin Marietta and Sandia Labs. However, it is probable that more basic materials work in this area would be helpful.

5) Creep/Fatigue of Receiver Tubes

Basic testing is presently in progress at Argonne Labs. It is important that this work continue particularly using 316, 316L and Incoloy 800.

6) Fluid Loop Testing

Constant temperature (1000°F) fluid loop testing was done at Martin Marietta for about 2000 hours. These tests showed no effects of erosion and verified the receiver tube heat transfer coefficients. If a molten salt system is selected for Phase II we plan to modify the loop so that it operates over the complete temperature range and contains the system

materials at the low and high temperature ends. The primary objective of these tests is to determine if there is any significant mass transport problems. Also, Sandia Labs is conducting small natural convection loop testing.

ALTERNATIVE CENTRAL RECEIVER POWER SYSTEM USING MOLTEN SALT AS THE HEAT TRANSFER AND STORAGE MEDIUM

Viewgraphs Presented

by

Tom Tracey

Martin Marietta Corporation

Denver, Colorado

PROGRAM OBJECTIVES

Primary

- Develop a system which is capable of producing electricity at a cost that is substantially less than the first generation system.

Secondary

- Provide higher capacity displacement when operating in a utility grid.
- Greater market penetration.
- Potential for future improvements.
- Reduced environmental impact.

SYSTEM SCHEMATIC

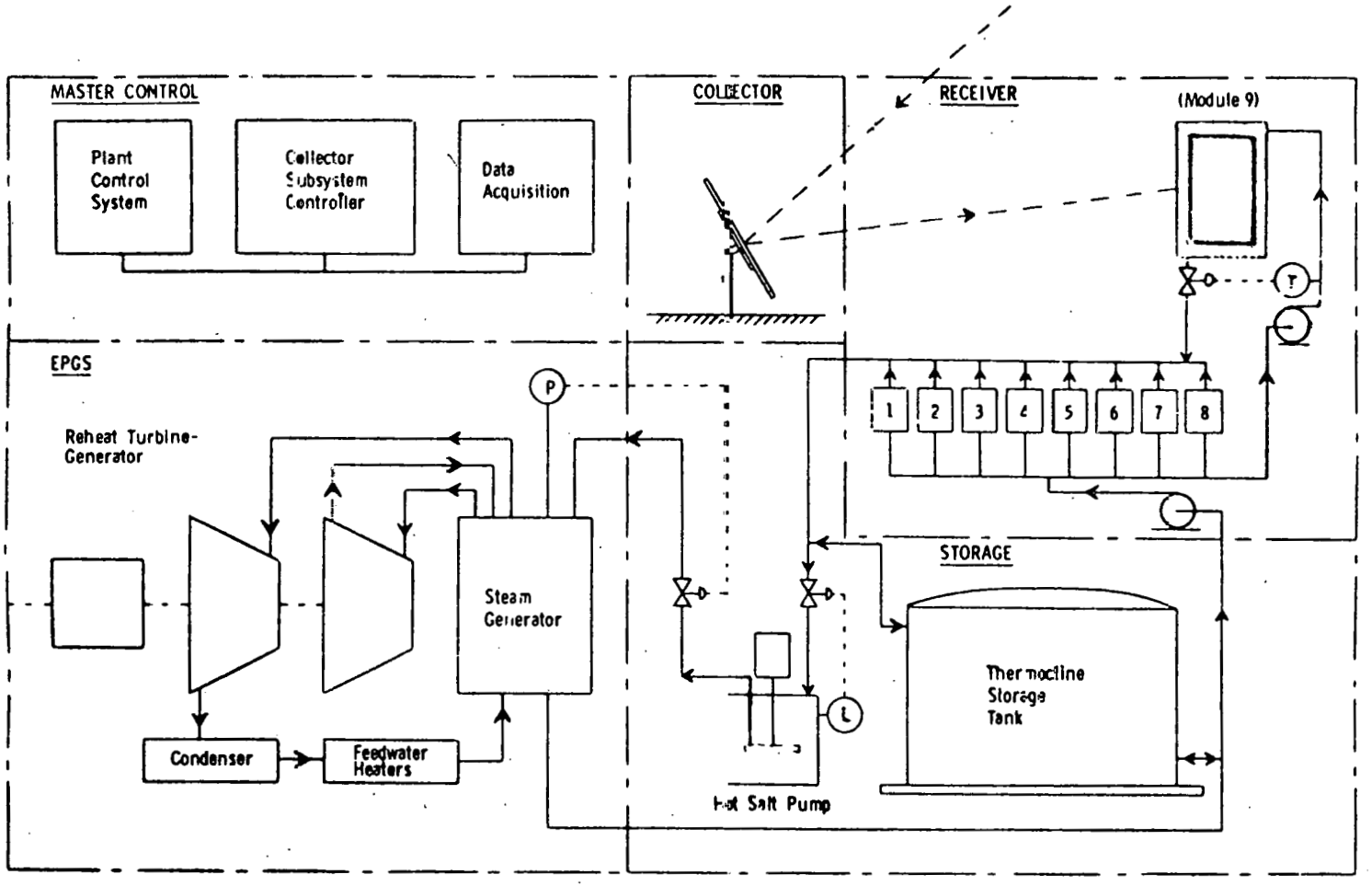
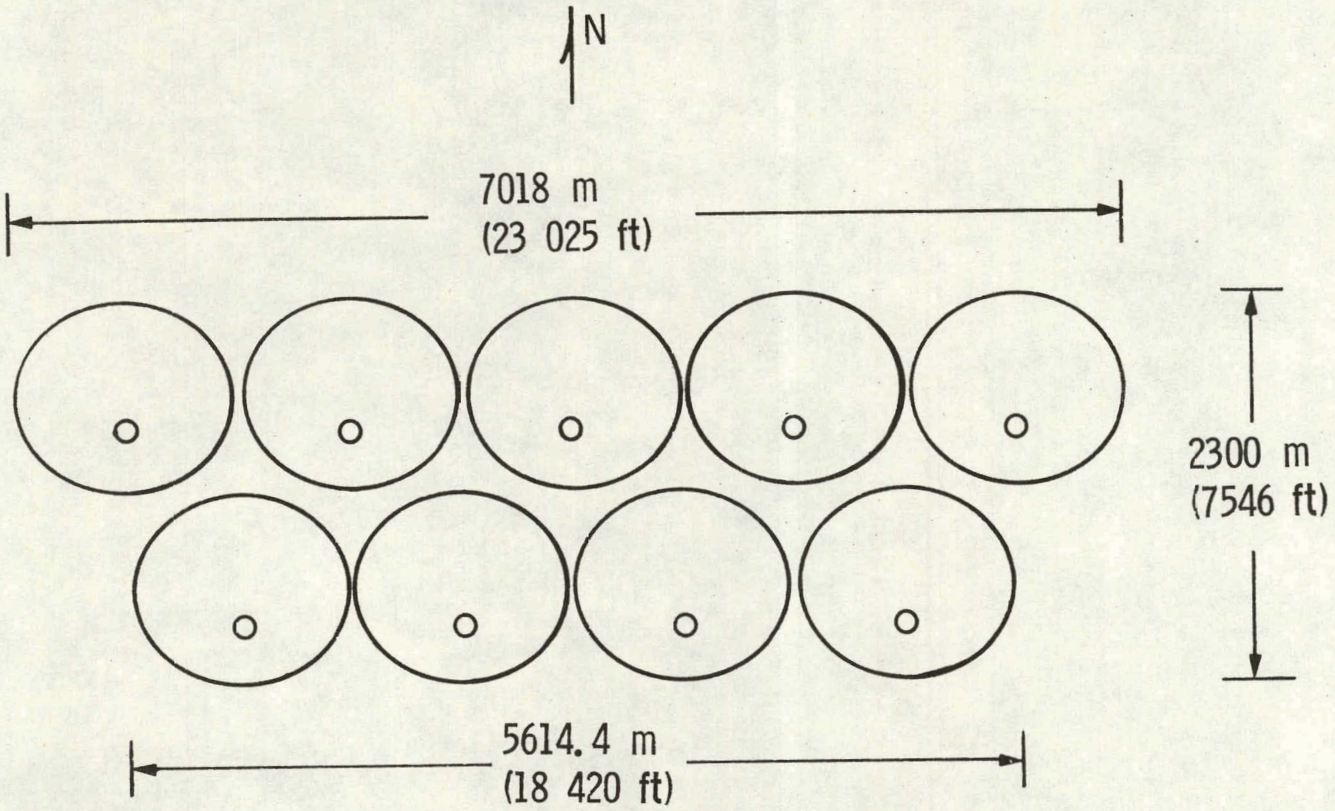
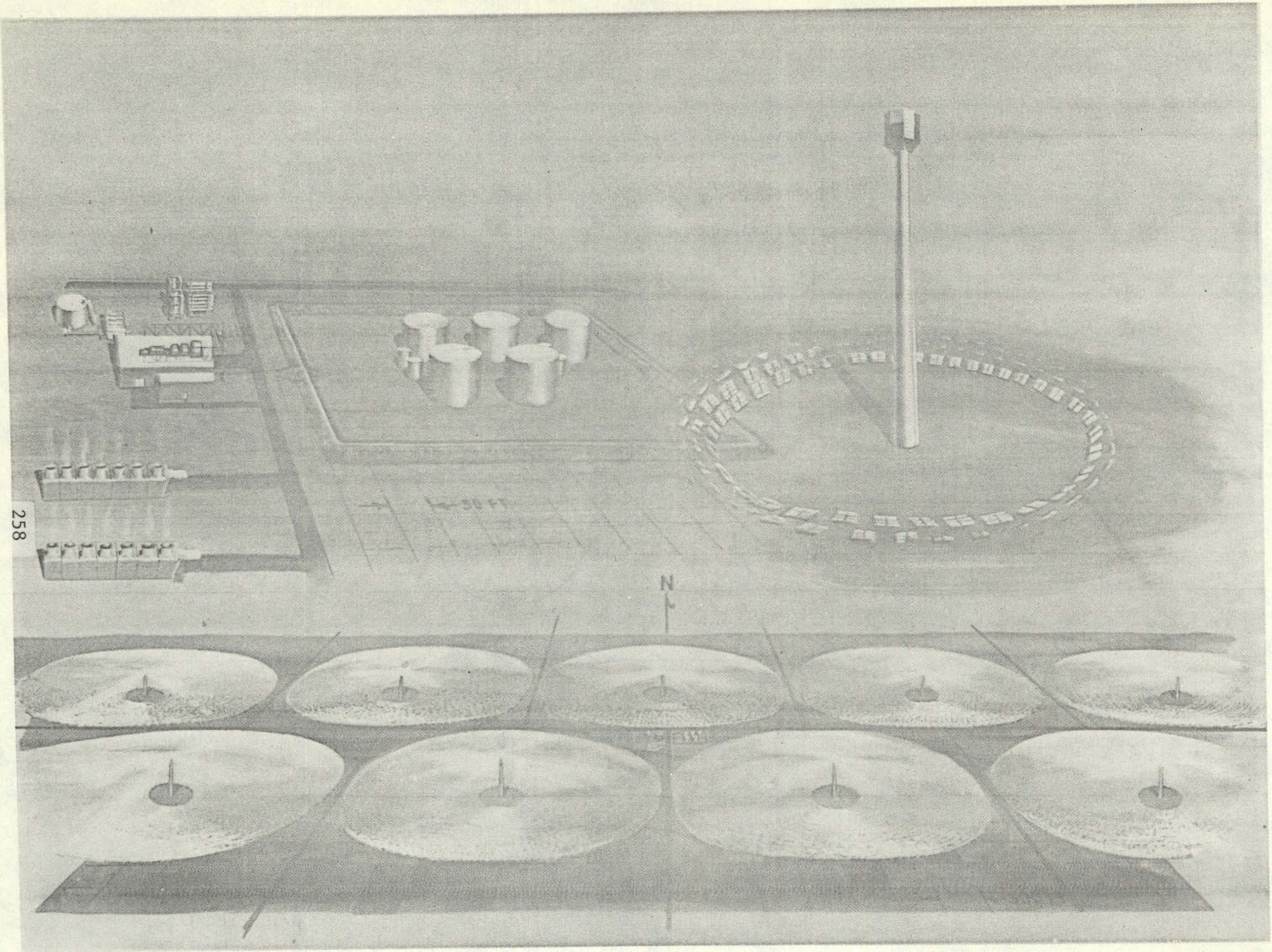


Figure 3

MARTIN MARIETTA

FIELD LAYOUT




N

PREFERRED CONFIGURATION

PLANT SIZE	- 300 MWe
STORAGE SIZE	- 24 HOUR OPERATION AT FULL LOAD ON 21 JUNE (11 HR STORAGE)
FIELD CONFIGURATION	- SURROUNDING FIELD - 7711 HELIOSTATS PER FIELD (40 SQ. METER PER HELIOSTAT)
PLANT CONFIGURATION	- 9 MODULES
RECEIVER TYPE	- FOUR APERTURE CAVITY
CONVERSION CYCLE	- WATER/STEAM RANKINE 783°K (950°F) 16,500 KPa (2400 psig) 783°K (950°F) REHEAT
STORAGE TANK TYPE	- SENSIBLE HEAT - THERMOCLINE TANK - SALT TEMPERATURE 561°K (550°F) TO 839°K (1050°F)
TOWER HEIGHT	- 166.4 m (546 ft) TO CENTERLINE OF APERTURE

PREFERRED SYSTEM PERFORMANCE (1976 BARSTOW TAPE)

Overall System Efficiency	= $\frac{\text{Net Output Electrical Power (MWHe)}}{\text{Heliostat Area x 1976 Barstow Insolation}}$	= 23.0%
EPGS Conversion Efficiency	Gross	43.9%
	Net	41.0%
Annual Plant Output	=	1.710×10^6 MWHe

MARTIN MARIETTA

BUSBAR ELECTRICITY COST

	Heliostat Cost - $/m^2 ($/ft^2)	
	$75.35/m^2 ($7/ft^2)	$107.64/m^2 ($10/ft^2)
Cost of Electricity (mils/KWh$_e$)		
- Cost of Money 7.5%	28.0	34.6
- Cost of Money 11%	38.4	47.2

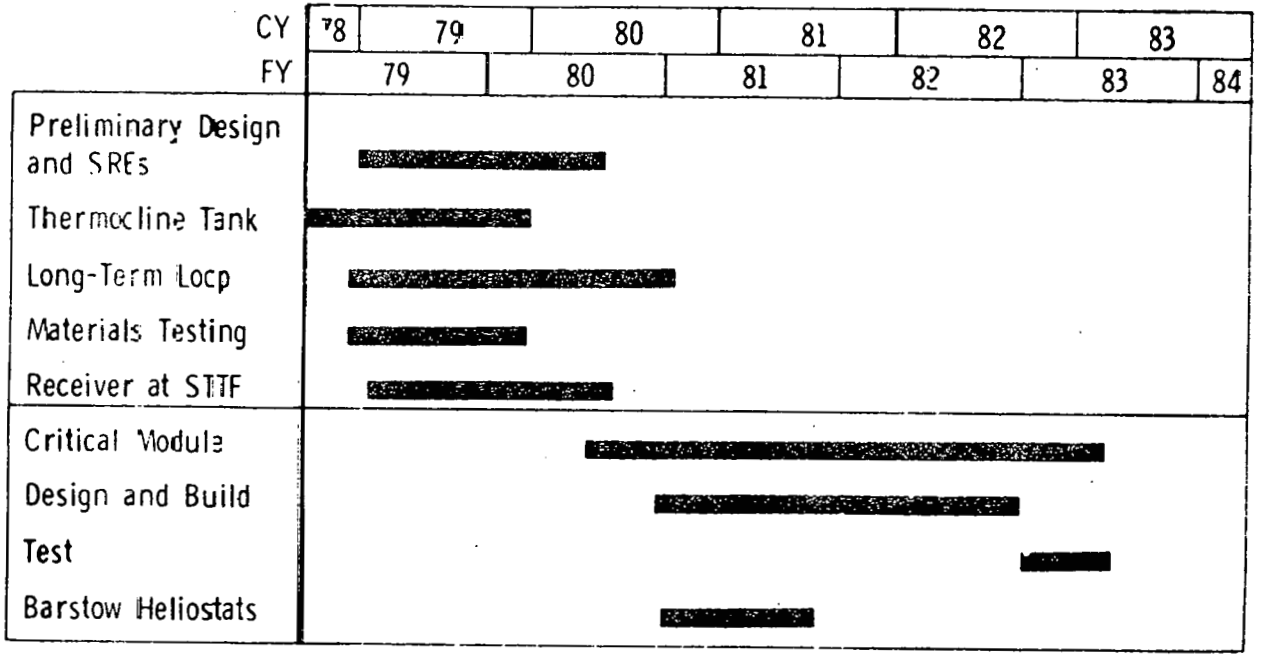
COST OF STORAGE

Thermal Storage ($/KWh$_{th}$)	-	3.40
Converted to Electricity ($/KWh$_e$)	-	8.20

RECOMMENDED PHASE II SMALL RESEARCH EXPERIMENTS (SREs)

- RECEIVER TEST AT STTF
- STATIC MATERIALS COMPATIBILITY TESTING
- LONG TERM FLUID LOOP
- SMALL SCALE INTERNALLY INSULATED STORAGE TANK TEST

CRITICAL MODULE DEVELOPMENT SCHEDULE



MARTIN MARIETTA

MATERIALS TEST STATUS

- Long Term Molten Salt Stability
  - Over 6000 hours of testing at 1100^{0}F shows negligible decomposition.
- Basic Molten Salt Chemistry
  - Measured equilibrium constants as a function of temperature and salt composition.
- Materials Compatibility
  - Incoloy 800 and 316 stainless steel useable to 1100^{0}F.
  - Carbon steel acceptable up to at least 750^{0}F.
- Fluid Loop Testing
  - Heat transfer coefficients verified for one-sided heating at design fluid velocity.
  - Receiver tube thermally cycles 10,000 times with no adverse effects.

THIS PAGE

WAS INTENTIONALLY

LEFT BLANK

MOLTEN SALT COMPATIBILITY

by

J. H. DeVan

Oak Ridge National Laboratory

Oak Ridge, Tennessee

MOLTEN SALT COMPATIBILITY

This summary is concerned with the chemical and physical properties of molten salt mixtures as they apply to the use of molten salts for thermal energy storage and transport. In current solar central receiver concepts, solar energy is concentrated and collected at a central tower and is transported as heat or kinetic energy to ground-based power generation equipment. To extend the power generating capability beyond diurnal hours, thermal energy is also stored during the day and fed back at night. Molten salts have application both as the heat transport medium conducting thermal energy from the receiver and also for thermal energy storage.

In the context of central receiver requirements, the term "molten salt" categorizes virtually any system of inorganic salts with melting points in the range from room temperature to the highest temperature of modern steam plants, approximately 570°C. This broad classification includes so many disparate chemical compounds that a cohesive treatment of the distinctive properties of relevant salt families would exceed the intended scope of this summary paper. For this reason, we will address the few generalizations that apply to the use of molten salts in power generation systems, but we will draw on background information from two specific salt systems in defining development program requirements.

General Considerations

Engineering criteria for the selection of salt systems for central receiver applications are not well established at this time. For example, questions of melting point, heat exchanger wall thicknesses, salt cost and availability can be addressed only qualitatively. Sensitivity analyses that treat these parameters in the context of their impact on capital and operating costs, so far as this writer is aware, remain to be accomplished. However, the following criteria[1] were used as guidelines in selecting salt systems for subsequent corrosion discussions, as well as to identify systems that do not appear applicable.

Freezing Point

In selecting molten salts for transferring sensible heat from the solar receiver to power generation equipment, freezing point becomes a seminal requirement. Any freezing point below 330°C would probably accommodate the feedwater temperature of conventional steam cycles.[2] Higher coolant freezing points could be tolerated, but with substantially higher cost and efficiency penalties.

The same temperature considerations hold for the selection of salts for sensible heat storage. However, salts which store thermal energy as latent heat (i.e., by melting and freezing) must meet a very different set of temperature requirements. For the latter salts, the freezing point is matched to the maximum evaporator and superheater temperature in the steam circuit and may be as high as 600°C.

Heat Transport and Fluid Transport Properties

For any coolant, there are important physical property requirements that are tied to the design of practical and economical heat transfer systems. These properties include high thermal conductivity and heat capacity, and low viscosity; such properties imply high heat-transfer coefficients and low pumping power requirements. Molten salts characteristically have much lower thermal conductivities but higher heat capacities than liquid metals. Viscosities of many molten salt systems are sufficiently high to seriously affect pumping power.

Vapor Pressure and Composition

One of the major attractions of molten salts is their potential for permitting relatively low system pressures. Vapor pressures over one atmosphere could be accommodated but would complicate engineering designs. Even pressures of 0.01 to 1 atmosphere will require recovery of coolant vapor from a cover or sweep gas to prevent coolant depletion. Such pressures also imply the formation or a solid from vapor in cooler regions with restrictions in vent lines, erosion of pump shafts and seals, etc.

Chemical Reactions

Leaks must be presumed to occur during the 30-year life of an operating power plant. Such leaks can put the coolant in contact with thermal storage salts, air, or steam. In each case, the resulting chemical reaction must not lead to destruction of structural components or permanently degrade the integrity of the system. Thus, leakage between the coolant and steam systems should not lead to an unacceptably high heat release or extensive metal corrosion in either the coolant loop or steam system. Even ppb quantities of chloride ions in water can lead to stress-corrosion cracking of 300-series steels, and the prospects of a steam leak would rule out the use of such alloys for chloride salt and steam containment.

Corrosion

The rate of corrosion of any thermal storage or heat transfer medium must be consistent with a 30-year plant lifetime. Molten salts which, because of predictably high corrosion rates, would lead to rapid failures

and replacement of plant components are obviously unacceptable. In essence, corrosion considerations amount to a comparison of the coolant cost and associated heat-transfer/fluid property benefits with the required metal thickness and composition to withstand corrosion. Such comparisons also must take into account the maintenance costs needed to control fouling and plugging of coolant passages resulting from corrosion product deposition.

In the absence of the cost-benefit studies discussed above, and without some guidelines as to classes of containment materials that are reasonable for solar thermal power stress and temperature conditions, one obviously can not treat corrosion behavior as a rigid index in the selection of viable salt candidates. Nevertheless, there are certainly some salt systems whose corrosiveness must be regarded as unacceptable, barring some major breakthrough in containment approach. Such salts as sulfates, sulfides, chlorates, and phosphates can reasonably be eliminated on this basis. Those salt systems for which a containment approach has been demonstrated in practice or can be argued theoretically include certain of the nitrates, chlorides, fluorides, bromides, carbonates, and hydroxides. Properties of typical salts from each of these chemical classes are compared in Table 1.

Among the latter classes, a considerable amount of corrosion data exist on the alkali metal and alkaline earth fluorides at temperatures up to 800°C. In most cases the systems studied have melting points higher than that desired for coolant applications (~330°C); however, they are among the most stable of all chemical compounds and consequently are relatively inert to most high temperature alloys. Nitrate, or more precisely, nitrate-nitrite salt mixtures have been widely used for industrial coolant applications, although the service temperatures have generally been below those required for modern utility steam supply systems. Information is lacking as to the chemical stability and corrosivity of these mixtures above 500°C, but the mixtures are attractive in terms of cost, freezing point, and fluid properties. Hydroxides have not been evaluated in detail for coolant applications, but the corrosion information available raises considerable doubt that they could be contained for long periods above 500°C using conventional alloys. The corrosion properties of carbonate salts are essentially unknown at present, at least over the temperature range of interest to utility boilers. Likewise, little information exists for chloride salts, although the mechanisms of corrosion are basically similar to those of fluoride salts.

Design Concerns

In addressing reliability questions and potential failure modes of molten salt heat transfer systems, the key concern must be the long-term corrosion effect of the salt on containment materials under controlled operating conditions. This concern includes questions of localized and stress-assisted attack as well as general corrosion. Moreover, the thermal conductivities of molten salts are sufficiently high that purely mechanical failures can be induced by thermal stresses in heat exchanger walls and mixing tees. Another

Table 1. Representative Molten Salts for Potential Solar Thermal Applications.

Salt system	Typical composition (mole %)	Melting point (°C)	Properties at 538°C (1000°F)		
			Viscosity (mPa·s)	Thermal conductivity (W/m·K)	Heat capacity (J/g·K)
$NaBF_4$-NaF	92-8	385	1.39	0.46	1.51
LiF-KF-NaF	46-42-12	455	6.84	1.30	1.85
NaF-KF-ZrF_4	10-48-42	385	9.40	1.00	1.05
LiCl-KCl	59-41	360	1.95	0.84	1.26
NaCl-$AlCl_3$	50-50	151	—	—	—
KCl-NaCl-$MgCl_2$	13-15-72	385	—	—	—
$NaNO_3$-$NaNO_2$-KNO_3	7-48-45	142	0.43	0.33	1.56
Li_2CO_3-Na_2CO_3-K_2CO_3	44-32-25	397	7.55	0.35	1.73
NaOH	100	318	1.57	1.05	2.12

important cause of mechanical failure results from the unscheduled freezing of salts in pipes and the large volume expansion associated with the solid-to-liquid phase change. Also, we have already pointed out the concern for accelerated corrosion produced by leakage between the salt and air or steam.

In any heat transfer circuit at high temperature, corrosion under normal service conditions is complicated by the temperature change occurring in the coolant, which gives rise to thermal gradient mass transfer. Because the kinetics of corrosion reactions tend to increase with temperature, corrosion products enter the circulating salt faster in the higher temperature parts of the circuit than at lower temperatures, and in effect there is a net flow of corrosion products from the hotter surfaces in the circuit to the colder. This process of mass transfer prevents the metal walls of the circuit from achieving passivity with the coolant, and corrosion characteristically shows linear or parabolic time dependence for the life of the system. Deposition of corrosion products in the cold leg is an adjunct problem which leads to fouling of heat transfer surfaces and tube plugging.

At the operating temperatures of modern utility steam supply systems (~570°C), corrosion of conventional engineering alloys will generally occur as selective leaching of the more reactive alloying components. If the diffusion rates of the affected component in the alloy are relatively fast, this selective leaching can produce microstructural and chemical changes within the alloy that degrade its load carrying ability far beyond the reduction attributable to wall thinning, per se.

Corrosion Mechanisms

Probably the best understood of all salt systems from a corrosion standpoint are solutions of alkali metal and reactive metal fluorides (e.g., NaF-LiF-KF, LiF-BeF_2, NaF-ZrF_4). These systems are comprised of some of the most stable salt compounds in nature and are relatively non-reactive toward most engineering materials. Corrosive attack stems largely from impurities carried in the salts, such as HF and NiF_2. The corrosion products formed by reaction with these impurities are soluble in the fluoride melt;[5] hence the rate of oxidation of a given alloy component is a function of (1) the free energy of the reaction between the component and impurities in the melt and (2) the diffusion rate of the component in the alloy. For a given fluoride ion potential in the melt, the relative nobility of potential alloying elements against fluoride salts increases in the order: aluminum (least noble) titanium, chromium, iron, nickel, molybdenum, tungsten (most noble). When conventional Ni-Fe-Cr alloys are exposed to chemically-stable fluoride salts with modest impurity levels, attack is selective toward chromium. Attack can be controlled by substituting a more noble element for chromium in the alloy, as was done in the development of Hastelloy N (17% Mo, 5% Fe, 7% Cr, bal Ni), designed specifically for fluoride salt containment. Alternatively, the fluoride ion potential of the melt can be lowered by buffering it with a reactive metal or a suitable redox couple, such as Ce^{+3}/Ce^{+4}. For example, by buffering with metallic beryllium, we were able to adjust the redox potential in a 316 thermal convection loop circulating Li_2BeF_4 to a point where the corrosion loss after 1000 h at 650°C was below our detectable weighing limit.[3] Over a period of 20,000 hours, with no further beryllium addition, the corrosion rate at 650°C has remained below 15 μm/year.

The latter approach should be applicable to chlorides as well as fluorides, but will be workable only in case of salt mixtures whose components are sufficiently stable to permit the imposition of highly reducing conditions. Such mixtures, whether fluorides or chlorides, tend to have melting points higher than desired for coolant applications. Thus, the approach for containing the lower melting, less stable, fluoride and chloride mixtures appears restricted to the development of more noble container materials (such as Hastelloy N).

From the standpoint of melting point and relative cost, nitrate or nitrate-nitrite salt mixtures appear better suited to central receiver coolant applications than do fluoride or chloride salt mixtures. Unfortunately, there are not sufficient corrosion data above 500°C to allow an assessment of the chemical compatibility of the nitrate salts with engineering materials for utility steam applications. Below 450°C the salts have performed quite satisfactorily in heat transfer systems used by the chemical processing industry, although quantitative corrosion rate data again are essentially lacking. We have conducted limited studies at ORNL of the compatibility of the salt mixture $NaNO_3$-$NaNO_2$-KNO_3 with 316 stainless steel and Hastelloy N in a closed loop with flow induced by thermal convection.[4] The loop operating temperature was varied in accordance with the schedule shown in Table II. Below a maximum temperature of 500°C, 316 stainless steel specimens showed an initial rapid weight loss, but there was no further loss after 1000 h. At 500°C, the weight loss increased linearly with time over a 4500-h interval. Increasing the temperature to 550°C resulted in an average maximum corrosion rate of 130 μm/year measured over a 6000-h interval. In all cases the specimens were covered by a relatively thin, non-porous oxide layer.

Table II. Operating Conditions for HTS Loop

Time interval after loop startup (h)	Maximum temperature (°C)	Temperature difference (°C)
0–3,000	431	70
3,000–9,000	505	81
9,000–10,000	432	78
10,000–16,000	550	92

In addition to concerns for thermal gradient mass transfer of stainless steels in nitrate salts, the prerequisites exist, at least in part, for the stress corrosion cracking of these materials. Considering the wide variations that are possible in the starting purity of the salts and in the concentrations of corrosion products, it can be argued on electrochemical grounds that the condition of unstable passivity, classically associated with aqueous stress corrosion cracking, could be reproduced in nitrate melts under some set of temperature and alloying conditions. Experience with nitrate salts to date has mainly involved low alloy and plain carbon steels, so the behavior of more highly alloyed materials remains an open question.

Program Requirements

The Martin Marietta central receiver conceptual design incorporates draw salt ($NaNO_3$-KNO_3) as the primary heat transfer medium in both the receiver and thermal storage subsystems. As discussed above, the major concern in the qualification of these salts for the intended application is the need for quantitative corrosion information above 480°C. Specifically, data are required in the following areas.

1. The mass transfer effects associated with the temperature change (ΔT) along the coolant flow path. (What is the rate of corrosion product dissolution and deposition in the salt as a function of temperature, flow rate, and ΔT?)

2. The potential stress-corrosion cracking effects associated with salt purity, alloy microstructure, and stress/strain/time relationships.

3. The effects of heat flux and thermal transients on the mechanical stability of oxidation reaction layers formed on stainless steels in HTS.

4. The changes in alloy chemistry and microstructure that accrue from selective leaching and their effects on mechanical properties.

It is probable that designers will seek similar information on the corrosion properties of HTS salts. The latter incorporate nitrites as well as nitrates; they are higher melting and are more subject to disproportionation (nitrogen evolution) above 540°C.

Interest in other salt mixtures appears to be confined to thermal energy storage applications, an area which is currently the province of DOE's Division of Energy Storage Systems. An extensive background of information exists on the generic properties of fluoride salts, which can serve to establish program requirements if and when an interest in these salts develops. Except for the general similarity in the chemical nature of chloride and fluorides, salt mixtures other than fluorides represent basically unknown technologies in terms of corrosion properties and system reliability. Carbonate salts are being studied for fuel cell applications, but the operating temperatures and chemical conditions endemic to these applications are only marginally relevant to central receiver conditions.

The present state of knowledge concerning the corrosion properties of draw salt and impurity effects is too limited to assess the requirements and possibilities for *in situ* measuring techniques. At ORNL we have found voltammetry to be a convenient and effective tool for monitoring the nature of corrosion reactions and concentration of corrosion products in fluoride salts.[5] The voltammetry approach could also be extended to the calculation of instantaneous corrosion rates based on anodic and cathodic polorization behavior.

For salt systems where the corrosion rate relates directly to the electrochemical properties (redox potential) of the salt, the use of more conventional electrochemical cells for measuring redox potentials is certainly feasible. Considering the relatively low system pressure, such cells are readily adapted to molten salts but would require the development of stable high temperature reference electrodes.

References

1. A. D. Kelmers, *et al.*, *Evaluation of Alternate Secondary (Tertiary) Coolants for the Molten-Salt Breeder Reactor*, ORNL/TM-5325, April 1976, Oak Ridge National Laboratory.

2. R. C. Robertson (ed.), *Conceptual Design Study of a Single-Fluid Molten-Salt Breeder Reactor*, ORNL-4541, June 1971, Oak Ridge National Laboratory.

3. J. R. Keiser, J. H. DeVan, and D. L. Manning, *The Corrosion Resistance of Type 316 Stainless Steel to Li_2BeF_4*, ORNL/TM-5782, April 1977, Oak Ridge National Laboratory.

4. J. H. DeVan and J. R. Keiser, "Compatibility Studies of Type 316 Stainless Steel and Hastelloy N in KNO_3-$NaNO_2$-$NaNO_3$", *Alloy Development for Irradiation Performance, Quarterly Progress Report January–March 1978*, DOE/ET-0058/1, August 1978, U.S. Department of Energy.

5. D. L. Manning and Gleb Mamantov, "Recent Electroanalytical Studies in Molten Salts", *Characterization of Solutes in Nonaqueous Solvents*, (Mamantov, ed.) Plenum Publishing Corp., New York, 1978.

THIS PAGE

WAS INTENTIONALLY

LEFT BLANK

ROLE OF MATERIAL VARIABLES IN THE THERMAL STRESS FRACTURE OF BRITTLE MATERIALS

by

D. P. H. Hasselman

Virginia Polytechnic Institute And State University

Blacksburg, Virginia

ABSTRACT

An overview is given of the role of material properties in the thermal stress resistance of brittle materials. A total of twenty-seven non-redundant figures-of-merit are presented for the selection of materials with optimum thermal stress resistance for a variety of thermal environments, performance criteria and failure modes.

I. INTRODUCTION

Many engineering structures or components operating at non-uniform temperatures frequently are subjected to thermal stresses of high magnitude. These thermal stresses exist in addition to the other mechanical stresses as the result of normal operating conditions. It is easily demonstrated that temperature non-uniformities of only a few tens of degree C are sufficient to create stresses well in excess of the failure stress of the material of construction. Especially under transient conditions such as the heat-up or cool-down of a structure, the thermal stresses can exceed the normal operating (and failure) stresses by an order of magnitude or more. The ability to survive thermal stress failure may well be the principal factor in determining the successful development of new engineering systems such as ceramic turbines, MHD-channels and others.

Brittle materials, because of the absence of stress-relieving mechanisms such as plastic flow, are particularly vulnerable to thermal stress failure. In brittle materials thermal stress failure frequently occurs in an explosive, catastrophic manner, rendering the structure or component totally incapable of continued satisfactory performance.

The analysis of thermal stress and optimum material selection represents an essential part of the engineering design and construction of engineering systems operating at non-ambient temperatures. Thermal stress analysis represents an inter-, if not multi-disciplinary problem involving principles of heat transfer, mechanics and materials science and engineering. The variables to be considered include the nature and magnitude of heat transfer, geometric factors, material properties, nature of the stress state, failure modes and the nature of crack pro-

pagation. Other performance criteria imposed on the structure need be considered as well.

For complex geometries coupled with non-uniform heating or cooling conditions and/or material properties which are strongly dependent on temperature, numerical methods are preferable and perhaps the only feasible method for assessing the magnitude and distribution of the thermal stresses.

For the development of guidelines for the selection of materials with optimum thermal stress resistance, the analytical approach is preferred, since it results in algebraic expressions in which the relative role of each individual material property in determining the magnitude of thermal stress is clearly identified. In general, the analytical approach requires simplifying assumptions, such as linear heat transfer and thermo-elastic behavior and temperature-independent material properties.

An analytical assessment of the optimum material to resist thermal stress failure requires a definition of the heat transfer environment as well as the geometry of the structure or component. Temperature distributions and resulting thermal stresses can then be derived. By defining the failure criterion, expressions can be derived for the maximum heat flux or temperature difference, etc, to which the material can be subjected without failure. These expressions permit the derivation of "thermal stress figures-of-merit" or "parameters" which form the basis for the material selection for a given thermal environment, performance criterion and/or failure mode.

The purpose of this paper is to present a summary of the currently available non-redundant literature equations for the maximum thermal conditions to which a materials can be subjected together with the

appropriate thermal stress resistance parameters. Since the choice of the optimum material is not affected by geometry, only one equation for a given thermal environment and performance criterion is presented. Furthermore, in order to keep the number of equations and parameters to a manageable total, factors containing Poisson's ratio such as $(1-\nu)$, $(1-2\nu)$, $(1+\nu)$ will be considered as part of the geometric term, to be combined in a single equation. For details of the underlying assumptions and boundary conditions for the equations to be presented, the reader is referred to the cited literature. This paper, with the exception of slight modifications, is identical to one[1] written by the present writer to be published shortly. Whenever possible, symbols used are those recommended by the American Ceramic Society.[2]

II. Equations and Figures-of-Merit

A. Steady-State Heat Flow

a. Circular hollow cylinder; radial heat flow, ΔT_{max} across wall[3,4]:

$$\Delta T_{max} = S_t(1-\nu)C/\alpha E \tag{1a}$$

Figure-of-merit:

$$R = S_t(1-\nu)/\alpha E \tag{1b}$$

b. In terms of maximum heat flow, Q_{max}, eq. 1a becomes:

$$Q_{max} = S_t(1-\nu)KC'/\alpha E \tag{2a}$$

Figure-of-merit:

$$R' = S_t(1-\nu)K/\alpha E \tag{2b}$$

c. Circular hollow cylinder, radial heat flow: Stress relaxation by linear creep. Maximum rate of temperature change[5]:

$$\dot{\Delta T}_{max} = S_t(1-\nu)C/\alpha\eta \tag{3a}$$

Figure-of-merit:

$$R_{cr} = S_t(1-\nu)/\alpha\eta \tag{3b}$$

d. In terms of maximum rate of change of heat flow, eq. 3a becomes[5]:

$$\dot{Q}_{max} = S_t(1-\nu)CK/\alpha\eta \tag{4a}$$

Figure-of-merit:

$$R'_{cr} = S_t(1-\nu)K/\alpha\eta \tag{4b}$$

e. Linear heat flow around spherical cavity. Maximum temperature gradient[6] can be derived to be:

$$\nabla_{max} = 2S_t(1-\nu)/\alpha Eb \tag{5a}$$

Figure-of-merit:

$$R = S_t(1-\nu)/\alpha E \tag{5b}$$

f. Eq. 5a in terms of maximum heat flow becomes:

$$Q_{max} = 2S_t(1-\nu)K/\alpha Eb \tag{6a}$$

Figure-of-merit:

$$R' = S_t(1-\nu)K/\alpha E \tag{6b}$$

From other solutions[7] figures-of-merit can be obtained for inclusions other than pores.

B. Internal Heat Generation

g. For solid circular rod with uniform internal heat generation (H), the maximum rate of heat generation is[8]:

$$H_{max} = 8S_t(1-\nu)K/\alpha Eb^2 \tag{7a}$$

Figure-of-merit:

$$R' = S_t(1-\nu)k/\alpha E \tag{7b}$$

C. Transient Heat Transfer

h. Flat plate; Linear rate of increase of surface temperature. Maximum rate of increase[9]:

$$\dot{T}_{max} = 3S_t(1-\nu)a/\alpha Eb^2 \tag{8a}$$

Figure-of-Merit:

$$R'' = S_t(1-\nu)a/\alpha E \tag{8b}$$

i. Convective (Newtonian) heat transfer. Spherical body subjected to heating and cooling over temperature range ΔT[10].

$$\Delta T_{max} = \frac{2.5\ S_t\ (1-\nu)}{\alpha E}\{1 + 2/\beta\} \quad \beta = bh/K \tag{9}$$

For severe heat transfer, $\beta \to \infty$

$$\Delta T_{max} = 2.5\ S_t(1-\nu)/\alpha E \tag{10a}$$

Figure-of-Merit:

$$R = S_t(1-\nu)/\alpha E \tag{10b}$$

For mild heat transfer, $\beta << 1$

$$\Delta T_{max} = 5S_t(1-\nu)K/\alpha Ebh \tag{11a}$$

Figure-of-merit:

$$R' = S_t(1-\nu)K/\alpha E \tag{11b}$$

j. Radiation heat transfer. Spherical body at low initial temperature and wavelength independent emissivity. Instantaneously uniformly subjected to black-body radiation. Maximum radiation temperature[11]:

$$T_{max} = \{5S_t(1-\nu)K/\rho b\alpha E\varepsilon\}^{1/4} \tag{12a}$$

Figure-of-merit:

$$R_{rad} = \{ S_t(1-\nu)K/\alpha E\varepsilon\}^{1/4} \tag{12b}$$

k. Radiation heat transfer. If body transparent to radiation at wavelength, $\lambda < \lambda_o$ eq. 12a becomes[12]:

$$T_{max} = \{5S_t(1-\nu)K/\rho b(1-\bar{F}_{\lambda o})\alpha E\varepsilon\}^{1/4} \tag{13a}$$

Figure-of-merit:

$$R_{trans} = \{S_t(1-\nu)K/(1-\bar{F}_{\lambda o})\alpha E\varepsilon\}^{1/4} \tag{13b}$$

l. Transient heat transfer with inertial effects. Rod of length L, freely suspended. Rod is very rapidly exposed to uniform temperature increase ΔT in time period, t_o. Compressive stresses will occur because of finite time required for expansion to take place.[13]

The maximum temperature increase of the rod, without compressive failure can be derived to be:

$$\Delta T_{max} = S_c/\alpha E \quad \text{for} \quad t_o \leq t_m \tag{14a}$$

Figure-of-merit:

$$R_{in} = S_c/\alpha E \tag{14b}$$

and

$$\Delta T_{max} = S_c c\ t_o/\alpha EL \quad \text{for} \quad t_o \geq t_m \tag{15a}$$

Figure-of-merit:

$$R'_{in} = S_c c t_o/\alpha E \tag{15b}$$

m. Transient heat transfer. Time-to-failure. Sphere. Surface temperature raised instantaneously by temperature difference, ΔT. Time to maximum stress[14]:

$$t^* = 0.0574\ b^2/a \tag{16a}$$

Figure-of-merit:

$$R_t = a^{-1} \tag{16b}$$

D. Thermal Buckling

n. Straight column prevented from expanding against rigid constraint. Heated by temperature difference ΔT. Critical temperature difference required for column instability[15]:

$$\Delta T_c = \pi^2 I/L^2 A\alpha \tag{17a}$$

Figure-of-merit:

$$R_{1b} = \alpha^{-1} \tag{17b}$$

o. Post-thermal buckling of straight column. Originally straight column prevented from expanding against rigid constraints, heated over temperature difference, $\Delta T > \Delta T_c$, to be subjected to bending in post-thermal buckling.

Maximum temperature difference required for failure of square column as the result of tensile bending stresses[16]:

$$\Delta T_{max} = \pi^2 d^2/12L^2\alpha + S_t^2 L^2/\pi^2 \alpha E^2 d^2 \qquad (18a)$$

Figure-of-Merit:

$$R_{2b} = S_t^2/\alpha E^2 \qquad (18b)$$

p. Column with slight initial curvature (radius R) prevented from expanding against rigid constraints. Heated by temperature difference ΔT. Critical temperature difference required for column fracture due to bending moment[17], can be obtained from:

$$\frac{5\alpha^2 (\Delta T)_{max}^2 EA^2 L^4 c}{384\ RI^2 S_t} + \frac{\alpha E \Delta T_{max}}{S_t}\left(\frac{AL^2 c}{8RI} - 1\right) - 1 = 0 \qquad (19a)$$

Figures-of-Merit:

$$R_{3b} = S_t/\alpha E \qquad R_{4b} = (S_t/\alpha^2 E)^{1/2} \qquad (19b)$$

q. Column initially straight subject to transverse temperature gradient ∇ and prevented from expanding against rigid constraints. Heated by temperature difference ΔT. Critical temperature difference ΔT_{max} for fracture of column due to bending moment (for given gradient ∇)[7] can be obtained by solving:

$$\frac{5\alpha^3(\Delta T)^2_{max} E\nabla A^2 L^4 C}{384 I^2 S_t} + \frac{\alpha E \Delta T_{max}}{S_t}\{\frac{\alpha \nabla A L^2 C}{8I} - 1 = 0 \qquad (20a)$$

Figures-of-Merit:

$$R_{5b} = (S_t/\alpha^3 E)^{\frac{1}{2}} \quad \text{and} \quad R_{6b} = (S_t/\alpha^2 E) \qquad (20b)$$

r. Initially straight column subjected to transverse temperature gradient ∇ and prevented from expanding against rigid constraints. Heated by temperature difference ΔT. Critical temperature gradient, ∇_{max} at fixed ΔT, required for column fracture can be obtained from:

$$\frac{5\alpha^3(\Delta T)^2 E\nabla_{max} A^2 L^4 c}{384 I^2 S_t} + \frac{\alpha E \Delta T}{S_t}\{\frac{\alpha \nabla_{max} A L^2 c}{8I} - 1\}-1 = 0 \qquad (21a)$$

Figures-of-Merit:

$$R_{7b} = (S_t/\alpha^3 E) \quad \text{and} \quad R_{5b} = (S_t/\alpha^2 E) \qquad (21b)$$

Expressing ∇_{max} in terms of maximum transverse heat flux, q_{max} with $Q_{max} = K\nabla_{max}$ yields the figures-of-merit

$$R_{8b} = S_t K/\alpha^3 E \quad \text{and} \quad R_{9b} = S_t K/\alpha^2 E \qquad (22)$$

E. Crack Propagation

s. Fatigue. Subcritical crack growth. Constant thermal stress. Material subjected at t = 0 to a steady-state thermal stress. $\sigma = C\alpha E\Delta T/(1-\nu)$, with $\sigma << S_t$, the fracture stress. The material undergoes subcritical crack growth with a crack velocity, $V = AK^n \exp(-Q_c/RT)$. For $K_i = Y\sigma_a\sqrt{\ell}$ and $K_i(t=o) << K_{Ic}$, for the condition that

over the total time period, the total extent of crack growth does not affect the compliance, the time to failure (t*) is[18]:

$$t_f \simeq \frac{2(1-\nu)^2 \exp(Q_c/RT)}{C(\alpha E \Delta T)^2 Y^2 A(n-2) K_i^{(n-2)}} \tag{23a}$$

Figure-of-merit:

$$R_f = \frac{(1-\nu)^2 \exp(Q_c/RT)}{\alpha^2 E^2 (n-2) A} \tag{23b}$$

If in analogy to eq. 2a, ΔT in eq. 23a is related to a heat flux Q, with $\Delta T = C'Q/K$, the time to failure becomes[18]:

$$t_f \simeq \frac{2(1-\nu)^2 K^2 \exp(Q_c/RT)}{C(\alpha E \Delta T C' Q)^2 Y^2 A(n-2 K_{Ii}^{(n-2)}} \tag{24a}$$

Figure-of-merit:

$$R_f' = \frac{(1-\nu)^2 K^2 \exp(Q_c/RT)}{\alpha^2 E^2 (n-2) A} \tag{24b}$$

t. Crack stability. Onset of catastrophic crack propagation. Flat plate with crack. Heat flow perpendicular to crack. Maximum temperature gradient to avoid crack propagation[19]:

$$\nabla_{max} = 8(G/2\pi\alpha^2 E \ell^3)^{\frac{1}{2}} \tag{25a}$$

Figure-of-merit:

$$R_{st} = (G/\alpha^2 E)^{\frac{1}{2}} \tag{25b}$$

Eq. 25a in terms of maximum heat flow becomes:

$$Q_{max} = 8(CK^2/2\pi\alpha^2 E \ell^3)^{\frac{1}{3}} \tag{26a}$$

Figure-of-merit:

$$R_{st}' = (GK^2/\alpha^2 E)^{\frac{1}{2}} \tag{26b}$$

u. Flat plate with N cracks per unit area. Plate cooled by temperature difference ΔT and prevented from shrinking by uniaxial rigid contraints. Critical temperature difference

of cooling[20]:

$$\Delta T_{max} = (2G/\pi \ell \alpha^2 E)^{1/2}(1+2\pi N \ell^2) \tag{27a}$$

Figure-of-merit:

$$R_{st} = (G/\alpha^2 E)^{1/2} \tag{27b}$$

For three-dimensionally constrained body with penny-shaped cracks[21] ΔT_{max} yields same figure-of-merit as eq. 22b.

F. Catastrophic crack propagation and resulting change in strength behavior:

v. Flat plate undergoing catastrophic (unstable) fracture by simultaneous propagation of N cracks per unit area. The final crack length at crack arrest[20]:

$$\ell_f = S_t^2/4NGE \tag{28a}$$

Minimum extent of crack propagation requires high values of the figure-of-merit:

$$R'''' = GE/S_t^2 \tag{28b}$$

The same figure-of-merit is obtained for penny-shaped crack undergoing crack propagation in three-dimensional body[21]. In order to avoid redundancy, the figure-of-merit, $R''' = E/S_t^2$, proposed previously is not included in the present review.

w. Strength retained (S_f) by plate which has undergone crack propagation with final crack length, ℓ_f can be derived to be:

$$S_f = \frac{GE}{S_t}\left(\frac{8N}{\pi}\right)^{1/2} \tag{29a}$$

Figure-of-merit:

$$R_f = GE/S_t \tag{29b}$$

For other geometries eq. 29a can take on somewhat different form[22].

III. Discussion and Conclusions

The expressions and figures-of-merit presented above indicate that the selection of a material with optimum thermal stress resistance can be a complex task. A total of twenty-nine independent equations are given for the thermal stress resistance of brittle materials for a number of different thermal environments, failure mechanisms and measures of thermal stress resistance. These twenty-nine equations lead to a total of twenty-seven different thermal stress figures-of-merit summarized in Table I. It should be noted that some of these figures-of-merit, such as R, R' and $R_{\varepsilon t}$, apply to more than one and in the case of R' to as many as four different thermal environments and criteria of thermal stress resistance. It should be noted that the present review does not include the figure-of-merit[23], $R''' = E/S_t^2$ which implicitly is contained within the figure-of-merit, R''''. For this reason, the figures-of-merit presented are non-redundant. On the other hand, a figure-of-merit, R_t is introduced, equal to the reciprocal of the thermal diffusivity. Other factors being constant, this figure-of-merit maximizes the time-of-maximum stress (i.e., time-of-failure) of a brittle material subjected to transient heating or cooling. Material selection on the basis of this parameter is appropriate to structures or components which have a specific function for a relatively short duration. Note also that the velocity of sound in a material has been introduced as a material property which can affect thermal stress resistance.

For the proper choice of figure-of-merit, it is essential that the heat transfer environment, the criterion of thermal stress resistance and failure mechanism be firmly established, before a choice can be made of the material with optimum thermal stress resistance. This choice of figure-of-merit is rendered even more complex by the temperature dependence of the physical properties, as well as the temperature dependence of heat transfer mechanisms. Due to these temperature dependencies, the relative thermal stress resistance of any two materials may well be interchanged for different levels of temperature at which the materials are susceptible to thermal stress failure.

In summary, a review is presented of all thermal-stress figures-of-merit available at the time of preparation of this paper. It is hoped that this review will make a contribution to the general understanding of the nature of thermal stress failure of brittle materials and the selection of the material with the best thermal stress resistance.

TABLE I

SUMMARY OF THERMAL STRESS FIGURES-OF-MERIT FOR BRITTLE MATERIALS

A. Steady State Heat Flow:

$S_{-}(1-\nu)/\alpha E$; $S_t(1-\nu)K/\alpha E$; $S_t(1-\nu)/\alpha\eta$; $S_t(1-\nu)K/\alpha\eta$

B. Transient Heat Transfer:

$S_{-}(1-\nu)a/\alpha E$; $S_t(1-\nu)/\alpha E$; $S_t(1-\nu)K/\alpha E$; $(S_t(1-\nu)K/\alpha E\varepsilon)^{1/4}$;

$(S_t(1-\nu)K/(1-F_{\lambda o})\alpha E\varepsilon)^{1/4}$; $S_c/\alpha E$; $S_c c/\alpha E$; a^{-1}

C. Thermal Buckling:

α^{-1}; $S_t^2/\alpha E^2$; $S_t/\alpha E$; $(S_t/\alpha^2 E)^{1/2}$; $(S_t/\alpha^2 E)$; $(S_t K/\alpha^2 E)$;

$(S_t/\alpha^3 E)^{1/2}$; $(S_t/\alpha^3 E)$; $(S_t K/\alpha^3 E)$

D. Crack Propagation and Change in Strength:

$(1-\nu)^2[\exp(Q/RT)]\alpha^2 E^2(n-2)A$; $(1-\nu)^2K^2[\exp(Q/RT)]/\alpha^2 E^2(n-2)A$;

$(G/\alpha^2 E)^{1/2}$; $(GK^2/\alpha^2 E)^{1/2}$; GE/S_t^2; GE/S_t

4. List of Symbols

A. Material Properties

α	-	coefficient of linear thermal expansion
A	-	constant in $V = AK^n \exp(-Q_c/RT)$
a	-	thermal diffusivity
c	-	speed of sound
ε	-	emissivity
E	-	Young's modulus
η	-	viscosity
G	-	fracture surface energy
K	-	thermal conductivity
K_{Ic}	-	critical stress intensity factor
λ_o	-	wave-length above which dielectric material is opaque and below which it is transparent
n	-	constant in $V = AK^n \exp(-Q_c/RT)$
ν	-	Poisson's ratio
Q_c	-	activation energy for sub-critical crack growth
S_c	-	compressive strength
S_t	-	tensile strength

B. Environmental, geometric variables and physical constants

A	-	cross-sectional area of column
b	-	thickness of plate, column, radius of cylinder, sphere or spherical cavity
β	-	Biot number, $\beta = bh/K$
C,C', c	-	geometric constants, neutral axis to outer fiber.
d	-	thickness of column
∇	-	temperature gradient
∇_{max}	-	maximum temperature gradient

$F_{\lambda o}$ - fraction of total energy from black-body radiation below frequency, λ_o

H_{max} - maximum rate of internal heat generation

h - convective heat transfer coefficient

I - cross-sectional moment of inertia of column

ℓ - crack half-length

L - length of column, rod

N - number of cracks per unit area of volume

Q_{max}, Q_c - maximum heat flux or flow, activation energy

$\dot{Q}_{max}$ - maximum rate of change of heat flux or flow

ρ - Stefan-Boltzmann constant

σ - stress

T_{max} - maximum temperature of black-body radiation

ΔT_c - critical temperature difference

ΔT_{max} - maximum temperature difference

$\dot{\Delta T}_{max}$ - maximum rate of change of ΔT_{max}

t_o - time period of rapidly heating rod by ΔT

t - time

t* - time-to-maximum stress

t_f - time-to-failure

References

1. D. P. H. Hasselman, Ceramurgia International, (in press).
2. See Symposium on Thermal Fracture, J. Amer. Ceram. Soc., 38 (1955) 1-54.
3. C. H. Kent, J. Appl. Mech., 54 (1932) 185.
4. R. L. Coble and W. D. Kingery, J. Amer. Ceram. Soc., 38 (1955) 33.

5. D. P. H. Hasselman, J. Amer. Ceram. Soc., 50 (1967) 459.

6. A. L. Florence and J. N. Goodier, J. Appl. Mech., 26 (1959) 293.

7. T. R. Tauchert, J. Comp. Mat., 2 (1968) 478.

8. Z. Zudans, T. C. Yen and W. H. Steigelmann, Thermal Stress Techniques in the Nuclear Industry, American Elsevier Publishing, New York 1965, p. 493.

9. W. R. Buessum, Sprechsaal, 93 (1960) 137.

10. W. B. Crandall and J. Ging, J. Amer. Ceram. Soc., 38 (1955) 55.

11. D. P. H. Hasselman, J. Amer. Ceram. Soc., 46 (1963) 229.

12. D. P. H. Hasselman, J. Amer. Ceram. Soc., 49 (1966) 103.

13. H. Bargmann p. 174 in Topics in Applied Continuum Mechanics, ed. by J. L. Zeman and F. Ziegler, Springer Verlag, Vienna (1974).

14. G. Gruenberg, Z. Phys. 35 (1925) 548.

15. Y. B. Fridman, Strength and Deformation in Nonuniform Temperature Fields, Consultants Bureau (1964) p. 3.

16. D. P. H. Hasselman, J. Amer. Ceram. Soc., 61 (1978).

17. D. P. H. Hasselman, J. Amer. Ceram. Soc., (in press).

18. D. P. H. Hasselman and W. Zdaniewski, J. Amer. Ceram. Soc., (in press)

19. J. N. Goodier and A. L. Florence, Proc. XIth Int. Cong. of Appl. Mech. Munchen (1964) p. 562.

20. D. P. H. Hasselman, pp. 89-103 in Ceramics in Severe Environments, ed. by W. W. Kriegel and Hayne Palmour III, Plenum Press, New York (1971).

21. D. P. H. Hasselman, J. Amer. Ceram. Soc., 52, 600 (1969).

22. J. A. Coppola, D. A. Krohn and D. P. H. Hasselman, J. Amer. Ceram, Soc., 55 (1972) 481.

23. D. P. H. Hasselman, J. Amer. Ceram. Soc., 46 (1963) 535.

ROLE OF MATERIAL VARIABLES IN THE THERMAL STRESS FRACTURE OF BRITTLE MATERIALS

Viewgraphs Presented

by

D. P. H. Hasselman

Virginia Polytechnic Institute And State University

Blacksburg, Virginia

THERMAL STRESS DESIGN AND MATERIAL SELECTION

- MULTIDISCIPLINARY PROBLEM
  - HEAT TRANSFER
  - STRESS ANALYSIS
  - MATERIALS ENGINEERING

- VARIABLES
  - NATURE OF HEAT TRANSFER
  - GEOMETRIC FACTORS
  - MATERIAL PROPERTIES
  - STRESS STATE
  - FAILURE MODE
  - CRACK PROPAGATION
  - OTHER PERFORMANCE CRITERIA

- METHODS OF SOLUTION
  - ANALYTICAL
  - NUMERICAL

DEVELOPMENT OF RULES OF SELECTION OF OPTIMUM MATERIAL TO RESIST THERMAL STRESSES.

- ANALYTICAL APPROACH
  - LINEAR HEAT TRANSFER
  - LINEAR THERMO-ELASTICITY
  - TEMP. INDEPENDENT PROPERTIES

- APPROACH
  - DEFINE HEAT TRANSFER
  - DEFINE GEOMETRY
  - CALCULATE $T(x,y,z;t)$
  - CALCULATE $\sigma(x,y,z;t)$
  - DEFINE FAILURE MODE
  - EQUATE MAX. σ TO FAILURE STRESS
  - DERIVE EQS. FOR MAX. THERMAL CONDITIONS TO WHICH MATERIAL CAN BE SUBJECTED

- q_{max}, T_{max}, ΔT_{max} ... $= f(S) \cdot g(\alpha, E...) \cdot h(t)$

$g(\alpha, E....)$ = THERMAL STRESS RESISTANCE PARAMETERS

SOLUTIONS OBTAINED FOR:

- STEADY-STATE HEAT FLOW
- TRANSIENT HEATING
  - CONVECTION
  - RADIATION
- THERMAL BUCKLING
- CRACK PROPAGATION
  - SUBCRITICAL
  - CRITICAL (UNSTABLE, STABLE)

THIRTY (30) NON-REDUNDANT THERMAL STRESS RESISTANCE PARAMETERS.

STEADY-STATE HEAT FLOW

CIRCULAR HOLLOW CYLINDER; RADIAL HEAT FLOW, ΔT_{max} ACROSS WALL :

$$\Delta T_{max} = S_t(1 - \nu)C/\alpha E \qquad (1)$$

IN TERMS OF MAXIMUM HEAT FLOW, Q_{max}, EQ. 1 BECOMES

$$Q_{max} = S_t(1 - \nu)KC^1/\alpha E \qquad (2)$$

EQS. 1 AND 2 YIELD THERMAL STRESS RESISTANCE PARAMETERS:

$$S_t(1 - \nu)/\alpha E \quad \text{and} \quad S_t(1 - \nu)K/\alpha E$$

STEADY-STATE HEAT FLOW (CONT'D):

CIRCULAR HOLLOW CYLINDER, RADIAL HEAT FLOW: STRESS RELAXATION BY LINEAR CREEP. MAXIMUM RATE OF TEMPERATURE CHANGE

$$\dot{\Delta T}_{max} = S_t(1 - \nu)C/\alpha\eta \qquad (3)$$

IN TERMS OF MAXIMUM RATE OF CHANGE OF HEAT FLOW, EQ. 3 BECOMES:

$$\dot{Q}_{max} = S_t(1 - \nu)CK/\alpha\eta \qquad (4)$$

EQS. 3 AND 4 YIELD THE THERMAL STRESS RESISTANCE PARAMETERS:

$$S_t(1 - \nu)/\alpha\dot{\eta} \quad \text{AND} \quad S_t(1 - \nu)K/\alpha\eta$$

STEADY-STATE HEAT FLOW (CONT'D)

LINEAR HEAT FLOW* AROUND SPHERICAL CAVITY
MAXIMUM TEMPERATURE GRADIENT:

$$\tau_{max} = 2S_t(1 - \nu)/\alpha Eb \qquad (5)$$

EQ. 5 IN TERMS OF MAXIMUM HEAT FLOW:

$$Q_{max} = 2S_t(1 - \nu)K/\alpha Eb \qquad (6)$$

EQS. 5 AND 6 YIELD THERMAL STRESS RESISTANCE PARAMETERS:

$$S_t(1 - \nu)/\alpha E \quad \text{AND} \quad S_t(1 - \nu)K/\alpha E$$

*ZERO THERMAL STRESS IN ABSENCE OF CAVITY.

STEADY-STATE HEAT FLOW (CONT'D)

INTERNAL HEAT GENERATION

FOR SOLID ROD WITH UNIFORM INTERNAL HEAT GENERATION (H), THE MAXIMUM RATE OF HEAT GENERATION IS:

$$H_{max} = 8S_t(1-\nu)K/\alpha Eb^2 \qquad (7)$$

EQ. 7 YIELDS THE PARAMETER:

$$R^1 = S_t(1-\nu)K/\alpha E$$

TRANSIENT HEAT TRANSFER

FLAT PLATE; LINEAR RATE OF INCREASE OF SURFACE TEMPERATURE. MAXIMUM RATE OF INCREASE:

$$\dot{T}_{max} = 3S_t(1 - \nu)a/\alpha Eb^2 \qquad (8)$$

EQ. 8 YIELDS THERMAL STRESS RESISTANCE PARAMETER:

$$S_t(1 - \nu)a/\alpha E$$

TRANSIENT HEAT TRANSFER (CONT'D

CONVECTIVE (NEWTONIAN) HEAT TRANSFER. SPHERICAL BODY SUBJECTED BY HEATING AND COOLING OVER TEMPERATURE RANGE ΔT.

$$\Delta T_{max} = \frac{2.5\ S_t(1-\nu)}{\alpha E}\{1 + 2/\beta\} \qquad \beta = Rh/K$$

FOR SEVERE HEAT TRANSFER, $\beta \to \infty$

$$\Delta T_{max} = 2.5\ S_t(1-\nu)/\alpha E \tag{9}$$

FOR MILD HEAT TRANSFER, $\beta << 1$

$$\Delta T_{max} = 5\ S_t(1-\nu)K\alpha ERh \tag{10}$$

EQS. 9 AND 10 YIELD THERMAL STRESS RESISTANCE PARAMETERS:

$S_t(1-\nu)/\alpha E$ AND $S_t(1-\nu)K/\alpha E$

TRANSIENT HEAT TRANSFER (CONT'D)

RADIATION HEAT TRANSFER. SPHERICAL BODY AT LOW INITIAL TEMPERATURE AND WAVELENGTH INDEPENDENT EMISSIVITY INSTANTANEOUSLY SUBJECTED TO BLACK-BODY RADIATION. MAXIMUM RADIATION TEMPERATURE:

$$T_{max} = \{5S_t(1 - \nu)K/\rho b\alpha E\epsilon\}^{1/4} \qquad (11)$$

IF BODY TRANSPARENT TO RADIATION AT WAVELENGTH $\lambda < \lambda_o$

$$T_{max} = \{5S_t(1 - \nu)K/\rho b(1 - F_{\lambda o})\alpha E\epsilon\}^{1/4} \qquad (12)$$

EQS. 11 AND 12 YIELD THERMAL STRESS RESISTANCE PARAMETERS:

$$\{S_t(1 - \nu)K/\alpha E\epsilon\}^{1/4} \qquad \{S_t(1 - \nu)K/(1 - F_{\lambda_o})\alpha E\epsilon\}^{1/4}$$

THERMAL STRESS RESISTANCE PARAMETERS FOR PARTIALLY ABSORBING BRITTLE MATERIALS SUBJECTED TO RADIATION HEATING

$$\left\{\frac{S_t(1-\nu)K}{\alpha E\mu\epsilon}\right\} \qquad \left\{\frac{S_t(1-\nu)K}{\alpha E\mu\epsilon}\right\}$$

$$\left\{\frac{S_t(1-\nu)K}{\alpha E\epsilon\mu^3}\right\} \qquad \left\{\frac{S_t(1-\nu)K}{\alpha E\epsilon\mu^3}\right\}^{\frac{1}{4}}$$

TRANSIENT HEAT TRANSFER (CONT'D)

SPHERE. SURFACE TEMPERATURE RAISED INSTANTANEOUSLY BY TEMPERATURE DIFFERENCE, ΔT. TIME TO MAXIMUM STRESS:

$$t^* = 0.0574\ b^2/a \qquad (13)$$

EQ. 13 YIELDS THE THERMAL STRESS RESISTANCE PARAMETER:

$$a^{-1}$$

INERTIAL EFFECTS

ROD OF LENGTH L, FREELY SUSPENDED. ROD IS VERY RAPIDLY EXPOSED TO UNIFORM TEMPERATURE INCREASE ΔT IN TIME PERIOD, t_o. COMPRESSIVE STRESSES WILL OCCUR BECAUSE OF FINITE TIME REQUIRED FOR EXPANSION TO TAKE PLACE.

THE MAXIMUM TEMPERATURE INCREASE OF THE ROD, WITHOUT COMPRESSIVE FAILURE:

$$\Delta T_{max} = S_c/\alpha E \qquad t_o \leq t_m \tag{14}$$

$$\Delta T_{max} = S_c c\, t_o/\alpha EL \qquad t_o \geq t_m \tag{15}$$

WHERE $t_m = L/c$, WHERE c IS THE SPEED OF SOUND WITH $c = (E/\rho)^{1/2}$

EQS. 13a and 13b YIELD THE PARAMETERS:

$Sc/\alpha E$ AND $S_c c/\alpha E$

THERMAL BUCKLING

STRAIGHT COLUMN PREVENTED FROM EXPANDING AGAINST RIGID CONSTRAINT. HEATED BY TEMPERATURE DIFFERENCE ΔT. CRITICAL TEMPERATURE DIFFERENCE REQUIRED FOR COLUMN INSTABILITY:

$$\Delta T_c = \pi^2 I/L^2 A\alpha \qquad (16)$$

EQ. 16 YIELDS THE THERMAL BUCKLING RESISTANCE PARAMETER:

$$1R_b = \alpha^{-1}$$

THERMAL BUCKLING (CONT'D)

COLUMN WITH INITIAL CURVATURE, PREVENTED FROM EXPANSION AGAINST RIGID CONSTRAINTS.

MAXIMUM TEMPERATURE DIFFERENCE, ΔT_{max} TO WHICH COLUMN CAN BE HEATED SO THAT FRACTURE INTENSION DUE TO BENDING CANNOT OCCUR, CAN BE OBTAINED FROM:

$$\frac{5\alpha^2(\Delta T)^2_{max} EA^2L^4c}{384\ RI^2S_t} + \frac{\alpha E\Delta T_{max}}{S_t}\left(\frac{AL^2c}{8RI} - 1\right)-1 = 0 \qquad (17)$$

EQ. 17 YIELDS THERMAL BUCKLING RESISTANCE PARAMETERS:

$(S_t/\alpha^2E)^{1/2}$, $S_t/\alpha E$

THERMAL BUCKLING (CONT'D)

COLUMN WITH SLIGHT CURVATURE DUE TO TRANSVERSE TEMPERATURE GRADIENT, PREVENTED FROM THERMAL EXPANSION AGAINST RIGID CONSTRAINTS.

MAXIMUM TEMPERATURE DIFFERENCE, ΔT_{max} TO WHICH COLUMN CAN BE HEATED TO AVOID FRACTURE IN BENDING, CAN BE OBTAINED FROM:

$$\frac{5\alpha^3(\Delta T)^2_{max} E\nabla A^2 L^4 c}{384 I^2 S_t} + \frac{\alpha E \Delta T_{max}}{S_t}\left\{\frac{\alpha \nabla A L^2 c}{8I} - 1\right\} - 1 = 0 \qquad (18)$$

EQ. 18 YIELDS THE PARAMETERS

$$(S_t/\alpha^3 E)^{1/2} \text{ and } S_t/\alpha^2 E$$

FOR ∇_{max}, PARAMETERS ARE: $S_t/\alpha^3 E$, $S_t/\alpha^2 E$ (19)

FOR Q_{max}, PARAMETERS ARE: $S_t K/\alpha^3 E$, $S_t K/\alpha^2 E$ (20)

THERMAL BUCKLING (CONT'D)

POST-THERMAL BUCKLING OF STRAIGHT COLUMN.

ORIGINALLY STRAIGHT COLUMN PREVENTED FROM EXPANDING AGAINST RIGID CONSTRAINTS, HEATED OVER TEMPERATURE DIFFERENCE, $\Delta T > \Delta T_c$ TO BE SUBJECTED TO BENDING IN POST-THERMAL BUCKLING.

MAXIMUM TEMPERATURE DIFFERENCE REQUIRED FOR FAILURE OF SQUARE COLUMN AS THE RESULT OF TENSILE BENDING STRESSES

$$\Delta T_{max} = \pi^2 d^2/12L^2\alpha + S_t^2 L^2/\pi^2 \alpha E^2 d^2 \qquad (21)$$

EQ. 21 YIELDS THERMAL POST-BUCKLING RESISTANCE PARAMETER:

$$6R_b = S_t^2/\alpha E^2$$

CRACK PROPAGATION

FLAT PLATE WITH CRACK. HEAT FLOW PERPENDICULAR TO CRACK. MAXIMUM TEMPERATURE GRADIENT TO AVOID CRACK PROPAGATION:

$$\tau_{max} = 8(G/2\pi\alpha^2 E\ell^3)^{1/2} \tag{22}$$

EQ. 18 IN TERMS OF MAXIMUM HEAT FLOW BECOMES:

$$Q_{max} = 8(GK^2/2\pi\alpha^2 E\ell^3)^{1/2} \tag{23}$$

EQS. 22 AND 23 YIELD THE THERMAL STRESS RESISTANCE PARAMETERS:

$$R_{St} = (G/\alpha^2 E)^{1/2} \quad \text{AND} \quad R_{St}^{\ 1} = (GK^2/\alpha^2 E)^{1/2}$$

CRACK PROPAGATION (CONT'D)

FLAT PLATE WITH N CRACKS PER UNIT AREA PLATE COOLED BY TEMPERATURE DIFFERENCE ΔT AND PREVENTED FROM SHRINKING BY RIGID CONSTRAINTS. CRITICAL TEMPERATURE DIFFERENCE OF COOLING:

$$\Delta T_{max} = (2G/\pi \ell \alpha^2 E)^{1/2}(1+2\pi N \ell^2) \qquad (24)$$

EQ. 24 YIELDS THE THERMAL STRESS RESISTANCE PARAMETER:

$$R_{St} = (G/\alpha^2 E)^{1/2}$$

CRACK PROPAGATION (CONT'D)

FLAT PLATE UNDERGOING CATASTROPHIC (UNSTABLE) FRACTURE BY SIMULTANEOUS PROPAGATION OF N CRACKS PER UNIT AREA. THE FINAL CRACK LENGTH OF CRACK ARREST:

$$\ell_f = S_t^2/4NGE \tag{25}$$

THE STRENGTH RETAINED FOR A FINAL CRACK LENGTH OF ℓ_f OF EQ. 21:

$$S_f = \frac{4GE}{S_t}\left(\frac{N}{\pi}\right)^{1/2} \tag{26}$$

EQS. 25 AND 26 YIELD THE "THERMAL STRESS DAMAGE RESISTANCE PARAMETERS":

GE/S_t^2 AND GE/S_t

THERMAL FATIGUE

MATERIAL SUBJECTED AT t = o TO A STEADY-STATE THERMAL STRESS, $\sigma_a = C\alpha E\Delta T/(1-\nu)$, WITH $\sigma_a << \sigma_f$, THE FRACTURE STRESS. THE MATERIAL UNDERGOES SUBCRITICAL CRACK GROWTH WITH A CRACK VELOCITY, $V = AK^n \exp(-Q/RT)$. FOR $K_I = Y\sigma_a \sqrt{a}$ AND K_{Ic} (t=o) << K_{Ic} THE TIME TO FAILURE (t*) CAN BE DERIVED TO BE:

$$t^* \simeq \frac{2(1-\nu)^2 \exp(Q/RT)}{C(\alpha E\Delta T)^2 Y^2 A(n-2) K_{Ic}^{(n-2)}} \tag{27}$$

FOR THE CONDITION THAT OVER THE TOTAL TIME PERIOD, THE TOTAL EXTENT OF CRACK GROWTH DOES NOT AFFECT THE COMPLIANCE.

IF ΔT IN EQ. 27 IS RELATED TO A HEAT FLUX Q, WITH $\Delta T = C'Q/K$, EQ. 27 CAN BE WRITTEN:

$$t^* \simeq \frac{2(1-\nu)^2 K^2 \exp(Q/RT)}{C(\alpha E\Delta TC'Q)^2 Y^2 A(n-2) K_{Ic}^{(n-2)}} \tag{28}$$

EQS. 27 AND 28 YIELD THE "THERMAL FATIGUE" RESISTANCE PARAMETERS:

$$R_f = \frac{2(1-\nu)^2 \exp(Q/RT)}{\alpha^2 E^2 (n-2) A} \quad \text{AND} \quad R_f' = K^2 R_f$$

SUMMARY OF THERMAL STRESS FIGURES-OF-MERIT FOR BRITTLE MATERIALS

A. Steady State Heat Flow:

$$S_t(1-\nu)/\alpha E;\quad S_t(1-\nu)K/\alpha E;\quad S_t(1-\nu)/\alpha\eta;\quad S_t(1-\nu)K/\alpha\eta$$

B. Transient Heat Transfer:

$$S_t(1-\nu)a/\alpha E;\quad S_t(1-\nu)/\alpha E;\quad S_t(1-\nu)K/\alpha E;\quad (S_t(1-\nu)K/\alpha E\varepsilon)^{1/4};$$

$$(S_t(1-\nu)K/(1-F_{\lambda o})\alpha E\varepsilon)^{1/4};\quad S_c/\alpha E;\quad S_c c/\alpha E;\quad a^{-1}$$

C. Thermal Buckling:

$$\alpha^{-1};\quad S_t^2/\alpha E^2;\quad S_t/\alpha E;\quad (S_t/\alpha^2 E)^{1/2};\quad (S_t/\alpha^2 E);\quad (S_t K/\alpha^2 E);$$

$$(S_t/\alpha^3 E)^{1/2};\quad (S_t/\alpha^1 E);\quad (S_t K/\alpha^3 E)$$

D. Crack Propagation and Change in Strength:

$$(1-\nu)^2[\exp(Q/RT)]\alpha^2 E^2(n-2)A;\quad (1-\nu)^2 K^2[\exp(Q/RT)]/\alpha^2 E^2(n-2)A;$$

$$(G/\alpha^2 E)^{1/2};\quad (GK^2/\alpha^2 E)^{1/2};\quad GE/S_t^2;\quad GE/S_t$$

CONCLUSIONS

MATERIAL SELECTION FOR THERMAL STRESS:

- IS COMPLEX, BUT NOT IMPOSSIBLE
- REQUIRES ANALYSIS OF:
  - HEAT TRANSFER
  - THERMAL STRESS
  - OTHER PERFORMANCE CRITERIA
  - MATERIAL PROPERTIES
  - FAILURE MODES
  - CRACK PROPAGATION BEHAVIOR
- REQUIRES EXPERIMENTAL TESTING PLUS COMPUTER SIMULATION
- REQUIRES TRADE-OFFS BETWEEN MATERIAL PROPERTIES AND DESIGN LIMITATIONS
- MULTI-DISCIPLINARY TEAM-WORK!!

THIS PAGE

WAS INTENTIONALLY

LEFT BLANK

LIQUID METAL HEATED STEAM GENERATORS

EFFECTS OF CORROSION ON PERFORMANCE

by

C. N. Spalaris

General Electric Company

San Jose, California

LIQUID METAL HEATED STEAM GENERATORS
EFFECTS OF CORROSION ON PERFORMANCE

C.N. Spalaris
Advanced Reactor Systems Department
General Electric Company, San Jose, CA

INTRODUCTION

Liquid metals have been used successfully to remove heat from high power density systems, such as nuclear reactors, and have recently been considered for use in solar-electric power plants. The use of sodium has dominated in engineering applications because of its desirable properties of heat transfer, large heat capacity, low vapor pressure and absence of corrosion in components where air and/or water are excluded. These benefits, plus the potential for using sodium to also store energy, make the liquid metal systems very attractive for solar plant applications.

To obtain high reliability required in an electricity generating plant, it will be necessary to at least equal and preferably exceed the on-line record of the presently operating sodium heated steam generators. Because corrosion is the main mechanism that has caused damage in the past, it is appropriate to review the conditions causing it and highlight the features of some systems that have thus far avoided corrosion altogether.

It is the purpose of this paper to (a) review the effects of corrosion upon the performance of sodium heated steam generators, (b) enumerate factors that lead to corrosive environments, and (c) list possible remedies that may be applied to future components to minimize or avoid damage and achieve high service availability.

Background

Heat removal in a liquid metal cooled reactor is accomplished by means of a primary and secondary circuits. Heat transfer from the liquid metal to produce steam is accomplished through the use of steam generators. Steam generator systems which have been designed thus far employ a single wall separating the water steam from the liquid metal, usually sodium. One successful steam generator, EBR II, employs a double wall arrangement for the heat transfer tubes.

In typical conditions, steam generator system modules are designed to transfer between 250-300 MWth to 750 MWth (new proposed designs).[1,2] The CRBR steam generator system is shown in Fig. 1. Three independent identical systems are used, each accepting sodium at 500°C, cools it to 344°C, and in the process, converts feedwater at 232°C to heated steam delivered to turbine throttle at 482°C and 10 MPa pressure. Each steam generator system for the Clinch River reactor was designed to transfer 300 MWth at full power with load following range from 40 to 100% at full power. Water recirculation is used in some units, others use no drum, but go directly from evaporator to superheater. Super Phenix reactor in France, will utilize a once-through type steam generator.

Extremely high reliability is desired for the systems. Apparently this reliability has been achieved at EBR II, presumably because of the double wall concept, and by the Phenix reactor due to extremely high degree of compartmentation.[3] The single wall tube steam generators for PFR and BN 350, have had to undergo modifications and repairs following extensive steam generator component failures. Most failures have been traced to weld defects which had gone undetected during fabrication (BN 350) or defects which occurred from neglect of known metallurgical requirements, such as omitting the post weld heat treatments for 2-1/4Cr-1Mo tube-to-tubesheet welds (PFR).[4]

Material Choice and Specifications

Most, if not all, sodium heated steam generators designed for use in large power producing reactors used 2-1/4Cr-1Mo for the evaporator portion of the steam generators.[3] The superheater portions are constructed either from 2-1/4Cr-1Mo, 2-1/4Cr-1Mo NB stabilized, or Types 316 or 321 stainless steel. The UK-PFR is now in the process of replacing Type 316 superheaters and re-

heater units because of severe damage from a caustic stress corrosion mechanism during the initial periods of operation.[4] The new construction material is 9Cr-1Mo, with a simultaneous introduction of a new design which avoids welds at the water/sodium interface. The Japanese plan to construct the Monju superheaters through the use of austenitic alloys Type 316 or 321, but final decision is yet to be made. Super Phenix once-through design utilizes Incoloy 800, while Super Phenix II will utilize ferritic alloys.[2]

The material used for CRBRP is 2-1/4Cr-1Mo for the evaporators, the steam drum and the superheaters.[1] The choice for this alloy was made on the basis of its proven resistence to chloride stress corrosion attack in boiler systems and extensive use in the boiler industry for the past 35 years. A projection was made that certain of its deficiencies could be accommodated through design allowances (general corrosion, decarburization, etc.). A national program was instituted in 1974 to acquire more knowledge for 2-1/4Cr-1Mo, with specific emphasis toward the design and operating needs for the CRBR steam generators. To achieve better weldability at the tube/tubesheet joints, it was decided to refine the material by either the Vacuum Arc Remelt (VAR), or the Electroslag Remelt (ESR) processes. A thorough product qualification program at GE-ARSD yielded ample information to indicate that all ASME Boiler and Pressure Vessel Code stipulations were met or exceeded by the melt-refined material.[6]

Design and Fabrication Issues

Full penetration, internal bore weld geometry was utilized to eliminate crevices and reduce stresses at the region of the weld.[1,7] The reference geometry permitted the use of high resolution radiography and the use of removable water/steam heads was chosen to provide direct access to the tube ends at the tubesheets for in-service inspection, and if necessary, plugging of the tubes from the water/steam side. Radiographic inspection using internal bore rod anode device allows resolution that reveals porosity of 0.002 inches in diameter. Ultrasonic, liquid penetrant, and helium leak inspection were mandatory to insure the highest possible quality. Post weld heat treatment will be done on each weld. Tubing was inspected by ultrasonic probes to 3% of the wall thickness.[8]

Although the above mentioned design and fabrication details are those pertinent to CRBRP steam generators, identical or similar specification have also been applied for the SNR (German/Netherlands) units, the replacement PFR units, and are contemplated for the Monju steam generators. The "extra" costs for high quality components have been accepted and demonstrated feasible. Lessons from operating PFR and BN 350 have been used in the repair of the steam generators for these plants. These two plants demonstrated what is truly necessary to achieve high reliability. Reference 1, Table I, lists the design criteria for the CRBRP steam generators; these are not much different, except in emphasis, from those stipulated for other power plant sodium heated units.

Performance Projection - Sodium Side

Pure sodium has been shown to be relatively non-corrosive to ferritic and/or austenitic materials. Design allowances for the sodium side are modest, provided that the presence of oxides, moisture or hydroxide are limited to minor quantities. Decarburization rates have been measured under prototypical operating conditions to be sufficiently low, so as to be accommodated by initial design allowances.[6]

The greatest concern from the sodium side is the presence or occurrence of small leaks, which if not detected and repaired during fabrication, are likely to grow to large sizes, capable of causing large scale Na/H_2O reactions. Studies in the U.S., U.K., France, Japan, Germany and the Soviet Union have demonstrated that micro leaks initially as small as 10^{-5} grams of water per second, first will plug, but then may grow to sizes allowing flow rates greater than tens and even hundreds of grams per second.[9] The mechanism involved was demonstrated[10] at GE, to be divided into three main stages. The first stage may or may not involve plugging by Na/H_2O reaction products (depending upon the original orifice size), followed by permeation of reacting species causing extremely high corrosion rates (presumably due to the formation of caustic), finally causing opening of the initial micro orifice to where the reaction products plug is washed away, allowing continuous injection, sustained by the water side pressure of 10 Mpa. Metal damage (self-wastage) rates during the "plugged" period have been measured to be as high as 2×10^{-2}mm/sec for 2-1/4 Cr-1Mo and 1.6×10^{-4}mm/sec* for austenitic materials under similar test conditions.[9]

*For calculating the above wastage rates, only the time of water injection is used.

"Unplugging" of micro leaks releases relatively large amounts of water or steam into the sodium side forming a high temperature, high velocity torch which impinges onto a neighboring tube causing it to fail. To minimize further damage, steam generators are equipped with rupture disks designed to fail under the water side pressure and the added pressure generated by the Na/H_2O reaction. Sodium is "dumped" into reaction products tanks while at the same time water and steam are also drained from the modules. Despite the water side higher pressures, systems that suffered large leaks (BN 350, KNK, etc.) have been found to contain large quantities of sodium and sodium reaction products on the water side of the system.

The PFR evaporators and superheaters did not experience a large Na/H_2O reaction, but small leaks (at welds and tubesheets) allowed sodium to flow and form caustic on the water side.

Thus, experience available from operating systems dictated that construction materials should be such as to offer reasonable resistance to caustic attack to allow repairs and recovery for normal operation. Components made of 2-1/4Cr-1Mo in the U.S.S.R and U.K have been repaired and returned to service.

Components of the Atomics International MSG (Module Steam Generator) were examined after 5 experimental Na/H_2O leak tests and found to contain no stress corrosion attack, no wastage to neighboring tubes, and even though the reaction products were allowed to stand for many hours at temperatures of 800 to 400°F.[11] In these cases, about 40 lbs. of water were injected into a large quantity of sodium, probably dissolving the reaction products to low concentrations. However, it indicates that if the protective system works as intended, the system can sustain certain types of Na/H_2O reactions, essentially without damaging the component.

Performance Projection - Water/Steam Side

Water and steam corrosion rates for 2-1/4Cr-1Mo even for temperatures up to 482°C, can be accommodated by initial tube wall thickness allowances. Experiments conducted under the influence of heat flux[12] typical of those present in the superheater regions, indicate the need for extra margins to be added to the steam corrosion allowance.[6] Even these added margins, usually a multiplier 1.5 of the isothermal corrosion rates, have been accommodated by

design. Similar allowances have also been found to be necessary for austenitic materials, as well as for high nickel alloys.[13]

Recent experiments indicated that steam corrosion rates for 2-1/4Cr-1Mo at 500°C cannot be extrapolated to define corrosion rates in lower temperature (water evaporator conditions).[14] Nevertheless, the proper rates are slightly less than 0.001 inches per year and can be accommodated by initial design allowances.

Off-chemistry conditions are more difficult to predict and make allowances at the design and fabrication stages. One potential off-chemistry condition investigated by teams in the U.S, Holland and France, is the Departure from Nucleate Boiling (DNB), which may occur in the evaporator under certain hydraulic and heat transfer conditions. The concern is that repeated wetting and drying DNB action will concentrate caustic impurities at a confined region subjected to thermal cycling stresses. Two separate experiments in the U.S[15,16] proved that the concern, under the conditions anticipated in the CRBRP steam generators, is minimal. During these two tests, sodium in the form of NaOH was deliberately added to feedwater at concentrations ranging from 1.5 to 6 times higher than those specified for the CRBRP normal operations. Post test examination of the DNB regions indicated normal corrosion product formation. Results from DNB tests in Holland have not been reported, whereas the tests run by the French at Grand Quevilly[17] did not result in excessive corrosion either, but the water chemistry was kept within specifications. Of the three ferritic alloy tubes tested at Grand Quevilly for up to 5,000 hours, none showed stress or fatigue type of cracking, although in some cases thicker than normal oxidation layers appeared at the DNB region and some oxide exfoliation was evidenced.

Off-chemistry caustic conditions were used to study 2-1/4Cr-1Mo in the U.S and U.K-Risley.[4] The U.S program at GE[18] included constant extension rate, straining electrode, as well as corrosion fatigue experiments. Most studies were performed at 316°C in NaOH solutions of 5%, 10% with specimens encompassing most metallurgical treatments expected present in a completed steam generator component. When tested at 316°C, the alloy was found to be extremely resistant to cracking. A few constant extension rate tests at 232°C in 5 and 10% NaOH caused 2-1/4Cr-1Mo to fail by intergranular and transgranular

stress corrosion.[18]

The corrosion fatigue studies were undertaken to confirm that the design basis (failure curve obtained from air tests) was adequate to also describe the effects of caustic environment. At 316°C, the results obtained[19] in 5% NaOH solution are above the design allowables, established from results obtained in air and the 2-20 safety factors stipulated by the ASME Boiler and Pressure Vessel Code. The corrosion fatigue tests are continuing during 1979 to explore additional sets of parameters in terms of temperatures, caustic concentrations and metallurgical conditions.

The U.K program to study stress corrosion cracking[4] is highly specific to the materials (2-1/4Cr-1Mo, 2-1/4Cr-1Mo NB stabilized and Type 316 stainless) and conditions prevalent in the PFR system. Leaks were detected after 14 days in one of the units and after 60 days in the other. A third unit has operated trouble-free since March 1974, the PFR start-up date.

The PFR 2-1/4Cr-1Mo evaporators were welded without the benefit of pre or post weld heat treatment, usually necessary for this material to reduce hardness (1340°F for 1 hour per inch of thickness). The metallographic work done is prodigious and of high quality involving tubular and tubesheet sections removed from the PFR units. Cracks in evaporators #1 and #2 are associated with tube/tubesheet welds and their heat affected zones. Some crack propagation into adjacent areas was also observed. Almost all of the cracks are intergranular, some follow the weld area around the tube circumference of the tube/tubesheet connectors.

Laboratory work at Risley verified that omitting post weld heat treatment is the most susceptible metallurgical condition. All U-bend non-post weld heat treated specimens tested in either "normal" water or in NaOH solutions (1-30%) at temperatures ranging from 120°C to 320°C, exhibited cracking. Some specimens crack while being heated to 320°C. In some experiments, stabilized and unstabilized 2-1/4Cr-1Mo alloy specimens cracked equally as rapid when the post weld heat treatment was omitted. Time to crack increased when the NaOH concentration was reduced from 10% to 1%, and below 1% the time to crack was increased significantly. Specimens welded in exact geometries of the PFR tube/tubesheet welds (7 tube) and exposed to 30% NaOH without the imposition of external stress. Correct post weld heat treatment,

prior to testing, resulted in no cracks after 7 days, whereas less proper post weld heat treated specimens cracked within 2-1/2 days. Introduction of small quantities of oxygen causes appearance and propagation of cracks in U-bend specimens.

The overall consensus is that 2-1/4Cr-1Mo, in the as-welded condition, is subject to SCC in caustic media, the degree of susceptibility and time for onset of cracking depends upon temperature (above 120°C), caustic concentration (above 1%), and introduction of traces of oxygen. The PFR evaporator troubles would have been significantly minimized and possibly avoided had the tube/tubesheet welds been properly heat treated.

Occurrence of Off-Chemistry Conditions

The reference water chemistry specification is the all-volatile treated (AVT) type, with a full-flow condensate polishing system for demineralization.[20] For steady state operation, the maximum allowable feedwater impurities are limited to oxygen to 7 ppb, chlorides to 9 ppb, copper to less than 1.5 ppb, and sodium to 1 ppb. Hydrazine is maintained at 5 ppb and ammonia is added to keep the pH at 8.7 to 9.1.

Loss of water chemistry control may occur when (a) there exists a condenser leak or many micro leaks that either go undetected or when operators fail to initiate corrective action, (b) break down in the ion exchange resins of the polishing units, or failure to initiate a resin regeneration step on time, (c) failure of instrumentation to register mandatory shutdown levels of certain ionic specie, (d) sodium/water reactions and intrusion of large quantities of sodium into the water side circuit, (e) sodium hydroxide incursions from resin regeneration operations, and (f) entry of harmful ions through impurities present in the chemical reagents used in water chemistry control (hydrazine and ammonia are additives).

Some of the harmful ions are not easy to detect at the low concentrations specified for control. Sodium and chloride are notable by their difficulty of detection; chloride ion must be measured through grab sampling schemes, whereas sodium ion on-line analysis has been recently demonstrated to sub ppb levels with a fair degree of success.[21] Due to concerns about DNB, sodium was specified at the 1 ppb level at the feedwater, and a 10% drain (blowdown) rate was set for the CRBRP system. Water entering the evaporator

will contain 6 ppb of sodium ion. Chloride limits have been set at 9 ppb in the feedwater, 50 ppb in the recirculation water, levels that are not easy to measure even with laboratory (batch sampling) techniques. Copper was recently set at less than 1.5 ppb, higher concentrations thought to promote high rates of corrosion for ferritic materials. If a condenser (such as in the case of CRBRP) is made from copper tubing (10Cu-90Ni), keeping copper limits in the feedwater at the level indicated as maximum may be difficult. Some fossil fired plants using 90-10 CuNi condenser tubing, show copper ions concentration less than 1 ppb in the condensate hot well (before polishing). Whether this is typical of all plants with Cu-Ni condensers is not known; nor is it known whether the low Cu concentration is typical for all time.

Remedies Offered to Avoid Sodium/Water Interface Imperfections

No system can be made immune to all possible damages, least of all a sodium heated steam generator. It is noted, however, that several large size steam generators have been made to work satisfactorily. EBR II (14 years), Phenix (4 years) have used large size systems that have operated flawlessly from the start. Other systems which were made to work after initial episodes are PFR (since 1977 with all 3 circuits), and BN 350 since 1976, KNK Germany since 1975. Large size (50 MWth) test rigs which operated for more than 4,000 hours include O-arai (Japan, 50 MWth, two units), Hengelo (Holland), and Les Renardieres, France. The MSG (30 MW, U.S.A) logged 4,000 hours of operation without problems.

Features that have been associated with successful systems are:

A. Design

- Make full use of up-to-date materials properties; provide sufficient margins.
- Tube-to-tube geometry fully radiographable, free porosity welds with no crevices. Minimize stresses.
- Double wall tubing and tubesheets.
- Avoidance of tube/tubesheet welds that separate Na from water. Under sodium butt welds have so far been successful if made properly (Hengelo, Renardieres, O-arai). (The French claim that elimination of tubesheet reduces weld stresses because of elimination of thick structural members.)

B. Choice of Materials

- Use of ferritic materials in almost all known evaporator units. Even after leaks occurred, clean-up and restart was possible (PFR, Hengelo, KNK, BN 350 and Fermi I).
- Avoidance of using austenitic materials--when leaks occur, entire components have been abandoned (PFR, Alco-BLH Experimental Unit, U.S.A).

C. Maximize Knowledge of Design Basis

- Through a well-thought-out program, obtain critical material properties needed in the design.
- Provide proper definition of critical areas and assign proper design margins.
- Examine metallurgical conditions (melt-refining, heat treating) that may enhance alloy resistance to aggravated corrosion conditions.

D. Material Specifications

- Metallurgically dirty material was claimed the culprit in failed porous welds of the BN 350.
- Melt refining (VAR) has been held responsible for the success of Hengelo tube/tubesheet and butt welds. Melt refining is also credited for the low rejection rates in the welding of tube/tubesheet joints for the SNR (Holland) steam generators.

E. Quality of Fabrication Steps

- Proper control of welding steps.
- Proper application of heat treatment of all welds.
- Use of high quality product forms such as tubing and tubesheets .
- Use of high reliability and high resolution weld inspection techniques.
- High degree of cleanliness during fabrication; dedicated staff.
- Real quality control (not just paper files).

F. Control of Pre-startup Conditions

- Proper storage, shipping and installation steps. (The Fermi I components were damaged prior to startup, although omitting post weld heat treatment of the 2-1/4Cr-1Mo may have been the original flaw.)
- Following well designed startup procedures.

G. Control of Conditions During Operation

- Provide adequate, high quality instrumentation to monitor water chemistry at all times.
- Take timely action to correct off-chemistry conditions.
- Maintain water chemistry control during low power, standby, and layup operations.

REFERENCES

1. J.C. Whipple and C.N. Spalaris, J. Nucl. Tech., Vol. 28, March 1976, p. 305.

2. Nuclear Engineering International, Vol. 23, No. 272, June 1978, p. 53.

3. M.G. Robin et al., BNES Trans. "Fast Reactor Power Stations", March 11-14, 1974, p. 205.

4. C.N. Spalaris, "UK Prototype Fast Reactor Evaporators", GEFR-00285, September 1977. Trip Report by C.N. Spalaris, J. Corum, E.E. Hoffman, and P. Patriarca.

5. J.S. Armijo et al., Ibid. Ref. 3, p. 189, Table I.

6. C.N. Spalaris et al., BNES Trans. "Int. Conference on Ferritic Steels for Fast Reactor Steam Generators", May 30-June 2, 1977, Paper No. 9.

7. R.W. McClung et al., Ibid. Ref. 1, p. 374.

8. R.A. Day and D.S. Kerr, "UT of The CRBR Steam Generator Tubing", submitted for publication to J. Materials Evaluation.

9. D.A. Greene, "Self-Waste Phenomena", GEFR-00051(1)-3, September 1977.

10. D.W. Sandusky, "Small Leak Behavior-Summary Report Scoping Tests", NEDM-14063, June 1975.

11. P. Ring and G.G. Gaul, personal communication, November 22, 1978.

12. J. DeVan et al., Ibid. Ref. 6, Paper No. 61. Also, J.C. Griess et al., "Oxidation of Heated 2-1/4Cr-1Mo Steel Tubing in Flowing Superheated Steam", ORNL-5373, April 1978.

13. W.L. Pearl et al., "General Corrosion of Materials for Nuclear Superheat Applications", GEAP-4760, March 1965.

14. P. Roy, D. Rodgers, and L.V. Hampton, personal communication. Also, see Nuclear Systems Materials Handbook Property Code 4103.

15. P.B. Stephens et al., "DNB Effects Test Program-Final Report", CRBRP-GEFR-00100, June 1977.

16. P. Cohen et al., Ibid. Ref. 6, Paper No. 65.

17. C.N. Spalaris Trip Report, Europe October 1975, p. 17.

18. M.E. Indig, "Constant Extension Rate Testing for LMFBR Steam Generators Applications", NEDO-12668, May 1977. Also, Ibid. Ref. 6, Paper No. 67.

19. A.R. McIlree et al., "Corrosion Fatigue of 2-1/4Cr-1Mo Steel in Caustic at 316°C", Paper to be presented at NACE 1979, Atlanta, GA, Symposium T3E/T11A. Also, GEFR-00375, June 1978.

20. D. Dutina, "A Survey of Modern Boiler Water Practice: Boiler Water Control to Minimize Corrosion of the Steam Generators CRBRP", GEAP-14042, April 1975.

21. C.N. Spalaris, An update of Ref. 20 to be issued.

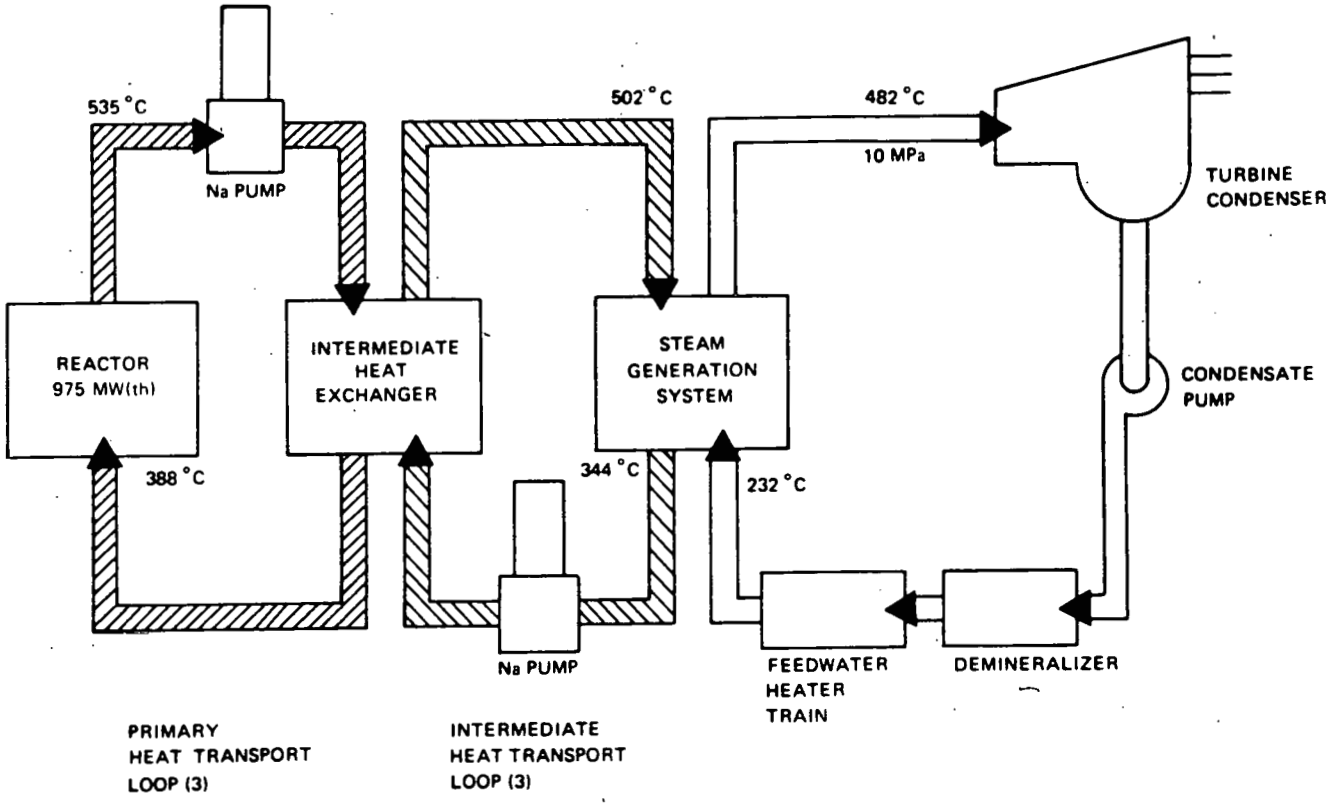


Fig. 1. CRBRP main heat transport system.

LIQUID METAL HEATED STEAM GENERATORS

EFFECTS OF CORROSION ON PERFORMANCE

Viewgraphs Presented

by

C. N. Spalaris

General Electric Company

San Jose, California

LIQUID METAL HEATED STEAM GENERATORS

EFFECTS OF CORROSION ON PERFORMANCE

C.N. SPALARIS

INTRODUCTION

- SODIUM DOMINANT IN SYSTEMS APPLICATIONS
- FUTURE COMPONENT RELIABILITY MUST EQUAL OR EXCEED SYSTEMS OPERATING NOW
- CORROSION DOMINANT MECHANISM IN CAUSING COMPONENT DAMAGE
- PURPOSE OF PAPER
    - RELATE CORROSION TO PERFORMANCE
    - FACTORS CAUSING CORROSION
    - POTENTIAL REMEDIES

LIQUID METAL HEATED STEAM GENERATORS

SIZE OF UNITS	250-750MW$_{TH}$
MAXIMUM TEMPERATURES	500-525°C
STEAM PRESSURE (TURBINE)	10-17MPa
STEAM TEMPERATURE	480-490°C
LARGE Na MASS-SECONDARY UNITS (SP)	1500 TONS

LIQUID METAL HEATED STEAM GENERATORS

MATERIAL CHOICES

- EVAPORATORS : FERRITICS
- SUPERHEATERS: FERRITICS AND AUSTENITICS

DESIGN FEATURES

- SINGLE WALL TUBES (EXCEPT EBR-II)
- FULLY RADIOGRAPHABLE WELDS
- NO CREVICES
- PFR REPLACEMENTS, SUPER PHENIX, NEW DESIGNS

FABRICATION FEATURES

- FULL PENETRATION WELDS
- HIGH RESOLUTION RADIOGRAPHY
- OTHER METHODS OF WELD INSPECTION
- FOR FERRITICS, POST WELD HEAT TREATMENTS
- CLEANLINESS OF OPERATIONS

LIQUID METAL HEATED STEAM GENERATORS

PERFORMANCE PROJECTION-SODIUM SIDE

- NECESSARY CORROSION ALLOWANCES ON Na SIDE ARE SMALL
- DECARBURIZATION RATES ACCOUNTED IN DESIGN

GREATEST CONCERNS

A. SMALL LEAKS DIFFICULT TO DETECT AT FABRICATION STAGE

B. GROWTH OF SMALL LEAKS

C. LARGE Na/H_2O REACTIONS, REACTION PRODUCTS RESIDUES

POSITIVE INDICATIONS

- LARGE SYSTEMS HAVE RECOVERED FROM Na/H_2O REACTIONS
- RECENT TESTS IN U.S., JAPAN, AND HOLLAND SHOW CONSEQUENCES OF Na/H_2O REACTIONS INNOCUOUS

LIQUID METAL HEATED STEAM GENERATORS

PERFORMANCE PROJECTION-WATER SIDE

- UNIFORM CORROSION ALLOWANCES CAN BE ESTABLISHED FOR MOST ALLOYS

MAJOR CONCERNS

A. RAPID STRESS CORROSION

B. CORROSION FATIGUE

C. CREEP-FATIGUE INTERACTION

CONDITIONS LEADING TO MAJOR CONCERNS

A. OFF-CHEMISTRY OF BOILER WATER

B. OCCURRENCE OF Na/H_2O REACTIONS

C. DNB (DEPARTURE FROM NUCLEATE BOILING)

LIQUID METAL HEATED STEAM GENERATORS

PERFORMANCE PROJECTION-WATER SIDE

CONDITIONS LEADING TO MAJOR CONCERNS (DETAILS):

A. OFF-CHEMISTRY OF BOILER WATER

- o CONDENSER LEAKS/NO TIMELY CORRECTIVE ACTION
- o BREAKDOWN OF ION EXCHANGE SYSTEM
- o FAILURE OF INSTRUMENTATION
- o CAUSTIC FROM RESIN REGENERATION
- o IMPURITIES FROM ADDITIONS OF CHEMICALS

B. Na/H_2O REACTIONS

- o ENTRY OF LARGE QUANTITIES OF SODIUM INTO WATER SIDE

C. DNB

- o CORROSION FATIGUE
- o CREEP/FATIGUE INTERACTIONS

LIQUID METAL HEATED STEAM GENERATORS

PERFORMANCE PROJECTION-WATER SIDE

- GIVEN THAT CONDITIONS LEADING TO RAPID CORROSION WILL OCCUR, THE SYSTEM MUST RECOVER AND CONTINUE OPERATION.

- VERIFICATION OF THE ABOVE CRITERION THROUGH EXPERIMENTAL WORK.

- MODELS FOR EXPERIMENTS BASED ON SYSTEM PERFORMANCE LESSONS.

LIQUID METAL HEATED STEAM GENERATORS

PERFORMANCE PROJECTION-WATER SIDE

LIST OF EXPERIMENTS CONSIDERED ESSENTIAL FOR SYSTEM VERIFICATION:

A. STRESS CORROSION IN CAUSTIC CONDITIONS

CONSTANT EXTENSION RATE, CONSTANT LOAD, AND STRAINING ELECTRODE (TEMPERATURE, METALLURGICAL CONDITION FOUND SIGNIFICANT FOR FERRITIC ALLOYS)

B. CORROSION FATIGUE

(CURVE NEEDED TO ESTABLISH DESIGN BASIS UNDER PROTOTYPIC CHEMISTRY AND OFF-CHEMISTRY CONDITIONS.)

C. CORROSION UNDER DNB*

ESTABLISH AN UPPER LIMIT, OR BRACKET OPERATING CONDITIONS THAT LEAD TO DISABLING CONDITIONS.

*IF PART OF DESIGN CONDITIONS

EFFECTS OF LIQUID METALS ON STRUCTURAL ALLOYS

by

N. S. Stoloff

Rensselaer Polytechnic Institute

Troy, New York

Session: High Temperature Thermal Conversion Liquid Metal/Molten Salt

EFFECTS OF LIQUID METALS ON STRUCTURAL ALLOYS

N. S. Stoloff
Materials Engineering Department
Rensselaer Polytechnic Institute
Troy, New York 12181

INTRODUCTION

This paper will briefly review three means by which structural metals in contact with liquid metals can experience deterioration or fracture. There are a) adsorption-induced embrittlement, which is most often encountered at relatively low exposure temperatures, b) cavitation and c) corrosion, which occurs at elevated temperatures. Cavitation and corrosion generally involve significant mass transfer, in contrast to adsorption-induced embrittlement, which is a very localized event.

ADSORPTION-INDUCED EMBRITTLEMENT

The literature of liquid metal embrittlement dates back to 1914. During the past six decades dozens of pure metals and their alloys have been shown to be embrittled by lower melting liquid metals. There are a number of reviews of this literature that are available.[1-4] The characteristics of embrittlement are demonstrated by the stress-strain curves of Fig. 1. Flow properties are unchanged by the liquid; both fracture stress and ductility are reduced, sometimes catastrophically. In recent years a number of instances of embrittlement by solid metallic films also has been reported;[5-8] all indications are that the same embrittlement mechanism is responsible, differing only in the means by which the embrittling species reaches the crack tip. A schematic diagram of the temperature dependence of such embrittlement appears in Fig. 2;[3] there is a trough denoting minimum ductility on either side of the melting point of the

liquid. Although most embrittlement studies have been conducted near room temperature with the low melting metals mercury, gallium, indium, etc., the higher melting metals copper (1083°C) and lead (326°C) produce catastrophic failures of steels at temperatures on either side of the respective embrittler melting points.

No method has yet been devised to predict accurately from first principles which solids are susceptible to LME. Part of the problem in this field is the sensitivity of embrittlement to both test variables (e.g. temperature, strain rate, notches) and material properties (e.g. grain size, solute content, phase distribution). Shunk and Warke,[3] who have published the most detailed analysis of observed embrittlement and non-embrittlement couples Tables 1 and 2, respectively, conclude that specificity of embrittlement is a questionable concept that is most difficult to demonstrate and is inadequately accounted for theoretically. Other researchers, to the contrary, both in the West[9-11] and in the Soviet Union[12-14] have suggested a number of theoretical approaches to embrittlement. One such approach, summarized in Fig. 3, relies on calculations of thermodynamic cycles involving s, p, d electrons of substrate and environment.[9] However, to date this approach has been more successful in rationalizing previously observed LME, rather than predicting new embrittlement couples.

The general features of adsorption induced LME are as follows: a state of tensile stress must exist in the solid, there must be barriers to plastic flow (e.g. grain boundaries, subboundaries or precipitate particles), and there must be good wetting between liquid and solid. Susceptibility to embrittlement is increased by coarse grain size, and by alloying additions that increase planarity of slip.[15] Examples are lowering of stacking fault energy of copper by Al, Zn or Ge, Fig. 4, and the addition of Si or Al to Fe, Fig. 5. Embrittle-

ment can also be influenced by the presence of alloying additions to the liquid.[16] In some cases, e.g. In added to Hg, the wetting characteristics of the liquid metal are improved, which much simplifies the experimental approach.

Fracture paths of single phase fcc base metals almost invariably are intergranular, see Fig. 6 a), whether testing is done in monotonic tension, bending, or fatigue. However, bcc and hcp metals and alloys, as well as precipitation hardened fcc alloys reveal transgranular fracture paths, as shown in Fig. 6 b). For many years transgranular embrittlement was associated with a cleavage mechanism of fracture (lowering of cohesion across low index fracture planes under the action of tensile stress).[16,17] However, Lynch[18,19] has recently shown that what looks like a cleavage fracture at low magnification actually may be a microvoid coalescence failure when viewed in the electron microscope. Examples of fine dimples on transgranular fracture surfaces of cadmium embrittled by gallium[18] and D6AC steel embrittled by lead[19] are shown in Fig. 7 a) and b) respectively. Fractographic evidence which is common to both hydrogen embrittlement and LME, together with analysis of slip traces at crack tips has led Lynch[18,19] to conclude that LME actually occurs in many cases by enhanced shear. For example, observations of LME in aluminum single crystals suggests that crack growth occurs by alternate shear on {111} slip planes intersecting crack tips. Insufficient general strain accompanies crack growth to produce some blunting and growth of microvoids. On this model, LME is a consequence of chemisorption of liquid metal atoms, thereby facilitating nucleation and movement of dislocations on slip planes intersecting crack tips.

CAVITATION

The formation and subsequent collapse of bubbles within a liquid can cause severe erosion of a solid surface in contact with the liquid. When the

local pressure in the liquid is reduced at constant temperature (e.g. at a constriction in a pipe), gas filled cavities can nucleate and grow within the liquid. If cavities formed in a low pressure region pass subsequently into a region of higher pressure, their growth is reversed and they will collapse as the vapor within condenses. It is the collapse of the bubbles that causes the damage. The mechanism most likely involves either shock waves that are produced by bubble collapse and immediate reformation (rebound), see Fig. 8,[20] or impingement of a microjet of liquid through the collapsing cavity onto the surface being damaged as a result of non-symmetrical cavity collapse, Fig. 9. Damage can be accelerated substantially by corrosion, but damage can occur even in the absence of corrosion.

Cavitation damage due to water has been observed on ship's propellers, hydraulic pumps and turbines, on dams and other hydraulic structures. Pitting, a plastically deformed surface layer and, in later stages, fracture of the substrate are characteristic of cavitation damage in ductile metals. Cavitation damage may be even more severe in the presence of liquid metals because damage increases with density of the fluid.[21] Pumps or piping systems utilizing a liquid metal as the working fluid are potential problem areas. An example of pitting due to cavitation damage to a ferritic stainless steel which contained boiling mercury at 1400°F is shown in Fig. 10.[22] Extensive damage with mercury or sodium has been noted also in laboratory tests with several structural materials, as shown in Fig. 11 a) for sodium at 800°F and 11 b) for mercury at 300°F.[21] It can be seen that cobalt-base Stellite B is the most resistant material of those tested in Na and Hg, and that Sicromo 9M, an Fe-Si-Mo alloy, is the most susceptible to damage. Comparisons of several materials in Pb-Bi at 500°F are shown in Table 3.[23] Tantalum alloys are the most resistant of those listed, Nb alloys are the least resistant. Similar results have been obtained at 1500°F,

except that 304 SS is much the worst of the alloys listed. Fig. 12 is a chart classifying 22 alloys or groups of alloys according to their normalized erosion resistance based on volume loss (relative to 18 Cr-8 Ni austenitic stainless having a hardness of 170 DPH).[20] The most resistant alloys: tool steels, stellites and maraging steels, have at least 10x greater erosion resistance than the reference material. The total range of resistance shown spans almost four orders of magnitude, which is far greater than any range of intrinsic material properties. Nevertheless, various properties such as hardness. fracture stress, strain energy to fracture and work hardening rate appear to be good qualitative measures of erosion resistance. Smith and co-workers[24] have investigated cavitation damage to three Inconel centrifugal pump impellors with sodium and with fused flouride in the range 1050-1400F. Although jets in excess of 1/4 in deep were formed, no change in performance of the pumps was detected in tests of less than 3500 hr duration. However, longer periods of exposure would have jeopardized hydraulic performance. Such findings illustrate the importance of time in the cavitation process (an incubation period sometimes needs to be exceeded). However, it is important to emphasize the detrimental effect of concurrent corrosion and erosion. Under such conditions failure is accelerated to a marked degree, since surface roughening due to corrosion, as well as mass transfer, accentuate the effect of erosion.

CORROSION AND MASS TRANSFER

Corrosion problems with liquid metals have previously received considerable attention in various liquid metal cooled nuclear reactor projects as well as for Rankine cycle turbines in nuclear auxiliary power engines for space applications. In the presence of a temperature gradient along a circulating system, mass transfer may occur in the direction of flow as more soluble alloying elements are leached out of the piping. This material is then deposited in

cool regions, leading to eventual failure of the system either by wall penetration in the hot zone or plugging of the passage in the cold zone. Also, when dissimilar metals are immersed in a liquid metal, transfer of a constituent from one material to the other is possible.

Corrosion of stainless steels by Na and NaK systems is mainly by oxidation, and is a function of the purity of the liquid metal. Generally austenitic stainless steels and nickel base alloys perform well in Na or NaK up to 800°C, while these materials as well as low carbon steels with up to 5% Cr suffer considerable attack in liquid mercury at 600°C. The corrosion rate of a solid metal into a liquid metal can be described by:[25]

$$R_i = [\lambda(S_o - S_i)]_{T = T_c}$$

when R_i is the dissolution rate at point i, α is a solution rate constant, S_o is the solubility of the solid metal and S_i the concentration of the solid metal in solution at point i. In most heavy liquid metals α is proportional to the diffusivity of the solid in the liquid and to the velocity of the liquid metal. In practice α will vary little from one metal to another at constant velocities, since diffusivities of most metal in liquid metal at 500°C are of the order of $5 \times 10^{-5} cm^2/sec$. Therefore, the corrosion rate of metals in Hg can be estimated by evaluating $S_o - S_i$ for each metal at constant T and velocity. Liquidus curves for a number of solid metals in mercury are shown in Fig. 13.[25] In general the bcc refractory metals are little soluble in mercury, while Zr, Ti, and Ni are highly soluble. Particularly noteworthy is the approximately 10 fold difference in solubility between Fe and Cr, suggesting that high Cr alloys will be susceptible to mercury corrosion. This has, in fact, been observed in 446 SS an Fe-25% Cr alloy, in contact with mercury at 1400°F.[22]

CONCLUDING REMARKS

The range of possible interactions between liquid metals and structural metals has been summarized in very general terms. The literature of LME is extensive, and several detailed review monographs are available.[1,2,4] For lack of space there has been no description here of embrittlement resulting from cyclic loading, for a general revision of which the reader is referred to two recent papers.[4,26] In addition, there is an extensive literature[27-32] on fatigue of austenitic stainless steels in liquid sodium which shows that fatigue lives are extended and crack growth rates reduced in sodium relative to air, see Figs. 14 and 15. This effect has been attributed to lack of oxygen at the crack tip when tests are run in sodium, since tests run in vacuum give the same results as tests in sodium.

REFERENCES

1. N. S. Stoloff in Surfaces and Interfaces II, J. J. Burke, et al Eds, p. 157, Syracuse Univ Press, Syracuse, N. Y. (1968).

2. M. H. Kamdar, Prog Mat Sci, V. 15, 1973, p. 289.

3. F. A. Shunk and W. R. Warke, Scripta Met., V. 8, 1974, p. 519.

4. N. S. Stoloff in Proc. Symp. on Environment-Sensitive Fracture of Engineering Materials, Chicago, Ill., Oct. 1977, to be published.

5. S. Mostovoy and N. N. Breyer, Trans. ASM, V. 61, 1968, p. 219.

6. D. N. Fager and W. F. Spurr, Corrosion, V. 26, 1970, p. 409.

7. J. C. Lynn, W. R. Warke and P. Gordon, Mat Sci and Eng., V. 18, 1975, p. 159.

8. D. N. Fager and W. F. Spurr, Corrosion, V. 27, 1971, p. 72.

9. M. Kelley and N. S. Stoloff, Met Trans A, V. 6A, 1975, p. 159.

10. A. R. C. Westwood, C. M. Preece and M. H. Kamdar in "Fracture", V. 3, H. Liebowitz, Ed., p. 589, Academic Press, New York (1971).

11. W. Rostoker, J. M. McCaughey and H. Markus, "Embrittlement by Liquid Metals", Reinhold Publ. Corp., New York, 1960.

12. M. M. Chaevskii, Sov. Mat. Sci., V. 1, 1965, p. 637 (p. 433, English Translation).

13. M. M. Chaevskii, Sov. Mat. Sci., V. 2, 1966, p. 143 (p. 102, English Translation).

14. N. V. Pertsov and P. A. Rebinder, DAN SSR, V. 123, 1958, p. 1068.

15. T. L. Johnston, R. G. Davies, and N. S. Stoloff, Phil Mag., V. 12, 1965, p. 305.

16. N. S. Stoloff and T. L. Johnston, Acta Met, V. 11, 1963, p. 251.

17. A. R. C. Westwood and M. H. Kamdar, Phil Mag., V. 8, 1963, p. 787.

18. S. P. Lynch, Materials Report 102, Aeronautical Res. Labs, Melbourne, Australia, Feb. 1977.

19. S. P. Lynch and N. E. Ryan, Proc Sec. Int. Congress on Hydrogen in Metals, 1977, Paris, France, paper 3 D 12.

20. F. G. Hammitt and F. J. Heymann, Metals Handbook, V. 10, 8th Ed., 1975, p. 160.

21. S. G. Young and T. R. Johnston in "Erosion by Cavitation or Impingement" ASTM STP 408, 1967, p. 186.

22. L. Klein, N. S. Stoloff, and D. J. Duquette, unpublished.

23. R. Garcia, F. G. Hammitt and R. E. Nystrom, in "Erosion by Cavitation and Impingement", ASTM STP 408, ASTM, Philadelphia, Pa., 1967, p. 239.

24. P. G. Smith, J. H. DeVan and A. G. Grindell, Trans ASME, J. Basic Eng., Sept. 1963, p. 329.

25. J. R. Weeks, Corrosion, April 1967, p. 98.

26. T. M. Regan and N. S. Stoloff, Met Trans. A, V. 8A, 1977, p. 885.

27. L. A. James and R. C. Knecht, Met Trans. V. 6A, 1975, pp. 109-116.

28. R. F. Koenig and S. R. Vandenberg, Met. Prog, V. 61, 1952, pp. 71-75.

29. J. W. Martin and G. C. Smith, Metallurgia, V. 56, pp. 227-232, 238.

30. J. K. Beddow, Metallurgia, V. 77, 1968, pp. 185-188.

31. L. H. Kirscher and R. C. Andrews, J. Basic Eng., Trans ASME, V. 91, 1969, pp. 785-791.

32. J. G. Y. Chow, Report BNL 50339, Brookhaven National Lab, 1971.

TABLE 1. (Ref. 3)

Summary of Embrittlement Couples.

P - element (nominally pure) C - commercial
A - alloy L - laboratory

Solid \ Liquid		Hg		Cs	Ga		Na	In		Li	Sn		Bi		Tl	Cd	Pb		Zn	Te	Sb	Cu
		P	A	P	P	A	P	P	A	P	P	A	P	A	P	P	P	A	P	P	P	P
Sn	P	x			x																	
Bi	P	x																				
Cd	P		x	x	x	x					x											
Zn	P	x	x		x						x						x					
	LA		x																			
Mg	CA						x												x			
Al	P	x	x		x			x				x				x						
	CA	x	x		x		x	x			x								x			
Ge	P				x			x			x		x		x	x	x				x	
Ag	P	x	x		x	x				x												
	LA									x												
Cu	CP	x	x				x			x			x	x			x					
	LA	x																				
	CA	x	x					x	x	x	x(?)		x				x					
Ni	P	x								x							x					
	LA									x												
	CA										x						x					
Fe	P																					x(?)
	LA	x	x							x												
	CA							x		x	x					x	x	x	x	x		
Pd	P									x												
	LA									x												
Ti	CA		x													x						

TABLE 2. (Ref. 3)

Summary of Non-Embrittling Couples

P - element (nominally pure)
A - alloy
C - commercial
L - laboratory

a - limited testing (known or inferred)
b - one test temperature (inferred)
c - no published information on test
e - also reported as embrittling

Solid \ Liquid		Hg		Ga	Na	In	Li	Se	Sn	Bi	Tl	Cd	Pb	Zn	Te
		P	A	P	P	P	P	P	P	P	P	P	P	P	P
Bi	P			c											
Cd	P	a	a												
Pb	P	c													
Zn	P												c,e		
Mg	CA		b	b		b	b	b	b	b	b	b	b		
Al	P								a						
	CA						b	b		b	b	b	b		
Au	P	b		b											
Cu	CP	a,e		c					c					c	
Fe	P	b	b			b									
	LA	b	b												
	CA		b	b	b			b	b,e	b	b		b,e		
Ti	CA			b	b	b	b	b	b	b	b		b	b	b

TABLE 3 Damage Data from Vibratory Tests of High-temperature Alloys Immersed in Molten Lead-Bismuth

TABLE 3 (A) Damage in Lead-Bismuth at 500 F

MATERIAL	AVERAGE WEIGHT-LOSS RATE (MG/HR)	AVERAGE MDP† RATE (MILS/HR)
T-111 Tantalum alloy	49.1	0.72
T-222 Tantalum alloy‡	51.6	0.76
Mo-½Ti	30.7	0.78
316 SS	26.6	0.88
304 SS	28.2	0.93
Cb-1Zr	55.1	1.63
Cb-1Zr‡	119.5	3.54

† MDP denotes (volume loss)/(specimen face area).
‡ Annealed condition.
SOURCE: Adapted from Garcia et al. (20,21).

TABLE 3 (B) Damage in Lead-Bismuth at 1500 F

MATERIAL	AVERAGE WEIGHT-LOSS RATE (MG/HR)	AVERAGE MDP† RATE (MILS/HR)
T-111 Tantalum alloy	57.1	0.84
T-222 Tantalum alloy‡ (annealed)	59.9	0.88
Mo-0.5Ti	42.6	1.08
Cb-1Zr	70.0	2.07
316 SS	83.3	2.80
Cb-1Zr‡	128.4	3.80
304 SS	342.0	11.30

† MDP denotes (volume loss)/(specimen face area).
‡ Annealed condition.

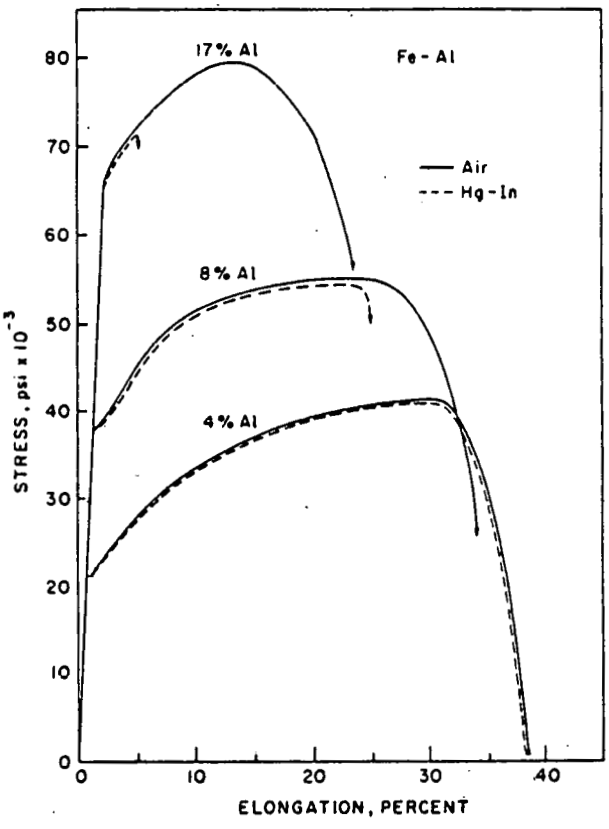


FIGURE 1. Mercury-induced embrittlement of Fe-Al alloys, illustrating lack of effect on yield stress and strain hardening rate (Ref. 1)

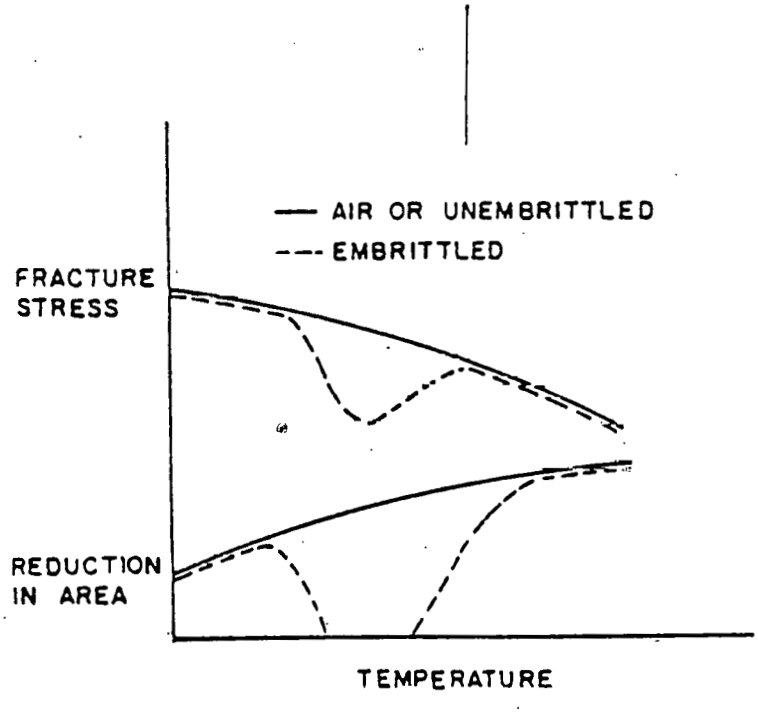


FIGURE 2. Effect of temperature on embrittlement due to solid and liquid metals (3).

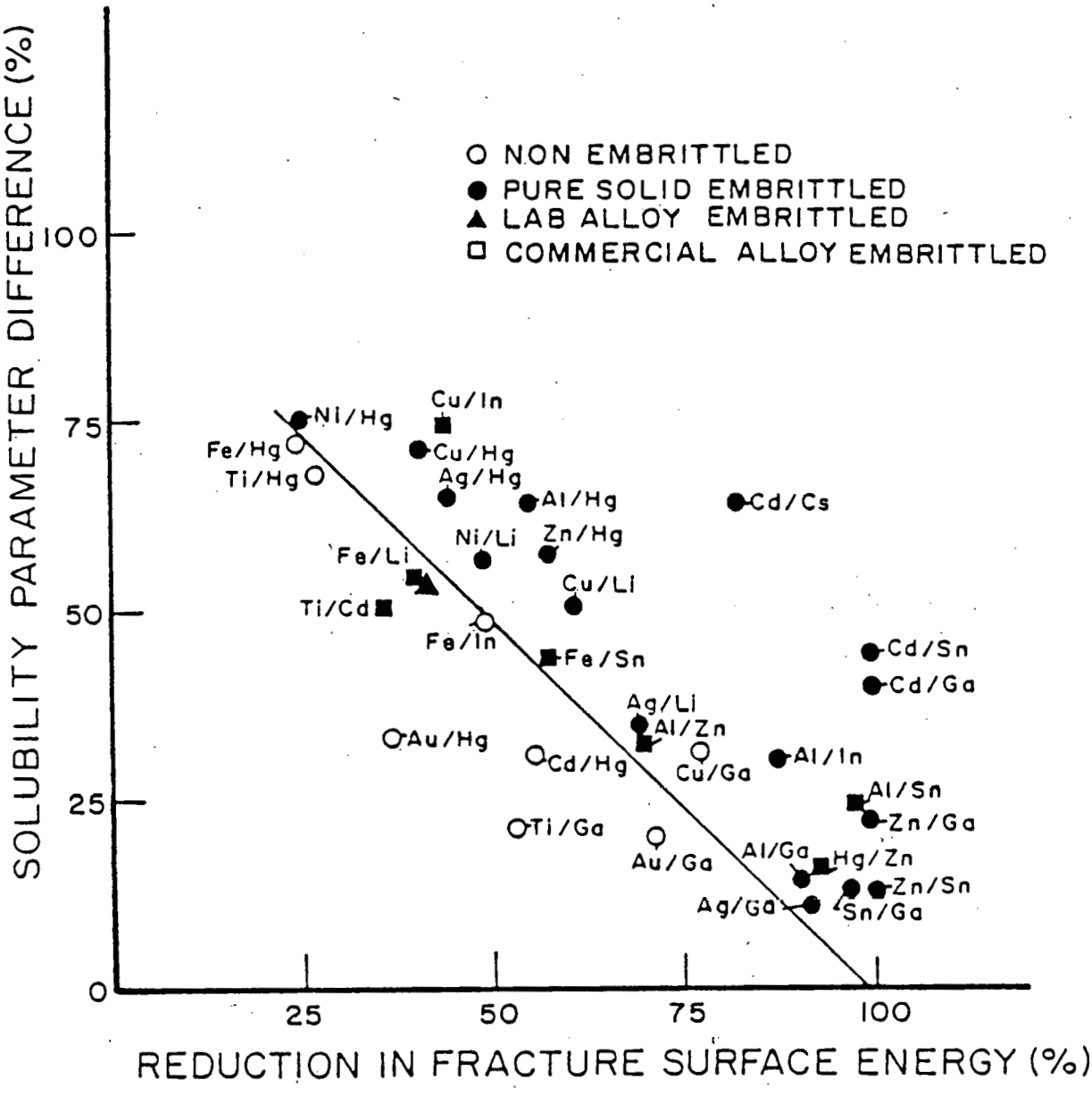


FIGURE 3. Calculated reductions in FSE relative to solubility parameter. (4)

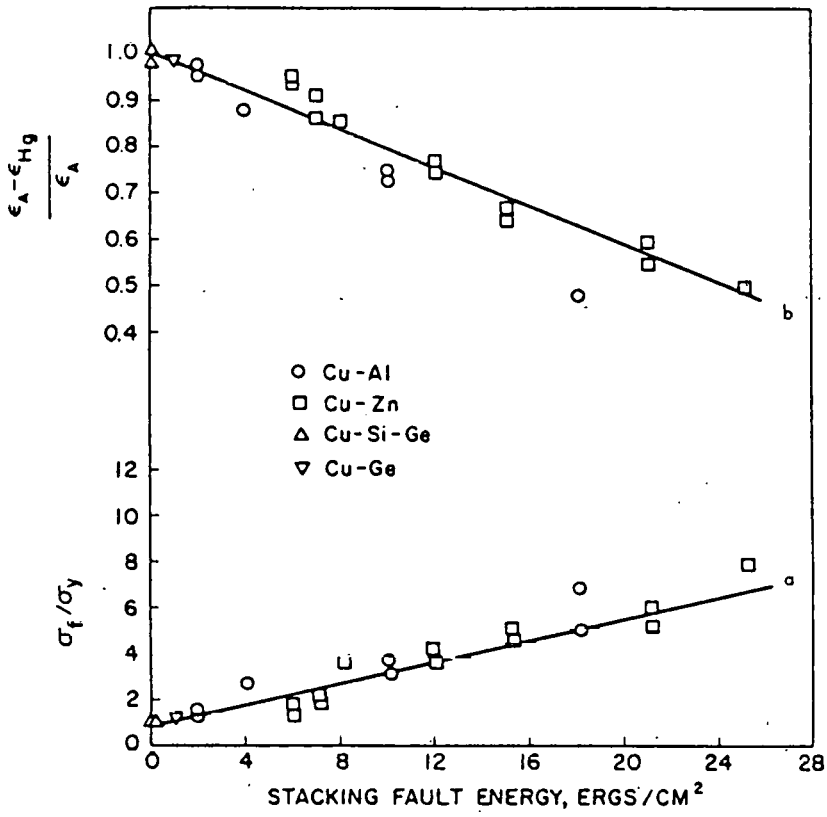


FIGURE 4. The effect of stacking fault energy on stress and strain embrittlement parameters for copper-base alloys tested in mercury (Johnston et al. [15]).

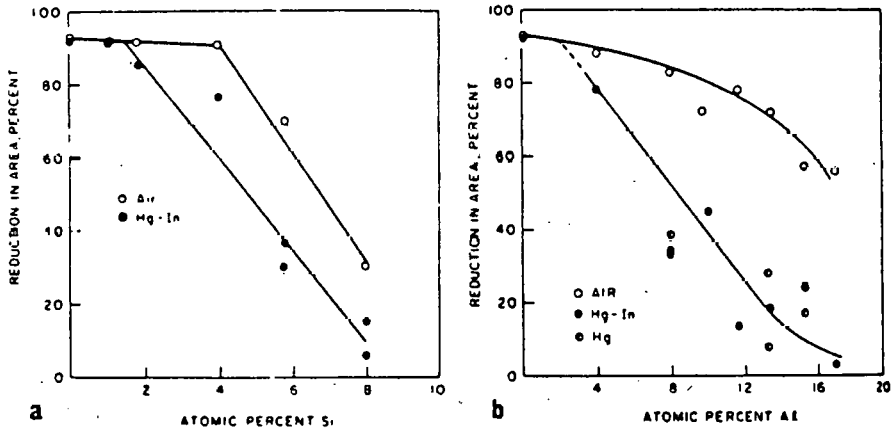


FIGURE 5. The influence of mercury-indium on the ductility of iron-base alloys (a) Fe-Si (b) Fe-Al (Ref. 1).



FIGURE 6 a). Microstructure illustrating intergranular cracks in coarse-grained 70/30 brass wetted with mercury. (X150) (Ref. 11)

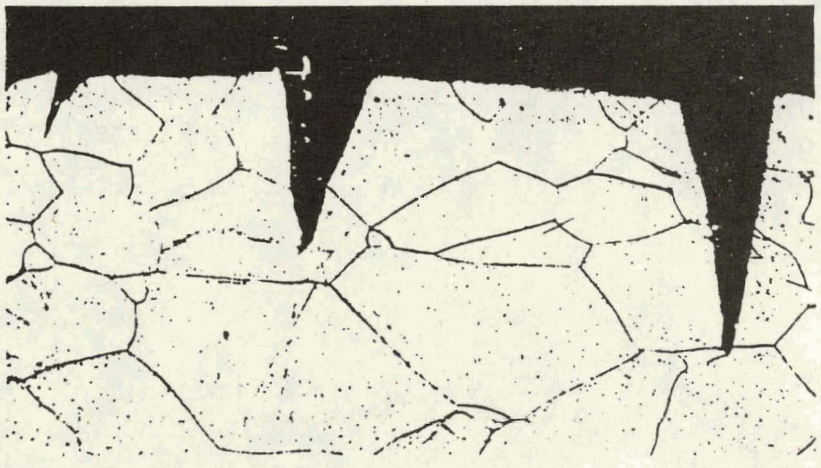


FIGURE 6 b). Edge cracks in necked region of Fe-5.7 pct Si, tested to fracture in mercury-indium, X1000. (Ref. 1)

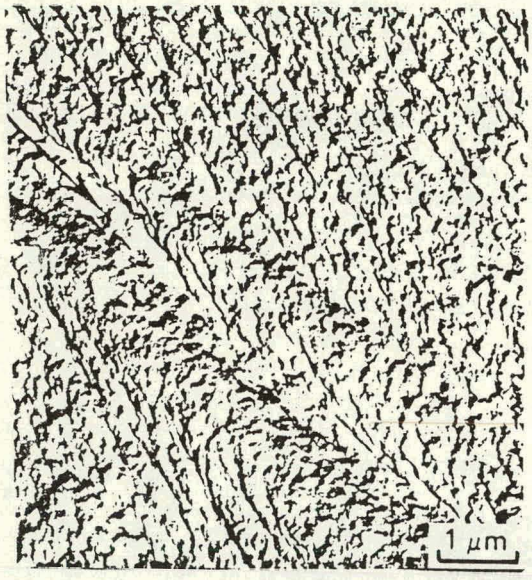


FIGURE 7 a). Dimples in Cd fractured in Ga. (18)

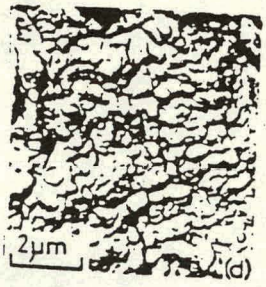


FIGURE 7 b). D6aC Steel, tested in Hg. (19)

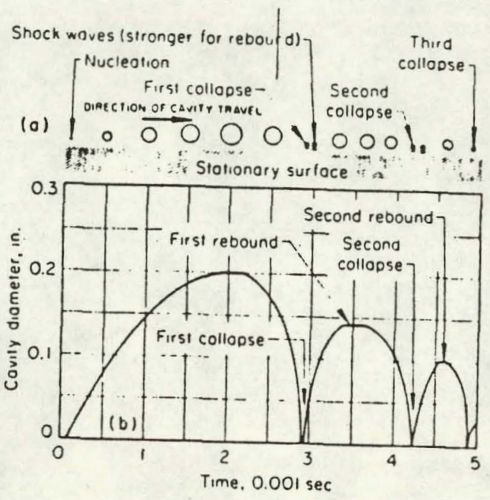


FIGURE 8. (a) Schematic representation of successive stages of growth, collapse and rebound of a single traveling cavity. (b) Graph of cavity diameter as a function of time for the cavity in (a).(Ref. 20)

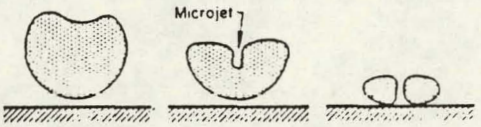


FIGURE 9. Schematic representation of successive stages of nonsymmetrical cavity collapse with microjet impingement against a metallic surface. (Ref. 20)

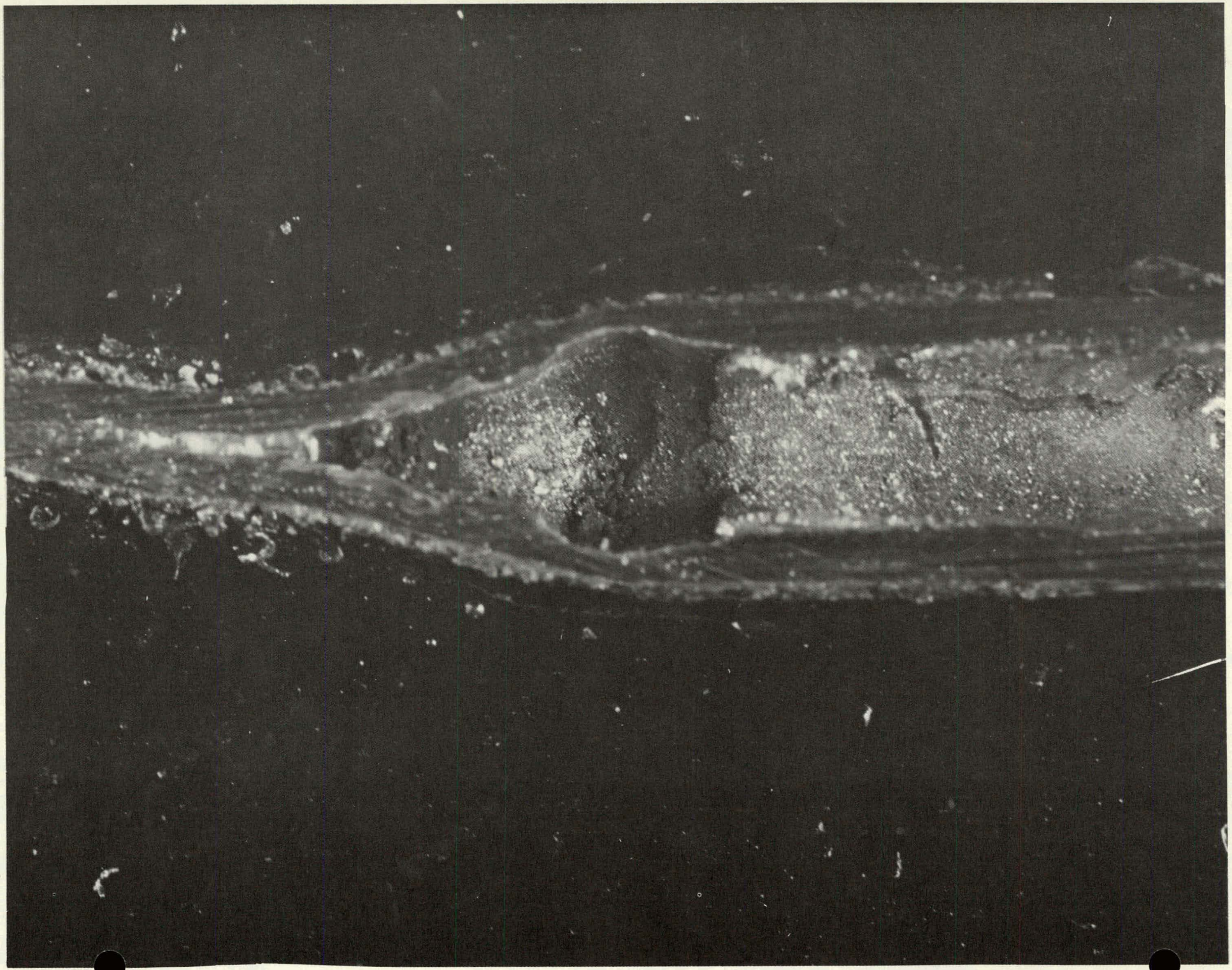


FIGURE 10. Type 446 Stainless Steel in contact with boiling Hg, 2.5 years. (22)

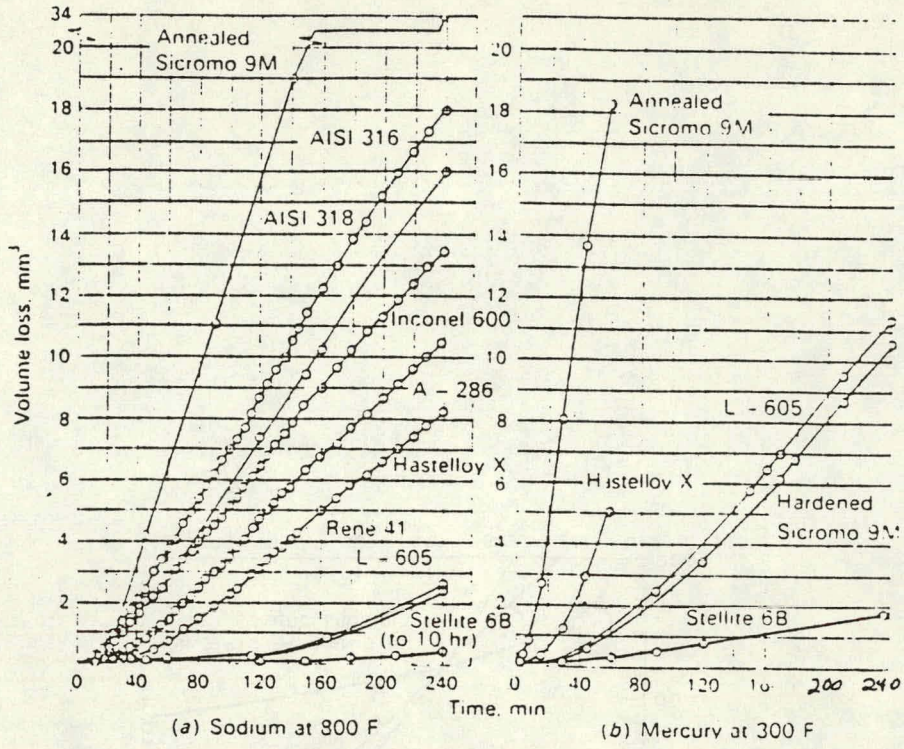


FIGURE 11. Vibratory-cavitation-damage results from tests in liquid metals (25 kc sec. 1.75-mil amplitude) at the NASA Lewis Laboratory. [Young and Johnston (21).]

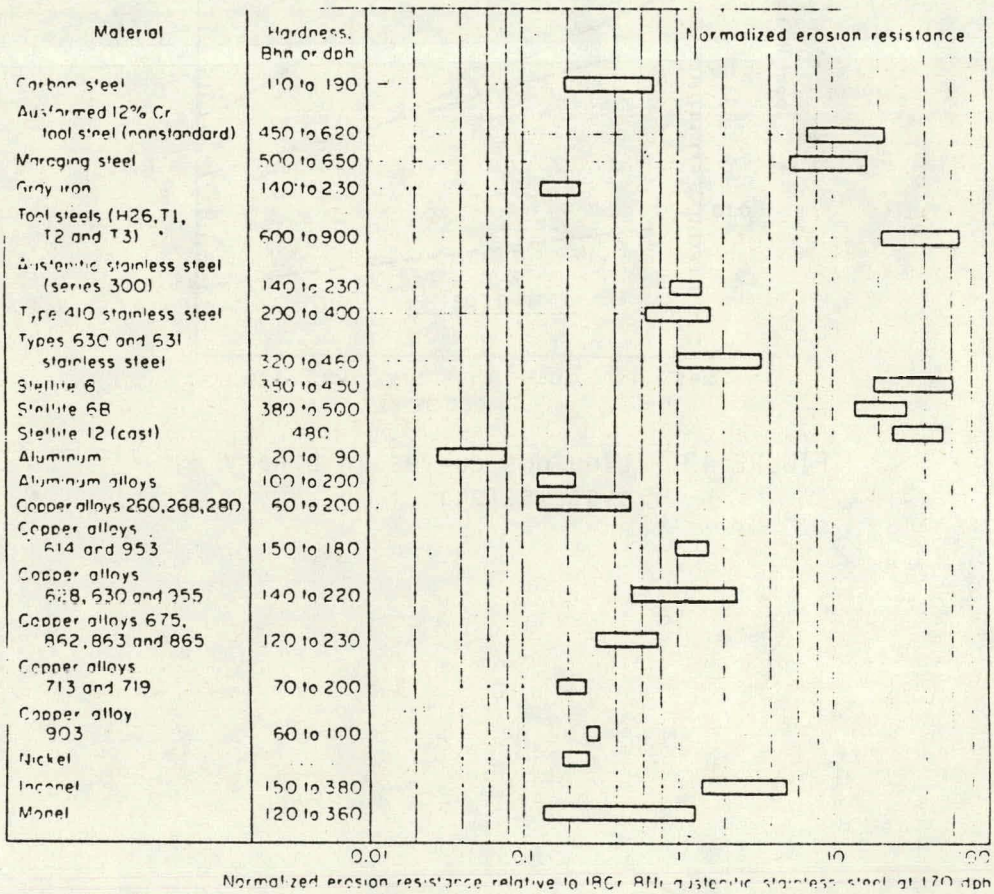


FIGURE 12. Classification of 22 alloys or alloy groups according to their normalized erosion resistance relative to 18Cr-8Ni austenitic stainless steel having a hardness of 170 dph. (20)

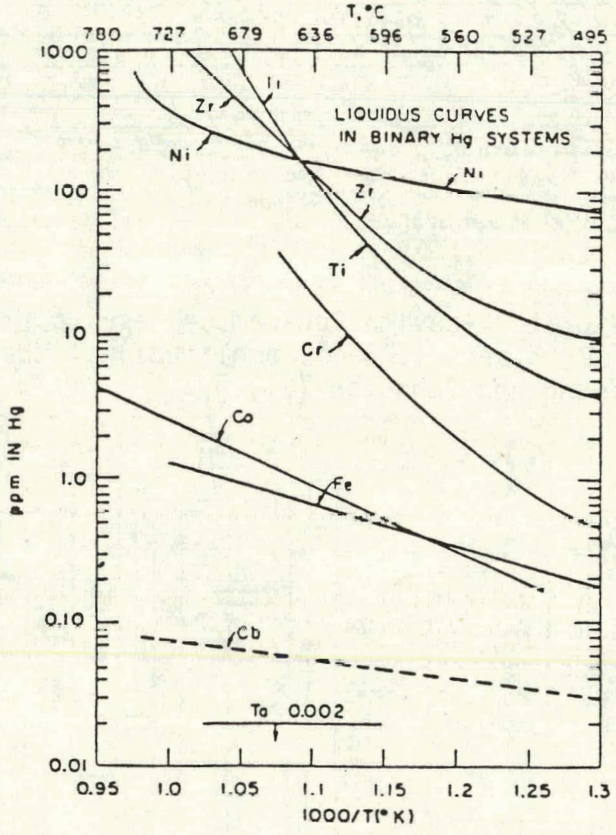


FIGURE 13. Liquidus curves in binary Hg systems.(25)

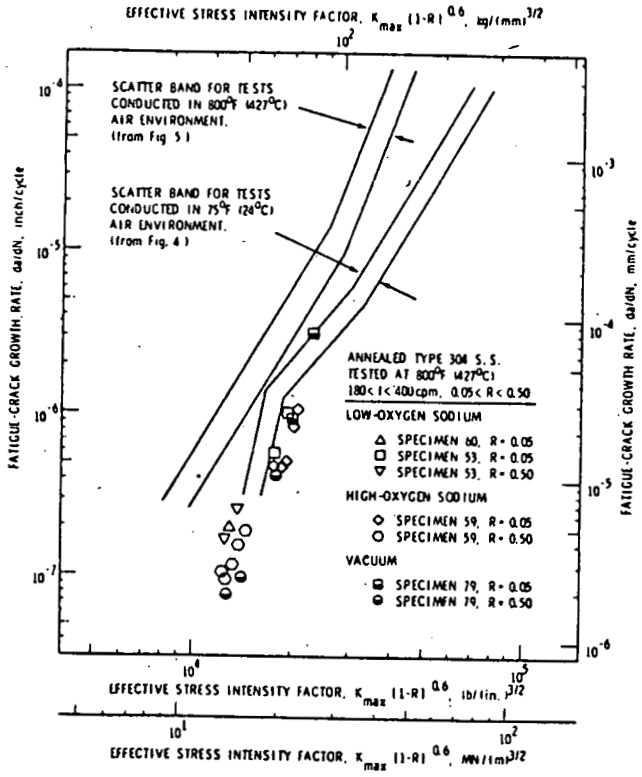


FIGURE 14. Fatigue-crack propagation behavior of annealed Type 304 stainless steel in sodium and vacuum environments at 800°F (427°C).

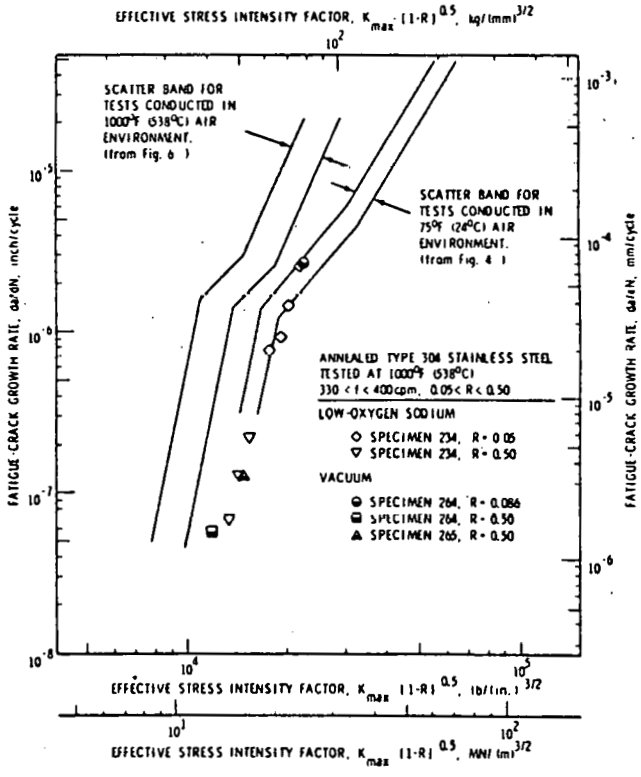


FIGURE 15. Fatigue-crack propagation behavior of annealed Type 304 stainless steel in sodium and vacuum environments at 1000°F (538°C).

EFFECTS OF LIQUID METALS ON STRUCTURAL ALLOYS

Viewgraphs Presented

by

N. S. Stoloff

Rensselaer Polytechnic Institute

Troy, New York

TABLE 1. (Ref. 3)

Summary of Embrittlement Couples

P - element (nominally pure) C - commercial
A - alloy L - laboratory

Solid \ Liquid		Hg		Cs	Ga		Na	In		Li	Sn		Bi		Tl	Cd	Pb		Zn	Te	Sb	Cu
		P	A	P	P	A	P	P	A	P	P	A	P	A	P	P	P	A	P	P	P	P
n	P	x			x																	
i	P	x																				
Cd	P		x	x	x	x					x											
Zn	P	x	x		x						x						x					
	LA		x																			
Mg	CA						x												x			
Al	P	x	x		x			x				x				x						
	CA	x	x		x		x	x			x								x			
Ge	P				x			x			x		x		x	x	x				x	
Ag	P	x	x		x	x				x												
	LA									x												
Cu	CP	x	x				x			x			x	x			x					
	LA	x																				
	CA	x	x					x	x	x	x(?)		x				x					
Ni	P	x								x							x					
	LA									x												
	CA										x						x					
Fe	P																					x(?)
	LA	x	x							x												
	CA							x		x	x					x	x	x	x	x		
Pd	P									x												
	LA									x												
Ti	CA		x													x						

TABLE 2. (Ref. 3)

Summary of Non-Embrittling Couples

P - element (nominally pure)
A - alloy
C - commercial
L - laboratory

a - limited testing (known or inferred)
b - one test temperature (inferred)
c - no published information on test
e - also reported as embrittling

Solid \ Liquid		Hg		Ga	Na	In	Li	Se	Sn	Bi	Tl	Cd	Pb	Zn	Te
		P	A	P	P	P	P	P	P	P	P	P	P	P	P
Bi	P			c											
Cd	P	a	a												
Pb	P	c													
Zn	P												c,e		
Mg	CA		b	b		b	b	b	b	b	b	b	b		
Al	P								a						
	CA						b	b		b	b	b	b		
Au	P	b		b											
Cu	CP	c,e		c					c					c	
Fe	P	b	b			b									
	LA	b	b												
	CA		b	b	b			b	b,e	b	b		b,e		
Ti	CA			b	b	b	b	b	b	b	b		b	b	b

TABLE 3 Damage Data from Vibratory Tests of High-temperature Alloys Immersed in Molten Lead-Bismuth

TABLE 3 (A) Damage in Lead-Bismuth at 500 F

MATERIAL	AVERAGE WEIGHT-LOSS RATE (MG/HR)	AVERAGE MDP† RATE (MILS/HR)
T-111 Tantalum alloy	49.1	0.72
T-222 Tantalum alloy‡	51.6	0.76
Mo-1Ti	30.7	0.78
316 SS	26.6	0.88
304 SS	28.2	0.93
Cb-1Zr	55.1	1.63
Cb-1Zr‡	119.5	3.54

† MDP denotes (volume loss)/(specimen face area).
‡ Annealed condition.
SOURCE: Adapted from Garcia et al. (20,21).

TABLE 3 (B) Damage in Lead-Bismuth at 1500 F

MATERIAL	AVERAGE WEIGHT-LOSS RATE (MG/HR)	AVERAGE MDP† RATE (MILS/HR)
T-111 Tantalum alloy	57.1	0.84
T-222 Tantalum alloy‡ (annealed)	59.9	0.88
Mo-0.5Ti	42.6	1.08
Cb-1Zr	70.0	2.07
316 SS	83.3	2.80
Cb-1Zr‡	128.4	3.80
304 SS	342.0	11.30

† MDP denotes (volume loss)/(specimen face area).
‡ Annealed condition.

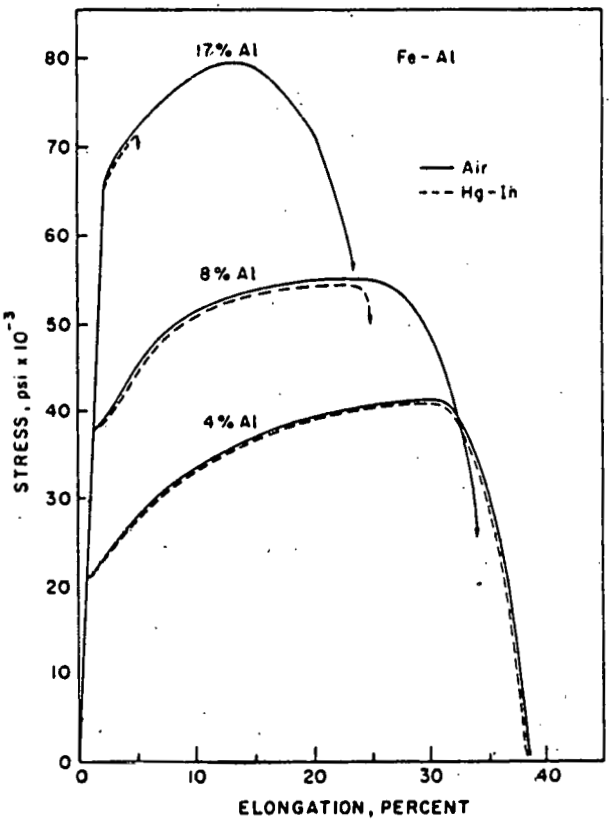


FIGURE 1. Mercury-induced embrittlement of Fe-Al alloys, illustrating lack of effect on yield stress and strain hardening rate (Ref. 1)

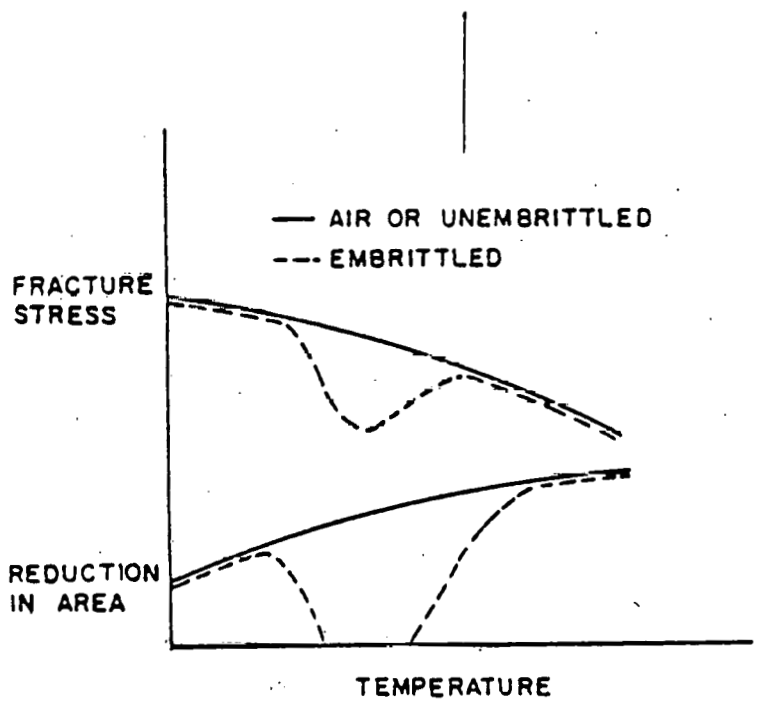


FIGURE 2. Effect of temperature on embrittlement due to solid and liquid metals (3).

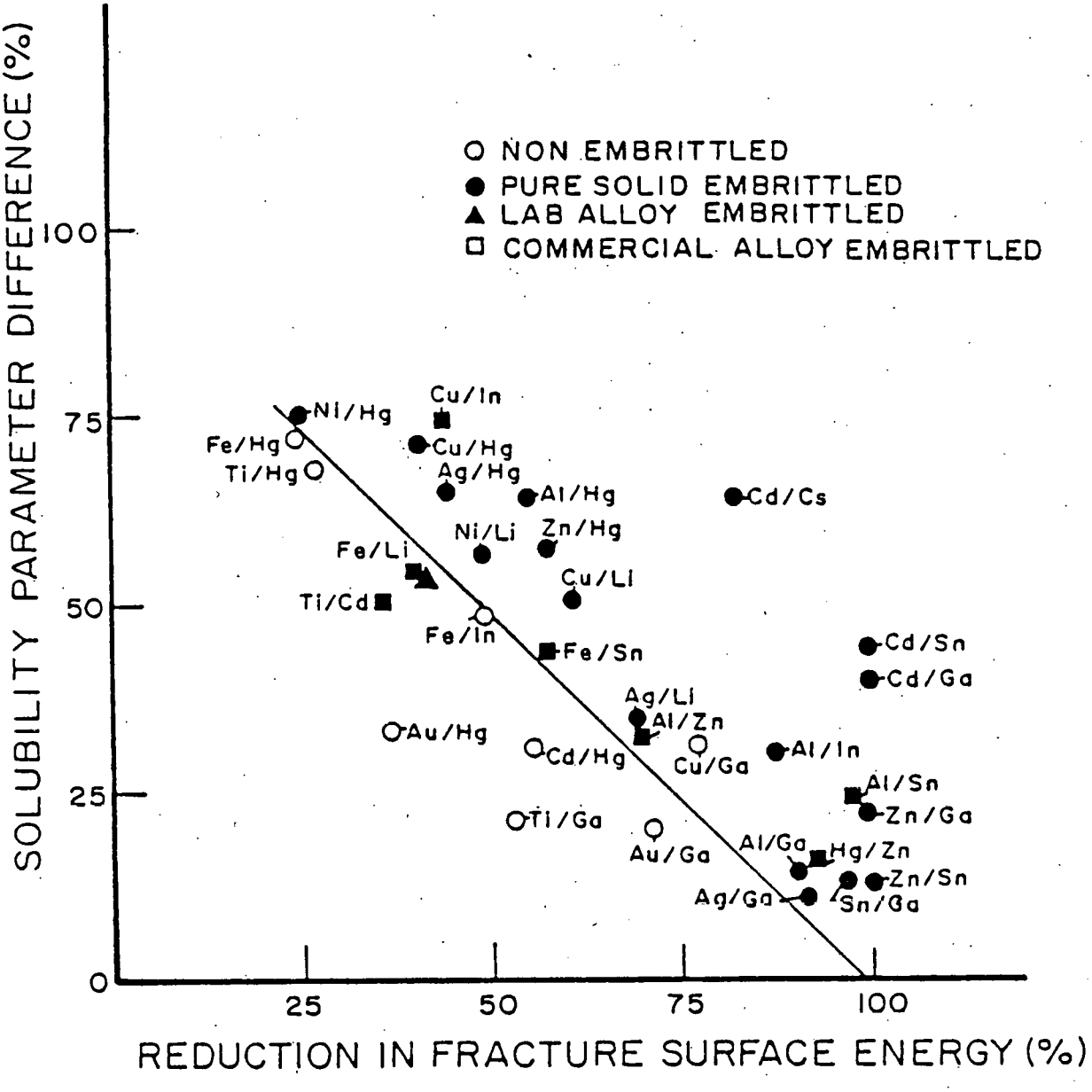


FIGURE 3. Calculated reductions in FSE relative to solubility parameter. (4)

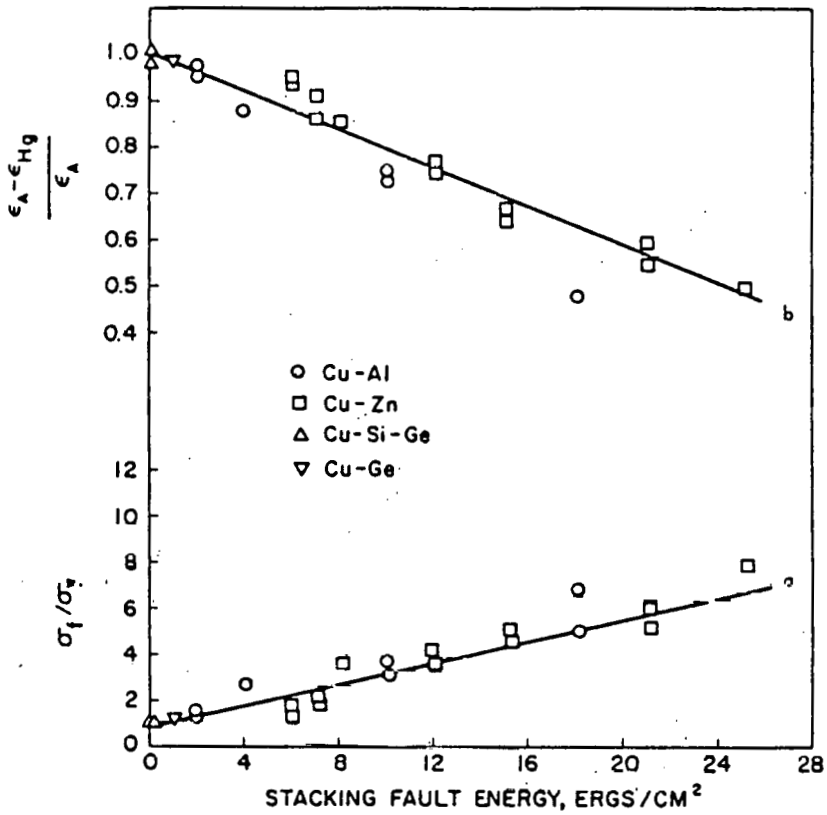


FIGURE 4. The effect of stacking fault energy on stress and strain embrittlement parameters for copper-base alloys tested in mercury (Johnston et al. [15]).

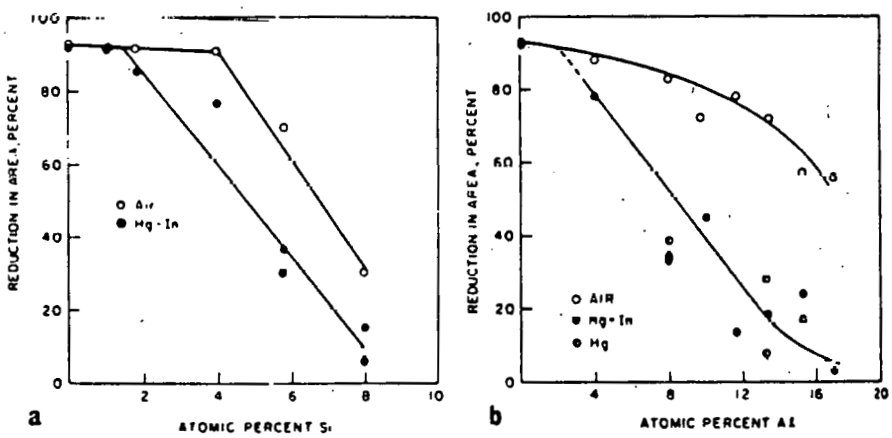


FIGURE 5. The influence of mercury-indium on the ductility of iron-base alloys (a) Fe-Si (b) Fe-Al (Ref. 1).

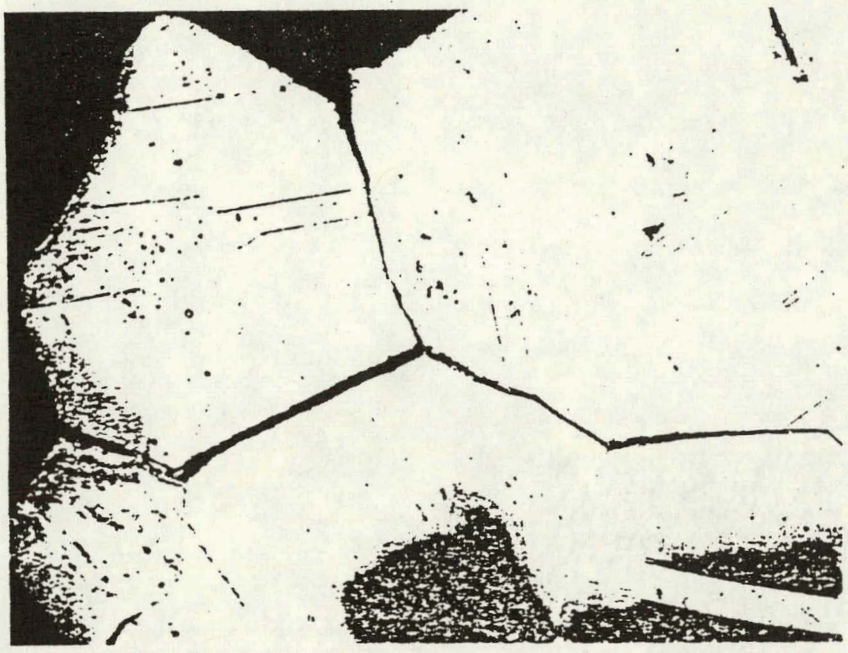


FIGURE 6 a). Microstructure illustrating intergranular cracks in coarse-grained 70/30 brass wetted with mercury. (X150) (Ref. 11)

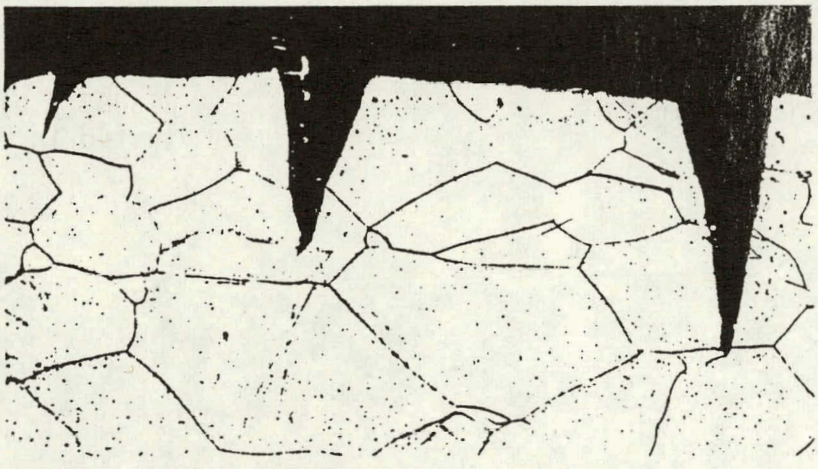


FIGURE 6 b). Edge cracks in necked region of Fe-5.7 pct Si, tested to fracture in mercury-indium, X1000. (Ref. 1)

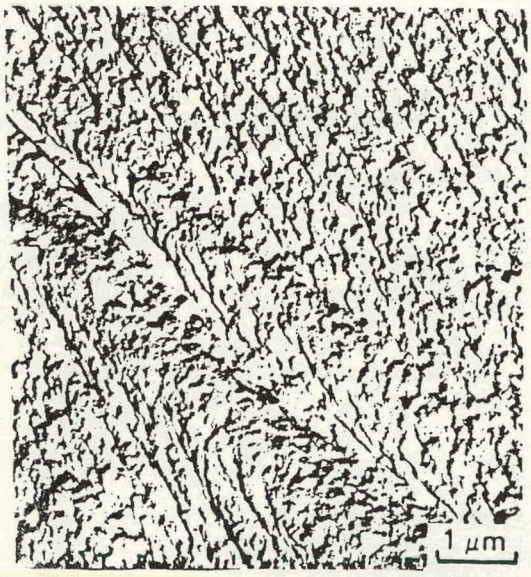


FIGURE 7 a). Dimples in Cd fractured in Ga. (18)

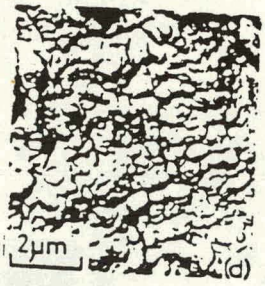


FIGURE 7 b). D6aC Steel, tested in Hg. (19)

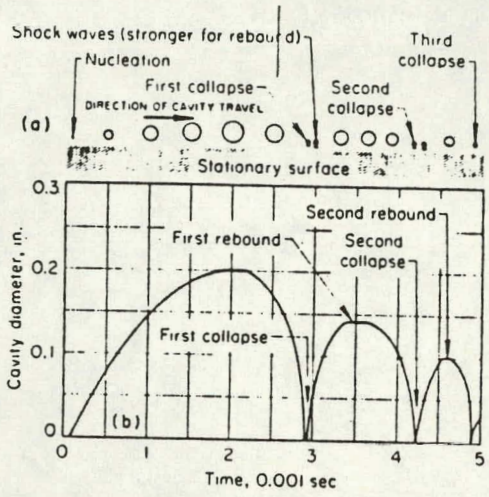


FIGURE 8. (a) Schematic representation of successive stages of growth, collapse and rebound of a single traveling cavity. (b) Graph of cavity diameter as a function of time for the cavity in (a).(Ref. 20)

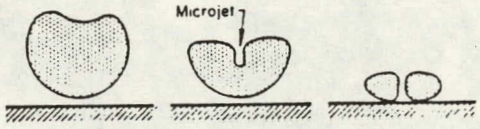


FIGURE 9. Schematic representation of successive stages of nonsymmetrical cavity collapse with microjet impingement against a metallic surface. (Ref. 20)

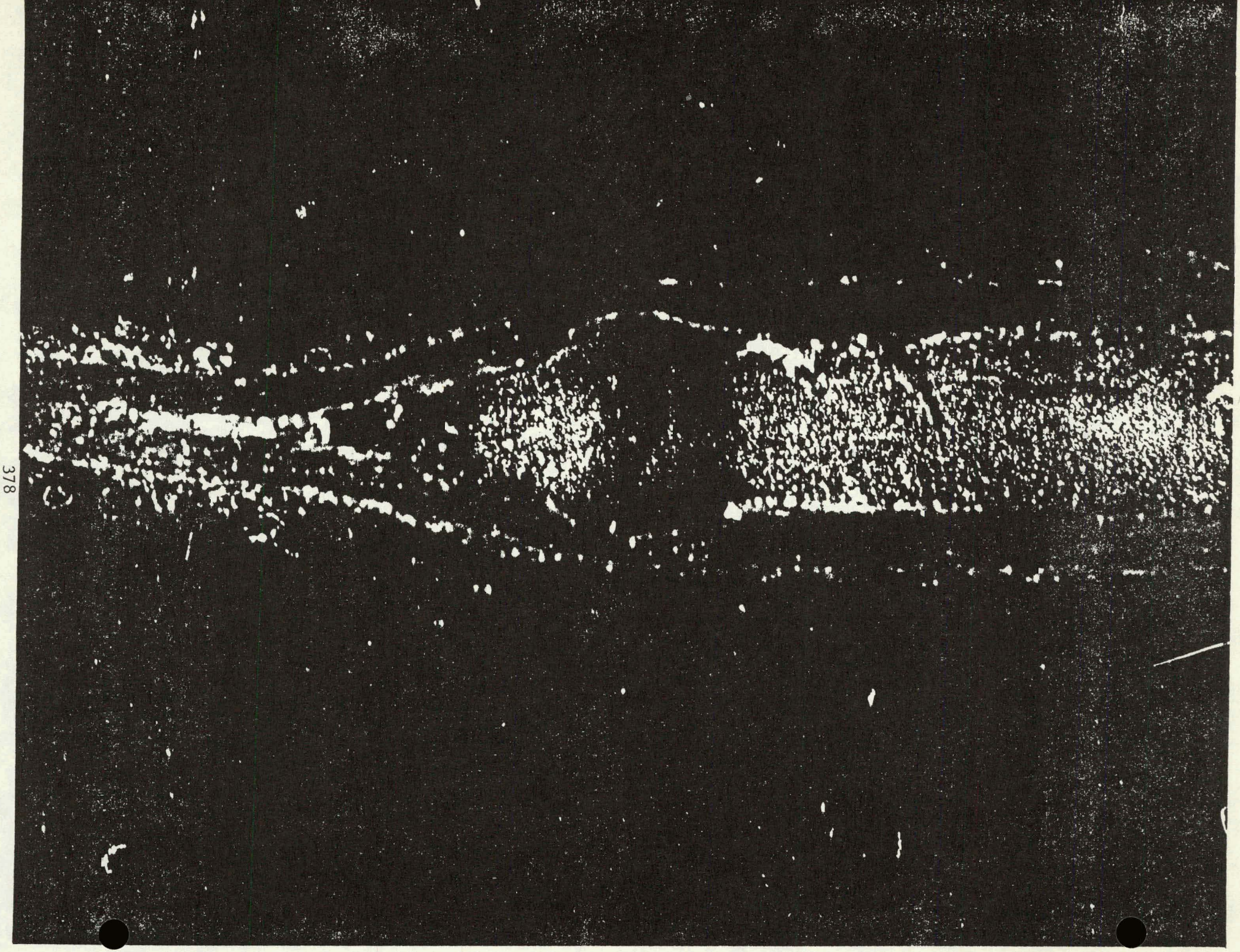


FIGURE 10 Type 446 Stainless Steel in contact with boiling Hg, 2.5 years. (9a)

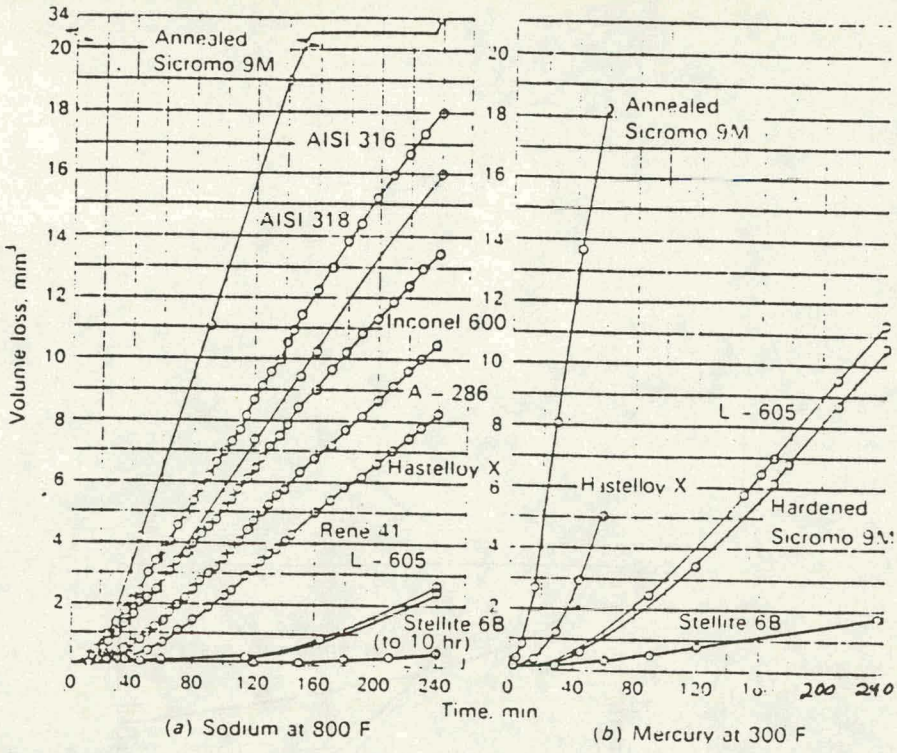


FIGURE 11. Vibratory-cavitation-damage results from tests in liquid metals (25 kc sec. 1.75-mil amplitude) at the NASA Lewis Laboratory. [Young and Johnston (21).]

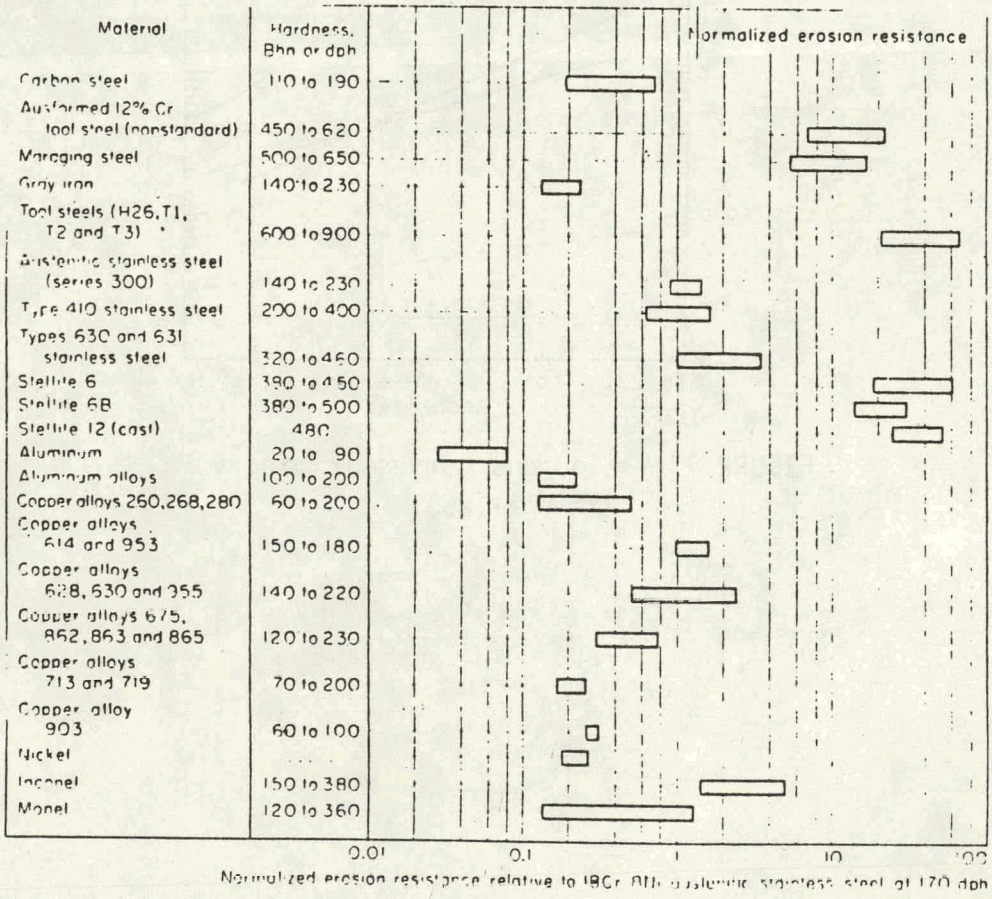


FIGURE 12. Classification of 22 alloys or alloy groups according to their normalized erosion resistance relative to 18Cr-8Ni austenitic stainless steel having a hardness of 170 dph. (20)

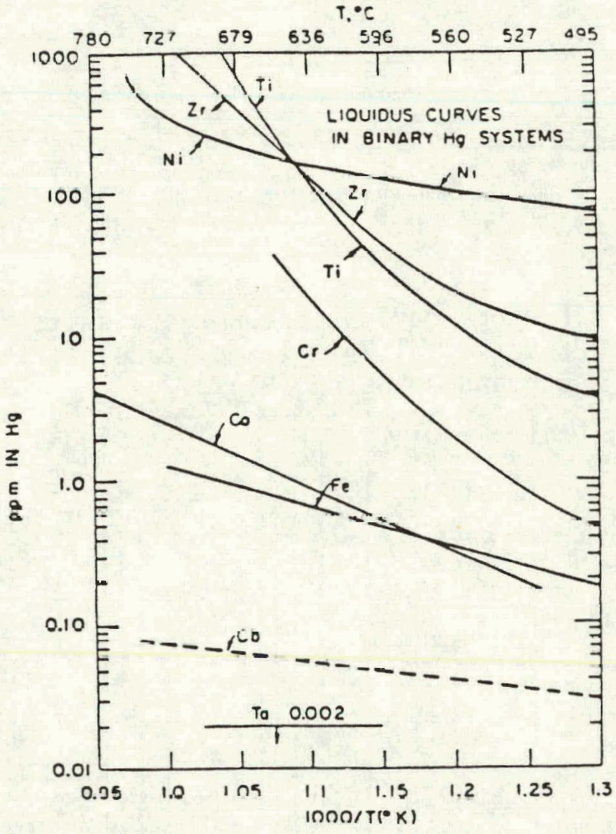


FIGURE 13. Liquidus curves in binary Hg systems.(25)

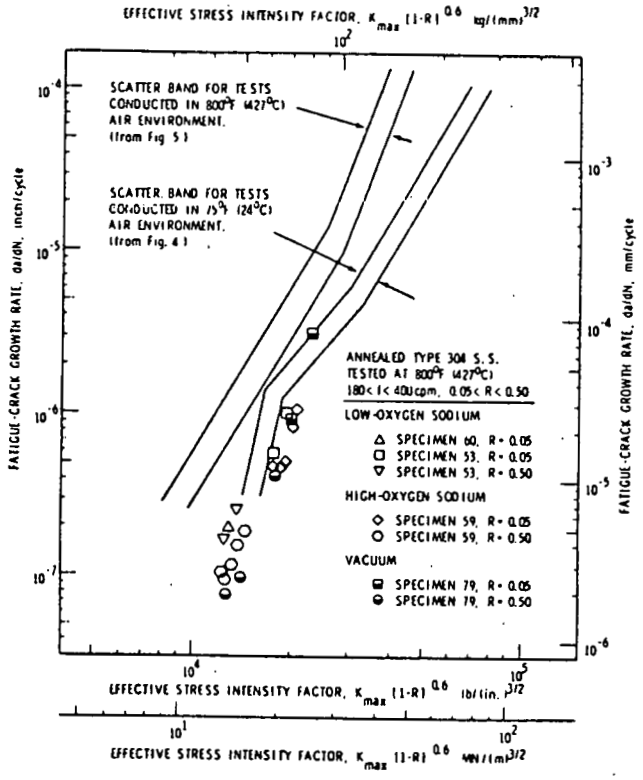


FIGURE 14. Fatigue-crack propagation behavior of annealed Type 304 stainless steel in sodium and vacuum environments at 800°F (427°C).

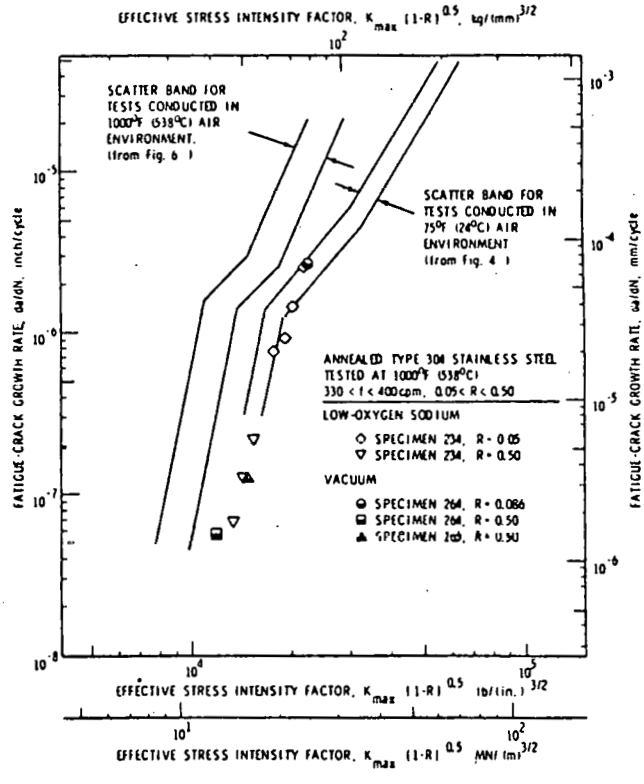


FIGURE 15. Fatigue-crack propagation behavior of annealed Type 304 stainless steel in sodium and vacuum environments at 1000°F (538°C).

SUPPLEMENTARY FIGURES

LME Variables

External

Temperature

Strain Rate

Notches

Cyclic vs. Monotonic loading

Internal

Crystal orientation

Grain size

Slip character

Phases

Solutes in liquid

Prestrain

Cavitation Resistance

Solid

- Hardness
- Tensile Strength
- Energy Density

Liquid

- Density
- Solubility

System

- Pressure drops
- Temperature

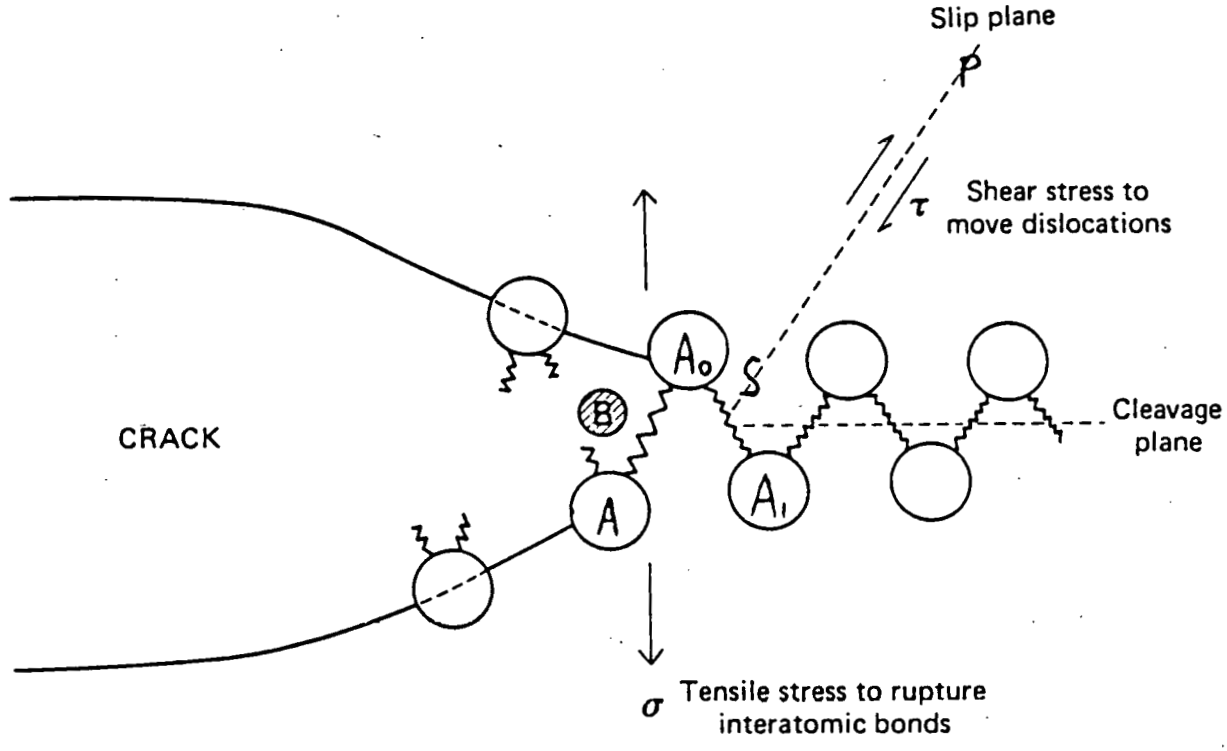


Fig.3. Schematic diagram illustrating commonly proposed mechanism of LME; adsorption of liquid-metal atom, B, at crack tip lowers the tensile stress, σ, required to rupture interatomic bond, A–Ao, but does not influence the shear stress, τ, necessary to move dislocations on slip plane (S–P).

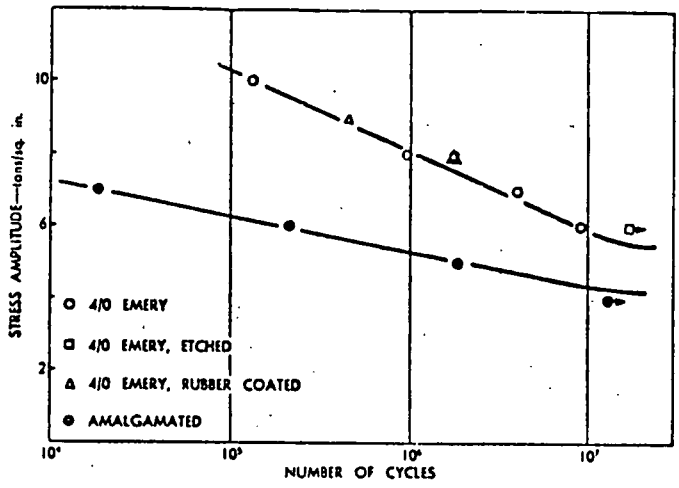


Fig. 1.—S–N curves for Wohler tests on 70/30 brass, before and after amalgamation with mercury.

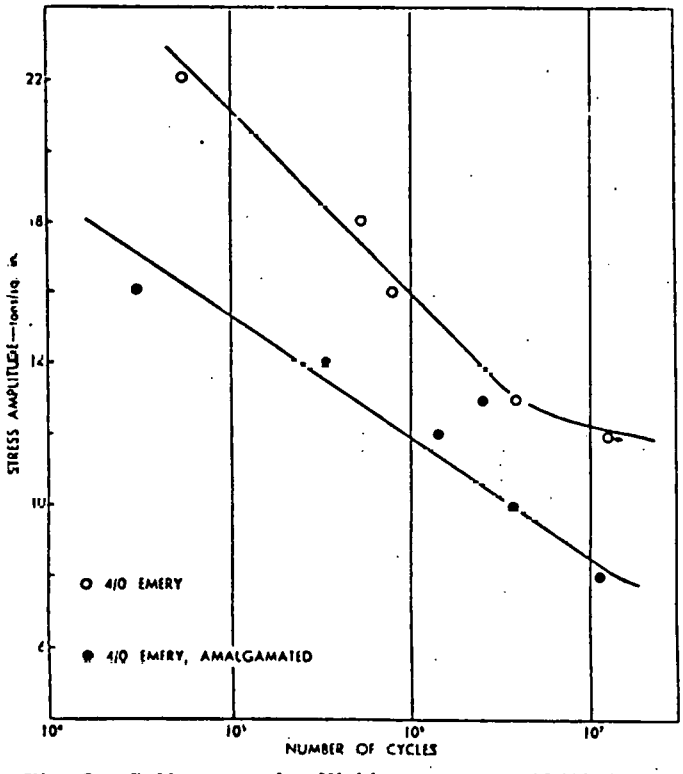


Fig. 3.—S-N curves for Wohler tests on 60/40 brass, before and after amalgamation with mercury.

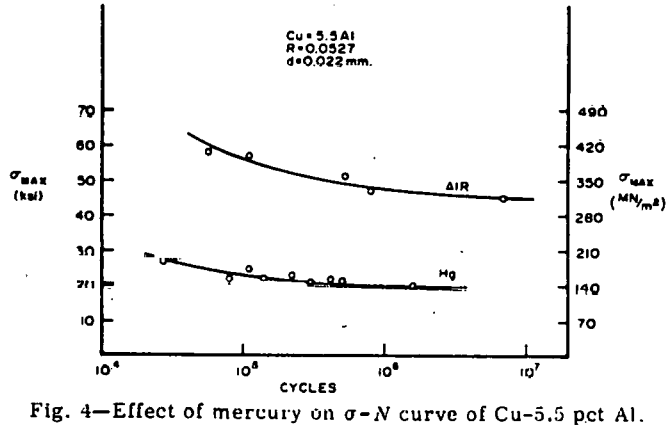


Fig. 4—Effect of mercury on σ–N curve of Cu–5.5 pct Al.

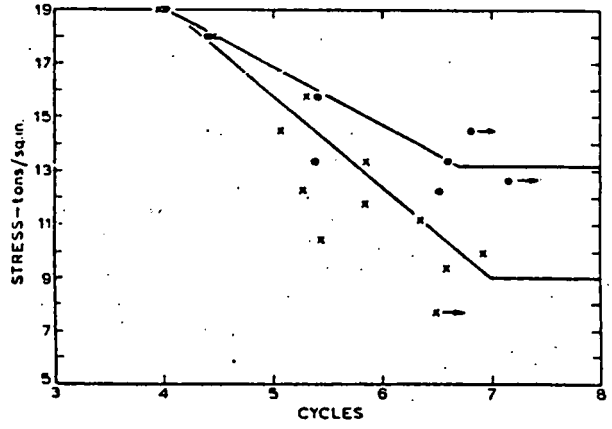


Fig. 1.—Mild steel fatigued at 500° C. Top curve in air, bottom curve in contact with sodium.

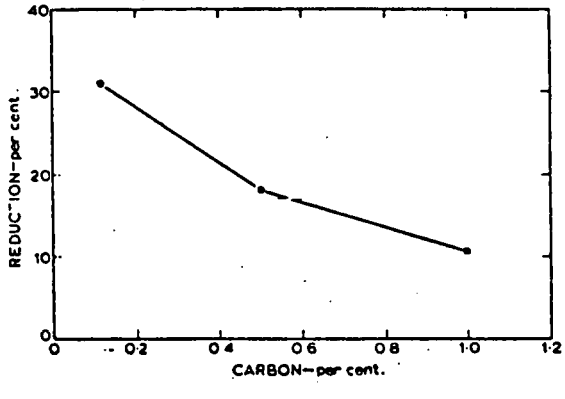
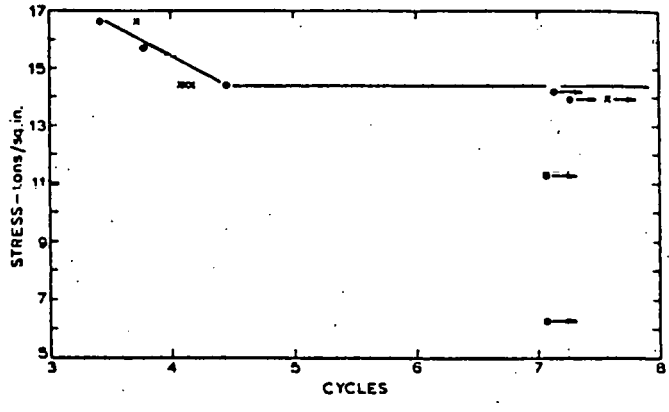


Fig. 3.—Effect of carbon content of plain carbon steels upon the reduction of endurance limit brought about by sodium at 500° C.



● Fatigued in air. X Fatigued in sodium.

Fig. 4.—Type 347 stainless steel fatigued at 500° C.

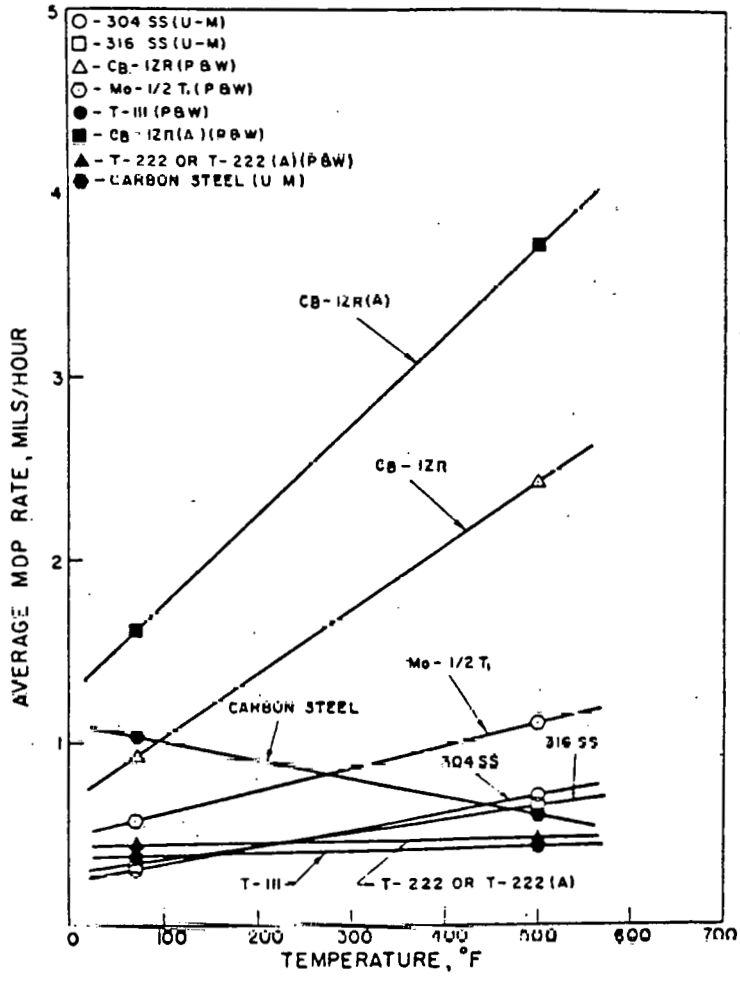


FIG. 12—*Effect of temperature on cavitation resistance in mercury.*

TABLE 4—*Summary of cavitation results in mercury at 500 F.*

Material	Average Weight-Loss Rate, mg/hr	Average MDP Rate, mils/hr
T-111 (P & W)	29.48	0.43
T-222(A) (P & W)	31.52	0.46
Carbon steel (U-M)	18.60	0.61
316 SS (U-M)	19.01	0.63
304 SS (U-M)	20.83	0.69
Mo-½Ti (P & W)	43.16	1.09
Cb-1Zr (P & W)	81.85	2.43
Cb-1Zr(A) (P & W)	125.78	3.73

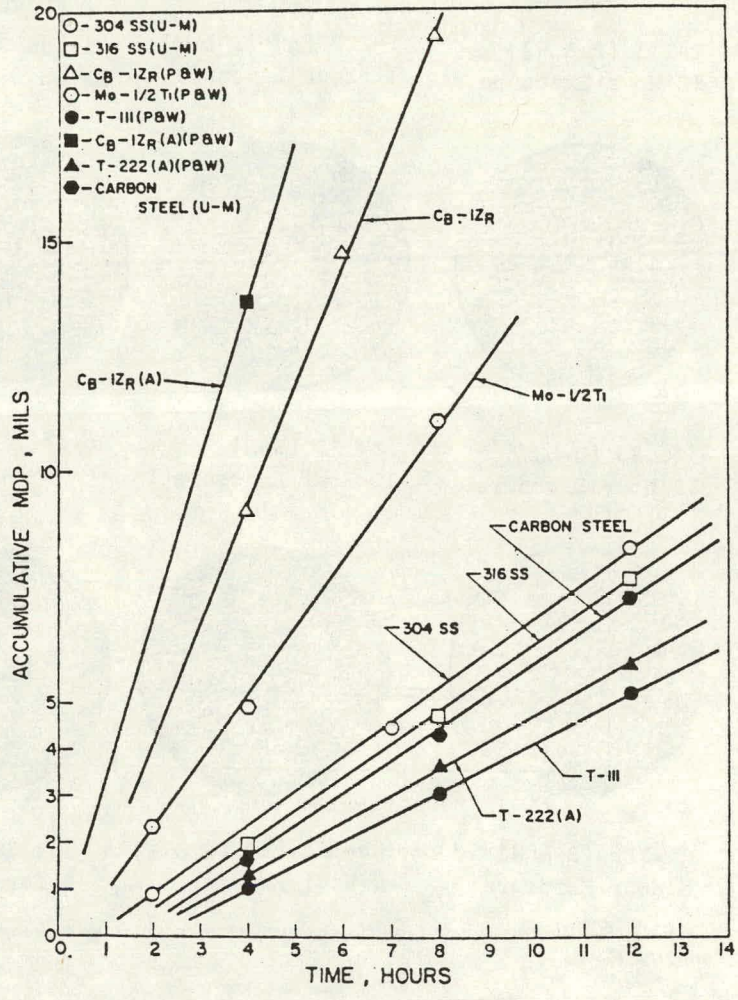


FIG. 8—*Effect of cavitation test duration on MDP at 500 F in mercury.*

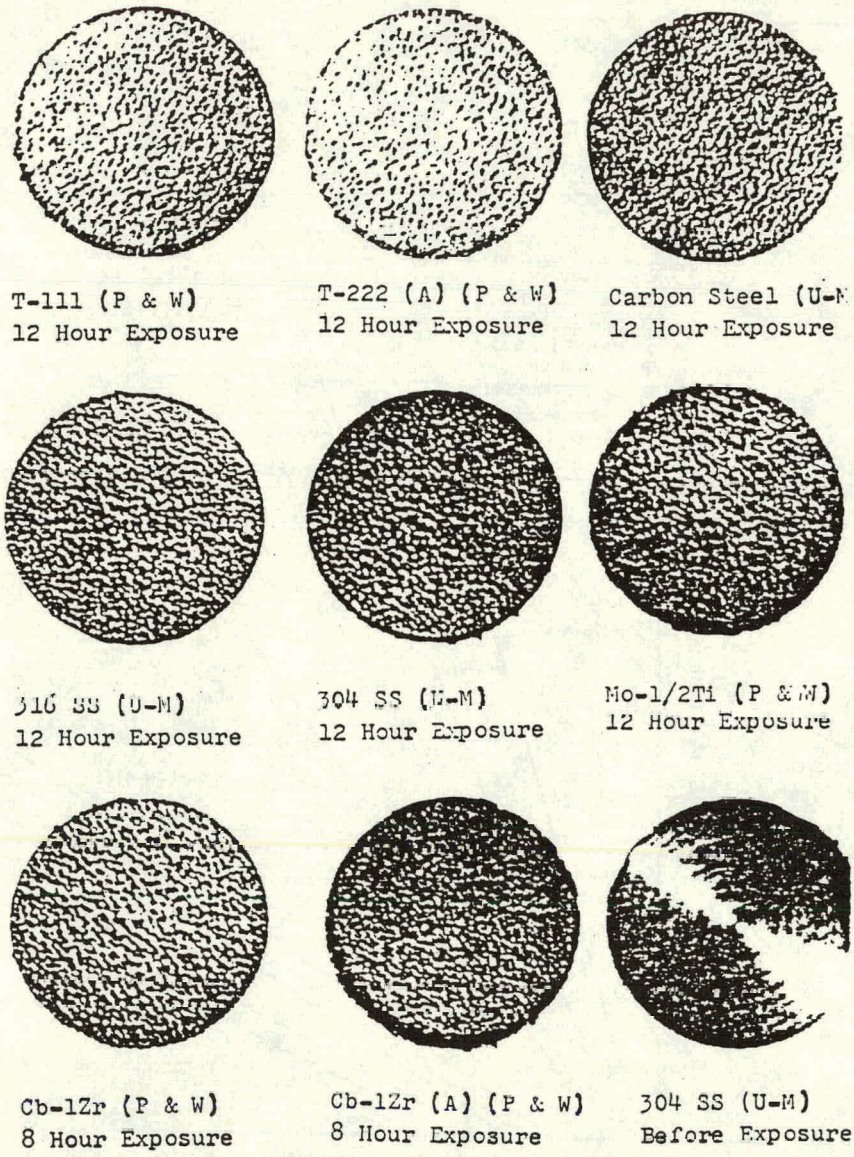


FIG. 9—*Photographs of specimens subjected to cavitation damage in mercu at 500 F.*

MATERIALS CONSIDERATIONS IN THE DESIGN OF A SODIUM COOLED CENTRAL RECEIVER SOLAR THERMAL POWER PLANT

by

Graham A. Whitlow

Westinghouse Electric Corporation

Madison, Pennsylvania

MATERIALS CONSIDERATIONS IN THE DESIGN OF A SODIUM COOLED CENTRAL RECEIVER SOLAR THERMAL POWER PLANT

GRAHAM A. WHITLOW

WESTINGHOUSE ELECTRIC CORPORATION
Advanced Reactors Division
P.O. Box 158
Madison, Pennsylvania 15663

ABSTRACT

Materials considerations are reviewed for a sodium cooled, central receiver, solar thermal power plant. Available information is summarized and data needs identified in the areas of materials-coolant compatibility, thermal and mechanical fatigue resulting from thermal cycling, friction, wear and self-welding and ASME Boiler Code requirements.

INTRODUCTION

The national solar energy program has as one of its objectives, the development of economically competitive central receiver, solar thermal power plants. A schematic of such a plant employing liquid sodium as the heat transport medium is illustrated in Figure 1. The collector system consists of a 360 degree flat field array of heliostats (mirrors), which redirect solar energy to the surface of the tower mounted, receiver.(1) Heat absorbed by the receiver is transferred to the liquid sodium energy storage system and/or the steam generators. The use of sodium as the primary coolant allows for maximum utilization of existing nuclear industry components technology, while taking advantage of heat transfer benefits, higher operating temperatures and consequential overall high efficiencies and reduced costs. The hardware base for such a solar plant is extensive with large sodium pumps, heat exchangers, steam generators and valves having been designed and tested. Major components are likely to be constructed of the austenitic stainless steels, Type 316 and 304; a ferritic steel such as the $2\frac{1}{4}$ Cr-1 Mo type will be used for the steam generator but may also find application in other system components.

The purpose of this paper is to review the materials aspects of the sodium heat transport system of a liquid metal cooled, solar thermal power plant, and to identify potential problem areas requiring attention with respect to reliability. Water side steam generator materials and water chemistry are subjects excluded from the scope of this paper.

SYSTEM PARAMETER DEFINITION

A schematic of a liquid sodium system, with the most significant parameters listed, is illustrated in Figure 2. The plant consists of a Collector System, Heat Transport System, Electrical Power Generation System, Master Control System, Buildings and Structures, and Miscellaneous Power Plant Equipment. The Heat Transport System is comprised of the Receiver System, Energy Storage System, Steam Generation System, and Auxiliary System. The Collector System shown in Figure 1 consists of a 360 degree, flat field array of heliostat units and their ancilaries. Heliostats are controlled to redirect solar energy continuously upon the surface of the receiver unit located atop the receiver tower. Heat absorbed by the receiver is transported through the Receiver

System to the Intermediate Heat Exchanger (IHX), where it is transferred to the liquid metal of the Energy Storage System. Application of an IHX is entirely a plant power generation cost consideration and is specifically dependent on receiver tower height. Advantages of an IHX include the possibility of using components with thinner walls in the energy storage and steam generation systems, because the IHX reduces the secondary system pressure. These factors may tend to offset the additional cost involved in the use of an IHX. The Energy Storage System liquid metal circuit is arranged to permit transfer of the heat into energy storage, to the Steam Generation System, or to both simultaneously, depending on the solar power available and the plant load demand. Also, the stored energy may be transported to the Steam Generators through the same pipe loop for partial or total utilization of stored energy. The maximum sodium temperatures in the primary and secondary loops are 593°C (1100°F) and 566°C (1050°F) respectively with a temperature difference in each loop of 223°C (400°F).

MATERIALS CONSIDERATIONS

In the following section, materials considerations are reviewed in the light of available sodium cooled breeder reactor experience. Problems to be addressed to permit materials to operate reliably in solar power plants are discussed and illustrative examples of materials problems common to solar and reactor sodium systems are described.

A. Materials - Coolant Compatibility

Major components of demonstration plants will most likely be fabricated from the austenitic 300 series stainless steels, Type 304 and 316. Temperatures in the secondary loop, assuming an intermediate heat exchanger (IHX) is required, are approximately 30°C (54°F) lower, and materials used will be austenitics for the IHX and ferritic steels such as the $2\frac{1}{4}$ Cr-1 Mo or 9 Cr-1 Mo alloys for the steam generator. Consideration may also be given to Alloy 800 for primary and secondary system application.

The corrosion potential of high temperature sodium is dependent primarily on the level of the major impurity i.e. oxygen. Consequently, it is necessary to reduce and then maintain the oxygen content at an acceptably low level e.g. 1 ppm by weight. In breeder reactor based studies, using low oxygen (0.5 to 1 ppm) sodium, it has been found that the 300 series stainless steels possess acceptably low corrosion rates.[2] There is a slight tendency of the flowing high temperature sodium to slowly remove the major metallic components of stainless steel (iron, chromium and nickel) from the hot section of the primary coolant loop. These species are transported in the sodium to cooler sections of the loop (IHX or steam generator), where compound deposition occurs. If Alloy 800 is selected, for example, for receiver tube application, then the sodium compatibility data base for this material will need to be expanded.

In a sodium cooled, solar plant the stringent nuclear standards and quality control for valves and piping, etc. may be somewhat relaxed permitting operation of the sodium system at oxygen levels greater than 1 ppm. If this occurs, corrosion rates will more than likely increase and crud and impurity control operations will need to be addressed for materials in higher oxygen level, sodium systems.

The sodium also serves as a medium through which the minor elements in the steel can migrate about the loop. Carbon is the element of principal concern, in as much as the high temperature strength of stainless steel is somewhat dependent on its carbon

level. Considerable effort has been expended to understand and predict carburization/decarburization rates in sodium coolant loops and is directly applicable to component design for a solar powered plant.[3] However, more work is needed in the area of ferritic materials behavior in sodium, particularly the 9 Cr-1 Mo alloys which have many attractive properties. In addition, the optimum heat treatments for ferritic alloy components with regard to long term metallurgical stability will require definition.

Another area of concern is the energy storage system, which in Figure 2 is depicted as a carbon steel sensible heat system.[1] Since the system will contain a very large carbon steel surface area, the degree and effects of mass transfer from the energy storage system to the balance of plant must be investigated. Both general corrosion and interstitial element transfer must be considered. Also, since the storage system should ideally maximize the steel to sodium mass ratio, flow channels should be narrow. Therefore, mass transfer deposit effects on heat transfer and pressure drop due to flow impedance must be considered. In addition, thermal cycling of the energy storage elements may lead to fretting corrosion. These concerns will necessitate theoretical and experimental modeling studies to be performed.

The proposed sodium solar receivers, as defined in system studies, will be subject to 0.3 to 0.8 MW/m^2 heat flux from the heliostat field. The maximum projected breeder reactor fuel core heat flux, where experimental sodium corrosion test loops have been operated is 0.3 MW/m^2. The research effort on sodium-material corrosion rate variation with heat flux is not extensive with available data indicating minor effects. However, it is important that the much higher heat flux proposed for the solar sodium-materials interface must be evaluated for its effect on corrosion potentials.

B. Thermal and Mechanical Fatigue

The response of materials to thermal cycling and hence, the occurrence of thermal fatigue damage has been accorded a high level of importance in breeder reactor studies. However, the problem of thermal cycling becomes more important in a solar plant, where diurnal as well as cloud cover thermal cycling of the central receiver tower and sodium system will occur. Transients up to 200°C (392°F) in a few seconds are anticipated. The most susceptible component will be the receiver itself, but components downstream of the receiver such as the hot leg piping and, if used, the IHX will also see shock conditions. Thermal shock or thermal fatigue damage has been observed in liquid metal systems and is of concern to the sodium system design community. Some examples of the type of damage that can result from thermal shock testing of the Type 300 stainless steels are shown in Figure 3.

Another important phenomenon occurs, when structures are subjected to alternating hot and cold sodium streams, giving rise to a thermal fatigue phenomenon, which is termed thermal striping. Careful design of piping components such as mixing tees will be mandatory, if damage of the type shown in Figure 4 is to be avoided. Thermal striping effects may occur in the receiver, if sodium streams at different temperatures (i.e. from different receiver locations) mix within a fluctuating temperature region. Likewise, simulation testing of materials, component joints, etc. will be necessary, mocking up the cyclic temperature history of a central receiver plant.

The effects of mechanical fatigue in liquid sodium at fixed temperatures both high and low cycle, have been extensively studied, such that base line fatigue data are available for use in design. Additional data may be required in this area if the 9 Cr-1 Mo alloy or the nickel based Alloy 800 are used in components subject to stress or strain cycle fatigue.

C. Friction, Wear and Self-Welding

Important materials properties to be considered in component design include friction, wear, and self-welding between metal parts submerged in the sodium coolant. High temperature sodium removes the protective "oxide" layer normally found on metal surfaces and thereby produces exceedingly clean surfaces. The absence of this protective film on metals in sodium can increase friction and wear at sliding interfaces because, generally speaking, these films have a lubricative nature. For this reason, moving parts in contact under sodium are either hardened surfaces, coated with low friction materials, or fabricated of wear resistant alloys such as Stellite 6. An extensive data base on low friction and wear materials for use in sodium environments is available.(4)

Friction and wear phenomena will occur in a sodium cooled solar plant, whenever contacting surfaces are required to move relative to each other. The sources of motion can be many and varied, i.e., deliberately induced motions in mechanical devices, flow induced vibrations, and expansion and contraction. Whether or not these motions give rise to galling or wear problems depends on the contact loads, the cumulative motion, the temperature, the environment and the materials selection. Large expansion and contraction movements will occur in a solar power plant, because the diurnal and cloud cover thermal cycling result in intermittent operation of this unit over a 24-hour period. For example, a 305 m (1,000 feet) tower may require the accommodation of 3-4m (10-12 feet) of expansion-contraction motion on the hot leg piping alone. The receiver piping, which could consist of lengths in the hundreds of feet range will be subjected to significant expansion-contraction movement. As the pipes will have to be supported in some manner, a condition conducive to friction and wear will exist between the pipe O.D. surface and the pipe support. Heat exchangers will also be subjected to this type of motion, in a sodium environment in this case. Added to the expansion-contraction motions will be those caused by flow induced vibration in piping and tubing. This will also affect the receiver and heat exchangers.

The problem of self-welding of contacting material surfaces in sodium becomes apparent, when the surfaces remain in intimate contact for extensive periods of time, before being required to move with respect to each other. An example of a component in which this may occur is in the seat of a hot leg valve—again an extensive data base is available, which can be used in the selection of self-welding resistant materials.(4)

D. Design and Construction Code Requirements

A central receiver solar thermal power plant utilizing sodium for heat transport must operate safely and reliably with high availability for 30-40 years. This requires great reliance upon analysis to extrapolate short time test results to predict long term structural behavior, and hence, the necessity for ASME code certification for commercial application. Solar powered plants will operate at low pressure, thus permitting the use of relatively thin-walled components, when compared to water/steam systems. Besides steady loadings due to pressure, thermal expansion and dead weight, there are cyclic loadings due to the thermal transients, pressure changes and seismic events requiring attention.

The existing ASME Boiler and Pressure Vessel Codes Sections I and VIII (Division 1) provide rules for high temperature design (>427°C (800°F), but do not address all possible material failure modes, particularly cyclic loading as in creep/fatigue.(5) In a solar powered plant, the failure modes which require ASME code consideration are:

1) Ductile rupture from short-term loadings.
2) Creep rupture from long-term loadings.
3) Creep-fatigue failure.
4) Gross distortion due to incremental collapse and ratcheting.
5) Loss of function due to excessive deformation.
6) Buckling due to short-term loadings.
7) Creep buckling due to long-term loadings.

These modes of structural failure are addressed in Code Case 1592 of Section III of the ASME Code, which was developed to provide the structural and quality requirements for the elevated temperature construction of nuclear components. This code case may be modified by tailoring the limits to suit the above requirements for solar plant components and by eliminating excessive conservatism, which was necessary based on the limited data available at the time the limits were developed.

Design and construction code requirements, therefore, require modification and simplification of Code Case 1592, to include an early definition of the quality and safety requirements for solar plants. In addition, the thermal transients and design limiting loads produced need to be established. Code development and component design must necessarily proceed simultaneously to ensure safe, reliable, long-term operation, consistent with economical construction and operation.

SUMMARY AND CONCLUSIONS

This paper has reviewed some of the more important material considerations for sodium cooled, central receiver, solar thermal power plants. It is readily apparent that there is available an excellent data base from the extensive research based on sodium breeder reactor development studies for the achievement of reliability in design. Specific areas, which have been identified as requiring resolution for the safe and reliable design and operation of a solar power plant are:

- Materials compatibility studies in sodium systems containing >1 ppm oxygen.
- Carbon transport in sodium and long term metallurgical stability, particularly with respect to the use of ferritic materials.
- Mass transfer effects in sodium when a carbon steel sensible heat, energy storage system is used.
- Effects of anticipated, solar heat fluxes on materials corrosion in sodium.
- Rapid thermal cycling effects on thermal and mechanical fatigue response of potential construction materials.
- Consequences of the expansion and contraction movement due to thermal cycling on the friction and wear behavior of tube and tube support materials.
- Development of a design standard based on ASME Section III Code Case 1592 concepts for application to solar thermal power plants. This code development must proceed simultaneously with component design to identify material data needs.

For a more comprehensive viewpoint on the advantages of using liquid sodium as the heat transport medium in a plant of this type, reference is made to the paper by Deegan et al.[1] In conclusion, it can be stated that a sodium heat transport system can operate reliably with respect to materials considerations at high temperatures, and provides a very simple, efficient and relatively inexpensive, low pressure heat transport and energy storage system.

ACKNOWLEDGEMENTS

The author would like to express his appreciation to coworkers at Westinghouse for their support and perceptive contributions to the preparation of this paper.

REFERENCES

1. P. B. Deegan, J. D. Mangus and G. A. Whitlow, "Liquid Metal Cooling Concepts in Solar Power Application", presented at Corrosion/78 Houston, March 1978, Paper #110 - to be published by NACE in "Materials Considerations in Liquid Metals Systems for Power Generation", (1978).

2. S. L. Schrock and G. A. Whitlow, in "Corrosion Problems in Energy Conversion and Generation", Ed. C. S. Tedmon, The Electrochemical Society, 225-239, (1974).

3. S. Janssen Editor, Proc. of Conf. on Chemical Aspects of Corrosion and Mass Transfer in Liquid Sodium, TMS-AIME, New York (1973) - See papers on pp. 130-155 and pp. 157-176.

4. M. H. Cooper Editor, Proc. of Int. Conf. on Liquid Metal Technology in Energy Production, Champion, Pa., CONF-76-0503, (1976) - See papers IIB-1, IIB-3 and IIB-7.

5. D. S. Griffin, "Structural Analysis for Elevated Temperature Design of the LMFBR", Proc. of 1976 ASME/ANS Int. Conf. or Advanced Nuclear Energy Systems", Pittsburgh, Pa., March 1976, ASME New York, pp. 237-249, (1976).

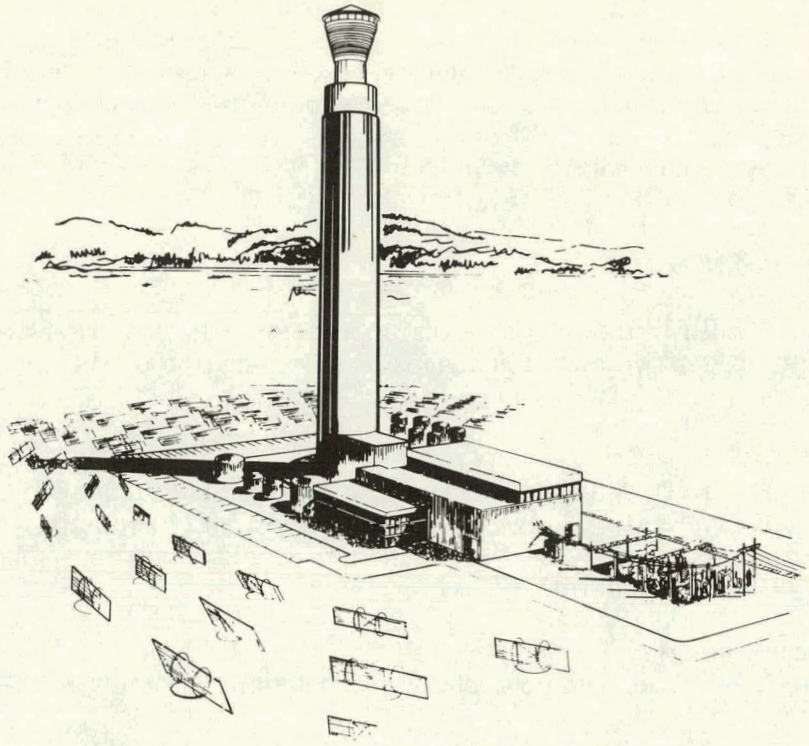


Figure 1. Advanced Central Receiver Power System

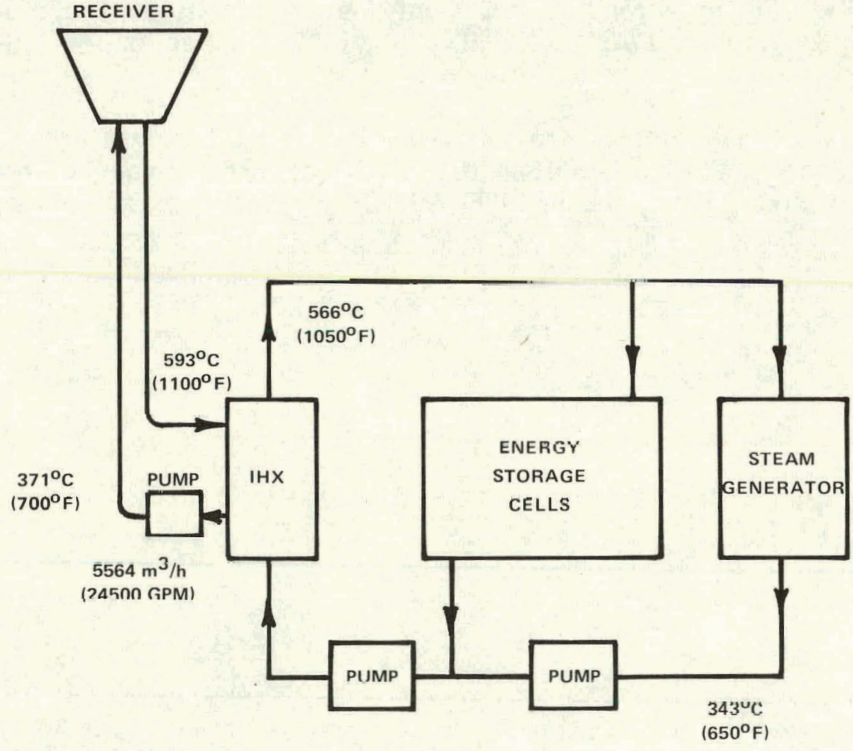


Figure 2. Advanced Central Receiver Power System – Schematic of Liquid Metal Cycle

1248-1

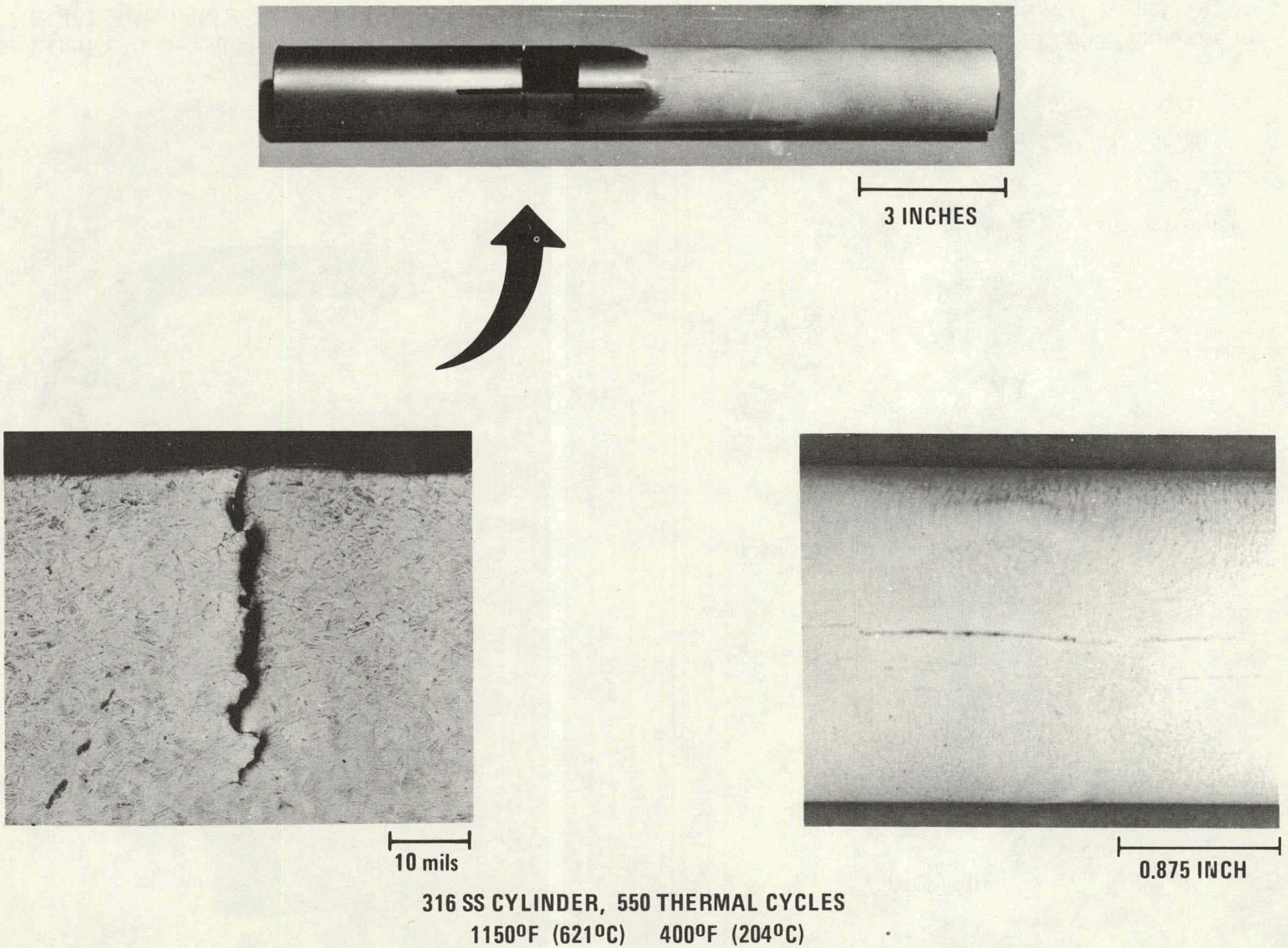


Figure 3. An Example of Damage Resulting from Thermal Cycling in Sodium. Courtesy R. L. Miller

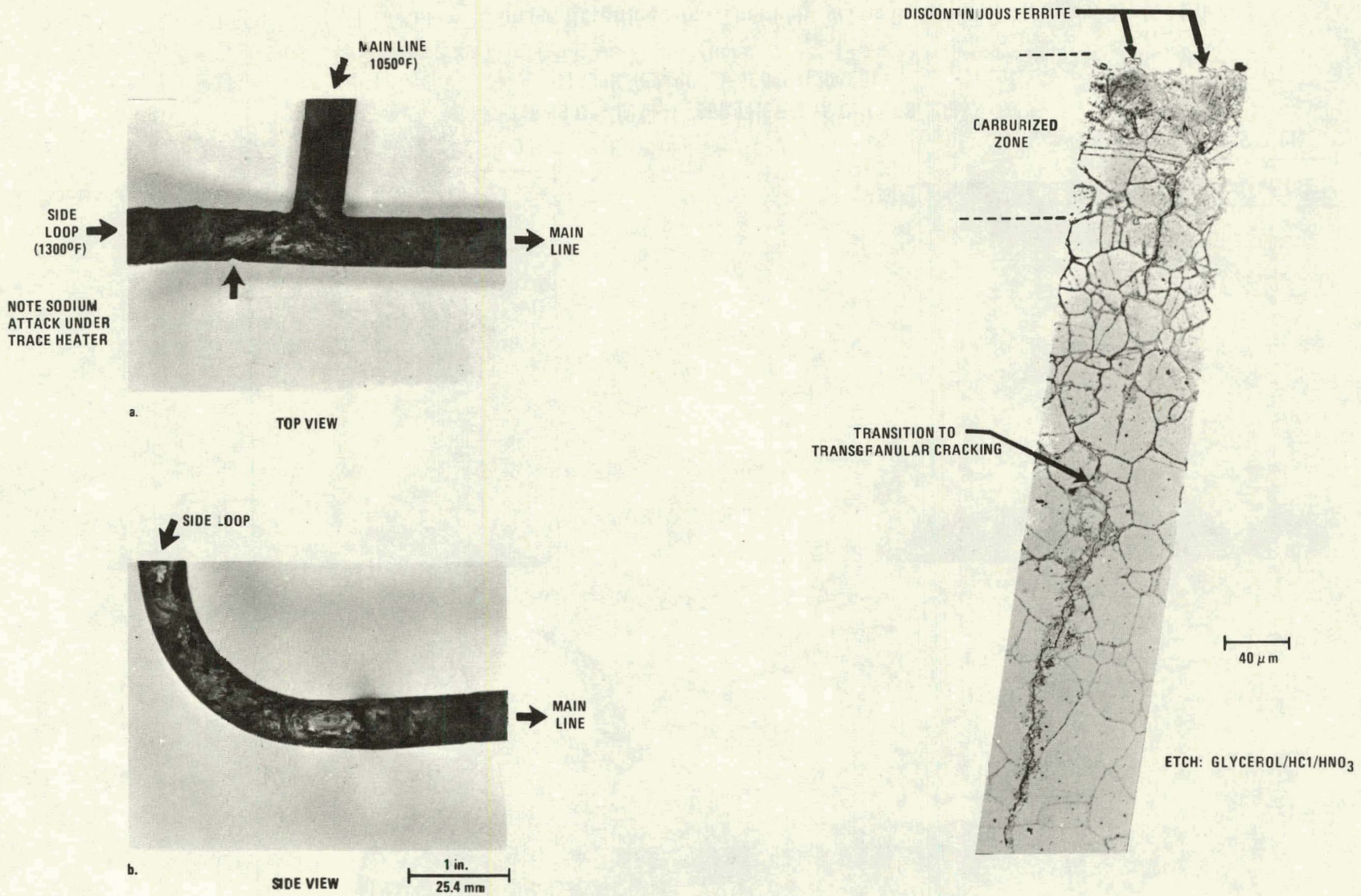


Figure 4. Exterior Views and Microstructure of a Failure, which Occurred at a Welded Tee Section, after 12,000h Exposure to High Temperature Sodium Streams (½" x 0.049" Wall Type 304 Stainless Steel Tubing) Courtesy C. Bagnal.

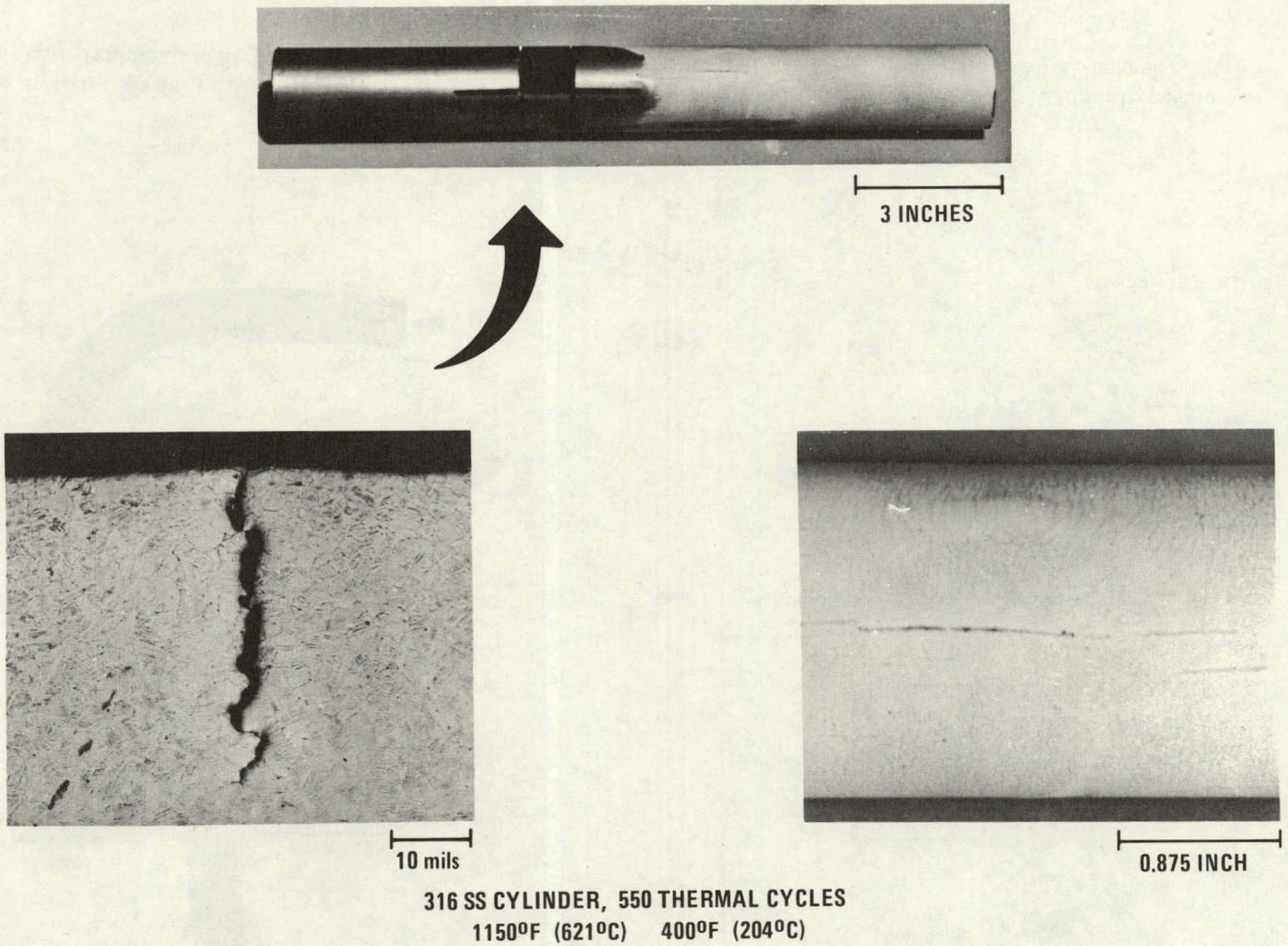
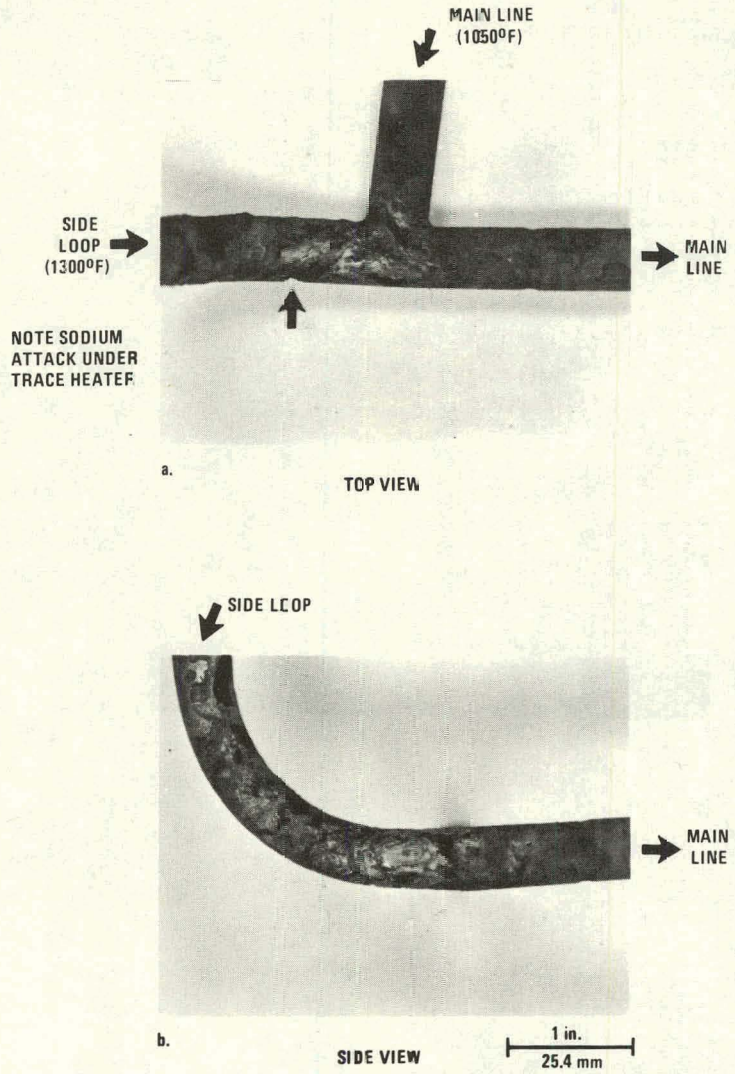


Figure 3. An Example of Damage Resulting from Thermal Cycling in Sodium. Courtesy R. L. Miller



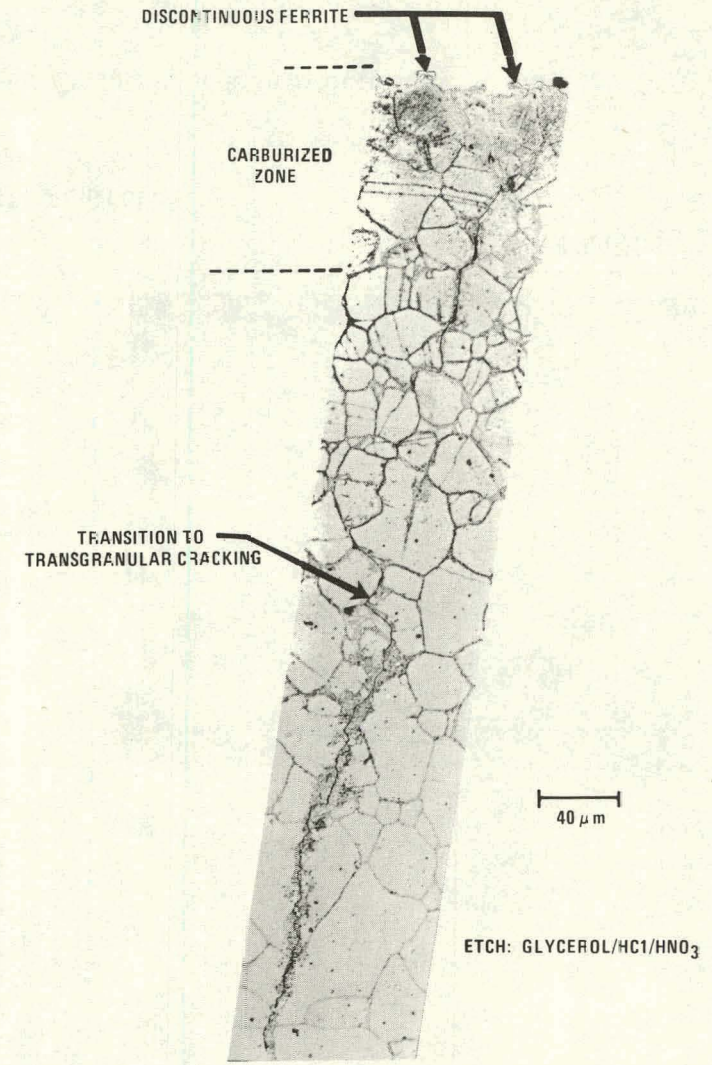


Figure 4. Exterior Views and Microstructure of a Failure, which Occurred at a Welded Tee Section, after 12,000h Exposure to High Temperature Sodium Streams. (½" x 0.049" Wall Type 304 Stainless Steel Tubing) Courtesy C. Bagnal.

EXTERNAL SINGLE PASS TO SUPERHEAT RECEIVER

by

J. M. Friefeld

Rockwell International

Canoga Park, California

and

G. C. Coleman

McDonnell Douglas Astronautics Co.

Huntington Beach, California

SUMMARY

This paper describes the external single pass to superheater receiver designed for use at the Barstow Pilot Plant (10 MWe Solar Thermal Power System). The receiver design is an integral part of the system designed and developed by a team headed by McDonnell Douglas Astronautics Company.

FORM 608-B-13 REV. 5-75

DISCUSSION

The system concept is as shown in Figure 1 which depicts the interaction of the major subsystem elements. Solar energy reflected by heliostats comprising the Collector Subsystem are absorbed by the Receiver Subsystem. The energy is absorbed in the form of superheated steam which is used to drive a conventional turbine/generator set. The energy not used by the turbine is directed to thermal storage for subsequent utilization. Thermal storage is accomplished by storing most of the energy as sensible heat in low cost rocks with an inorganic heat transfer oil as the transport medium.

The receiver design is shown in Figure 2. It is comprised of 24 independent panels, 18 of which serve as boiler/superheaters; the remainder (south side) are used as preheaters. A panel fabricated and tested is shown in Figure 3. The end nearest is the water end which shows a detail of the tube to header joints. The tubes, headers, and integral appendages are all made from Incoloy-800, an approved Section I boiler material. The tubes are mounted to a backup structure so as to allow free lateral and longitudinal expansion during elevated temperature operation.

Receiver design parameters are as follows:

Inlet Conditions:
- Temperature - 400F
- Pressure - 2000 psia

Exit Conditions
- Temperature - 960F or 660F
- Pressure - 1515 psia

Power Absorbed
- Maximum - 37.1 MW_t
- Minimum - 7.26 MW_t

FORM 608-B-13 REV. 5 75

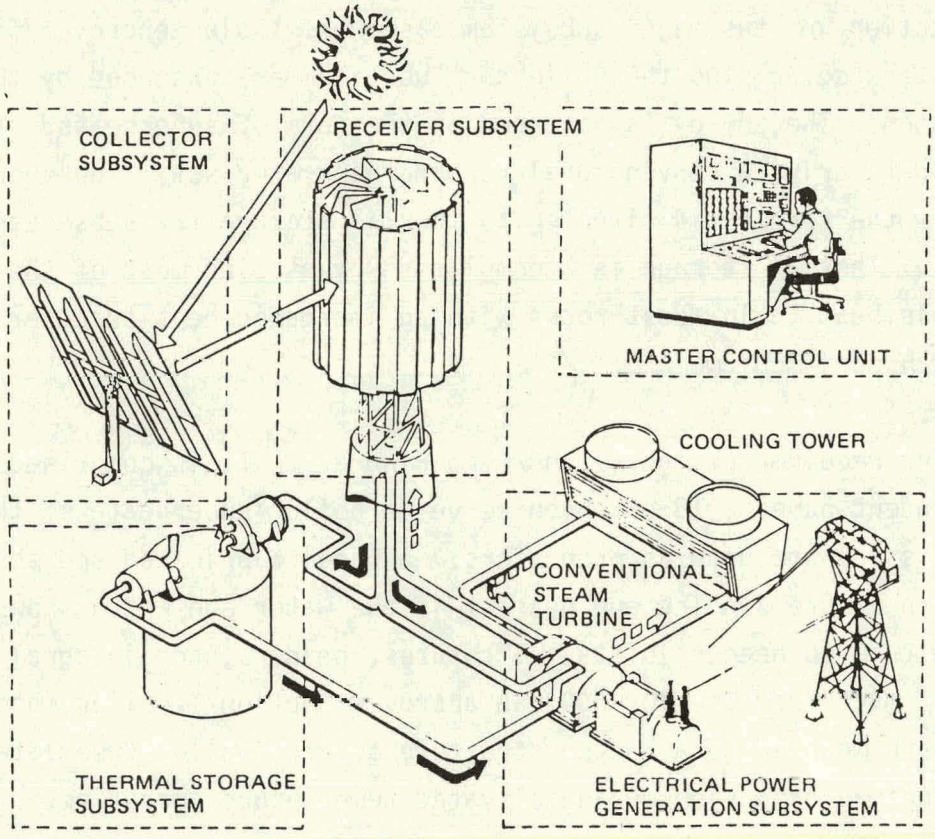


Figure 1. Central Receiver Baseline Concept

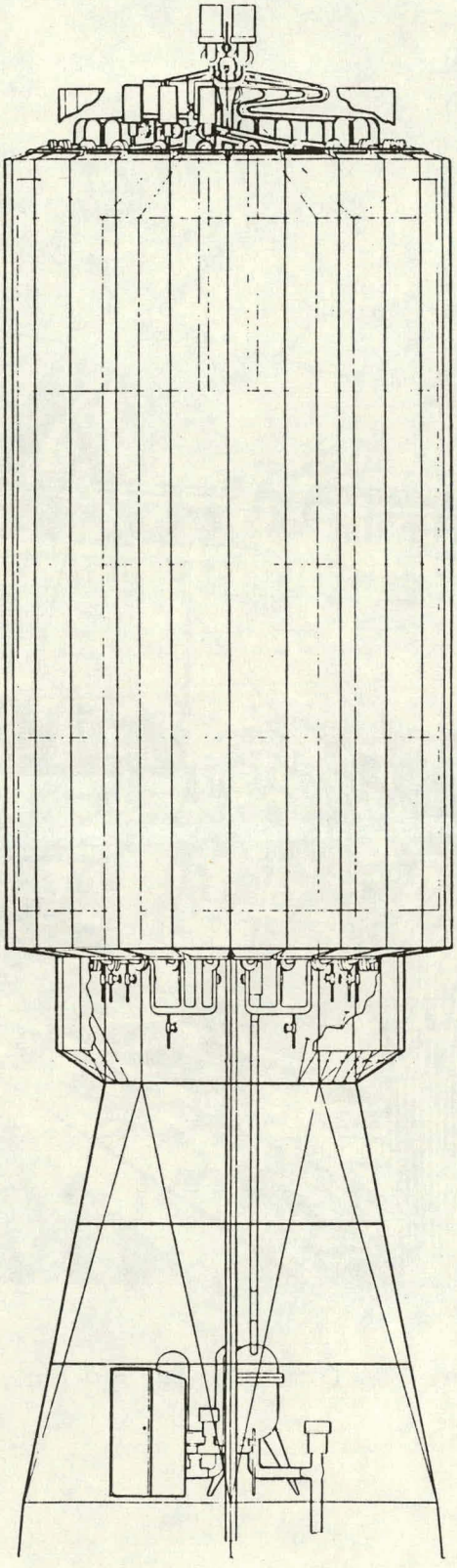


Figure 2. Pilot Plant Receiver Unit External View (Looking North)

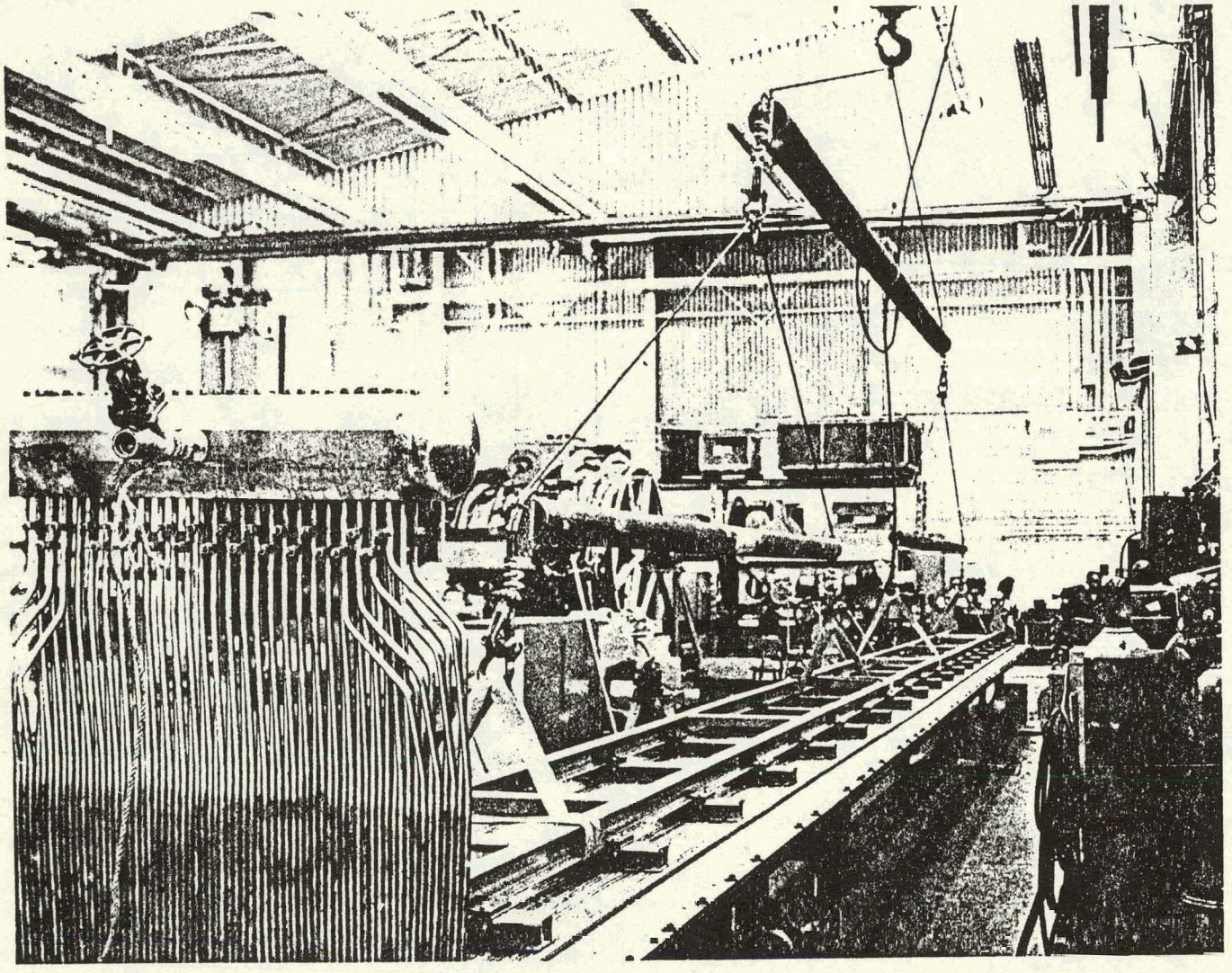


Figure 3. Completed Pilot Plant Panel

Peak Heat Flux
0.29 MW/M^2

The receiver tubes were designed in accordance with the above conditions utilizing Section I of the ASME Boiler and Pressure Vessel Code. The most severe thermal strain occurred in the two-phase zone as shown in Figure 4 (235 in. from inlet) with a resultant strain of 0.3%. The predicted life for the pilot plant tubing is nearly 100,000 cycles. (Figure 5). As noted, the life criterion was developed from Section 3 of the code since Section 1 does not allude to fatigue life.

Alloys considered for receiver construction are shown in Table I. It was found that Incoloy 800 had the best combination of strength, ductility, corrosion resistance and resistance to chloride attack of those considered. Other experiences using Incoloy 800 are shown in Table II.

A receiver panel was built and tested under infrared heating conditions at conditions approximating those anticipated in the pilot plant. No adverse results were obtained. Currently the panel is in the process of being interfaced to the STTF at Sandia Laboratories in Albuquerque for tests in concentrated sunlight. Data from these tests will be available shortly.

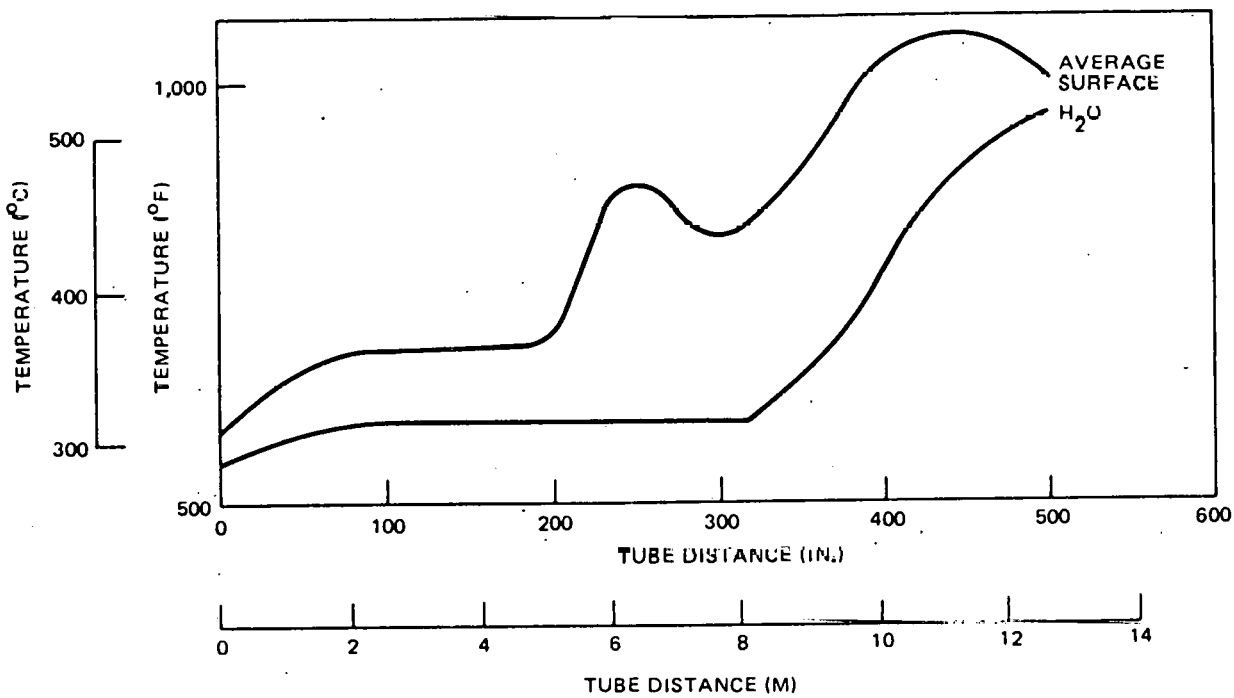


Figure 4. Pilot Plant Temperature Profiles, Equinoz Noon, North Tube

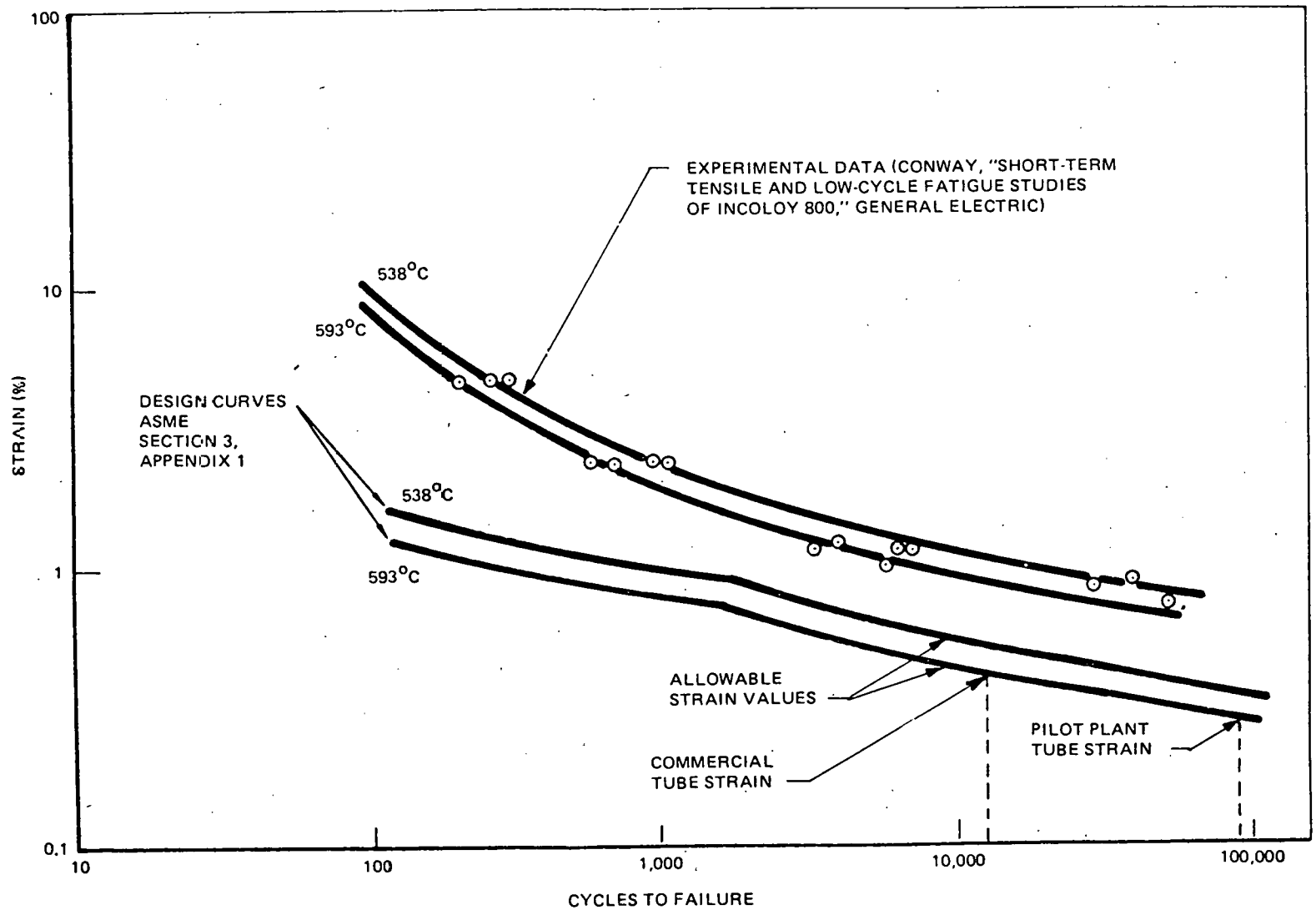


Figure 5. Fatigue Data and Design Curves

TABLE I

RECEIVER ALLOY COMPOSITION COMPARISON

Alloy Designation	Nominal Composition*
Incoloy 800	32 Ni - 20 Cr
Low Alloy Steel	2 1/4 Cr - 1 Mo
Stainless** 304	18 Cr - 8 Ni
Stainless** 316	16 Cr - 13 Ni - 3 Mo
Stainless** 321	18 Cr - 8 Ni - 1 Ti
Stainless** 347	18 Cr - 8 Ni - 1 Cb

*Remainder Iron
**Austenitic Stainless Steels

TABLE II

STEAM SERVICE CORROSION DATA (SUMMARY) INCOLOY 800

Location	Steam Temp	0_2 Content	0_2 Removal Method	Results
Ohio Power Beverly, Ohio	(1,025°F)	0.2 ppm	Mechanical dearation Only	30 mo, no scaling or oxidation
Sc. Calif. Edison Hermosa Beach, CA	565°C (1,050°F)	5 ppb	Dearation; hydrazine and ammonia	22 mo, nonspalling oxide (0.004 in.) 0.1 mm
Commonwealth Edison	565°C (1,050°F)	---	Hydrazine	24-48 mo, no scaling
Electric Energy, Inc. Joppa, Ill. Boiler No. 2	570°C (1,055°F)	0.003-0.007 ppm	Hydrazine and sulfite	32 mo, tight adherent scale (0.004 in.) 0.1 mm
Electric Energy, Inc. Joppa, Ill.	570°C (1,055°F)	0.003-0.007 ppm	Hydrazine and sulfite	66 mo, tight adherent scale (0.004 in.) 0.1 mm
Electric Energy, Inc. Joppa, Ill. Boiler No. 1	540°C (1,005°F)	0.003-0.007 ppm	Hydrazine and sulfite	42 mo, tight adherent scale (0.004 in.) 0.1 mm

THIS PAGE

WAS INTENTIONALLY

LEFT BLANK

Thermal Conversion - Aqueous/Steam Coolant

MATERIAL PROBLEMS RELATED TO HIGH TEMPERATURE STRUCTURAL DESIGN OF WATER/STEAM SOLAR RECEIVERS

by

Dr. A. C. Gangadharan

Foster Wheeler Development Corporation

Livingston, New Jersey

MATERIAL PROBLEMS RELATED TO HIGH TEMPERATURE STRUCTURAL DESIGN OF WATER/STEAM SOLAR RECEIVERS

by

Dr. A. C. Gangadharan
Foster Wheeler Development Corporation
12 Peach Tree Hill Road
Livingston, NJ 07039

1. Solar Design Conditions

In the context of the ASME Boiler and Pressure Vessel Code, a high temperature design is defined as the one in which metal temperatures exceed 700°F in ferritic steels and 800°F in austinitic steels. This is the threshold temperature above which time-dependent creep deformation becomes significant in structural metals. Increase in metal temperature also reduces the yield point of the material resulting in cyclic plasticity under repeated loading conditions. Design and analysis of structures at high temperature service conditions therefore become very complex.

One critical component in a water/steam solar system which operates at a high temperature is a superheater tube. These tubes are heated from one side by the incoming solar flux. Tubes will be heated non-axisymmetrically with a maximum temperture, about 1200°F, at the outside tube surface facing the mirror field. The backside (shadow side) of the tube will be at a temperature close to the steam temperature, 950°F to 1000°F. The internal pressure may range from 1500 psi to 3200 psi. The loads are cyclic in nature. This happens due to diurnal flux variation as well as due to intermittant cloud covers. In a 30-year life time the superheater tubes may undergo as many as 14,000 thermal cycles and close to 90,000 hours of steady state hold time. Under these conditions the tubes undergo cyclic elastic-plastic creep deformation.

The related failure modes to be guarded against are:

creep rupture
creep and fatigue damage
creep ratcheting
creep buckling.

2. ASME Code Requirements

Under a broad definition of terms, a solar water/steam receiver may be considered as a Section I pressure vessel. However, a closer look would reveal that Section I is not adequate to design pressure vessel parts subjected to a high temperature cyclic condition. Section I does not have rules to evaluate cyclic thermal loads. It also does not have explicit rules for creep. Nor does the other sections such as Section VIII and Section III consider all the failure modes associated with high temperature cyclic service conditions. The only document that deals with these conditions is Code Case 1592 which is an appendage to Section III rules for nuclear power components. Code Case 1592 provides detailed design rules to safeguard against all significant failure modes associated with high temperature design conditions. Some key reasons for the inapplicability of Code Case 1592 in solar designs are listed below:

a. Legality: The ASME Code when invoked is a legal document. Section III and Code Case 1592 are a nuclear system document. They do not apply to a solar design.

b. Design Margins: Rules of Code Case 1592 are compatible with the high reliability and safety requirements of a nuclear system. Because of this, Code Case 1592 rules are very conservative. The level of safety and the required design margins in a solar design need not be as high as in a nuclear design. A set of rules consistent with the desired level of safety and reliability in a solar plant should therefore be established.

c. Adequacy of Rules: Design rules and design analysis methods of Code Case 1592 were developed considering the general loading conditions in a nuclear pressure parts. For example a heat transfer tube in a nuclear steam generator is subjected to axisymmetric thermal loads; the maximum significant stresses in a nuclear tube are tensile. A solar superheater tube is heated non-axisymmetrically. The major stress in the tube is compressive. There are more thermal cycles in a solar system than in a nuclear system. Because of these differences, the rules in Code Case 1592 may be too conservative or inadequate for a solar design.

d. Design Cost: High temperature elastic-plastic designs are generally very costly. The Code Case 1592 recognizes this fact and,therefore; it has provided exceptions to certain criteria when some specified conditions are met. Many of these exception criteria cannot be met in a solar design because of the large number of thermal cycles or high steady state thermal stresses existing in a solar design. New exception criteria must be found based on comparable design experience in fossil power plant system and a consideration of the desired reliability and safety levels in a solar design. This will minimize solar high temperature design cost.

From the foregoing discussion it is clear that high temperature design rules for solar design must be established based on solar design conditions and other relevant considerations.

3. A New Solar Structural Design Standard

With funding from DOE-Sandia Laboratories, Foster Wheeler Development Corporation has been working on a project to prepare an interim structural design standard for solar power system design application. The final report

of the work containing the interim standard is currently under preparation. This interim standard, we hope, will form the nucleus for further discussion and deliberation on a final set of Code rules for solar boiler and pressure vessel components that will be established by appropriate code committees.

The interim set of rules adopts Section VIII of the ASME Code as the basis. The high temperature design rules are based mostly on Code Case 1592, with appropriate modifications to suit the solar design conditions and design philosophy. The rules proposed in the interim standard are preliminary. They can be finalized only after careful review, test, and evaluation.

A number of material problems exists in high temperature design. These problems are identified in the final report containing the interim standard. Appropriate tests and development works are recommended. These works are needed in order to verify and substantiate high temperature design rules; to simplify the design approaches; and to upgrade the rules for additional material service conditions. A description of these works are given below.

4. Test and Development Needs

The material tests that are identified below fall under two categories:

a. Tests to substantiate and verify the recommended high temperature rules.

b. Tests to upgrade the standard to other materials and design conditions.

4.1 Effect of Compressive Stress on Creep Damage

The proposed interim standard chooses the maximum tensile principal stress for the calculation of creep damage as opposed to the effective stress used in Code Case 1592. The effective stress approach assumes that a tensile and a compressive stress are equally damaging under a creep condition.

The superheater tubes in solar designs usually exhibit high compressive stress. Use of effective stress for creep damage calculation will make solar design very conservative and costly. There are some test results that show compressive stress has little or no effect on creep life of certain materials. A comprehensive test program to evaluate all candidate high temperature materials used in solar design are recommended.

4.2 Effect of Multiaxial Stresses on Creep and Fatigue

Multiaxiality effects on creep-fatigue damage is an important question in solar applications. Multiaxial tests in general are complex and expensive. As a minimum, biaxial creep-fatigue tests are recommended. Argonne National Laboratory is currently conducting such tests on 316SS tubes. Such tests using other candidate materials will be useful.

4.3 Elevated Temperature Fatigue Data

For temperatures in the subcreep regime, fatigue curves are available in ASME Code Section VIII, Division 2. However, acceptable fatigue curves at elevated temperatures are available only for three materials, viz., Type 304 SS and 316 SS, Incoloy 800H (Code Case 1592). For other candidate materials such as Incoloy 800, Inconels, Haynes 188 etc.; fatigue data and design curves at elevated temperatures are needed.

4.4 Creep Ratcheting Tests

The proposed Interim Standard does not have any specific requirements to prevent excessive thermal or creep ratcheting. This rule in the solar standard is different from the Nuclear Code, where there are requirements for ratcheting analysis and limiting the ratcheting strain. The assumption for the solar standard is that the requirements to prevent ductile and creep rupture, the

limit of stress range and the creep-fatigue limit will preclude excessive ratcheting. This assumption, however, needs to be verified by ratcheting tests on solar tubes.

4.5 Creep Rupture Data

Code Case 1592 gives creep rupture times for 4 materials: Incoloy 800H, Type 304 SS and 316 SS and 2 1/4 Cr - 1Mo. For other candidate materials such as Incoloy 800, Inconels, Haynes 188 etc. tensile creep rupture data are needed.

4.6 Structural Tests on Solar Receiver Tubes, Tube Panels, and Weld Joints

Tests on solar receiver tubes under nonaxisymmetric flux conditions are useful to evaluate the validity of the criteria proposed in the Interim Structural Design Standard. These tests may be performed in a solar thermal test facility STTF or under simulated conditions with infrared heating. Similar tests should be conducted on tube panels and weld joints.

5.0 Closure

The high temperature material tests are generally complex and time consuming. The tests proposed in this paper all require a coordinated long-term test and development program at a national level. Equally important is the need to start such a test program immediately so that the most basic element of creep tests, viz., time, is not wasted. High temperature test facilities at the government labs, e.g. ANL, ORNL, and many private industries which were established in recent years for nuclear power programs can be utilized to conduct the proposed solar high temperature material tests.

THIS PAGE

WAS INTENTIONALLY

LEFT BLANK

A CENTRAL RECEIVER USING NATURAL CIRCULATION STEAM GENERATION FOR HIGH TEMPERATURE SOLAR THERMAL CONVERSION

by

David N. Gorman

Martin Marietta Corporation

Denver, Colorado

A CENTRAL RECEIVER USING NATURAL CIRCULATION STEAM GENERATION FOR HIGH TEMPERATURE SOLAR THERMAL CONVERSION

David N. Gorman
Martin Marietta Corporation

Presented At

SOLAR ENERGY RESEARCH INSTITUTE WORKSHOP
ON RELIABILITY OF MATERIALS FOR SOLAR ENERGY SYSTEMS

18 December 1978

I. INTRODUCTION

A Central Receiver Solar Thermal Power System (CRSTPS) concept having broad operational flexibility and low technical risk has been developed. A preliminary design for a 10 MW_e pilot plant was performed by Martin Marietta Corporation under contract to the United States Department of Energy. Detailed design of the receiver, as well as design and fabrication of a 5 MW_t demonstration receiver, was performed by the Foster Wheeler Development Corporation under contract to Martin Marietta. The concept utilizes an integral solar collector/receiver module consisting of focused, tracking heliostats and a tower-mounted, steam generating receiver to maximize the combination of optical and thermal absorption efficiencies. Technical feasibility of this concept has been established by analysis and testing of the non-conventional subsystems--collector, receiver and thermal storage. Economic studies indicate such a system to have a strong potential for electrical power production in the competitive commercial market.

Although the purpose of this paper is to discuss the design and operational characteristics of the receiver, a brief description of the entire system will provide background and perspective. Energy flow through the system is shown schematically in Figure 1. Radiant solar energy is reflected and concentrated by the heliostat collector field and is used to generate superheated steam within the receiver. The steam can be routed directly to a conventional turbine/generator for immediate electrical power production or to a thermal storage subsystem where thermal energy is extracted and stored for later regeneration of steam and power production. Thermal storage is accomplished by a sensible heat gain of oil and a mixture of alkaline salts as the steam is cooled and condensed in the two heat exchangers. To produce power from thermal storage, the flow processes are reversed; the oil and salts are cooled in the

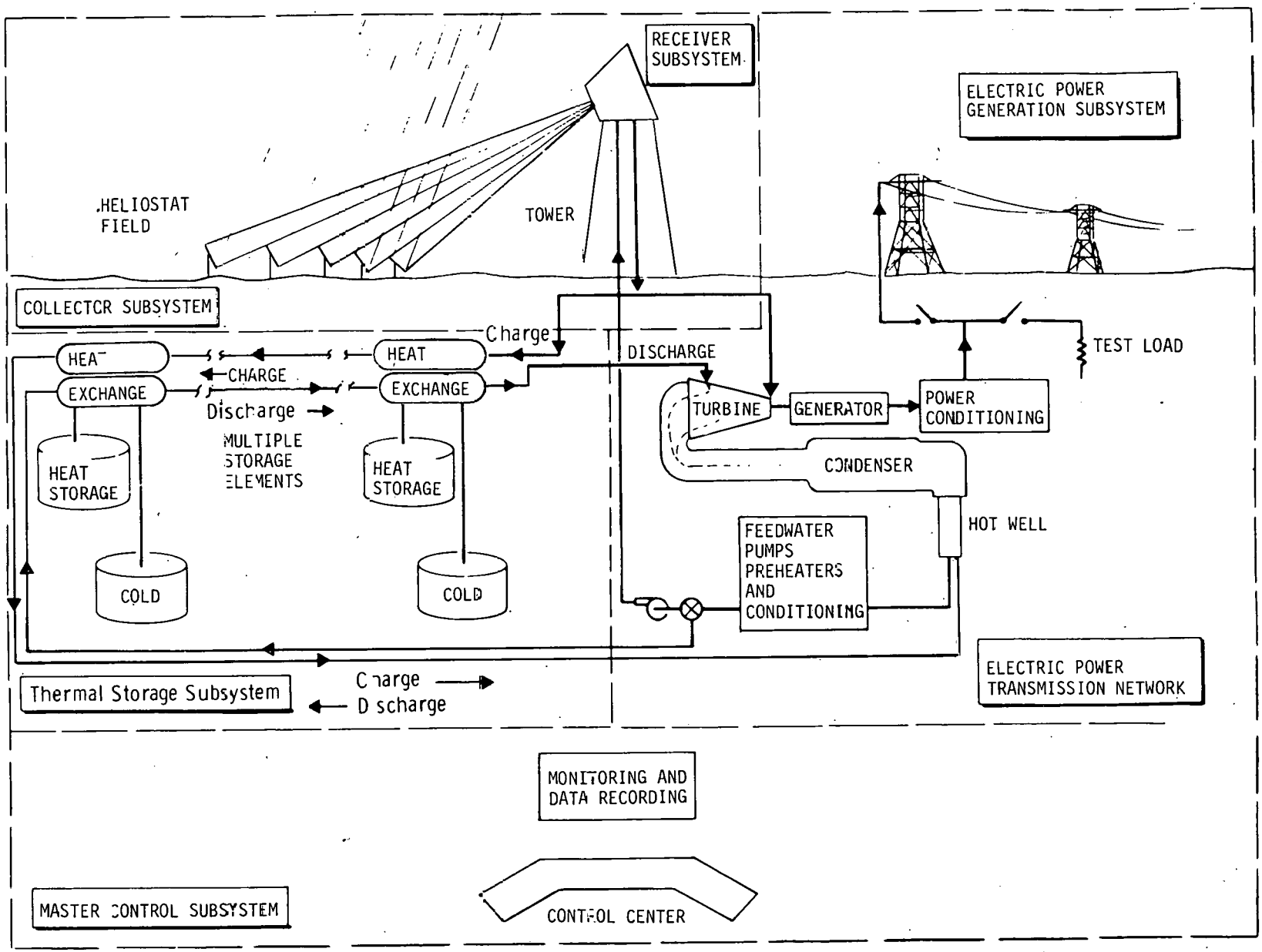


Figure 1 Central Receiver Solar Thermal Power System Concept Schematic

heat exchangers producing superheated steam which is routed to the turbine. Water from the condenser and/or the thermal storage subsystem is conditioned and recycled for continued generation of steam.

The receiver design must be very closely coordinated with collector field design. The collector field consists of multi-faceted heliostats arranged in a pattern which, together with receiver placement and elevation, provides optimum optical performances. Each facet of each heliostat is contoured to produce minimum reflected image size and pre-aligned so that images from all facets are concentrically coincident at the receiver aperture. The heliostats are individually driven by computer command to properly track the sun throughout the day. The receiver is a natural circulation steam generator whose boiler and superheater panels are geometrically arranged for proper exposure to the concentrated solar energy. Adiabatic roof, floor and side surfaces are added to complete the cavity enclosure, leaving a square aperture on the north side of ingress of the projected solar energy. The cavity arrangement minimizes radiant and convective heat loss from the absorbing surfaces. The entire cavity is insulated and includes aperture doors for heat retention during periods of cloudiness and overnight shutdown, minimizing normal startup time and reducing cyclic stress levels.

Design and operating characteristics of this receiver concept have been proven through the fabrication and testing of two small scale units: a 5 MW_t unit was tested using infra-red lamps to simulate solar input at the Sandia Laboratories radiant heat facility in Albuquerque, New Mexico; and a 1 MW_t unit was tested in the Centre Nationale de la Recherche Scientifique (CNRS) solar facility at Odeillo, France.

II. RECEIVER DESIGN REQUIREMENTS AND RATIONALE

The key requirements necessary to design the receiver include site location, environmental conditions, steam output characteristics operational considerations, and collector field-related factors. Some of the more pertinenet requirements for the pilot plant receiver are shown in Table 1. One of the most severe requirements is that of cycle lifetime. The diurnal cycle is the normal mode of operation, and occurs due to overnight and cloud-induced shutdowns. The minimum receiver temperature for startup during diurnal cycles is about 205°C (400°F). Cold start cycles occur when the receiver has been shutdown for extended periods, and the receiver temperature at startup can be equal to the local ambient.

Another requirement which can result in significant receiver design impact is the seismic criteria. Depending upon tower design, and the dynamic response characteristics of the tower/receiver combination, seismic loads can be greatly amplified from the ground level values to the point where these dominate design of major support structure.

Rationale behind the development of this receiver concept is based upon the specified requirements along with other considerations of safety reliability and acceptability in the commercial power generation market.

The receiver subsystem consists of a natural-circulation, side-opening-cavity receiver supported by an enclosed and roofed structural-steel tower (Figure 2). It has a number of features that contribute to low cost, low risk, and safe operation and maintenance.

The side-opening cavity, which is equipped with an aperture door, has a high-energy absorption efficiency and low thermal losses, both while in operation and also overnight when the cavity

Table 1 Pilot-Plant Receiver Requirements

Site Location	Barstow, California
Aperture Elevation	90 m above ground level
Aperture Opening	7.498 m (24.6 ft) square
Maximum Solar Energy to Receiver	52.3 MWt
Feedwater Input:	
Flow Rate	76,050 kg/h (161,600 lb/h)
Pressure	13,460 kPa (1950 psig)
Temperature	467 K/503 K (390°F/445°F)
Receiver Output:	
Flow Rate	75,300 kg/h (160,000 lb/h)
Temperature	789 K (960°F)
Pressure	10687 kPa (1550 psig)
Cycle Life:	
Diurnal	13,000
Cold Starts	1,300
Start-Up Time:	
Overnight	45 min
Cold	6 h
Winds (Ground Level)	3.5 m/s (8 mi/h) Maximum Operating 40.0 m/s (90 mi/h) Maximum
Ambient Temperature	243 K/323 K (-20°F/120°F)
Seismic Activity (Ground Level)	0.25 g

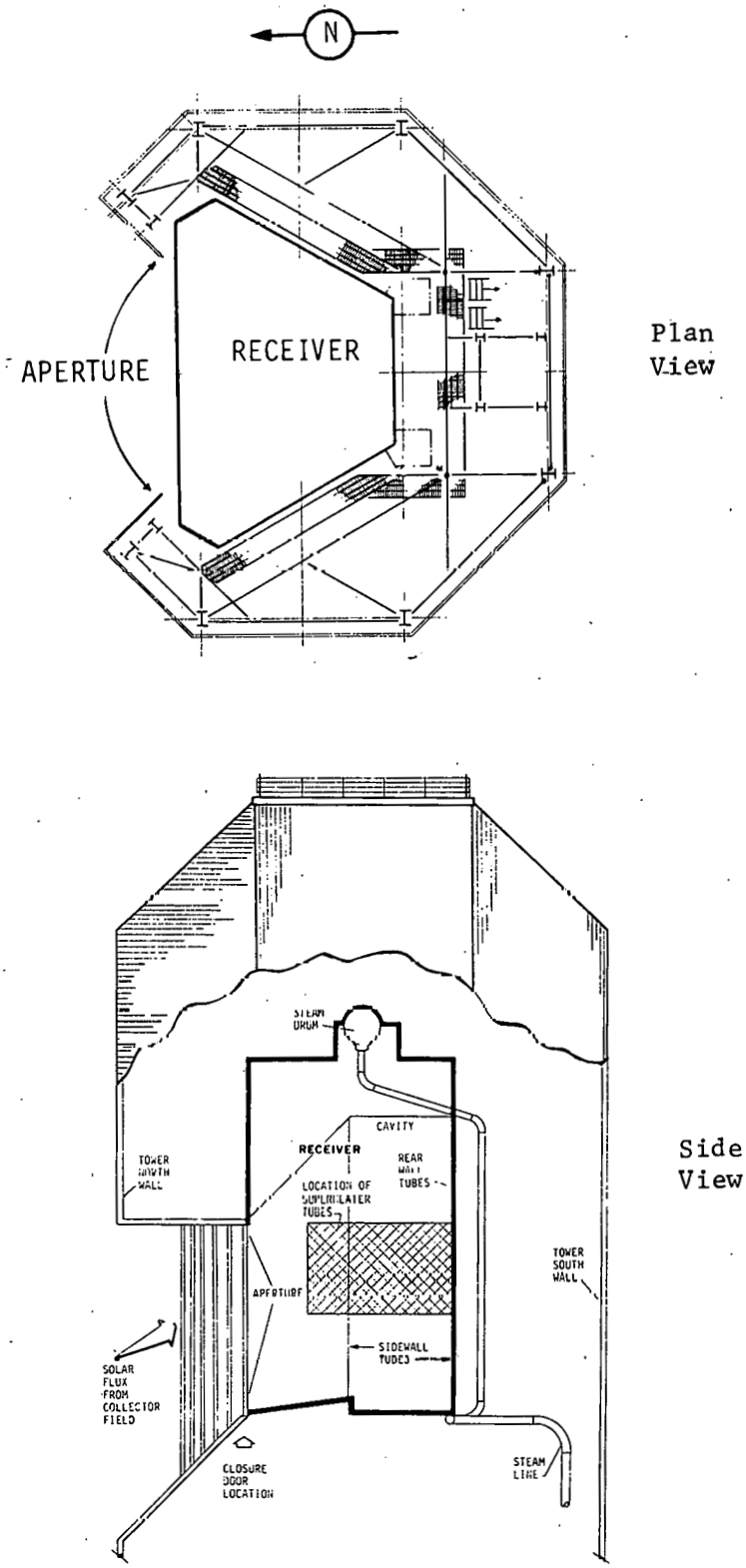


Figure 2 Receiver Installation in Tower

door is closed. The exterior surfaces of the receiver are easily protected from stray solar flux by a shield mounted on the tower. There are no structural supports to be protected. The side-opening cavity also permits use of a single focal point for the collector subsystem.

Natural circulation has a history of high reliability in fossil-fueled boilers. Using it eliminates capital and maintenance costs, reliability considerations, and power consumption associated with a forced-circulation pump. The boiler tubes are relatively large in diameter and no small orifices prone to plugging are needed to control flow distribution. Flow circuitry and valving are inherently uncomplicated. The receiver is relatively tolerant to impure feedwater because of its large tubes and sizeable water inventory. The circulation is inherently self-compensating for energy input variations. Heat-transfer characteristics in boiler and superheater are well known by the designer. Conventional, reliable, low-cost systems are used for feedwater and steam temperature control.

The receiver is similar in design to a fossil-fueled steam generator and would be designed, manufactured and constructed using conventional, well-established materials and techniques.

The tower places the receiver at the proper elevation with respect to the collector field in order to optimize sun angles. It is enclosed to provide protection for equipment and maintenance personnel; however, an open and more optimized structural design would be more economical for commercial plants.

Figure 3 depicts the selected cavity configuration. Dimensions shown are for inside surfaces at ambient temperature. Also shown are the projections of heliostat solar beams which bound the directly radiated surfaces of the cavity. This figure illustrates that the active steam-generating tubing must occupy most of

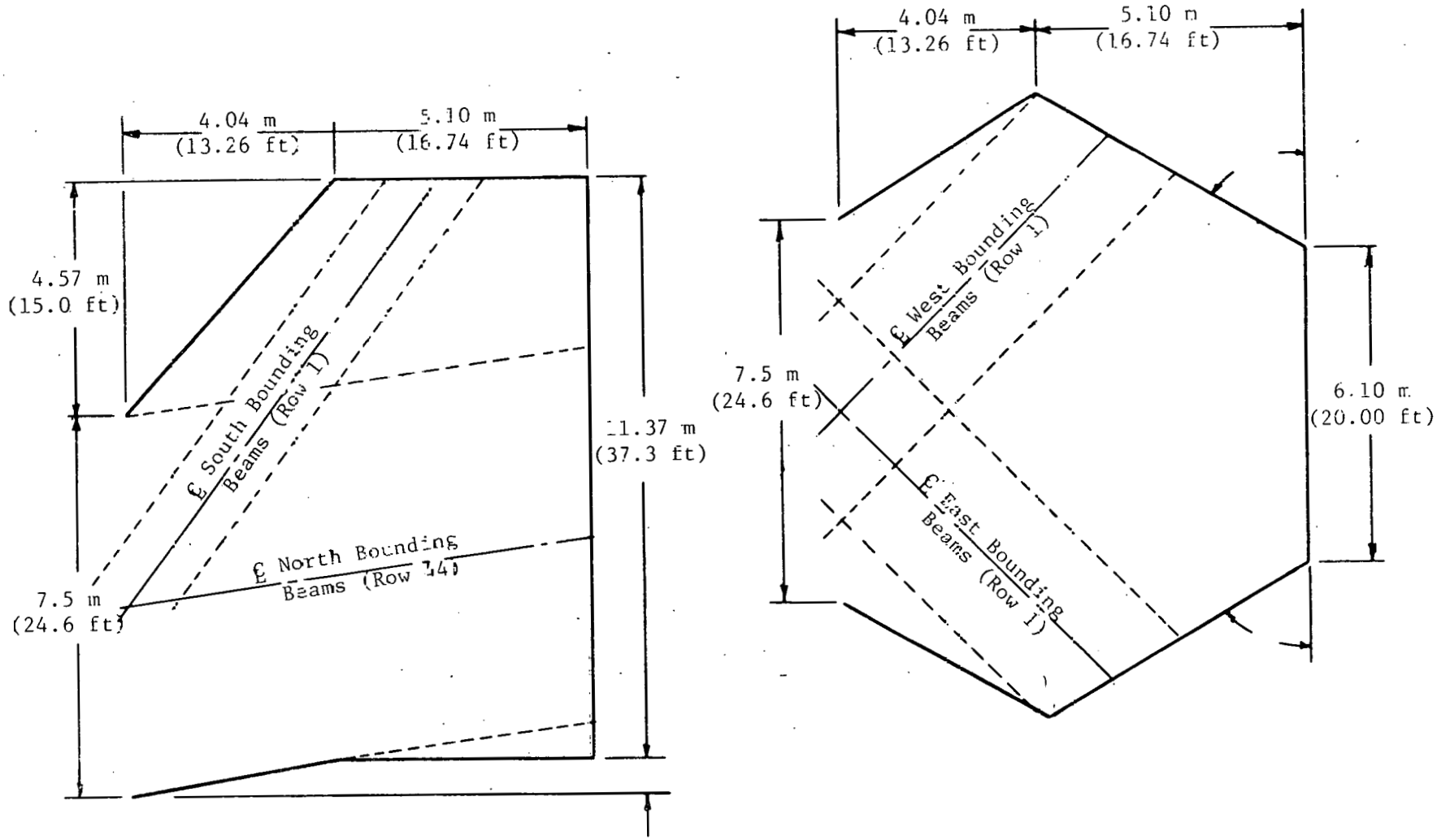


Figure 3 Cavity Configuration

the two side walls and the rear wall. The remaining walls, floors and ceiling will be inactive, with reflective surfaces to redirect radiant energy to the three active walls.

The aperture was sized to accommodate two divergent considerations. The opening must be large enough to capture most of the reflected energy from all heliostats. However, increasing the aperture size also increases thermal losses from the cavity by radiation and convection. Therefore, the optimum aperture size is that which allows the most energy to enter and yet minimizes direct radiation and convection losses from the cavity. The 7.498-m square aperture captures an annual average of 97.7 percent of the energy projected from the heliostat field and losses about 6 percent by radiation (both reflected and re-radiated) and convection from the cavity.

The depth and width of the cavity and the orientation of the three active walls with respect to the aperture were established to attain a reasonable compromise between receiver size and active surface heat-flux distribution. A larger cavity could result in lower peak heat fluxes and a somewhat more uniform distribution of energy over the active walls, but it would also be heavier (a detriment to tower design), costlier, and less efficient as a result of increased heat losses through the insulated walls.

III. RECEIVER DESIGN SUMMARY

A. Description

The receiver is designed to generate up to 20.55 kg of steam at 10,687 k Pa and 789 K outlet conditions. The essential instrumentation, valving and controls of the receiver are shown in the schematic flow diagram (Figure 4). Water flows from the steam drum through external downcomer pipes and branching feeders to the lower headers of the boiler where the flow is divided among

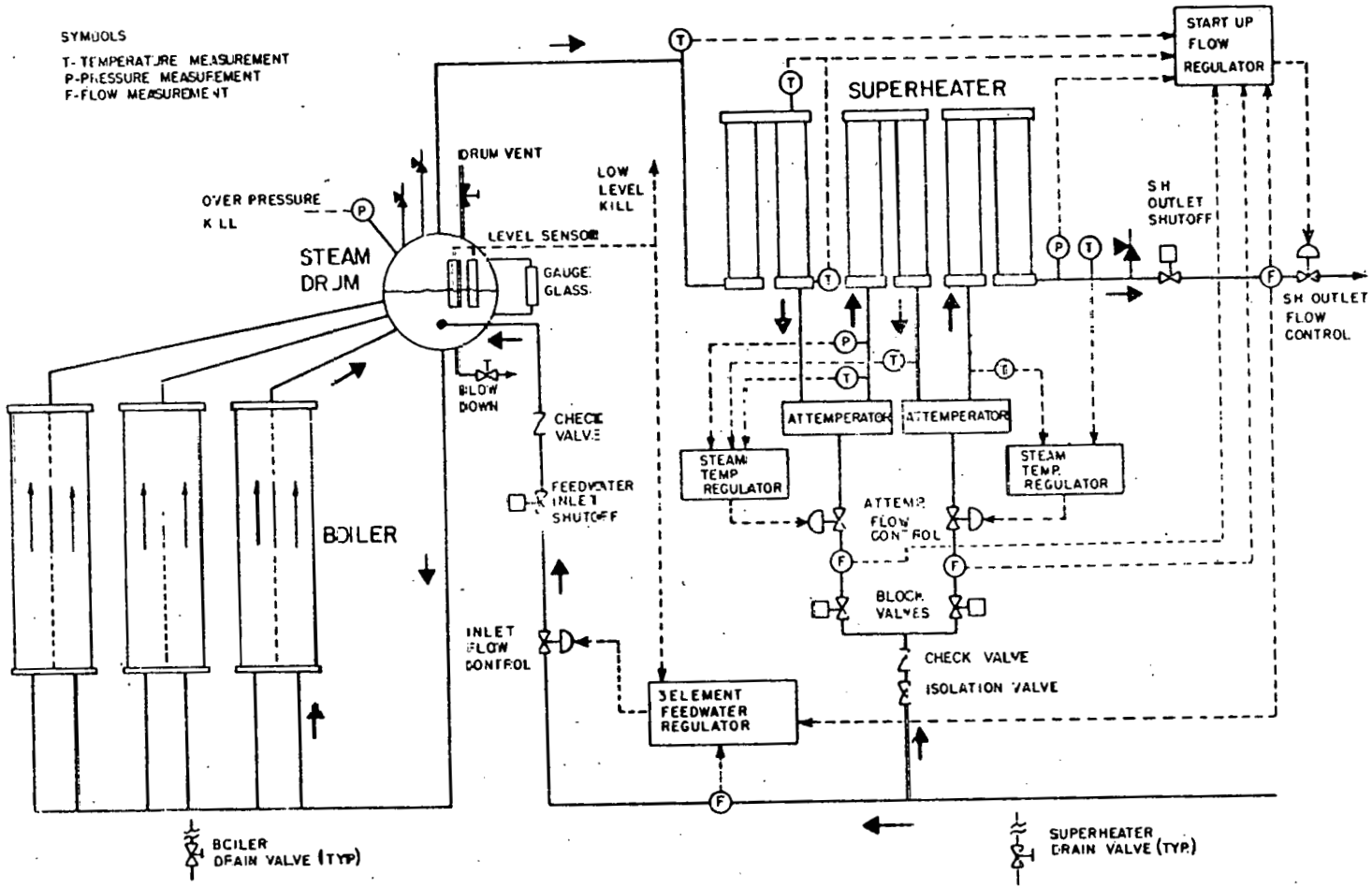


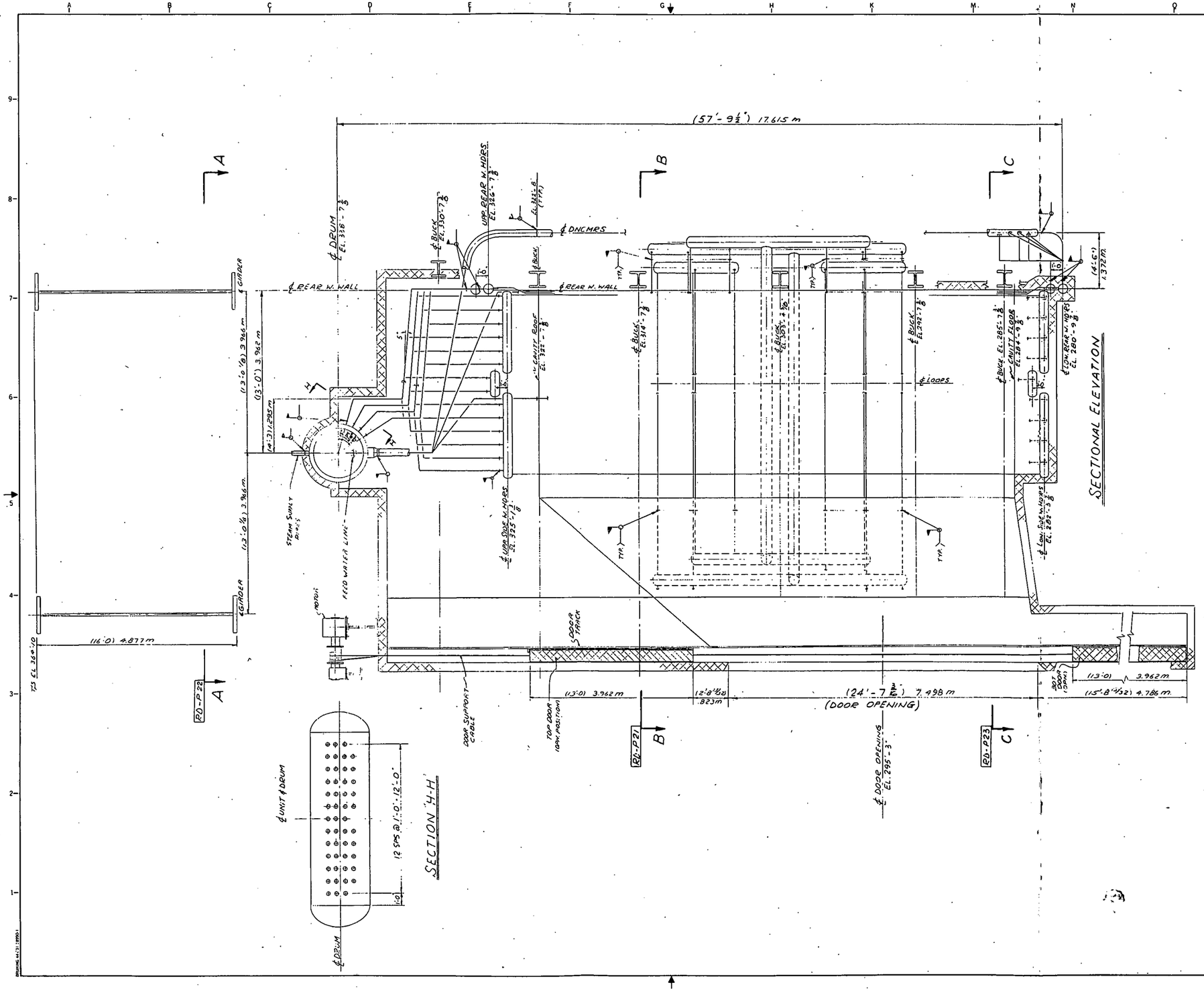
Figure 4 Natural Circulation Receiver Schematic

the various upflow circuits in the waterwalls (boiler tubes). As the water flows upward through the tubes, a portion of it is converted into steam by the absorbed heat. The resultant mixture of water and steam leaving the tubes is collected in the upper side- and rear-wall headers and carried to the steam drum through riser tubes. In the drum the mixture passes through centrifugal separators which separate the steam from the water. The water, after mixing with incoming feedwater, enters the downcomers for another trip around the circuit while the steam passes through chevron-type driers (mist eliminators) for removal of any entrained water droplets. From the drum the dry, saturated steam flows through a number of pipes to the six-pass superheater where it is heated to its specified outlet temperature.

Feedwater flow to the receiver is controlled by a conventional three-element feedwater regulator that matches feedwater flow to steam flow, with a trimming override in response to drum level.

Superheated steam temperature is controlled by attemperators in which feedwater is sprayed into the superheated steam and evaporated, thus lowering the steam temperature. Two attemperators are used--one between the second and third passes and another between the fourth and fifth passes. Attemperation is required during start-up not only to control steam temperature but also to prevent excessively high tube temperatures. During normal operation it is required because the fraction of the total solar flux incident on the superheater varies with the time of day and season of the year.

Sectional side elevation and plan views of the receiver are shown in Figures 5 and 6. All walls of the cavity are vertical. The rear wall and a large portion of both side walls are covered with 38.0-mm O.D. carbon steel boiler tubes on 44.5-mm centers, using Monowall^{TM} construction in which the tubes are jointed together along their length by continuous-weld integral fins to form



NOTES

1. DO NOT SCALE THIS DRAWING. USE FIGURE DIMENSIONS ONLY.
2. ABBREVIATIONS USED ON THIS DRAWING ARE IN ACCORDANCE WITH AMERICAN STANDARD "ABBREVIATIONS FOR USE ON DRAWINGS".

Figure 5

REV	DATE	BY	CK	DESCRIPTION
A	5-17-77			FIRST SUBMITTAL

REVISIONS

GENERAL ARRANGEMENT
SECTIONAL ELEVATION
COMMERCIAL/PILOT PLANT
RECEIVER

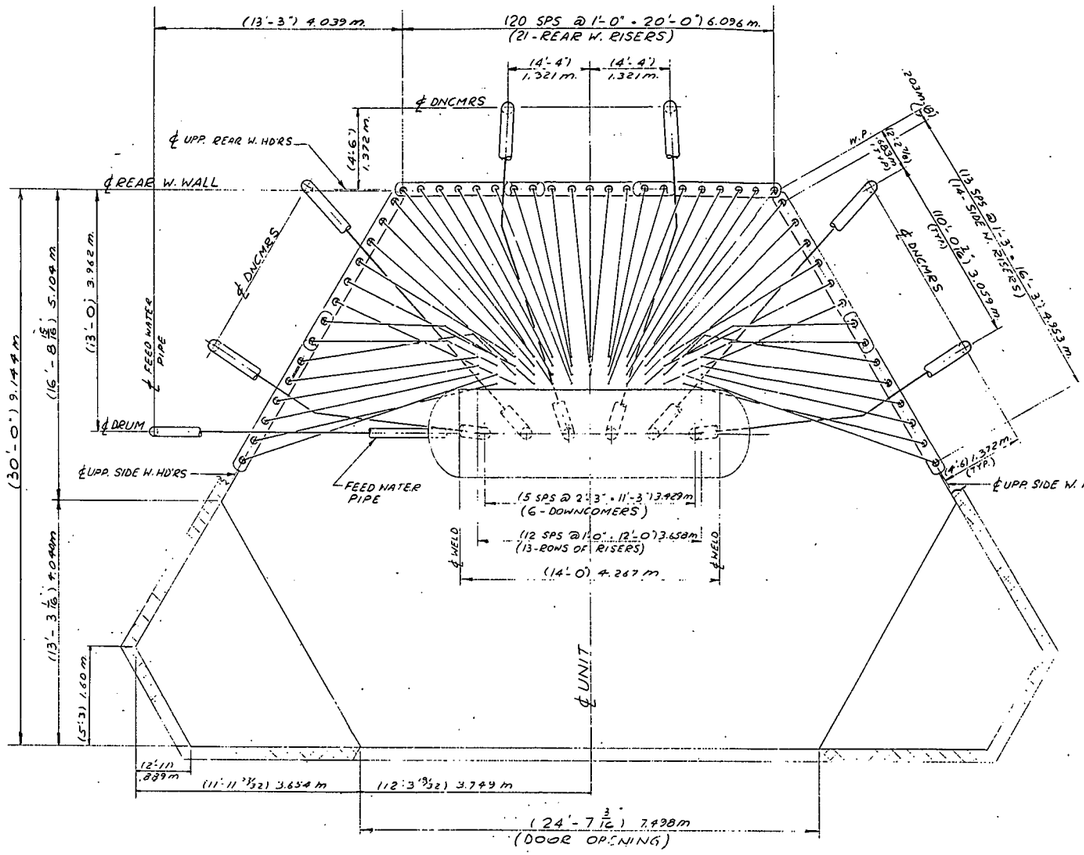
DRAWING NUMBER	SCALE	REVISION
59-6026-5-P 20	3/8" = 1'-0"	A

DRAWN BY	P.L.K. 11-22-76	0-59-6026
CHECKED BY		
APPROVED BY		

This Drawing is the Property of the FOSTER WHEELER ENERGY CORPORATION 110 S.Bd. BRIDGE AVE., LIVINGSTON, N. J.

AND IS LOANED SUBJECT TO RETURN ON DEMAND. IT IS TO BE USED ONLY IN CONNECTION WITH WORK DONE FOR THE COMPANY AND IS NOT TO BE LOANED TO OTHERS EXCEPT UNDER AGREEMENT THAT IT SHALL NOT BE REPRODUCED LOANED USED, OR DISCLOSED DIRECTLY OR INDIRECTLY FOR ANY PURPOSE OTHER THAN THAT FOR WHICH IT IS SPECIFICALLY FURNISHED. THE APPARATUS SHOWN IN THE DRAWING IS COVERED BY PATENTS.

436



SECTION "A-A" [20-P20]

NOTES

1. DO NOT SCALE THIS DRAWING. USE FIGURE DIMENSIONS ONLY.
2. ABBREVIATIONS USED ON THIS DRAWING ARE IN ACCORDANCE WITH AMERICAN STANDARD "ABBREVIATIONS FOR USE ON DRAWINGS".

Figure 6

REV.	DATE	BY OR APP.	DESCRIPTION
A	3-17-77	ZLK	FIRST SUBMITTAL

REVISIONS

GENERAL ARRANGEMENT
PLAN VIEW "A-A"
COMMERCIAL/PILOT PLANT
RECEIVER

DRAWING NUMBER	SCALE	REVISION
59-6026-5-P22	3/8" = 1'-0"	A

DRAWN BY	ZLK	12-15-76	0-59-6026
CHECKED BY			
APPROVED BY			

FOSTER WHEELER ENERGY CORPORATION
110 SO ORANGE AVE. LIVINGSTON N. J.

© 1977 FOSTER WHEELER ENERGY CORPORATION
THIS DRAWING IS THE PROPERTY OF THE CORPORATION AND IS LENT WITHOUT CONSIDERATION UNLESS OTHERWISE AGREED, UPON THE UNDERSTANDING THAT IT SHALL NOT BE REPRODUCED COPIED LENT OR DISPOSED OF DIRECTLY OR INDIRECTLY NOR USED FOR ANY PURPOSE OTHER THAN THAT FOR WHICH IT IS SPECIFICALLY FURNISHED THE APPARATUS SHOWN IN THE DRAWING IS COVERED BY PATENTS

437

flat panels. This construction was adopted because it is structurally rigid, can be handled in shipment and during erection with relative ease, and is impenetrable to solar flux.

The superheater consists of six passes in series, two passes on each of the side walls and two on the rear wall. Each pass is made from a number of parallel 25.4-mm O.D. austenitic stainless steel tubes arranged side by side on 28.6-mm centers to form one or more platens. These tube platens are placed in front of the waterwall panels (on the cavity side) as shown in Figure 7. The heat-flux pattern requires that the passes on all three walls be approximately aligned horizontally at two elevations. All passes are divided into two subpasses each, and steam flow is split into one upper and one lower subpass. This reduces the vertical heat-flux variation in each pass and, therefore, effects a more uniform flow distribution and steam temperature rise among the tubes. All superheater headers and transfer lines between passes are located behind the waterwall panels. Superheater tubes penetrate through openings in the waterwall panels at the inlet and outlet of each pass and at intervals along each pass where expansion loops and intermediate supports are located.

The inner surfaces of the cavity that are not lined with boiler tubes are lined with either steel coated with reflective material or with refractory material, depending on the intensity of incident solar flux on the particular surface. The outside surface of the entire cavity, as well as the steam drum and exterior piping, is encased in weather-proofed insulation.

The entire receiver is suspended from a structural-steel grid made up of large girders that are attached to the columns of the tower. The receiver is free to expand downward from the support grid, rearward from the front, and sideward about its centerline. The waterwalls are held in position and braced against externally

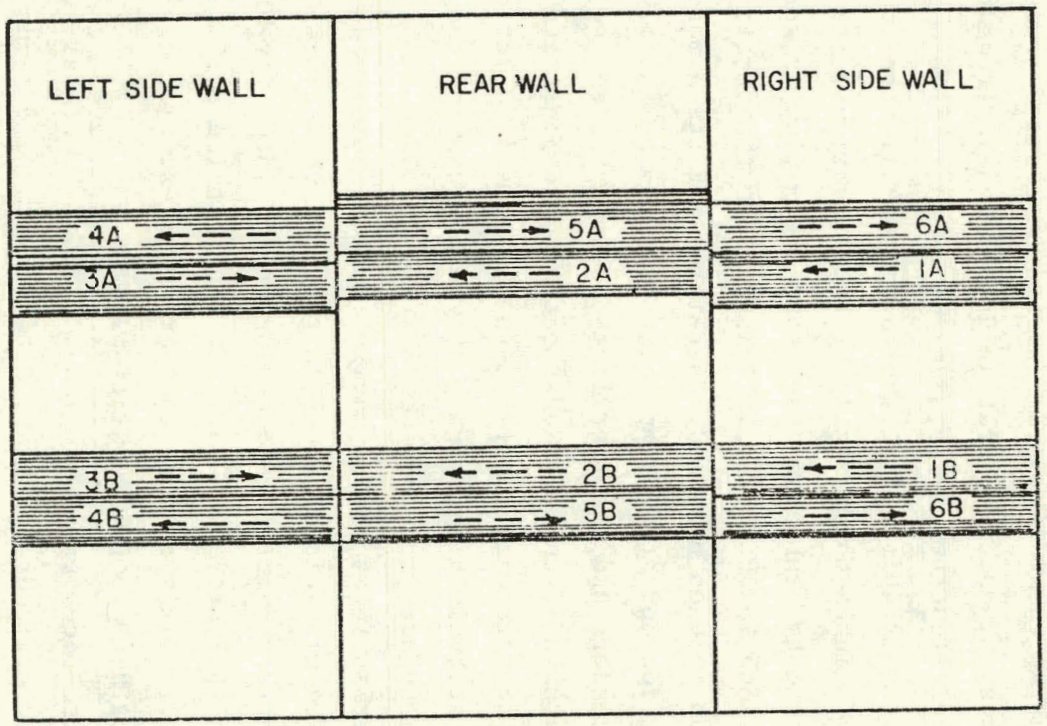


Figure 7 Arrangement of Superheater Passes

applied loads (wind and seismic) by horizontal, structural-steel buckstays located at five elevations. These buckstays also support the enclosure. The superheater headers are supported by brackets welded to the enclosure. Support points for the superheater tubes are located at the expansion loops and where the tubes penetrate the waterwalls. Mechanical snubbers attached to the buckstays transmit seismic loads to the tower structure while still permitting movement of the receiver parts caused by thermal expansion.

The aperture of the cavity is provided with an insulated door that can be closed to minimize heat loss and resultant cooling when the receiver is out of service. This door is mounted inside the receiver enclosure and is made up to two pieces which abut each other at the horizontal centerline of the aperture when the door is closed. The two pieces of the door counterbalance each other through the operating mechanism to minimize operating power.

B. Principal Materials

The primary materials of interest from the metallurgy/mechanics standpoints are those which contain the water/steam working fluid and undergo cyclic temperature and pressure variations. A listing of those materials is provided in Table 2, along with nominal operaing temperatures and size data for the various components.

Of particular concern are those components which are exposed to direct, concentrated solar heating--the boiler and superheater tube panels. The cyclic, assymetric heating incurred by these components result in more complex differential temperature induced stress loading and creep/fatigue characteristics. For this particular receiver design, the most severe condition in the boiler occurs at the peak heat flux of 722 kW/m^2 (229,000 $Btu/hr\text{-}ft^2$) which results in a maximum tube metal temperature of 437°C (818°F), about 112°C (200°F) above the adiabatic backside of the tube. The critical location in the superheater section is in pass 5A where the

Component	Material	O.D. mm (in.)	Wall Thickness mm (in.)	Maximum Operating Temperature °C (°F)
Superheater Section				
Pass 1	SA-213 TP304H	25.4 (1.0)	2.77 (0.109)	555 (1030)
Passes 2 thru 6	SA-213 TP316H	25.4 (1.0)	2.77 (0.109)	638 (1181)
Headers	SA-335 P-11	273.0 (10.75)	28.6 (1.125)	516 (960)
Outlet Pipe	SA-335 P-11	273.0 (10.75)	28.6 (1.125)	516 (960)
Boiler Section				
Waterwall Tubes	SA-210 A1	38.1 (1.5)	3.76 (0.15)	437 (818)
Headers	SA-106C	219.1 (8.625)	7.95 (0.313)	325 (617)
Risers	SA-210 A1	101.6 (4.00)	7.95 (0.313)	325 (617)
Feeders	SA-210 A1	88.9 (3.50)	7.15 (0.281)	325 (617)
Downcomers	SA-106C	168.0 (6.625)	11.0 (0.432)	325 (617)
Steam Drum	SA-515 GR-17	1422.4 (56)	101.6 (4.00)	325 (617)

TABLE 2 Principal Materials in Receiver

maximum heat flux is 422 kW/m^2 (134,000 $Ftu/hr\text{-}ft^2$), the metal temperature reaches 638°C (1181°F) and the front-to-back temperature differential is a maximum of 172°C (311°F).

C. Water Quality

1. Feedwater

The feedwater to the receiver should be of high quality to minimize the possibility of internal boiler corrosion and tube deposits. Tube deposits can lead to tube failures, particularly at the high heat-flux levels in this receiver.

The recommended maximum limits on critical feedwater characteristics entering the receiver are:

- o Iron - 10 ppb
- o Copper - 5 ppb
- o Oxygen - 7 ppb (but preferably low enough to be undetectable using a carmine-indigo color comparator)
- o Hardness - Minimum detectable by ASTM Procedure D-1126, Method B, or equivalent.
- o pH - 9.0 to 9.2

Oxygen scavenging is accomplished by injection of hydrazine and ammonia is used for pH control.

2. Boiler Water

The concentration of impurities in the boiler water must be limited by continuous blowdown. The rate of blowdown, as a percentage of the feedwater flow, is a function of the concentration of impurities in the feedwater relative to their concentration in the boiler water. The recommended maximum limits on critical impurities in the boiler water are:

- o Total dissolved solids - Limit specific conductivity of blowdown to 100 μmho
- o Silica - 1 ppm

The total dissolved solids are limited to avoid unacceptable priming and carry-over. The limit on silica is kept low not because higher concentrations would be detrimental to the boiler, but because silica dissolves in the steam and is transported to the turbine, where it forms insoluble deposits requiring costly, mechanical cleaning.

CHARACTERISTICS OF HOT WATER AS A CHEMICAL SOLVENT

Viewgraphs Presented

by

J. Cobble

San Diego State University

San Diego, California

Characteristics of Hot Water as a Chemical Solvent

- Ionizing solvent
- pH leveling solvent
- Gas dissolving solvent
- Hydrolysis inducing solvent
- Complex ion inducing solvent
- Faster kinetics in hot water
- Rapid changes in thermodynamic functions of solutes over relatively small temperatures
    - rapid changes in redox couples
    - rapid changes in chemistry

Little difference in chemical properties of steam and water at high temperatures

<u>These properties frequently operate to make high temperature water a corrosive solvent.</u>

$$\Delta F^{\circ}_{T_2} = \Delta F^{\circ}_{T_1} - \Delta S^{\circ}_{T_1} (T_2 - T_1) + \Delta C_p \Big]_{T_1}^{T_2} \left(\Delta T - T_2 \ln \frac{T_2}{T_1} \right)$$

For ordinary reactions

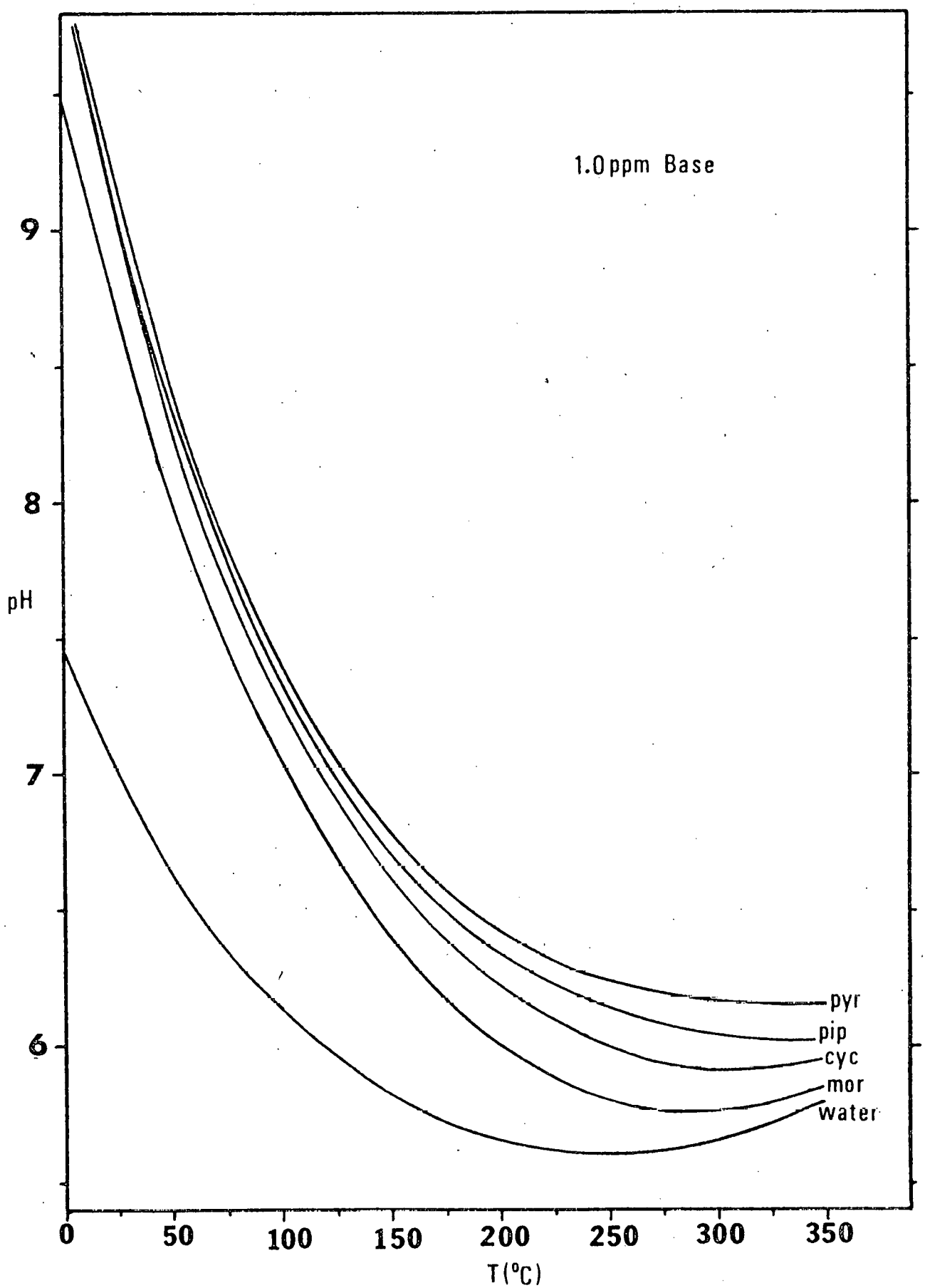
ΔS can be very + or -

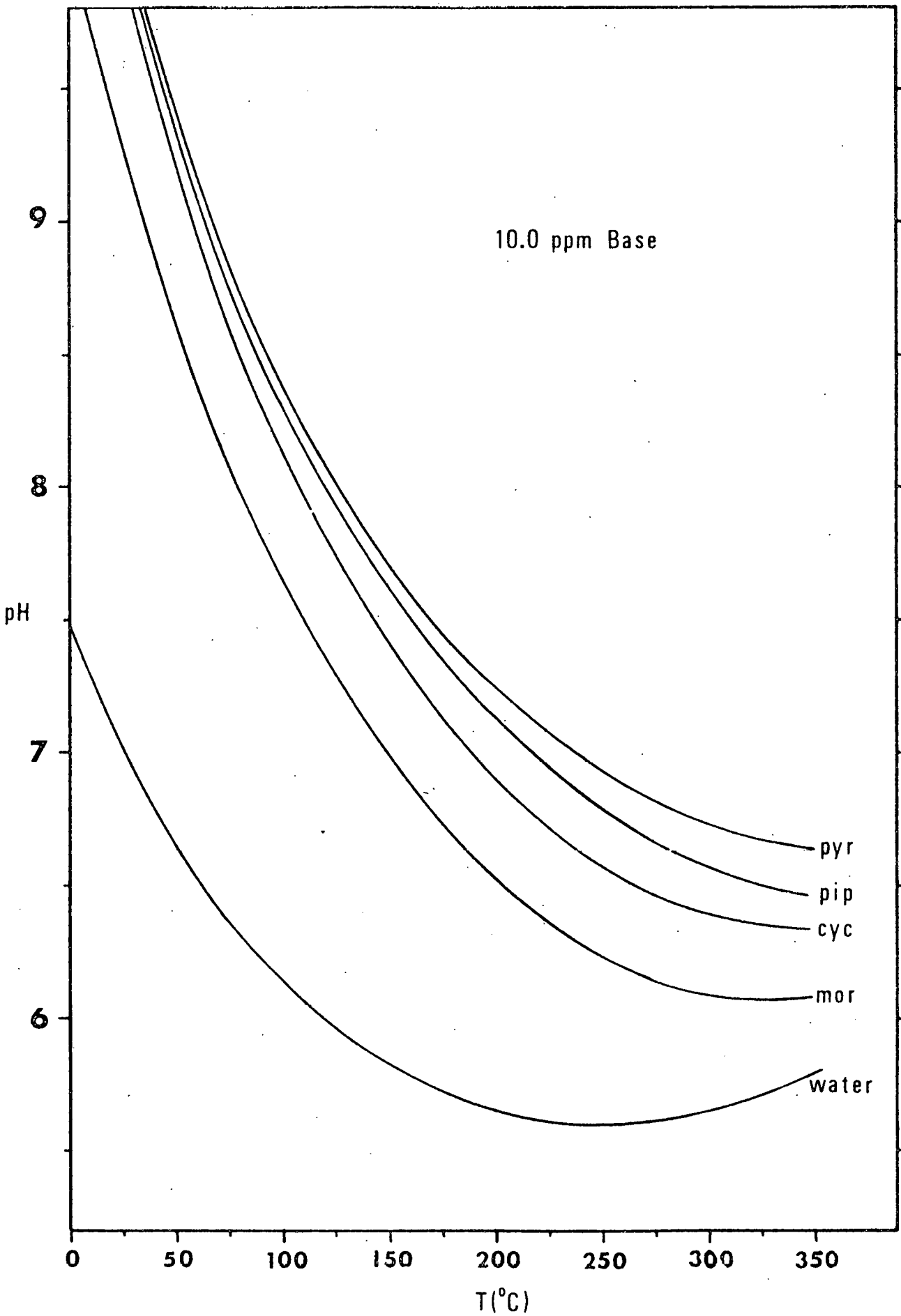
ΔC_p small

For reactions in water

ΔS can be very + or -

ΔC_p can be very + or -


1.0ppm Base
9
8
7
6
pH
pyr
pip
cyc
mor
water
0
50
100
150
200
250
300
350
T(°C)


10.0 ppm Base
pH
9
8
7
6
0
50
100
150
200
250
300
350
T(°C)
pyr
pip
cyc
mor
water

$$\text{Gas} \rightleftharpoons \text{Gas (dissolved)} \qquad K = \frac{\text{Conc}}{\text{Pressure}}$$

t°(c)	K_{CO_2}	K_{O_2}	K_{H_2}
0	7.9×10^{-2}	2.2×10^{-3}	9.8×10^{-4}
25	3.5×10^{-2}	1.3×10^{-3}	8.0×10^{-4}
100	1.1×10^{-2}	8.2×10^{-4}	7.9×10^{-4}
150	8.4×10^{-3}	1.0×10^{-3}	1.0×10^{-3}
200	8.7×10^{-3}	1.7×10^{-3}	1.5×10^{-3}
250	1.1×10^{-2}	3.1×10^{-3}	2.2×10^{-3}
300	1.4×10^{-2}	6.2×10^{-3}	3.6×10^{-3}

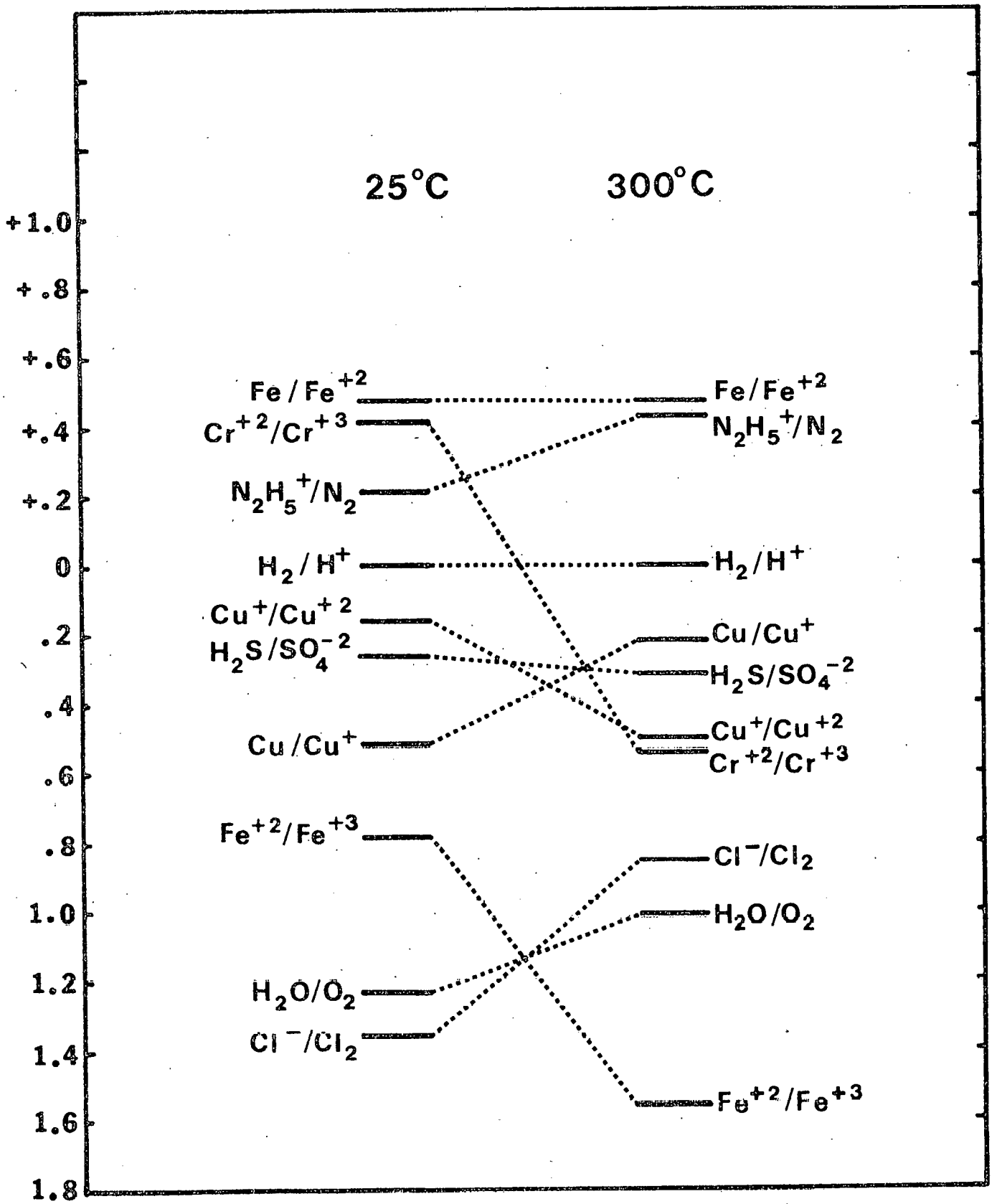
Increasing Temperature Effect on Complex Ion Formation

$$Fe^{+2} + OH^{-} = Fe(OH)^{+} \longrightarrow$$

$$Cr^{+3} + 2Cl^{-} = CrCl_2^{+} \longrightarrow$$

$$Ni^{+2} + 3OH^{-} = Ni(OH)_3^{-} \longrightarrow$$

$$Fe^{+2} + SO_4^{-2} = FeSO_4^{\circ} \longrightarrow$$


25°C
300°C
+1.0
+.8
+.6
+.4
+.2
0
.2
.4
.6
.8
1.0
1.2
1.4
1.6
1.8
Fe / Fe+2
Cr+2/Cr+3
N2H5+/N2
H2 / H+
Cu+/Cu+2
H2S/SO4-2
Cu /Cu+
Fe+2/Fe+3
H2O/O2
Cl-/Cl2
Fe/Fe+2
N2H5+/N2
H2/H+
Cu/Cu+
H2S/SO4-2
Cu+/Cu+2
Cr+2/Cr+3
Cl-/Cl2
H2O/O2
Fe+2/Fe+3

Solubility of Salts in Steam

$$NaCl(c) + nH_2O(g) = NaCl \cdot nH_2O(g)$$

$$K(T) = \frac{[\text{Salt in steam}]}{P_{H_2O}^{n}}$$

$$\log \text{Solubility} = n \log P_{H_2O} + \log K(T)$$

when $T = 300°C$

$P \sim 1000$ psi

$$\log S_{(ppb)} = 0.8 \log P_{(psi)} - 2.38$$

THIS PAGE

WAS INTENTIONALLY

LEFT BLANK

POSSIBLE ENVIRONMENTALLY-ENHANCED CRACKING PROBLEMS IN SOLAR-POWERED STEAM-GENERATORS

by

F. P. Ford

General Electric Company

Schenectady, New York

The proposed design of a solar-powered steam generator[1] is based essentially on that for a medium powered drum-boiler incorporating water chemistries and specifications currently used in fossil-fuel powered plant. Identification of possible areas of cracking due to stress-corrosion, corrosion-fatigue or hydrogen damage involves a review of current problems due to these modes of failure in operating fossil-fuel plant and a decision as to whether the use of solar energy is likely to make the problem worse or less. For instance, the higher frequency of load cycles due to cloud movement, etc., might be expected to increase the danger of corrosion-fatigue in the solar powered steam generator. This short discussion document reviews the fundamental requirements for environmentally enhanced cracking, correlates these requirements with the conditions and incidences of cracking in medium-powered sub-critical boiler plant, and points out the possible changes in these patterns due to the use of solar-energy in the steam generator.

1. Fundamental Requirements for Environmental Cracking

The delayed failure of ductile alloys under tensile stress in aqueous environments due to crack propagation is normally associated with pH/electrode potential conditions where a protective film (normally an oxide) is thermodynamically stable. Crack propagation is faradaically related to the dissolution which occurs at the crack tip where the protective film is continuously ruptured due to the creep processes concentrated there. Thus fundamentally the crack propagation rate will be a function of the potential dependent dissolution and passivation rates and the stress-dependent oxide-rupture rate. This simple model may be modified at higher temperatures where the thermodynamic stability of the oxide in a crack may be decreased, but the role of a protective mechanism for the sides of the crack is essential for the advancement of a sharp crack. This protective mechanism may be oxide formation or some other process, e.g., concentration polarization, formation of a salt, etc., but regardless of the precise nature, its requirement is important, for it is the main reason for differences in stress-corrosion behavior between stainless- and carbon-steels in the dilute aqueous environments nominally present in power generation operations.

The dependence of the crack propagation rate on electrode potential (and hence concentration of such oxidizing species such as, oxygen, nitrates, ammonia, etc) will be complicated due to the competing effects of dissolution and passivation, but in general there will be a potential range where the propagation rate of a sharp crack is high. (See, for instance[2] Figure 1 for stainless steel in dilute sulphate; similar relationships exist for carbon steel). Since the dissolution and passivation rates can be dependent on anion content, the range of potentials and the crack propagation rates may be extended by the presence of specific anions, (e.g., Cl^-, OH^- for stainless steel; OH^-, NO_3^- for carbon steel), but it should be emphasized that cracking, (at least for stainless and carbon steels) is possible in pure water, albeit at slower propagation rates than in concentrated environments.

Since the crack-propagation rate is also fundamentally related to the oxide-rupture rate at the crack tip, the susceptibility, both in terms of the potential range in which cracking is observed and the crack propagation rate, will increase with applied strain rate due to either monotonic or cyclic stresses (Figure 2 and 3). This fact offers a natural connection between stress-corrosion cracking and corrosion fatigue phenomena, and intimates that in operating power generation plant corrosion-fatigue problems, or failures during transient load conditions such as start up, should be far more common than stress-corrosion cracking, which requires more specific operating conditions to be severe. That this is the case is shown by the statistics[3] in Figure 4, which indicate the predominant role corrosion fatigue plays in the environment-enhanced failure of low and medium powered boiler-plant.

2. Practical Considerations vis à vis Cracking in Solar-Powered Steam Generators

In light of the above fundamental considerations, the danger of cracking in boiler plant, whether it be fossil-, nuclear- or solar-powered will be related to (a) the metallurgical condition of the alloy, (b) the environment - both bulk and localized, (c) the stress state, or more fundamentally, the strain rate at the crack tip. In comparing the danger of cracking in the proposed solar-powered boiler with conventional alternative, items (a) and (b) will not be changed, since the proposed design is similar to fossil-or nuclear powered boilers; the main difference will occur due to the higher incidence of fluctuating load cycles in the solar unit associated with, for incidence, cloud movements. The possible effect of these differences is briefly discussed below under failure mode/component headings.

2.1. Stress Corrosion Cracking

2.1.1. Boiler Tubes, Steam Drum and Superheaters

Failures of carbon-steel pipework or drums in medium powered boiler plant due to stress-corrosion cracking are not common, and when they do occur they are usually associated with caustic cracking due to localized hydroxide concentration caused by steam blanketing and the associated poor heat transfer or with leaks at welds in newly fabricated plant, or at rivets (in older drums).

The failure of stainless steel superheaters are also rare since the degree of superheat (>100^{0}C) precludes the presence of an aqueous phase. Such incidents that have occurred are normally associated with precommissioning operations, such as inadequate flushing of cleaning solution (e.g., Hcl), the exheuded exposure of the tubes to town-water ($\sim$10-15 ppm Cl^-), or the leaching of chloride from external lagging.

There is little likelihood of the incidence of stress-corrosion cracking in solar-powered steam generators under steady load conditions being greater than that observed in conventional power plant, especially when a zero-solids chemistry is employed. However, questions which should be addressed are:

(i) The variation of stress-corrosion susceptibility with load fluctuations, i.e., the effect of stress ripple plus a high mean load on the crack propagation rate. There is little data at present for the specific alloy/environment systems in the boiler, but there is evidence from both gas-pipeline[4] and turbine operations that such a stress variation (which may occur in the solar-powered boiler due to cloud movement) will increase the crack propagation rate at a given mean stress-intensity.

(ii) The variation of stress corrosion susceptibility of both stainless and carbon steel with the different oxygen-temperature combinations expected during start-up operations. In the design document the oxygen temperature combinations are not stated - they should be determined.

(iii) The time-concentration relationships for various anions (Cl^-, OH^-) should be determined for various operations, e.g., condenser leakage, boiling zones, etc. Particularly the relationship should be determined for wick-boiling conditions at sites of high oxide buildup, which might be expected in tubes heated primarily on one side.

2.2. Corrosion-Fatigue

2.2.1. Boiler Tubes and Superheaters

Incidences of corrosion-fatigue can occur relatively frequently (Figure 4), especially at tube/header joints or other tube attachment points. This can be expected in the solar-powered boiler unless the design specifically adjusts for the high bending stresses expected for tubes heated predominantly on one side, and which are undergoing frequent load cycling. Factors which will be of importance in determining the corrosion fatigue crack propagation rate will be (1) stress amplitude (2) mean stress; the higher the mean stress the greater the propagation rate (3) frequency; the slower the frequency the greater the penetration per cycle; note that the cyclic frequencies in the solar-powered boiler are likely to be low. (4) Environment; the same remarks for stress corrosion apply for corrosion fatigue, although as pointed out in Section 1, severe corrosion fatigue damage is not dependent as the formation of an aggressive environment.

2.2. Hydrogen Damage

2.3.1. Boiler Tubes

Failure of carbon steel boiler tubes by hydrogen damage is also relatively common[5] (listed under 'waterside on-load corrosion' in Figure 4). This mode of failure occurs in the temperature range 600^0 - 950^0F and is manifested by window-type blow-out of the tube. The hydrogen damage mechanism depends on a high hydrogen-ion activity at the surface, and since the bulk pH 25^0 may be ∿9.0, this acidity requirement can only be satisfied at isolated regions in the boiler tube. These regions are normally adjacent to surface protuberances (such as welds) where localized tubulence can lead to poor heat transfer and deposition of compacted crud on the tube surface. Under this crud, a cyclic process of cation-hydrolysis, acidity build-up and localized corrosion occurs. This leads to a certain amount of hydrogen atom absorption, diffusion down the grain boundaries and interaction with grain boundary cementite to form methane gas bubbles, which can cause grain boundary cracking due to their high internal pressures. The interaction of the systems stresses and natural defects at welds with this internal cracking then results in the catastrophic tube failure.

There is no reason to suppose that the incidence of hydrogen damage failure in solar-powered boilers will be any less than in conventional boilers if low chromium carbon steels are used and the weld finishing procedures are

inadequate. Indeed the incidence of failures may be higher if the oxide build-up is accelerated by the preferential heating on one side of the tube.

Remedial actions would involve annealing cold bent tubes and the use of higher chromium containing steels, e.g., 1% Cr ½% Mo or 2% Cr steels.

REFERENCES

1. W. J. Oberjohn & W. T. Southards - report issued at meeting.
2. F. P. Ford & M. Silverman - to be published.
3. J. Melville & G. G. Foster, Int. J. Pressure Vessel & Piping 3, 1, 1975.
4. R. R. Fessler Pipe Line Industry 44, 37, 1976.
5. See for instance series of papers in J. of Engineering for Power (Trans ASME), July 1964.

WATER CHEMISTRY AND HIGH TEMPERATURE THERMAL CONVERSION WITH AQUEOUS/STEAM COOLANT

Viewgraphs Presented

by

W. T. Lindsay, Jr.

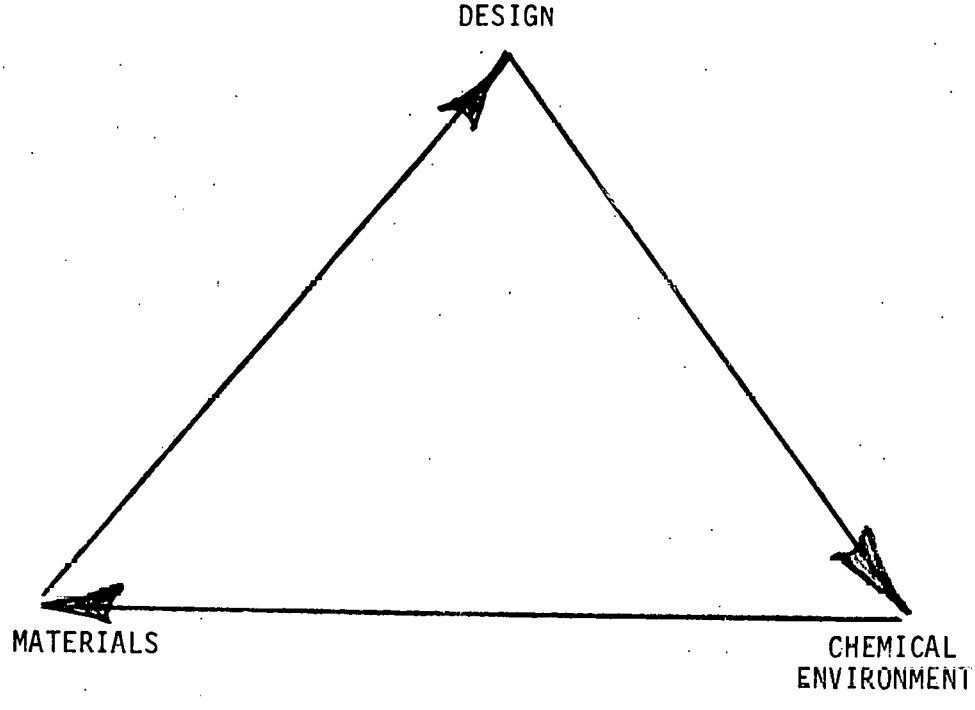
Westinghouse Research and Development Center

Pittsburgh, Pennsylvania

THE ISSUES OF

- WATER CHEMISTRY
- MATERIALS
- PLANT AND COMPONENT DESIGN

ARE INTERDEPENDENT AND INSEPARABLE



THE TYPE OF WATER CHEMISTRY THAT IS

NEEDED/OBTAINABLE/TOLERABLE

DEPENDS ON

DESIGN

(both overall and in detail)

FOR EXAMPLE:

- SEPARATE OR COMBINED FUNCTIONS AND SYSTEMS
  - RECEIVER COOLING
  - STEAM GENERATION FROM INCOMING ENERGY
  - STEAM GENERATION FROM STORED HEAT
- BOILER TYPE
  - ONCE-THROUGH
  - RECIRCULATING
- BOILER DESIGN
  - CONFIGURATION
  - HEAT FLUX DISTRIBUTION
  - INTERNAL FLOW DISTRIBUTION

STEPHEN WILCOX'S TWELVE REQUIREMENTS
FOR A PERFECT STEAM BOILER (1875)
INCLUDE THE FOLLOWING AS THE FIRST FIVE:

1. PROPER WORKMANSHIP AND SIMPLE CONSTRUCTION WITH EXPERIENCE-PROVEN MATERIALS.

2. A MUD DRUM TO RECEIVE ALL IMPURITIES DEPOSITED FROM THE WATER, PLACED AWAY FROM THE ACTION OF THE FIRE.

3. CAPACITY SUFFICIENT TO AVOID FLUCTUATIONS IN WATER LEVEL AND STEAM PRESSURE.

4. ADEQUATE SURFACE FOR STEAM DISENGAGEMENT.

5. CONSTANT AND THOROUGH INTERNAL CIRCULATION OF WATER TO KEEP ALL PARTS AT THE SAME TEMPERATURE.

THE "PERFECT" BOILER IS TOLERANT WITH RESPECT TO WATER CHEMISTRIES

- MINIMAL HIDEOUT
- NO LOCAL SUPERHEAT TO FORM CORROSIVE CONCENTRATES
- GOOD STEAM PURITY
- RESISTANT TO SCALING

IT MAY NOT BE POSSIBLE TO DESIGN A PERFECT BOILER AS A TOWER MOUNTED, CENTRAL-RECEIVER COOLER

- SIZE AND WEIGHT LIMITATIONS
- UNUSUAL CONFIGURATIONS
- HIGH HEAT FLUXES
- HEAT FLUX VARIATION WITH TIME AND POSITION
- CYCLIC OPERATION

PURPOSES OF WATER CHEMISTRY TREATMENT AND CONTROL

- CORROSION CONTROL
  - IN BOILER
  - IN TURBINE
  - IN CONDENSER
  - IN FEEDWATER SYSTEM
- CLEANLINESS CONTROL
  - SCALE PREVENTION FOR HEAT TRANSFER SURFACES
  - MANAGEMENT OF INSOLUBLE SLUDGES
  - AVOIDANCE OF TURBINE BLADE AND VALVE DEPOSITS

SOME CHEMICAL ADDITIVES THAT HAVE BEEN USED FOR BOILER WATER TREATMENT, AND THEIR FUNCTION

- OXYGEN SCAVENGING
  - HYDRAZINE
  - CATALYZED HYDRAZINE
  - SODIUM SULFITE
- pH CONTROL IN BOILER
  - SODIUM PHOSPHATE
  - SODIUM CARBONATE
  - SODIUM HYDROXIDE
- pH CONTROL IN CONDENSATE AND FEEDWATER
  - AMMONIA
  - MORPHOLINE
  - CYCLOHEXYLAMINE
- REDOX POTENTIAL CONTROL
  - HYDROGEN
  - OXYGEN
  - HYDRAZINE
- SLUDGE CONDITIONING
  - SODIUM PHOSPHATE
  - POLYELECTROLYTES
- SCALE CONTROL
  - CHELATES

SOME TYPES OF BOILER CHEMISTRIES THAT HAVE HAD SUBSTANTIAL APPLICATION

- COORDINATED PHOSPHATE AND "CONGRUENT CONTROL" PHOSPHATE
  - WIDELY USED WITH DRUM-TYPE, FOSSIL-FUEL UNITS
  - LESS THAN COMPLETELY SUCCESSFUL WITH PWR STEAM GENERATORS

- ALL VOLATILE TREATMENT (AVT)
  - MANDATORY FOR ONCE-THROUGH UNITS
  - COMMON ALSO FOR DRUM-TYPE BOILERS
  - PREFERRED NOW FOR PWR STEAM GENERATORS, BUT DEMANDING

- HIGH PURITY, HIGH OXYGEN
  - FORCED CHOICE FOR BWR'S
  - USE IN GERMANY FOR FOSSIL-FUEL UNITS

- CHELATE TREATMENT
  - EXPERIENCE MAINLY WITH LOW PRESSURE INDUSTRIAL BOILERS

- "PRECISION CONTROL" (LOW PHOSPHATE WITH FREE CAUSTIC)
  - REPORTED SUCCESSFUL USES LIMITED TO MODEST PRESSURE UNITS, BUT
  - FREE CAUSTIC SHOULD BE AVOIDED IN ANY UNIT

CONDENSERS

VS.

CONDENSATE POLISHERS

VS.

TURBINES

A DILEMMA IN COST/BENEFIT/RISK TRADE-OFFS

CONCLUSIONS

- IT WOULD BE UNWISE TO ASSUME IN ADVANCE THAT ANY CENTRAL-RECEIVER-COOLING STEAM GENERATOR WILL TOLERATE A WIDE SPECTRUM OF WATER CHEMISTRIES, INTENTIONAL OR UNINTENDED.

- PRELIMINARY CHOICES LEAST LIKELY TO BE TROUBLESOME:
  - DRUM BOILER
  - ALL VOLATILE TREATMENT WITH
    - HYDRAZINE FOR O_2 SCAVENGING
    - AMINES FOR pH CONTROL IN STEAM MOISTURE, CONDENSATE AND FEEDWATER
  - GOOD CONDENSER DESIGN, MATERIALS, MAINTENANCE
  - (CONDENSATE POLISHERS?)

- MODEL AND PILOT SCALE TESTS ARE NEEDED TO EVALUATE THE EFFECTS OF WATER CHEMISTRY VARIATIONS/DEVIATIONS/ ALTERNATIVES IN UNFAMILIAR BOILER CONFIGURATIONS.

HYDROGEN EMBRITTLEMENT IN HIGH PRESSURE STEAM

by

Joe Lux

Babcock & Wilcox

Alliance, Ohio

Paper or viewgraphs not available.

THIS PAGE

WAS INTENTIONALLY

LEFT BLANK

DESIGN CONSIDERATIONS FOR PARABOLIC-CHLINDRICAL SOLAR COLLECTORS

by

George W. Treadwell

Sandia Laboratories

Albuquerque, New Mexico

SAND76-0082
Unlimited Release
Printed July 1976

Distribution
Category UC-62

DESIGN CONSIDERATIONS FOR PARABOLIC-CYLINDRICAL SOLAR COLLECTORS

George W. Treadwell
Solar Energy Project Division 5712
Sandia Laboratories
Albuquerque, NM 87115

ABSTRACT

This report presents in some detail the various significant factors which influence the design of parabolic-cylindrical solar collectors.

Printed in the United States of America

Available from
National Technical Information Service
U. S. Department of Commerce
5285 Port Royal Road
Springfield, Virginia 22161
Price: Printed Copy $5.00 ; Microfiche $2.25

ACKNOWLEDGMENT

The foundation for much of the work described in this report comes from the efforts of a number of technical research personnel within Sandia Laboratories. An exhaustive listing is not practical, but appreciation for their contributions is extended to the following:

Coating Development - D. M. Mattox, 5834, R. R. Sowell, 5834

Optical and Thermophysical Properties - R. B. Pettit, 5842

Reflector Characterization - B. L. Butler, 5844

Code Development - M. W. Edenburn, 5719, W. H. McCulloch, 5711. F. Biggs, 5231

CONTENTS

	Page
Summary	7
Introduction	8
Considerations	9
Solar Coating	9
Sizing of Glass Annulus	13
Insulating or Silvering of Glass	16
Reflection and Transmittance	17
Receiver Tube Sizing	21
Collector Sizing	20
Influence of Asymmetric Heating	30
Other Design Considerations	30
Miscellaneous Considerations	33
APPENDIX A - CALCULATION OF RIM ANGLE FOR MINIMUM AVERAGE DISTANCE FROM FOCUS TO PARABOLA	35
Bibliography	37

TABLES

Table		Page
I	Average Collector Efficiency Percentage at 316°C (600°F)	16
II	Phase IVB Collector Sizing Considerations	26
III	Collector Efficiency (%) and Arc Length Changes (%) Compared to 1.57 Radians (90°) Rim Angle	27
IV	Figure of Merit vs Collector Rim Angle	28

FIGURES

Figure		Page
1	Parabolic-Cylindrical Solar Collector	8
2	Reflector With Receiver Tube Suspended at Focal Line	10
3	Reflector With Glass-Jacketed Receiver Tube Suspended at Focal Line	10
4	Input Temperature vs Percent Efficiency for 25.4 mm OD Receiver With 57.1 mm OD Glass Jacket at No Vacuum	11
5	Input Temperature vs Percent Efficiency for 25.4 mm OD Receiver With 57.1 mm OD Glass Jacket at 0.2 mm Hg Pressure	11
6	Solar Collector Test Results	12
7	Total Hemispherical Emittance of Receiver vs Collector Efficiency	12

CONTENTS (cont)

FIGURES

Figure		Page
8	Harshaw Black Chrome on Electroplated Sulfamate Nickel (4 Minute Treatment Time)	13
9	Harshaw Black Chrome (4 Minute Treatment Time)	14
10	Steel Receiver With Glass Jacket	15
11	Results Obtained From Equation (1)	15
12	Receiver Cross Section	17
13	Collector Power Losses	18
14	Collector Power Losses	18
15	Probable Collector Efficiency Range	19
16	Solar Spectrum Reflectance vs Aperture For Various Reflector Materials	20
17	Collector Efficiency vs Non Non Normal Sun Position (Assuming Attenuation at Solar Noon Applied to All Sun Angles)	20
18	Receiver Tube Assembly Cross Section	21
19	Various Rim Angles for Common Aperture	22
20	Energy Distribution vs Collector Efficiency	23
21	Apparatus for Characterizing Slope Errors of Parabolic Reflector Surfaces	24
22	Scans Resulting From Use of Apparatus Shown in Figure 21	24
23	Collector Efficiency vs Receiver Tube Outer Diameter	26
24	Influence of Off-Center Receiver Tube Mounting	28
25	Energy Input Influence on Receiver Sizing	29
26	Predicted Maximum Therminol 66® Film Temperatures	31
27	Influence of Plug on Predicted Maximum Therminol 66® Film Temperatures (Phase IVA Northwest Quadrant)	31
28	Receiver Tube and Support Assembly	32
29	Alternate Receiver Tube Assembly Design	33

DESIGN CONSIDERATIONS FOR PARABOLIC-CYLINDRICAL SOLAR COLLECTORS

Summary

The solar collector is an important component in the solar powered system presently being designed and installed at Sandia Laboratories. This report describes some of the key considerations which have an influence upon collector design.

The relative importance of the solar coating absorptance and total hemispherical emittance for linear-focusing collectors is described. A high absorptance has a much more important effect on collector efficiency than does a low emittance. The evacuation of a glass-jacketed receiver design achieves approximately a 5% efficiency improvement, and the design is shown to be sized with the least thermal loss strategy when the annulus gap between the steel receiver and glass is approximately 10 mm (0.4 in.). The tradeoffs between an insulated or silvered glass jacket and total hemispherical emittance are also shown. When the emittance is greater than 0.5 an insulated glass jacket is desirable. Silvering the glass is of dubious benefit under any conditions because of processing and durability considerations.

The present state of the art in reflecting materials is used in energy balance calculations, and the calculated results are compared to test results to illustrate plausible improvements in collector efficiency. Durable specular reflective surfaces with reflectivity between 0.90 and 0.95 are presently being fabricated in laboratory sizes. It is reasonable to expect that efficiencies of 70% at 315°C and solar noon can be achieved in the near future. The interrelationships between reflector rim angle and receiver size are shown to result in rim angle selections which maximize energy collection for minimal costs. Although a 2.09 radians (120°) rim angle has the minimum average parabola-to-focus distance, a reasonable rim angle is shown to be 1.57 radians (90°) because of minimal collector efficiency improvements with accompanying increased construction costs for 2.09 radians (120°). The characterization of parabolic reflector shapes and reflector materials are part of this selection process. Mirror slope standard deviations of less than 9 milliradians (0.5°) are achievable. The relationship between optical congruency and thermal non-congruency in establishing optimal collector sizing is also demonstrated. A 2-metre wide aperture is shown to be reasonable for systems which allow 1% of the collected energy to be used for pumping.

The importance of asymmetric heating on the receiver design is described in some detail as is the importance of flow control when organic heat transfer liquids are used. With a 25 mm OD receiver, a 2-metre aperture width, and a 1.57 radian rim angle, flow rates of greater than 0.00019 m^3/sec (3gpm) are required in order to prevent local overheating and eventual destruction of the organic liquid. A lower flow rate could be achieved by incorporating internal liquid turbulence generators.

A limited discussion of collector orientations and off-axis receivers is included. Collector fields oriented north-south collector more energy than do east-west oriented fields but are less economical in land utilization because of nonshadowing spacings, in pipeline costs, in structural costs, and in thermal losses.

Introduction

Sandia Laboratories has been funded by the Energy Research and Development Administration to analyze, design, and build a solar total energy experimental system to provide the energy needs for a 1100 square-metre building.

A significant contributor to a successful solar-powered system is the design of the solar collector. The design of the collector must be such that energy capture is high, thermal losses are low, and cost/effectiveness ratio is as small as practicable. This report addresses the design of parabolic-cylindrical solar collectors (Figure 1) using Therminol 66® heat transfer liquid in uniflow receiver tubes and examines in some detail those aspects most important to high collector efficiency; it briefly examines cost aspects since production quantities have such a large influence upon unit costs.

One of the purposes of this report is to portray the relationships between the sizes and shapes of these collectors. An understanding of these relationships will allow comparisons and analyses to be drawn for other focusing collector designs. It should be noted that this report examines, only cursorily, matters such as collector orientation, equitorial mount tracking, and collector field layouts. These matters have been more properly treated in detail in other reports.

Some of the work described in this report is extracted from the sources listed in the bibliography particularly with respect to the use of the listed computer codes, spectrum definitions, material characteristics, and heat transfer phenomena. Other opinions and results are based upon nearly three years of experience in testing, measuring, construction, and analyses at Sandia Laboratories. This report is not intended to be a parametric sensitivity analysis, but it does examine what is believed to be the more important facets of design in a 315°C (600°F) maximum operating temperature system. Reference to the bibliography will permit a more thorough examination of some of these aspects.

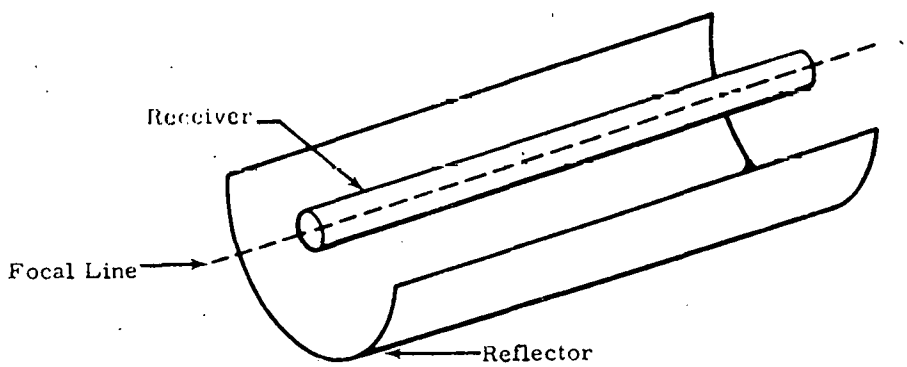


Figure 1. Parabolic-Cylindrical Solar Collector

Considerations

Solar Coating

Several authors have attempted to describe the importance of a coatings' high average solar energy absorptance (α_S) and total hemispherical emittance (ϵ_{TH}) ratio (α_S/ϵ_{TH}). In reality, the ratio is not very important and this will be illustrated by reference to test results and to analysis. A Pyromark® - painted ($\alpha_S = 0.98, \epsilon_{TH(300°C)} = 1.0$) receiver tube suspended at the focal line of a 1.57 radians (90°) rim angle Alzak® reflector (Figure 2) oriented normal to the sun, was unable to capture sufficient reflected energy to compensate for thermal losses at 315°C (600°F) and operated at a negative efficiency (defined as: energy into liquid in receiver/energy into aperture). The addition of a glass jacket (Figure 3) allowed a positive efficiency to be obtained (Figure 4). The use of a modest vacuum in the annulus improved the efficiency approximately 5% (Figure 5). The range of analytical-model predicted results compared with some test results are shown in Figure 6. Since the Alzak has a specular reflectance within the portrayed range, there is reasonable agreement between predictions and test results

Since the test results and analytical model have reasonable agreement, an analytical model was used to calculate the data appearing on Figure 7 and to portray the influence of α_S and ϵ_{TH}. From these data, a clear relationship between solar absorptance and total hemispherical emittance can be seen. The higher the α_S, the higher the collector efficiency; the lower the ϵ_{TH}, the higher the collector efficiency, but the improvement is not so pronounced. The collector efficiency with

$$\alpha_S = 0.85 \text{ and } \epsilon_{TH} = 0.05 \left(\frac{\alpha_S}{\epsilon_{TH}} = 17\right)$$

is 50%; the collector efficiency with

$$\alpha_S = 0.95 \text{ and } \epsilon_{TH} = 0.3 \left(\frac{\alpha_S}{\epsilon_{TH}} = 3.17\right)$$

is 51%. It is obvious from these data that a high absorptance is far more important than a low emittance, and the ratio of α_S/ϵ_{TH} not so important. In other words, it is far more effective to initially capture the sun's energy and attempt to decrease those thermal losses controlled by the emittance through proper design.

Coating development work at Sandia and NASA/Lewis has demonstrated that a thin (0.15-0.20 μm) black chrome (Cr_2O_3) layer electrodeposited over dull nickel can achieve $\alpha_S \geq 0.95$ and $\epsilon_{TH} \leq 0.25$ and not degrade rapidly at operating temperatures of at least 315°C whether exposed to air, moisture, and/or ultraviolet energy. The coating's total hemispherical emittance determined by calorimetric techniques is displayed as a function of temperature in Figure 8. In general, the emittance is directly proportional to the electrodeposition time and

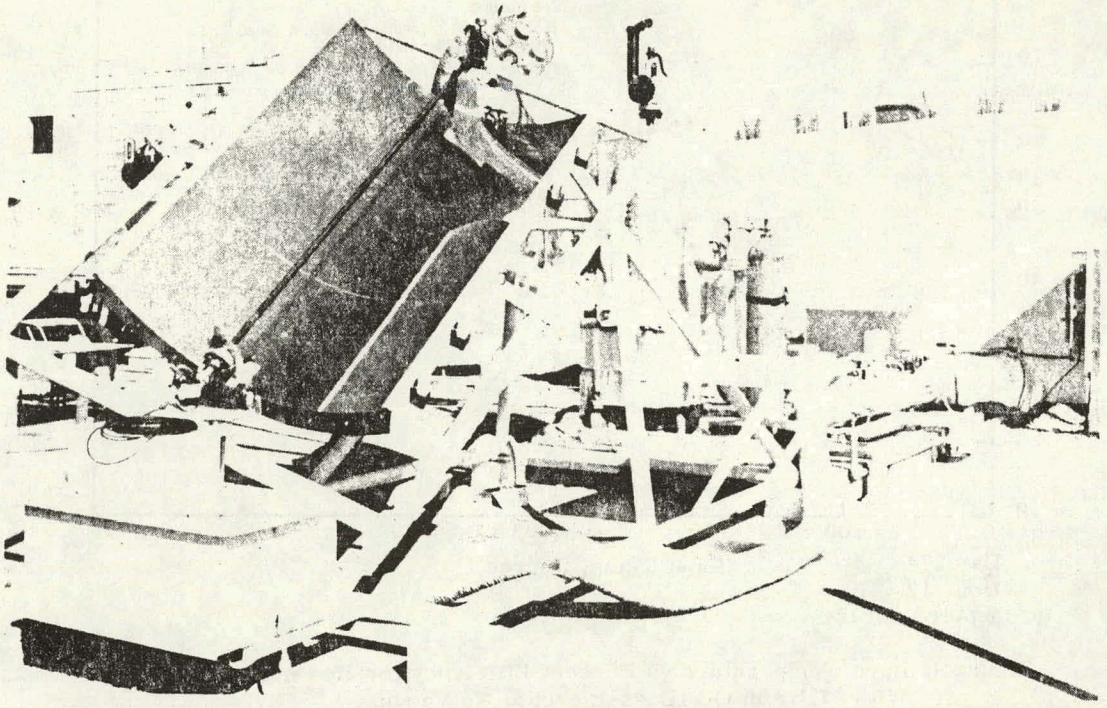


Figure 2. Reflector With Receiver Tube Suspended at Focal Line

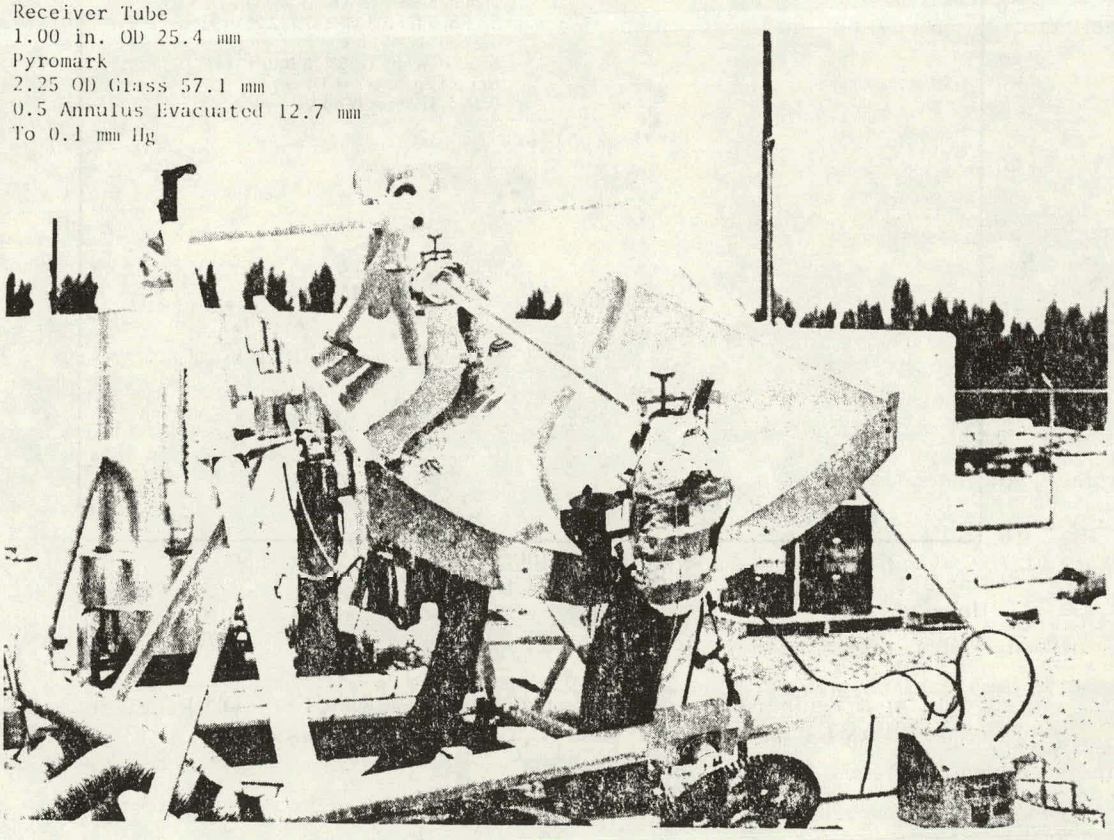


Figure 3. Reflector With Glass-Jacketed Receiver Tube Suspended at Focal Line

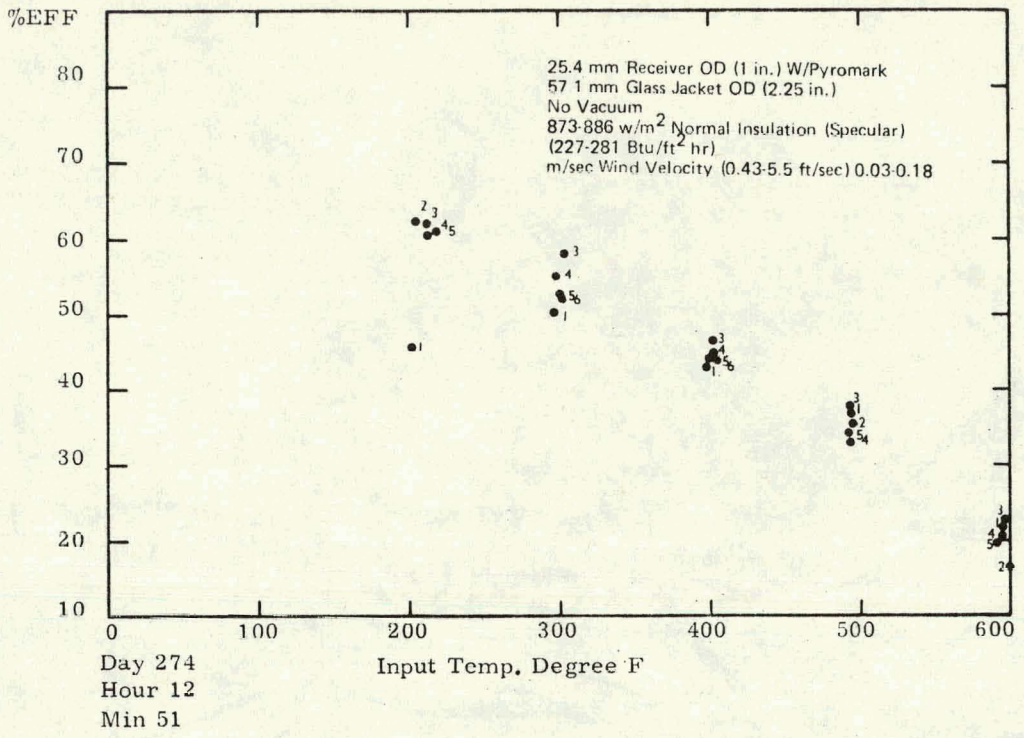


Figure 4. Input Temperature vs Percent Efficiency for 25.4 mm OD Receiver With 57.1 mm OD Glass Jacket at No Vacuum

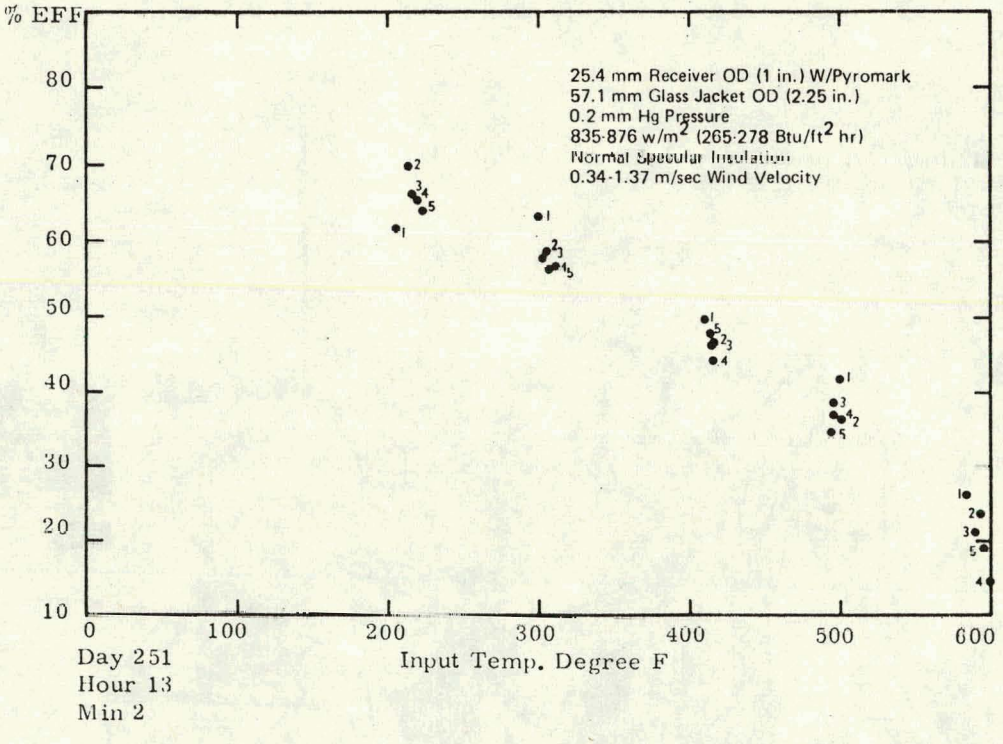


Figure 5. Input Temperature vs Percent Efficiency for 25.4 mm OD Receiver With 57.1 mm OD Glass Jacket at 0.2 mm Hg Pressure

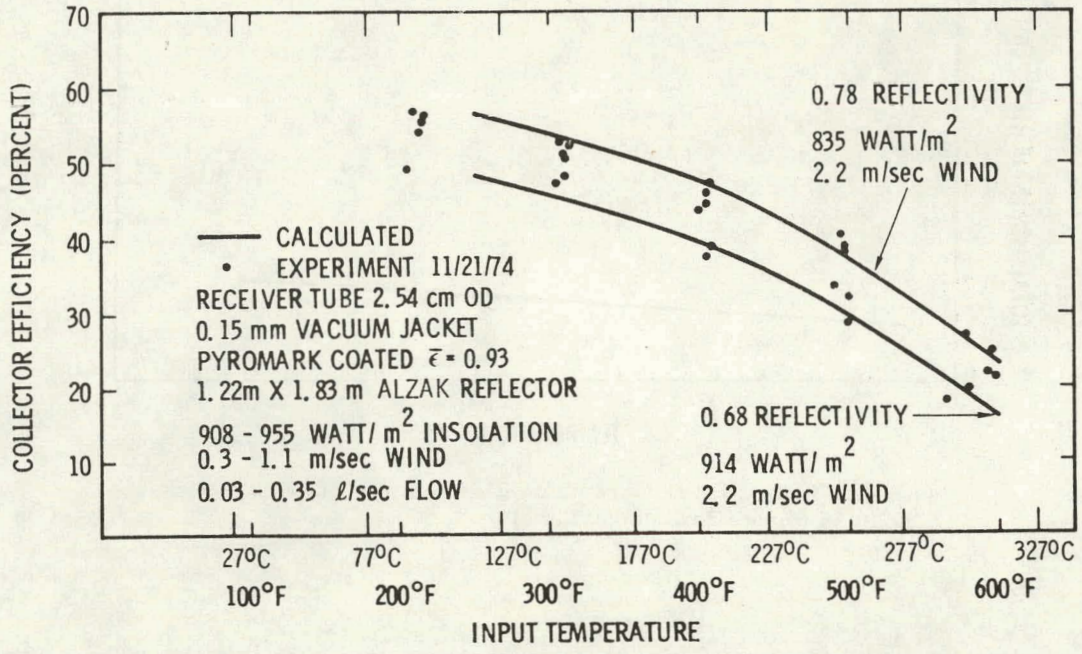


Figure 6. Solar Collector Test Results

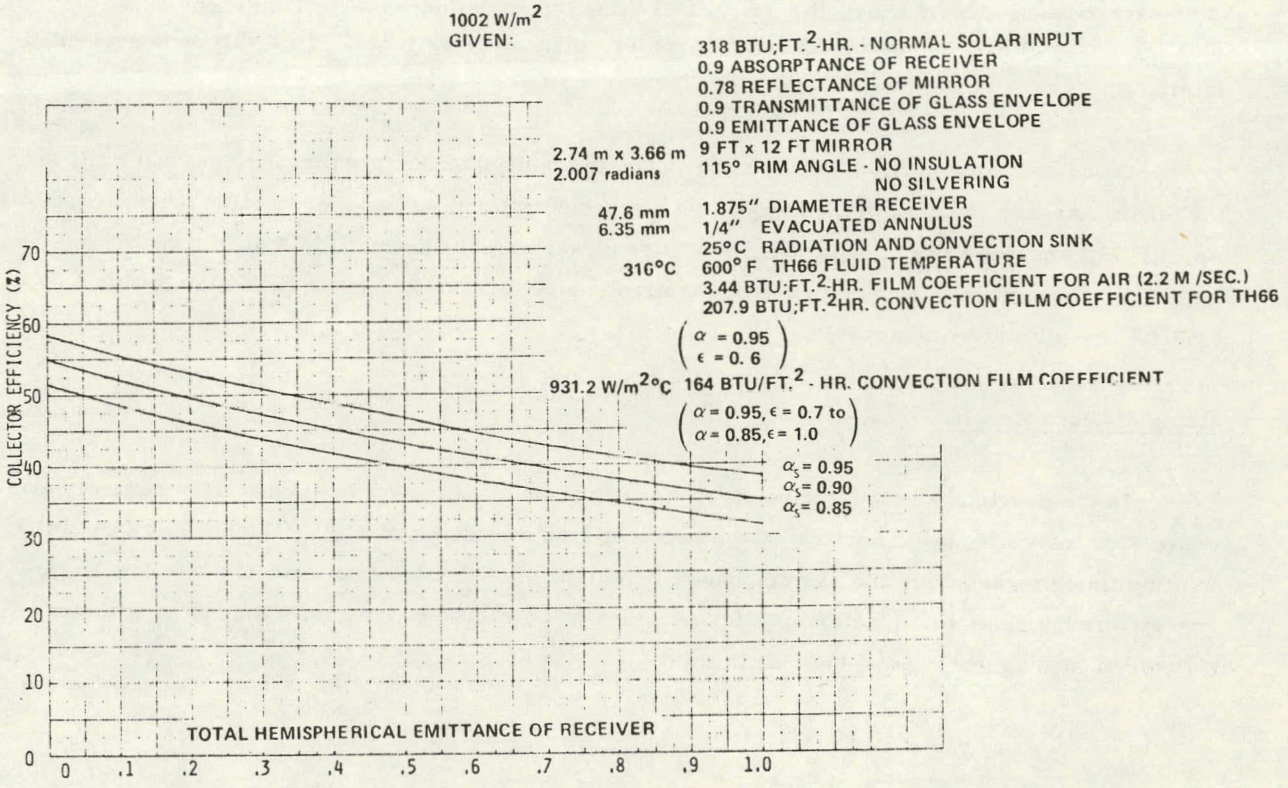


Figure 7. Total Hemispherical Emittance of Receiver vs Collector Efficiency

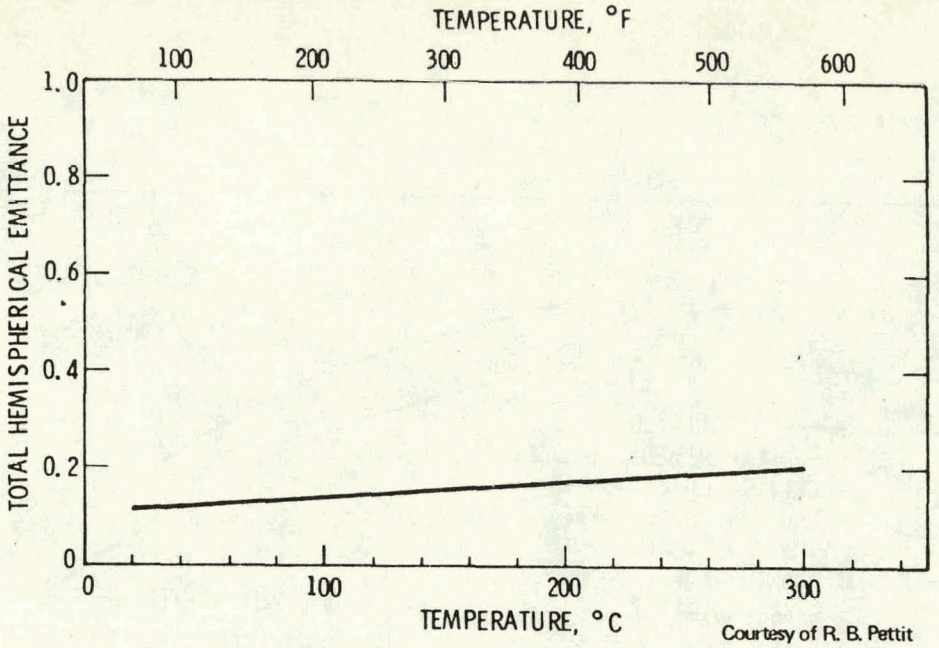


Figure 8. Harshaw Black Chrome on Electroplated Sulfamate Nickel (4 Minute Treatment Time)

current levels in the bath. On the other hand, the absorptance increases to a plateau maximum with increases in plating times. The plating time for black chrome is established to achieve $\alpha_s \geq 0.95$ and, with that timing and current density, achieves $\epsilon_{TH(300°C)} \leq 0.25$. Solar absorptance of a solar coating decreases with increasing angles of incidence, and black chrome is no exception. Figure 9 shows the changes in α_S as the angle increases. This phenomenon must be factored into the sizing considerations for solar receiver tubes. This will be described later.

Other coatings, particularly vacuum-deposited multiple interference coatings, can achieve the solar characteristics of black chrome but not necessarily at as low a production price. As of April 1975, a quoted price for black chrome over nickel was $\$13.89/m^2$ ($\$1.29/ft^2$) in 23 226 m^2 (250,000 ft^2) quantities. Projections from available data suggest production prices as low as $\$.50/ft^2$ are ultimately achievable.

Sizing of Glass Annulus

In the previous section, the need for a transparent glass jacket to significantly reduce thermal convection losses from the surface of the receiver tube was demonstrated. The annulus size which will minimize losses from the system can be determined. Since the transmission of solar energy through glass is a function of thickness, the glass should be only thick enough to withstand structural loading and reasonable hail threats.

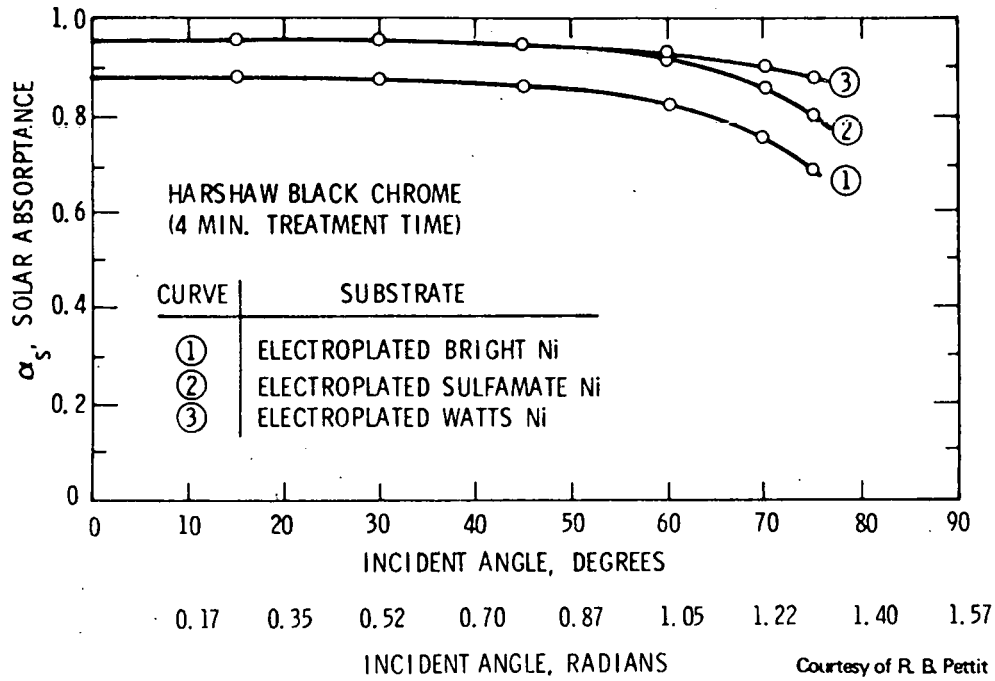


Figure 9. Harshaw Black Chrome (4 Minute Treatment Time)

A simplified technique used for annulus sizing is somewhat analogous to the determination of critical insulation thickness for small-diameter circular tubes. An energy balance for a given operating temperature can be constructed as follows: Radiation loss from the coated receiver tube + air conduction and convection loss from the coated receiver tube = convection loss to environment from glass tube + radiation loss to environment from the glass tube. The algebraic formulation of the configuration shown in Figure 10 is as follows:

$$\frac{\sigma A_1 \left(T_1^4 - T_2^4\right)}{\frac{1}{\epsilon_1} + \frac{A_1}{A_2}\left(\frac{1}{\epsilon_2} - 1\right)} + \frac{2\pi k_e L \left(T_1 - T_2\right)}{\ell n \left(\frac{r_2}{r_1}\right)} = h_2 A_2 \left(T_2 - T_a\right) + \sigma \epsilon_2 F_{2a} A_2 \left(T_2^4 - T_a^4\right) \qquad (1)$$

where

h = heat transfer coefficient
σ = Stefan-Boltzmann constant
ε = emittance
A = area
L = length
k_e = effective thermal conductivity
F = radiation shape factor

In the case of a vacuum in the annulus, the second expression on the left is not considered since $k_e \rightarrow 0$.

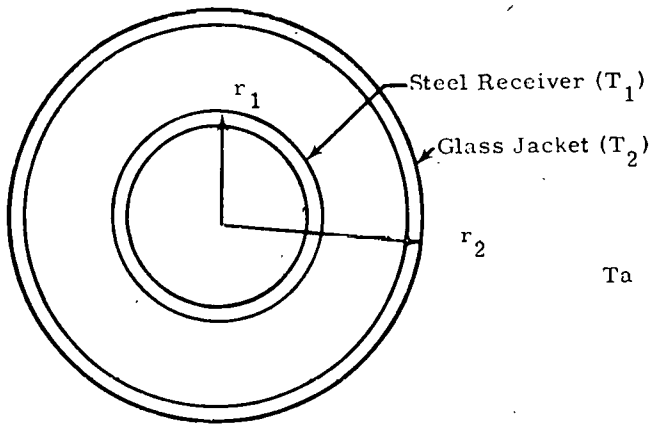


Figure 10. Steel Receiver With Glass Jacket

Some of the results from this equation are shown in Figure 11. The optimum annulus gap is established through a review of these data. If operation with a vacuum could be guaranteed, it would be desirable to establish the annulus gap as its minimum possible size to minimize the unit length thermal losses, as per Curve B. However, if the vacuum is lost, the losses would be expressed by Curve D for that particular gap. From this, it is evident that the gap should be selected to be at the minimum of Curve D since Curve B (vacuum) losses for that larger gap (~11mm) are slightly greater but vacuum failure will result in the minimum system thermal losses. At an operating temperature of 204°C, the conduction-convection losses shown by Curve A still are minimum at a gap of approximately 11 mm (0.44 in.). A doubling of the convection film coefficient (h_2), and a halving of the receiver diameter still results in an optimum gap of between 9.5 and 11 mm.

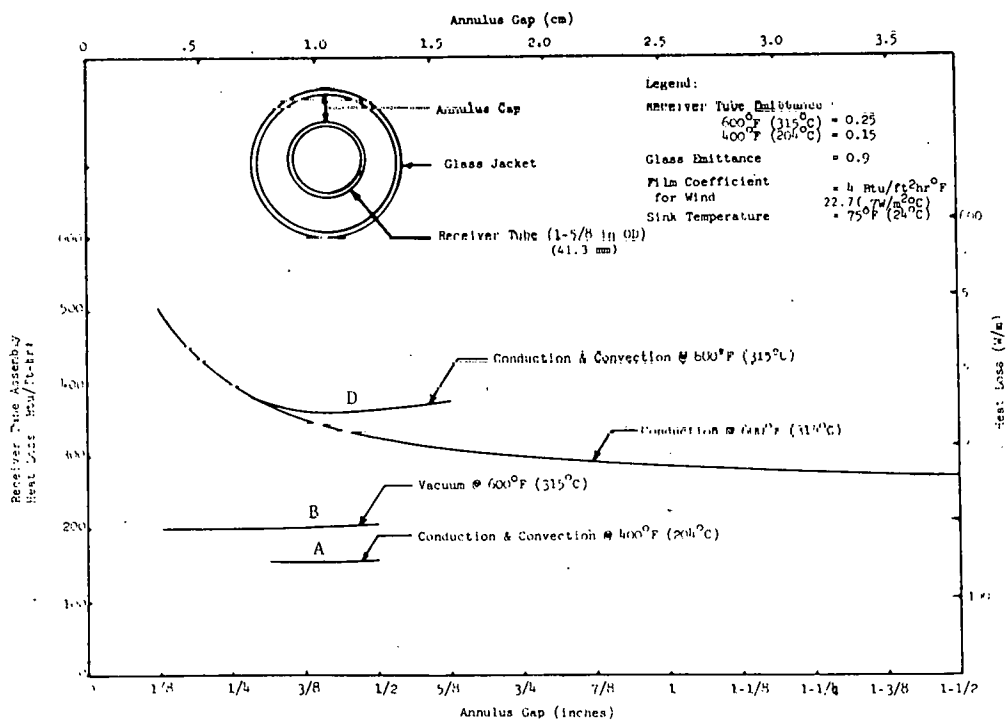


Figure 11. Results Obtained From Equation (1)

Curve B has only a slight positive slope and Curve D has a broad trough so with consideration of production tolerances and gravity sag, an annulus size of between 9.5 mm and 12.7 mm would be adequate for the parameters used in the calculations.

Insulating or Silvering of Glass

Upon initial consideration, it might seem appropriate to either silver or insulate an arc of glass opposite the reflector (Figure 12) to decrease thermal losses. Actual test results, reported in Table I, refute that supposition as a general conclusion. Only in the case of high total hemispherical emittance (> 0.5) is there an improvement in collector efficiency. With a 1.57 radians arc of insulation to preclude additional reflector shadowing, a high-emittance receiver increased in efficiency; an insulated low-emittance receiver decreased in efficiency for the same test configuration. With a high-emittance coating, the insulating strip more than compensates in thermal savings for the loss of the direct sun on the receiver tube. With a low-emittance coating, the thermal losses are already so low that decreasing them still further cannot compensate for the occlusion of the direct sun.

TABLE I

Average Collector Efficiency Percentage at 316°C (600°F)

Receiver Tube Coating	No Vacuum	Vacuum	Vacuum w/Insulator	Vacuum w/Plug	No Vacuum w/Plug	Remarks
Pyromark (Tempil) (α= 0.98, ϵ = 1.0)	16.2	18.32	23.9	X	X	Average of 10 days' data for vacuum no vacuum. Average of 4 days' data for vacuum w/insulator.
Intermediate Black Chrome on Bright Nickel (α = 0.88, ϵ = 0.24)	32.1	34.6				Average of 8 days' data.
AMA (Honeywell) (α = 0.97, ϵ = 0.38)	39.0	43.1	42.2			Average of 5 days' data; vacuum w/insulator, 1 day average
Black Chrome on Sulfamate Nickel (α = 0.97, ϵ = 0.28)	41.6	46.2	43.1		X	Average of 9 days' data for vacuum/no vacuum. Average for 6 days' data for vacuum w/insulator.

NOTES:
1. Volume flow rate approximately 5.7 l/min (1.5 gpm) (Re > 12,000).
2. Test temperature varied between 302°C (575°) and 311°C (591°F).
3. Collector Efficiency Percentage -

$$\frac{\dot{m}\, C_p\, (T_{OUT} - T_{IN})}{(\text{Aperature Area})\,(\text{Direct Insolation})}$$

4. Direct Insolation Range: 861-990 W/m^2 (273-314 Btu/ft^2/hr).
5. Wind Velocity Range: 0.24-3.46 m/sec (0.73-11.4 ft/sec).
6. Internal cylindrical plug of 1.59 cm (5/8") dia.
7. X = To be tested.
8. Alzak Reflector ($\rho \cong 0.7$).

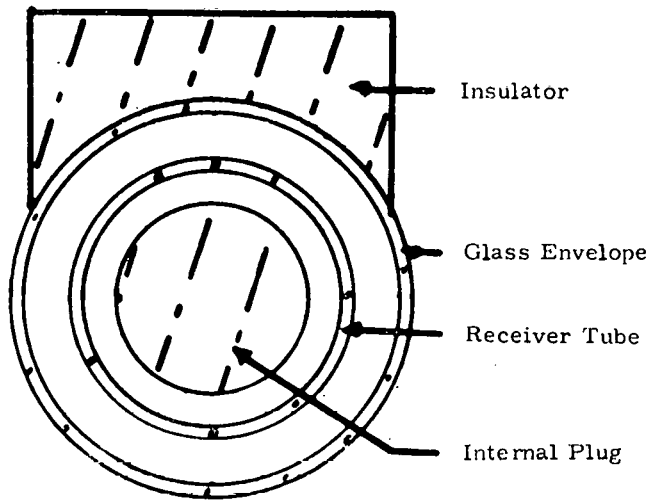


Figure 12. Receiver Cross Section

This analogy would hold for the silver coating also. In addition, the silver should be deposited on the inner surface of the glass which means a diffuse surface would face the receiver and not necessarily reflect the infrared energy due to radiation back to the receiver. Further, as time passes, the silver would change in infrared reflectance as imperfect vacuums allow oxygen to attack the surface.

With these considerations, neither insulation nor silvering are recommended for the low-emittance coatings comtenplated for use.

Reflection and Transmittance

Examination of the collector energy losses for normal incidence, (Figure 13) indicates that significant improvements in collector efficiency can be made through improvements over the present technology for parabolic mirror reflectance and glass jacket transmission. Figure 14 illustrates the influence of a ten percentage point change in mirror reflectance. The coating losses shown are given by $(1 - \alpha_S)$, and can be improved only slightly by increasing the coating absorptance. The thermal losses, convection and radiation, are substantially only a function of operating temperature as long as the receiver internal design effectively permits energy to be delivered into the energy collecting liquid. Should the desired improvements be made in the optics losses (coating absorptance, mirror reflectance, and glass transmission), Figure 15 illustrates the collector efficiency improvements which can be realized. For every percentage point increase in either reflectance or transmission, the collector efficiency increases nearly a percentage point.

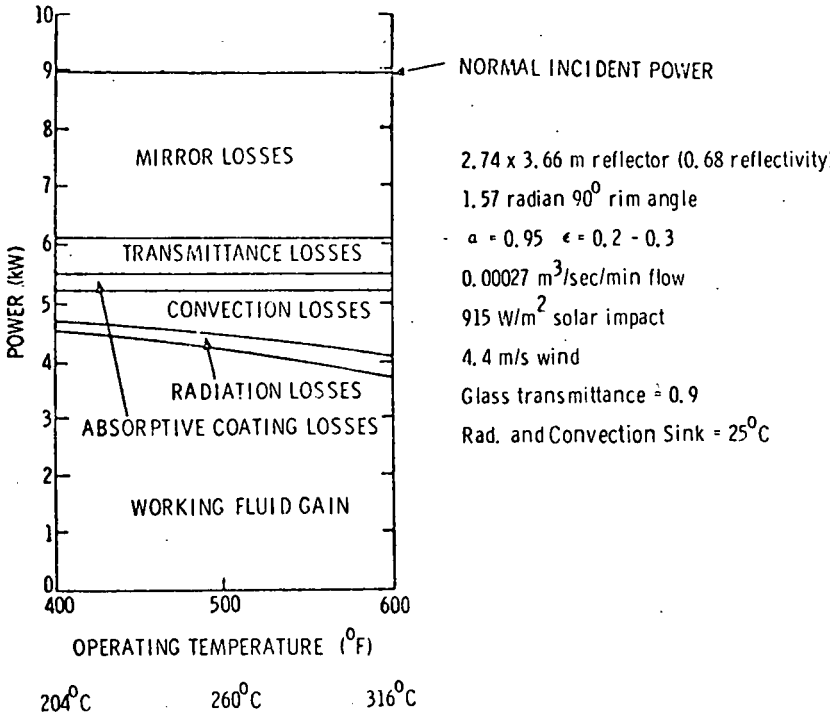


Figure 13. Collector Power Losses

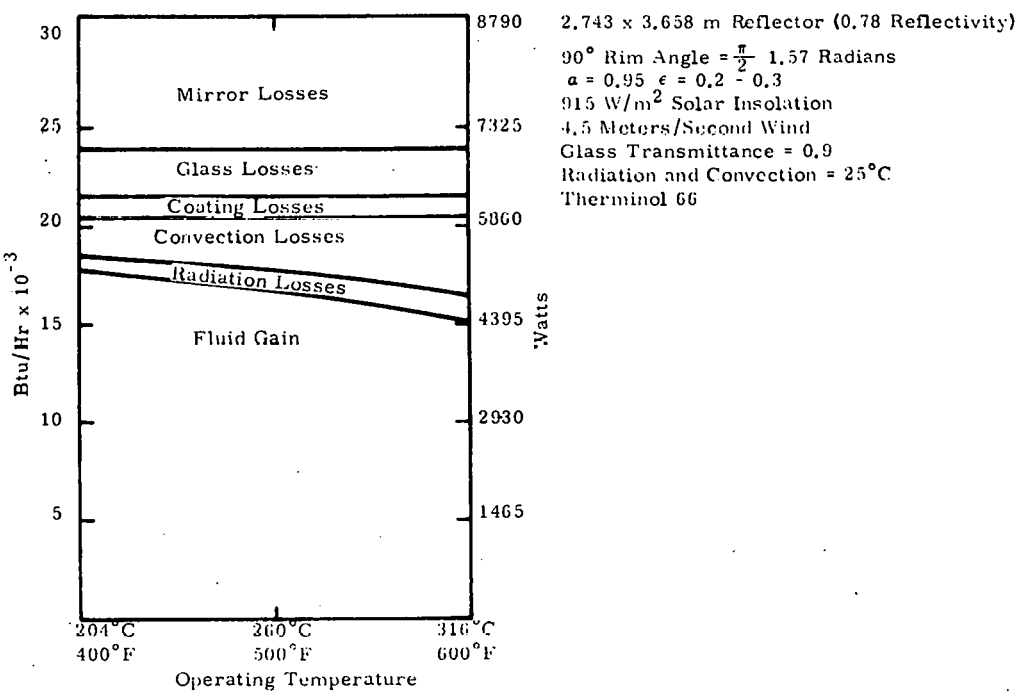


Figure 14. Collector Power Losses

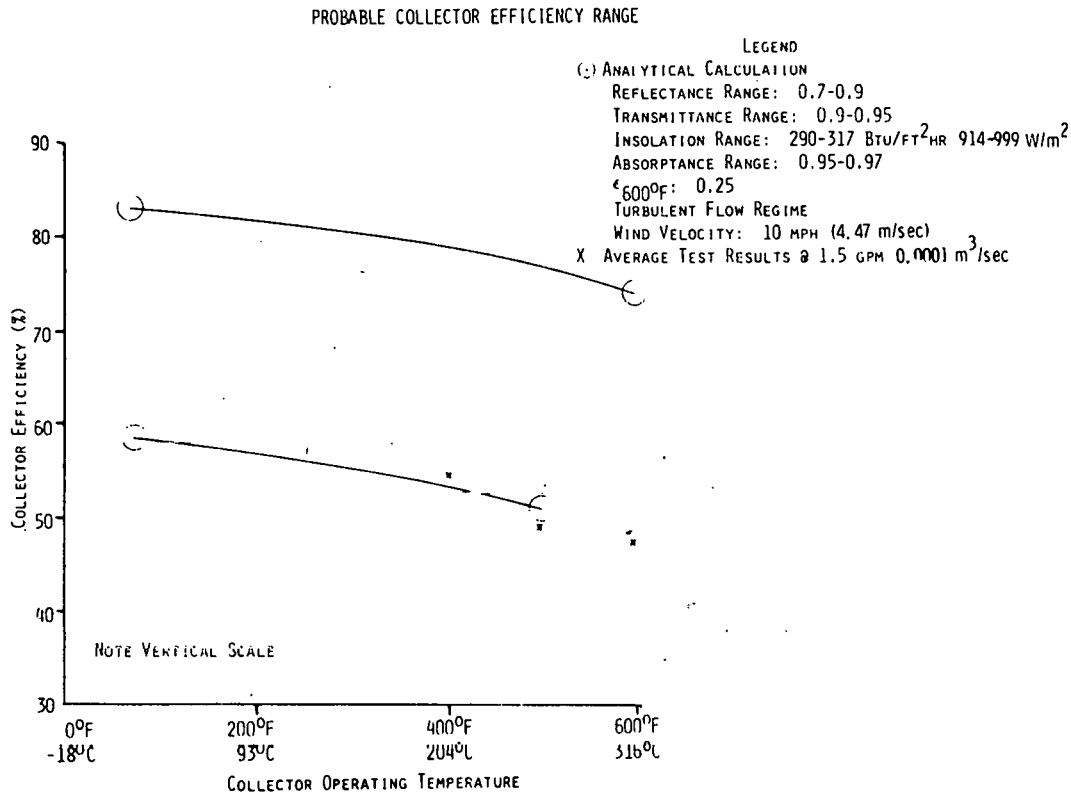


Figure 15. Probable Collector Efficiency Range

Although durable reflectors with a specular reflectance, ρ, of 0.95 are not presently available in large size, laboratory-sized specimens are available and development efforts are underway to increase size. An important characteristic of the reflectance is its specularity, and this is measured as a function of angular aperture. Figure 16 illustrates the solar reflectance versus aperture of several reflector materials of the present and near future. The aperture angle occluded by a receiver tube dictates the specular reflectance characteristics that are appropriate for use in analytical calculations. It can be seen that Alzak® has directional characteristics that must be taken into consideration in design.

The influence of energy reflections off the glass jacket if the sun is non-normal, as is the preponderant situation for east-west oriented parabolas, is shown in Figure 17. The maximum attainable efficiency curve is also displayed to illustrate the magnitude of improvement that could be obtained with no reflectance loss off the glass and coating. This chart does not include end loss effects whereby energy reflected off the end of the reflector is lost in space. The application of an inexpensive antireflection coating on, say, soda-lime glass could increase the transmission, τ, from 0.90 to 0.95. Present efforts indicate a fluoroboric acid vapor attack of soda-lime glass can achieve this improvement. If an antireflection coating is not applied, significant decreases in daily energy collection can be expected for east-west oriented collectors in addition to the cosine and end losses.

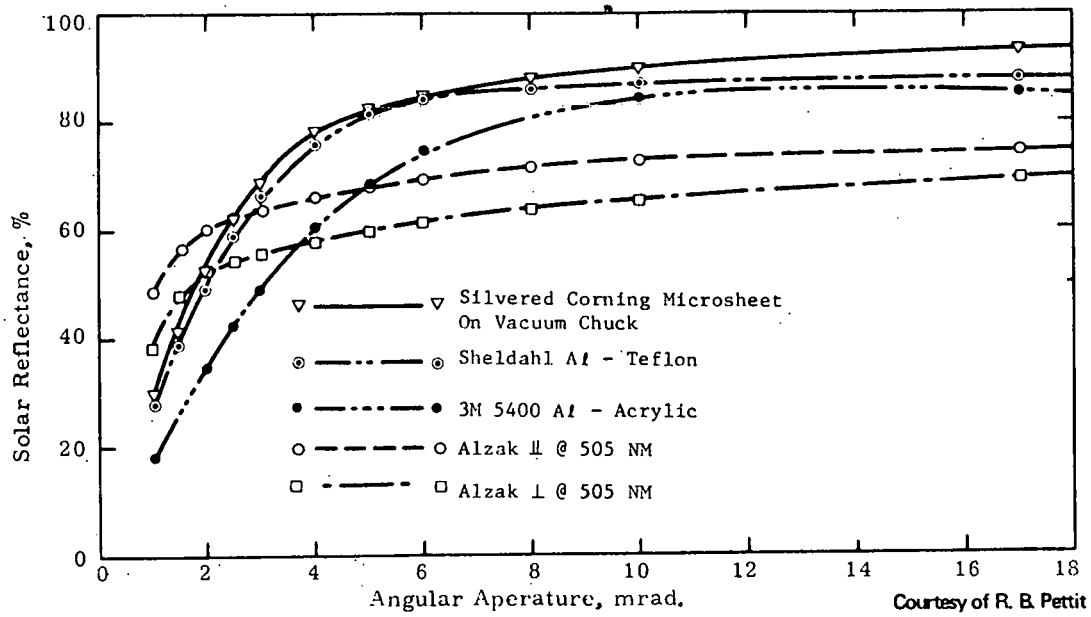


Figure 16. Solar Spectrum Reflectance vs Aperture For Various Reflector Materials

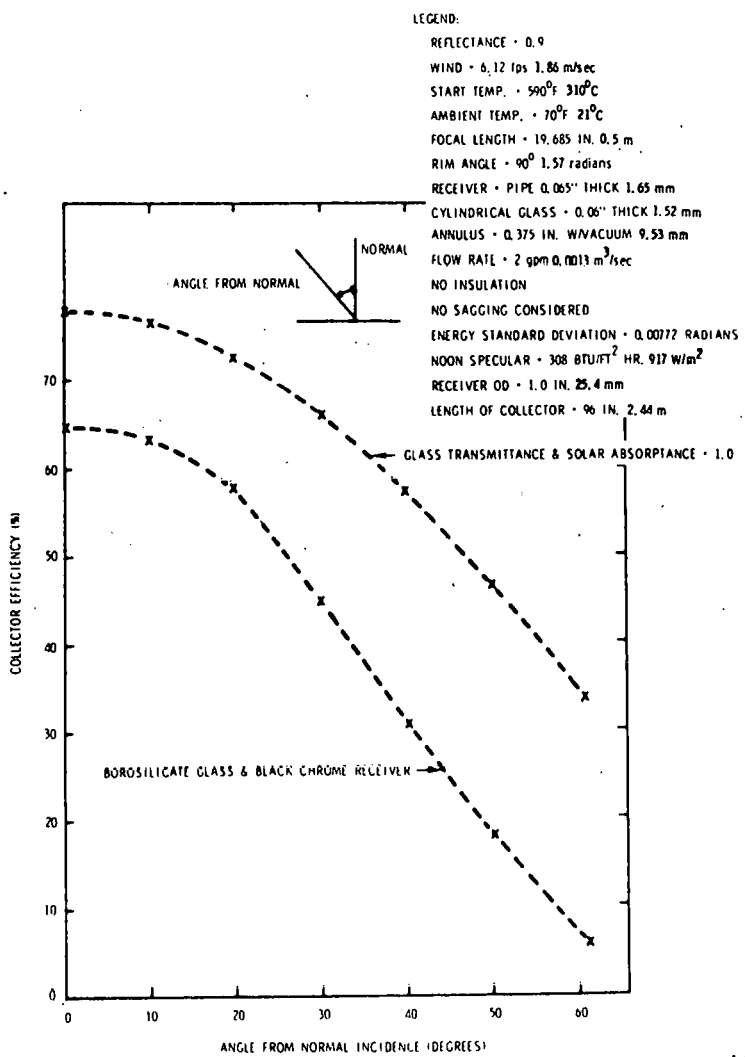
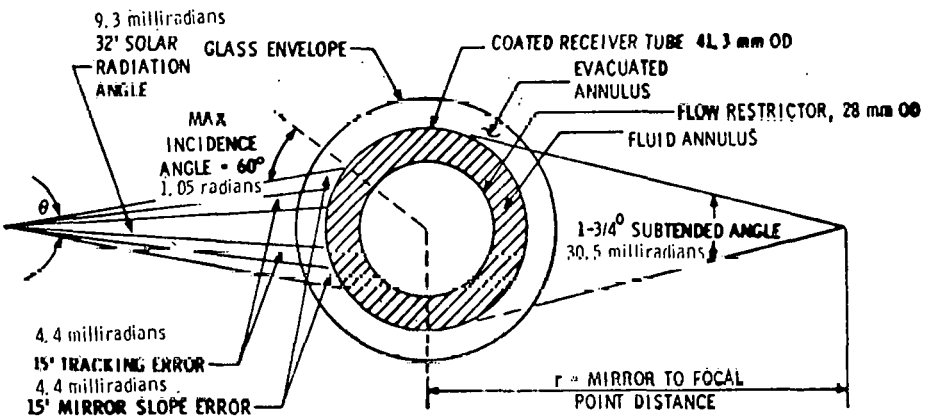


Figure 17. Collector Efficiency vs Non-Normal Sun Position (Assuming Attenuation at Solar Noon Applied to All Sun Angles)

Receiver Tube Sizing

In an initial approximation for the sizing of the receiver tube diameter, the assumption can be made that it is appropriate to attempt to capture all of the energy reflected from the parabola. The receiver tube size would then be dependent upon the sun's angular width (0.009 radians of arc), the magnitude of the tracking error, the mirror slope error (i.e., the angular departure from a tangent to a theoretical parabola), the irregularity of the reflective surface, and the angular absorptance characteristics of the solar coating. Figure 18 sums these influencing factors in a conservative arithmetic manner since the potential magnitude of tracking and slope errors is not completely known. The 1.05 radians maximum incidence angle conservatively compensates for photon reflection off the solar coating. From this figure, since the sizing is in terms of angular aperature, it can be seen that the receiver diameter is proportional to the distance from the reflector.

It is also apparent from Equation (1) that thermal losses are directly proportional to the receiver diameter, so the obvious goal would be to select a parabolic rim angle which would result in the smallest maximum distance from parabola to focus. A review of several rim angles for a common aperture (Figure 19) results in the selection, by calculation from Figure 18 and by inspection, of a rim angle of 1.57 radians. This angle will minimize the maximum reflector-to-focus distance and therefore require the smallest receiver diameter. When the aperture width is established, the receiver diameter can then be calculated. For example, with a 2-metre aperture the calculated receiver diameter is 30.9 mm.



THERMAL LOSSES PROPORTIONAL TO RECEIVER TUBE DIAMETER

$$\text{RECEIVER TUBE DIAMETER} = \frac{2r \sin \theta/2}{\sin 60^\circ \sin (\text{RIM ANGLE})}$$

Figure 18. Receiver Tube Assembly Cross Section

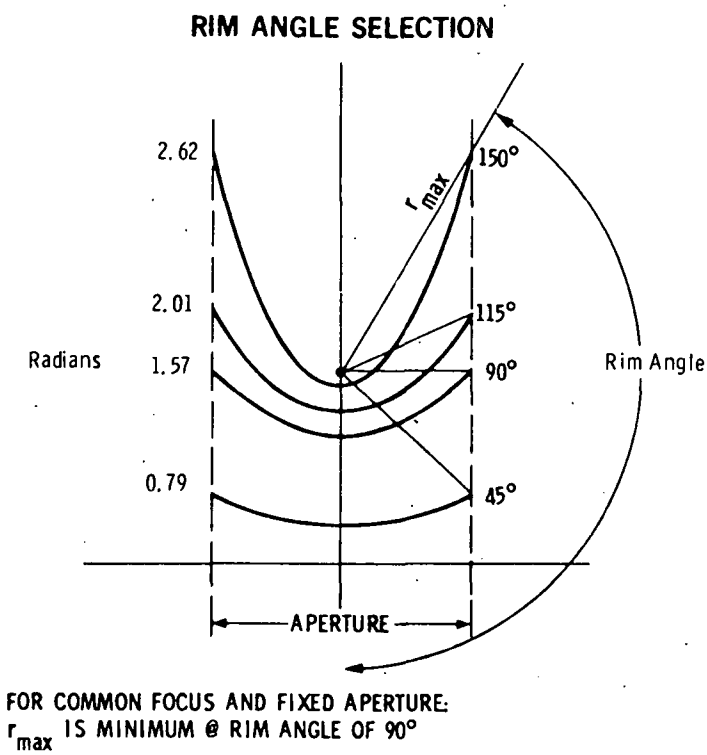


Figure 19. Various Rim Angles for Common Aperture

When one considers the implication of the central limit theorem, i.e., the distribution of the sum of several random variables can be closely approximated by a normal distribution, it is possible that receiver tubes sized in accordance with the preceding conservative rationale may not be of optimum size. While assumptions must still be made regarding the tracking and slope error potential and mirror non-specularity, trade-offs can be made between the amount of solar eenergy which can be allowed to miss a smaller receiver tube and the compensating savings in thermal losses through diameter reduction. A portrayal of such trade-offs for assumed errors and normal solar incidence is shown on Figure 20. For an energy distribution standard deviation* ranging from minimum (the sun's quarter-width) to 12 milliradians, it can be observed that the optimum receiver diameter is a function of the energy distribution. The use of the apex connecting line permits the determination of an optimum diameter once the energy distribution is known. Since thermal losses are a function of the receiver surface area, it also can be observed that for a given energy distribution other shapes of receivers to decrease surface area, (i.e., triangular or flattened circles) would have a modest influence on collector efficiency because of the broad shapes of the curves. For example, with an energy distribution of 7.72 milliradians, small efficiency differences are observed within a receiver diameter range of between 22.2 mm and 30.9 mm. As the energy distribution arc becomes smaller, the receiver diameter becomes of greater importance.

*The statistical blending of the sun's width, tracking errors, slope errors, and mirror diffuseness:

$$\sigma_{\text{Total}} = \sqrt{\sigma^2_{\text{Slope}} + \sigma^2_{\text{Tracking}} + \sigma^2_{\text{Reflector}} + \sigma^2_{\text{Sun}}} \quad .$$

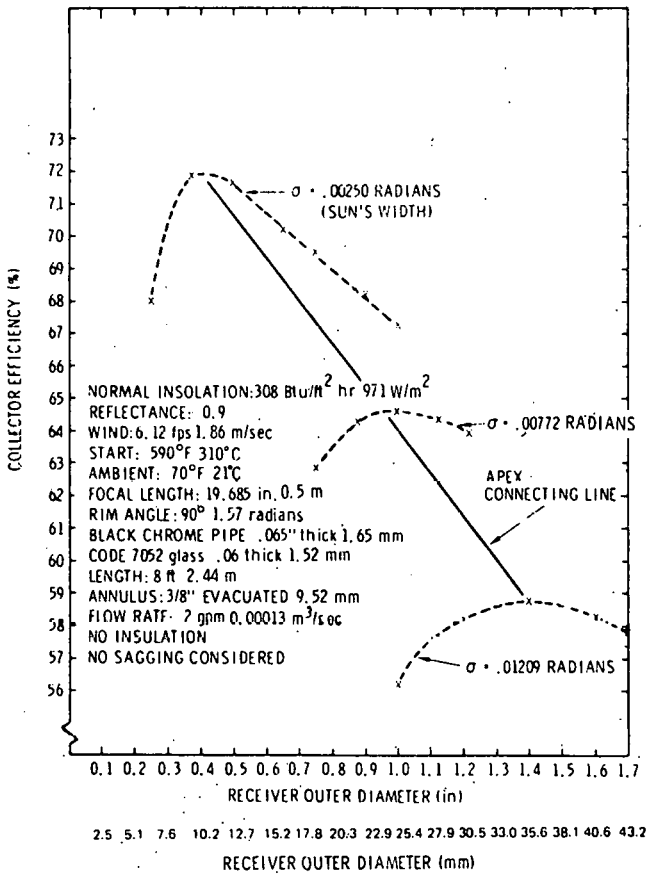


Figure 20. Energy Distribution vs Collector Efficiency

Efforts to characterize the slope errors of parabolic reflector surfaces have been made through the use of the apparatus illustrated in Figure 21. The laser is scanned in the X direction, and the resulting reflection is captured at a particular location on the detector which is located at the focal point such that the angular deviation from the calculated focus can be measured. After each scan, the parabolic mirror is translated to a new Y position. The resulting scans can be portrayed as illustrated in Figure 22 and statistically reduced to a deviation representative of that mirror.

With a $\pm 2\sigma$ normal distribution (95.46% of the area under a normal curve), recent extremes of measurements on 0.79 radian rim angle parabolas (0.61 m x 1.22 m) can be used as follows:

$$\text{Beam } \sigma = \left[(\text{Sun } \sigma)^2 + (\text{Tracking } \sigma)^2 + (\text{Slope Error } \sigma)^2 + (\text{Reflector } \sigma)^2 \right]^{1/2}$$

$$\sigma = \left[(2.5 \text{ mrad})^2 + (2.5 \text{ mrad})^2 + (7.9 \text{ mrad})^2 + (2 \text{ mrad})^2 \right]^{1/2}$$

$$\sigma = 8.9 \text{ milliradians.}$$

With this energy distribution, an optimum diameter of 27.4 mm results from entry into Figure 20.

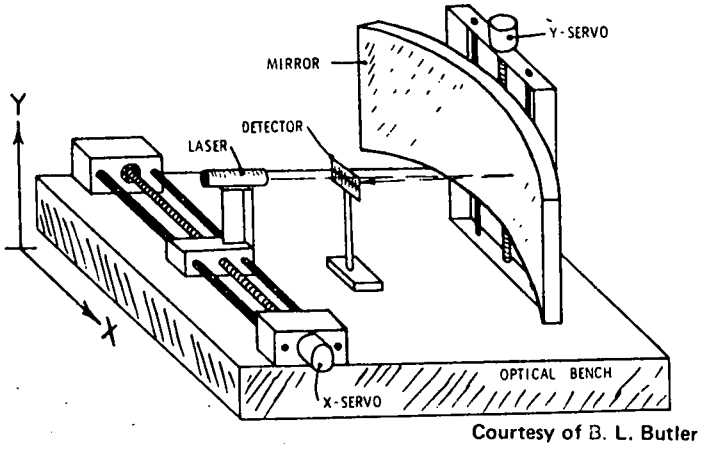


Figure 21. Apparatus for Characterizing Slope Errors of Parabolic Reflector Surfaces

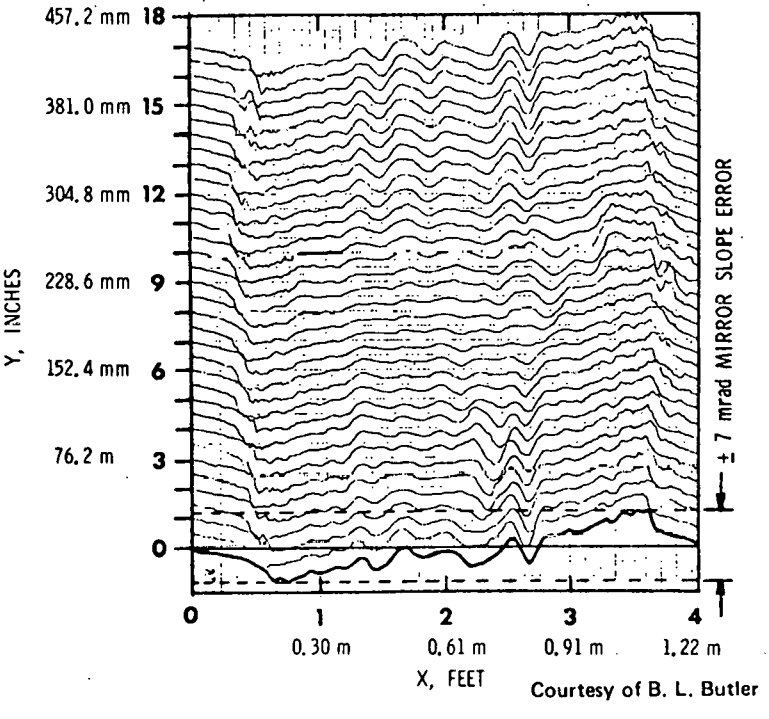


Figure 22. Scans Resulting From Use of Apparatus Shown in Figure 21

With an occluded angle aperture calculated from this receiver, an appropriate specular reflectance can be selected from Figure 16.

The selection of the 1.57 radians (90°) rim angle is now brought back into question since it can be shown that a 2.09 radians (120°) rim angle yields the shortest average distance from the reflector to the focus (See Appendix A) and, ostensibly, the least reflected beam spread. Reference to Figure 23 shows that slight efficiency improvements can be obtained by increasing the rim angle to greater than 1.57 radians with an optimum occurring between a 1.83 radians and a 1.92 radians rim angle. Rim angles less than 1.57 radians; which are not displayed in Figure 23, result in efficiencies lower than that for 1.57 radians. The reason for the slight departure from the 2.09 radians theoretical optimum is due to the thermal considerations and beam spreading at larger angles. The slope and tracking error influences become more prounounced with larger rim angles.

There is a penalty associated with the use of larger rim angles since the arc length changes of reflector required for a given aperture are not in proportion to the increase in efficiency. The sectors of the parabola which have significant slope angles are not contributing as much to solar energy interception. Where the slope of the parabola is 0.79 radian, its aperture for the same reflector arc length is only 70.7% of the parabola aperture near the vertex. An alternative to restricting the parabola slopes would be to trim, figuratively, a 1.57 radians rim angle parabola to 1.40 radians or 1.22 radians while retaining the focus. This removes the most arc length for the least change in aperture. These considerations are reflected in the calculated results given in Tables II and III. Obviously a "trimmed" width must have compensating length to capture the same amount of energy.

It would be desirable to establish a figure-of-merit to use for comparison of these alternatives. All other things being equal, the cost of collector construction is proportional in some manner to the weight or surface area, while the energy collected is proportional to the collector efficiency. Alternative figures-of-merit could be constructed as follows.

$$\text{Figure of Merit} \propto \frac{\text{Construction Cost}}{\text{Energy Collected}} \propto \frac{(\text{Average Receiver Circumference} + \text{Reflector Arc Length})(\text{Collector Length})}{(\text{Collector Efficiency})(\text{Standard Collector Length})};$$

or if it could be determined that reflector arc length had more influence on total cost it could appear as follows:

$$\text{Figure of Merit} \propto \frac{(1/4\ \text{Average Receiver Circumference} + 3/4\ \text{Reflector Arc Length})(\text{Collector Length})}{(\text{Collector Efficiency})(\text{Standard Collector Length})}$$

Table IV lists some results from such calculations using data from Tables II and III. The calculations suggest a "trimmed" collector may be desirable, but they should be viewed with caution since other non-considered factors are not necessarily equal. For "trimmed" rim angles, the smaller diameter receiver tubes may mean greater heat transfer liquid pumping losses, and the longer collector may require more intermediate supports. For larger rim angles, the influence

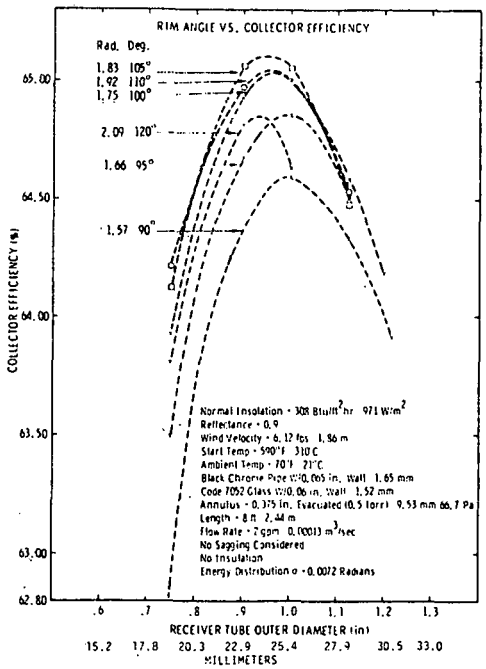


Figure 23. Collector Efficiency vs Receiver Tube Outer Diameter

TABLE II

Phase IVB Collector Sizing Considerations

Rim Angle (rad)	Rim Angle (deg)	Approximate Collector Efficiency (%)	Focal Length (mm)	Focal Length (in)	Approx. Optimum Receiver OD (mm)	Approx. Optimum Receiver OD (in)	Arc Length (mm)	Arc Length (in)	Remarks
1.22	70 (Trimmed 90°) 1.57 rad	63.7	500	19.68	22.9	0.9	1.51	59.36	90° Rim Angle Focal Length 1.57 radian 1.4 Metres Aperture
1.40	80 (Trimmed 90°) 1.57 rad	64.3	500	19.68	22.9	0.9	1.85	73.16	90° Rim Angle Focal Length 1.57 radian 1.678 Metres Aperture
0.79	45	55.97	1207	47.52	40.6	1.6	2.06	80.94	2 Metres Aperture
1.05	60	60.6	866	34.10	35.6	1.4	2.11	82.92	2 Metres Aperture
1.22	70	62.4	714	28.11	26.7	1.13	2.15	84.77	2 Metres Aperture
1.40	80	63.6	596	23.46	26.7	1.05	2.21	87.19	2 Metres Aperture
1.57	90	64.6	500	19.68	25.4	1.00	2.30	90.38	2 Metres Aperture
1.66	95	64.9	458	18.04	25.4	1.00	2.35	92.35	2 Metres Aperture
1.75	100	65.0	420	16.52	24.1	0.95	2.40	94.64	2 Metres Aperture
1.83	105	65.1	384	15.10	24.1	0.95	2.47	97.31	2 Metres Aperture
1.92	110	65.0	350	13.78	24.1	0.95	2.55	100.46	2 Metres Aperture
2.09	120	64.8	289	11.37	24.1	0.95	2.76	108.67	2 Metres Aperture

Normal Insulation - 308 Btu/ft^2 hr 971 W/m^2
Reflectance = 0.9
Wind Velocity = 6.12 fps 1.86 m/sec
Start Temp = 590°F 310°C
Ambient Temp = 70°F 21°C
Black Chrome Pipe W/0.65 m Wall 1.65 mm
Code 7052 Glass W/0.06 in. Wall 1.52 mm
Annulus = 0.375 in. Evacuated (0.5 Torr) 9.53 mm 66.7 Pa
Length = 8 ft 2.44 m
Flow Rate = 2 gpm 0.00013 m^3/sec
No Sagging Considered
No Insulation
Energy Distribution σ = 0.00772 Radians

of tracking and slope errors becomes more pronounced. Upon brief consideration of these factors, there appears to be no compelling reason at the present time to depart from 1.57 radians (90°) rim angle although indicators point more toward smaller than larger rim angles.

TABLE III

Collector Efficiency (%) and Arc Length Changes (%)
Compared to 1.57 Radians (90°) Rim Angle

Rim Angle		Change in Collector Efficiency (%)	Change in Arc Length (%)
Degrees	Radians		
45°	0.79	-13.50	-10.44
60°	1.05	- 6.24	- 8.25
70°	1.22	- 3.39	- 6.21
80°	1.40	- 1.32	- 3.53
95°	1.66	+ 0.40	+ 2.18
100°	1.75	+ 0.63	+ 4.71
105°	1.83	+ 0.73	+ 7.67
110°	1.92	+ 0.62	+11.15
120°	2.09	+ 0.34	+20.24
80° @ 90° focus	1.40 @ 1.57 radian focus	- 0.46	-19.05
70° @ 90° focus	1.22 @ 1.57 radian focus	- 1.38	-34.32

Since the influence of aiming and slope errors has been briefly mentioned, another influencing factor in effective collector design is the accuracy with which the true focal line can be determined. The laser technique mentioned earlier can establish the true focal line for a given parabola and, presumably, such a technique can be used for production acceptance and quality control. However, if separate collectors are arranged in a contiguous manner and "gang" driven, the receiver tube assembly positioning will probably be along an average focal line. The influence of mislocation of a receiver tube assembly is illustrated in Figure 24. For the conditions shown, the receivers can be mislocated only by ± 10% of their diameter without suffering a significant loss in effectiveness. The receiver diameter could be made slightly larger to compensate for mislocation without a significant efficiency penalty as shown in Figure 20.

In summary, a 1.57 radians (90°) rim angle appears reasonable, and the receiver tube diameter can be sized based uponthe techniques resulting in the data shown in Figure 20.

TABLE IV

Figure of Merit vs Collector Rim Angle

Rim Angle (rad)	(deg)	Aperture, (m)	Figure of Merit*	Figure of Merit**
1.22	90 (Trimmed to 70) 1.22 rad	1.4	1.419	1.095
1.57	90 (Trimmed to 80) 1.40 rad	1.678	1.431	1.036
0.79	45	2	1.560	1.114
1.05	60	2	1.461	1.050
1.22	70	2	1.434	1.038
1.40	80	2	1.442	1.044
1.57	90	2	1.466	1.066
1.66	95	2	1.491	1.085
1.75	100	2	1.522	1.109
1.83	105	2	1.557	1.137
1.92	110	2	1.612	1.176
2.09	120	2	1.739	1.273

*Based On: (Average Receiver Circumference + Reflector Arc Length)/(Collector Efficiency) (Standard Collector Length)

**Based On: (1/4 Average Receiver Circumference + 3/4 Reflector Arc Length) (Collector Efficiency)(Standard Collector Length)

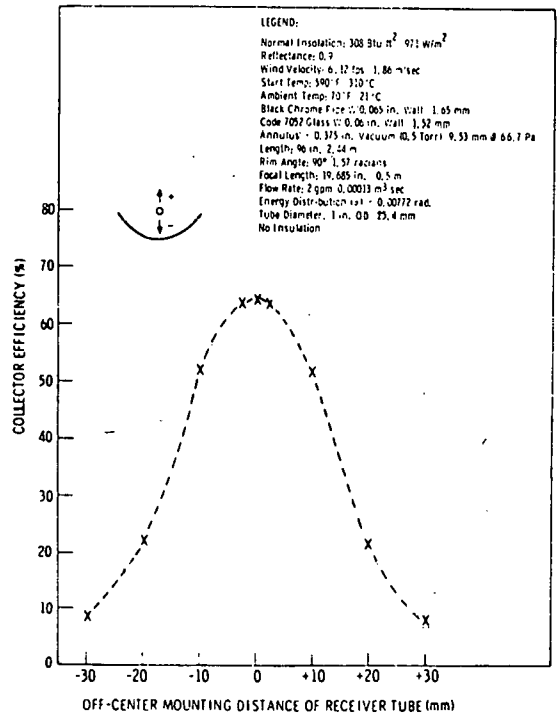


Figure 24. Influence of Off-Center Receiver Tube Mounting

Collector Sizing

The discussions on receiver sizing have been, to a large extent, based upon the fact of optical congruence. The collector aperture could have been 1 metre or 10 metre wide, and the same conclusions would hold. Once the energy delivery requirements for a collector field are established, other factors must be considered. For a given energy delivery requirement at a specified temperature, the flow rate is established. Heat transfer into the working fluid at a given flow rate is a function of diameter and is not linearly proportional (congruent). To a limit, the energy transfer into the working fluid is enhanced by a smaller receiver diameter. Since this is the situation, the collector aperture can be adjusted to achieve the proper receiver diameter to optimize the collection efficiency. It must be kept in mind that energy delivered is energy collected less energy required to drive the fluid through the collector system. If the pumping losses are kept to some limit, say 1% of the collected energy, and the flow is maintained in the turbulent regime to maintain effective heat transfer, it is possible to establish some collector sizing limits. One such attempt is portrayed on Figure 25. A 2 metre aperture has a higher collector efficiency than a 2.74 metre aperture collector although both collectors have a 1.57 radians rim angle. The 25.4 mm receiver OD associated with a 2 metre aperture is a practical minimum size because of friction losses at the 1% level. As previously suggested, the number or length of collectors must be increased to capture the same quantity of solar energy. More narrow apertures mean smaller supports and frames and smaller structures due to smaller bending moments in wind-loading. Whether those cost reductions compensate for greater numbers or length of collectors remains to be seen. However, if costs are the same, the 2 metre aperture is potentially more effective.

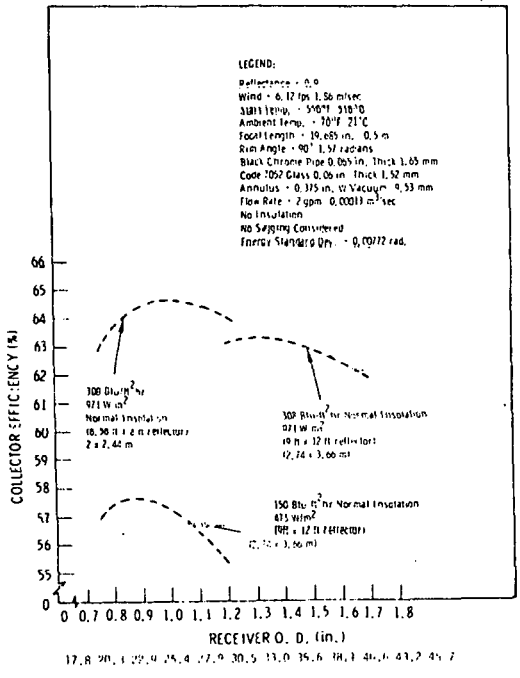


Figure 25. Energy Input Influence on Receiver Sizing

Influence of Asymmetric Heating

With 1.57 radians rim angle line-focus reflectors, a much greater amount of energy is deposited upon one half of a receiver tube than upon the other half. If the heat transfer liquid and receiver material cannot effectively transfer this energy into the lower energy-deposition areas of the receiver, significant asymmetric heating of the fluid and receiver distortion can occur. For organic heat transfer liquids, allowable film temperature limits can be exceeded which will result in lower heat transfer, viscosity increases, and greater pumping losses. If the liquid boils, the collector system must be designed to withstand the pressures without venting and loss of energy and fluids. The heat transfer ability of a liquid-gas system would not normally be as good as a liquid system due to mass flow considerations. With respect to the foregoing, water is an excellent heat transfer liquid but requires nearly 11 x 10^6 Pa (1600 psi) overpressure at 315°C to prevent boiling. Any storage system for high temperature water has significant safety hazards.

Several possible techniques for better distribution of the energy have been considered. Copper receiver tubes would circumferentially transfer the energy better than steel tubes but are more expensive, more ductile, and require more supports to prevent sagging. Increasing the thickness of the steel tubes would increase the weight of the tube at a greater rate than the moment of inertia is increased and more supports would also be required. The use of internal rods to force annular flow is a technique to better transfer the energy into the liquid by decreasing the hydraulic radius and thereby increasing the film coefficient of heat transfer. Other mixing techniques that require lower pumping work are being investigated. As an indication of the distortion caused by asymmetric temperatures in steel receiver tube 1.6 mm thick, a diametral temperature difference ΔT of 56°C can cause an additional 25.4 mm sag over a 3.66 metre span.

Calculations for the organic liquid Therminol 66 (Figure 26) indicate that a ΔT of this magnitude can occur. Obvious solutions to prevent the ΔT are to use internal rods and to increase the flow rates. These effects are shown in Figure 27. The internal rod delays larger ΔT's until much lower volumetric flow rates are reached. In both cases shown in Figure 27, increasing flow rate decreases the ΔT in the liquid. Flow rate control is an important parameter in the use of organic liquids.

Other Design Considerations

If collectors are oriented on an east-west axis, it is prudent to arrange them contiguously to minimize the energy losses at morning and evening due to high non-normal incidence angles causing end losses. An 18.3 metre length of receiver tubes when heated from ambient to 315°C can expand nearly 76 mm in length. Flexible end joints and linear slides must accommodate this expansion. One design which can be used is illustrated in Figure 28. The pins which fix the receiver tube position also accommodate the expansion by allowing sliding. The pin-hole clearances also allow some end flange rotation due to the receiver ΔT. The expansion bellows accommodate the linear expansion differences between the glass and the steel receiver tube.

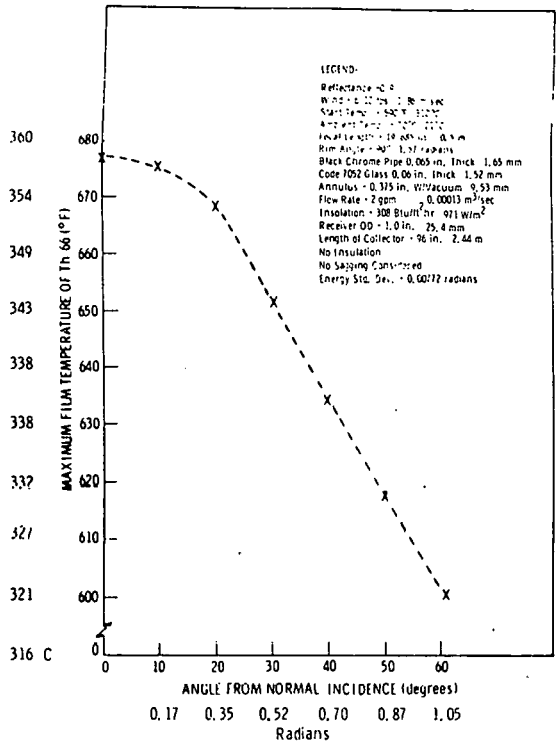


Figure 26. Predicted Maximum Therminol 66Ⓣ Film Temperatures

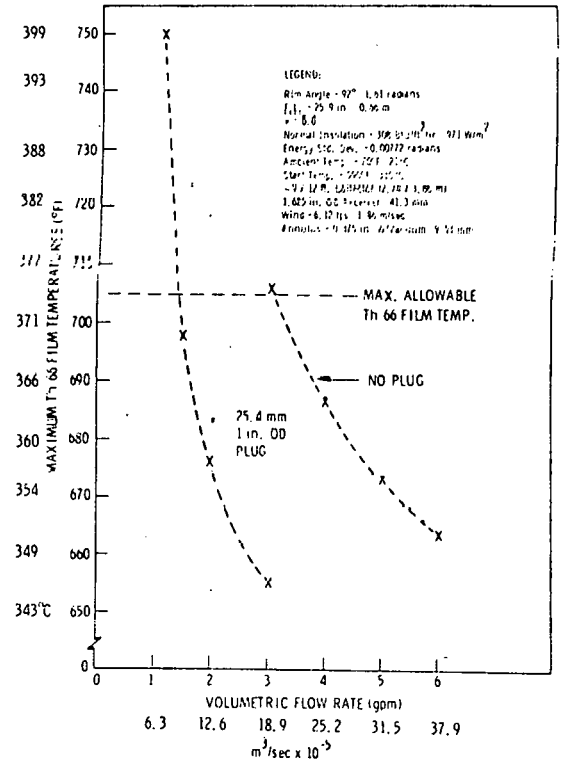


Figure 27. Influence of Plug on Predicted Maximum Therminol 66Ⓣ Film Temperatures (Phase IVA Northwest Quadrant)

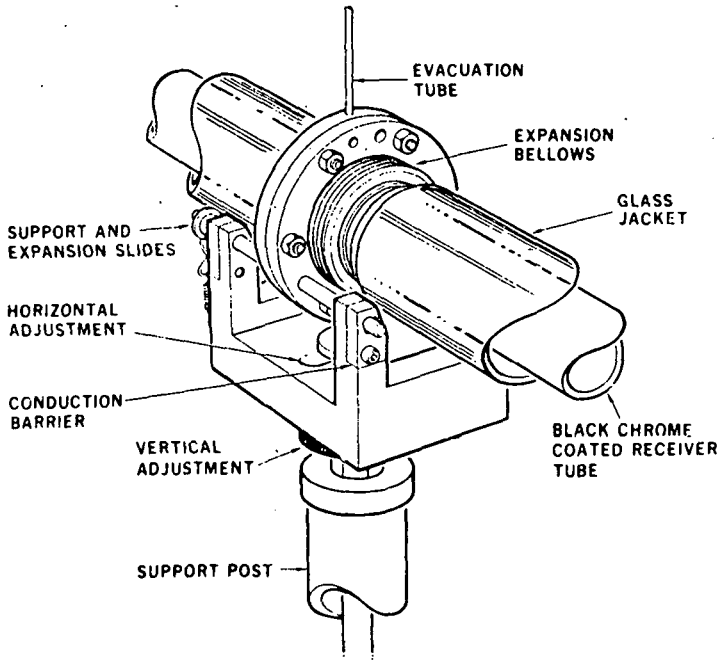


Figure 28. Receiver Tube and Support Assembly

The glass should reach temperatures of less than 110°C although the receiver reaches 315°C. The glass-to-metal seal is formed by expansion-matched borosilicate glass and Kovar. Operation with liquids at 315°C requires durable leak-proof seals. Hollow metal "O" rings are adequate for this design.

The thickness of the receiver tube has been briefly mentioned. The span of the receiver between supports represents a trade-off between deflection and circumferential energy transfer. The thicker the tube material, the greater the sag and the better the energy transfer, and vice versa. The internal rod for obtaining high film coefficients of heat transfer is hollow such that it will "float" in the liquid and not sag against the internal diameter of the receiver tube and exaggerate the receiver sag from the focal line.

Another receiver tube assembly design which appears to be capable of satisfying all requirements is illustrated in Figure 29. In this design, commerical tube fittings and silicone "O" rings replace the flanges, welded joints, expansion bellows, and glass-to-metal seals. Calculations prior to testing and temperatures obtained during testing indicate "survival" of the seal for long periods. In addition, broken glass tubes are easily replaced so repair is inexpensive.

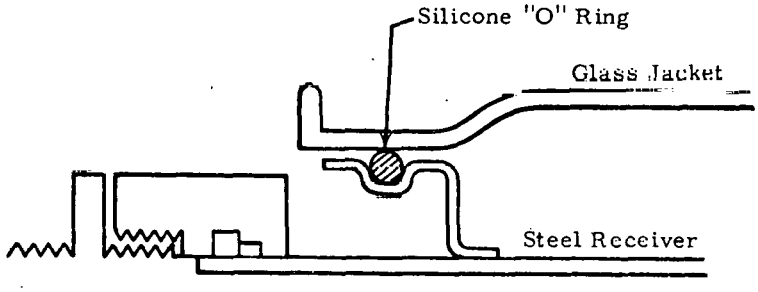


Figure 29. Alternate Receiver Tube Assembly Design

Miscellaneous Considerations

The orientation of collectors (N-S axis versus E-W axis) also is involved with trade-offs. The east-west oriented collector arrangement will typically collect less energy than the north-south, but it is more economical in land utilization because of shadowing considerations, lower in construction and pipeline costs, and has less pumping and thermal losses from one collector bank to the next because they can be closer without shadowing. Another consideration is that the east-west collector sunset position is almost exactly the position for sunrise. The north-south must be driven from the evening to the morning position. East-West orientations lend themselves to uniflow receiver designs. An option for counterflow receivers appears to be more appropriate for north-south orientations. At that, the proposed use of counterflow receivers should require detailed thermal analysis because of the asymmetry of energy deposition for parabolic-cylindrical collectors.

East-West linear-focusing collectors with off-axis receivers may offer some promise of construction cost reductions in exchange for less energy collection due to solar aperature and cosine effects. Certainly off-axis receivers can have lower thermal losses due to the insulation which can be used. The selection of the orientation and collector design is a function of the importance of these considerations, the latitude, and the expected amount of sunshine at the site.

APPENDIX A
CALCULATIONS OF RIM ANGLE FOR MINIMUM AVERAGE DISTANCE FROM FOCUS TO PARABOLA

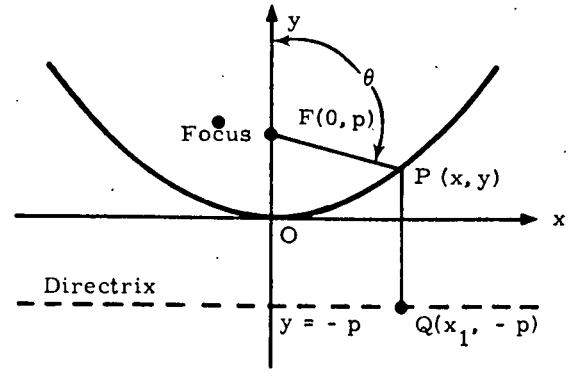
General Formula for Parabola: $y = \frac{x^2}{4p}$

$$\overline{FP} = r = \left[x^2 + (p - y)^2\right]^{1/2}$$

$$r = \left[x^2 + \left(p - \frac{x^2}{4p}\right)^2\right]^{1/2}$$

$$r = \left[\frac{x^2}{2} + p^2 + \frac{x^4}{16p^2}\right]^{1/2}$$

$$r = p + \frac{x^2}{4p}$$



Average distance from focus to parabola:

$$\overline{r} = \frac{\int_o^{Xmax} \left(p + \frac{x^2}{4p}\right) dx}{\int_o^{Xmax} dx}$$

$$\overline{r} = \frac{px + \frac{x^3}{12p}\Big|_o^{Xmax}}{x\Big|_o^{Xmax}} = \frac{px_{max} + \frac{x^3_{max}}{12p}}{x_{max}}$$

$$\overline{r} = p + \frac{x_{max}^2}{12p}$$

Minimum average distance for $x = x_{max}$:

$$\bar{r} = p + \frac{x_{max}^2}{12p}$$

$$\frac{d\bar{r}}{dp} = 1 - \frac{x_{max}^2}{12p^2}$$

$$0 = 1 - \frac{x_{max}^2}{12p^2}$$

$$p = \frac{Xmax}{2\sqrt{3}}$$

@ $x_{max} = 1$

$p = 0.288675$

Distance from focus to parabola expressed in polar coordinates:

$$\overline{OF} = p = \frac{r(1 - \cos\theta)}{2}$$

@ $\theta = 60°$ (i.e., rim angle = 120°)

$x_{max} = 1.$

$r = 1.1547$

and $p = \frac{1.1547(1 - \cos 60°)}{2}$

$p = 0.288675$

∴ Minimum average distance occurs at 120° rim angle

Bibliography

Eldon C. Boes, Solar Radiation Availability to Various Collector Geometries, A Preliminary Study, SAND76-0009, Sandia Laboratories, Albuquerque, New Mexico, March 1976.

R. B. Pettit, Total Hemispherical Emittance Measurement Apparatus for Solar Selective Coatings, SAND75-0079, Sandia Laboratories, Albuquerque, New Mexico, June 1975.

D. M. Mattox, et. al., Selective Solar Photothermal Absorbers, SAND75-0361, Sandia Laboratories, Albuquerque, New Mexico, July 1975.

E. R. G. Eckert, Robert M. Drake, Jr., Analysis of Heat and Mass Transfer, McGraw-Hill, New York, 1972.

William H. McAdams, Heat Transmission, 3rd Edition, McGraw-Hill, New York, 1954.

G. W. Treadwell, Selection of Parabolic Solar Collector Field Arrays, SAND74-0375, Sandia Laboratories, Albuquerque, New Mexico, May 1975.

M. W. Edenburn, Performance of a Focusing Cylindrical Parabolic Solar Energy Collector: Analysis and Computer Program, SLA-74-0031, Sandia Laboratories, Albuquerque, New Mexico, April 1974.

G. W. Treadwell, et. al., Test Results from a Parabolic-Cylindrical Solar Collector, SAND75-5333, Sandia Laboratories, Albuquerque, New Mexico, July 1975.

W. H. McCulloch, G. W. Treadwell, Design Analysis of Asymmetric Solar Receivers, SAND74-0124, Sandia Laboratories, Albuquerque, New Mexico, August 1974.

M. W Edenburn, N. R. Grandjean, Energy System Simulation Computer Program-SOLSYS, SAND75-0048, Sandia Laboratories, Albuquerque, New Mexico, June 1975.

Frank Biggs, EDEP: A Computer Program for Modeling the Parabolic Trough Solar Concentrator, SAND76-0106, Sandia Laboratories, Albuquerque, New Mexico, to be published.

D. M. Mattox, Coatings and Surface Treatments in Solar Energy Applications, Plating and Surface Finishing, January 1976, pp. 55-59.

D. M. Mattox, Solar Energy Materials Preparation Techniques, Journal of Vacuum Science Technology, Vol. 12, No. 5, Sept/Oct. 1975, pp. 1023-1031.

DISTRIBUTION:

TID-4500-R64, UC-62 (274)

US ERDA
Division of Solar Energy
Washington, DC 20545
Attn: G. Kaplan

US ERDA
Albuquerque Operations Office
P.O. Box 5400
Albuquerque, NM 87115
Attn: D. K. Nowlin

Watt Engineering Ltd
RR 1, Box 183-1/2
Cedaredge, CO 81413
Attn: A. D. Watt

1100 C. D. Boyles
Attn: J. D. Kennedy, 1110
G. E. Hansche, 1120
1280 T. B. Lane
1283 H. C. Hardee
1284 R. T. Othmer
1300 D. B. Shuster
1330 R. C. Maydew
1400 A. Y. Pope
2300 L. D. Smith
2320 K. L. Gillespie
Attn: L. W. Schulz, 2324
2541 G. E. Gobeli
3620 R. S. Wilson
3622 E. R. Frye
5000 A. Narath
Attn: J. K. Galt, 5100
5110 F. L. Vook
5130 G. A. Samara
5150 J. E. Schirber
5200 E. H. Beckner
5231 J. H. Renken
Attn: F. Biggs
5420 J. V. Walker
5700 J. H. Scott
5710 G. E. Brandvold
5711 R. P. Stromberg
5712 J. A. Leonard
5712 G. W. Treadwell (100)
5735 M. M. Newsom
5740 V. L. Dugan
5800 R. S. Claassen
Attn: R. L. Schwoebel, 5820
5830 M. J. Davis
Attn: D. M. Mattox, 5834
5840 D. M. Schuster (3)
Attn: R. C. Heckman, 5842
F. P. Gerstle, 5844
E. K. Beauchamp, 5846
8100 L. Gutierrez
8180 C. S. Selvage
Attn: A. C. Skinrood, 8184

9300 L. A. Hopkins, Jr.
9330 A. J. Clark, Jr.
9336 J. V. Otts
9340 W. E. Caldes
Attn: J. L. Mortley, 9344
9400 H. E. Lenander
9410 R. L. Brin
Attn: R. K. Petersen, 9412
9515 J. T. Hillman
8266 E. A. Aas (2)
3141 C. A. Pepmueller (Actg) (5)
3151 W. L. Garner (3)
For ERDA/TIC (Unlimited Release)

CORROSION PROBLEMS IN MEDIUM TEMPERATURE THERMAL CONVERSION SYSTEMS WITH AQUEOUS/OIL COOLANTS

by

Jerome Kruger

National Bureau of Standards

Washington, D.C.

Corrosion Problems in Medium Temperature Thermal Conversion Systems with Aqueous/Oil Coolants

Jerome Kruger
Chemical Stability and Corrosion Division
National Bureau of Standards
Washington, D.C. 20234

The solar technology to which this brief discussion of corrosion is directed is dispersed solar thermal power systems. Such systems are applied to irrigation pumping, solar total energy systems, small (less than 10 MW) solar electric power plants, and high-temperature process heat applications. Three regimes have to be considered in discussing corrosion problems of medium temperature thermal conversion systems: 1) that surrounding the collector surfaces, 2) that surrounding the outer receiver surfaces, and 3) that to which the interior of the receiver tubes are subjected. The corrosion problems of the first two parts of the system are not serious, especially in those cases where evacuated envelopes are used to protect surfaces exposed to ambient atmospheres. They will, however, be discussed briefly along with the more serious problems occurring in the aqueous and oil environments to which the interior of the receiver tubes and the systems to which such tubes are attached are subjected.

Collector Surfaces

These surfaces which are designed for temperatures of 300°C utilize three families of materials, polished metals, metallized films and silvered glass. The primary materials involved are polished aluminum, silver, glass, polymeric films of mylar, teflon and acrylic. Their corrosion problems are as follows:

Aluminum - Al and aluminum alloys have atmospheric corrosion rates of ambient temperatures approaching maximum values of 10 mpy. At the

higher temperatures to which collector surfaces are exposed the corrosion rate would be considerably higher. It is for this reason that polished aluminum surfaces are coated or are surrounded by evacuated envelopes.

Silver - Surface silver will degrade somewhat by oxidation with the oxide film that forms decomposing around 300°C. Continual oxidation and decomposition can lead to roughening and a lowering of reflectivity.

Polymerics and glass - Mylar can suffer degradation by ultraviolet radiation. Glass can undergo "weathering" by exposure to the atmosphere. This will lead to a decrease in transmittance because of clouding.

Receiver Surfaces

The receivers are usually steel pipes coated with black chrome plate. The black chrome is said to suffer degradation at temperatures above 300°C.

Parts of Surfaces Exposed to Aqueous and Oil Fluids

It is these surfaces that undergo the greatest amount of corrosion problems. Three metals are mainly used in such systems, steel, aluminum and copper. Many of the problems found for the aqueous systems are common to nuclear energy systems, parts of which are exposed to high purity water at temperatures of 300°C or lower and at comparable flow rates (∿3 ft/sec.) Oil systems kept free of water and other impurities especially halides may present no problems. With breakdown products or impurities wholly unexpected failures may result such as the unsuspected stress corrosion of titanium in methanol found around 10 years ago in space applications.

Carbon and Low Alloy Steels - Of major importance in the use of steel in hot aqueous environments is the nature of the oxide film that forms on its surface in room temperature water. This depends strongly on the oxygen content of the water (1). At low initial oxygen contents more protective films tend to form at room temperatures that will promote the

formation of protective films altering high temperature operation. On the other hand, high initial oxygen contents promote the formation of less protective films at high temperatures. Thus, what happens during shut down is of crucial importance.

Coupled with the role played by oxygen concentration and of equal or greater importance is pH. Corrosion rates of steel at pH 8 to 9.5 are six times greater than the rates at pH 10.5 to 11.5 (3). Tackett et al have reported that if the pH is the proper value, compositional differences, surface finish, water resistivity, water velocity as high as 15 to 35 ft/sec, thermal cycling, temperature (260 to 310°C) and other variables have little effect on the corrosion rate. When oxygen content and pH are not at optimal values the following corrosion failure mechanisms may be possible:

1) Pitting - This type of failure can occur if the water inadvertantly contains damaging species such as chlorides or if the steel was exposed to high oxygen initially producing poorly protective mounds of γ or α FeOOH where pits can start. Potential monitoring and other techniques can be used as an alert to pitting situations that develop in the environment.

2) Crevice Attack - If confined or shielded sites exist in the system, especially in the presence of certain inhibitors, the growth of magnetite can take palce. Such growth can lead to a phenomenon called "denting" that can lead to cracking or distortion of tubing.

3) Stress Corrosion-Corrosion Fatigue - In most of the environments contemplated for dispersed solar power systems, the possibility of stress corrosion (SCC) of carbon or low alloy steels is low. Only when the introduction of nitrates or the build up of high alkalinity becomes

a possibility could stress corrosion become a failure mechanism. A cautious note must be struck, however, because it was not suspected that austenitic stainless steels were susceptible to SCC when the oxygen level in nuclear BWR systems went above a few ppm. Adequate testing for SCC as a function of pH, pO_2, inhibitor nature and content is very necessary. The slow strain rate test is an excellent tool for assessing environmental effects on SCC susceptibility. Corrosion fatigue may also not be a problem. It should, however, be recognized that the superposition of the cyclic stresses needed for corrosion fatigue upon the static stress encountered in SCC may create a dangerous situation.

4) Erosión Corrosion - The coupling of flowing fluids with the possibility of particulates produced by the dislodgement of corrosion product films can result in erosion corrosion failures, especially at bends in a tubing system.

Aluminum Alloys - Nuclear system experience (2) indicates that commerical purity Al and most alloys have no corrosion problems at about 200°C in pure water. Above 200°C the aluminum alloys fail rapidly because of intergranular attack (4). The remarks made for the corrosion of steels in oils applies to aluminum. The following failure mechanisms can be suggested for aluminum:

1) Pitting - Pitting can occur at temperatures below 100°C when small concentrations of heavy metal ions are present in the water.

2) General Corrosion - A major factor influencing general corrosion of aluminum is pH. The optimal pH is between 5 and 6. At higher pH values (9.7-9.9) the role of additives becomes important. LiOH causes a considerably higher rate of attack then NH_4OH for a pH of 9.9 (2). Heat flux also affects corrosion rate by influencing the rate of oxide film dissolution.

3) Stress Corrosion and Corrosion Fatigue - The introduction of damaging species such as chloride ions can cause SCC and corrosion fatigue problems.

Copper and Copper Alloys - Oxygen content in water systems is of crucial importance in the corrosion of copper alloys. Rapid attack occurs in aereated high temperature water (2).

1) Stress Corrosion - The use of oxygen controlling additions such as hydrazine can lead to the production of ammonia in some water systems. Many copper alloys are susceptible to SCC in ammonia or ammonia-like compound solutions.

2) Pitting - Damaging species such as chlorides can lead to pitting problems.

References

1. Strauss, M. B., and Bloom, M. C., "Corrosion Mechanisms in the Reaction of Steel with Water and Oxygenated Solutions at Room Temperature and 316 C", J. Electrochem. Soc., 107 (2), 73-79 (February, 1960).

2. Berry, W. E., "Corrosion in Nuclear Applications", John Wiley and Sons, New York, 1971.

3. Tackett, Donald E., Brown, Paul E., and Esper, Richard T., "Review of Carbon Steel Corrosion Data in High-Temperature, High-Purity Water in Dynamic Systems", USAEC Report WAPD-LSR(C)-134 (October 14, 1955).

4. Draley, Joseph E., and Ruther, Westley E., "Aluminum Alloys", USAEC Report TID-8540, pp 215-223 (1964).

THIS PAGE

WAS INTENTIONALLY

LEFT BLANK

ABSORBER COATINGS

by

P. Call

Solar Energy Research Institute

Golden, Colorado

*Paper or Viewgraphs

Not Available

*Publications available:

"National Program Plan for Absorber Surfaces R&D", Patrick J. Call, SERI/TR-31-103 (1978).

Proceedings DOE/DST Thermal Power Systems Workshop on Selective Absorber Coatings, P. J. Call (ed.), SERI/TP-31-061, (August, 1978).

Proceedings Second Annual Conference on Absorber Surfaces for Solar Receivers, P. J. Call (ed.), SERI/TP-49-182, (1979).

THIS PAGE

WAS INTENTIONALLY

LEFT BLANK

ANHYDROUS ORGANIC HEAT TRANSFER FLUIDS IN MEDIUM TEMPERATURE SOLAR CONVERSION

by

David R. Miller

Monsanto Company

St. Louis, Missouri

INTRODUCTION

Organic heat transfer fluids have come into wide-spread industrial use in the past few decades in such diverse operations as:

making styrene, polyester & plastics
spinning nylon
dehydrating natural gas
refining petroleum, petrochemicals
barging asphalt

In these and numerous other uses, the organic medium accepts and rejects heat, generally within the temperature band of 175 to 400°C (350 to 750°F). Above about 400°C, the organics lack the chemical stability demanded in practical systems. Below about 175°C, water and water/organic solutions are frequently chosen over anhydrous organics for economic reasons.

Ease of containment explains much of the appeal of the organics. Compared to water, they are practically non-corrosive to common materials of confinement. In addition, they possess much lower vapor pressures, with consequent reduction in strength, weight and cost of confining hardware.

Within the 175 to 400°C cost-performance window (Figure 1), about 20 trademarked organic fluids are sold into the North American industrial market by about 8 domestic chemical and oil companies. Oil companies offer petroleum cut oils, whereas chemical companies supply chemically synthesized fluids. Collectively, they are often called "heat transfer oils". Around these products has grown a practical technology of materials, design, operation and maintenance

which is fairly mature, but highly invisible and fragmented. Well designed and intelligently operated industrial organic systems are about as reliable now as water-steam systems at much lower temperatures.

The same factors explaining the industrial popularity of the organic media pertain to the medium temperature solar conversion application. Transfusion of the industrial technology to the solar sector is a clear and urgent need in the acceleration of solar medium temperature conversion development.

STATE OF KNOWLEDGE

Comparisons of representative operating parameters for an industrial radiant heater and a mid-temperature solar collector field heating the same organic fluid appear in Figure 2. While these data give an inkling of the technical challenges in collector development, they do not hint at the areas where solar system development transcends industrial experience, especially:

- transiency of insolation (and control)
- necessity to store heat
- novel and unfamiliar material compatibility demands
- modified safety/environmental concerns
- dispersal, piping network complexity, pumping
- photochemical implications (transparent receivers)

These subjects need R&D attention.

FLUID RELIABILITY

System reliability as relates to the heat transfer fluid is a complex interactive function of a) fluid chemical composition, b) containment materials and c) conditions of use. It is impossible to consider any one or two of these isolated from the other(s). Each of these factors changes inexorably with time under the influence of:

chemical and physical-chemical degradation
deposit formation, fouling
leakage, evaporation
corrosion
wear, fatigue, erosion, creep
contamination

The benign result of these forces is gradual deterioration of system performance: the malignant result is rapid deterioration and/or failure.

The chemical composition of the system fill fluid is fixed, within limits, when the fluid choice is made. Ideally, the choice is the outcome of a careful cost-benefit analysis, involving difficult trade-offs and a few candidate products and substances of established functionality. Again ideally, fluid reliability should enter into the analysis in an objective and quantitative way. This is not presently possible, for want of an acceptable meterstick (yardstick). It is not too surprising, then, to observe a proliferation of unique ad hoc reliability gaging tests in the shops of the solar fluid choosers.

Once chosen, the fluid is susceptible to change within the system. Good design, operating and maintenance practices limit such change to an acceptably low level. Failures, defined as unacceptably fast changes in fluid or function, are perceived to occur for reasons listed in Figure 3. This is a distillation of some 7 years experience in diagnosing industrial heat transfer system ills, mostly by analyzing "blood" samples.

While the immediate causes of failure are usually revealed by chemical and condition analyses, a degree of speculation enters into assigning ultimate causes. There can be little doubt, though, that human frailties and poor communications have far outranked technology gaps and deficient materials. Any program to improve material reliability needs take this into proper account.

TECHNOLOGY TRANSFER

Figure 4 shows a hypothetical solar system project in terms of technical resources (boxes) and information/product exchanges (arrows). Accomplishment travels fromtop to bottom through the usual definition, design, build and operate sequence. In the extreme, these are in four distinct and separate organizations. On the cross arms are the component suppliers and the open (generally available) technology, all feeding information and most feeding products to the builder and designer. Again in the extreme, there are no duplications of organizations (which will actually exceed in number the four depicted).

This dispersion of know-how is further aggravated by a paucity of reliable organic media data in the open technology block (although it is rich in the science of heat transmission). This leaves the suppliers as the repositories of a major portion of the technical information on organic systems, a situation not generally apparent to the newcomer.

Now, if this hypothetical solar project proceeds true to industrial tradition, the arrows will almost all point in one direction, the loop will not be closed, and many opportunities to learn from experience, and thereby advance technology will be lost.

Another dimension to the technology transfer problem appears in Figure 5. This side-by-side listing of the principal participants in the various functional blocks of the previous figure reveals a near-total separation between the industrial and solar system technical fraternities, at least above the fluid producer level. Will the solar "newcomers" learn anything from the industrial "oldtimers" on the industrial side? Or will they reinvent the wheel along the way?

Establishing new lines of two-way communication between all participants is felt to be the most effective way to improve fluid reliability in solar systems. Corollary to this is tapping industrially-grown technology to advance and accelerate solar.

EXPERIMENTAL TECHNIQUES AND NEEDS

Figure6 lists test methods used to characterize organic fluids in terms of properties, stability and compatibility, and health, handling and environmental. Of particular pertinence here are the stability and compatibility tests, for these are the primary measures of fluid permanence in various environments. All these methods involve measuring changes in the properties, compositions and amounts of a fluid sample exposed to a defined environment at a given temperature for a specified time.

The simplest static exposure test uses a hermetically sealed steel vessel in place of the glass ampoule called out in ASTM D2160. Vessels of various capacities made of pipe or tubing have found use. The smallest, holding 3 cc, is shown in Figure 7. Other static vented or gas sparged vessels have found use in testing compatibilities of fluids in contact with various solid thermal storage media.

A point of issue with all static exposure tests is how well they simulate real system conditions. One way to find out is to compare such measurements with others made with the same materials in a more simulative dynamic test loop, as listed in Figure 6.

All such exposure and loop tests are in need of standardization, refinement, and cross checking. Similitude theory needs to be brought to this area with the idea of developing scaling rules and methods.

FLUID MANAGEMENT

Fluid management is a concept worthy of attention at every major step of a development starting with system design. Too often it appears that the first person to pay it heed is the system user just after the installers leave. Every aspect of selection, purchase, receipt storage, fill and top-off, drain, reclaim or disposal and system cleanout should be considered. Regular monitoring of the condition of the fluid is a most effective way to detect changes and forestall system failure.

The simple in-situ tests listed in Figure 8 are adequate for most monitoring purposes. Quite often, even these few relatively simple tests are considered too complicated for use by on-site operating personnel. When this is the case, samples can be sent to any of many commercial laboratories equipped to run the needed tests.

D.R.M.
12-13-78

SUMMARY OF NEEDS
MID-TEMPERATURE SOLAR SYSTEM MATERIALS

INFORMATIONAL

- WHO, WHAT, WHERE, WHY, HOW OF MATERIALS TECHNOLOGY.
- EFFECTIVE 2-WAY COMMUNICATION; TECHNOLOGY TRANSFUSION.
- INFORMATION CENTER; DATA; MATERIALS, EXPERIENCE BANKS.
- SOLAR RECOMMENDED PRACTICES, MATERIALS.
- SOLAR-SPECIFIC SAFETY, HEALTH, ENVIRONMENTAL GUIDES.

EXPERIMENTAL

- SOLAR-SIMULATIVE COMPATIBILITY/STABILITY TEST METHODS.
- COMPATIBILITY/STABILITY TEST RESULTS ON NEW MATERIALS, NEW COMBINATIONS OF MATERIALS, NEW CONDITIONS.
- DEVELOPMENT OF TEST SCALING RULES, SIMILARITY THEORY.
- TRANSLATION OF SOLAR-UNIQUE DEMANDS INTO NEW MATERIAL REQUIREMENTS (TRANSIENCY, STORAGE, PHOTODEGRADATION, ETC.)
- MATERIALS MONITORING OF OPERATING SOLAR SYSTEMS; REPORTING, FAILURE/RELIABILITY ANALYSES.

ORGANIZATIONAL

CENTRALIZED PUBLIC LABORATORY & FACILITY FOR SOLAR MATERIALS

- INFORMATION CLEARING HOUSE AND RESOURCE.
- CATALYZE, SUPPORT, PROMOTE THE NORMAL CHANNELS OF MATERIALS DEVELOPMENT.
- TESTING OF MATERIALS NEEDED IN SYSTEM DEVELOPMENT.
- GUIDANCE AND SUPPORT OF EFFORTS NEEDED TO ESTABLISH ACCEPTABILITY OF NEW MATERIALS.
- MATERIALS-IN-USE MONITORING AND REPORTING.

ANHYDROUS ORGANIC HEAT TRANSFER FLUIDS IN MEDIUM TEMPERATURE SOLAR CONVERSION

Viewgraphs Presented
by

David R. Miller

Monsanto Company

St. Louis, Missouri

FIGURE I

ORGANIC HEAT TRANSFER MEDIA
IN
MEDIUM TEMPERATURE SOLAR THERMAL
CONVERSION

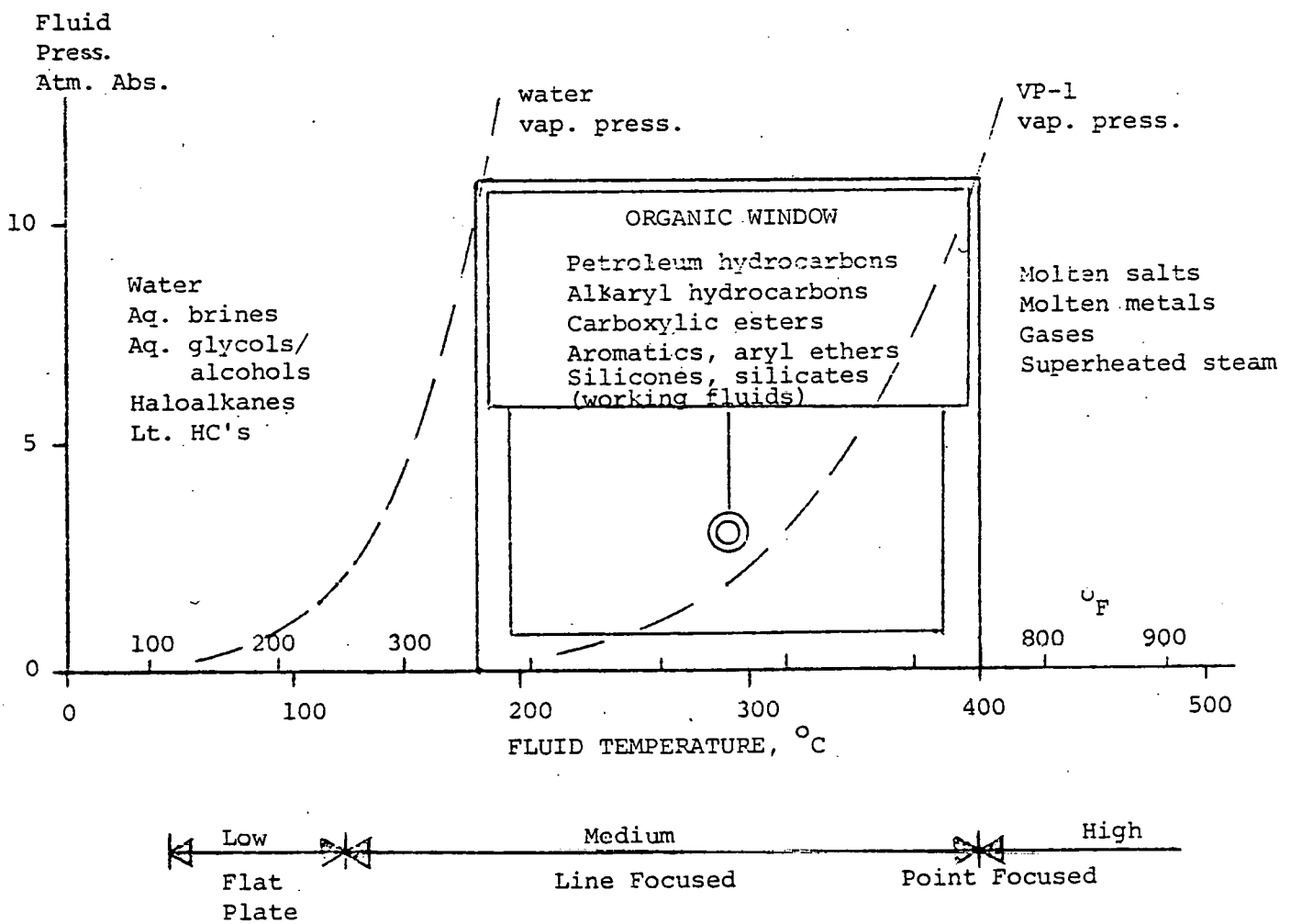


FIGURE II

STATE OF THE ART
ORGANIC HEAT TRANSFER SYSTEMS

Fluid Temperature, Bulk	400°C (750°F) max.
Representative Medium Size Industrial Organic Fluid Heater (non-boiling, gas/oil fired, radiant)	
Heat rate (fluid pick-up)	1 MW (3.5M Btu/h)
Heat flux, mean (at fluid interface)	20 kW/m^2 (7 kBtu/h.ft.^{2}) or 35 suns (360° avg.)
Exchange surface area	50 m^2 (500 ft^2)
Organic flow rate	2 m^3/min. (500 gpm)
Organic velocity	2 m/sec. (7 fps)
Thermal efficiency	85%
Heater volume (radiant encl.)	50 m^3 (1700 ft.^{3})
Representative Mid-Temperature Solar Collector Field (non-boiling, line focused, E-W parabolic trough)	
Heat rate, peak (fluid pick-up)	0.1 MW (0.35M Btu/h)
Heat flux, mean peak (at fluid interface)	6 kW/m^2 (2 kBtu/h.ft^2) or 10 suns
Collector aperture	200 m^2 (2000 ft.^{2})
Exchange surface area	18 m^2 (180 ft.^{2}) ?
Organic flow rate	
Organic velocity	
Thermal efficiency, peak	55%
Collector volume	600 m^3 (20,000 ft.^{3})

FIGURE III

FLUID ASSOCIATED FAILURE MODES

FLUID ABUSE

- NEGLECT
- OVERHEATING (THERMAL DECOMPOSITION)
- EXPOSURE TO AIR (OXIDATION)
- CONTAMINATION

  MOST OFTEN WITH WATER, MINERAL ACIDS, ALKALIES, CLEANERS, LUBRICANTS, OTHER H.T. MEDIA, PROCESS FLUIDS
- LEADING TO:

  PUMP CAVITATION, FLOW LOSS, TWO LIQUID PHASES, SOLIDS DEPOSITION, EXCESSIVE VENTING, ALTERED H.T. RATES, INSTABILITIES, CORROSION, FLUID LOSS, VISCOSITY INCREASE.

CONTAINMENT FAILURE

- STATIC & DYNAMIC SEAL LEAKAGE.
- WEAR, FATIGUE, CORROSION, EROSION, CREEP, OVERSTRESS
- INCOMPATIBLE WETTED MATERIALS
- LEADING TO:

  FLUID LOSS, ENVIRONMENTAL CONTAMINATION/HAZARD, CONTAMINATION OF FLUID, OTHER CONSEQUENCES ABOVE.

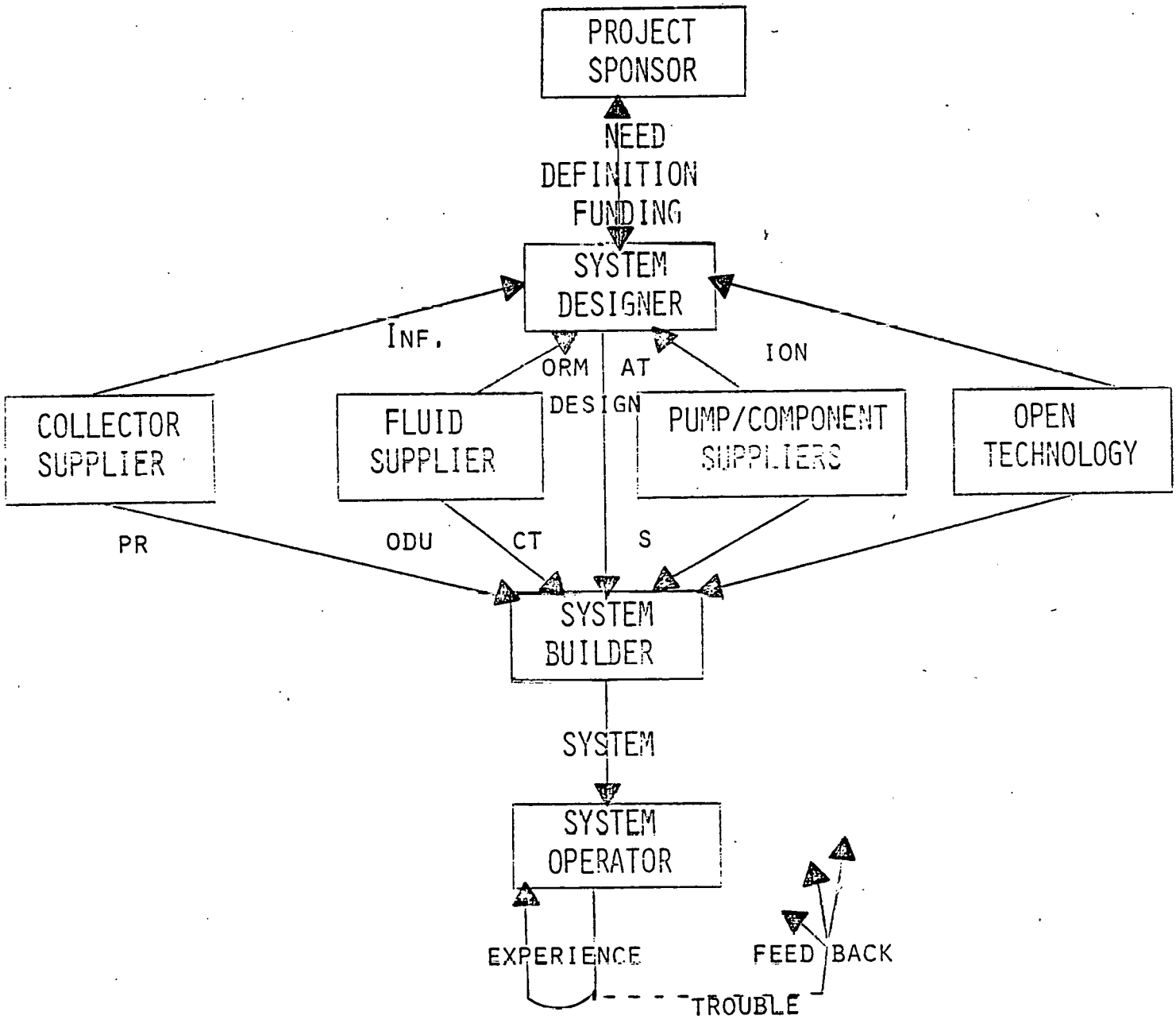
ULTIMATE CAUSES

- SLOTH
- IGNORANCE
- TECHNICAL GAPS
- MATERIAL IMPERFECTIONS

FIGURE IV

TECHNOLOGY FLOW

"TYPICAL" PROJECT



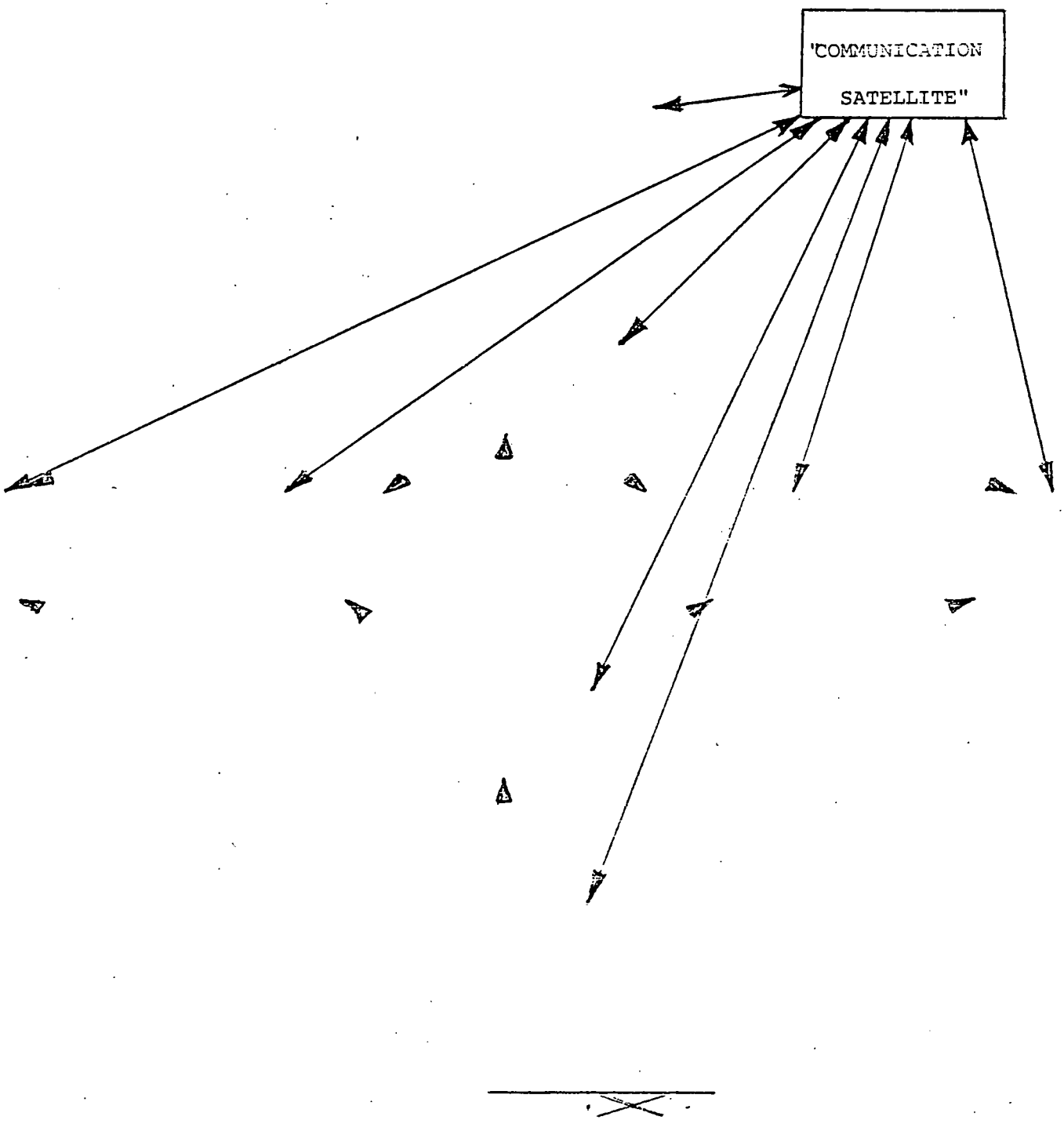

'COMMUNICATION
SATELLITE"

FIGURE V

WHO'S WHERE? - MID TEMPERATURE ORGANIC THERMAL SYSTEMS

INDUSTRIAL		SOLAR
SYSTEM OPERATORS		
REFINERIES, CHEM/PETROCHEM/TEXTILE PLANTS, BARGES/SHIPS, PIPELINES/TERMINALS, OIL/GAS WELLS, METAL TREATERS/COATERS, RUBBER/PLASTIC/PAPER PROCESSORS.		NATIONAL LABS, PUBLIC UTILITIES, COM'L & LIGHT INDUST., CENTERS/COMPLEXES/INSTITUTIONS/BUILDINGS, FARM COOPS, MILITARY INSTAL.
SYSTEM DESIGNERS/BUILDERS		
AM. HYDROTHERM, BRIGHTON, CAROTEK, G.E.A. AIREXCHANGERS, GRUENBERG-UDOLF, IND. PROC. ENG., SIVALS TANK, FALLON ENGR., COMBUSTION EQUIP. ASSOC., STONE & WEBSTER.		NATIONAL LABS, MCDONNELL DOUGLAS, ROCKETDYNE, WESTINGHOUSE, G.E. HONEYWELL, BOEING, MARTIN MARIETTA, ATOMICS INTL., ACUREX, GRUMMAN, MIDWEST RESEARCH
HEATERS	**DESIGNERS/BUILDERS**	**COLLECTORS/RECEIVERS**
AM. HYDROTHERM, BLACK/SIVALLS/BRYSON, BROWN FINTUBE, CLEAVER BROOKS, ECLIPSE BOILER, ECONO-THERM, FULTON BOILER, INT'L. BOILER WORKS, C.E. NATCO, STRUTHERS WELLS, VAPOR CORP.		AAI, ACUREX, HEXCEL, JACOBS-DEL SOLAR, SOLTRAX, SCIENTIFIC ATLANTA, NORTHRUP, G.E., OWENS ILLINOIS, 3M, SOLAR KINETICS, FMC, ITEK, GEN. ATOMIC, MCDONNELL DOUGLAS, SUNTEC, RAYTHEON, BOEING, EPRI
FLUID PRODUCERS		
PETROLEUM: MOBIL, EXXON, SUN, TEXACO, SHELL. SYNTHETICS: DOW, MONSANTO		SAME, PLUS DOW CORNING, G.E., RESOURCE TECHN., UNIROYAL, NUCLEAR TECH., MARK ENTER.
PUMP & COMPONENT MANUFACTURERS		

HIGH DEGREE OF COMMONALITY

APOLOGIES TO: ANYONE OMITTED OR INCORRECTLY PIGEON-HOLED.

FIGURE VI

CREDIBLE EXPERIMENTAL METHODS

ROPERTIES	METHODS
ENSITY	WESTPHAL BALANCE, THERMOSTATED
ISCOSITY (KIN.)	ASTM D445/2515, GLASS CAPILLARY
PECIFIC HEAT	DIFFERENTIAL THERMAL ANALYZER
HERMAL CONDUCTIVITY	PULSED HOT WIRE TECHNIQUE (SPECIAL)
APOR PRESSURE	GLASS PIEZOMETER, PROGRAMMED (SPECIAL)
EAT OF VAPORIZATION	CALCULATED FROM VAPOR PRESSURE
OILING RANGE	ASTM D86 OR 1160 (ATM OR VAC)
LASH/FIRE POINTS	ASTM D92 OR 93 (COC OR PM)
UTO IGNITION TEMP.	ASTM D2155
OUR POINT.	ASTM D97
TABILITY/COMPATIBILITY	
TATIC AMPOULE, OVEN EXPOSURE (3-300 CC SAMPLE IN STEEL OR SS)	ASTM D2160 MODIFIED, ANALYSES BY ASTM D445, D664, D1744, GLC, MASS SPEC., WEIGHINGS AND ETC.
ENTED OR GAS-SPARGED VESSEL, THERMOSTATED	SPECIAL AD HOC APPARATUS, ANALYSES AS ABOVE
IMULATIVE THERMAL TEST LOOPS (30 GPM, 26 KW, 20 GAL.)	SPECIAL RIG, ANALYSES AS ABOVE
EALTH, HANDLING & ENVIRONMENTAL	
NHALATION & TLV	LEGAL TEST PROTOCOLS USED IN HAZARDOUS/TOXIC MATERIALS TESTING (OUTSIDE ANIMAL TEST LABS) TOSCA, EPA, OSHA
KIN & EYE CONTACT (DLD 50)	
RAL INGESTION (OLD 50)	
ARCINOGEN, MUTAGEN, TERATOGEN	
ISH & BIRD EXPOSURE	
XTENDED (2 YR.) FEEDING	
IOACCUM., BIODEGRAD., WATER & SOIL	

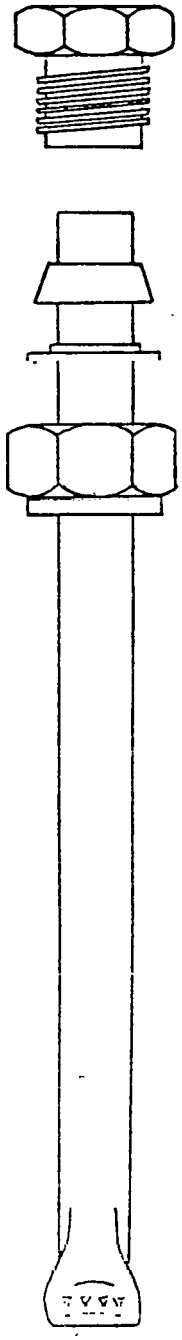


FIGURE VII

Tube Specifications

SAE 1008 low carbon steel tubing

6 inches long

0.375 in. OD x 0.035 in. wall thickness

Total volume 7.0 ml

Top Fitting - Swagelok S 600-C

Bottom - Crimped and Heliarc Welded

FIGURE VIII

FLUID CONDITION MONITORING

IN SITU

APPEARANCE, ODOR

KINEMATIC VISCOSITY*, 100°F (ASTM D445)

THERMOSTATED GLASS CAPILLARY

ACIDITY* (ASTM D664)

POTENTIOMETRIC TITRATION WITH KOH REAGENT

MOISTURE CONTENT* (ASTM D1744)

KARL FISCHER TITRATION

PARTICULATE CONTAMINATION* (ARP 785, MODIFIED)

CONTROL FILTER GRAVIMETRIC PROCEDURE

* - NOTE: REQUIRES SPECIALIZED LABORATORY EQUIPMENT, OFTEN NOT FOUND NEAR WORKING SYSTEMS.

EX-SITU

GAS-LIQUID CHROMATOGRAPHY

FULL RANGE OF ANALYTICAL INSTRUMENTS, TECHNIQUES FOR IDENTIFICATION OF CONTAMINANTS, DECOMPOSITION AND CORROSION PRODUCTS,

X-RAY FLUORESCENCE/DIFFRACTION

IR/VISIBLE/UV SPECTROSCOPY

MICROCOULOMETRY

SUMMARY OF NEEDS
MID-TEMPERATURE SOLAR SYSTEM MATERIALS

INFORMATIONAL

- WHO, WHAT, WHERE, WHY, HOW OF MATERIALS TECHNOLOGY.
- EFFECTIVE 2-WAY COMMUNICATION; TECHNOLOGY TRANSFUSION.
- INFORMATION CENTER; DATA, MATERIALS, EXPERIENCE BANKS.
- SOLAR RECOMMENDED PRACTICES, MATERIALS.
- SOLAR-SPECIFIC SAFETY, HEALTH, ENVIRONMENTAL GUIDES.

EXPERIMENTAL

- SOLAR-SIMULATIVE COMPATIBILITY/STABILITY TEST METHODS.
- COMPATIBILITY/STABILITY TEST RESULTS ON NEW MATERIALS, NEW COMBINATIONS OF MATERIALS, NEW CONDITIONS.
- DEVELOPMENT OF TEST SCALING RULES, SIMILARITY THEORY.
- TRANSLATION OF SOLAR-UNIQUE DEMANDS INTO NEW MATERIAL REQUIREMENTS (TRANSIENCY, STORAGE, PHOTODEGRADATION, ETC.)
- MATERIALS MONITORING OF OPERATING SOLAR SYSTEMS; REPORTING, FAILURE/RELIABILITY ANALYSES.

ORGANIZATIONAL

CENTRALIZED PUBLIC LABORATORY & FACILITY FOR SOLAR MATERIALS

- INFORMATION CLEARING HOUSE AND RESOURCE.
- CATALYZE, SUPPORT, PROMOTE THE NORMAL CHANNELS OF MATERIALS DEVELOPMENT.
- TESTING OF MATERIALS NEEDED IN SYSTEM DEVELOPMENT.
- GUIDANCE AND SUPPORT OF EFFORTS NEEDED TO ESTABLISH ACCEPTABILITY OF NEW MATERIALS.

- MATERIALS-IN-USE MONITORING AND REPORTING.

A SURVEY OF ORGANIC COOLANT EXPERIENCE IN NUCLEAR REACTORS

Viewgraphs Presented
by

H. Pearlman, J. Jacobson, and C. A. Trilling

Rockwell International

Canoga Park, California

HIGHLIGHTS OF ORGANIC COOLED REACTORS

- FOJR REACTOR SYSTEMS REPORTED BUILT 1957-1965. ONE STILL OPERATING IN 1978 (13 YEARS)

- EXPERIENCE WITH MIXED TERPHENYLS; PARTIALLY HYDROGENATED TERPHENYLS; AND PETROLEUM DISTILLATE FRACTIONS

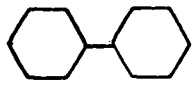
- MAXIMUM COOLANT TEMPERATURE ~ 400°C, SYSTEM PRESSURE ~200 PSIG, HEAT TRANSFER ~135,000 B/HR-FT^2

- CARBON STEEL, LOW ALLOY STEEL, ALUMINUM ALLOYS ARE COMPATIBLE WITH COOLANT AND DECOMPOSITION PRODUCTS AT SERVICE TEMPERATURES

- DECOMPOSITION MOSTLY (> 90%) BY RADIOLYSIS. COMPOSITION MAINTAINED BY SIDESTREAM ADSORPTION, FILTRATICN, AND/OR DISTILLATION

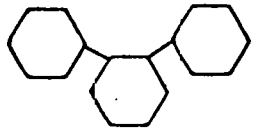
- ATOMICS INTERNATIONAL (ROCKWELL) PIQUA NUCLEAR POWER FACILITY GENERATED 150,000 LB/HR OF SUPERHEATED STEAM AT 550°F AND 450 PSIA, AND DELIVERED 11.4 MW_E (1963-1966)

SOME PROPERTIES OF PURE POLYPHENYLS

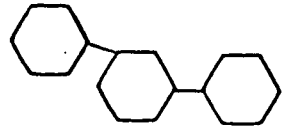


BIPHENYL

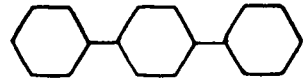
$C_{12}H_{10}$



ORTHO-TERPHENYL



META-TERPHENYL



PARA-TERPHENYL

$C_{18}H_{14}$

	BIPHENYL	ORTHO-TERPHENYL	META-TERPHENYL	PARA-TERPHENYL
M.P. (°C)	71	56.1	87.2	212
(°F)	(160)	(133)	(189)	(414)
B.P. (°C)	255.9	332	365	400
(°F) AT 760 TORR	(492.6)	(630)	(689)	(752)
T_c (°F)	(960)	(1144)	(1205)	(1210)
P_c (PSIA)	551	566	508	506

Rockwell International
Energy Systems Group

COMMERCIAL POLYPHENYLS AND DERIVATIVES

--APPROXIMATE COMPOSITIONS AND MELTING POINTS

	SANTOWAX OM	SANTOWAX OMP	SANTOWAX WR	SANTOWAX R	OM2	HB40
BIPHENYL (WT %)	3	<2	<2	1	<1	0
o-TERPHENYL (WT %)	65	10	15-20	7	20	18
m-TERPHENYL (WT %)	30	60	75	50	76	0.5
p-TERPHENYL (WT %)	2	28	4	22	4	0.5
HYDROG. TER. (WT %)	-	0	0	0	0	82
HIGH BOILERS (WT %)[A]	-	<1	0	20	0	0
MELTING RANGE (°C)	~50	~175	~85	83-110	85	<ROOM TEMP

[A]NOT VOLATILE AT OVERHEAD CONDENSER TEMPERATURE ~ 525°F (274°C) IN A STANDARD FRACTIONAL DISTILLATION COLUMN

SANTOWAX OMP COOLANT IN PNPF

- SPECIFICATIONS (MAX. PERMISSIBLE PPM IN NEW COOLANT)

AL	BA	CA	CL	CR	CU	FE	MG	MO	NI	P	PB	S	SI
1	2	10	(A)	1	2	10	1	1	3	8	4	60	3

- QUALITY CONTROL CRITERIA, IN REACTOR

ASH (PPM)	≤ 5
FE (PPM)	≤ 2
CL (PPM)	≤ 2
CARBONYL OXYGEN (PPM)	≤ 100
MEMBRANE STAIN TEST (A/MG)	$\leq 50 \times 10^{-5}$ (B)

NOTES: (A) AS LOW AS POSSIBLE. OMP FROM MONSANTO CONTAINED ~3 PPM

(B) AN EMPIRICAL TEST WHICH MEASURED CHANGE IN OPTICAL ABSORBANCE OF A FILTER MEMBRANE AFTER PASSAGE OF A KNOWN QUANTITY OF COOLANT IN SOLUTION

FOULING AND FILM FORMATION

- NOT SIGNIFICANT WHERE DECOMPOSITION IS BY PYROLYSIS ALONE
- IN RADIATION FIELDS, FILMS ARE PREDOMINATELY ORGANIC, WITH SOME Fe CONTENT
- MECHANISM
  1) DECOMPOSITION AND CORROSION PRODUCTS → COLLOIDAL PRODUCTS SUSPENDED IN COOLANT
  2) COLLOIDAL PARTICLES AGGLOMERATE ON HOTTER METAL SURFACE
  3) AGGLOMERATED LAYER → FILM, UNDER INFLUENCE OF RADIATION AND TEMPERATURE
- EFFECTS OF IMPURITIES
  1) ACCELERATED BY TRACES OF Cl, AND O COMPOUNDS SUCH AS CARBONYL ORGANICS. LATTER FORM BY REACTION WITH AIR (THEREFORE, MAINTAIN AIR-FREE SYSTEM)
  2) PREVENTED BY ~100 ppm WATER IN COOLANT. EMPIRICALLY EFFECTIVE, MECHANISM NOT CLEAR

HEAT TRANSFER WITH POLYPHENYLS AND RELATED COMPOSITIONS

FORCED CONVECTION

CORRELATED BY: $Nu = 0.023\ Re^{0.8} Pr^{0.4}$ (TO 875°F) WHERE Nu, Re AND Pr ARE THE NUSSELT, REYNOLDS AND PRANDTL NUMBERS

BOILING

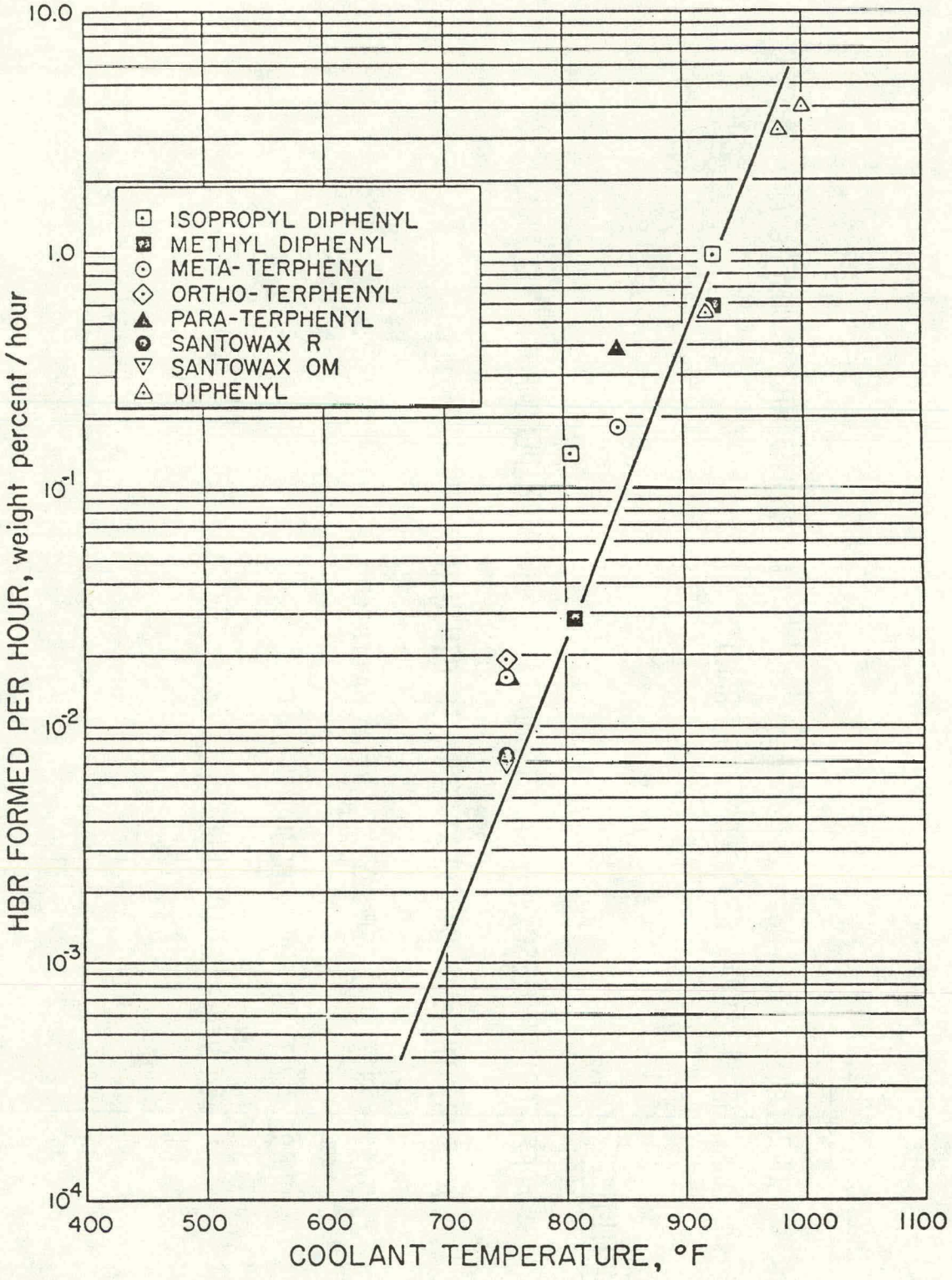
AFFECTED BY DISSOLVED GASES AND LIGHT ENDS OF DECOMPOSITION PRODUCTS

AT DNB, THE MAXIMUM HEAT FLUX IS GIVEN BY:

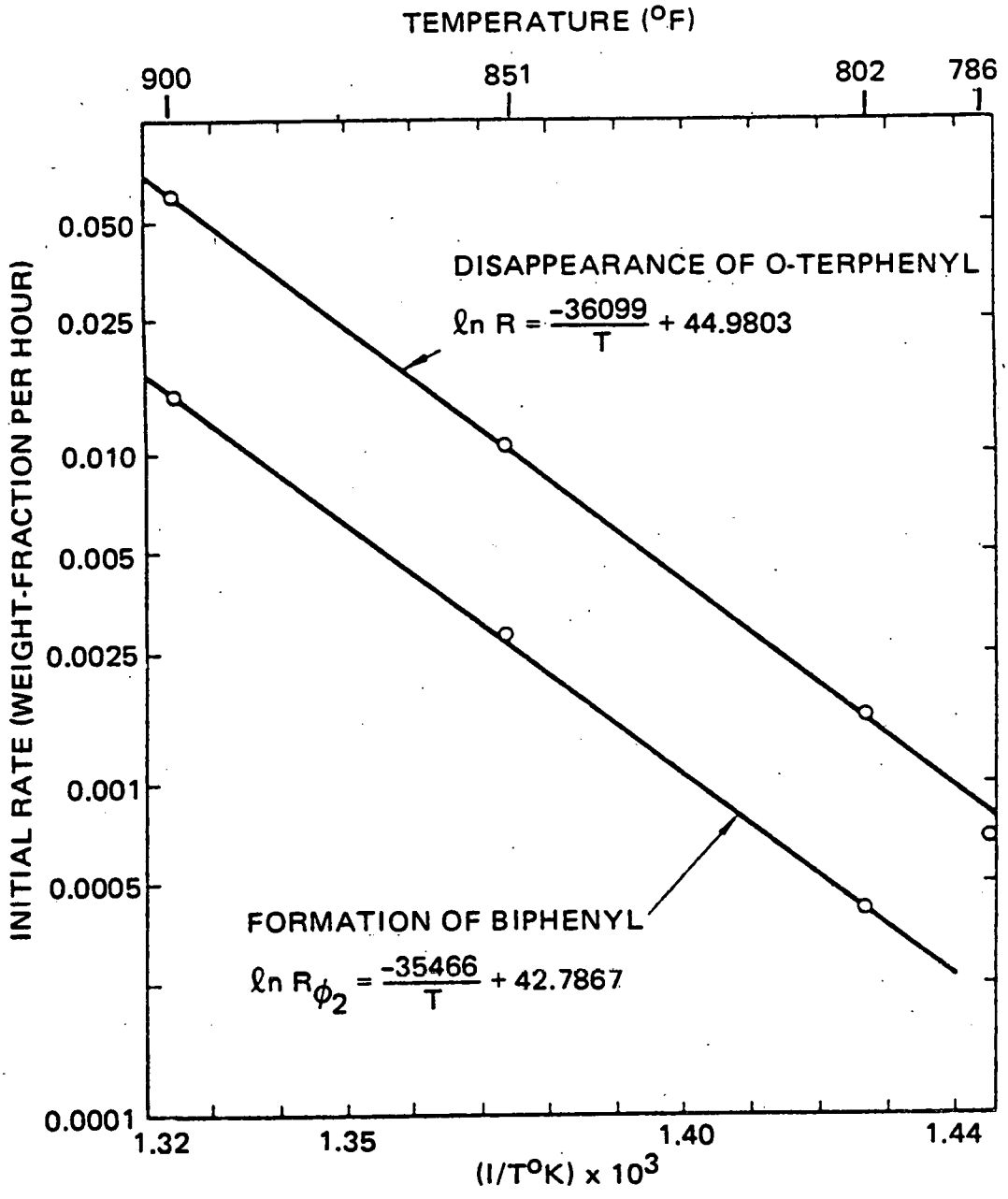
$$Q/A = 98.3 + 0.696\ \Delta T_{SUB}\ V^{2/3}\ \text{WATTS/CM}^2$$

WHERE ΔT IS THE SUBCOOLING, °C

V IS FLUID VELOCITY, M/S



PYROLYSIS OF POLYPHENYLS



PYROLYSIS OF O-TERPHENYL

Rockwell International
Energy Systems Group

DESIGN PARAMETERS, PNPF

--REACTOR PLANT--

THERMAL/ELECTRICAL POWER OUTPUT -- 45.5 Mw/11.4 Mw

COOLANT -- SANTOWAX OMP

SYSTEM PRESSURE (AT CORE INLET) -- 120 PSIA

SYSTEM DESIGN PRESSURE -- 300 PSIA

COOLANT TEMPERATURE INTO CORE -- 523^{o}F

COOLANT TEMPERATURE OUT OF CORE -- 575^{o}F

COOLANT FLOW TO STEAM GENERATOR -- 5.5×10^{6} LB/HR (12,000 GPM)

STEAM FLOW FROM GENERATOR -- 150,000 LB/HR

STEAM CONDITIONS -- 550^{o}F, 450 PSIA

--HEAT TRANSFER--

MAXIMUM TEMPERATURE FUEL ELEMENT SURFACE -- 718^{o}F

BURN OUT HEAT FLUX -- 640,000 BTU/HR-FT^{2}

MAXIMUM HEAT FLUX -- 132,000 BTU/HR-FT^{2}

AVERAGE HEAT FLUX -- 34,300 BTU/HR-FT^{2}

HEAT TRANSFER COEFFICIENT TO COOLANT -- 1300 BTU/HR-FT^{2}-^{o}F

--COOLANT--

TOTAL -- 10,500 GALLONS (80,000 LB)

DECOMPOSITION RATE AT FULL POWER -- 91 LB/HR (AT 7% HB)

PURIFICATION FLOW RATE -- 195 LB/HR

PURFICATION PROCESS -- DISTILLATION AND FILTRATION

EXPERIENCE IN WR-1 REACTOR

- D_2O MODERATED, ORGANIC-COOLED, 60 MW_T RESEARCH REACTOR
  NO POWER GENERATION
- COOLANT
  - FEED -- SIMILAR TO MONSANTO HB-40
  - STEADY STATE REFERENCE -- 30% HB, 28% H-TERPHENYLS, 11% METHYL BIPHENYL, 10% M-TER., 7% QUATERPHENYLS, 5% BIPHENYL, 5% P-TER., 3% < BIPHENYL AND 1% O-TER.
  - TOTAL INVENTORY -- 127,000 LB
- MAX COOLANT TEMPERATURE -- 400°C (752°F), MAX PRESSURE -- 315 PSIA
- TIME AT MAX TEMPERATURE -- 7 YEARS
- FOULING -- AFTER THIN FILM FORMS, FURTHER DEPOSITION ELIMINATED BY MAINTAINING C_L < 50 PPB, O <100 PPM, Fe <500 PPB, PARTICULATES <1000 PPM, AND WATER BETWEEN 200 AND 600 PPM
- MAX METAL TEMPERATURE -- 640°C, MAX HEAT FLUX -- 510 W/CM^2
- PURIFICATION -- DISTILLATION, ABSORPTION ON CLAY, FILTRATION

A SUMMARY OF TABULATED DATA FOR POLYPHENYL COOLANTS

- PHYSICAL PROPERTIES
  - MELTING POINTS, VAPOR PRESSURES, CRITICAL CONSTANTS
  - PVT DATA, COMPRESSIBILITIES
  - DENSITY, VISCOSITY, SURFACE TENSION
  - HEAT CAPACITY, ENTHALPY, HEATS OF FUSION AND VAPORIZATION, FREE ENERGY, ENTROPY
  - THERMAL CONDUCTIVITY (LIQUID AND VAPOR), HEAT TRANSFER CORRELATIONS
- CHEMICAL PROPERTIES
  - COMPOSITIONS OF COMMERCIAL PRODUCTS
  - THERMAL DECOMPOSITION (PYROLYSIS) RATES AND MECHANISMS
  - DETAILED ANALYTICAL PROCEDURES FOR IMPURITIES AND DECOMPOSITION PRODUCTS
- SYSTEM PROPERTIES
  - PURIFICATION PROCEDURES AND MAKE-UP RATES
  - FOULING RATES, MECHANISM AND CONTROL
  - COMPATIBILITY WITH MATERIALS OF CONSTRUCTION

LOW TEMPERATURE FLAT-PLATE COLLECTOR SPACE/WATER HEATING

by

S. W. Moore

Los Alamos Scientific Laboratory

Los Alamos, New Mexico

LOW TEMPERATURE FLAT-PLATE COLLECTOR SPACE/WATER HEATING

Design Presentation

by

S. W. Moore
Los Alamos Scientific Laboratory
P. O. Box 1663, M/S 571
Los Alamos, NM 87545

ABSTRACT

Low temperature flat plate collector designs can take many different forms and make use of a variety of materials. Collectors can be liquid heaters, air heaters, heat-pipe heat exchanged, or a hybrid arrangement when combined with passive systems. They can be factory-manufactured modules, site assembly of factory-manufactured components, factory-manufactured into transportable housing, or completely site-constructed. Material selection for all components must be evaluated with respect to operating parameters, performance, durability, and above all, life-cycle costing.

INTRODUCTION

Solar collector design and development is at a point where there is a worldwide effort to study, develop and determine the performance of solar collectors and collector systems. Flat plate solar collector designs range from the more inexpensive plastics and general construction materials to the high thermal performance flat plates and evacuated tube collectors. Much effort, both commercial and government-supported, is being aimed at improving the thermal performance, durability, and reducing costs. All of these results must be carefully evaluated from a "cost of energy delivered to the end use" standpoint.

BASIC FLAT PLATE COLLECTOR DESIGN

Many types of solar collectors have been designed and built. At the low temperatures used for water or space heating, flat plate types work with reasonable efficiency and are relatively easy to construct.

The major functional parts of a collector are the absorber surface, coolant passages, cover glazing and back insulation as shown in Figure 1.

Collectors are designed to maximize absorption of solar radiation and minimize heat losses. The predominant heat loss mechanisms from the front face are by convection and radiation. Convection losses can be controlled by the use of transparent covers or by using convection suppression honeycombs or evacuated collectors. Radiation losses are sometimes reduced by means of a "selective" coating on the absorber surface which has a high absorptance for the solar spectrum and a low emittance for the infrared re-radiation spectrum. Other minor heat loss mechanisms are conduction to the collector backside and edge.

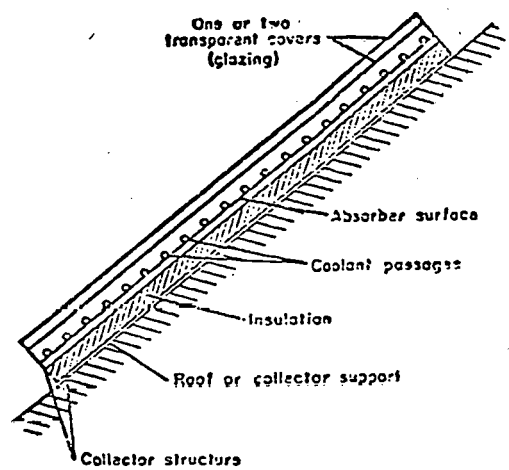


Fig. 1. Basic collector.

Some of the many variations in geometry are shown in Fig. 2. Not shown are the tubular non-concentrating type of collectors.

MAJOR DESIGN CONSIDERATIONS

Absorbers:
- Temperature capability
- Pressure
- Corrosion resistance
- Compatibility w/fluids and absorber coatings
- Fatigue and creep resistance
- Specific heat
- Thermal expansion
- Cost/Durability

*Work performed under the auspices of the U.S. Department of Energy, R&D Branch for Heating and Cooling, Office of the Assistant Secretary for Conservation and Solar Energy.

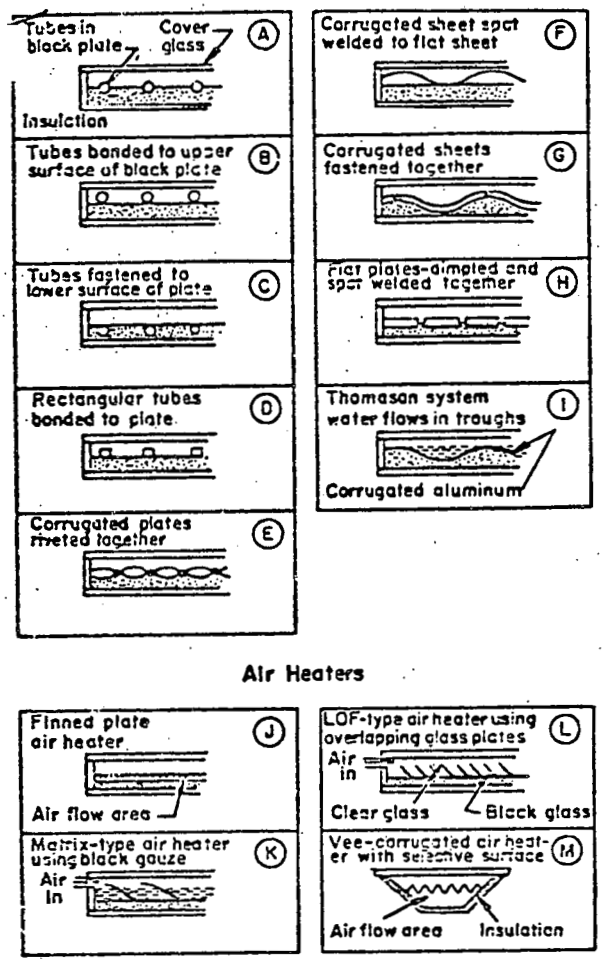


Fig. 2. Flat plate collector types.[1]

Absorber Coatings:
- Optical properties
- Temperature limits
- UV stability
- Moisture resistance
- Cost/Durability

Insulating Materials:
- Thermal Conductivity
- Density
- Temperature limit
- Coefficient of expansion
- Dimensional stability
- Fire and flashpoint
- Flame spread
- Smoke evolution
- Outgassing products
- Cost/Durability

Sealing Materials:
- Temperature limits
- Thermal conductivity
- Flammability
- Compatibility with mating components/fluids
- Elastic properties
- Adhesion thermal stability
- Cost/Durability

Glazing Materials:
- Hemispherical optical transmission
- Temperature capability and resistance to thermal gradients
- UV resistance
- Strength
- Impact properties
- Weight
- Abrasion resistance
- Moisture resistance
- Thermal expansion
- Cost/Durability

Fluids:
- Viscosity
- Temperature limit
- Specific heat
- Flash point
- Boiling point
- Freezing point
- Toxicity, fluid and combustion
- Volumetric expansion
- Density
- Cost/Durability

Examples of basic collector performance and operating limits as functions of varying properties are shown in Figs. 3 through 10 for the following model:[2]

Symbol	Description	Engineering Units	SI Units
QIN	Incident solar flux	300 BTU/hr ft^2	946 W/m^2
TAMB	Ambient temp.	40 °F	4°C
WCP	Flow rate x specific heat or fluid	10 BTU/hr °F ft^2	57 w/m^2°C
VEL	Wind velocity	2 mph	1 m/s
G	Number of glass panes	2	
K	Extinction coeff. of glass	0.8 in.$^{-1}$	31.5 m
t	Glass thickness	0.125 in./pane	3.2 mm
α	Surface absorptivity	.98	
ε	Surface emissivity	.89	
R_B	Back surface thermal resistance	12 hr ft^2 °F/BTU	2.1 m^2 °C/w

All results are based on the model derived by Hottel & Woertz.[3]

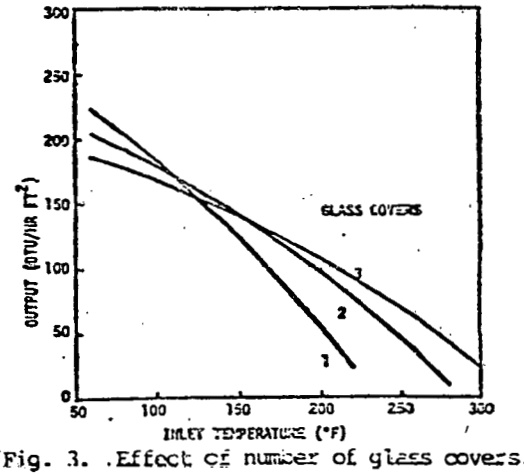


Fig. 3. Effect of number of glass covers.

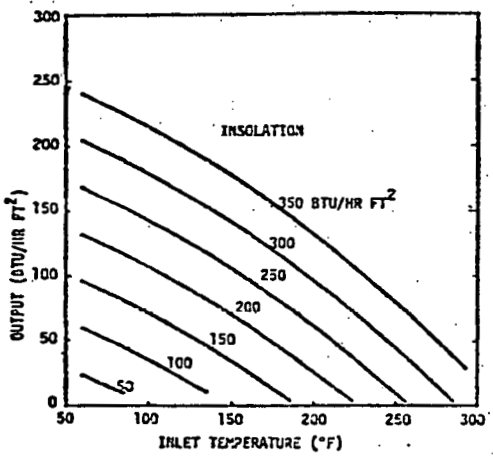


Fig. 4. Effect of insolation.

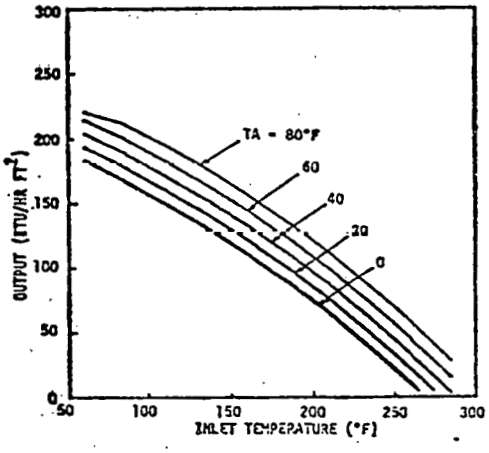


Fig. 5. Effect of ambient temperature.

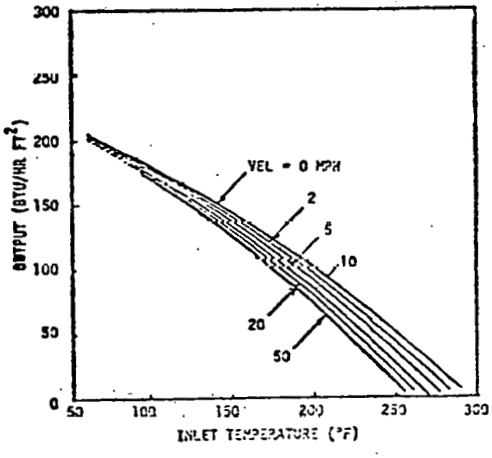


Fig. 6. Effect of wind velocity.

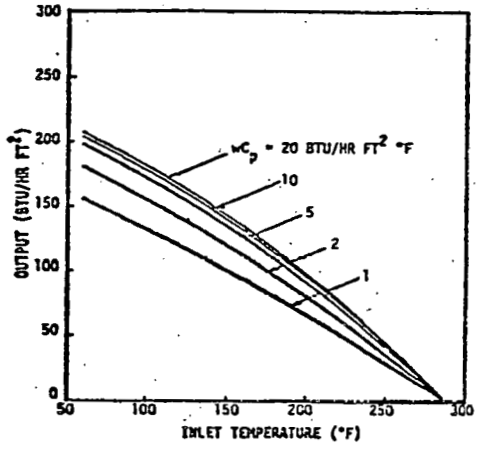


Fig. 7. Effect of collector flow rate.

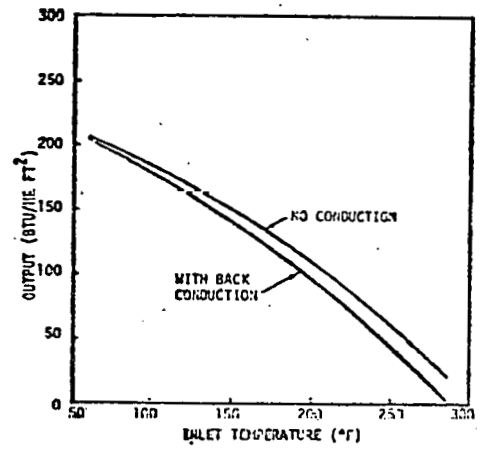


Fig. 8. Effect of back conduction.

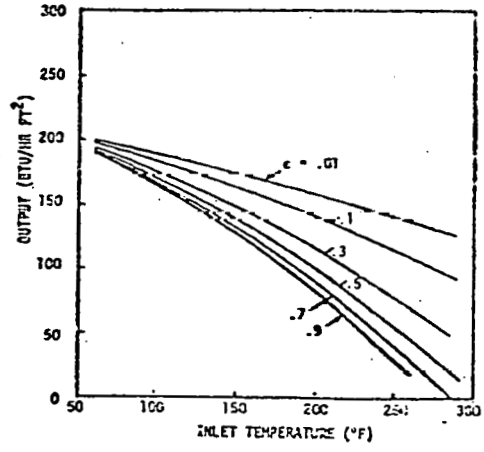


Fig. 9. Effect of emissivity ($\alpha = 0.9$).

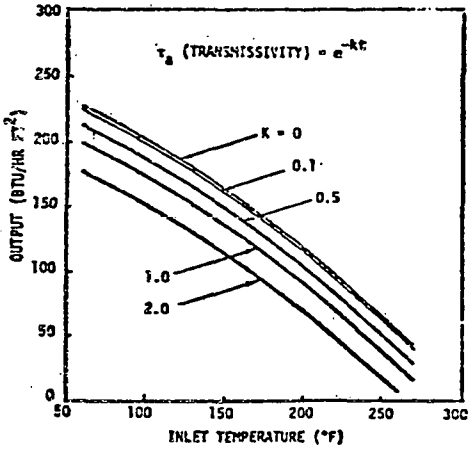


Fig. 10. Effect of glass absorption.

The preceding variations are representative of a specific type of collector and can vary depending upon the actual type and geometry. They do, however, represent the wide range of performances and temperatures dependent upon the basic design and properties selected.

SOLAR ASSESSMENT[4]

In order to assess in detail the state of the technology for solar heating and cooling of buildings, five 2-day meetings were held during December, 1975. Experts were recruited for these meetings from industry both large and small, universities, and government laboratories. The meeting subjects were solar collectors, thermal storage, air conditioning and heat pumps, systems and controls, and non-engineering aspects of solar energy. The meetings based on each topic, discussed the details of the state of the art, the problem areas, and the objectives of necessary research and development.

Solar collectors' needs, materials problems, material capabilities and objectives were established. Results of this assessment were factored into the National Plan for Research and Development in Solar Heating and Cooling[5] and established the framework for the PRDA and RFP solicitations.

DOE COLLECTOR MATERIALS R&D PROGRAMS[6]

There are presently 32 projects funded by DOE specifically focused on evaluating or developing new materials for solar collectors. These projects fall into the following basic six categories:

Development of Selective Surfaces
Cover Plate Study and Development
Coolants and Corrosion
Sealants and Breathing
Freeze Protection
Exposure Testing

These programs, which will be of great assistance in the design of collectors by providing better materials and a greater understanding of solar materials are as follows.

DEVELOPMENT OF SELECTIVE SURFACES

- Berry Solar Products
  "Commercial selective surfaces applicable to copper, aluminum, and stainless steel, their cost effective improvement and evaluation of potential durability in solar absorbers."
- De Soto, Inc.
  "Solar selective absorber coatings by the electrodeposition of paint."
- Honeywell Systems & Research Center
  "Selective paint and black chrome coatings development."
- Lockheed Missiles & Space Company
  "Study of metal/metal oxide and other selective surfaces, coating techniques, stability, optical performance and costs."

COVER PLATES

Honeycomb

- Battelle Pacific Northwest Labs
  "Development of improved cover plates for solar collectors."
- University of California
  "Transparent glass honeycomb for energy loss control."
- Lockheed Missiles and Space Company
  "Optimization of thin film transparent plastic honeycomb covered flat-plate solar collector."

Anti-Reflectance and I.R. Coatings

- General Electric
  "A.R. and I.R. coatings on glass."
- Honeywell, Inc.
  Selective I.R. reflective coatings development", and "Low-cost solar anti-reflection coatings."
- Hughes Aircraft Company
  "Non-glass glazings and surface coatings."
- Research Triangle Institute
  "Non-glass glazings."
- Springborn Laboratories
  "Study of non-glass glazings, surface coatings and UV protective coatings for plastic glazing."
- Tufts University
  "Studies for predictably modifying the optical constants of doped indium oxide films for solar energy applications."

- University of Wisconsin
  "Polymer surface coatings for down-conversion of UV radiation and inhibition."

Glazing Protection

- Altas Corporation
  "Development of cost effective techniques and concepts for the protection of glazings against breakage caused by hail, vandals or thermal stresses."

COOLANTS AND CORROSION

- Battelle Memorial Institute
  "Study corrosion processes of coolants and interaction of fluids, additives and systems."

- Dow Corning Corporation
  "Development of superior liquid coolants."

- E I C Corporation
  "Corrosion protection of solar-collector heat exchangers with electro-chemically deposited films."

- University of Florida
  "Vegetable oils: a superior liquid coolant."

- Giner Corporation
  "Aluminum corrosion studies for solar heat collectors."

- Monsanto Research Corporation
  "Study of superior liquid coolants."

INSULATING MATERIALS

- Dow Corning Corporation
  "Development of improved insulation materials."

- Solar, IHC
  "Development of polyimide materials for use in solar energy systems."

- Versar
  "Study and survey of thermal insulating materials."

SEALANTS & BREATHING

- Products Research & Chemical Corporation
  "Development of 400°F resistant sealants for flat plate solar collector construction and installation."

- Westinghouse Electric Corporation.
  "Study of collector sealants and collector breathing."

- Ametek, Inc.
  "Development of improved breathing control techniques.

FREEZE PROTECTION

- Polyset, Inc.
  "Development of a freeze-tolerant solar water heater using cross-linked polyethylene."

EXPOSURE TESTING

- I I T Research Institute
  "Exposure testing and evaluation of solar collector materials."

One of the major program outgrowths, besides the basic materials development, will be the dissemination of information in the form of User Handbooks.

COLLECTOR PROBLEM AREAS

Many people have begun looking at collector systems which have been operational for some time and have published their findings. Of these, Skoda and Masters[7], DOE (NASA, ASHRAE and UAH)[8] and CASH[9] have provided a good compilation of some of the pitfalls to avoid.

REFERENCES

1. J. E. Yellott, "Solar Energy Utilization for Heating and Cooling," ASHRAE Handbook, 1974.

2. J. D. Balcomb, J. C. Hedstrom, and S. W. Moore, "Research on Integrated Solar Collector Roof Structures," LA-5859-PR, Progress Report, Jan., 1975, Los Alamos Scientific Laboratory.

3. H. Hottel and B. Woertz, Paper No. 64, p. 91. Transactions of the ASME, Feb., 1942.

4. J. D. Balcomb and J. E. Perry, "Assessment of Solar Heating and Cooling Technology," LA-6379-MS, Informal Report, Los Alamos Scientific Laboratory.

5. "National Program Plan for Research and Development in Solar Heating and Cooling for Buildings, Agricultural and Industrial Applications," DOE/CS-0008, U.S. Department of Energy, August, 1978.

6. S. W. Moore, "Collector Materials R&D Overview, 3rd Annual Solar Heating and Cooling R&D Contractors Meeting, Los Alamos Scientific Laboratory, September, 1978.

7. L. F. Skoda and L. W. Masters, "Solar Energy Systems - Survey of Materials Performance," NBSIR 77-1314, October, 1977.

8. Mitchell Cash, "Hardware Problems Encountered in Solar Heating and Cooling Systems," DOE/NASA TM-78172, May, 1978.

9. "Solar Heating and Cooling Project Experiences Handbook," PRELIMINARY ISSUE, Sponsored by DOE, July, 1978.

LOW TEMPERATURE FLAT-PLATE COLLECTOR

SPACE/WATER HEATING

Viewgraphs Presented

by

S. W. Moore

Los Alamos Scientific Laboratory

Los Alamos, New Mexico

RELIABILITY OF MATERIALS

FOR SOLAR ENERGY SYSTEMS WORKSHOP

Denver, Colorado

December 18-20, 1978

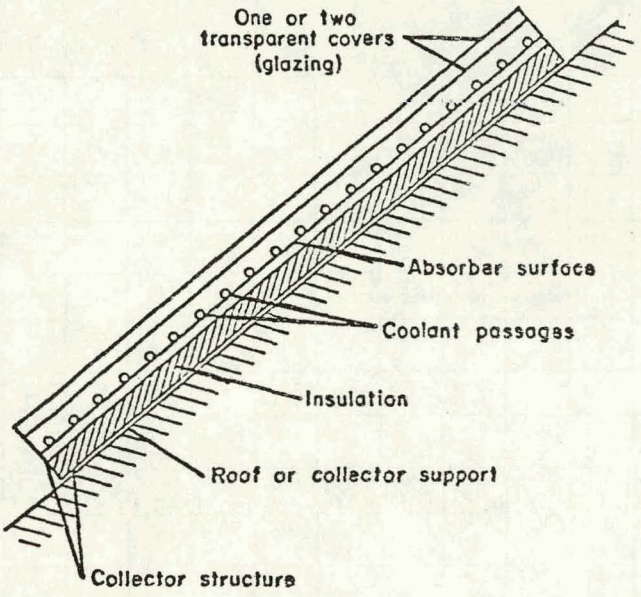
PRESENTATION MATERIAL

FLAT PLATE COLLECTOR

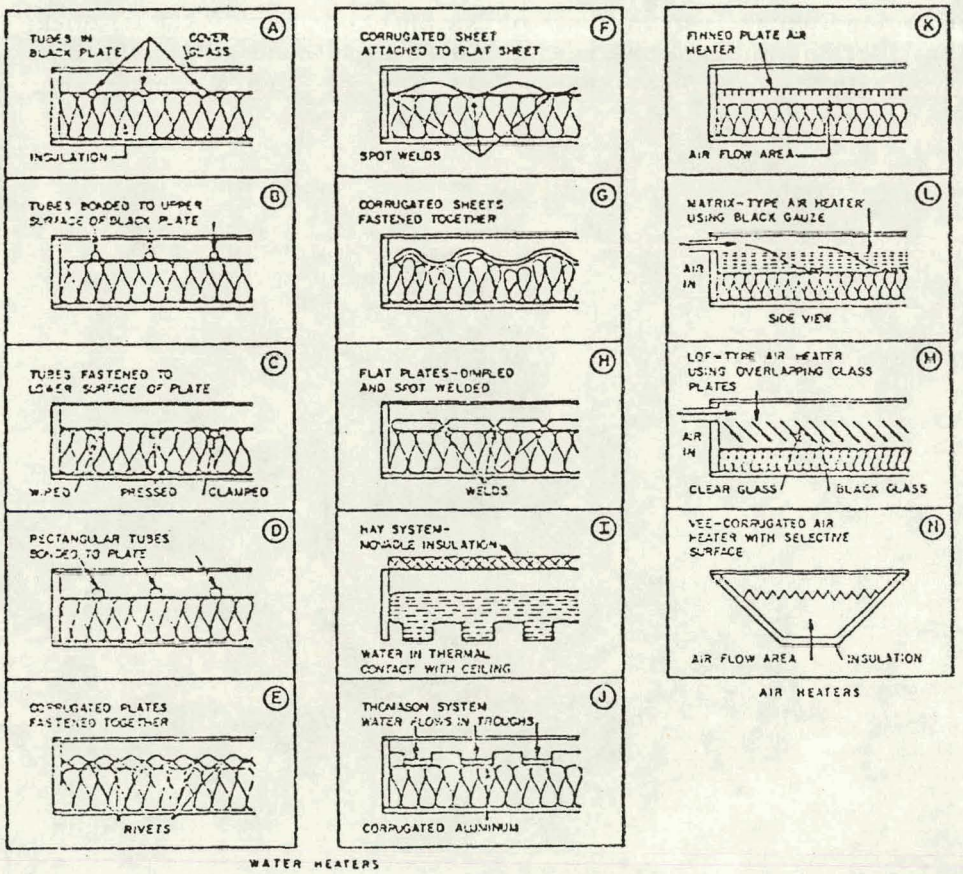
DESIGN PRESENTATION

S. W. Moore

Los Alamos Scientific Laboratory



COLLECTOR TYPES



This potpourri of collector types is taken from Chapter 59 of the ASHRAE Handbook, 1974, "Solar Energy Utilization for Heating and Cooling," by John I. Yellott

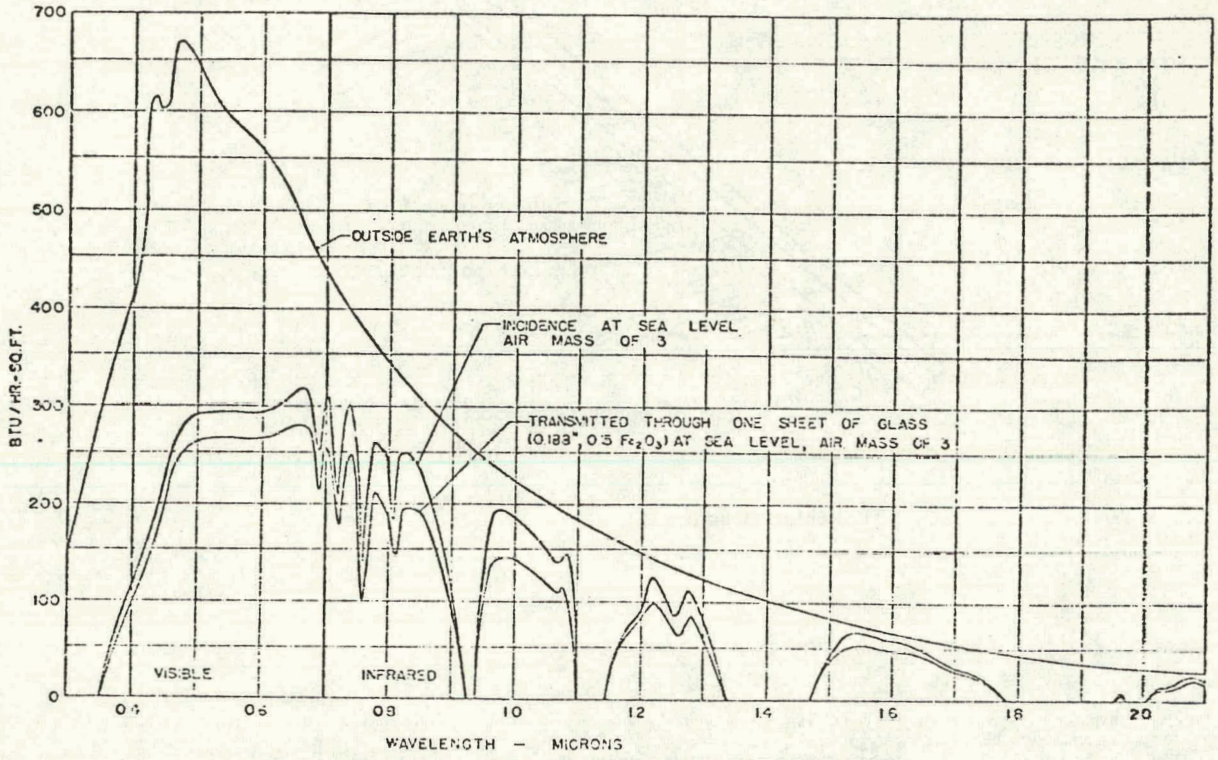


Figure 15. Curves Showing Solar Energy Transmittance of One Sheet of Glass (0.188 in. thick, 0.15 Fe_2O_3) at Sea Level, for Solar Radiation Transmitted Through Standard Air Mass of 3. Curves are Compared with Standard Solar Energy Curve Outside Earth's Atmosphere.

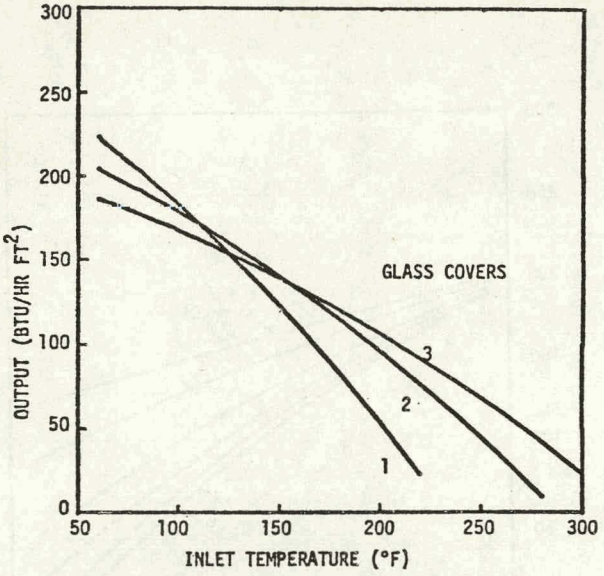


Fig. 5. Effect of number of glass covers.

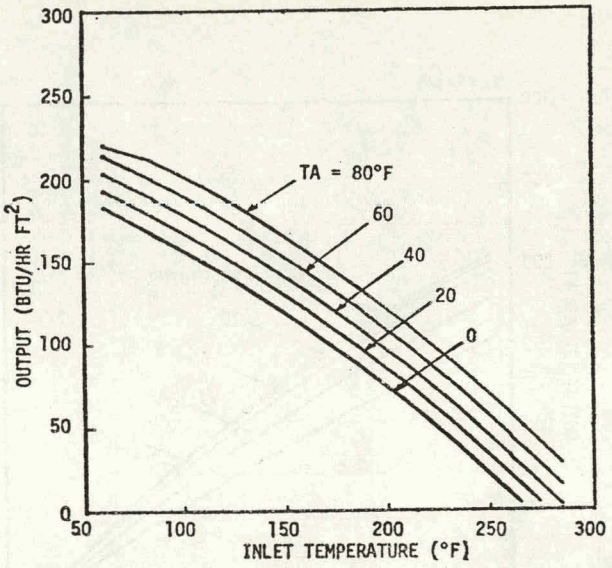


Fig. 7. Effect of ambient temperature.

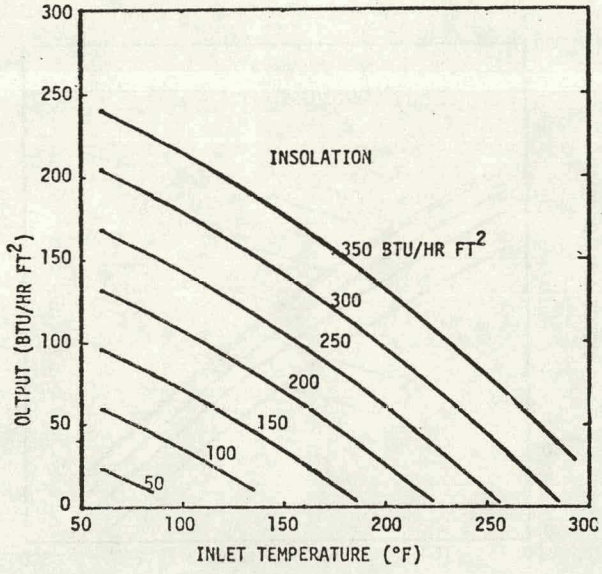


Fig. 6. Effect of insolation.

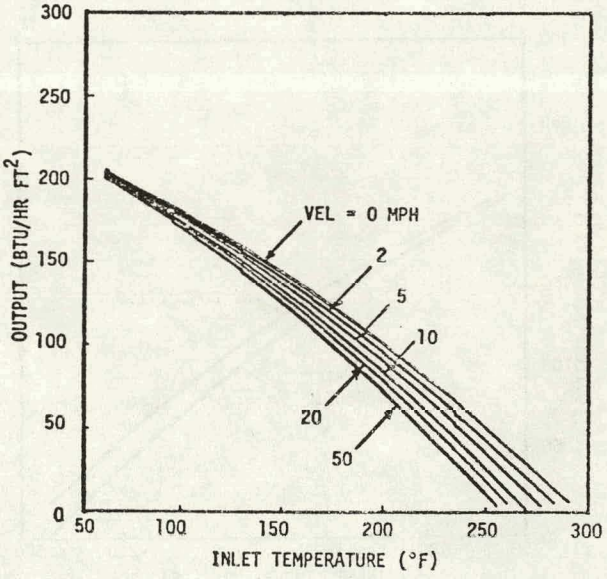


Fig. 8. Effect of wind velocity.

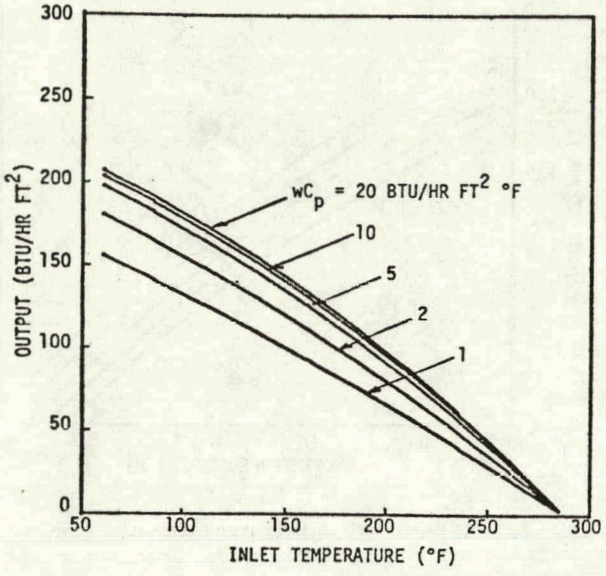


Fig. 9. Effect of collector flow rate.

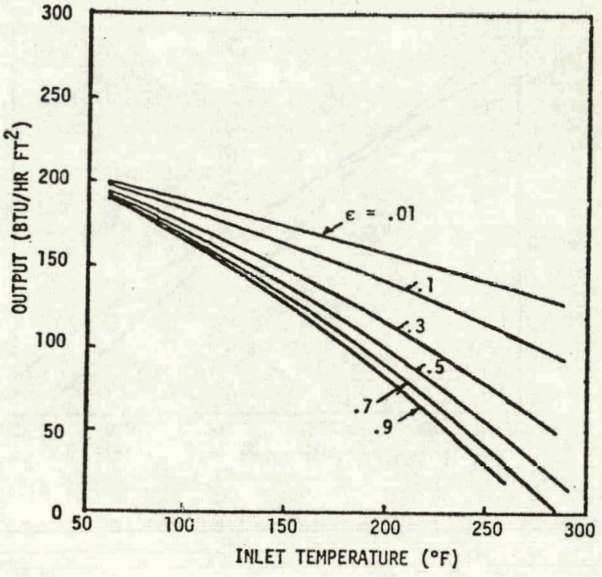


Fig. 11. Effect of emissivity (α = 0.9).

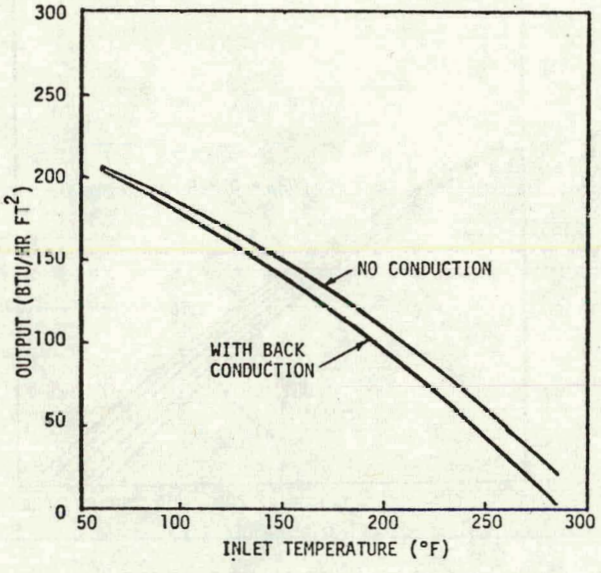


Fig. 10. Effect of back conduction.

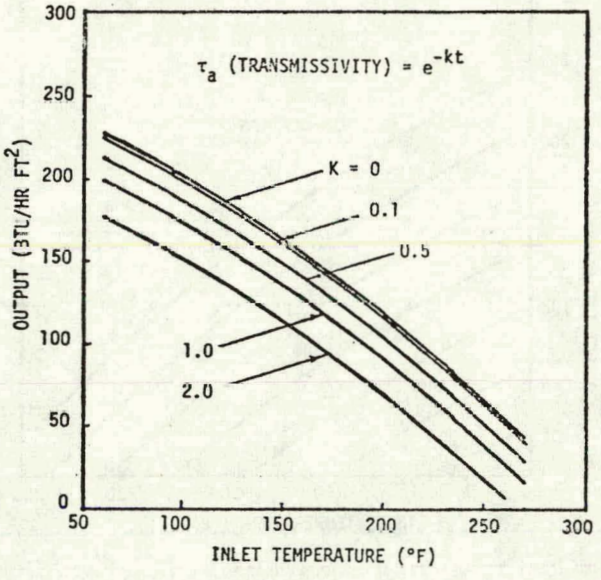
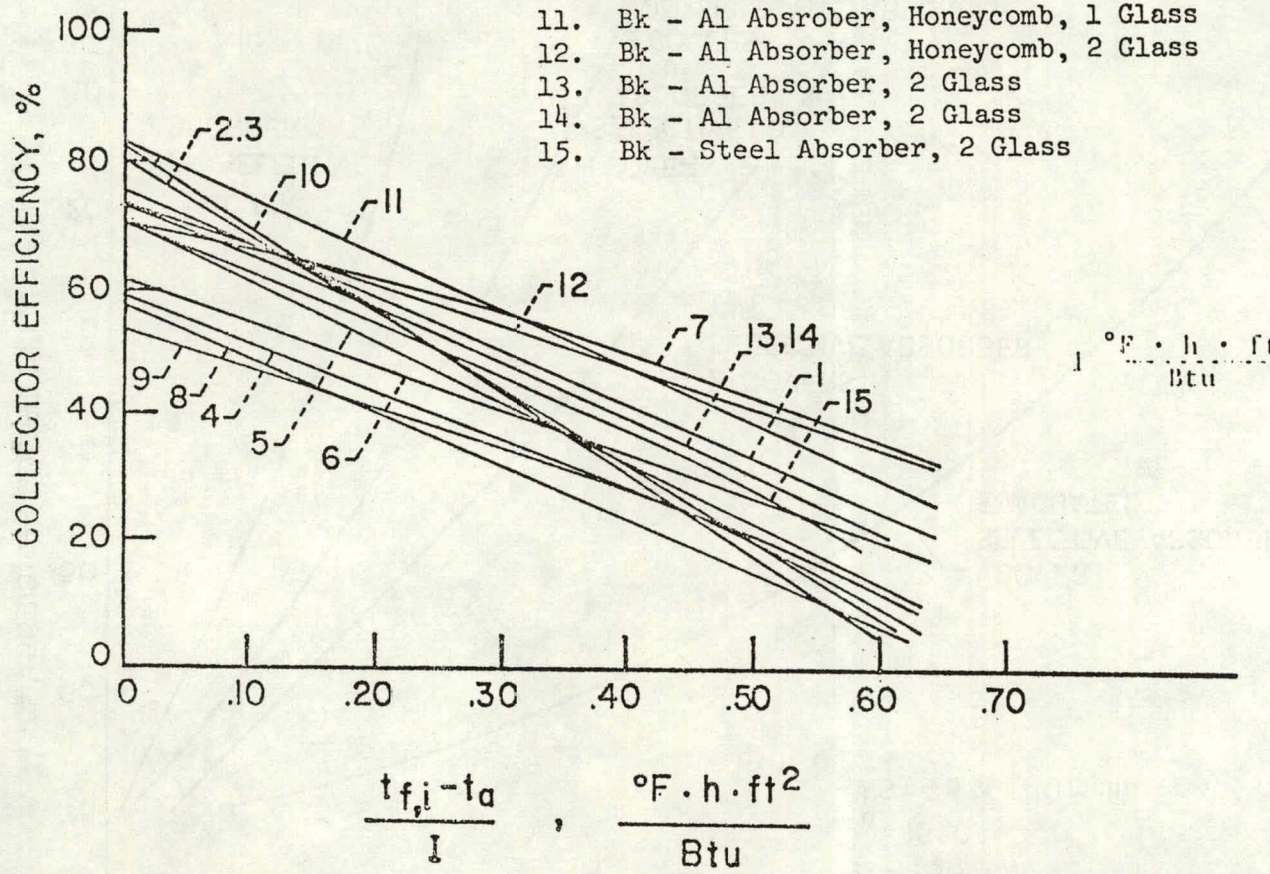


Fig. 12. Effect of glass absorption.

1. Bk-Cu Absorber, 2 Glass
2. CuO-Cu Absorber, 1 Glass
3. CuO-Cu Absorber, Honeycomb, 1 Glass
4. CuO-Cu Absorber, 2 Glass
5. Bk Ni - Al Absorber, 1 Glass
6. Bk Ni - Al Absorber, 2 Glass
7. Bk Ni - Al Absrober, 2 Glass
8. Bk Ni - Al Absorber, 1 Tedlar
9. Bk Ni - Al Absorber, 2 Tedlar
10. Bk - Al Absorber, 1 Glass
11. Bk - Al Absrober, Honeycomb, 1 Glass
12. Bk - Al Absorber, Honeycomb, 2 Glass
13. Bk - Al Absorber, 2 Glass
14. Bk - Al Absorber, 2 Glass
15. Bk - Steel Absorber, 2 Glass



$$1 \frac{°F \cdot h \cdot ft^2}{Btu} = 0.176 \frac{°C \cdot m^2}{W}$$

Figure 31 Efficiency Curve for Fifteen Liquid-Heating Solar Collectors Determined using the Indoor Test Facility at the NASA Lewis Research Center [29]

Ref: NBS TECHNICAL NOTE 899

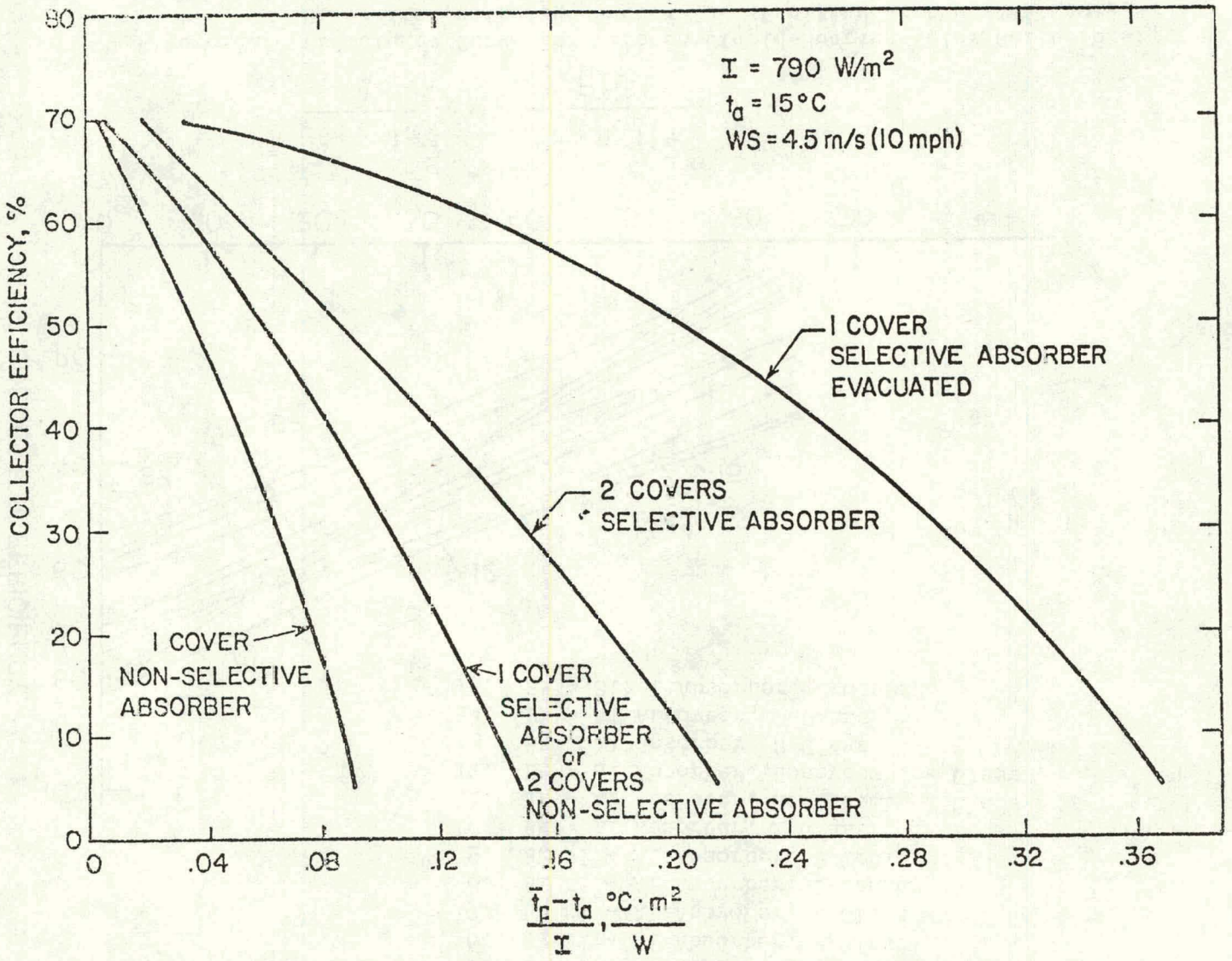


Figure 47 Efficiency Curves for Flat-Plate Solar Collectors of Various Designs

Ref: NBS TECHNICAL NOTE 899

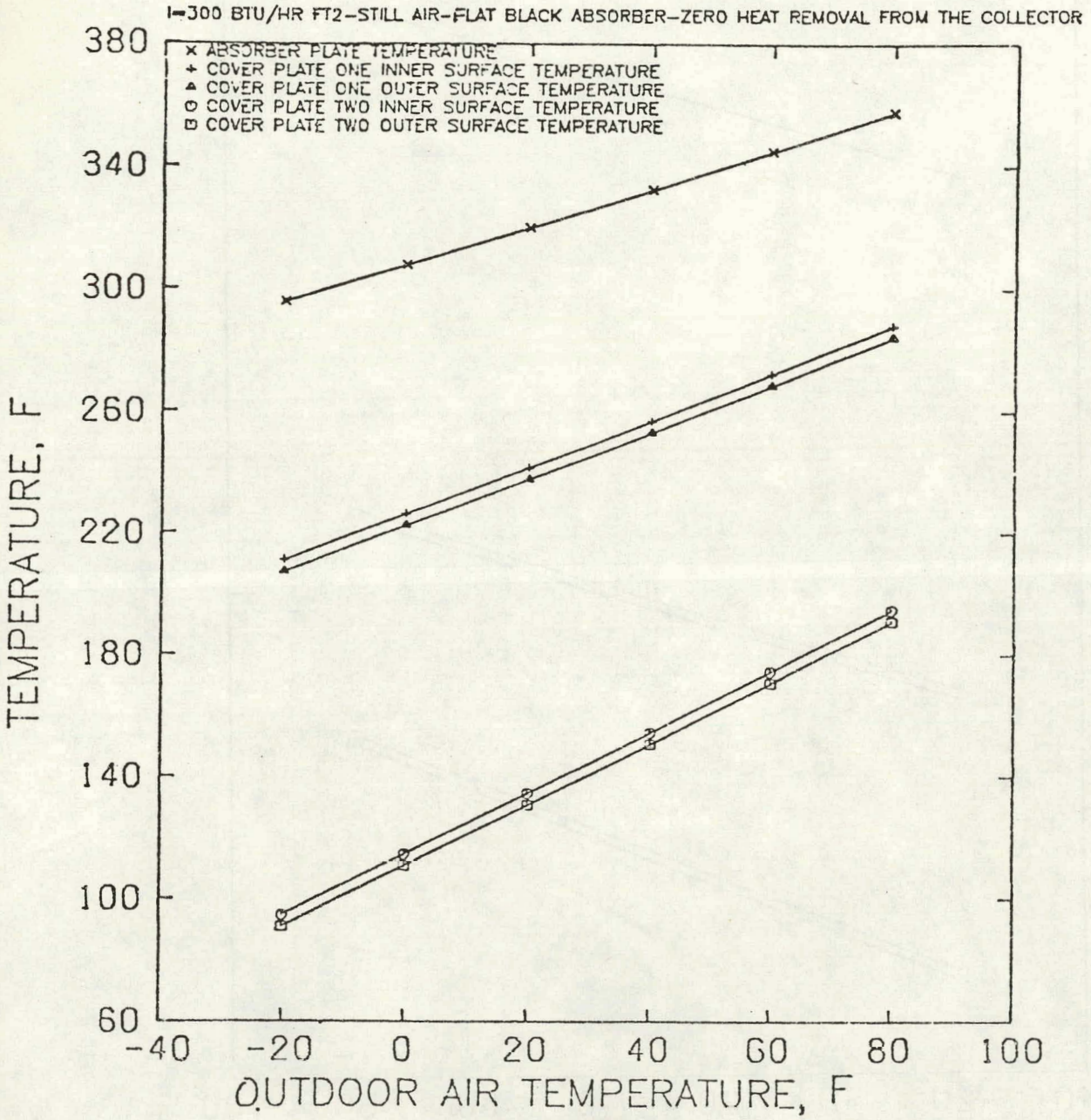


Figure A-1. Temperatures at Various Locations in a Collector with a Flat Black Absorber and Two Glass Cover Plates (Absorptivity = 0.9, Emissivity = 0.9, I = 300 BTU/Hr. ft.^{2})

Re- NBS/HUD Interim Performance Criteria for Solar Heating and Combined Heating/Cooling Systems and Dwellings

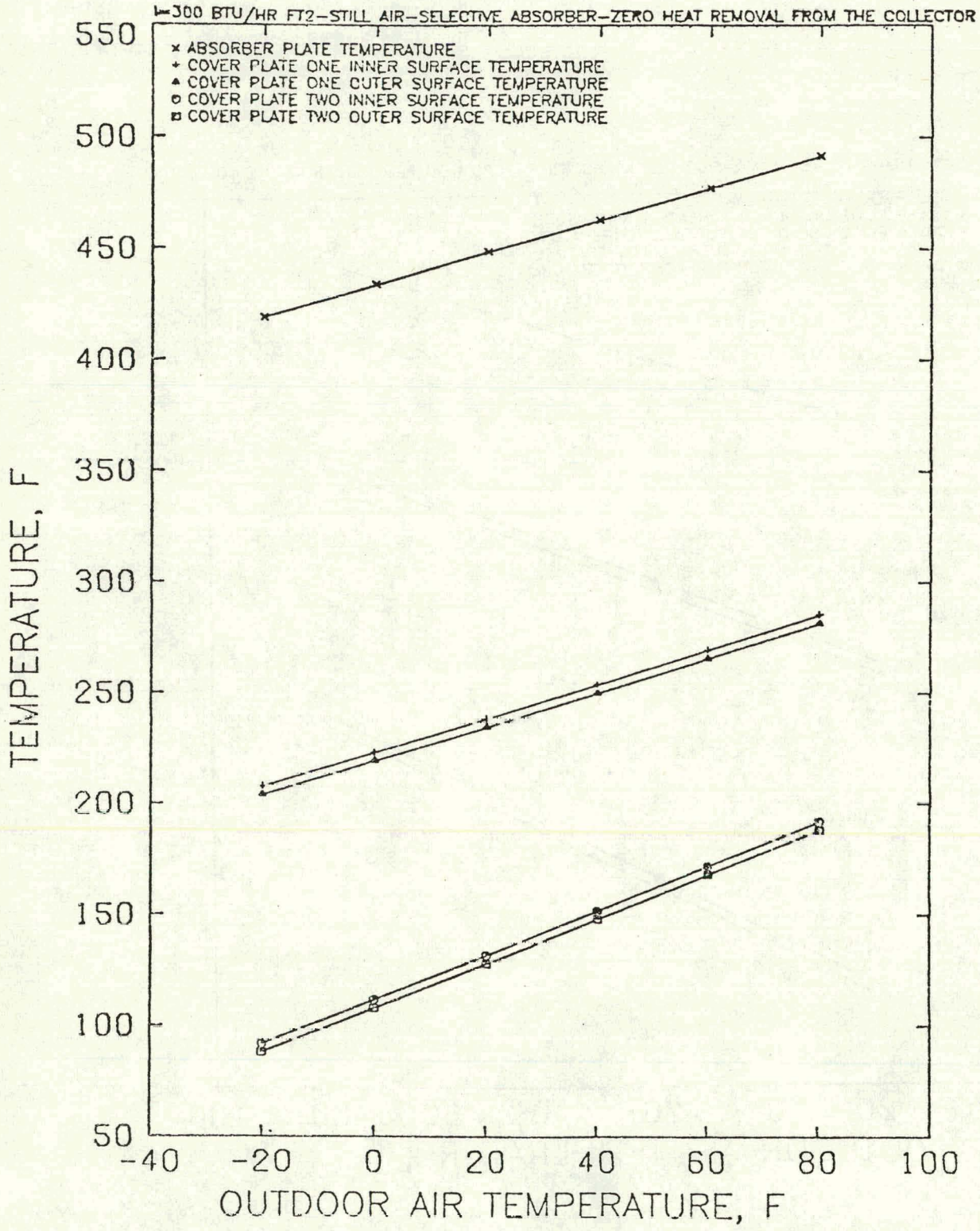
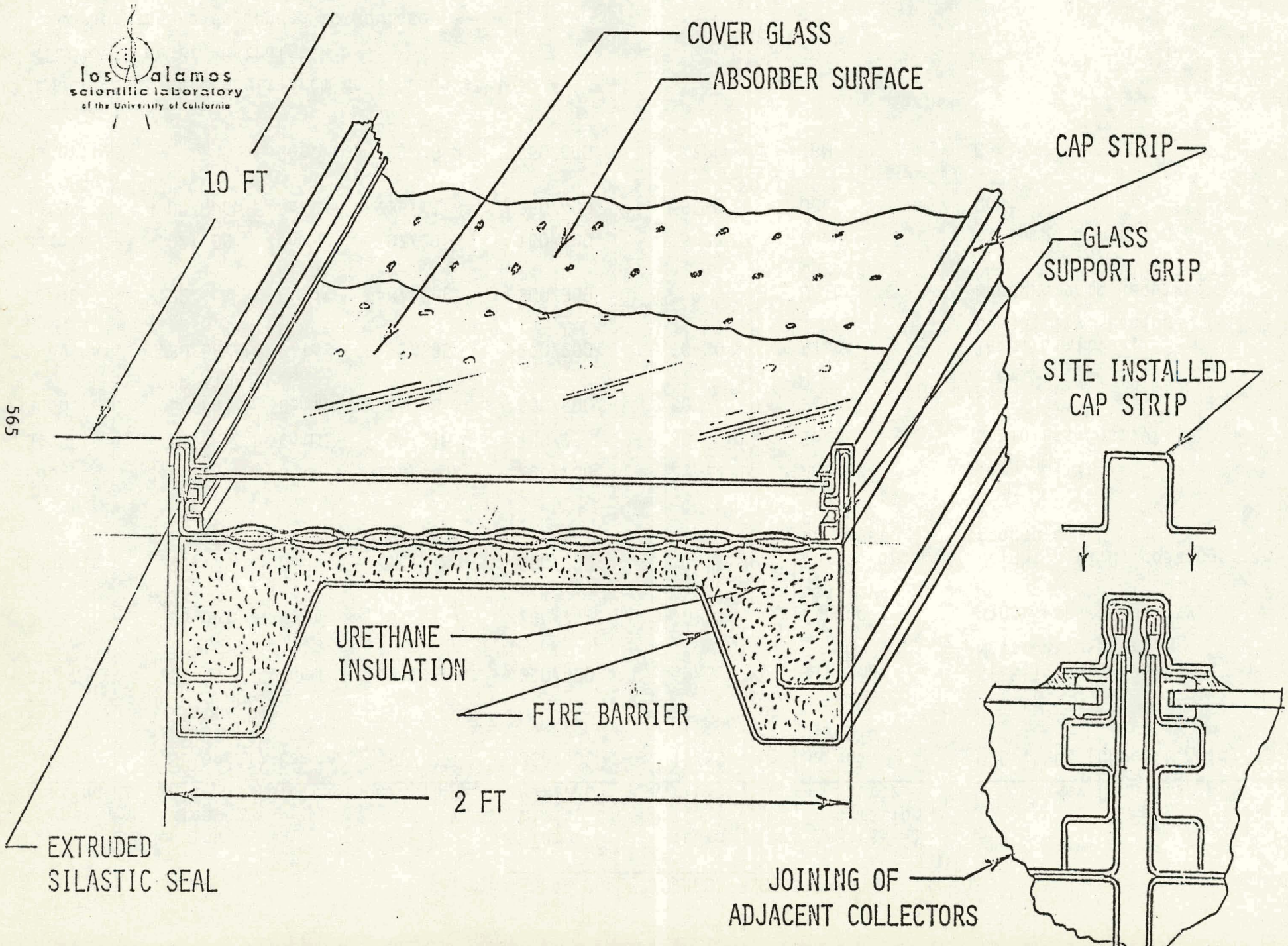


Figure A-3 Temperatures at Various Locations in a Collector with a Selective Absorber and Two Glass Cover Plates (Absorptivity = 0.9, Emissivity = 0.1, I = 300 BTU/Hr. ft.^{2})

Ref: NBS/HUD Interim Performance Criteria for Solar Heating and Combined Heating/Cooling Systems and Dwellings

SOLAR COLLECTOR DETAILS



SOLAR COLLECTOR COATINGS

Type Coating	Coating Price $/ft^2	Status	α/ε 150°C	Temp. Limit(°C) Air/Vac.	Years Durability Air/Vac.	Additional Information Source	Key Problems
Bl. Cr.	1.95 on Al) 1.55 on Fe)* 1.25 on Cu)	Comm.	.96/.12	350/400	15/30	Harshaw Olympic	Q.C., EPA (Chromic Acid)
Bl. Ni.	.55	Comm.	.9 /.05	350/400	0/30	Mirromet	Stability--Degrades in Moist Atmosphere
CuO	.25 on Cu	Comm.	.9/ .1	200/?	10+/?	Ethone Beasley	High Temp. Stability
Enamels	.25-.75	Comm.	95+/.85	500/500	∞	Ferro, Porc. En. Inst. Pemco	Weight, (I.R. coatings can reduce ε
PbO_2	> 2.00	Comm.	.98/.30	200/200	20/?	Ametek	Temp. Limit
St. Stl.	.20**	Comm.	.9 /.16	150/?	30	Inco	Stainless Costly?
Anod. Al.	.50 batch (one side)	Comm.	.95/.8	500/500	50	Permalloy	ε
Conv. Al.	.30 batch	Pilot Plant	.93/.35	200/200	10-20	Alcoa	Temp. Limit, ε, Durability, Fading
Carbon***	.02	Pilot Plant	≥Bl.Cr(?)	500/300	?	Union Carbide	Measurements Required
Paint	.02/.50	Comm	.97/.9	150/200	5-20	Many	ε, Temp. Limit
Inter-ference	4.00/Quan 100,000	Res. +	.95/.?	350/400	5/30	OCLI	Cost
Dendrite	?	Res.	.99/.3 @ 550°C	250/600	?	IBM	Cost

*Lower costs can result from continuous strip.

**F.O.B. Sidney, Australia

***Carbon spheroids bonded to surface.

Table 4

SEALANTS: MANUFACTURERS AND PROPERTIES

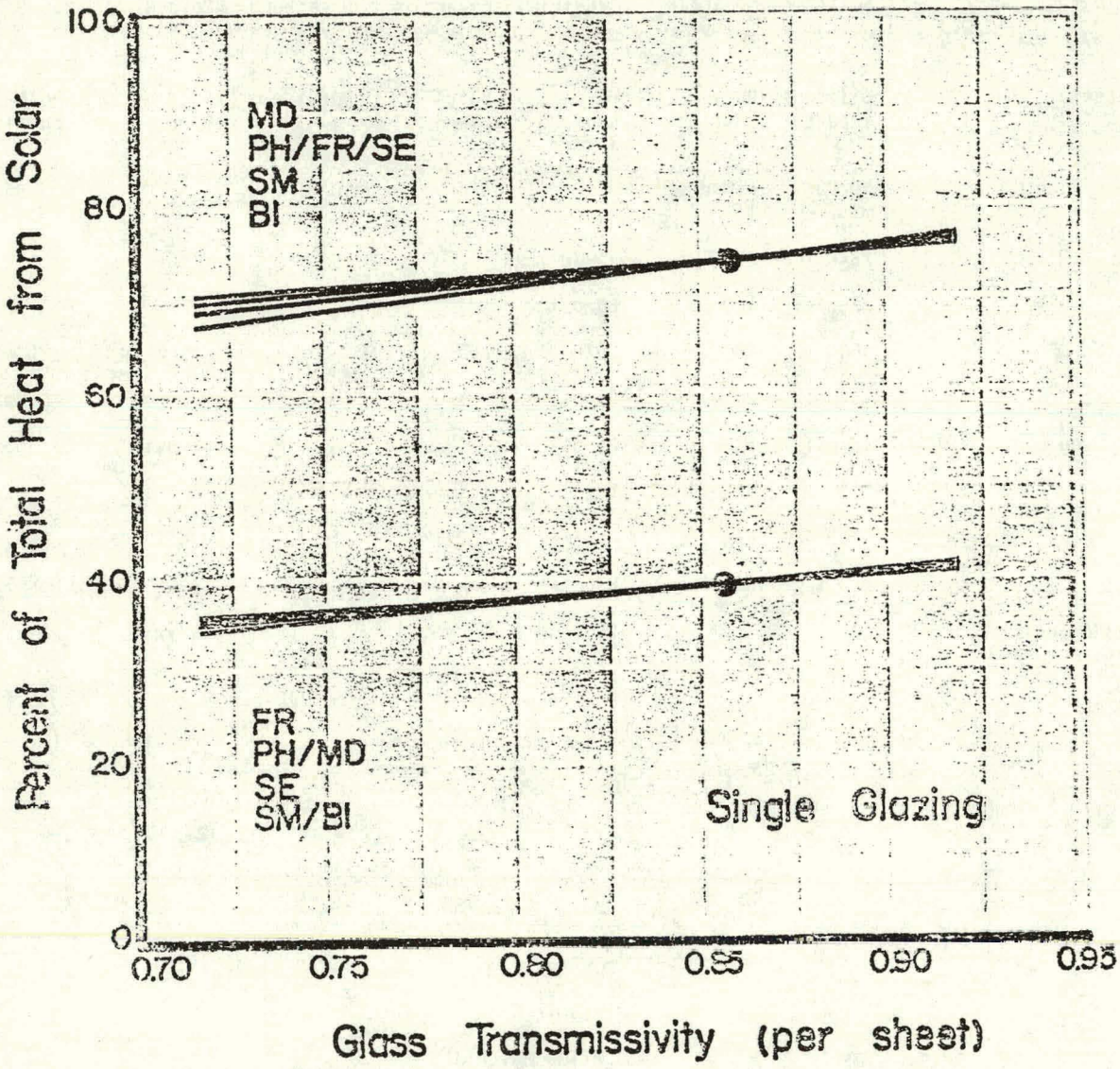
Manufacturer	Dow Corning	Novagard	Thorson	Novagard	Novagard	Novagard	Pecora
Product Name	Silastic 732	Novacalk 600	TPC-101	Novacalk 400	Novatherm 415 (Hot Melt)	Novacalk 444	GC-9
Base Material	Silicone 1 part	Poly-sulfide	Poly-sulfide 1 part	Butyl Blend	Butyl	Butyl Blend	Poly-sulfide
Tack Free Time	10-20 min.	4-8 hrs.		1 hr.	10 min.	1 hr.	to 96 hrs.
Hardness	25A	25A	20-30A		30A		35A
Tensile	275 psi	140	60 psi				NA
Elongation	450%	800%	85%	25%		25%	350%
Peel-Glass	15 ppi	20 psi	25 psi		10-12 psi		10 ppi
Peel-Aluminum	15 ppi	22 psi	25 psi			20 psi	20 ppi
Shrinkage		None	None	15% max.	None	15% max.	3% max.
Service Temp., ^{o}F	-100+450	-40+200	-60+212	-20+180	-100+325	-20+180	-20+180
Viscosity	Non Sag	Non Sag	Non Sag	Non Sag	Non Sag	Non Sag	Non Sag
Life Expectancy (yrs) (per Manufacturer)			20 yrs	20 yrs		20 yrs	10-20 yrs
Cost/Gallon	$25.00		$17.50		$13.00		$19.00

28

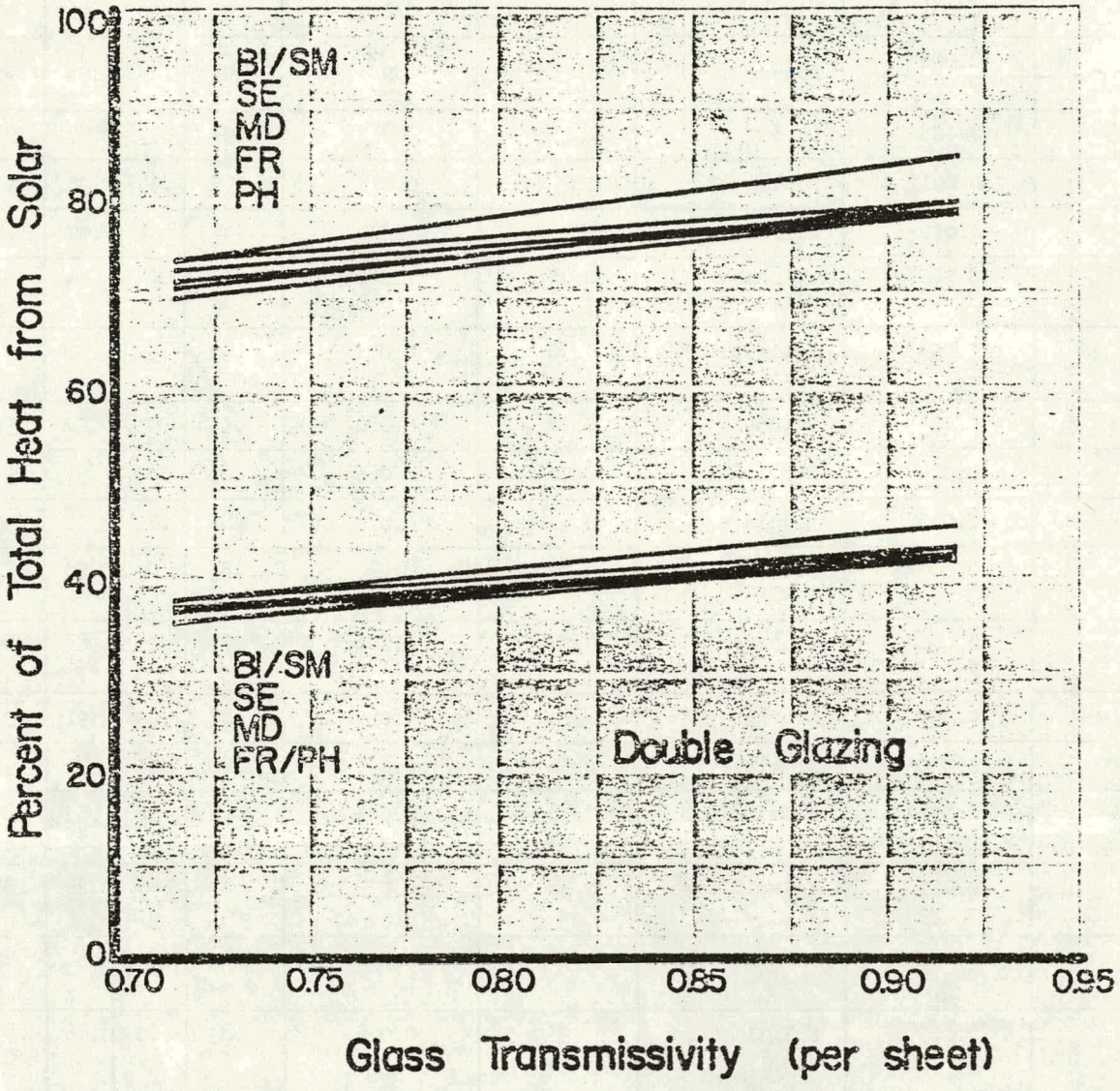
Table 5

INSULATION MATERIALS

Material	Density (lb/ft^3)	K at $200^{o}F$ (BTU-in./ ft^2-^{o}F-hr	Upper Temp. Limit (^{o}F)	Outgassing Temp. (^{o}F)	Cost (in qty) ($/Board Foot)
Fiberglass with Organic Binder	0.6	.41	350	340	.05
	1.0	.35	350		.08
	1.5	.31	350		.12
	3.0	.30	350		.16
Fiberglass - No binder	1.5	.31	850	> 400	.32
Ceramic Fiber Blanket	3.0	.40 at $400^{o}F$	2300	> 400	.59
Mineral Fiber Blanket	10.0	.31	1200	> 400	.12
Calcium Silicate	13.0	.38	1200	> 400	.60
Urea-Formaldehyde Foam	0.7	.20 at $75^{o}F$	210	280	.04
Urethane Foam	2-4	.20	250-400	350	.15-.30



Ref: ERDA's Pacific Regional Solar Heating Handbook



Ref: ERDA s Pacific Regional Solar Heating Handbook

HEMISPHERICAL SOLAR TRANSMITTANCE

Material	Thickness	Supplier	Cutoff Wavelength μm	Hemis. Reflectance	Hemis. Solar Transmittance m*=0	m=1	m=2	m=3	m=4
Teflon 100 C	0.001"	Dupont	0.25<	0.031	.96	.96	.96	.96	
Teflon 200 C 300 C	0.002" 0.003"	Dupont	0.25<	NM†	.95	.95	.95	.95	.95
Teflon 500 C	0.005"	Dupont	0.25<	NM	.94	.94	.94	.94	.94
Teflon 100 A	0.001"	Dupont	0.25<	0.035	.95	.95	.95	.95	.95
Teflon 1000 A	0.010"	Dupont	0.25<	NM	.94	.94	.94	.94	.94
Aclar #22A	0.002"	Rainhart; Allied Chem.	0.25<	0.060	.94	.94	.94	.94	.94
Corning Ultra-microsheet	0.0045"	Butler; Corning	0.30	0.071	.91	.92	.92	.92	.92
Tedlar, Polished	0.004"	Dupont	0.30	0.080	.91	.91	.92	.92	.92
Tedlar, Unpolished	0.004"	Dupont	0.30	0.065	.89	.90	.91	.91	.91
Rhom-Haas Korad C	0.003"	Brumleve	0.38	0.070	.86	.89	.90	.90	.91
Rhom-Haas Korad A, Std. Clear	0.003"	Brumleve	0.38	0.082	.85	.87	.89	.89	.90
Rhom-Haas Korad A, Std. Clear	0.006"	Brumleve	0.38	0.088	.84	.86	.88	.89	.89
Rhom-Haas Exp 55D-62A	0.002"	Brumleve	0.38	0.075	.87	.90	.91	.91	.92
Rhom-Haas Exp 55D-62A	0.010"	Brumleve	0.30	0.070	.90	.91	.91	.91	.91
Filon A748 Tedlar Coated	0.028"	Filon Corp.	0.38	0.082	.82	.84	.85	.86	.86
Kalwall Sunlite Regular	0.025"	Kalwall Corp.	0.38	0.079	.83	.85	.86	.86	.87
Kalwall Sunlite Regular	0.040"	Kalwall Corp.	0.38	0.079	.81	.83	.84	.84	.85
Kalwall Sunlite Premium	0.025"	Kalwall Corp.	0.38	0.078	.83	.85	.86	.87	.87
Kalwall Sunlite Premium	0.040"	Kalwall Corp.	0.38	0.087	.77	.79	.80	.80	.80
Swedlow Continuous Cast Acrylic	0.076"	Swedlow Corp.	0.38	0.070	.83	.86	.87	.88	.88
Swedlow Continuous Cast Acrylic	0.103"	Swedlow Corp.	0.38	0.070	.84	.87	.88	.88	.88
Swedlow Coated Acrylic (Cell Cast)	0.273"	Swedlow Corp.	0.38	0.058	.80	.85	.86	.87	.87
Acrylic Safety Glazing ANSIZ 97.1-1966.100 U	0.224	Sandia Stores	0.35	0.068	.83	.86	.86	.87	.86
Lucite 147	0.120"	Dupont	0.38	NM	.81	.86	.87	.87	.87
Mylar D	0.010"	Dupont	0.33	0.112	.84	.86	.86	.86	.86
Mylar A	0.002"	Dupont	0.32	0.13	.82	.83	.84	.84	.89
Mylar A	0.005"	Dupont	0.35	0.19	.74	.76	.77	.77	

† NM = Not Measured;

* m = effective air mass for the solar spectral irradiance.

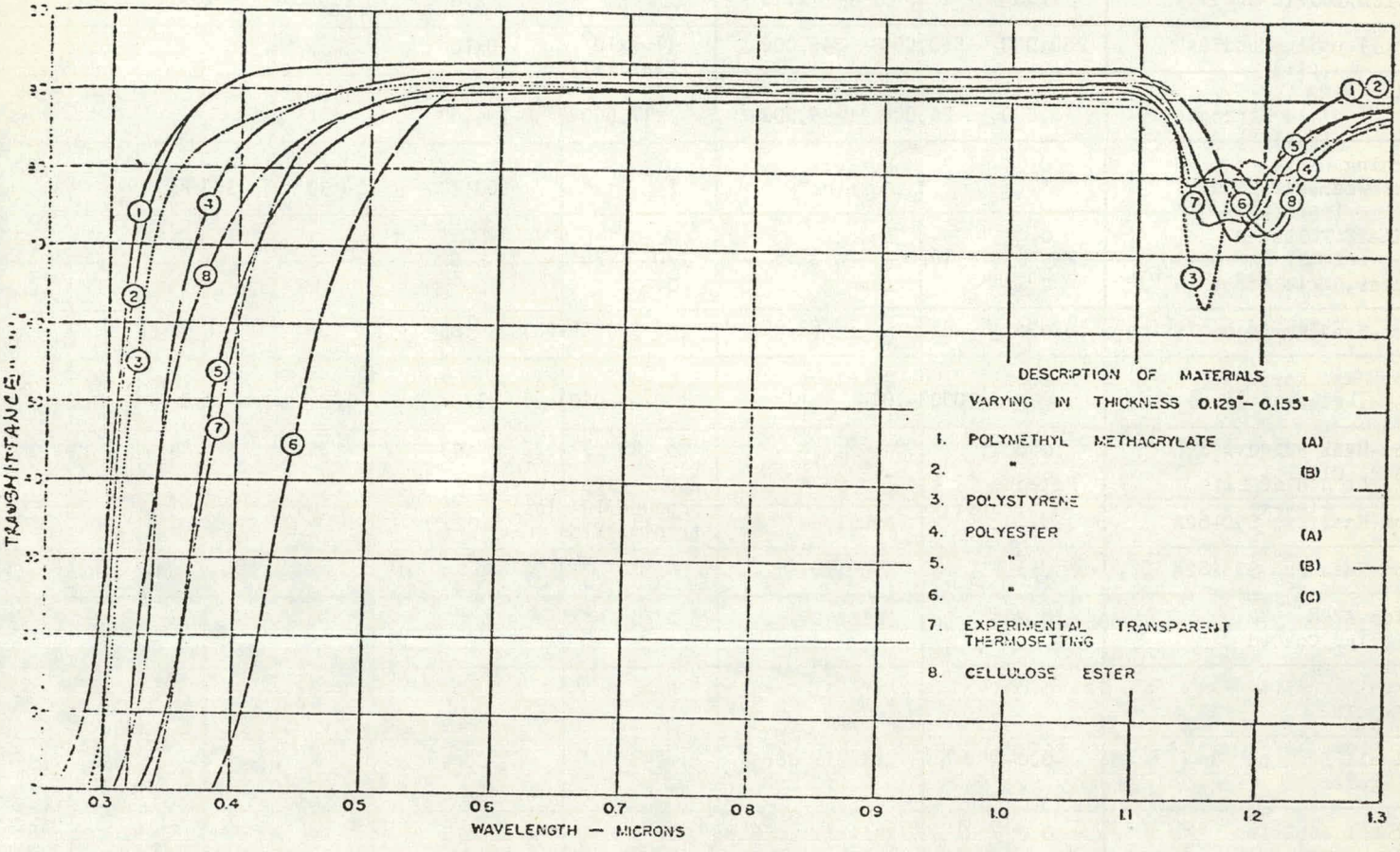


Figure 21. Spectral Transmittance of Various Transparent Plastics Versus Wave Length.

Table 2

PROPERTIES OF PLASTIC FILMS AND GLASS

	Tedlar (4 mil)	Mylar (W)	Lexan (MR-4000)	Kalwall Sunlite Reg.	Kalwall Sunlite Prem.	PPG Herculite Sheet	ASG Annealed	ASG Tempered
Specific Gravity	1.38	1.39	1.25	*	*	2.5	2.5	2.5
Tensile Modulus (psi)	260,000	550,000	345,000	(1.1×10^6 Flexural)		10×10^6		
Tensile Strength (psi)	13,000	24,000	9,500	17,000		29,000	*	*
Greatest Load ($psf:ft^2$)	*	*	*	*	*	100:28	20:30	100:28
Thermal Expansion ($in./in./^oF \times 10^{-6}$)	24.	15.	37.5	20	20	8.6		
% Solar Transmission	92-94	85	82-89	(85-90)	(85-88)	85	85	91
Thickness (in.)	*	.0003-.014	1/8	(.025-.040)		1/8	1/8	1/8
Cost Approx. $\$/ft^2$	.15	.08	*	.25-.29	.32-.38	.43	.35	.85
Length of Life (Years)	Retains 95% trans. in 5 yrs.	4	*	200^oF exposure will produce 10% loss in transmission		*	*	*

4

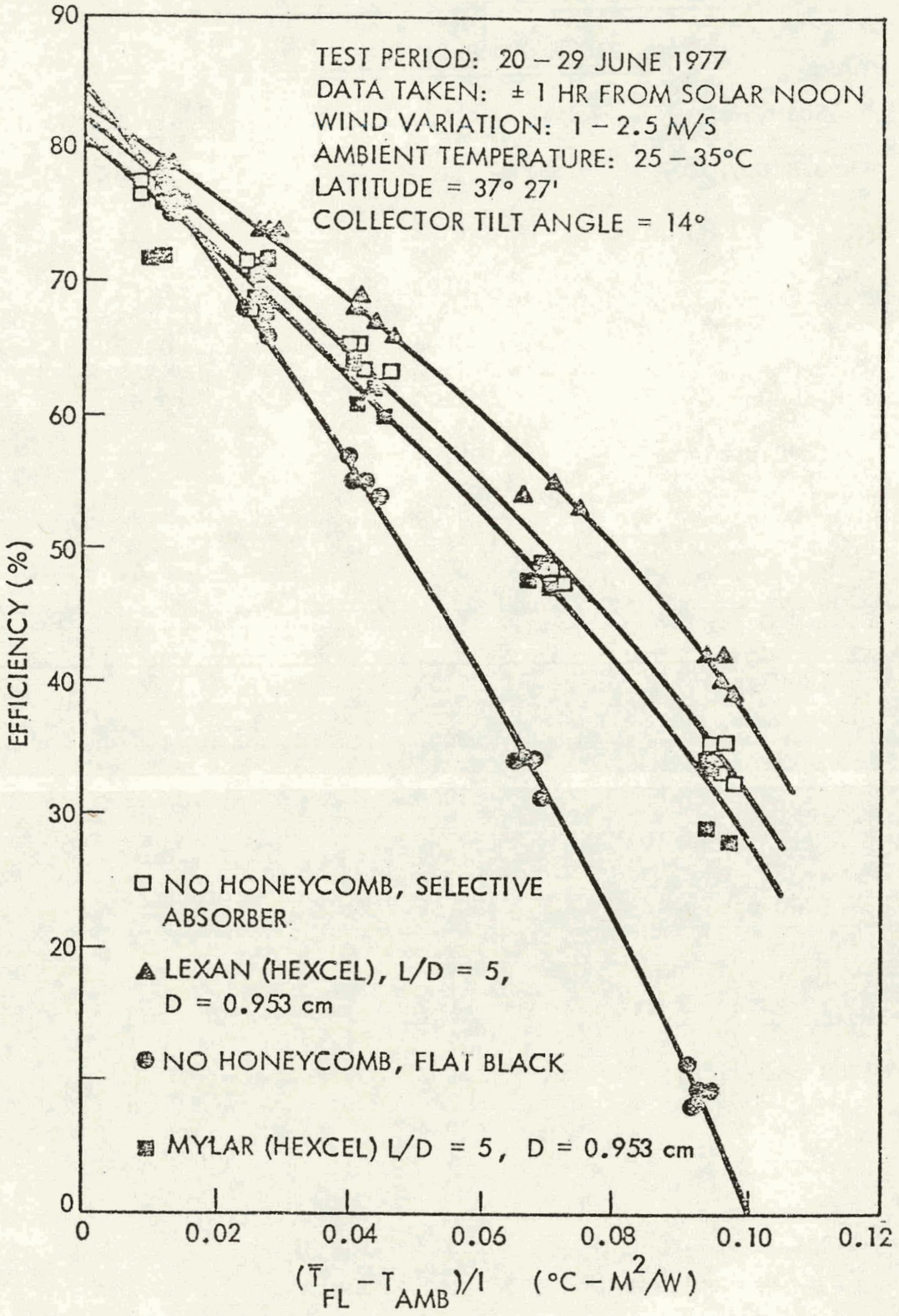


Fig. 3-19 Comparison of Efficiency Between a Glass Covered Flat Black Collector With and Without Hexcel Lexan Honeycomb and a Selective Black, No Honeycomb Collector

TABLE I

OVERALL CORROSION RATES OF ALUMINUM

AT 210°F UNDER LAMINAR FLOW

Solution	Alloy	R_{corr} (mpy)
Pure E.G./H_2O	1100	0.19
(35 Vol.%)	99.9%	0.16
	3003	0.13
	3004	0.10
E.G./H_2O + Cl^-	1100	8.5
(200 ppm)	99.9%	7.0
	3003	9.9
	3004	3.5
E.G./H_2O + Cu^{+2}	1100	5.5
(200 ppm)	99.9%	17
	3003	4.5
	3004	14
E.G./H_2O + Fe^{+3}	1100	30
(200 ppm)	99.9%	18
	3003	14
E.G./H_2O + Fe^{+3} + Cl^- + Cu^{+2}	99.9%*	71
(200 ppm each)	3003	74
	3004	120

* Under turbulent flow.

Ref: Giner, Inc. DOE Contract No. EY-76-C-02-2934

CONCLUSIONS

- ALL ALUMINUM ALLOYS SHOWED MARGINAL CORROSION RESISTANCE IN PURE UNINHIBITED ETHYLENE GLYCOL SOLUTIONS.
- COMMON IMPURITIES, SUCH AS CHLORIDE, CUPRIC, AND FERRIC IONS, CAUSE SIGNIFICANT REDUCTION IN ALUMINUM CORROSION RESISTANCE IN UNINHIBITED ETHYLENE GLYCOL SOLUTIONS.
- PROPYLENE GLYCOL IS LESS CORROSIVE TO ALUMINUM THAN ETHYLENE GLYCOL. ATTACK ON ALUMINUM DUE TO THE PRESENCE OF IMPURITIES WAS STILL FOUND TO BE SERIOUS.
- ALUMINUM CORROSION WAS FOUND TO BECOME LESS SEVERE WITH INCREASING GLYCOL (ETHYLENE AND PROPYLENE) CONCENTRATION.
- INHIBITORS USED IN AUTOMOTIVE COOLANTS WERE FOUND TO PROVIDE SATISFACTORY PROTECTION TO ALUMINUM AT TEMPERATURES BELOW 100°C WITH ALL THREE SPECIES OF CONTAMINANTS PRESENT.
- ZINC METAL WAS FOUND TO BE AN EFFECTIVE SCAVENGER OF HEAVY METAL IONS IN WATER GLYCOL MIXTURES.
- ZINC POWDER IN SOLUTION SERVES NOT ONLY AS A HEAVY METAL ION SCAVENGER BUT ALSO AS A SACRIFICIAL ANODE WHICH CATHODICALLY PROTECTS ALUMINUM EVEN WITH CHLORIDE PRESENT.
- INHIBITED ETHYLENE GLYCOL SOLUTION WITH ZINC POWDER WAS FOUND TO RENDER EXCELLENT PROTECTION TO ALUMINUM AT TEMPERATURES UP TO 160°C EVEN WHEN CHLORIDE AND HEAVY METAL IONS WERE PRESENT.

Toxicity of Heat Transfer Fluids

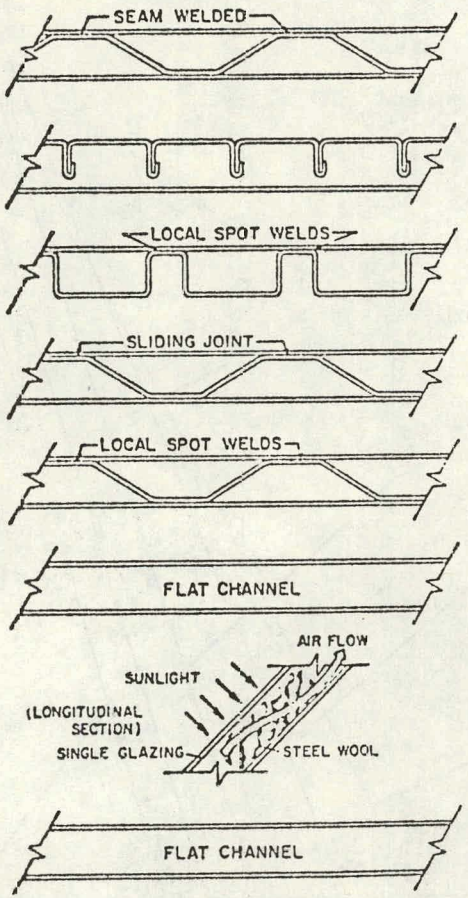
Commercial Name	Composition	Acute Oral Toxicity
Mobiltherm Light	Paraffinic oil, high aromatic	LD_{50} 20,000 mg/kg
Mobiltherm 603	Paraffinic neutral oil	LD_{50} 64 ml/kg, 57,000 mg/kg
Suntemp 1	Paraffinic oil, low aromatic	LD_{50} > 50 ml/kg
Caloria HT-43	Paraffinic oil, low aromatic	-
Thermia 33	Paraffinic oil	-
Exxon Process, Oil 3029	Napthenic mineral oil	-
Dowthern A	Diphenyl and diphenyl oxide mixture	LD_{50} 5600 mg/kg
Therminal 66	Terphenyls mixture	LDLo 500 mg/kg (p-terphenyl only)
SF-96, DC-200, DC Q2-1132	Polydimethylsiloxanes	TDLo 1500 mg/kg (subcutaneous) oral > 30 ml/kg
Dowtherm SR-1, UCAR-17	Ethylene glycol	LD_{50} 5840 mg/kg*
Dowfrost, UCAR-35	Propylene glycol	LD_{50} 21,000 mg/kg
UCON 50-H-280-X	Polethylene glycol	LD_{50} 6130 mg/kg
UCON 500	A polyglycol	
Methanol	Methanol	LD_{50} 13,000 mg/kg

Human Data

*Ethylene glycol - human LDLo 1500 mg/kg
Diethylene glycol - human LDLo 1000 mg/kg

Key to Figure 7.

Line Number	Collector Designation	Flow CFM
1a 1b	LASL Seam-Welded Internally Corrugated	2.8 2.2
2a 2b	Nichols Semi-Rib	3.2 2.1
3	LASL-1	2
4	LASL Mobile-1	2
5	LASL Mobile-1a	2
6	LASL Flat Channel	2
7	FUZZ-1 (Aztech)	2
8	ISE Flat Channel	2.1



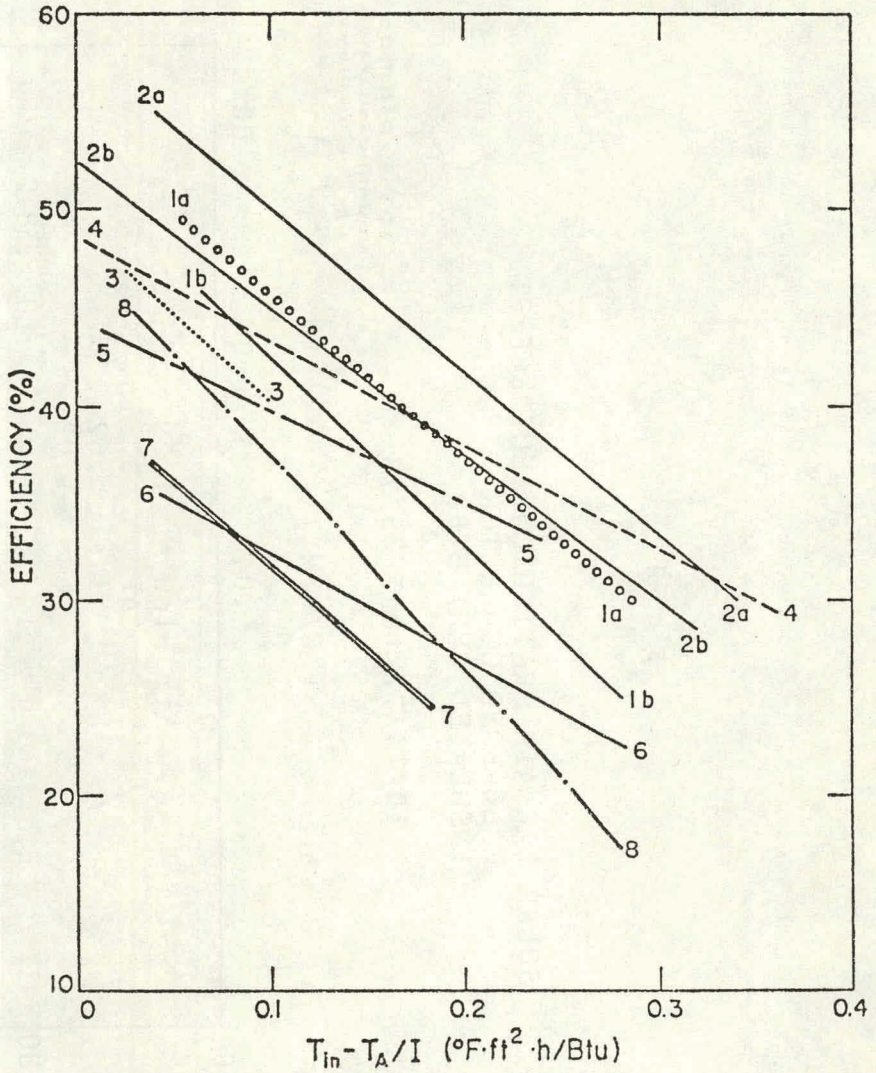


Fig. 7. Summarized results of efficiency measurements on single-glazed air heaters of various designs.

Fig. 27

SOLAR LAB AIR-HEATING COLLECTOR TEST
ROLL-BOND COLLECTOR
INSULATED PERIMETER

10/14/77 to 1/25/78

los alamos scientific laboratory of the University of California

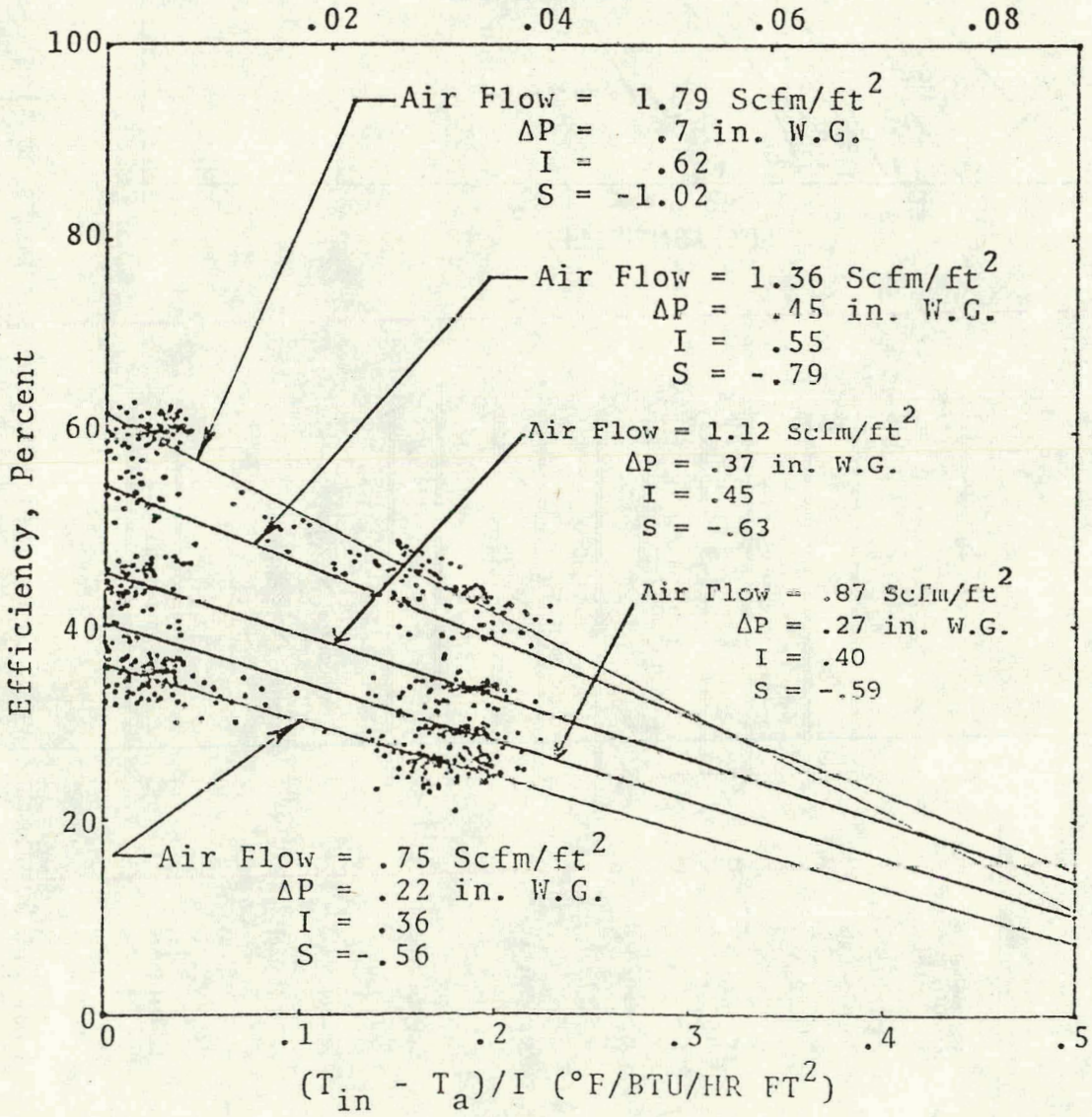
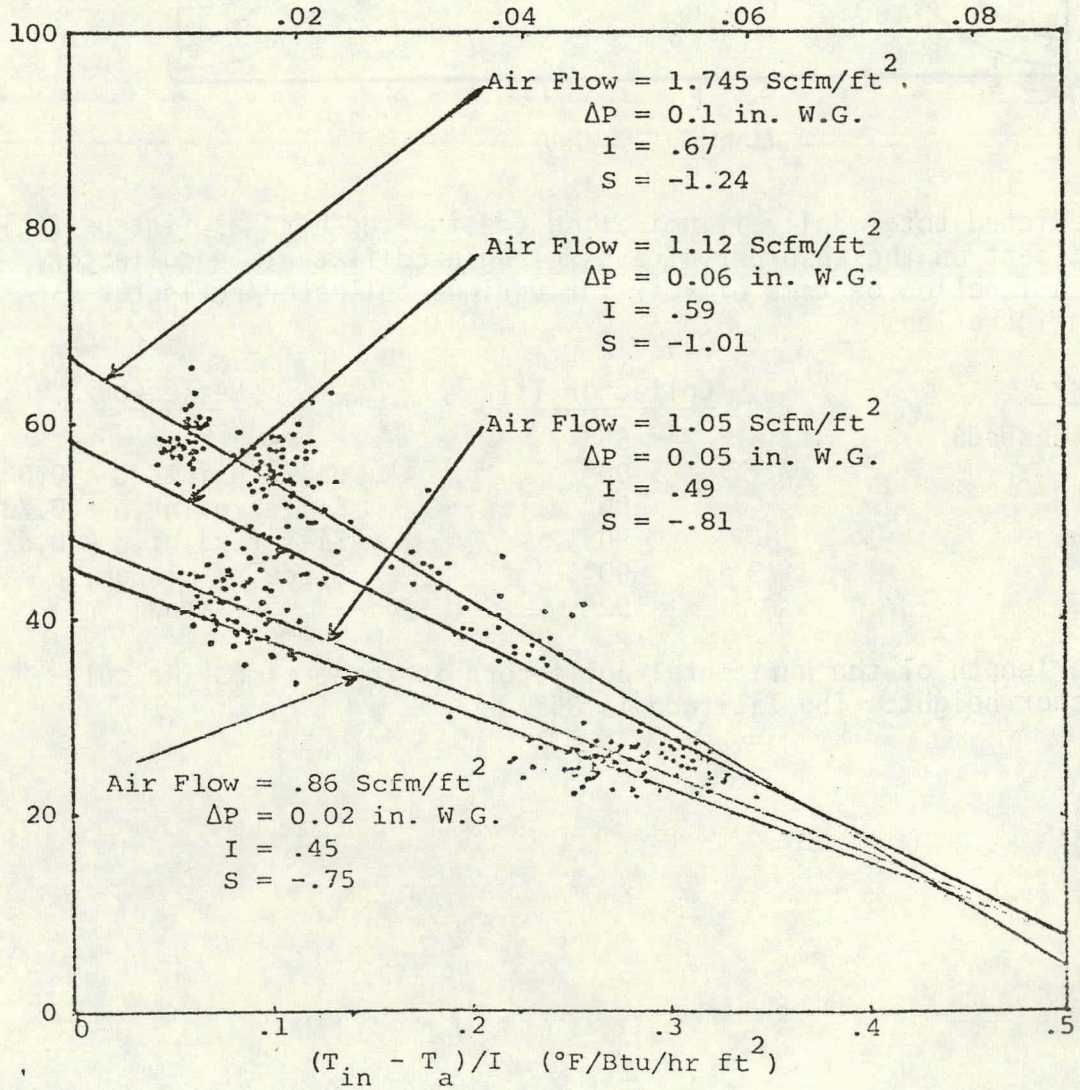


Fig. 28

LASL SEAM WELDED INTERNAL
CORRUGATED AIR COLLECTOR

11/12/77 to 4/6/78



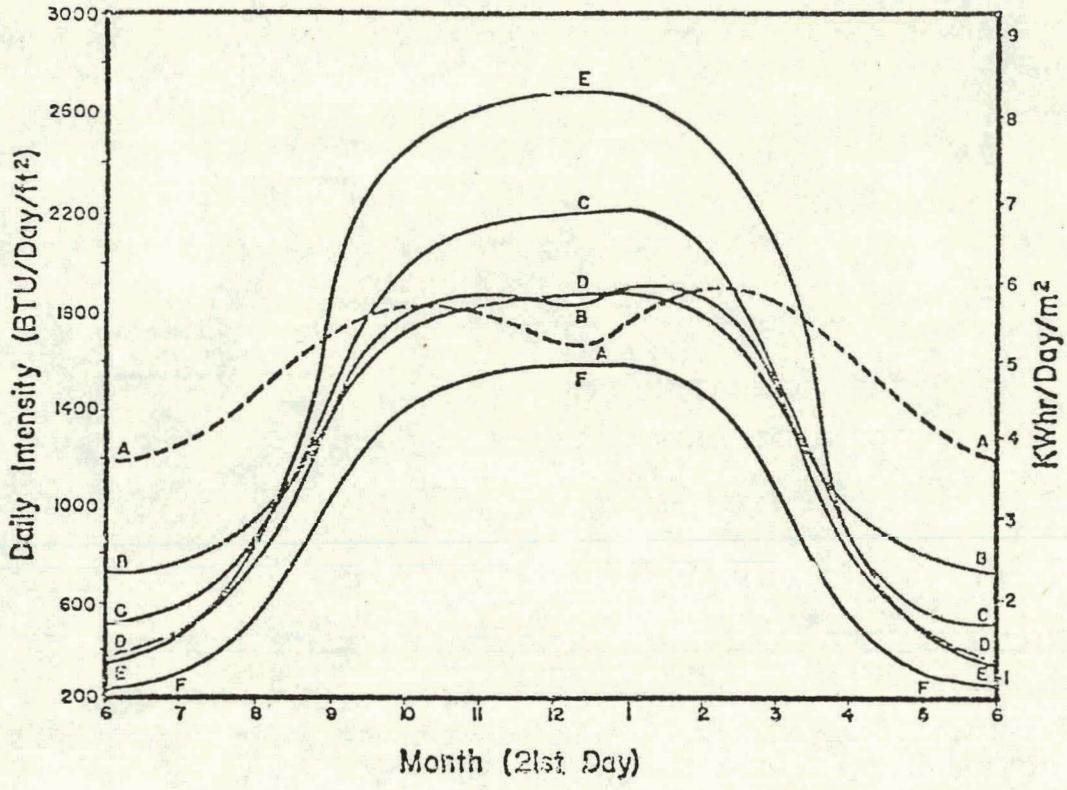


Fig. 10. Predicted total daily illumination (designated here as "intensity") incident on the absorber of a single-glazed flat-plate collector, as a function of time of year for various collector/reflector configurations.

Curve	Collector Tilt	Reflector
A (dashed)	55°	None
B	90°	White paint, ρ = 0.8
C	90°	Silver paint, ρ = 0.73
D	90°	Silver paint, ρ = 0.52
E	90°	Specular mirror, ρ = 0.8
F	90°	None

The length of the horizontal collectors is three times the collector height. The latitude is 35°.

TABLE 9-II

Specular Reflectance Properties of Various Mirror Materials

Material	Supplier	Wavelength (nm)	R_1	σ_1 (mrad)	R_2	σ_2 (mrad)
Alzak	Alcoa	670.	0.65	0.39	0.20	9.7
perpendicular to rolling marks		505.	0.54	0.42	0.31	10.1
		407.5	0.44	0.53	0.41	9.8
parallel to rolling marks	Alcoa	670.	0.68	0.24	0.17	7.7
		505.	0.60	0.29	0.25	7.1
		407.5	0.53	0.40	0.32	7.0
3M 5400 laminated to 0.64 mm (0.025 in.) Al sheet	3M	550.	0.85	1.9	-	-
3M 5400 special mounting on 0.64 mm (.025 in.) Al sheet	3M	690.	0.85	0.87	-	-
		550.	0.85	0.87	-	-
		410	0.85	0.89	-	-
Al-Teflon laminated to 0.64 mm (0.025 in.) Al sheet	Sheldahl	690.	0.87	1.2	-	-
		550.	0.87	1.2	-	-
		410.	0.87	1.3	-	-
Silver - 2 mil (0.05 mm) Teflon, mounted on optically flat plate	Sheldahl	550.	0.69	0.77	0.28	6.9
Silver - 5 mil (0.127 mm) Teflon, mounted on optically flat	Sheldahl	690.	0.77	0.26	0.20	4.7
		550.	0.75	0.26	0.22	7.0
		410.	0.62	0.33	0.35	8.2
Silvered Corning Microsheet 0.0045 in. (0.11 mm) mounted on optically flat plate	Sandia	550.	0.78	1.1	0.18	6.2
Double coat acrylic-Al-mylar on 0.64 mm (0.025 in.) Al sheet	Sheldahl	550.	0.49	0.89	0.37	12.7
Double coat acrylic silver on glass	Sheldahl	550.	0.93	0.21	-	-
High purity Al bright	Metal Fabrication, Waterbury, Conn.	550	0.38	1.2	0.46	9.6
Kinglux reflector sheet	Kingston Industries	493	0.62	0.37	0.23	15.1

Ref: Sandia Laboratories Report No. SAND76-0078

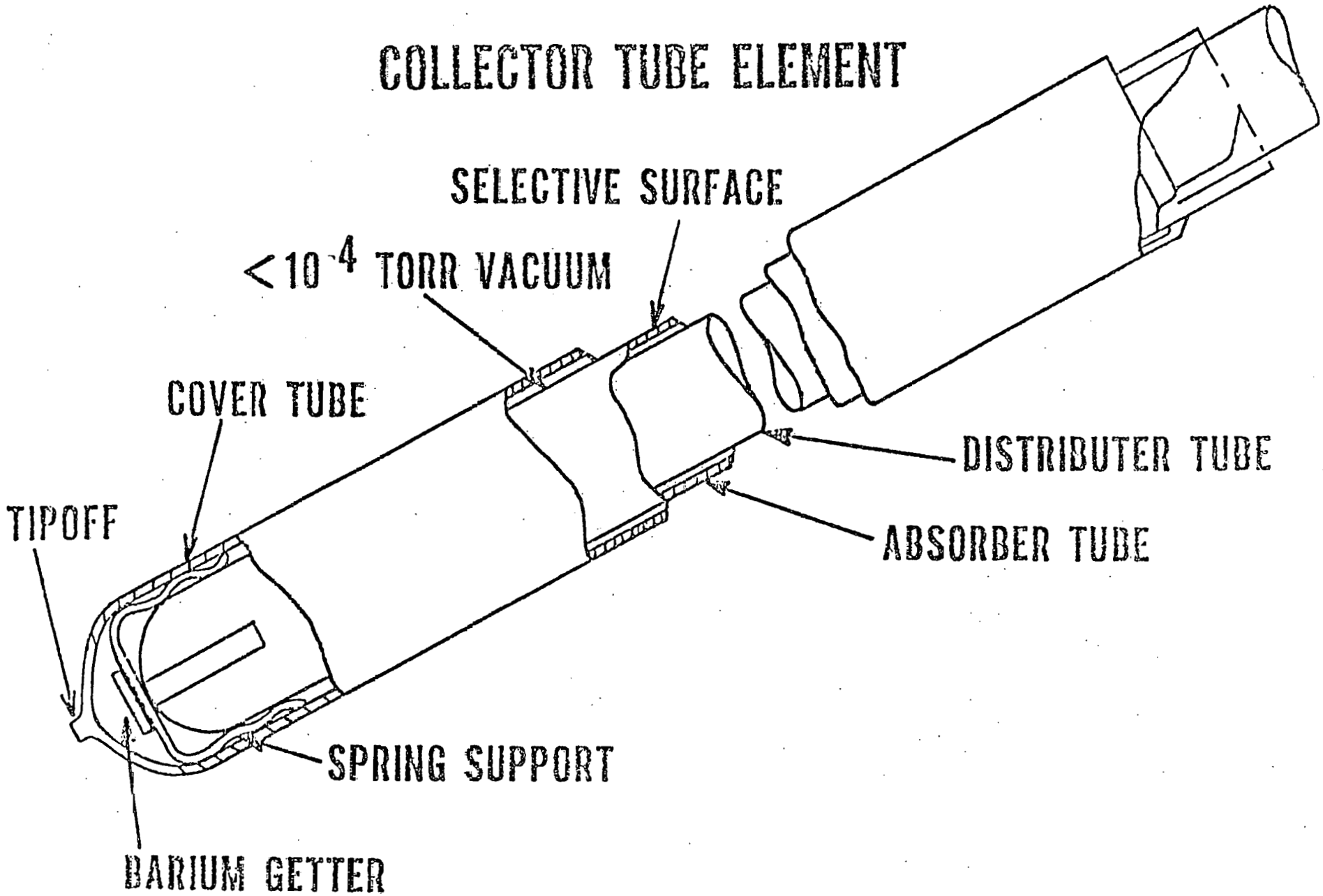


Fig. 4. Schematic of typical all-glass evacuated tube solar collector construction.

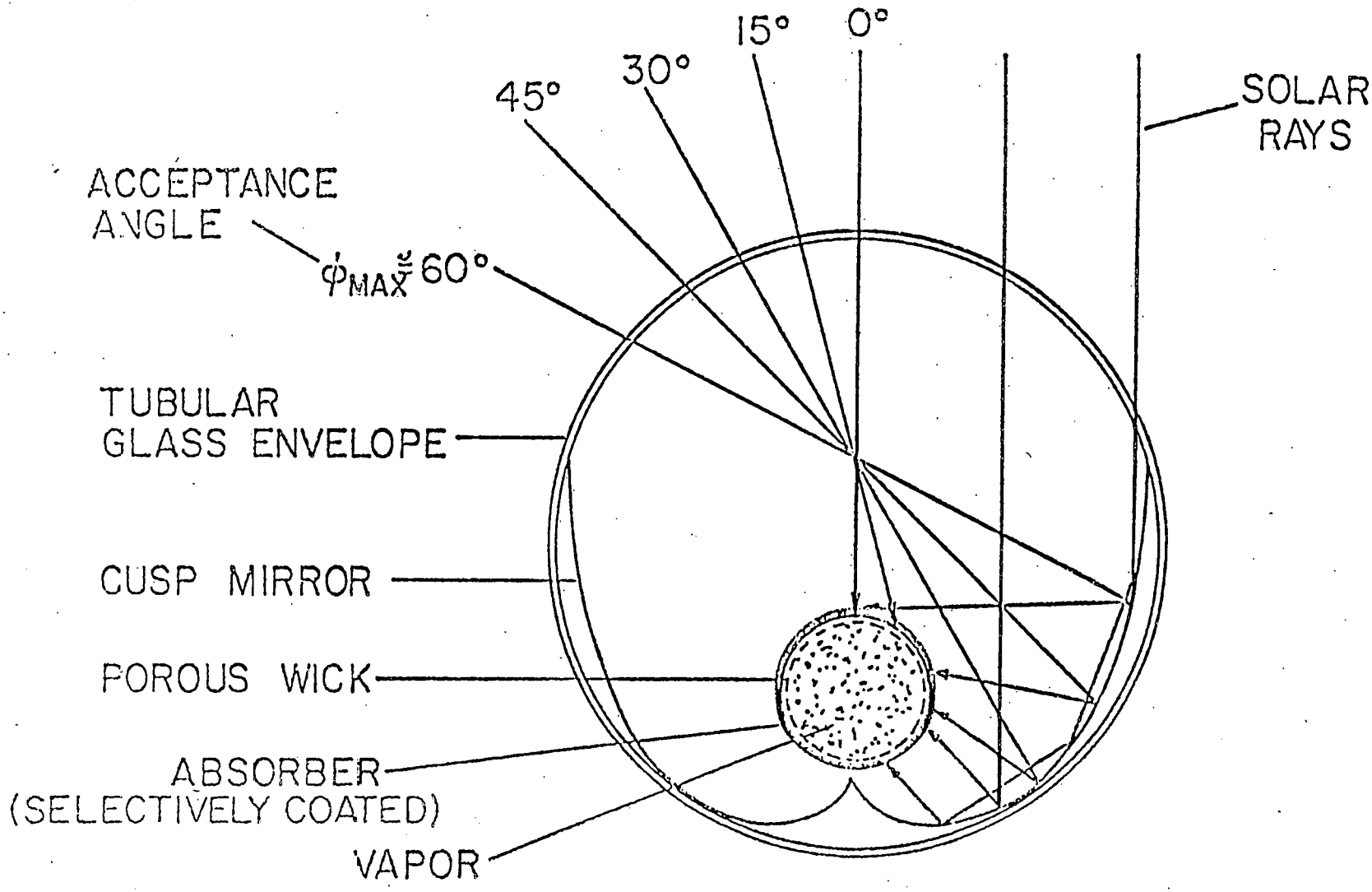


Fig. 15. Cross-sectional view of the Corning cusp reflector, heat pipe absorber, evacuated tube solar collector.

THIS PAGE

WAS INTENTIONALLY

LEFT BLANK

FLUID CORROSIVITY SENSOR FOR SOLAR SYSTEMS

by

R. Baboian and G. S. Haynes

Texas Instruments Incorporated

Attleboro, Massachusetts

Copper, aluminum or iron alloys are commonly used in the construction of flat plate solar collectors. Advantages of these materials include high strength, ease of fabrication and joining and high thermal conductivity. These materials, however, are vulnerable to internal corrosion due to interaction with the heat exchanging fluid and failures due to corrosion can significantly reduce the design life of the system. Contamination of internal surfaces from residual soldering or brazing flux as well as the use of mixed metal systems can accelerate corrosion.

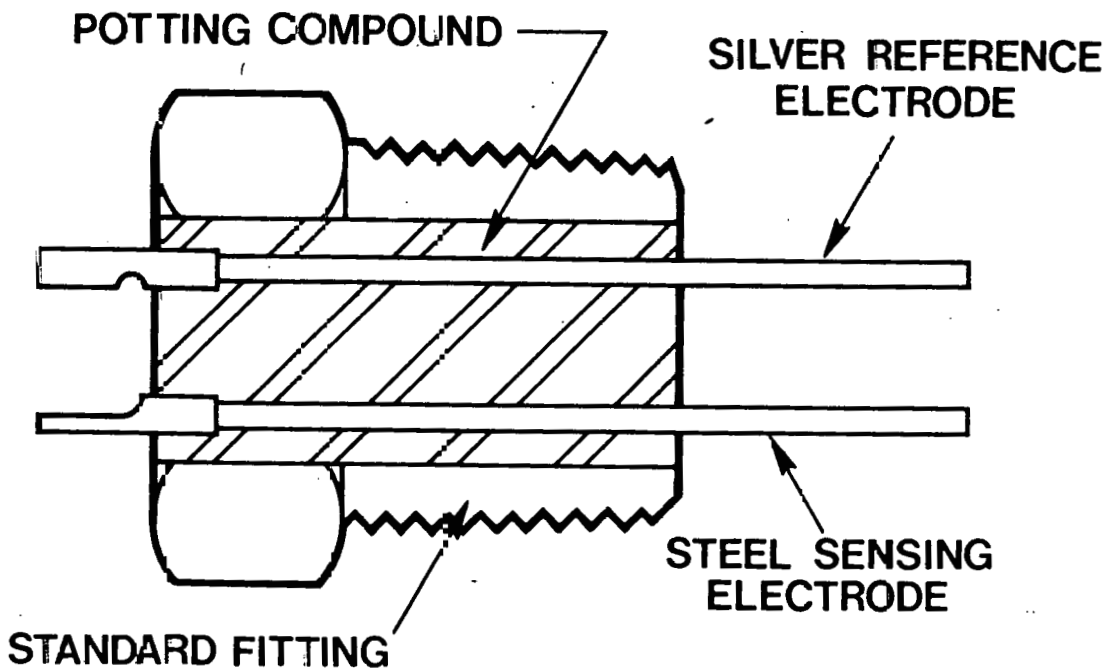
Inhibitors are added to the heat exchanging fluids to prevent internal corrosion. A variety of inhibitors are extremely effective in sufficient concentration, however, degradation of inhibitors occurs due to hot spots, air entrainment, thermal breakdown or other causes. After the inhibitor concentration has dropped below a minimum level corrosion can occur at a rate greater than would occur without inhibitors, this is due to the fact that inhibitors maintain passive films on the metal surfaces. If these films cannot be maintained due to lack of inhibitor localized corrosion of the metal surfaces occurs and penetration rates are high. Aluminum alloys are particularly susceptible to pitting and other forms of localized corrosion although localized corrosion as well as uniform corrosion of other materials can occur.

Automotive experience with inhibited heat exchanging fluids has not been a reliable indicator of their performance in flat plate solar collectors. There is a strong demand in the solar industry for a reliable method of determining the effectiveness of inhibitors. This has led to the development of a fluid corrosivity sensor capable of detecting, in situ, the effectiveness of inhibitors.

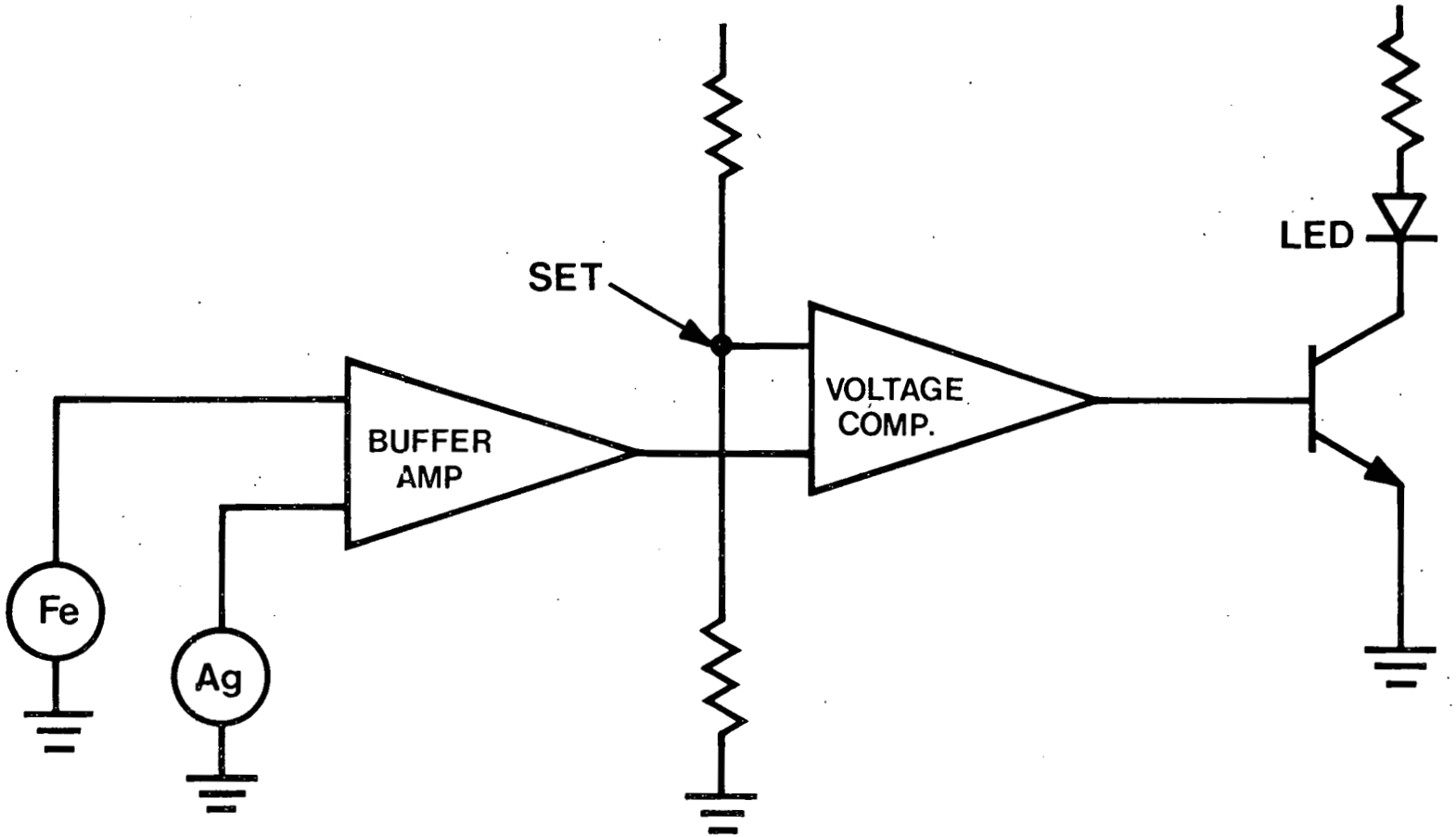
This sensor is capable of detecting when the inhibitors in a system have been depleted to the point where corrosion of the materials in the system is imminent. The sensor is based on electrochemical principles and consists of a sensing probe, electronic package, and an indicating device. In practice, the potential between a sensing electrode and a reference

electrode is monitored. A fully inhibited system exhibits a potential which is 0.5 volts less negative than an uninhibited system. Results of laboratory and field tests have shown that the sensor is responsive to all passivating inhibitors. Data has been generated which allows the device to trigger an indicating device when this potential difference exceeds a preset value where corrosion is imminent.

COOLANT CORROSIVITY SENSOR



CIRCUIT DIAGRAM FOR COOLANT CORROSIVITY SENSOR



THIS PAGE

WAS INTENTIONALLY

LEFT BLANK

PRELIMINARY MATERIALS ASSESSMENT IN SOLAR DEMONSTRATION SYSTEMS

by

Craig F. Cheng

Argonne National Laboratory

Argonne, Illinois

*Not presented at this workshop.

PRELIMINARY MATERIALS ASSESSMENT IN SOLAR DEMONSTRATION SYSTEMS

CRAIG F. CHENG

ARGONNE NATIONAL LABORATORY

ABSTRACT

This paper reviews data on materials performance in solar heating and cooling demonstration systems from the published literature and from limited service experience. It includes a preliminary list of materials recommended for use in collector and transport systems.

TABLE OF CONTENTS

1	Introduction	1
2	Solar Demonstration Systems	1
3	Collector Subsystems	1
	3.1 Batten/Enclosure	5
	3.2 Cover Plates	8
	3.3 Reflective Coating	11
	3.4 Insulation	12
	3.5 Absorber Coating/Substrate	13
	3.6 Absorber Panel	16
4	Energy Transport Subsystems	16
	4.1 Heat Transfer Fluid	16
	4.2 Internal Corrosion	17
	4.3 Localized Corrosion	21
	4.4 Storage Tanks	22
	4.5 Organic Hose	22
5	Summary and Conclusions	23

LIST OF FIGURES

Figure 1 DOE Solar Demonstration Systems Summary 2

Figure 2 Active Solar System 3

Figure 3 Passive Solar System 3

Figure 4 Active/Passive Solar System 3

Figure 5 Solar Collector Types in Solar Demonstration Systems 4

Figure 6 Detailed Construction of Solar Collectors 6

Figure 7 Typical Solar Collector With *In-Situ* Atmospheric Corrosion Monitoring 7

Figure 8 Atmospheric Corrosion Monitoring Data 9

Figure 9 Voltage Corrosivity Sensor--Solar Collector Piping System 18

Figure 10 Thermal Breakdown of Solar Fluid--Solution Potential vs. Time.19

1 INTRODUCTION

The major costs of solar energy systems are the capital investment in components and ongoing maintenance requirements. The economic consequences of material degradation and system unreliability are significant impediments to the commercial utilization of solar energy. Accordingly, the National Solar Heating and Cooling Demonstration Branch of the Department of Energy (DOE) has initiated the Solar Data Project at Argonne National Laboratory (ANL). The Project objective is to collect, evaluate, and publish reliability, maintainability, and material performance data on solar demonstration systems.[1] This paper is a preliminary review of the literature on critical materials in solar heating and cooling systems. Reliability and maintainability of solar demonstration systems are covered by other conference papers[2] [3] and ANL reports.[4] [5] [6]

2 SOLAR DEMONSTRATION SYSTEMS

The DOE sponsors 182 solar demonstration projects (operational or under construction), 81 of which include instruments for automatic remote monitoring of thermal performance via the National Solar Data Network (NSDN) through the Site Data Acquisition System (SDAS) at IBM, Huntsville, Alabama.[7] Figure 1 is a bar chart showing the distribution of projects with respect to:

energy application - 63% are for hot water and heating and hot water applications

system design - 95% are active systems

collector medium - 90% use a liquid medium

collector type - 76% use flat plate collectors

storage type - 91% use liquid storage

Figures 2, 3, and 4 are typical schematic diagrams for active, passive, and active/passive systems, respectively.

3 COLLECTOR SUBSYSTEMS

Typical solar collectors (flat plate, concentrating linear trough, and evaucated tube) are shown in Figure 5, and the details of their

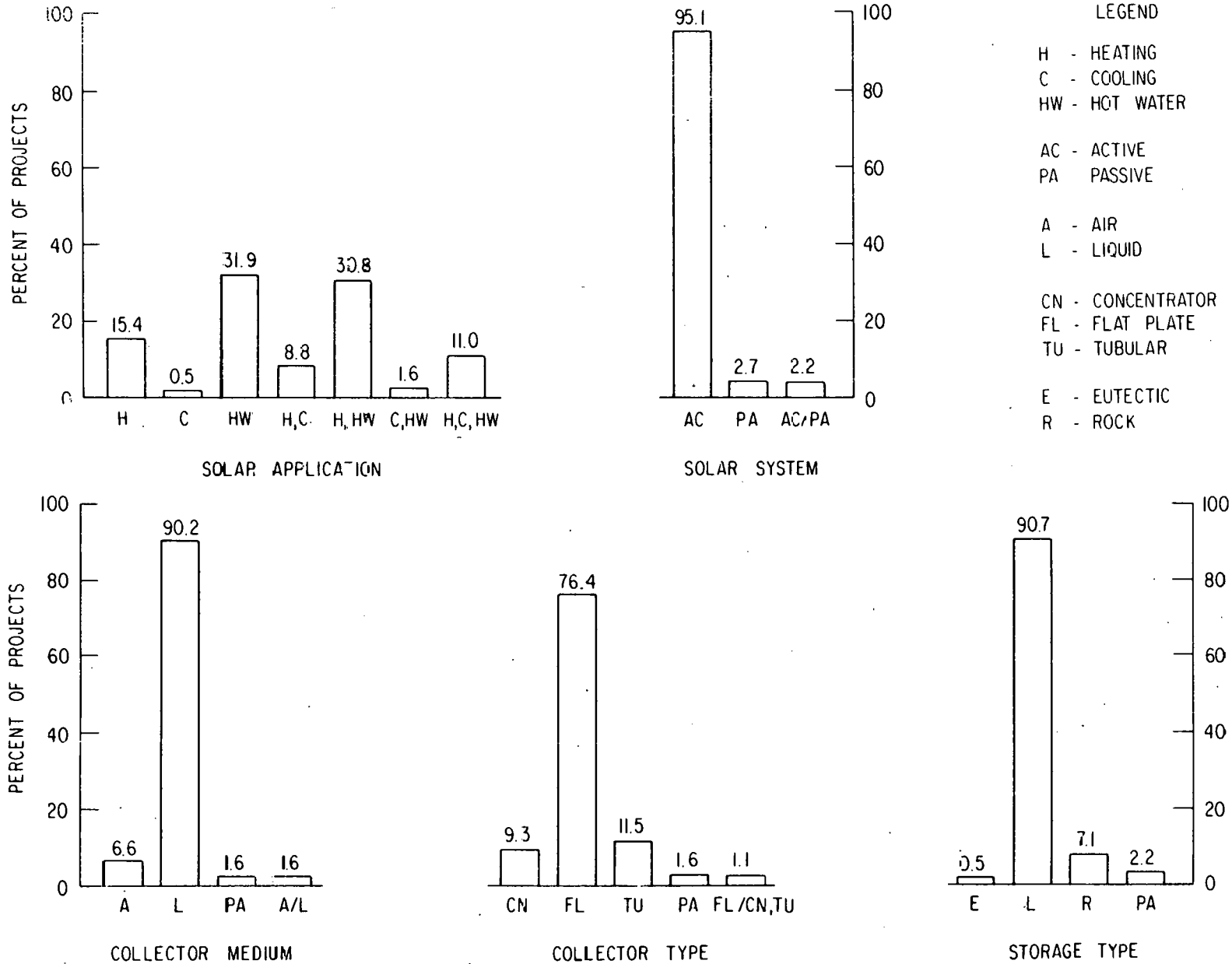


Fig. 1 DOE Solar Demonstration Systen Summary

OWNER: CITY OF SANTA CLARA

LOCATION: SANTA CLARA, CA.

SYSTEM: ACTIVE

APPLICATION: HEATING, COOLING & HOT WATER

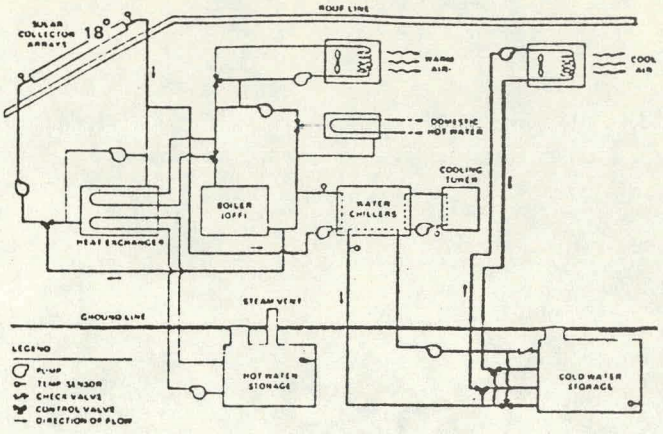


FIG. 2 ACTIVE SOLAR SYSTEM

OWNER: AM. ORNAMENTAL METAL CO.

LOCATION: AUSTIN, TX

SYSTEM: PASSIVE

APPLICATION: HEATING

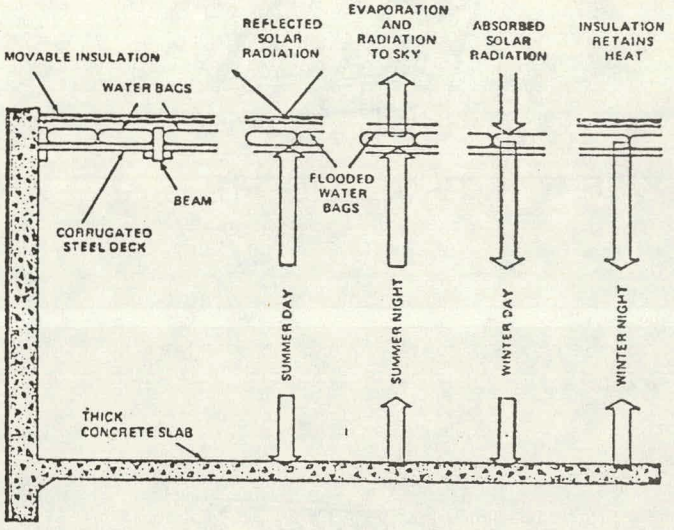


FIG. 3 PASSIVE SOLAR SYSTEMS

OWNER: RENAULT & HANDLEY

LOCATION: SANTA CLARA, CA

SYSTEM: ACTIVE/PASSIVE

APPLICATION: HEATING & HOT WATER

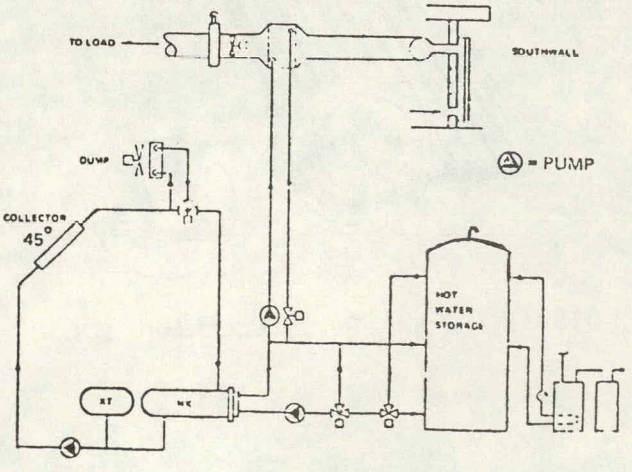
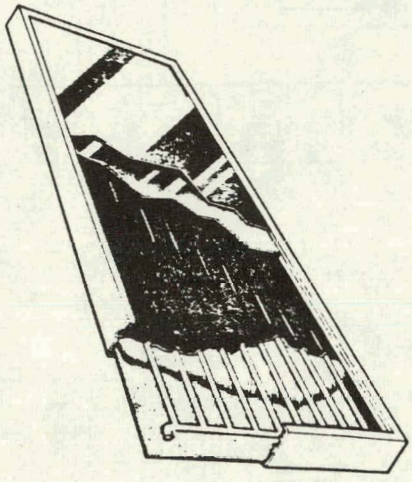
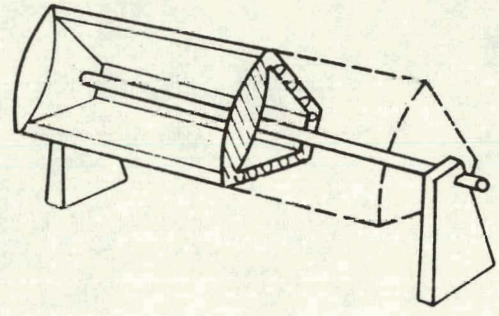


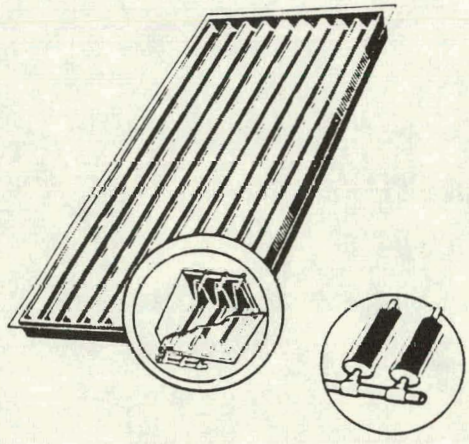
FIG. 4 ACTIVE/PASSIVE SOLAR SYSTEM



FLAT PLATE COLLECTOR (LIQUID)



CONCENTRATING LINEAR TROUGH COLLECTOR (LIQUID)



CONCENTRATING PARABOLIC COLLECTOR (LIQUID)

Fig. 5 Solar Collector Types in Solar Demonstration Systems

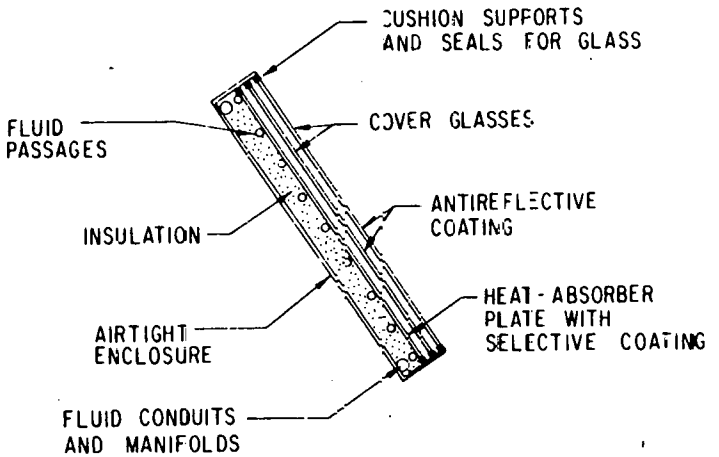
construction are shown in Figure 6. The principal materials used for different components of the collector are discussed below.

3.1 BATTEN/ENCLOSURE

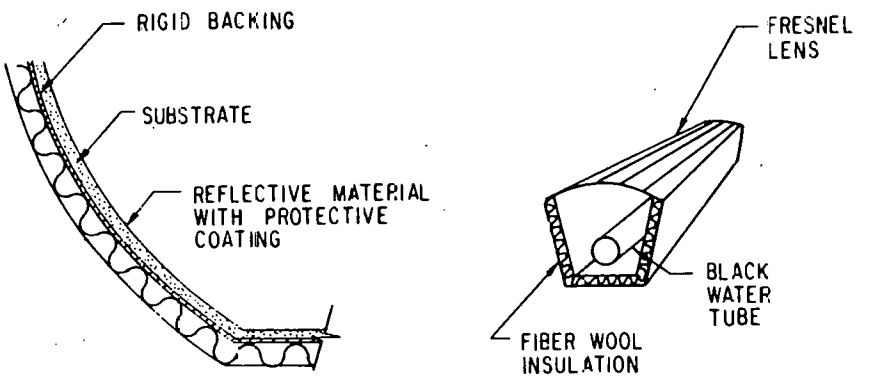
The batten holds down the cover plate(s) and provides a weather-tight seal between the enclosure and the cover in a flat plate collector (Figure 6a). The batten and enclosure are made of aluminum, galvanized steel, or epoxy-painted steel. These materials have successfully resisted atmospheric corrosion at demonstration sites for a short time in some climatic regions. However, severe salt-air corrosion of the mechanically cut edge (unprotected surface) of galvanized steel battens/enclosures is already being reported.[8] At a North Sea offshore drilling site, a number of dramatic premature failures of a structural steel platform, painted with a zinc silicate primer and vinyl top coats, have been reported, but a similarly treated platform has been satisfactory in the Gulf of Mexico.[9] These examples illustrate that climatic conditions and exposure time (~20 years) are important factors in selecting materials for battens and enclosures.

As part of the materials assessment program in the ANL Solar Data Project (ASDP), atmospheric corrosion study of metallic supports (batten/enclosure) through *in-situ* monitoring is being conducted at 15 selected NSDN sites located in representative climatic regions.[2] The sensor data from each site will be transmitted through SDAS to the central IBM data processing facility at Huntsville, Alabama. The atmospheric corrosion monitoring illustrated in Figure 7 is being carried out by two complementary *in-situ* experiments:

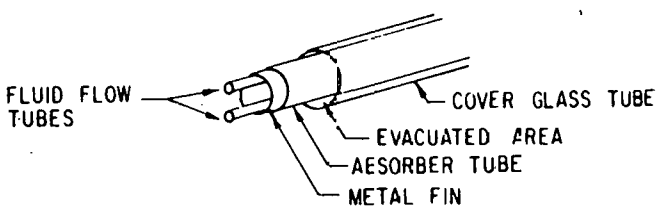
1. Accelerated Corrosion Test - Monitoring the telemetry from an atmospheric corrosion monitor (ACM), a relative humidity sensor, and an ambient temperature sensor.
2. Long Time Exposure Test - Determining the weight loss and pitting characteristics from metallic coupons housed in an atmospheric corrosion rack (the metallic coupons include aluminium, galvanized steel, aluminized steel, and painted steel).

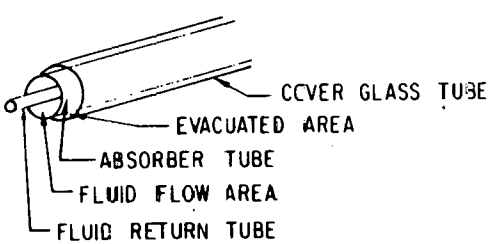


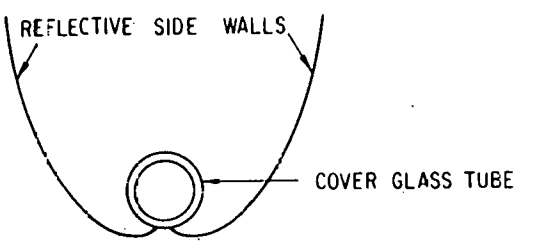
FLAT PLATE COLLECTOR



CONCENTRATING LINEAR TROUGH COLLECTOR







CONCENTRATING PARABOLIC COLLECTOR

Fig. 6 Detailed Construction of Solar Collectors

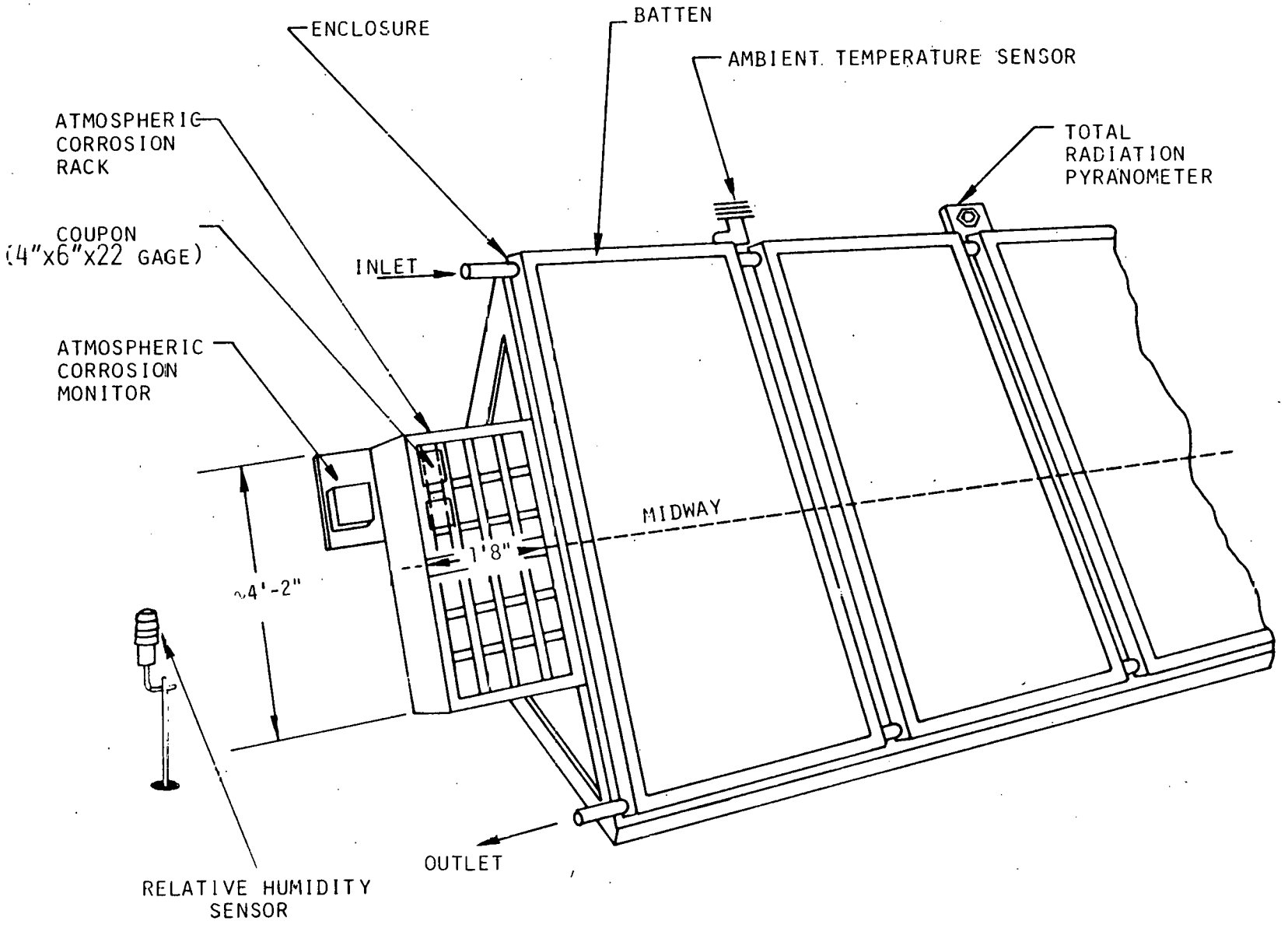


Fig. 7 Typical Solar Collector with In-Situ Atmospheric Corrosion Monitoring

The experiment is based on the theory that atmospheric corrosion of metal is a discontinuous process attributed to the synergistic effects of humidity, temperature, and atmospheric constituents.[10] Corrosion occurs only when electrolyte layers are present; these layers cause anodic and cathodic reactions that lead to corrosion. The total weight loss (ΔM) is the sum of corrosion that occurs during separate corrosion periods, i.e. time of wetness (τ). The ACM generates a galvanic current during τ due to corrosion between a stack of Cu/Zu plates,[11] and the magnified current is recorded by SDAS.

Figure 8 shows the relationship between the ACM galvanic current (Ig), the relative humidity, and the temperature for an atmospheric corrosion monitoring site on the roof of Rockwell International Science Center. Because all three data sets fluctuate in the same manner, it is possible to correlate Ig with τ, relative humidity, and site temperature at each test site. Since Ig is proportional to the corrosion rate for a diffusion controlled process, the maximum Ig during τ indicates the maximum corrosion rate. The total electrical charge in coulombs obtained by integrating Ig over τ relates to the amount of zinc metal dissolved during τ. The loss (ΔM_{zn}) can be calculated from Faraday's law. All these data can be correlated with weight loss data from test coupons exposed on an adjacent atmospheric corrosion rack. The combined results will indicate how rapidly various materials will corrode as a function of relative humidity, time of wetness, temperature, and atmospheric constituents at each site.

3.2 COVER PLATES

Cover plates minimize convections and radiation from the flat plate collector to the environment. A second cover plate will always increase thermal efficiency, but its cost of installation might offset the savings from increased efficiency. The best way to choose between one or two covers is to compare the thermal efficiencies of each over an extended period and examine the cost effectiveness of the second cover.

When the outdoor temperature is 38°C (100°F): (1) the stagnation temperature is 150°C (302°F) for the inner cover and 100°C (212°F) for the outer cover; and (2) the operating temperature is 70°C (167°F) for the inner plate and 50°C (122°F) for the outer plate. The maximum operating temperature for a single cover plate is 92°C (~~67°C + 25°C~~).

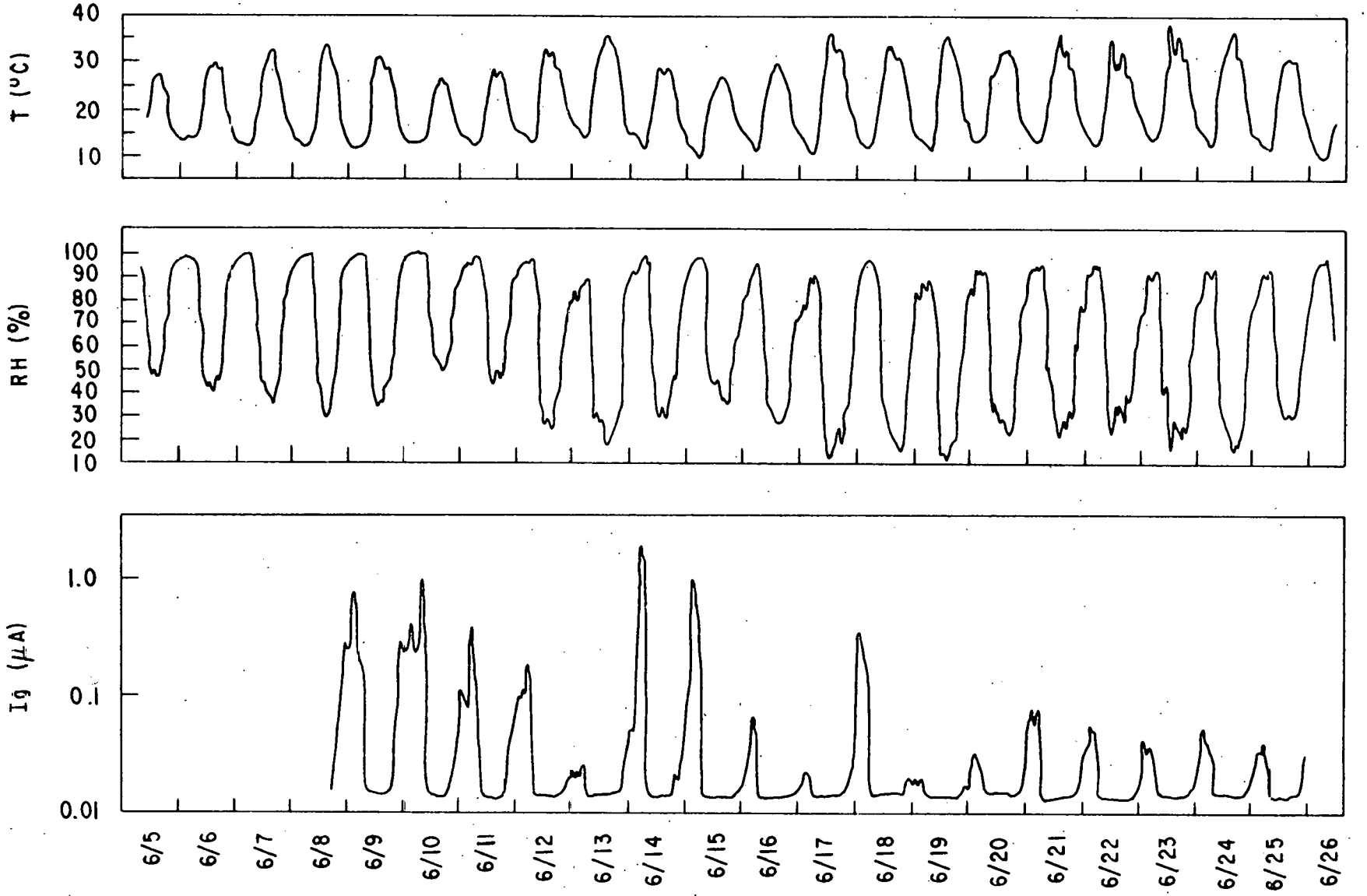


Fig. 8 Atmospheric Corrosion Monitoring Data

At the demonstration sites, glass and/or self-supporting plastic sheets are used for the single or double cover plate, and plastic film is employed for the inner cover plate. The mechanical, thermal, and radiative properties of cover plate materials have been reviewed and summarized by several authors. (12,13,14)

Glass resists ultraviolet radiation and absorbs long wave reradiation emitted from the absorber coating. Untempered glass cover is structurally strong enough to carry wind, rain, and snow loads, but is susceptible to shattering under the force of ice ball projectiles. Tempering improves shatter resistance, (14) and the tempered low-iron glass covers used in the demonstration sites have good transmission in the range of 86%. With acid etching, transmission can be increased to 90%.

However, dirt and grime deposits over time or during stagnation pose one of the most serious threats to the durability of glass. These deposits reduce the optical transmission of etched and unetched glass alike. It had been thought that grime deposits would be more difficult to remove from etched glass due to the porous nature of the surface. However, experiments have shown that the problems of dirt and grime are no worse for etched than for unetched glass.(15) In an experiment exposing a glass panel to an outdoor urban environment for six months, transmission degradation from dirt and grime was 4 percent, and washing with a mild detergent easily restored the original transmission level. If dirt deposits remain on the exterior surface of the glass cover, they should be cleaned twice a year.

Deposits on the underside of cover plates can result either from condensation (contaminant inclusion) or outgassing products from an internal source (insulation).(16) If the effect of such deposits on cover plate transmission exceeds 10 percent, the question of cleaning is a matter of relative cost.

Self-support plastic sheets, such as Lexan (a polycarbonate) are not as heavy or breakable as glass. Lexan is highly shatter-resistant, but fairly soft. Thus, excessive warpage was observed in several systems using polycarbonate covers. Also, stress carcking of polycarbonate cover plate was observed at the edge of stiffening ribs.(16) Furthermore, although Lexan has a fairly good initial transmission range (84.5% to 88%), yellowing due to surface weathering and ultraviolet degradation will cause this level to drop over

a five year period.[13,14]

Plexiglass (an acrylic) has adequate transmission in the solar wavelength region, but plexiglass is not very opaque in the infrared region. This effectively cancels its transmission advantage. Since plexiglass softens at 75°C (162°F), it can only be used as an inner cover with a support frame.

Plastic films are attractive because of their low cost. However, they need supplementary support systems to stretch and hold them in position, and these support devices increase their cost. Plastic films are not generally very durable when exposed to radiation; however, if used as an inner cover, ultraviolet durability may not be required. Tests have shown that glass/Teflon collector covers are more efficient than double glass covers.[17] The following plastic films are ranked in order of preference according to their transmission rates and durability: Teflon F.E.P. (flourocarbon, DuPont), Tedlar P.V.F. (fluorocarbon, DuPont), Sunlite Premium (fiberglass, Kalwall), and Mylars (polyester, DuPont).[13]

3.3 REFLECTIVE COATING

Solar reflectors have different optical requirements depending on the concentrator design--central receiver, parabolic trough, or compound-parabolic systems. The performance of a material in a solar concentrator will depend upon both the solar reflectance value and the specularity of the reflected beam, as well as the environmental stability and cost of the reflector. At Sandia Laboratories [18] the specular reflectance properties of a variety of solar reflector materials were measured using a hemispherical reflecto-meter together with a specially designed bi-directional reflectometer. The solar averaged hemispherical reflectance of silvered and aluminum mirrors were typically in the range of 90-96% and 85-90% respectively. However, the specular reflectance values could be significantly lower as a result of scattering and/or absorption in protective cover films, scattering at the reflecting interface, or scattering from surface irregularities which result from laminating the reflector to a support structure. An understanding of the scattering and absorption properties of these particles and their effect on the specular reflectance properties of the reflectors are required for a complete understanding of this problem.

Current studies of reflector materials[18] concentrate on determining their dust accumulation characteristics and on developing procedures for cleaning the reflector surface. Initial results indicate that after a relatively short outdoor exposure, dust accumulation can reduce the specular reflectance up to 25%. Particulates deposit onto the reflector surface through the complex fluid mechanical interaction of the dust laden air stream with the mirror structure. Once deposited, initial adhesion under dry conditions is dominated by surface energetic phenomena. In the presence of moisture or high humidity, the adhesion is dominated by capillary effects and water-induced chemical and physical bonding. Several continuous and periodic cleaning procedures show promise, but their effectiveness will depend upon the technique used, the environmental conditions, the amount of time the mirror has been exposed, and the mirror material.

Information about long term environmental degradation of the mirror due to abrasion, ultraviolet aging, moisture penetration, edge protection, or reflector surface deterioration is not available at present. So far, only service failures of front surface mirrors have been reported.[19] They sometimes flake, craze, or have edge corrosion. In another incidence, self-adhering aluminized film was used as a reflective coating in a collector, and the film peeled off in service.[16]

3.4 INSULATION

Collector insulation design requirements[14] to minimize the heat loss to the collector housing are:

Maximum temperature of 204°C (400°F)

Temperature cycling endurance between -29°C and 121°C (-20°F and 250°F)

Thermal conductance less than 0.57 $W/m^2-°C$ (0.1 $Btu/hr-ft^2-°F$)

Many insulation materials designed for the construction industry should be modified to meet solar industry requirements. The outgassing of binders at higher temperatures and the subsequent effects of this upon the transmissivity of the cover plate have been identified at numerous sites. Also freon-blown materials have a problem over 177°C because hydrofluoric and

hydrochloric acids are liberated and this corrodes selective coatings.[20]

Four basic types of insulation are considered below: mineral fiber, ceramic fiber, form glass and plastic, and fiberglass. Their thermal and their physical properties have been summarized and discussed by several authors.[13,14]

The mineral and ceramic fibers are comparable to fiberglass in thermal conductivity. The former are generally used for higher temperatures and cost much more. The exception is mineral wool, a loose fill material with relatively low thermal conductivity. It tends to settle under its own weight, eventually leaving an air gap behind the absorber panel. This decreases the efficiency of the collector by increasing the heat loss from the absorber plates. Mineral wool also loses its insulation qualities if it is subjected to humidity cycling. Therefore, the collector housing must be hermetically sealed to prevent such cycling. Loose insulation is undesirable during repair or maintenance operations.

Fiberglass is the lowest cost insulation available today. It is produced in a variety of densities (affecting thermal conductance) and a variety of binder conditions depending on the application. Semi-rigid fiberglass board for high temperature application with hardly any binder is recommended. Furthermore, this insulation material should be preheated above 177°C (351°F) to drive off the volatile binder prior to laying the cover plate over the collector housing. Then the insulation can be used at temperatures around 371°C (700°F), provided it is not compressed.

Exposed polyurethane foam is not recommended as insulation material. Field experience reported degradation of the material from ultraviolet radiation followed by swelling.[16]

3.5 ABSORBER COATING/SUBSTRATE

The design of the absorber/substrate must ensure the following:

- High solar absorption
- High thermal conduction
- Low thermal emittance
- Durability over collector life

Temperature cycling endurance from -29°C to 121°C (-20°F to 250°F) for flat plate collector and 170°C (338°F) for concentrating collector

The absorber coating for a flat plate collector may be either selective or nonselective, and at low temperatures the collector will perform comparably with either kind. The maximum stagnation temperature is less than 200°C (392°F) for nonselective material and 250°C (482°F) for selective materials. If the collector is to be used solely for heating, then a nonselective coating is preferable because it is less costly and more durable. If the collector is to be used for heating and cooling, then a selective coating is preferable. The improvement in collector performance will more than offset the expense of high performance selective coatings. In concentrating collectors at high temperatures, selective coating is also used.

3.5.1 Non-Selective Coatings

Non-selective black coatings are of three types: paints, fused vitreous porcelain enamels, and metal conversion coatings. Paints may be either organic or inorganic; porcelain enamels and metal conversion coatings are both inorganic.

Of about 80 organic and inorganic pigments evaluated at Honeywell Inc. System and Research Center, [21] the iron-manganese-copper oxide (feno F-6331) had the best optical properties. Paint coatings made with this metal oxide have 0.92 absorbtivity (α) and 0.13 emissivity (ε) when in an aliphatic urethane binder. The material cost is estimated at 0.1¢/ft^2 and the total coating cost (material and fabrication) is about 5¢/ft^2. The paint coatings show good environmental stability, but their mechanical durability is poor. Their adhesion to substrates and their abrasion resistance need improvement. In service, peeling and cracking of paint coatings seem to be confined to absorber plate edges (within 2 or 3 inches of the edge) and to the lower portions of the absorber plate. [16]

Fused vitreous porcelains have the advantage of high temperature and long term durability, but non-glossy, "flat" coatings are difficult to formulate and require firing at from moderate to high furnace temperatures.

Among the chemically blackened coatings evaluated by NASA, [22] only

Ebonol C* treated copper, and Ebonol S-34 treated steel appear satisfactory. The other coatings (Ebonol Z treated zinc, Electroless Black Magic** treated aluminum, and anodized coatings of aluminum and titanium) lacked the right combination of optical properties.

3.5.2 Selective Coatings

Black iron plate is less costly than either chrome or nickel plate. The optically efficient black iron plate ($\alpha = 0.90$ $\varepsilon = 0.07$) can be made durable by applying a silicone overcoat with very little increase in ε. Black iron plate is attractive for low-cost collector applications. Besides, it uses non-strategic materials.(21)

Black chrome plate (Harshaw Process) and black iron plate (Ebonol S Process) are the most promising selective coatings for flat plate solar collector applications. Black chrome plate has good optical properties ($\alpha = 0.95$ $\varepsilon = 0.09$) and is most durable. The coating life was estimated to be longer than 30 years when a half-mil nickel (Harshaw NUSAT) undercoat was used. Quarter-mil nickel has been verified to provide enough protection to the steel substrate.(21)

Double layer black nickel on nickel plated steel can be routinely made with $\alpha = 0.95$ and $\varepsilon = 0.07$. However, this coating is relatively expensive and has proven highly susceptible to degradation when exposed to humidity in laboratory tests and service.(2,16)

Two problems of selective coatings that must be overcome are: (1) their need for antireflection coatings and (2) their reliability during short or long-term exposure under use conditions.(12) The durability of most selective coatings is a function of photo-oxidation processes at the conductive metal substrate -- processess that are generally accelerated by moisture and other volatile contaminants. Selective coatings of demonstration site collectors will have to be evaluated after five or more years of exposure in order to correlate service data with accelerated laboratory tests.

---

* Trade name of Euthone, Inc.

** Trade name of Michell-Bradford Company

Antireflection (AR) coating is needed because the high absorption coefficient for solar radiation of many selective coatings gives rise to a high complex refractive index and, therefore, high Fresnel reflection at solar wavelengths. This phenomenon requires an additional, antireflection (AR) coating to couple the system's refractive index with that of air in a non-evacuated system. The coupling can be achieved by both single and multiple layers (stacks) of thin film. Recent laboratory tests [21] indicate that dipped organic AR coating on glass is promising. It increases the solar transmission by about 5% (0.35 μm to 0.75 μm) at an estimated material cost of about 0.15¢/ft^2. However, the coating adhesion and its abrasion resistance are poor and need further improvement.

3.6 ABSORBER PANEL

The design considerations for the absorber substrate of a cost effective collector configuration are: (a) thermal performance, (b) reliability, (c) operating pressure flow distribution in large arrays and pumping power, and (d) fabrication and materials costs. Since demonstration-site absorber panels are all made of high conductive metals (copper, aluminum, iron and steel), the premature failures of collector panels are not anticipated, except for corrosion by heat transfer liquid at the internal passage. (See Section 4.1)

4 ENERGY TRANSPORT SUBSYSTEMS

The energy transport subsystem transfers heat energy from the collector subsystem to the storage subsystem and from the storage subsystem to the point of use.

4.1 HEAT TRANSFER FLUID

When aqueous liquid is used as the heat transfer fluid, the degradation of the liquid/inhibitor with time and temperature will initiate metallic corrosion at the inside surface of the containment material and localized corrosion of dissimilar metal interconnections. Nonaqueous liquid is not corrosive to containment material unless the liquid is contaminated by corrosive products or water. Liquid decomposition generates corrosive products. Water can be initially present or picked up from the solar systems.

The corrosion damage is more severe at the internal surface of the absorber tubing that emits heat to the liquid than at the piping surface heated by the fluid.[23] At the demonstration sites, the aqueous liquids include inhibited water, ethylene glycol/water and propylene glycol/water, and the nonaqueous liquids include silicone oil and hydrocarbon oil. If the breakdown of the aqueous liquid or its inhibitor can be *in-situ* monitored and adjusted then subsequent corrosion-erosion of collector and transport subsystems can be prevented. The "voltage corrosivity sensor" (an experimental sensor developed by Texas Instruments Company) measures the static potential by detecting the difference in voltage between a sensing and a reference electrode (Figure 9). Any degradation of the heat transfer fluid or its inhibitor is indicated by a lowering of solution potential, and a signal is amplified by the "voltage corrosivity sensor." The development of the original sensor, designed for use in automotive coolant, will be discussed at the AES meeting in April, 1979.[24]

As a part of the materials assessment program in the ASDP, *in-situ* "voltage corrosivity sensors" are being installed in transport subsystem lines at 5 selected demonstration sites using inhibited water or anti-freeze (ethylene glycol/water) as the heat transfer liquid.[2] Figure 10 is a typical illustration of a laboratory test on the thermal breakdown of inhibited 50% antifreeze (ethylene glycol) when the fluid temperature is raised from the normal collector (flat plate) operating range (between 85°F and 228°F) to stagnation condition (278°F). It is seen that the potential is suddenly lowered to the corrosive regime of carbon steel (below -0.5 volt). In addition, the sensor potential does not return to its original value when the fluid is cooled back to the operating temperature range.

4.2 INTERNAL CORROSION

At the solar demonstration sites, aqueous liquid is in contact with internal surfaces in single or mixed metal systems. The metals are (a) aluminum, (b) copper and brass, and (c) iron and steel. A cursory review of the literature on inhibitors against metallic corrosion used in ethlylene glycol formulation is given below:[2]

1. Copper and Brass - 2 mercaptobenzothiazole (MBT), benzotriazole (BTZ), and tolyltriazole (TTZ) all form insoluble copper complexes

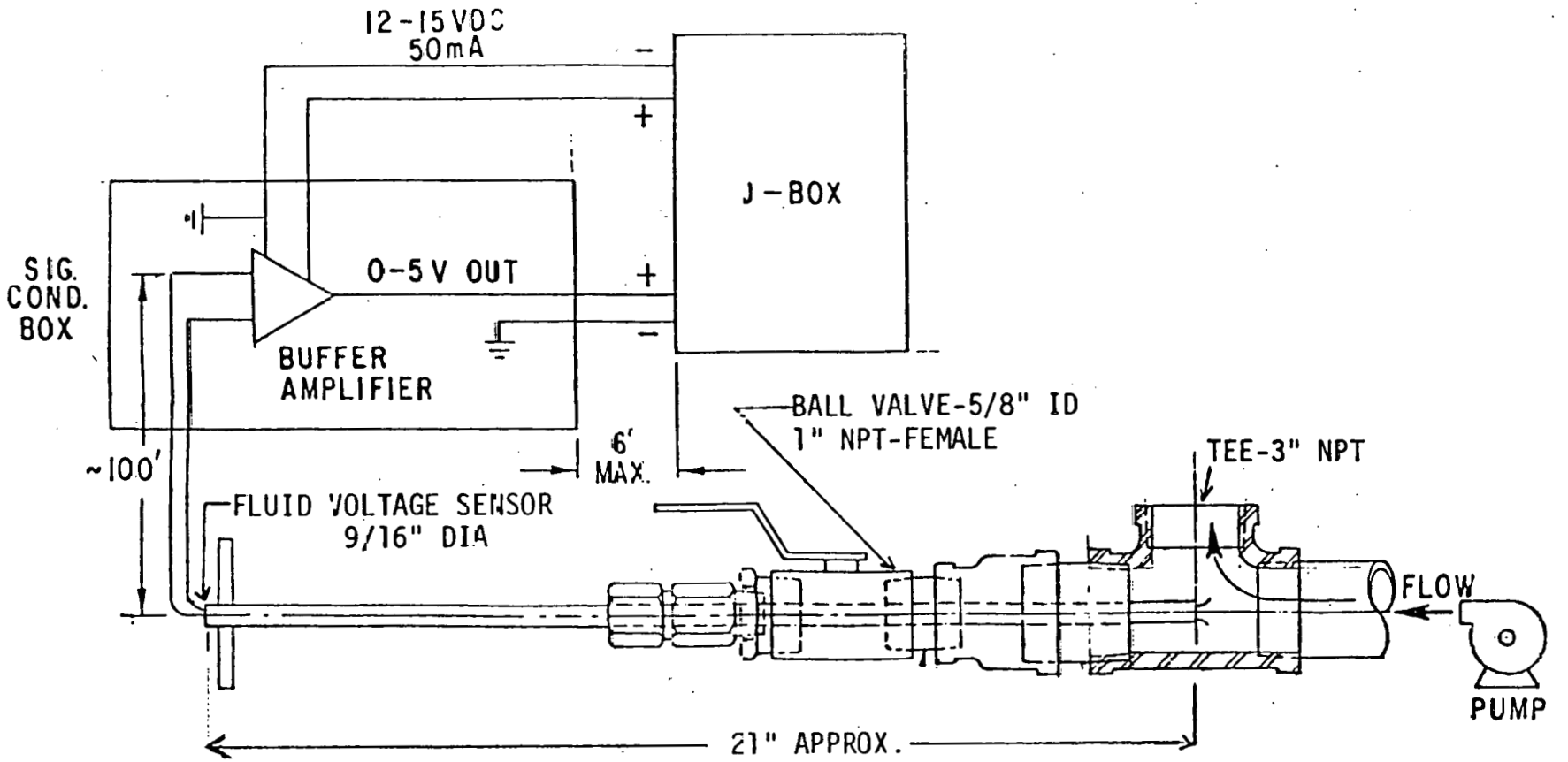


Fig. 9 Voltage Corrosivity Sensor--Solar Collector Piping System

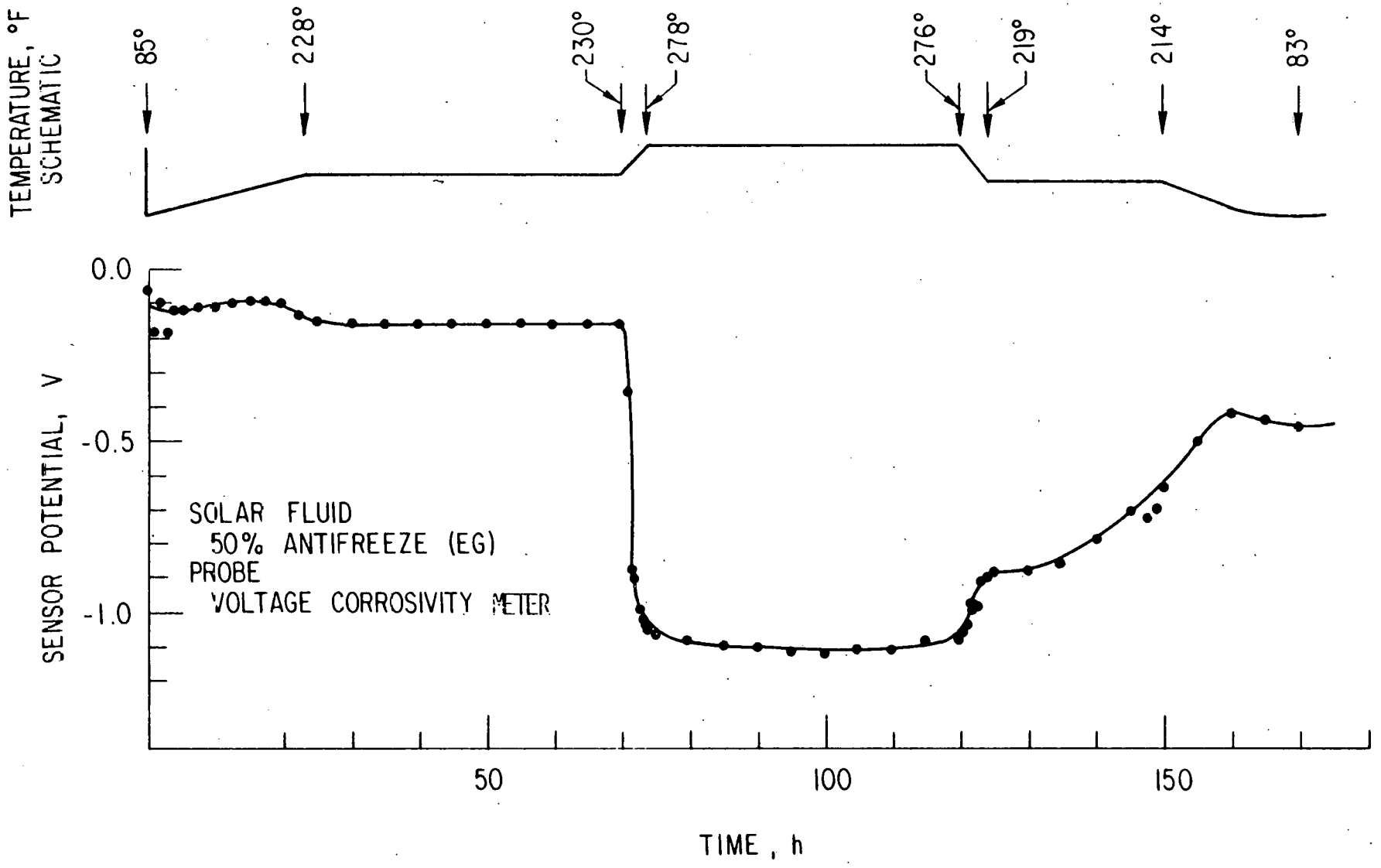


Fig. 10 Thermal Breakdown of Solar Fluid--Solution Potential vs. Time

on metal surfaces. These copper inhibitors indirectly protect less noble metals in the same system by suppressing copper ions in solution, thereby preventing galvanic corrosion and pitting due to copper plating on the other metal surface. TTZ and BTZ are preferable to MBT because they have better thermal stability. Also MBT converts to insoluble and ineffective disulfide via oxidation reactions and photochemical excitation by the absorption of visible or ultraviolet light.

2. Aluminum - Phosphates in various forms and silicate in silicone silicate copolymer are used to protect aluminum because they form insoluble metal phosphate. Sodium nitrate is also used in forming or repairing the protective oxide film on aluminum.

3. Iron and Steel - Borates, phosphates, benzoates, arsenites and silicates all function as ferrous metal inhibitors by forming protective films. Additionally, borates and phosphates stabilize the pH of the solution.

4. Solder - There is no generally recognized inhibitor specifically for lead alloys, but corrosion protection is usually achieved by using either a silicate to form an insoluble film by controlling the pH of the solution, or by the use of a polar type oil which will absorb on the metal surface with a consequent inhibitor effect.

5. Sodium Nitrate ($NaNO_3$) - This iron inhibitor has to be used with care because under certain conditions it may have a deleterious effect on solders.

6. Chromates - The oxidizing action of chromates for iron protection not only depletes the inhibitor but the redox products may be detrimental to solar systems.

This review is in agreement with the recently formulated antifreeze (ethylene glycol) product developed for the automotive industry for use in aluminum engines.[25] This product contains the following concentration of inhibitor by weight percent in the antifreeze concentrate:

0.21 sodium nitrate ($NaNO_3$);
0.98 sodium borate ($Na_2B_4O_7 5H_2O$)
0.17 sodium silicate ($Na_2SiO_3 \cdot 5H_2O$):

0.43 trisodium phosphate ($Na_3PO_4 \cdot 12H_2O$);
0.55 of a 50% water solution of sodium salt of MBT and 0.19 sodium hydroxide (NaOH).

This combination of inhibitors was selected after evaluating a large number of candidate formulas. Each chemical serves a particular purpose:

1. Nitrate for protection of aluminum and solder,
2. Borate for its buffering action, reserve alkalinity and protection of ferrous metals,
3. Silicate for general protection of all metals,
4. Phosphate for its protection of ferrous metals and aluminum and its buffering action,
5. MBT for protection of copper and brass,
6. NaOH for additional reserve alkalinity.

Furthermore, silicate and phosphate are effective against cavitation.

This type of formulated antifreeze provided excellent corrosion protection at a 44% concentration, using corrosive water for dilution, in 10 test cars for a two-year period with an accumulated mileage in each car of 20 to 25,000 miles. Normal depletion of silicate, MBT, and phosphate occurred, but the pH and reserve alkalinity of the coolant solutions showed only a nominal change in two years. The product has reasonably good storage stability, good compatibility with other antifreezes, good high temperature stability, and good protection against cavitation.

4.3 LOCALIZED CORROSION

Failure to provide dielectric separation between dissimilar metal interconnections can initiate localized galvanic corrosion. Where copper tubing has been connected to an aluminum collector, corrosion of the more active aluminum has been reported. Similarly, material incompatibility between the threaded copper pipe and connecting steel flange accelerated localized corrosion of the more active steel flange face to the extent of leaking aqueous liquid. The problem was resolved by refitting with brass flange. Leakage of soldered connections in joining copper piping was traced to the use of low temperature flux. The resoldered joints using nonacid organic flux (95-5)

exhibited no leaking.

4.4 STORAGE TANKS

The problems in storage subsystems are predominantly system problems. Some material failures of storage tanks are:[26]

1. Leaking of fiberglass tank due to threads perforating the tank wall permitting "wicking" of water.
2. Wetting of insulation and loss of insulation properties due to water leakage.
3. Use of a fiberglass-reinforced epoxy tank which cannot stand maximum tank temperature.
4. Galvanic corrosion of underground steel tank in acid soil due to failure to provide cathodic protection.

4.5 ORGANIC HOSE

Organic hose materials must be able to withstand temperature cycling endurance from -29°C to 121°C (-20F to 250°F), ultraviolet radiation, and ozone. At some sites, sulphur dioxide resistance might be required. Finally the amount of compression set is an important parameter in maintaining leak-tight hose joints.

With these requirements in mind, several major hose manufacturers were contacted, and they agreed that the life expectancy of organic hoses would be 5 to 7 years. Their consensus on hose materials is summarized below:

RECOMMENDED	ACCEPTABLE	NOT RECOMMENDED
EPDM Rubber (ethylene Propylene-diene terpolymer)	Butyl (isobutylene isoprene)	Natural Rubber (polyisoprene)
Viton (Fluorelastomer)	Neoprene (chloroprene)	Buna N (butadiene-acrylonitrile)

RECOMMENDED	ACCEPTABLE	NOT RECOMMENDED
Hyphon (chloro-sulfonyl polyethylene)	-	Buna S (styrene butadiene)
Silicone (polysilofane polymer)	-	-

5 SUMMARY AND CONCLUSIONS

A preliminary review of the literature assessing materials used in solar demonstration systems was made. The following were highlighted for collector subsystems:

1. Accelerated atmospheric corrosion experiments on batten/enclosure materials are monitored *in-situ* at 15 sites with representative climatic conditions. Telemetry from atmospheric corrosion monitors (Cu/Zn Couple), relative humidity meters, and ambient temperature sensors are recorded by the National Solar Data Network. Data will be calibrated against the weight loss of coupons housed in an adjacent atmospheric corrosion rack.

2. Tempered and etched low-iron glass is preferred for the outer cover plate. Plastic film (e.g. Teflon FEP, Tedlar PVF, Sunlite Premium, and Mylar) is recommended for the inner cover plate.

3. Low-cost semi-rigid fiberglass block is recommended as insulation material, if preheated above 177°C to drive off volatile binders prior to collector assembly. Polyurethane foam is not recommended as exposed insulation material since it degrades by ultraviolet radiation.

4. Among the numerous chemically blackened coatings, Ebonol C treated copper and Ebonol S-34 treated steel appear satisfactory as non-selective coatings.

5. Black chrome plate with 1/4 mil nickel plate undercoat and black iron plate with silicone overcoat are the two most promising selective coatings for the absorber panel.

In energy transport systems, the following were discussed:

1. "Voltage Corrosivity Sensors" can detect the early breakdown of the transport liquid/inhibitor. Experimental models are being installed in the transport systems of 5 selected demonstration sites.
2. The role of different inhibitors (in ethylene glycol formulation) to prevent internal piping corrosion of (a) aluminum, (b) copper and brass, and (c) iron and steel are discussed.
3. Localized galvanic corrosion at dissimilar metal interconnections was attributed to the absence of a dielectric separator between the connections.
4. Galvanic corrosion of an underground steel tank in acid soil can be prevented by cathodic protection.
5. Natural rubber hoses (Buna N and Buna S) degrade by ultraviolet radiation and ozone. The recommended list of organic hoses from manufacturers data includes EPDM rubber, Viton, Hyphlon and silicone.

ACKNOWLEDGEMENT

The work described in this paper was performed under the auspices of the Department of Energy as part of the National Solar Data Program under the direction of H. Jackson Hale, Program Manager, Demonstration Program Branch.

REFERENCES

(1) *ANL Solar Data Project Plan,* Argonne National Laboratory report ANL/SDP-TM-78-1 (September 1978).

(2) Chopra, P.S., C.F. Cheng, and R.M. Wolosewicz, *Preliminary Evaluation of Selected Reliability, Maintainability and Materials Problems of Solar Heating and Cooling Systems,* Argonne National Laboratory report ANL/SDP-TM-78-2 (September 1978).

(3) Chopra, P.S. and R. Wolosewicz, *Freezing Problems in Operational Solar Demonstration Sites,* to be presented at Solar Heating and Cooling Systems Operational Results Conference, Colorado Springs (November 29 - December 1, 1978).

(4) Wolosewicz, R., et al, *Reliability and Maintainability Evaluation of Freezing in Solar Systems,* Argonne National Laboratory report ANL/SDP-TM-78-3 (September 1978).

(5) Wolosewicz, R., et al, *Reliability and Maintainability Evaluation of Collector to Manifold Leaks,* Argonne National Laboratory, unpublished information (1978).

(6) Wolosewicz, R., et al, *Reliability and Maintainability Evaluation of Control Systems,* Argonne National Laboratory, unpublished information (1978).

(7) *National Solar Data Network, Solar - 77-17, Dec. 1977: Solar Heating and Cooling Demonstration Project Summaries* DOE/C5-0009, May 1978, DOE, Washington D.C.

(8) Middleton, R.E., *The Solar Heating and Cooling Demonstration Program at Marshall Space Flight Center - Some Problems and Conclusions,* 15th Space Conference, Cocoa Beach, Florida (April 1978).

(9) Deacon, D.H., and A.J. Sansum, *Full Time Inspection Minimizes Paint Failures in the North Sea,* Materials Performance, August 1977, p. 25.

(10) Barton, F., *Schutz Gegan Atmospherische Korrosion,* Verlag Chemie ed., Weinheim/Bergsta, West Germany, Chap. 3 (1973).

(11) Mansfeld, F., and J.V. Kenkel, *Electrochemical Measurements of Time-Of-Wetness and Atmospheric Corrosion Rates,* Corrosion, 33:13-16 (1977).

(12) Zerlaut, G.A., *Fundamental Material Considerations for Solar Collectors,* in Critical Material Problems in Energy Production, Charles Stein, ed., Academic Press, Inc., New York, Chap. 13 (1976).

(13) Ratzel, A.C. and R.B. Bannerat, *Commercially Available Materials Suitable For Use in Flat-Plate Solar Energy Collectors,* in Proc. 1977 Flat-Plate Solar Collector Conference, D. B. Ward, ed., pp 387-394, Florida Solar Energy Center, Cape Canaveral, Florida (February 28 - March 2, 1977).

(14) Holland, T. H., *Design, Fabrication, and Testing of Low-Cost Flat-Plate Collector,* in ibid., pp. 47-62.

(15) Baldwin, A. J., *Performance and Durability of Acid-Etched Solar Glass,* presented at ANL Solar Materials Conference, 1978.

(16) Skoda, L.F., and L.W. Masters, *Solar Energy System - Survey of Material Performance,* NSSIR 77-1314, October 1977, p. 4.

(17) Ribbans, R. C. III, *Teflon FEP Fluorocarbon Film for Flat-Plate Solar Collectors,* in Proc. 1977 Flat-Plate Solar Collector Conference, pp. 367-376.

(18) Pettit, Richard B., *Characterization of the Refelected Beam Profile of Solar Mirror Materials,* Solar Energy, 19: 733-741, and personal communication.

(19) Davis, M. J., Sandia Laboratory, personal communication, 1978.

(20) Streed, E. R., *Tests and Standards for Solar Energy Systems, A State-of-Solar-Technology Summary Report,* in Proc. 1977 Flat-Plate Solar Collector Conference, pp. 37-38.

(21) Lin, R. J. H., and P. B. Zimmer, *Optimization of Coatings for Flat Plate Solar Collectors,* Honeywell Inc., Systems and Research Center, Minneapolis, Minnesota, COO-2930-13 for ERDA Contract No. EY-76-C-02-2930.*000 (July 1977).

(22) Lowery, J. R. *Solar Absorption Characteristics of Several Coatings and Surface Finishes,* Marshall Space Flight Center, NASA TMX-3509 (Mar. 1977).

(23) Walker, M. S., *Effect of Inhibitor in Antifreeze on Corrosion of Heat Rejecting Surfaces,* Materails Protection Performance, 12:29 (1978).

(24) Baboian, Bob and J. S. Hayne, *Detecting Coolant Corrosion With Electrochemical Sensors,* to be presented at ASTM Symposium on State-of-the-Art of Engine Cooling Testing, Atlanta, Ga. (April 9-11, 1979).

ELECTROCHEMICAL MEASUREMENTS OF TIME-OF-WETNESS AND ATMOSPHERIC CORROSION RATES

by

F. Mansfeld and J. V. Kenkel

Rockwell International Science Center

Thousand Oaks, California

Electrochemical Measurements of Time-of-Wetness and Atmospheric Corrosion Rates★

F. MANSFELD and J. V. KENKEL *

Abstract

An atmospheric corrosion monitor has been developed which allows monitoring of time-of-wetness and corrosion behavior in outdoor exposure. This device is being used in exposure studies in Southern California and has also been applied to laboratory studies of atmospheric corrosion, in which the effects of salt particles, gaseous pollutants, impurities in rust, temperature, and relative humidity are evaluated.

Following the finding of Vernon[1] in 1931 that beyond a "critical relative humidity" corrosion of a material exposed to the atmosphere will take place, it has become apparent that measurements of the time at which this critical humidity is exceeded are very important. Sereda[2] has developed a method for measuring the so-called "time-of-wetness" of test panels and has carried out a number of investigations of atmospheric corrosion this this method. A summary of his work has been given recently.[3] Sereda's method is based on the measurement of the galvanic current flowing between zinc and platinum during atmospheric exposure. This galvanic current develops in the presence of moisture, and time-of-wetness is somewhat arbitrarily defined as the period during which the galvanic current measured as the voltage drop across a 10 MΩ resistor exceeds 0.2 V. Gutman[4] has used Sereda's measuring device and has concluded that for a 4 year average, the time-of-wetness corresponds to the time during which the relative humidity (RH) exceeds 86.5% at the test site in Birchbank, British Columbia, Canada.

In Sereda's measuring device,[2-4] a timer is started when the potential difference exceeds 0.2 V, and the total time-of-wetness is

★Submitted for publication May, 1976.

*Science Center, Rockwell International, Thousand Oaks, California.

Reprinted from CORROSION, Vol. 33, No. 1, pp. 13-16 (1977) January
Copyright 1977 by the National Association of Corrosion Engineers, 2400 West Loop South, Houston, Tx. 77027

recorded for a given test period. While this approach is certainly useful, it does not allow continuous monitoring of the corrosion behavior of a metal exposed to atmospheric conditions. Kucera and Mattson[5] have made some progress in this direction by developing an electrochemical technique which can be used to monitor atmospheric corrosion rates. They use a galvanic cell or an electrolytic cell and record the cell current during exposure. In the galvanic cell, a zero resistance ammeter (ZRA) as described by Lauer and Mansfeld[6] and additional electronic equipment are used which allow continuous recording up to 3 months in outdoor exposure. Kucera and Mattson[5,7] found that their instrument could distinguish between wet periods, when the galvanic current (I_g) is high as a result of surface moisture resulting from rain, dew, fog, or snow, and dry periods when the cell current was low. It was assumed that the surface becomes wet for $I_g > 1\ \mu A$.

Experimental Approach and Results

The approach taken by Kucera and Mattson[5,7] has been evaluated further by the authors in laboratory studies and outdoor exposure and some preliminary results have been reported.[8,9] The basic design of the atmospheric corrosion monitor (ACM) (Figure 1) has been described in detail elsewhere.[8,9] A number of galvanic couples have been used for construction of ACMs, such as Cu/steel, Cu/Zn, steel/Zn, Al/steel, and Al/Zn. For outdoor exposure studies, Cu/steel and Cu/Zn ACMs have been found to be most suitable since they show large variations of the current between "wet" and "dry" periods. Such ACMs have been exposed up to 4-1/2 months with continuous monitoring of the galvanic current. Due to the large variations of I_g between 10^{-2} and $10^{3}\ \mu A$, it has been found necessary to use a logarithmic convertor between the output of the ZRA and the strip chart recorder which is used to monitor the galvanic current. In this way, a direct plot of log I_g vs time (t) is obtained. The electrical arrangement is shown in Figure 2. The galvanic current is measured by the ZRA (A1), the output of which ($V_g = I_g R_m$) is fed into the log converter (A2). Since the log converter used accepts only positive or negative voltages and shows a very large negative output for very low input voltages, it was necessary to add a small constant voltage $V_o = 3$ mV to the input of A2, which will be measured when the surface becomes dry ($V_g \rightarrow 0$).

A program was started in January, 1975 in which one or two ACMs were exposed for various times on the Science Center roof to provide a continuous record of atmospheric corrosion over a 2 year period. Simultaneously, samples of weathering steel and galvanized steel were exposed which will be removed at different times in order to provide correlations between ACM readings and corrosion behavior. Starting in October, 1975, RH and temperature are also monitored at the exposure site of the ACM. Figure 3 shows results obtained for two Cu/steel ACMs exposed at an angle of 30° to the south for a 24 hour period in July, 1975. The purpose of the experiment in Figure 3 was to find out whether the length of exposure influences the results obtained with ACMs. The devices used in the experiment of Figure 3 had been exposed for 32 and 105 days, respectively, with only traces of rain recorded during this time period. Due to the nightly occurrence of dew, both ACMs had a thick rust layer. The curves in Figure 3 shows that even small details are recorded very similarly by both ACMs. The galvanic current rises in the early evening hours and decreases sharply in the morning. These results show that ACMs will give similar results independent of exposure time once a corrosion product layer has been formed on which an electrolyte layer can be formed at RH < 100% by the mechanism discussed earlier.[9] A freshly polished ACM would have shown only minor current peaks during the 24 hour period of Figure 3.

Figure 4 shows galvanic current, relative humidity, and temperature measurements for the 20 day period between October 27, 1975 and November 16, 1975 using a Cu/steel ACM which had been first exposed on July 16, 1975. During the period covered in Figure 4, it rained only 1 day (October 30, 1975). The sharp rise of the galvanic current which occurred every evening—except for a 3 day period from November 11 to November 13, 1975—is therefore due to condensation of dew. The galvanic current-time curve is, in most cases, very similar to that shown in more detail in Figure 3. There is a striking correlation between I_g and RH values as a function of time, maxima and minima of I_g corresponding to maxima and minima of RH, respectively. There is also a correlation between RH and temperature, in this case a maximum in temperature corresponds to a minimum of RH. This correlation between temperature and RH does not hold for the period between November 11, 1975 and November 13, 1975 when due to Santa Ana wind conditions the RH stayed below 20% and no signal was observed from the ACM.

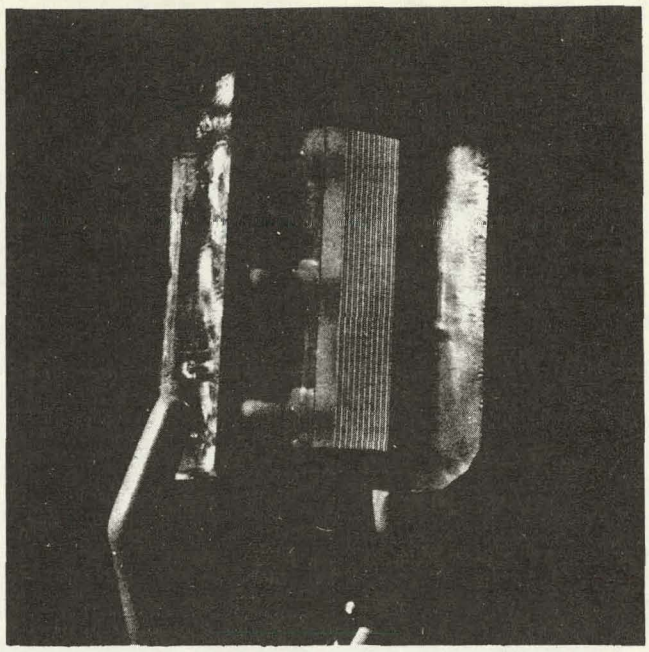


FIGURE 1 — Atmospheric Corrosion Monitor (ACM).

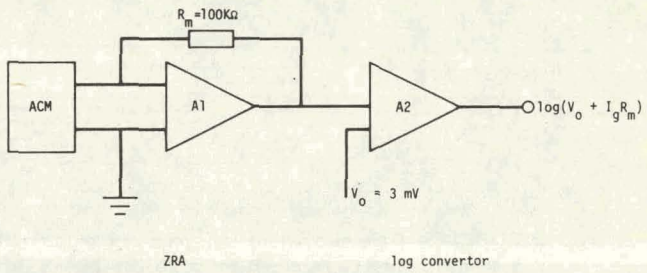


FIGURE 2 — Sketch of electrical arrangement.

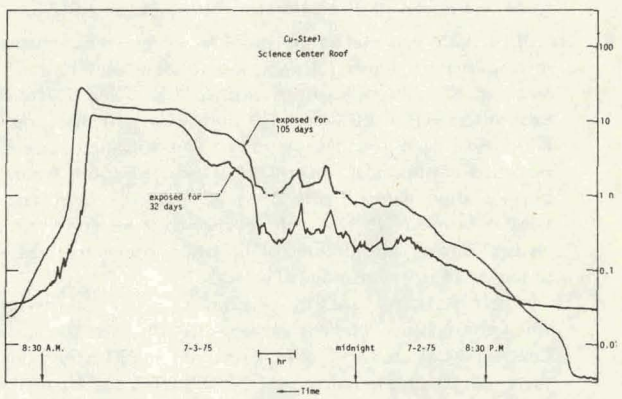


FIGURE 3 — Galvanic current (I_g)—time traces for two Cu/steel ACMs exposed for different lengths of time on the Science Center roof.

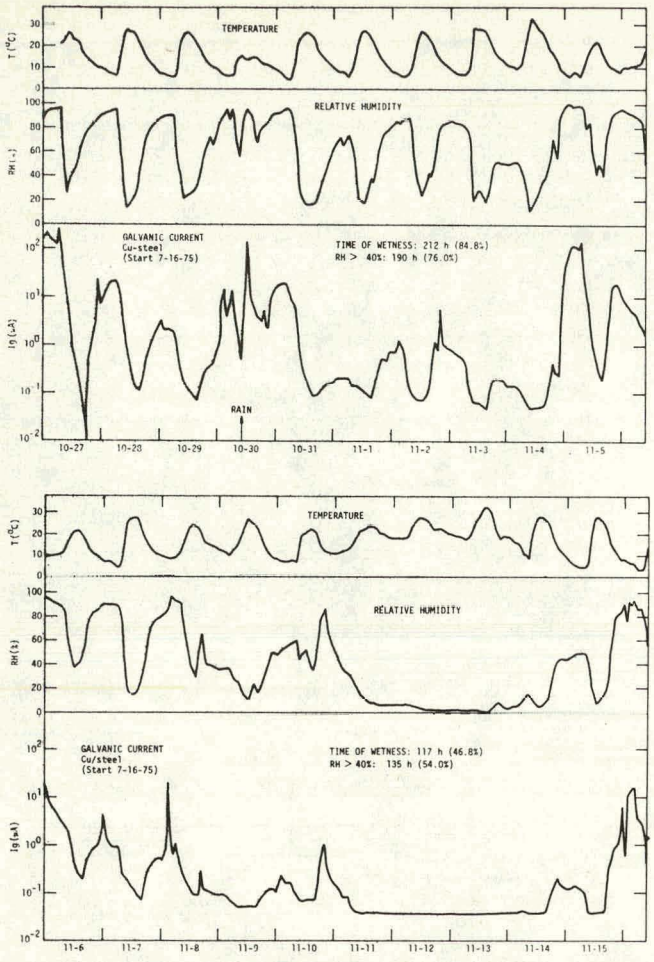


FIGURE 4 — Galvanic current (I_g), relative humidity (RH), and temperature (T) recorded for a 20 day period on the Science Center roof.

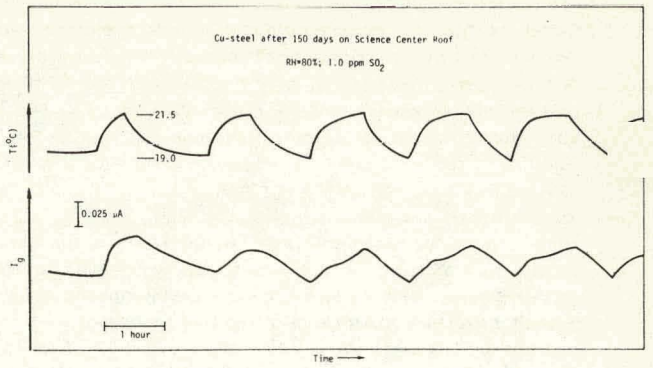


FIGURE 5 — Effect of temperature fluctuations on signals (I_g) recorded with Cu/steel ACM in laboratory experiment (SO_2 = 1.0 ppm, RH = 80%).

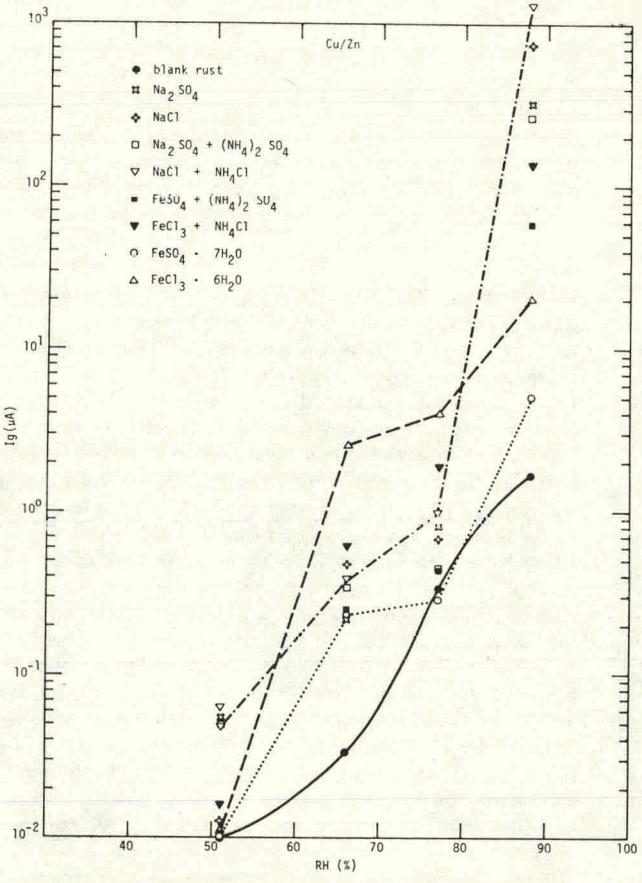


FIGURE 6 — Galvanic current (I_g) for Cu/Zn ACM covered with rust containing various additives (2.5 Wt%) total) for various relative humidities (RH).

The effect of temperature on the galvanic current of a Cu/steel ACM was observed in a laboratory study of the ACM used in Figure 4. This ACM was placed in a test cell which was connected to a gas mixing system which allows one to control RH and add small amounts of pollutants to the air or nitrogen. The Cu/steel ACM was exposed at RH = 80% and 1.0 ppm SO_2, which is the maximum SO_2 level used in these studies. The galvanic current (I_g) was recorded continuously overnight as was the room temperature (T) using a thermistor. Figure 5 shows that the fluctuations of the temperature due to the night cycle of the air conditioning system leads to similar fluctuations of I_g, which shows the great sensitivity of the ACM to environmental effects.

If it is assumed that the test surface is wet and corrosion occurs when the galvanic current exceeds 0.1 μA, then the surface of the Cu/steel ACM used in Figure 4 was wet for 212 hours or 84.8% of the total 10 days between October 27, 1975 and November 5, 1975 and for 117 hours or 46.8% of the total time between November 6, 1975 and November 15, 1975. If one compares the changes of I_g and RH in Figure 4, one finds that the I_g values exceed 0.1 μA at the time when RH exceeds 40%. Figure 4 shows a close correlation between time-of-wetness and RH $>$40%. These findings suggest that the usually accepted "critical humidity"[1] of 60 to 70% is by far too high, probably because it does not take into account the effect of pollutants in formation of corrosion product layers which cause condensation of electrolyte. The finding of Gutman[4] that the time-of-wetness corresponds to RH $>$ 86.5% is surprising in the light of the results presented here. It is possible that at a site, which is relatively free of atmospheric pollutants, corrosion products are formed which condensate moisture only at higher RH. The authors have shown for example[8,9] that chloride ions on ACM surfaces lead to condensation and current flow at lower RH than sulfates. In further laboratory experiments (Figure 6), it was shown for Cu/steel and Cu/Zn ACMs that rust, when doped with chloride ions, produced higher currents than rust doped with sulfates. The rust was prepared similar to Chandler's procedure,[10] and various salts were added at a total concentration of 2.5 Wt%. This mixture was placed on a freshly polished ACM, and the current measured over an 8 hour period at 4 RH levels. At the highest RH level, the spread of I_g values reaches almost three orders of magnitude, showing the tremendous effect of impurities in corrosion products on corrosion behavior. If it is again assumed that the surface becomes wet f $>$0.1 μA, then the "critical RH" would be about 73% for rust ... of additions, and as low as 55% for doped rust. In the cases of Zn, which is used in Sereda's device, condensation should occur at RH = 10% provided $ZnCl_2 \cdot H_2O$ is formed[11] as discussed by

Bukowiecki.[12,13] Considering these results, the critical humidity reported by Gutman seems to be unusually high. An analysis of the data of Kucera and Mattson[5,7] is more difficult since in this case I_g is sometimes seen to decrease when RH increases and vice versa. For the remaining time, the current is exceeding 0.1 μA for RH $\geqslant$ 75%.

Discussion

The parameter measured with the use of ACMs is the galvanic current (I_g). The relationship of I_g with the dissolution rate of the anode in a galvanic couple and the corrosion rate of the uncoupled metal has been given by the authors in a series of papers concerning galvanic corrosion of Al alloys[14-16] and other metals.[17,18] For the case of a corrosion reaction in which the cathodic (reduction) reaction is under diffusion control, as one would expect in neutral, aerated solutions, it was shown that the galvanic current density (i_g^A) with respect to the anode is related to the limiting diffusion current density (i_L) for oxygen by:

$$i_g^A = i_L \frac{A^C}{A^A} \quad (1)$$

where A^C/A^A is the area ratio of cathode to anode and $i_g^A = I_g/A^A$. Since for this system the corrosion current density (i_{corr}^A) of the uncoupled anode equals the limiting current density (i_L):

$$i_{corr}^A = i_L \quad (2),$$

the galvanic current density (i_g^A) is a measure of the corrosion rate of the anode in the couple:

$$i_g^A = i_{corr}^A \cdot \frac{A^C}{A^A} \quad (3)$$

For an area of one as used in the ACM, the measured galvanic i_g^A equals the corrosion current density of the uncoupled anode:

$$i_g^A = i_{corr}^A \quad (4)$$

This analysis shows that in the present application use is made of a galvanic corrosion phenomenon in order to measure the corrosion rate a metal would have without any coupling to a dissimilar metal, whereas in the more common studies of galvanic corrosion the same measurement would be used to assess to increase of the dissolution rate of an anode due to coupling to a cathode.[15-18] The results presented in Figure 3-6 show, therefore, the changes of the corrosion rate of steel or Zn as a function of time or RH, since according to Equations 1-4:

$$I_g = k_1 r \quad (5)$$

where r is the corrosion rate, and k_1 a constant.

It is clear from the experimental data that the ACM readings provide detailed information concerning time-of-wetness of test panels as discussed for Figure 3. In addition, it has become apparent that one obtains also a measurement of the corrosivity of a given test site since the corrosion rate is measured directly according to Equation 5. The recording of ACM data, therefore, results in time-of-wetness *and* corrosion rate or corrosivity data, thereby exceeding the possibilities of Sereda's device.[2] It has to be cautioned that these calculations are based on the theoretical analysis of galvanic current data (Equations 1-5) which is derived for the ideal case of pure diffusion control. Comparison of electrochemical and weight loss data is necessary to evaluate this concept. Such measurements are presently carried out in the laboratory, while further evaluations of ACMs is carried out by exposure in St. Louis, Missouri, where exposure tests for a large number of metals are carried out at 9 test sites,[19] at which all important air quality parameters are measured continuously under the Regional Air Pollution Study (RAPS) for the Environmental Protection Agency.

Acknowledgment

This work was sponsored by the Office of Naval Research under Contract N00014-75-C-0788, NR036-108.

References

1. W. H. J. Vernon. Trans. Far. Soc., Vol. 27, p. 265 (1931); Vol. 31, p. 1668 (1935).
2. P. J. Sereda. ASTM Bulletin No. 246, p. 47 (1960).
3. P. J. Sereda. Corrosion in Natural Environments, ASTM STP 558, p. 7 (1974).
4. H. Gutman. Metal Corrosion in the Atmosphere, ASTM STP 435, p. 223 (1968).
5. V. Kucera and E. Mattsson. Corrosion in Natural Environments, ASTM STP 558, p. 239 (1974).
6. G. Lauer and F. Mansfeld. Corrosion, Vol. 26, p. 504 (1970).
7. F. Mansfeld and J. V. Kenkel. Corrosion/75, April 14-18, 1975, Toronto, Canada, Paper No. 161.
8. F. Mansfeld and J. V. Kenkel. Electrochemical Monitoring of Atmospheric Corrosion Phenomena, Corrosion Science, Vol. 16, p. 111 (1976).
9. V. Kucera and E. Mattsson. 7th Scand. Corr. Cong., Trondheim Norway, May 26-28, p. 202 (1975).
10. K. A. Chandler. Brit. Corrosion J., Vol. 1, p. 264 (1966).
11. K. Barton. Schutz gegen Atmospharische Korrosion, Verlag Chemie, Weinheim, West Germany (1973).
12. A. Bukowiecki. Schweiz. Archiv., Vol. 23, p. 97 (1957).
13. A. Bukowiecki. Oberflache–Surface, Vol. 13, p. 219 (1972).
14. F. Mansfeld, D. H. Hengstenberg and J. V. Kenkel. Corrosion, Vol. 30, p. 343 (1974).
15. F. Mansfeld and J. V. Kenkel. Corros. Sci., Vol. 15, p. 183, 239 (1975).
16. F. Mansfeld. Werkstoffe und Korrosion, Vol. 25, p. 518 (1974).
17. F. Mansfeld and J. V. Kenkel. Corrosion, Vol. 31, p. 298 (1975).
18. F. Mansfeld and J. V. Kenkel. Werkstoffe und Korrosion, Vol. 26, p. 699 (1975).
19. F. Mansfeld. Study of the Effects of Airborne Sulfur Pollutants on Materials–One-Year Exposure Report, Rockwell International Air Monitoring Center, Creve Coeur, Mo. 63141, SC553.T026AR-1, January 1976.

THIS PAGE

WAS INTENTIONALLY

LEFT BLANK

Flat-Plate Collector

RESULTS OF THIRTY MONTHS ATMOSPHERIC CORROSION TESTING IN ST. LOUIS, MO., USA

by

F. Mansfeld

Rockwell International Science Center

Thousand Oaks, California

RESULTS OF THIRTY MONTHS ATMOSPHERIC CORROSION TESTING IN ST. LOUIS, MO., USA

F. Mansfeld
Rockwell International Science Center
Thousand Oaks, California 91360

ABSTRACT

Samples of galvanized steel, weathering steel, Al 2014 and 7079 tension samples, silver, marble, and two types of house paint have been exposed for various lengths of time Atmospheric data which include wind speed and direction, temperature, relative humidity, total sulfur, SO_2, H_2S, O_3, NO_x, total hydrocarbon, total suspended particulates, sulfate and nitrate concentrations have been collected at each of the nine exposure site under the Regional Air Monitoring System (RAMS).

For galvanized steel and weathering steel, four different sets have been exposed in order to study the effect of the atmospheric conditions at first exposure on subsequent corrosion behavior. For galvanized steel a pronounced effect of time of first exposure was observed, while the corrosion behavior of weathering steel did not seem to depend on t seasonal effects.

House paint showed discontinuous corrosion behavior with time. Exposure to the south was more corrsive than exposure to the north for both latex and oil base paint. The integral corrosion rates for latex base paint were higher than those for oil base paint.

Tarnishing of silver plated samples was measured by the reflectance loss and by an electrochemical technique. At some sites 50% reflectance loss occurred after 3 months exposure. The Al tension samples showed different behavior, Al 2014 showing a larger dependence of time-to-failure on test site.

A first attempt has been made to provide a statistical correlation between corrosion and atmospheric data using a multiple regression model. Some of the apparent inconsistencies which seem to occur in the estimated effects of pollutants on corrosion behavio are believed to be due to multi-collinearity. Corrosion (CCN) and Pollutant Code Numbers (PCN) have been assigned to each test site based on the average corrosion values and pollutant levels. No obvious correlations between corrosion behavior and atmospheric conditions can be obtained by comparison of these numbers.

INTRODUCTION

A thirty months exposure study starting in October 1974 has been performed for the United States Environmental Protection Agency (EPA) as part of the Regional Air Pollution Study (RAPS) with the purpose to determine the effects of airborne sulfur pollutants on the corrosion behavior of materials. Table I lists the materials, exposure conditions, sample preparation and methods for assessment of the corrosion damage. The samples were exposed at nine sites on ASTM exposure racks at 30 degrees facing south, except for the paint samples which were exposed vertically facing north and south and the silver plated discs which were exposed vertically in louvered shelters. Exposure sites #103, 105, 106, 108 and 112 are close to the inner city, while sites #115, 118, 120 and 122 are located in rural or partially industrial areas further away from the center of St. Louis. Exposure occurred on the roof of the monitoring stations which recorded continuously a large number of air quality parameters. For the intended correlation between corrosion behavior and pollution, the following air quality parameters were chosen: wind speed, wind direction, temperature, relative humidity and the concentrations of: ozone, total hydrocarbon (THC), NO_x, total sulfur (TS), SO_2, H_2S, sulfate, nitrate and total suspended particulates (TSP).

At selected test sites, atmospheric corrosion monitors (ACM) of the type described by Mansfeld and Kenkel (1,2) were exposed to determine the time-of-wetness and atmospheric corrosion rates. These data (5) and all atmospheric data were stored on computer tape. For analysis, the atmospheric data were received from the Rockwell Air Monitoring Center in St. Louis in the form of hourly averages which were then further processed into a suitable format.

Samples were removed after 3, 6, 12, 18, 24 and 30 months exposure except for the silver samples which were removed every three months. The Al tension samples were removed as soon as failure had occurred. In order to evaluate the effects of seasonal variations, new sets of galvanized steel and weathering steel were exposed in October 1974, January, April and July 1975 at all nine test sites. A new set of silver was exposed at the start of the second year.

The weight loss data were analyzed following the approach suggested by Bohnenkamp (3) and Schwenk (4). From the experimental data the integral corrosion rate v_i which is defined as:

$$v_i = \frac{\Delta m}{t} \qquad (1)$$

where Δm is the weight loss per sample area, has been calculated. Provided that v_i can be expressed as:

$$v_i = kt^{-n}, \qquad (2)$$

where $0 \leqslant n \leqslant 1$, the true, differential corrosion rate v_d can be calculated from v_i-values. From Eqs. (1) and (2) one finds:

$$\Delta m = v_i \cdot t = kt^{1-n}. \qquad (3)$$

Since

$$v_d = \frac{d\Delta m}{dt} = k(1-n)t^{-n} \qquad (4)$$

$$= (1-n)v_i \quad , \qquad (5)$$

it follows that differential corrosion rates can be calculated from the experimental v_i-values provided that the parameter n has been determined. This determination has been carried out from log Δm-log t plots from which the value of the parameter k is also obtained as the weight loss after one month.

The corrosion behavior of a material of a given test site is characterized by a set of empirically determined n and k values. The parameter n gives information about the corrosion mechanism, a value $n \approx 0.5$ indicating that the corrosion rate is determined by diffusion of species involved in the corrosion process, such as oxygen through the corrosion product layer. While n is a parameter which is mainly material dependent, k gives information about the corrosivity of a test site. Based on the n and k values determined over a given test period, extrapolations for longer exposure times can be made. It has to be considered, however, that k and n depend on the atmospheric conditions which can change significantly over longer time periods. A detailed discussion of the experimental corrosion and air quality data has been given in the Final Report of this project (5). This report also contains a first attempt of a statistical correlation between corrosion and pollution data.

CORROSION DATA - RESULTS AND DISCUSSION

1. Galvanized Steel

Some of the results obtained for galvanized steel are shown in Figs. 1 and 2. The results for the first set exposed in October 1974 (Fig. 1) show that after 30 months the weight loss was the highest at site #108 and the lowest at site #120. Assuming linear behavior between 6 and 30 months, corrosion rates are seen to fall between 1.04 and 0.84μm/year.

The weight loss data in Fig. 2 for the four sets exposed at site #103 show the effect of the time of the year at which galvanized steel is first exposed on the corrosion rate during further exposure. The highest weight loss is observed for the samples which had been first exposed in October 1974, while samples exposed in April and July 1975 had the lowest weight loss. The data also show that there is a slight decrease of corrosion rates with time for the first two sets.

The curves extending to 36 months in Fig. 2 have been constructed using Eq. (3) and the appropriate n and k values (Table II). Table II shows the interesting result that n, which indicates formation of protective films, is the highest for the first two sets and approaches zero for the third and fourth set. A value n=0 indicates corrosion without film formation at a constant corrosion rate. The constant k is also larger for the first and second set. The combined influence of n and k leads to initially higher corrosion rates with film formation for the first two sets, corrosion rates approaching those of the third and fourth set at longer times. The range of corrosion rates observed assigns a degree of corrosivity of 3 (0.1 to 1.0 μm/yr) on a scale of 5 as defined by Barton (6) to all test sites.

2. Weathering Steel

Figure 3 shows the weight loss data for the first set at all nine test sites as a function of time. After 24 and 30 months the highest weight loss is observed at site #122, while the weight loss is the lowest at site #105. There is a pronounced decrease of corrosion rates with time and, as also observed for galvanized steel, the weight loss is higher for the first and second sets. The curves in Fig. 4 have been constructed with Eq. (3) with the values of n and k listed in Table III. While the average value of n is close to 0.5 for the first three sets indicating a diffusion controlled mechanism, $n \approx 0.6$ to 0.7 for the fourth set at all sites.

Differential corrosion rates as calculated according to Eq. (4) fall between 32.4μm/yr for site #115 after 3 months for the second set and 2.3μm/yr for site #105 after 30 months for the fourth set. The differential corrosion rates obtained in this way contain a certain error due to the error in the determination of n and k which assumes that all weight data for a given site and set fall on a straight line in a log Δm-log t plot. In fact, as shown in Fig. 5, a distinct pattern is observed at all nine sites in the log v_i-log t curve with different slopes for different time periods for the first set. The decrease of corrosion rates was slower between April and October 1975 than expected for n=0.5. For the last 18 months, n > 0.5 for all sites except sites #115, 118 and 122.

3. House Paints

For both paints and at all sites a higher weight loss is observed for exposure to the south. Latex paint showed higher weight loss than oil base paint. A plot of weight loss as a function of time (Fig. 6) shows discontinuous corrosion behavior with larger slopes for the first 3 months and between 6 and 12 months exposure. This is also shown in Fig. 7 for the integral corrosion rate v_i at site #103. The highest corrosion rates for latex base paint are found at site #122 for exposure to north and south, while the highest values for oil base paints are found at site #122 for exposure to north and at site #105 for exposure to south. The lowest v_i-values for latex base paints are found at site #105 after 6 months exposure to the north and south. For oil base paint the lowest values are found at sites #112 (north) and #106 (south) after 30 months exposure.

4. Marble

The time dependence of the weight loss for two sites is shown in Fig. 7. The decrease of corrosion rates with time in the early stages of exposure indicates formation of a protective film. Between 12 and 30 months the corrosion rate seems to be constant; for site #122, where the highest weight loss was observed in general, it was about 126 μg/cm^2 month, while for site #106, where weight loss data are the lowest, it was found to be 107 μg/cm^2 month as determined by a straight line through the data points between 12 and 30 months.

The characteristic constants n and k have been obtained for sites #103, 115 and 122. Site #103 has the lowest values of n and k, while site #122 has the highest values. The constants for site #122 have been used to calculate a weight loss-time curve in Fig.

5. Silver

The silver samples were evaluated by reflectance loss measurements and by electrochemical reduction of the tarnish film in 3.5% NaCl. Figure 8 shows the correlation between reflectance loss RL and amount of electricity Q consumed for reduction of the tarnish film.

Most of the points fall close to the straight line in Fig. 8 for the first nine months. For longer exposure times a deviation from linearity has to occur with increasing film thickness since RL cannot exceed 100% while the thickness of the tarnish film seems to increase continuously. This becomes evident especially in the results for the second year, where RL did not exceed 80 to 90%, while the film thickness varied from 300 to 500 Å. The slope in the linear region was similar for both sets of samples. The reflectance loss was somewhat higher in the second year of exposure.

6. Aluminum Tension Samples

Nine samples each of Al 2014 at 25 and 45 Ksi and of Al 7079 at 15 and 25 Ksi had been exposed originally. Al 2024 showed a larger spread of time-to-failure than Al 7079. The number n_s of samples surviving as a function of time is shown in Figs. 9a and b for sites #103 and #112 as an example. All samples of Al 7079 at 25 Ksi have failed in the first 255 days. At the lower stress level of 15 Ksi all samples failed in less than 630 days except at site #120, where two samples remain. Time-to-failure for Al 2014 at 45 Ksi showed much wider variations. At site #103 all nine samples have failed in 66 days, while one sample each remains unbroken at sites #112 and 115. Not many samples of Al 2014 at 25 Ksi have failed in 30 months. Only at sites #105 and 108 have all samples failed. At site #106 only one sample has cracked. Less than fifty percent of all samples have failed at sites #106, 108, 112 and 115 (Table IV).

AIR QUALITY PARAMETERS

The pollution levels in St. Louis were found to be rather low. The quarterly SO_2 averages exceeded 20 ppm only at sites #105, 108, 115 and 122 between November 1974 and April 1975. For many days during the thirty month test period the SO_2, H_2S and total sulfur levels did not exceed the detection limit of the instruments.

A detailed analysis of the air quality data for all nine test sites over the thirty months periods has been given in the Final Report (5). The effects of seasonal variations were especially evident for ozone, NO_x, TSP, sulfates and nitrates. While the ozone levels

are higher in the summer, the NO_x levels are higher in the winter. In the center of the city, higher NO_x concentrations are observed than in the outlying areas. TSP showed maxima in the April/July quarter of 1975 and July/October quarter of 1976 which parall those found for sulfates except that the 1975 maxima occur in the April/July quarter for sites #118 and 122, which are on the outer ring of test sites and in the July/October quarter at sites #103 and 106, which are on the inner ring. The average nitrate concentrations have broad maxima in the October/January and January/April quarters.

CORRELATION BETWEEN CORROSION BEHAVIOR AND ATMOSPHERIC DATA

1. Corrosion and Pollution Code Numbers

In order to provide a simple survey of the ranking of the nine test sites according to corrosion rates and pollutant concentrations, tables have been prepared in which the test sites are ranked according to the severity of corrosion and amount of pollution (5). The highest corrosion rates and highest pollution concentrations were ranked as 1. For the Al alloys, results for 100% failure taking into account the number of unbroken samples were used. For the pollutant data, the average values at the end of the four exposure periods were considered. For galvanized steel, pronounced changes in ranking can occur for the four sets, while for weathering steel the ranking of a site is more or less independent of the start of exposure. As a summary of these tabulations, Corrosion and Pollution Code Numbers have been prepared for all sites and materials. For the Corrosion Code Number (CCN), the sequence of numbers corresponds to the ranking of galvanized steel, weathering steel, house paint, marble, silver and stressed aluminum alloys. The rankings for different sets of materials or the two Al alloys at different stress levels have been combined to give one number for each material. In the Pollution Code Number (PCN), the sequence is SO_2, TS, H_2S, O_3, NO_x and THC. The particulate matter data were not considered in the PCN. In this way two six digit numbers have been prepared:

Site #	CCN	PCN
103	336652	676644
105	494431	432931
106	868977	227712
108	123223	355553
112	779799	X6X815
115	544518	111378
118	652375	X9X189
120	987856	782466
122	211134	534297

Based on the CCN, sites #108 (CCN = 123223) and #122 (CCN = 211134) are by far the most corrosive sites. For these two sites the two corresponding PCNs are 355553 and 534297, indicating average or low pollutant concentrations. On the other hand, for site #106, CCN 868977 and PCN = 227712 indicate low corrosivity but high concentrations in SO_2, TS, NO_x, and THC. A comparison of CCNs and PCNs does, therefore, not show any obvious correlations between corrosivity and pollution. It has to be considered, however, when comparing CCNs and PCNs that high concentrations of some pollutants might have an inhibiting effect.

2. Statistical Analysis

A first attempt has been made to relate the integral corrosion rate to various atmospheric pollutants, duration of exposure and other atmospheric factors (5). It was postulated that the logarithm of the integral corrosion rate v_i for each material is linear proportional to the pollutants and other corrosive atmospheric factors and linear in the logarithm of time of exposure. The model is thus a multiple regression model with the dependent variable being log corrosion rate and the so-called independent variables being the atmospheric parameters and log time. The coefficients in the model represent the marginal effects of the pollutants, exposure time and other atmospheric factors. The analysis was done for all materials except silver and Al alloys at all test sites and has been presented in tabular form (5). Some of the apparent inconsistencies in the estimated effects for different materials or different sets of materials are clearly due to the interdependence of the so-called independent variables in the multiple regression model. This situation is known as the problem of multi-collinearity.

As the analysis now stands, there is a high degree of uncertainty in the estimated regression coefficients. This makes it very difficult to determine if the linearity assumptions for the explaining variables are valid. Further efforts are necessary to perform an extensive residual analysis to identify distributional characteristics or multi-dimensional outliers.

ACKNOWLEDGEMENT

This project was carried out under Contract No. 68-02-2093 with the Environmental Protection Agency.

REFERENCES

1. F. Mansfeld and J. V. Kenkel, Corr. Sci. 16, 111 (1976).
2. F. Mansfeld and J. V. Kenkel, Corrosion 33, 13 (1977).
3. K. Bohnenkamp, G. Burgmann and W. Schwenk, Stahl und Eisen 93 (22), 1054 (1973).
4. W. Schwenk and H. Ternes, Stahl und Eisen 88, 318 (1968).
5. F. Mansfeld, "Study of the Effects of Airborne Sulfur Pollutants on Materials", Rockwell International AMC 7010.T0112FR, 1978.
6. K. Barton, "Schutz gegen atmosphärische Korrosion", Verlag Chemie, West Germany, 1976.

TABLE I. Materials, Preparation, Exposure Conditions and Assessment of Corrosion Damage

MATERIAL	Exposure Condition	Sample Preparation	Assessment
Galvanized Steel (4"x6"x0.036")	30° from horizontal facing south	Degrease, clean, weigh	Gravimetric
Weathering Steel (Corten A) (4"x6"x0.036")	30° from horizontal facing south	Degrease, descale, weigh	Gravimetric
Al 7079-T651 (tension specimen* 15 and 25 Ksi stress level)	30° from horizontal facing south	Degrease, stress	Time-to-failure
Al 2014-T651 (tension specimen* 45 and 25 Ksi stress level)	30° from horizontal facing south	Degrease, stress	Time-to-failure
House Paint on stainless steel (4"x6"x0.036")	Vertical facing north and south	Degrease, clean, apply paint, condition, weigh	Gravimetric, loss of reflectance
a. oil base, 2.5 mil.			
b. latex, 1.5 mil			
White Cherokee Marble (4"x6"x3/8")	30° from horizontal facing south	Clean, condition, weigh	Visual, gravimetric
Silver (6" diameter plated discs)	Open to ambient air but protected from direct environmental factors	Degrease	Visual, loss of reflectance, electrochemical

* in short transverse direction

TABLE II Air Quality Data Used for this Project

Parameter
Wind Speed
Wind Direction
Temperature
Ozone Concentration
Total Hydrocarbon Concentration
NO_x Concentration
Total Sulfur Concentration
H_2S Concentration
SO_2 Concentration
Relative Humidity
Sulfate
Nitrate
Total Suspended Particulates

FIGURE CAPTIONS

1. Weight loss of galvanized steel, first set, for the nine test sites.
2. Weight loss for four sets of galvanized steel at sites #103 and #112.
3. Weight loss of weathering steel, first set, for the nine test sites.
4. Weight loss for four sets of weathering steel at sites #103 and #112.
5. Log v_i-log t plot for the first set of weathering steel at all test sites.
6. Weight loss Δm and integral corrosion rates v_i for house paints at site #103.
7. Weight loss of marble at sites #106 and 122 over a thirty months period.
8. Relationship between reflectance loss RL and coulombs Cb or film thickness d for first year of exposure of silver plated discs.
9. Percent of Al tension samples surviving (n_s) as a function of time for site #103 (a) and site #112 (b).

Table III. Corrosion Parameters n and k for Galvanized Steel (k in mg/cm^2 month)

	First Set		Second Set		Third Set		Fourth Set	
Site	n	k	n	k	n	k	n	k
103	0.26	0.135	0.23	0.12	0.17	0.076	0.15	0.071
105	0.13	0.097	0.21	0.11	0.07	0.050	0.10	0.063
106	0.13	0.094	0.22	0.083	0.13	0.050	0.03	0.043
108	0.11	0.097	0.10	0.077	0.08	0.072	0.11	0.060
112	0.13	0.083	0.17	0.081	0.05	0.042	0.00	0.040
115	0.13	0.087	0.14	0.079	0.00	0.042	0.12	0.066
118	0.17	0.087	0.17	0.087	0.01	0.076	0.03	0.083
120	0.12	0.076	0.14	0.074	0.03	0.037	0.02	0.039
122	0.07	0.079	0.00	0.055	0.00	0.053	0.02	0.069
Average	0.14	0.093	0.15	0.085	0.06	0.055	0.06	0.059
	± 0.03	±0.012	±0.05	±0.014	±0.05	±0.013	±0.05	±0.012

Note: k = 0.1 mg/cm^2 month corresponds to 1.68 μm/year

Table IV. Corrosion Parameters n and k for Weathering Steel (k in mg/cm^2 month)

Site	First Set		Second Set		Third Set		Fourth Set	
	n	k	n	k	n	k	n	k
103	0.58	8.1	0.53	6.8	0.51	6.3	0.67	9.5
105	0.52	5.1	0.49	5.0	0.55	4.8	0.76	8.2
106	0.51	4.8	0.35	4.0	0.46	5.0	0.69	7.8
108	0.53	7.0	0.38	4.4	0.59	8.0	0.67	9.5
112	0.48	4.8	0.52	5.5	0.73	8.9	0.66	7.4
115	0.44	5.4	0.35	4.8	0.64	8.9	0.64	8.7
118	0.41	4.4	0.29	3.9	0.44	4.8	0.64	8.1
120	0.58	5.9	0.51	5.0	0.58	5.9	0.70	8.1
122	0.48	6.5	0.50	6.9	0.58	8.4	0.64	9.7
Average	0.50	5.8	0.44	5.1	0.56	6.8	0.67	8.6
	±0.05	±1.0	±0.08	±0.8	±0.07	±1.6	±0.03	±0.7

Note: k = 1.0 mg/cm^2 mo corresponds to 15.25 μm/yr.

Table V . Time-To-Failure of Al Tension Samples, (Days)

I. 50% of All Samples

Site #	Al 7079 25 Ksi	Al 7079 15 Ksi	Al 2014 45 Ksi	Al 2014 25 Ksi
103	125	224	<48	575
105	150	245	60	450
106	160	370	230	
108	165	250	<48	
112	210	270	410	
115	225	270	100	
118	160	260	105	822
120	155	320	75	755
122	160	133	75	822

II. 100% of All Samples

103	172	382	66	(2)*
105	160	360	230	822
106	210	622	505	(8)
108	210	381	225	871
112	240	622	(1)	(6)
115	255	346	(1)	(7)
118	220	630	155	(1)
120	224	(1)	83	(3)
122	201	277	814	(4)

* Number of samples left.

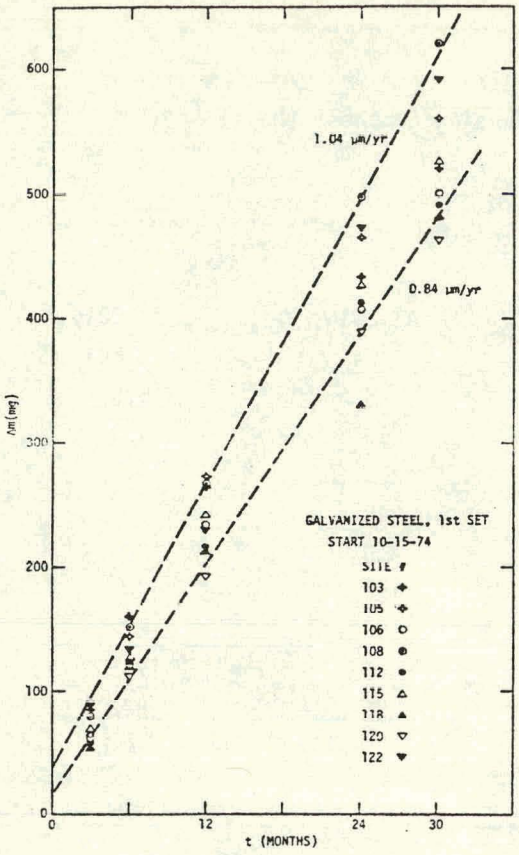


Figure 1

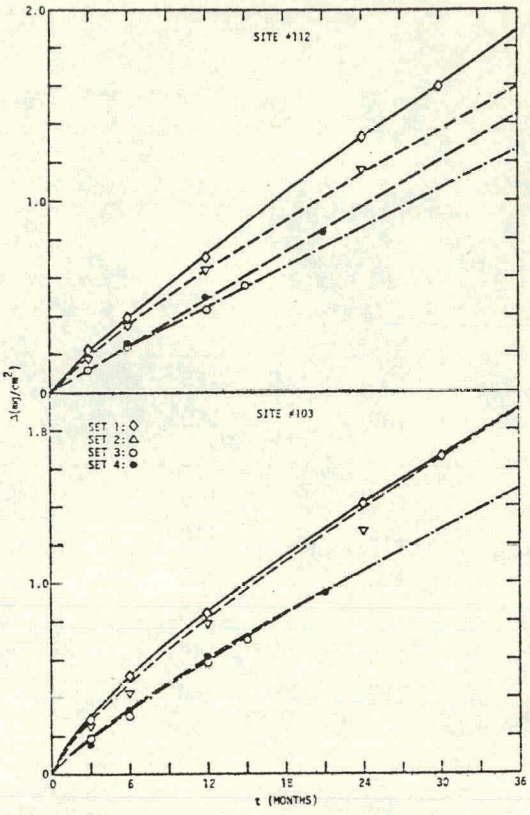


Figure 2

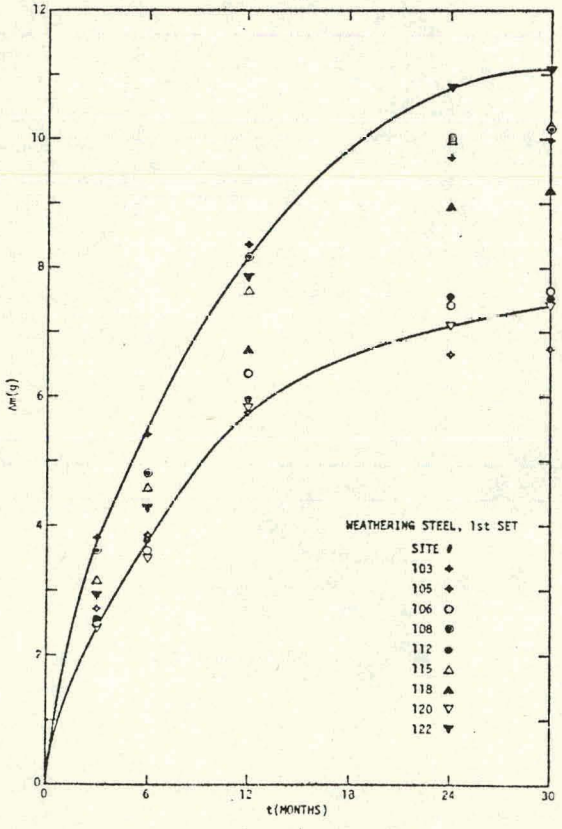


Figure 3

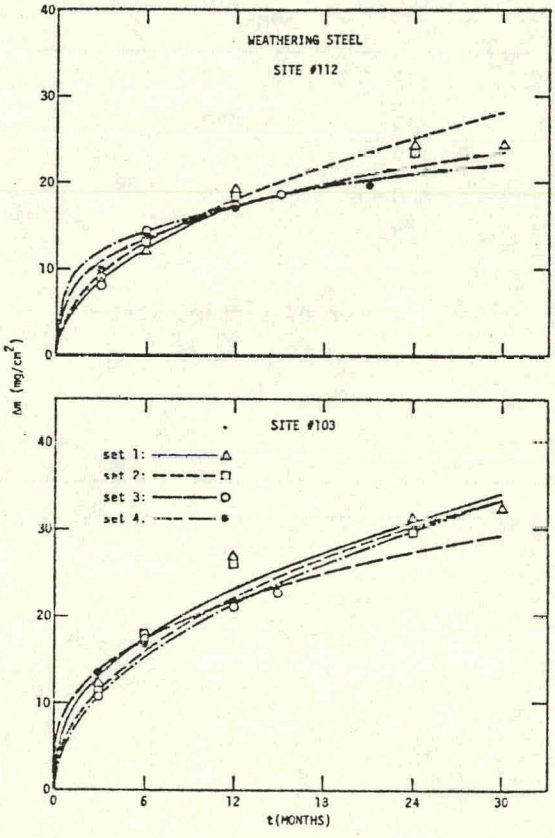


Figure 4

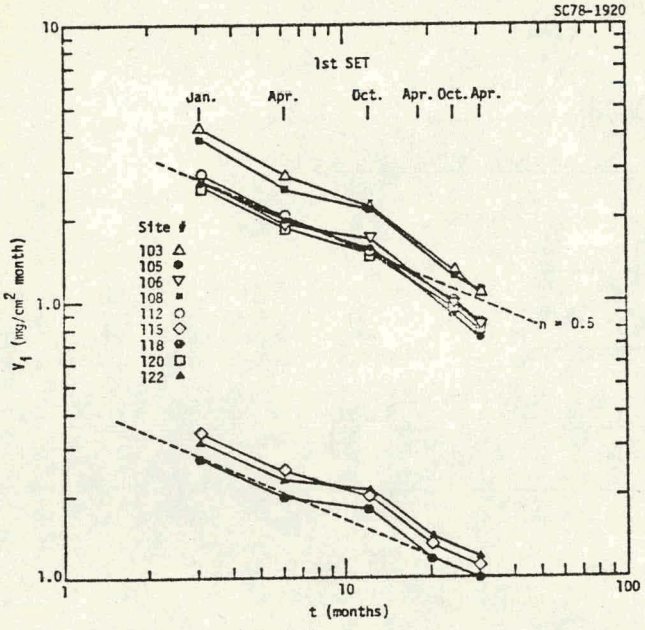


Figure 5

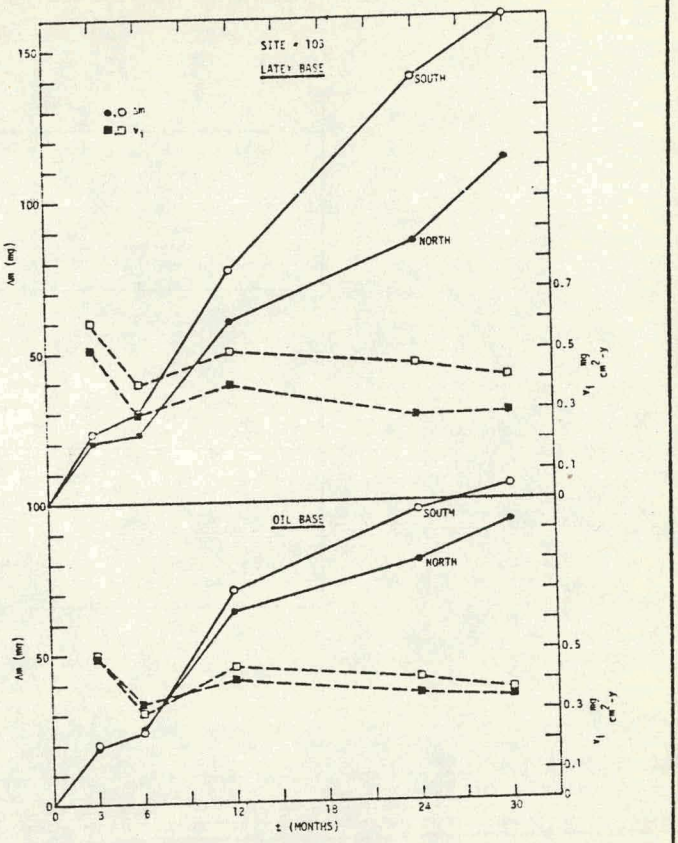


Figure 6

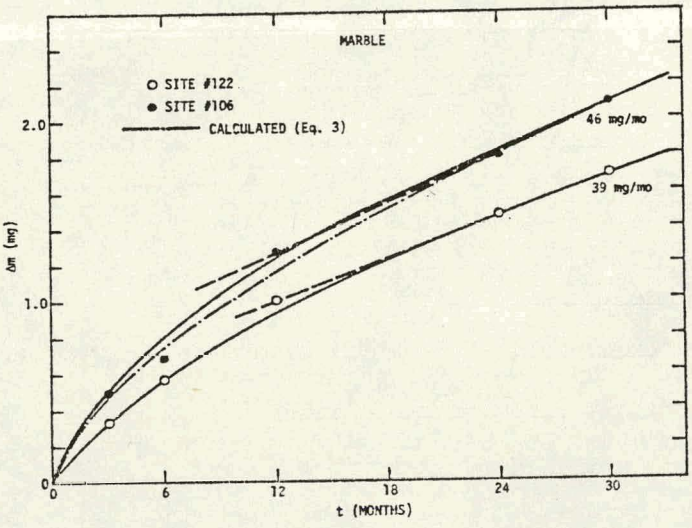


Figure 7

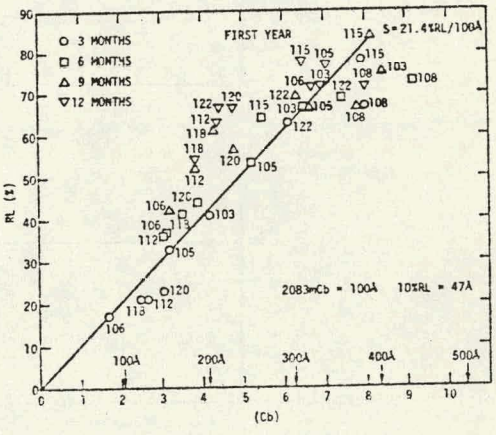


Figure 8

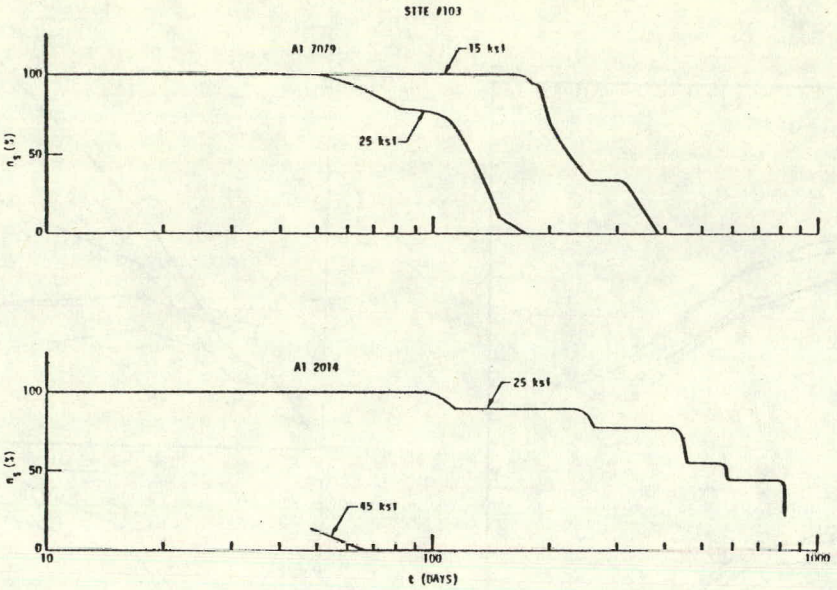


Figure 9a

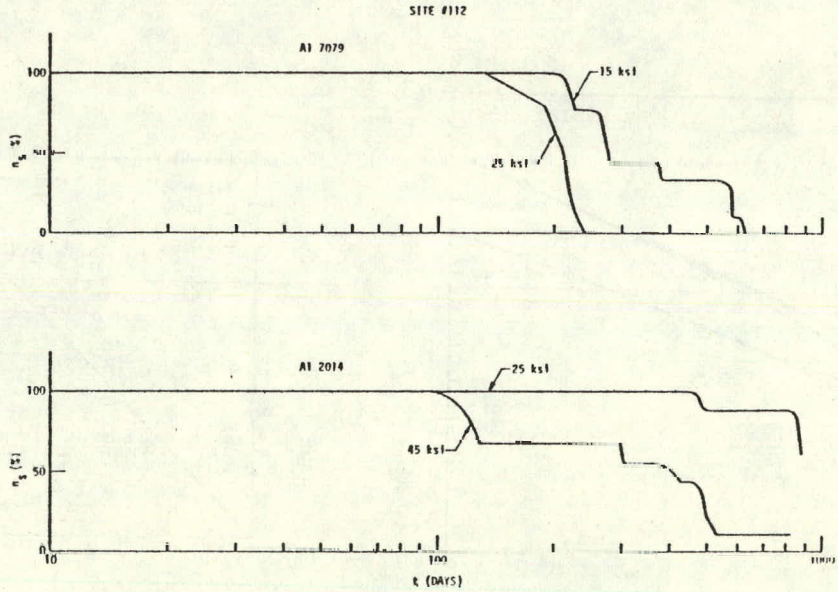


Figure 9b

RESULTS OF THIRTY MONTHS ATMOSPHERIC CORROSION TESTING IN ST. LOUIS, MO., USA

Viewgraphs Presented

by

F. Mansfeld

Rockwell International Science Center

Thousand Oaks, California

MONITORING OF ATMOSPHERIC CORROSION PHENOMENA

ATMOSPHERIC CORROSION IS A DISCONTINUOUS PROCESS WHICH IS CHARACTERIZED BY THE FORMATION AND DISAPPEARANCE OF THIN ELECTROLYTE LAYERS:

$$\Delta M = \Sigma R_I T_{W,I}$$

T_W = TIME-OF-WETNESS

T_W CAN BE MEASURED BY ELECTROCHEMICAL TECHNIQUES:

- SEREDA (ZN - AU)
- KUCERA AND MATTSON (CU-STEEL, CU-ZINC, FE-FE, ZN-ZN, ETC.)
- MANSFELD (CU-STEEL, CU-ZINC)

R = CORROSION RATE DURING T_W

R CAN ALSO BE MEASURED BY ELECTROCHEMICAL TECHNIQUES.

NO DEFINITE DATA REPORTED DUE TO PROBLEMS WITH INTERPRETATION OF ELECTROCHEMICAL DATA AND EXPERIMENTAL PROBLEMS.



KINETICS OF ATMOSPHERIC CORROSION REACTIONS

EXPLAIN TIME DEPENDENCE OF CORROSION RATES BY SIMPLE EXPRESSION WHICH CONTAINS MATERIALS AND ATMOSPHERIC FACTORS

$$\Delta M = KT^{1-N}$$

$$R = KT^{-N}$$

K = MEASURE OF CORROSION SUSCEPTIBILITY OF METAL, CORROSIVITY OF TEST SITE

N = FUNCTION OF CORROSION MECHANISM

$0 \leq N \leq 1$

N = 0 CORROSION PROCEEDS WITHOUT FORMATION OF PROTECTIVE CORROSION PRODUCT FILMS (ZINC)

N = ½ PROTECTIVE FILM FORMS, CORROSION RATE LIMITED BY DIFFUSION OF CORROSIVE SPECIES (E.G. OXYGEN) (WEATHERING STEEL)

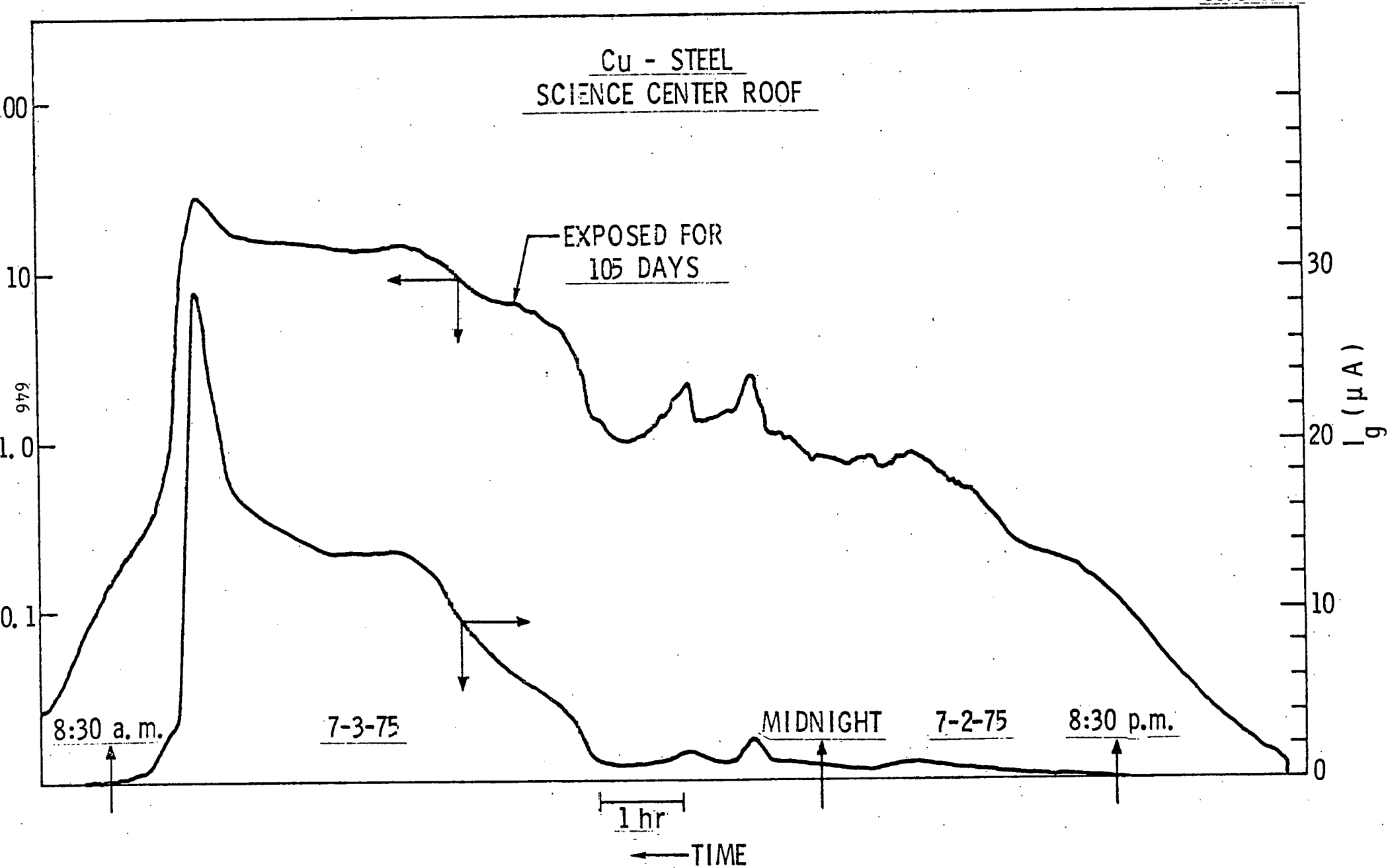
<u>EFFECT OF POLLUTANTS</u>:

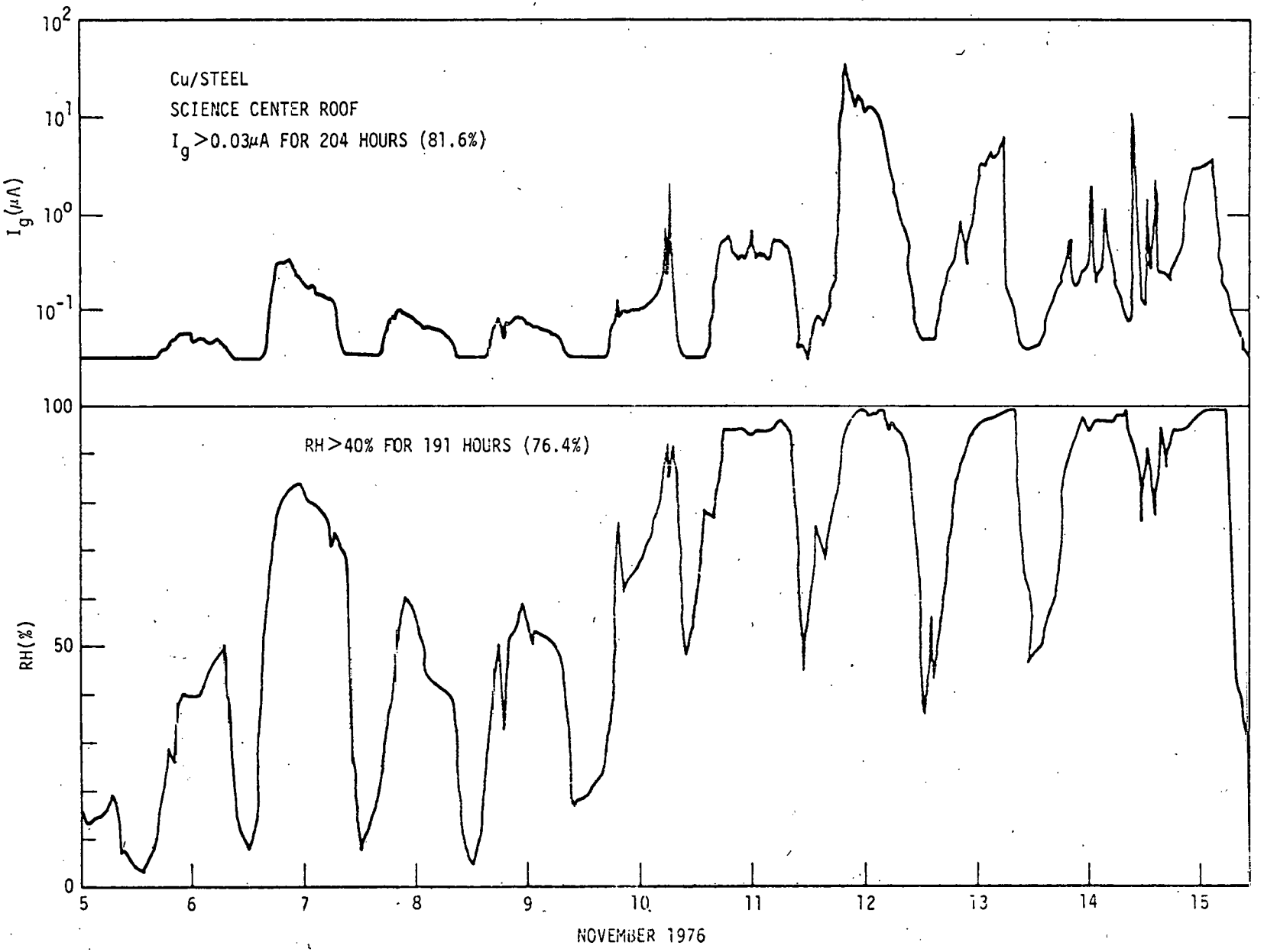
$$R = KT^{-N} \cdot E^{\Sigma \beta_I P_I} = K \cdot T^{-N}$$

β_I = EFFECT OF P_I ON R

$P_I(T)$ = CONCENTRATION OF POLLUTANT I AT TIME T

Rockwell International
Science Center


Cu - STEEL
SCIENCE CENTER ROOF
EXPOSED FOR
105 DAYS
00
10
1.0
0.1
646
30
20
10
0
I_g (μA)
8:30 a.m.
7-3-75
MIDNIGHT
7-2-75
8:30 p.m.
1 hr
TIME


Cu/STEEL
SCIENCE CENTER ROOF
I_g>0.03μA FOR 204 HOURS (81.6%)
I_g(μA)
10^2
10^1
10^0
10^{-1}
RH>40% FOR 191 HOURS (76.4%)
RH(%)
100
50
0
5
6
7
8
9
10
11
12
13
14
15
NOVEMBER 1976

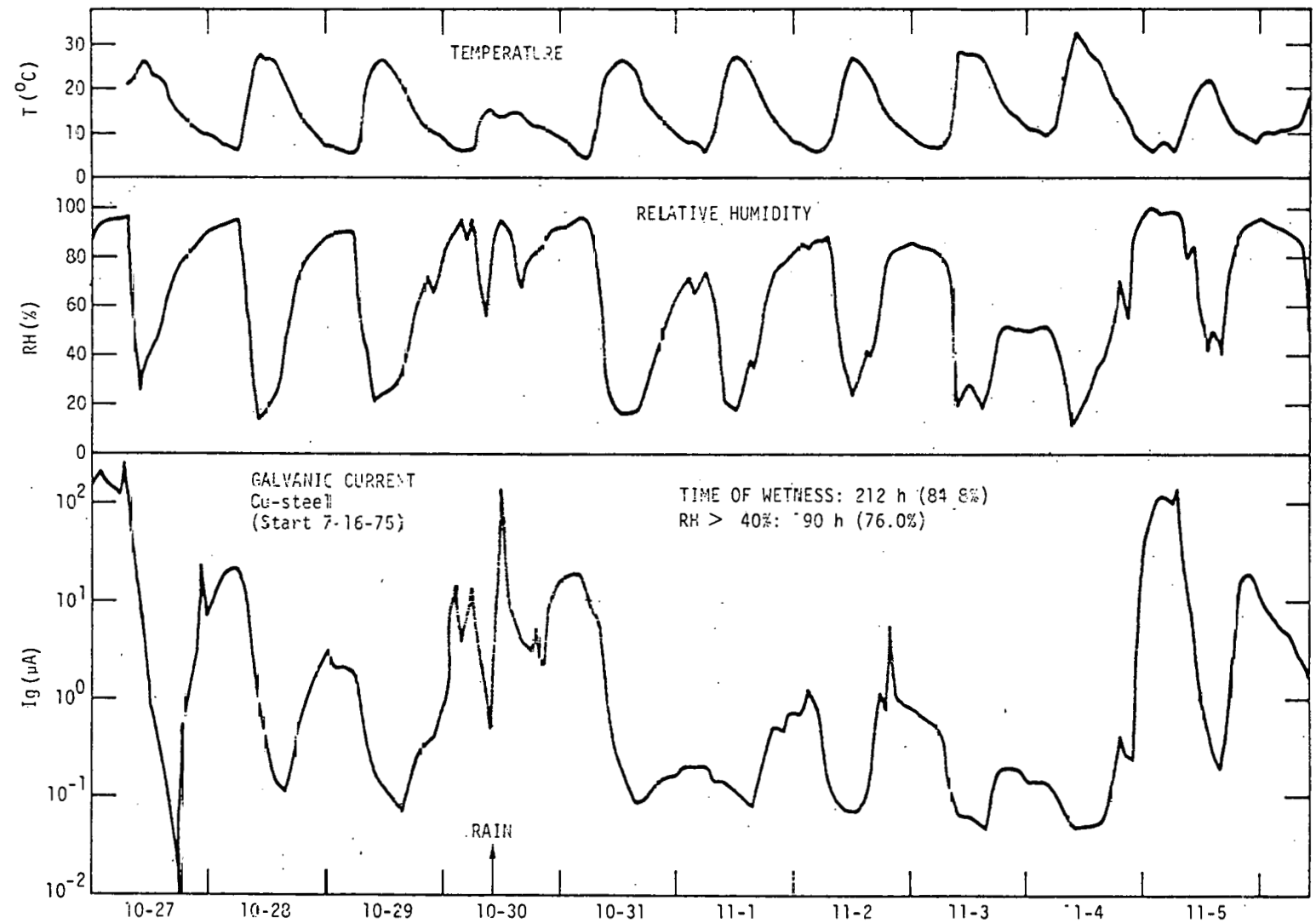


Fig. 4. Temperature, relative humidity and ACM output for a 20 day period or Science Center roof. The time-of-wetness corresponds to $I_g \geq 0.1$ μA.

Science Center
Rockwell International

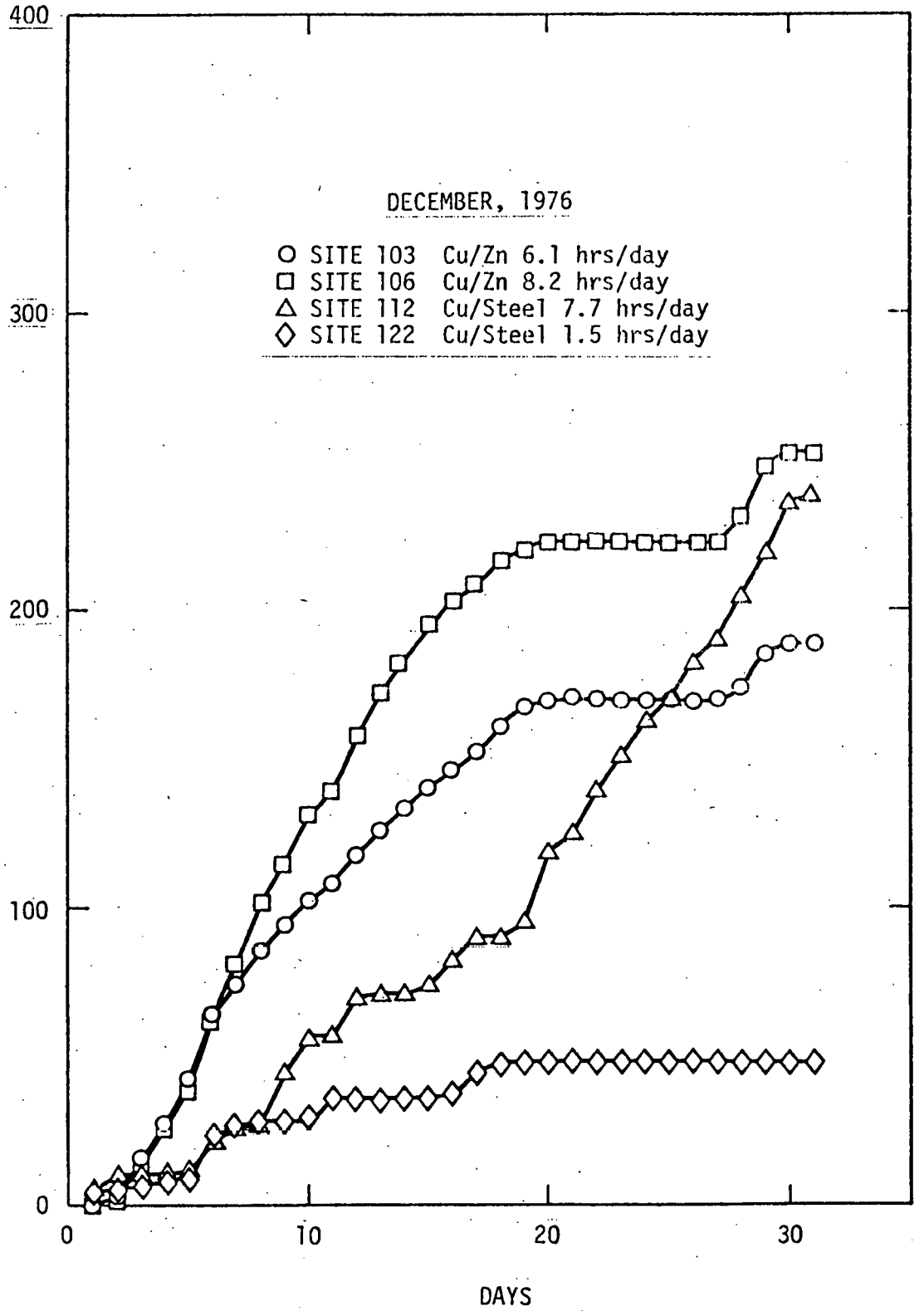

DECEMBER, 1976
SITE 103 Cu/Zn 6.1 hrs/day
SITE 106 Cu/Zn 8.2 hrs/day
SITE 112 Cu/Steel 7.7 hrs/day
SITE 122 Cu/Steel 1.5 hrs/day
400
300
200
100
0
0
10
20
30
DAYS
Σt_w, Hours

Fig. 10

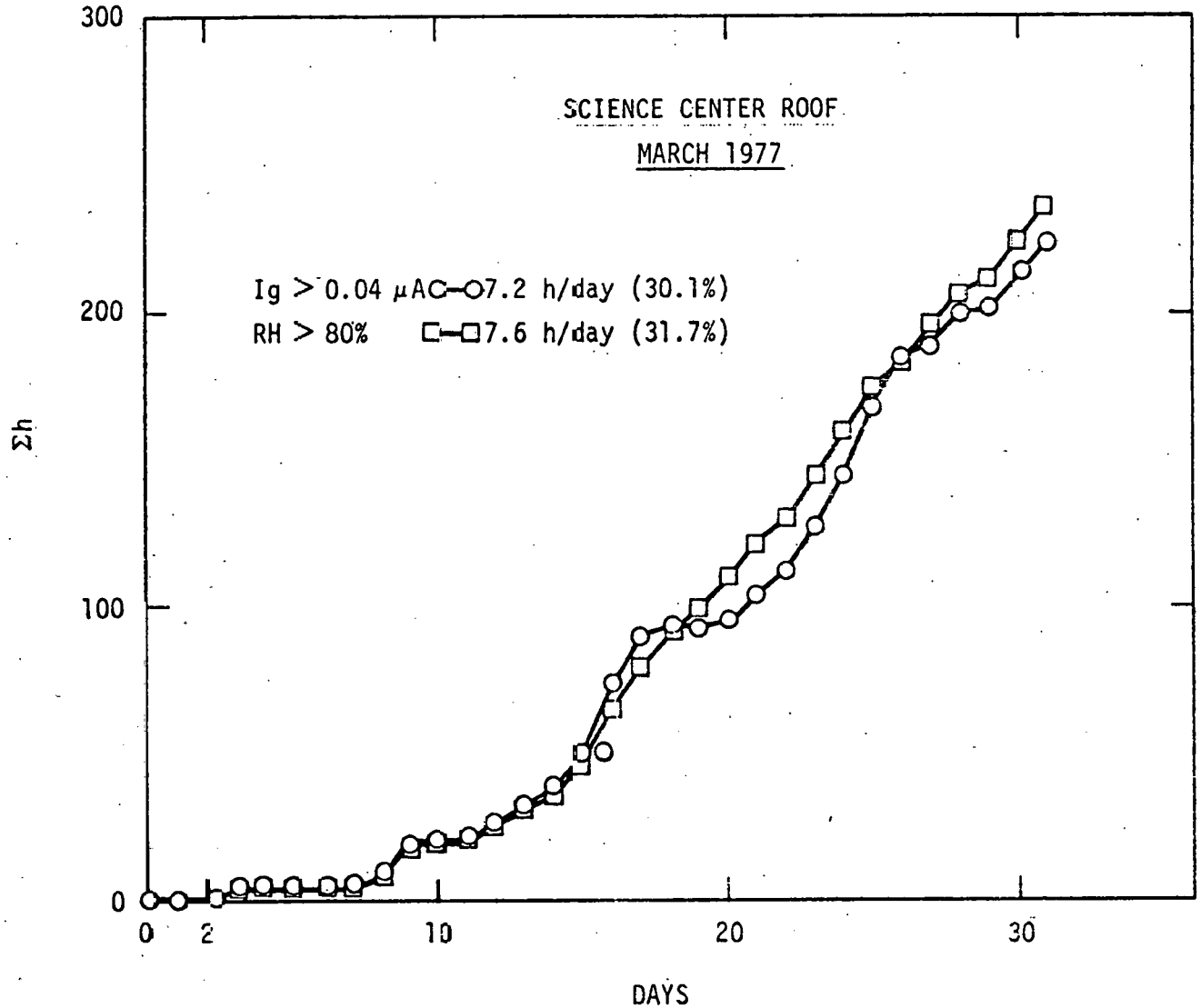
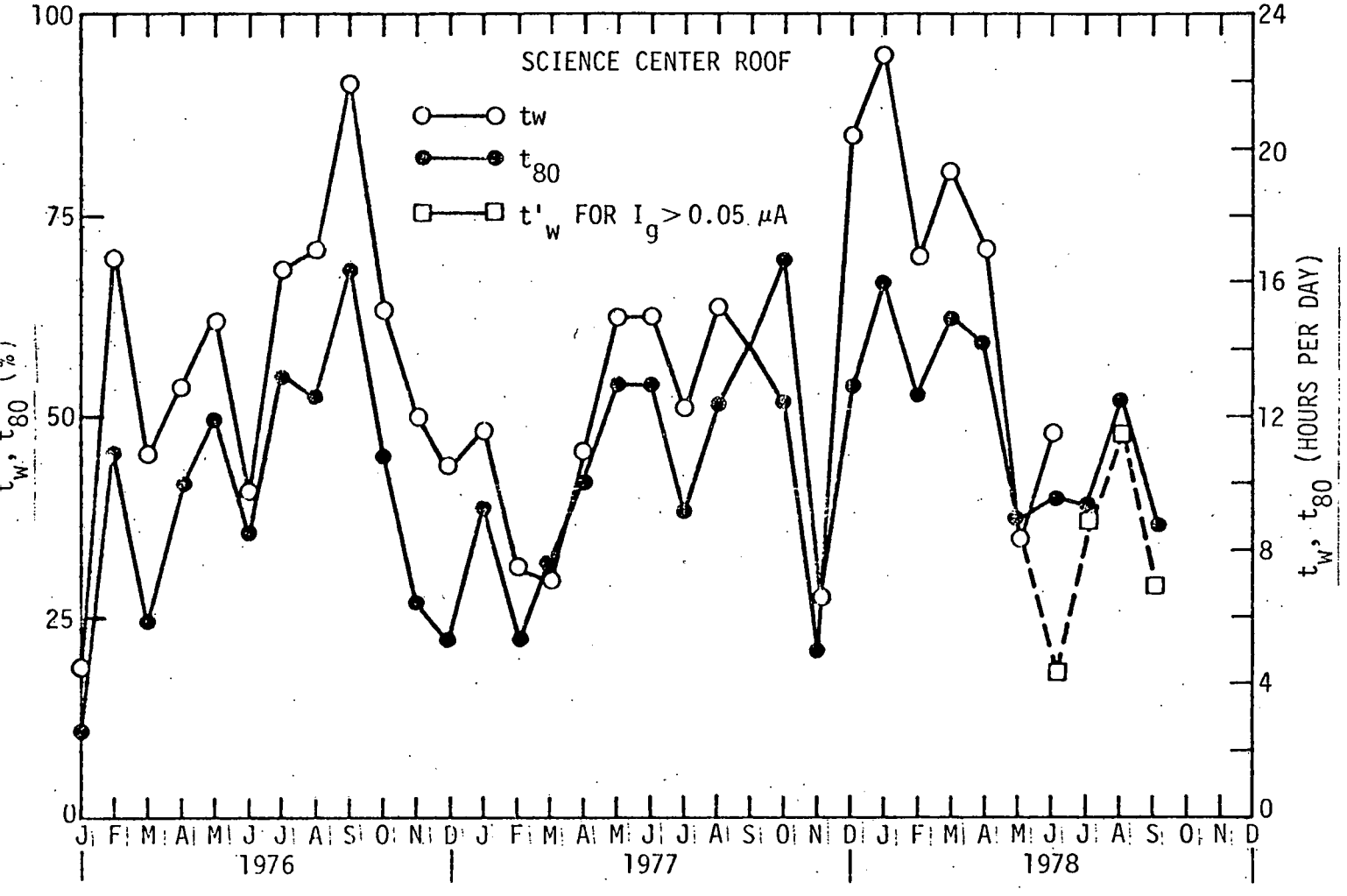
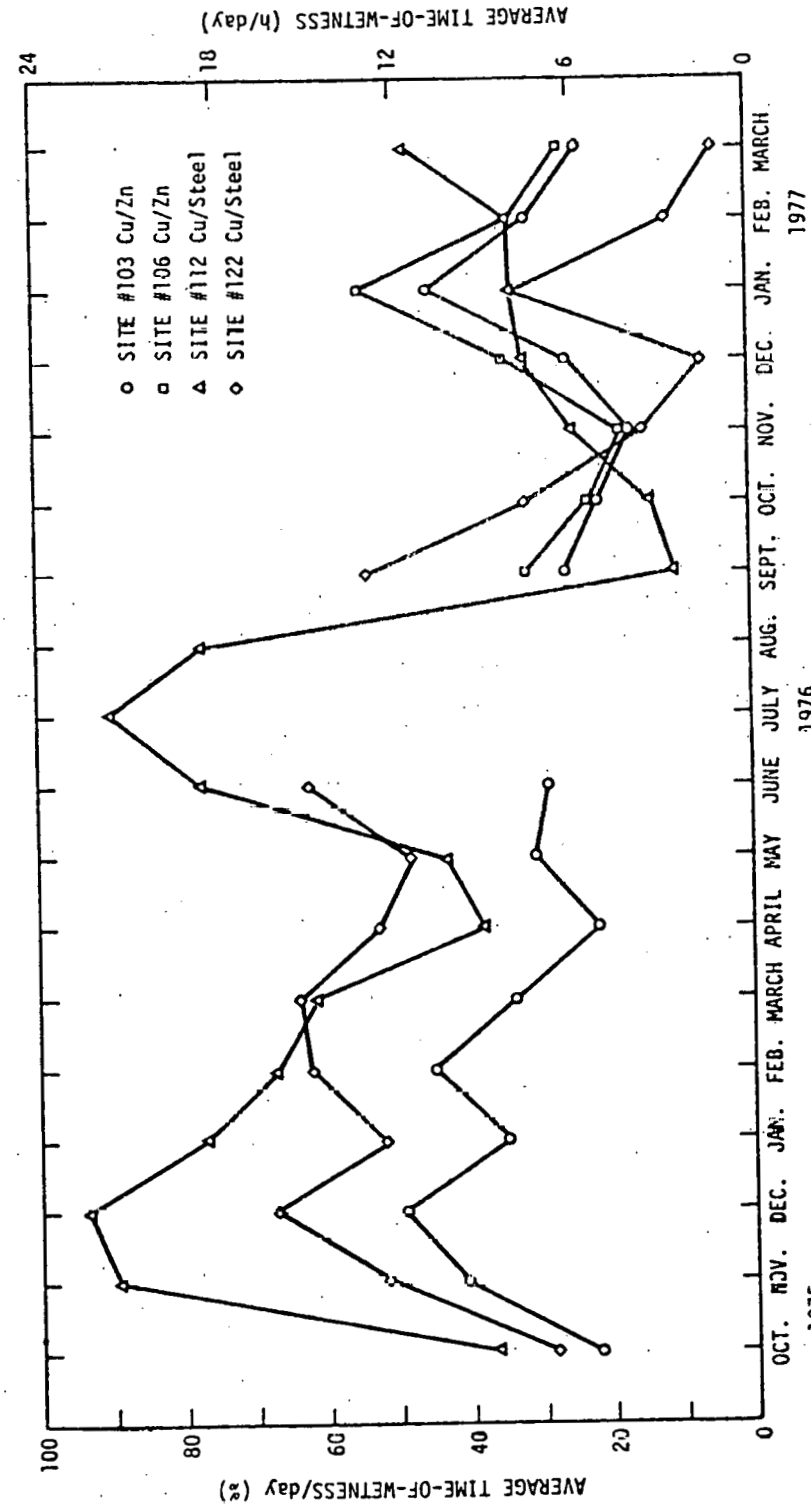


Fig. ~~13~~ 4

Rockwell International
Science Center
SC[illegible]-640

SC78-3215


SCIENCE CENTER ROOF
tw
t_{80}
t'_w FOR $I_g > 0.05\ \mu A$
t_w, t_{80} (%)
t_w, t_{80} (HOURS PER DAY)
100
75
50
25
0
24
20
16
12
8
4
0
J F M A M J J A S O N D J F M A M J J A S O N D J F M A M J J A S O N D
1976
1977
1978

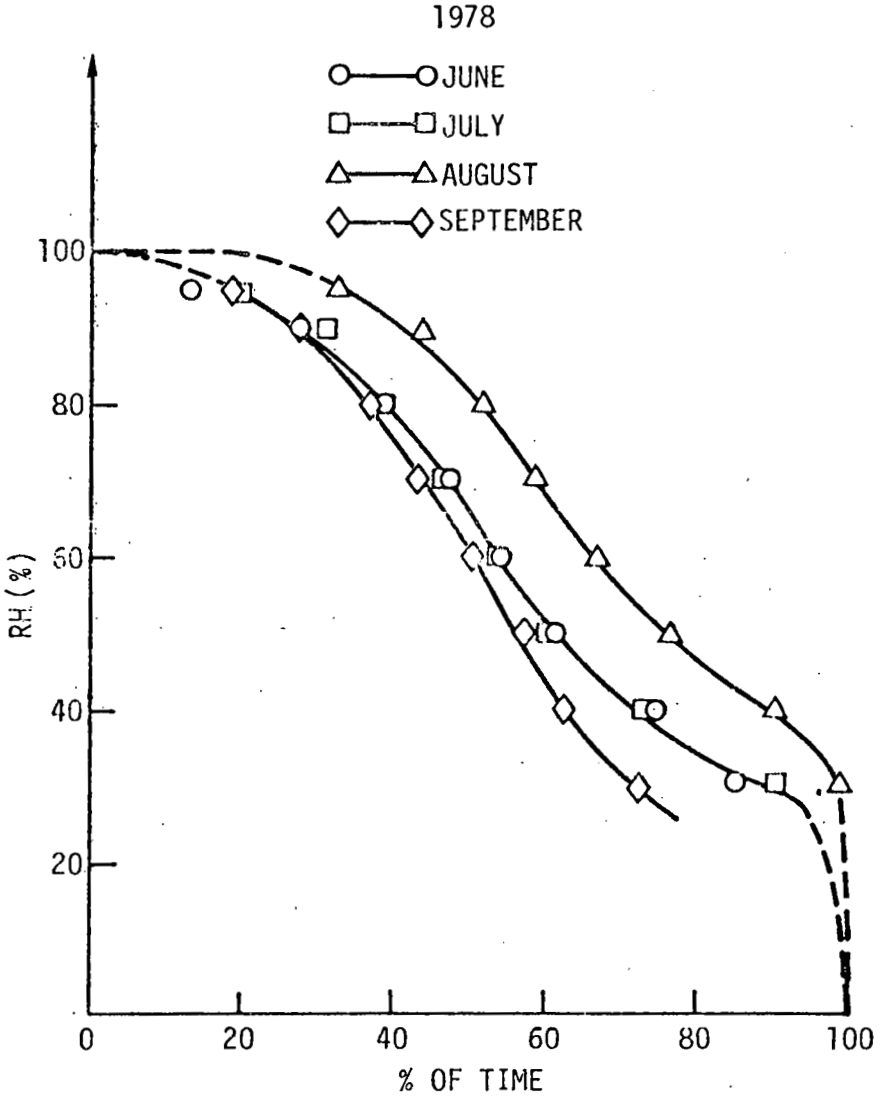


SC78-253

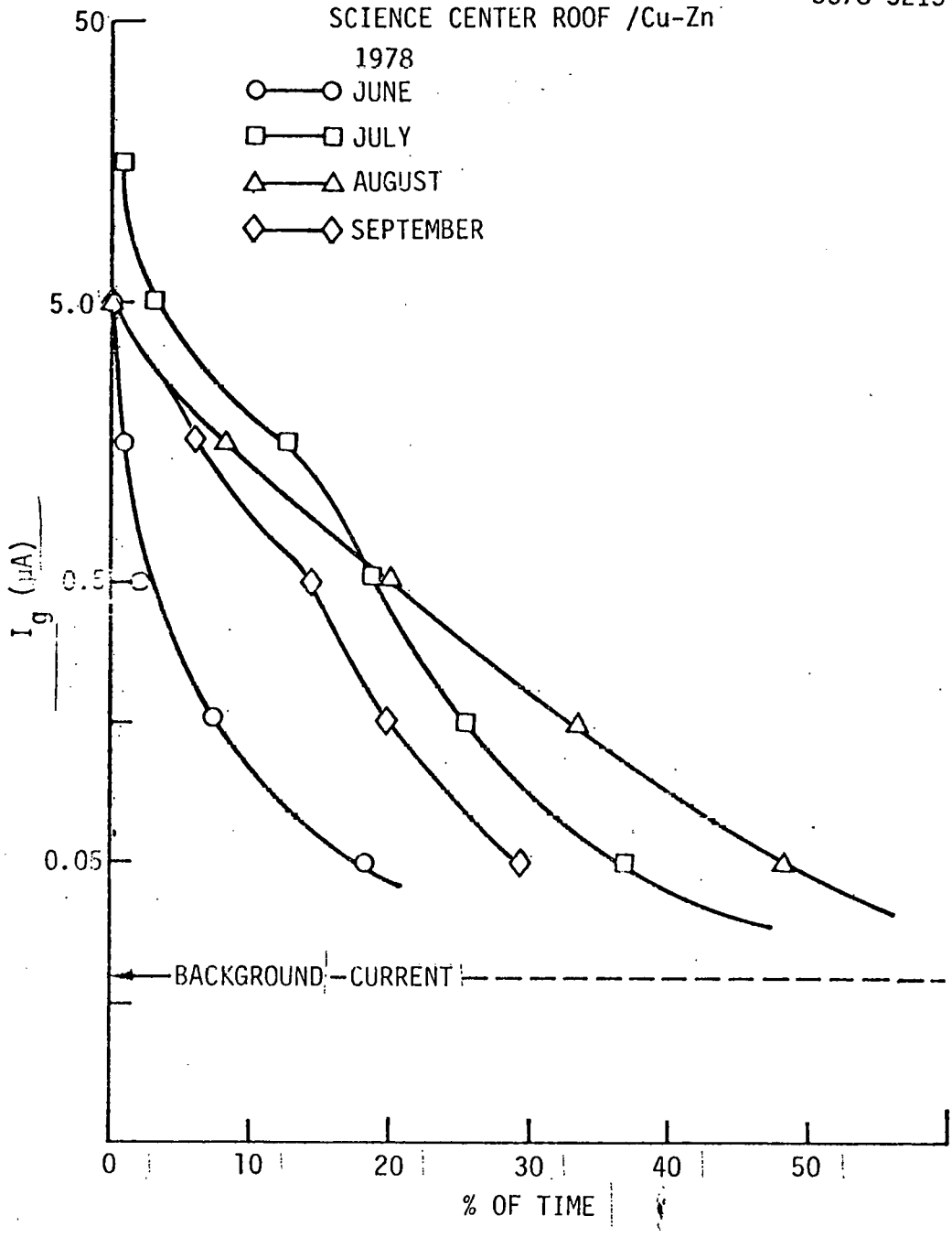
Fig. 12

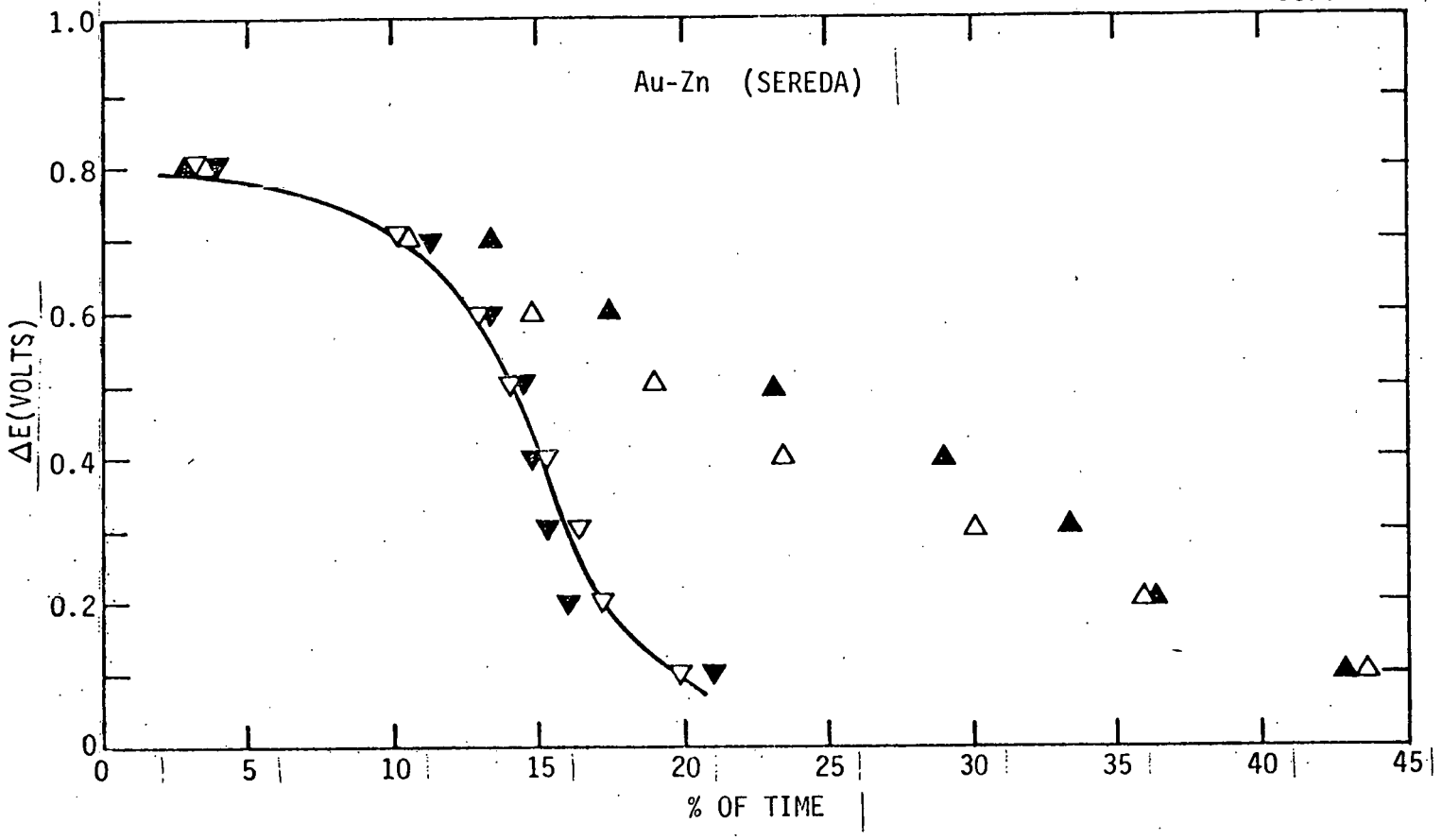
SC78-3212

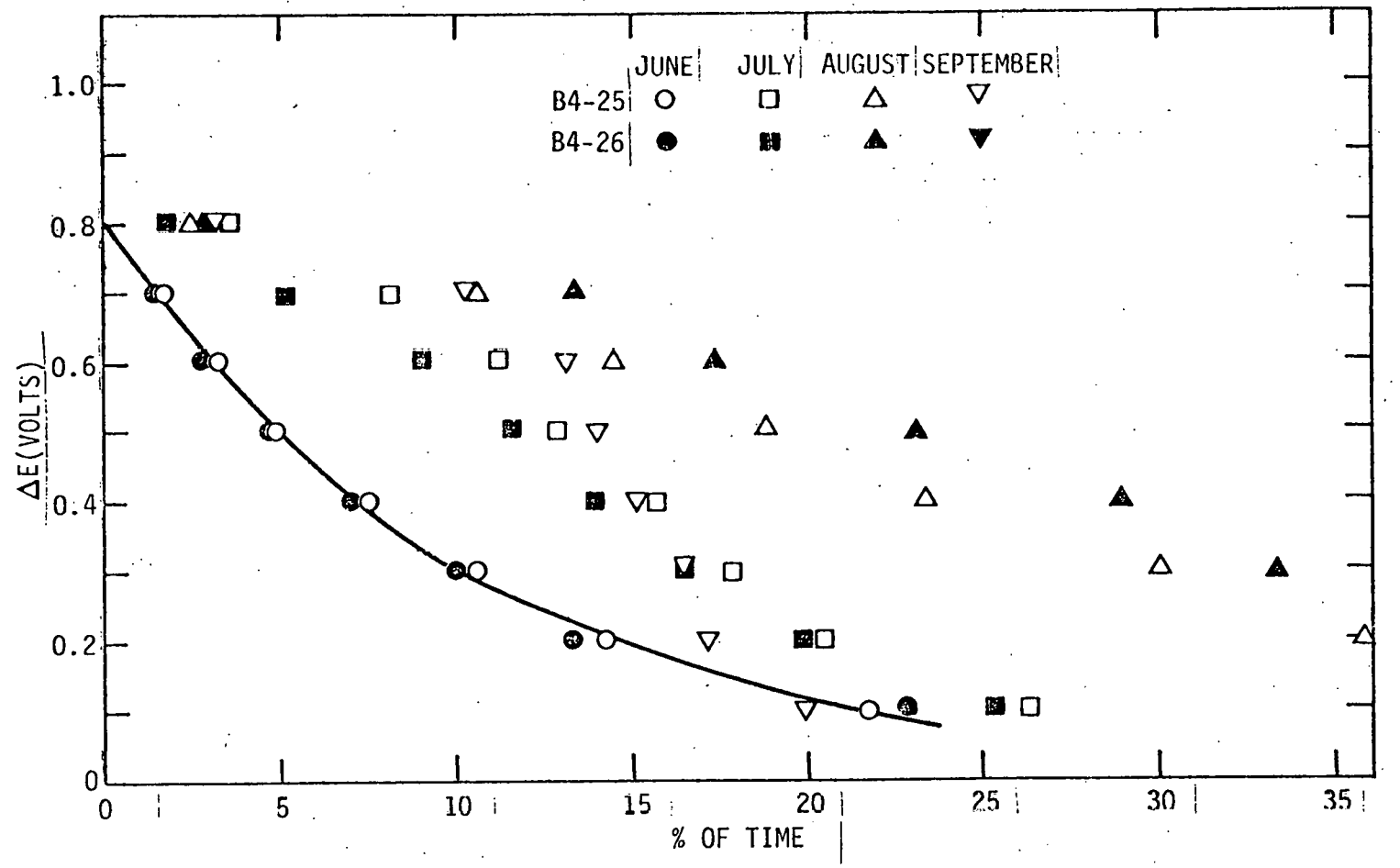
SCIENCE CENTER ROOF / Cu-Zn

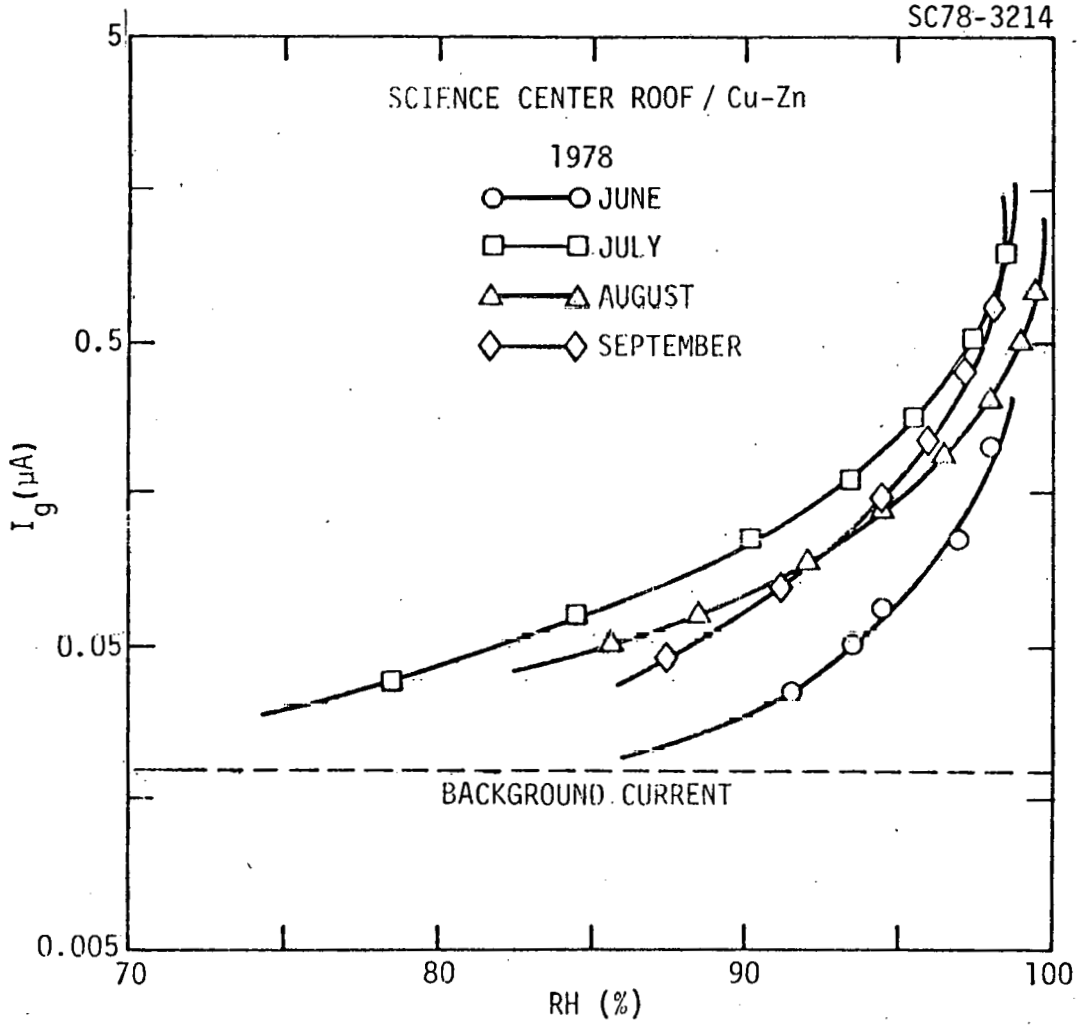


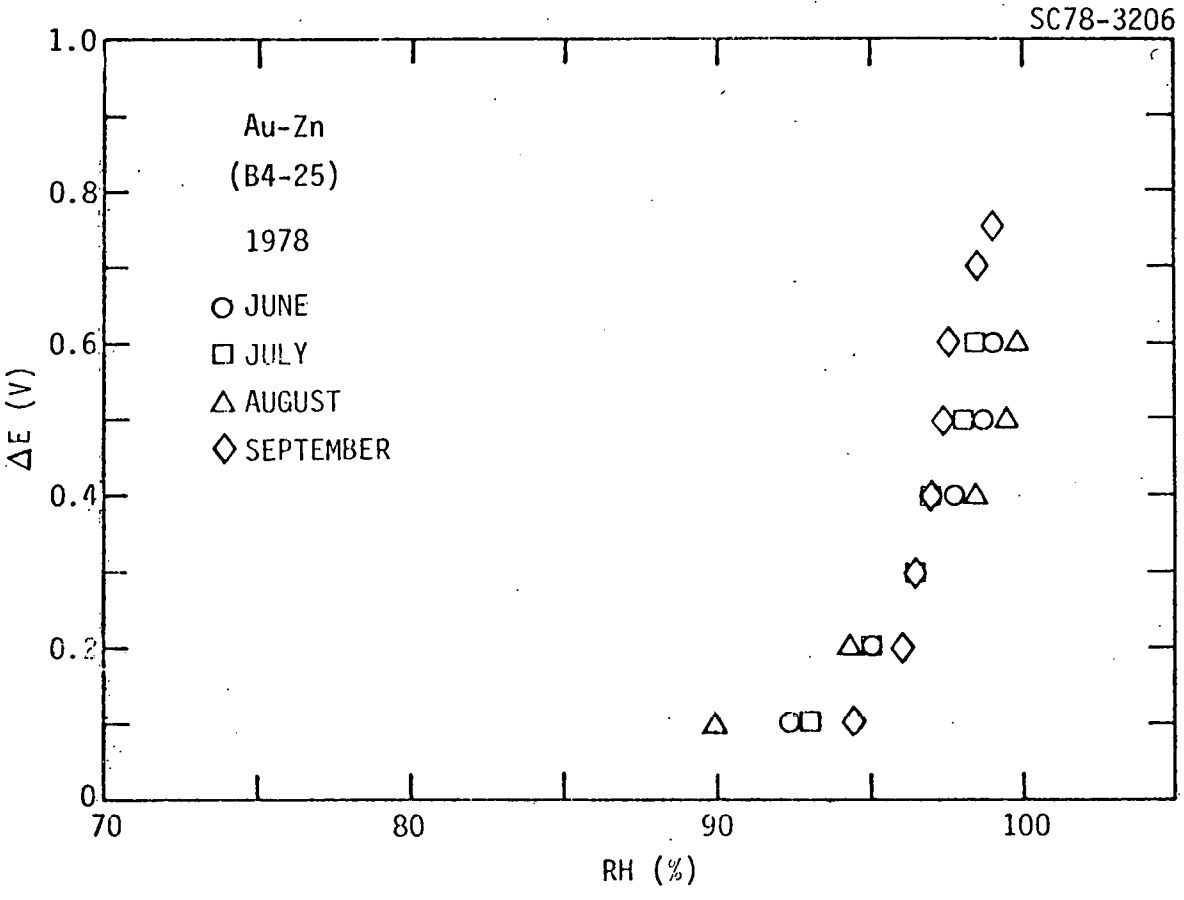
SC78-3213


SCIENCE CENTER ROOF /Cu-Zn
1978
JUNE
JULY
AUGUST
SEPTEMBER
50
5.0
0.5
0.05
I_g (μA)
BACKGROUND CURRENT
0
10
20
30
40
50
% OF TIME


Au-Zn (SEREDA)
ΔE(VOLTS)
1.0
0.8
0.6
0.4
0.2
0
0
5
10
15
20
25
30
35
40
45
% OF TIME


JUNE
JULY
AUGUST
SEPTEMBER
B4-25
B4-26
ΔE(VOLTS)
1.0
0.8
0.6
0.4
0.2
0
0
5
10
15
20
25
30
35
% OF TIME


SC78-3214
SCIENCE CENTER ROOF / Cu-Zn
1978
JUNE
JULY
AUGUST
SEPTEMBER
BACKGROUND CURRENT
5
0.5
0.05
0.005
I_g (μA)
70
80
90
100
RH (%)


SC78-3206
Au-Zn
(B4-25)
1978
JUNE
JULY
AUGUST
SEPTEMBER
ΔE (V)
RH (%)
1.0
0.8
0.6
0.4
0.2
0
70
80
90
100

THIS PAGE

WAS INTENTIONALLY

LEFT BLANK

INHIBITORS FOR LOW TEMPERATURE FLAT-PLATE SOLAR COLLECTORS IN SPACE/WATER HEATING

by

Charles C. Nathan

New Mexico Energy Institute at New Mexico Tech

Socorro, New Mexico

INHIBITORS FOR LOW TEMPERATURE FLAT-PLATE SOLAR COLLECTORS IN SPACE/WATER HEATING

Charles C. Nathan, Director
New Mexico Energy Institute at
New Mexico Tech
Socorro, New Mexico 87801

To date there is but little open literature covering the problems of corrosion and its prevention in low-temperature, flat-plate collectors; however, the several published articles which will be mentioned in this review cover the subject well, and extensive references will be made to them. The use of inhibitors has received some study in both the laboratory and field; a number of well known materials as well as proprietary treatments are already on the market, and preliminary test data are presented. It is the feeling of this author that such systems do not present any formidable conditions or problems, and that inhibitors when properly utilized and monitored, should be readily applicable to the solar systems under discussion. Before discussing the use of inhibitors in these systems, the principal factors causing corrosion will be mentioned as well as design and operating parameters recommended to minimize corrosion either without the use of inhibitors or when supplemented by inhibitor usage.

Thompson and Hayden (1) have stated that, "The most pressing problem in solar heating system design is control of corrosion in aluminum absorbers. Absorbers cannot be opened for inspection, coating, or descaling, so corrosion treatment must be foolproof. Any extremes of pH, dissolved heavy metal or chloride ion in the water, 'hard' water, and dissolved oxygen increase the risk of corrosion in aluminum absorbers."

As is well known to corrosion investigators, aluminum is a very

active metal and is thermodynamically unstable in most aqueous systems. Practical use of aluminum in such systems is dependent on the stability of a thin, adherent, protective film which is formed rapidly on initial exposure of the metal to the atmosphere and/or process fluids and acts as a barrier to further attack on the base metal. Because of the amphoteric nature of aluminum, the oxide/hydroxide film is unstable and dissolves at pH values removed from neutrality. Minimum corrosion rates in these systems occur at pH of 6.5. Large excursions from this value must be controlled by use of buffers, etc. Chlorides inactivate the protective oxide film on aluminum; accordingly, water of high salinity should be avoided when possible. "Hard" waters are known to cause pitting attack on aluminum through the formation of deposits which set up or aggravate differential oxygen cells. High fluid velocities coupled with high oxygen contents also accelerate aluminum corrosion as does alternate drainage and filling of the fluids in freezing systems through deterioration of the protective film on aluminum.

Reference (1) also states, "A second problem is the difficulty of building single-metal systems. Although it is possible, for example, for one to build an all-iron conventional hot-water system, the plumbing components for a solar heating system generally include some copper or brass (particularly in valve bodies, piping components, and heating coils) some iron (tanks and pump housings), and some aluminum (collectors)." The use of iron and copper, themselves corrodible in the aqueous fluids, allows for the presence of soluble ions of Cu and Fe, which because Cu and Fe are noble to aluminum, can plate out on the aluminum to set up active bimetallic galvanic cells. These cells cause rapid corrosion of the aluminum in the proximity of the deposits. Additional difficulties are caused by the presence of lead and tin-bearing solders, weld metal spatter and other detritus. The situation has many similarities to automotive

radiator fluids in which the development of satisfactory corrosion inhibitors is complicated by the presence of a variety of active metals. Inhibitors for some metals may accelerate the corrosion of others.

It should be emphasized that no cases of failure of aluminum have been reported by general wastage of the metal through uniform attack. Rather is the action in the form of isolated areas of pitting, crevice attack, etc., which result in complete perforation. This is of particular importance with the thin metals sections used, of the order of ten mils. The metal thickness is dictated by reasons of economy in construction, maintenance of high heat transfer rates and other design factors.

Copper collectors are also being advocated (2,3) as being competetive with aluminum in solar hot-water collectors, and generally are relatively free of corrosion problems on the copper per se. This is due to the protective oxide films on copper which are quite stable in such systems. Increased initial costs of copper units may very well be offset by the advantages of longer life without the need for such close control of operating parameters including the use of inhibitors.

The references herein cited point out the need for system cleanliness, sufficient liquid velocity, at least four fps to prevent stagnant areas and deposits, use of insulating couplings between different metals, use of getters to remove oxygen, and inert gas or oil blanketing of storage tanks exposed to air. Cathodic protection has not been utilized because of unfavorable geometrical factors.

INHIBITOR TREATMENTS IN FREEZING SOLUTIONS

Chromates, well-known in various water treatments, are effective

but because of environmental hazards, must be used with caution. The possibility of the circulating fluids in the solar system contaminating potable water must be considered. Also, the eventual discharge of the fluids containing chromates or other toxic inhibitors is a factor in the use of such materials. Sodium silicate does not possess the disadvantages of chromates and has long been used in residential water supplies. Certain organic materials, such as soluble oils, have been and are employed in automotive cooling systems, and a combination of silicate-organic at 200 ppm is recommended (4). Limits of pH are held between 8.0-9.5 for either chromate or silicate treatments. In common with other anodic type inhibitors, these materials are "dangerous" in the sense that dosages below the desired level can accelerate pitting in treated systems over and beyond that observed in systems with no inhibitor treatment. Accordingly, proper monitoring of inhibitor concentrations and pH, as well as dissolved oxygen is desirable. The use of corrosion test coupons and the more sophisticated electrical instruments should be considered in critical and/or expensive systems, especially during start-up of the systems. Since measurements and monitoring as just described usually require time and skill on the part of the operator, the use of the services of a competent water-treating firm may be advisable.

FREEZE-PROOF SYSTEMS

Freeze-proof systems employ ethylene glycol or other glycol and pose some additional problems over the aqueous systems without anti-freeze. This is mainly due to the long-term decomposition of the glycols under the action of oxygen, high temperatures and contact with active metals. Decomposition products include aldehydes, organic acids and other organics. Their presence, if untreated, results in a lowered pH and

accelerated attack on both aluminum and copper. Additionally, some of the decomposition products can chelate with corrosion products and cause high corrosion of the base metal. Accordingly, although as stated above, copper can be used satisfactorily without an inhibitor in freezing solutions, an inhibitor must be added in antifreeze solutions (5). See Figure 1 attached.

INHIBITORS IN FREEZE-PROOF SYSTEMS

A rather comprehensive review of the various organic and inorganic materials used or proposed in solar systems is given by Beynon (6). Most of these materials are well known from other applications including automotive cooling systems.

A condensation follows:

Copper and Brass: 2-mercaptobenzothiazole (MBT) is well known as an inhibitor through forming insoluble copper-containing films. In recent years, triazoles, such as benozotriazole (BZT) and tolyltrazole (TTZ) are finding increased usage because of better thermal stability and reduced toxicity to various aquatic species.

Aluminum: Anions such as phosphates and silicates are used. Silicate, which forms a gelatinous, poorly protective film on Al, is enhanced greatly through formulating a silicone-silicate (4) copolymer. Sodium nitrite is used to form and/or repair the oxide film on aluminum. Arsenite is effective but requires special labelling because of its toxicity.

Iron and Steel: Borates, phosphates, arsenites and silicates all function as oxidizing agents to form a protective oxide film on iron. Borates and phosphates also have buffering action against the breakdown products of the glycol; benzoate has some buffering action but is less effective. Nitrite can be used to supplemant the oxide film formation, but may attack solders. Note that all of the inhibitors mentioned above are "dangerous" as previously defined. Close control of inhibitors concentration is essential.

Chromates are not used in antifreeze solutions because of their oxidizing action on the glycols.

Solder: This is difficult to inhibit and specific materials have not been developed for lead alloys; however, silicate at the proper pH gives a protective film, and polar oils also adsorb on the metal to give oily, protective barriers.

Proprietary Formulations and Inhibitor Testing

Popplewell (5) describes test apparatus and methods for evaluation of a number of proprietary anti-freeze solutions for corrosion on copper alloy CA 122 and aluminum alloys 3003 and 1100. Inhibitors are formulated in some of these fluids. Data are also given for inhibitors in freezing fluids. In general, the inhibited systems give satisfactory results on all three metals tested. Specific differences are pointed out. He also gives corrosion data employing as the heat transfer media nonaqueous fluids such as silicones. These were found to have very low corrosion rates under the test conditions.

Tests were of short duration, three months, relative to the desired service life of the solar systems of twenty years.(7) The possibilities of breakdown of the organic fluids, water pick-up, etc., are pointed out with subsequent deleterious effects on performance.

SUMMARY AND FUTURE DIRECTIONS

The concepts previously found of value for corrosion control in aqueous systems at moderate temperatures on common materials of construction appear applicable with few modifications to solar collectors. The need for proper control of operating parameters is emphasized. Materials used in other aqueous systems as inhibitors appear promising in the solar collector systems based on limited, short-term data. By following up on present knowledge and ideas, improvements can be expected in technology and in economics so that long-term, reliable service life of these units is assured.

REFERENCES

(1) Paul D. Thompson and Michael B. Hayden. "Corrosion Problems in Solar Energy Systems," Materials Performance 16 28, February 1978.

(2)James M. Popplewell and Stephen F. Hager. "Corrosion of Copper Alloys in Recirculating Cooling Tower Systems And Its Effect on Copper in the Effluent," Paper #122 Presented at CORROSION/77 - NACE - San Francisco, Ca. - March 14-18, 1977.

(3) Anon. "Solar Heating No Pie in Sky for Specialties," - Chemical Week, p. 54, Sept. 21, 1977.

(4)A.N. Pines and E.A. Zientek (Union Carbide Corporation), U.S. Patents 3,312,622; 3,337,496; 3,341,469.

(5)James M. Popplewell, "Corrosion And Its Prevention in Flat Plate Absorber Solar Systems," - Presented at the October 18-20, 1977 - NACE North Central Regional Meeting - Chicago, Ill.

(6)Eric Beynon, "Inhibited Ethylene Glycol As the Solar Nexus,"- Presented at CORROSION/77 - NACE - San Francisco, Ca. - March 14-18, 1977.

(7)Anon. "Battelle Studying Ways to Prevent Corrosion in Solar Collectors," Materials Performance 16, 54, October 1978.

TABLE 1 (Reference 5)

Substance	Potential mv*
Magnesium	1730
Zinc	1050
Al-4% Zn	1020
Al-1% Zn	960
Al-4% Mg	870
99.95% Al	850
Al-11.9% Si	830
Al-1.25% Mn	830
Al-Si-Cu-Ni-Fe (DTD 133B)	810
Al-7% Mg	690
Al-4% Cu	690
Iron	580
Copper	220

* vs S.C.E.

TABLE 2 (Reference 6)

GENERAL COMPOSITION OF
INHIBITED ETHYLENE GLYCOL CONCENTRATES

Ingredient	Weight %
Ethylene Glycol	95
Inhibitors (Anhydrous)*	2
Total Water	3
Antifoam	present
Dye	trace

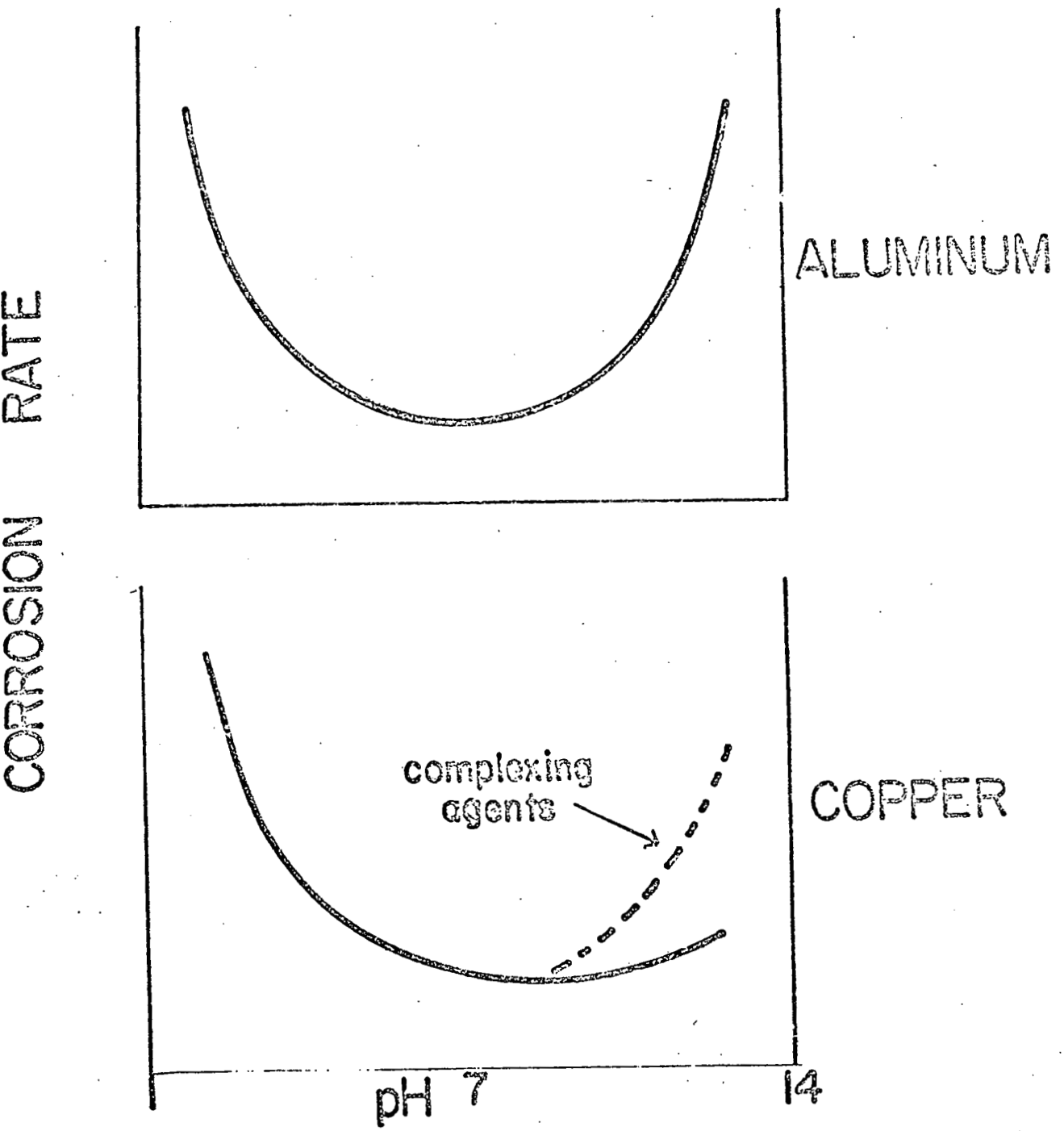
* The actual weight percent of soluble inhibitors added is greater than the figure shown because some of these compounds contain water of hydration.

TABLE 3

CURRENTLY USED ETHYLENE GLYCOL INHIBITORS

Inorganic	Organic
Borates	Phosphates
Phosphates	Benzoates
Nitrites	Mercaptans
Nitrates	Triazoles
Silicates	Amines
Arsenites	Polar Oils

Figure 1 (Reference 5)



Corrosion rate versus pH for copper and aluminum

THIS PAGE

WAS INTENTIONALLY

LEFT BLANK

ALUMINUM ALLOYS

by

Ellis C. Verink

University of Florida

Gainesville, Florida

Introduction

Chemical compositions limits for a number of wrought aluminum alloys are given in Table I. The asterisks indicate the compositions most likely to be considered for construction of solar energy apparatus. The individual components will normally be constructed of alloys shown in Table II. A generalized listing of comparative characteristics of the most useful alloys is given in Table III.

Atmospheric Weathering Resistance

The alloys marked with an asterisk in Table I (and listed again in Table III) are generally similar in their resistance to atmospheric weathering. These alloys exhibit a high degree of resistance to corrosion and generally may be used without added protection in even severe industrial or marine atmospheres. The following is quoted from Aluminum Association Publication #60.

"ATMOSPHERES. Most aluminum alloys have excellent resistance to the atmosphere and are widely used without protection for architectural and structural purposes. The earliest known example of aluminum exposed to the weather is the cap piece on the well-known Washington, D.C., monument erected in 1884. When examined in 1934 the original inscription could still be read. The first known aluminum roof was erected on a church in Rome in 1897 and is still in service. Recent inspections confirm its good resistance to the weather. The Al-Cu-Mg and Al-Zn-Mg-Cu groups of alloys require protection in more corrosive atmospheres but with these exceptions the performance of the other alloys is remarkably similar. The corrosiveness of the atmosphere to aluminum and other metals varies greatly from place to place. The most important factors are the degrees of industrial pollution; the proximity of the sea, the amount and frequency of rain and sunshine, the amount of humidity and fog, the direction of the wind and the average temperature. In rural atmospheres there is no appreciable corrosion of aluminum over very long periods and the corrosion rate is less than 0.01 mpy. In marine atmospheres the rate is usually less than 0.1 mpy and

and aluminum exhibits very good corrosion behavior. Hundreds of ships have been constructed with painted aluminum superstructures including the 52,000-ton passenger liner UNITED STATES which was launched in 1951 and contains over 2,000 tons of aluminum. The 12,700-ton freighter SUNRIP has been at sea since 1954 with an unpainted aluminum superstructure. Up to March, 1963, three more freighters have gone into service with unpainted aluminum superstructures. Unprotected aluminum dockside structures have given good mpy and after several decades some loss of properties of thin sections will occur. However, the corrosion rate of aluminum under these conditions is less than that of most other metals. In corrosive atmospheres there is more corrosion of sheltered areas than in the case of bold exposure. Attention should be paid in the design of aluminum structures to the presence of other metals and to the filling of crevices, especially for service in marine atmospheres. See following table and also Figure 1."

Resistance to Water

Aluminum cooking utensils (in particular, tea kettles) have been used throughout the world for potable water. In most natural fresh waters, 3003 (and the other non-clad tubing, pipe and plate alloys listed in Table II) provides adequate resistance to corrosion by fresh waters. In certain waters however (e.g., Altoona, Pennsylvania) severe pitting and perforation of 3003 sheet occurred. Analysis revealed the presence of heavy metal ions, notably Cu, Ni and Co in the water which plated out on the aluminum surfaces caused local galvanic cells which in turn stimulated the observed pitting. Alclad 3003 (cladding alloy 7072) was developed to combat this problem. Where heavy metal corrosion is expectable, alclad products are preferred to prevent perforation. The situation is similar for saline water environments. For more detail refer to Aluminum Association Publication #74, entitled "Aluminum in Desalination Equipment."

The following comments regarding resistance to water are quoted from Aluminum Association Publication #60, entitled "Aluminum With Food and Chemicals," 4th Edition.

"WATER. H_2O

Aluminum is resistant to high purity water including distilled, deionized, uncontaminated rain water, and heavy water used in nuclear reactors. A slight reaction occurs initially between aluminum and high purity water, but after a few days it almost completely ceases and aluminum pick-up by the water becomes negligible.

Aluminum alloys are especially suitable for handling steam and steam condensate because they are not adversely affected by carbon dioxide and oxygen nor by chemical agents such as hydrazine, sodium sulfite and filming amines added to protect steel. The rate of corrosion over the pH range 4.0 - 9.5 is very low.

Aluminum is also compatible with most natural fresh waters, but a few cause pitting. The rate of pitting is a function of the relatively small amounts of dissolved minerals present in natural waters. The most important of these are chlorides, sulfates, bicarbonates, and heavy metals such as copper, nickel, cobalt, tin, iron, and mercury. Bicarbonate ion has been shown to promote pitting when present with other ions. Heavy metal salts which have appreciable solubility in acidic waters are reduced by aluminum; when reduced, they promote further corrosion, generally in the form of pitting by galvanic action. In alkaline waters, their effect is considerably less because of their decreased solubility.

Deaeration generally reduces the rate of corrosion of aluminum in natural waters because the absence of oxygen eliminates a good cathodic reaction (reduction of oxygen) required for the corrosion process.

The rate of pitting of aluminum in most fresh waters generally decreases with time and has been shown to follow the equation $d=Kt^{1/3}$, where d is the maximum pit depth. K is a constant which depends on the particular water and alloy, and t is the time.

Pitting of aluminum in natural waters can be minimized by the use of alclad products, inhibitors, cathodic protection, and, where feasible, by cleaning with abrasive materials such as steel wool that produce numerous scratches.

Aluminum equipment is used in various industries to handle different types of water. For instance, aluminum alloy storage

tanks, tubes, fittings, and valves are commonly used for handling and storing distilled water. Aluminum surface condenser tubes, condensate lines and condensate tanks are used in power plants. Aluminum steam-jacketed kettles and steam traced product lines are used by chemical and food industries. Aluminum heat exchangers using sea water cooling are in service and aluminum irrigation tube has wide application."

Designing to Prevent Corrosion

When dissimilar metal couples between aluminum and copper, lead, nickel-copper alloys, brass, etc., exist in the presence of an electrolyte, galvanic corrosion of the aluminum part is likely. This implies that the use of copper tubes on aluminum flat plate collectors may be dangerous unless provision is made to exclude the electrolyte from the dissimilar metals. As a matter of practical fact, there are a number of successful applications employing this combination because of careful avoidance of electrolyte. Naturally, the use of aluminum tubing with aluminum plates provides a simpler design. Dissimilar metal corrosion also may occur between aluminum and mild steel however the difference in electrode potential (the driving force) is less than for copper-base alloys.

Couples between aluminum alloys such as 3003 and austenitic stainless steels normally are satisfactory in fresh water, however in strong electrolytes such as sea water, special provisions are recommended (see desalination booklet). Where dissimilar metals must be selected, one should try to select materials whose electrode potentials are as nearly the same as possible in the expected electrolyte at temperature in order to reduce the driving force for galvanic corrosion.

It is good design practice to provide drainage for moisture which may tend to collect. Where feasible avoid crevices and pockets which can trap moisture and dirt. Thermal insulation should be of a composition which is not water soluble and which will not trap or hold moisture against metal parts. Otherwise, differential aeration cells will be formed which can cause crevice corrosion of metal parts.

Closed systems with recirculated fluids may be inhibited to avoid corrosion. There are a number of proprietary inhibitors and inhibited solutions which have been designed for use with polymetallic systems such

as automotive cooling systems. Normally these glycol solutions are compatible with systems having aluminum parts. High temperature heat transfer media such as silicone oils, Dowtherm, etc., also have been used successfully with aluminum alloys.

TABLE I. Chemical Composition Limits of Wrought Aluminum Alloys (1) (2)

AA DESIGNATION	SILICON	IRON	COPPER	MANGANESE	MAGNESIUM	CHROMIUM	NICKEL	ZINC	TITANIUM	OTHERS Each	OTHERS Total	ALUMINUM Min.
1050	0.25	0.40	0.05	0.05	0.05			0.05	0.03	0.03		99.50
1060	0.25	0.35	0.05	0.03	0.03			0.05	0.03	0.03		99.60
* 1100	1.0 Si + Fe		0.05-0.20	0.05				0.10		0.05	0.15	99.00
1145 (3)	0.55 Si + Fe		0.05	0.05	0.05			0.05	0.03	0.03		99.45
1175 (3)	0.15 Si + Fe		0.10	0.02	0.02			0.04	0.02	0.02		99.75
1200	1.0 Si + Fe		0.05	0.05				0.10	0.05	0.05	0.15	99.00
1230 (3)	0.7 Si + Fe		0.10	0.05	0.05			0.10	0.03	0.03		99.30
1235	0.65 Si + Fe		0.05	0.05	0.05			0.10	0.03	0.03		99.35
1345	0.30	0.40	0.10	0.05	0.05			0.05	0.03	0.03		99.45
* 1350 (4)	0.10	0.40	0.05	0.01		0.01		0.05		0.03 (5)	0.10	99.50
2011	0.40	0.7	5.0-6.0					0.30		0.05 (6)	0.15	Remainder
2014	0.50-1.2	0.7	3.9-5.0	0.40-1.2	0.20-0.8	0.10		0.25	0.15 (7)	0.05	0.15	Remainder
2017	0.20-0.8	0.7	3.5-4.5	0.40-1.0	0.40-0.8	0.10		0.25	0.15 (7)	0.05	0.15	Remainder
2018	0.9	1.0	3.5-4.5	0.20	0.45-0.9	0.10	1.7-2.3	0.25		0.05	0.15	Remainder
2024	0.50	0.50	3.8-4.9	0.30-0.9	1.2-1.8	0.10		0.25	0.15 (7)	0.05	0.15	Remainder
2025	0.50-1.2	1.0	3.9-5.0	0.40-1.2	0.05	0.10		0.25	0.15	0.05	0.15	Remainder
2036	0.50	0.50	2.2-3.0	0.10-0.40	0.30-0.6	0.10		0.25	0.15	0.05	0.15	Remainder
2117	0.8	0.7	2.2-3.0	0.20	0.20-0.50	0.10		0.25		0.05	0.15	Remainder
2124	0.20	0.30	3.8-4.9	0.30-0.9	1.2-1.8	0.10		0.25	0.15 (7)	0.05	0.15	Remainder
2218	0.9	1.0	3.5-4.5	0.20	1.2-1.8	0.10	1.7-2.3	0.25		0.05	0.15	Remainder
2219	0.20	0.30	5.8-6.8	0.20-0.40	0.02			0.10	0.02-0.10	0.05 (8)	0.15	Remainder
2319	0.20	0.30	5.8-6.8	0.20-0.40	0.02			0.10	0.10-0.20	0.05 (8)	0.15	Remainder
2618	0.10-0.25	0.9-1.3	1.9-2.7		1.3-1.8		0.9-1.2	0.10	0.04-0.10	0.05	0.15	Remainder
* 3003	0.6	0.7	0.05-0.20	1.0-1.5				0.10		0.05	0.15	Remainder
* 3004	0.30	0.7	0.25	1.0-1.5	0.8-1.3			0.25		0.05	0.15	Remainder
3005	0.6	0.7	0.30	1.0-1.5	0.20-0.6	0.10		0.25	0.10	0.05	0.15	Remainder
* 3105	0.6	0.7	0.30	0.30-0.8	0.20-0.8	0.20		0.40	0.10	0.05	0.15	Remainder
4032	11.0-13.5	1.0	0.50-1.3		0.8-1.3	0.10	0.50-1.3	0.25		0.05	0.15	Remainder
4043	4.5-6.0	0.8	0.30	0.05	0.05			0.10	0.20	0.05 (9)	0.15	Remainder
4043 (10)	9.0-11.0	0.8	0.30	0.05	0.05			0.10	0.20	0.05	0.15	Remainder
4047 (10)	11.0-13.0	0.8	0.30	0.15	0.10			0.20		0.05 (11)	0.15	Remainder
4145 (10)	9.3-10.7	0.8	3.3-4.7	0.15	0.15	0.15		0.20		0.05 (12)	0.15	Remainder
4343 (10)	6.8-8.2	0.8	0.25	0.10				0.20		0.05	0.15	Remainder
4643	3.6-4.6	0.8	0.10	0.05	0.10-0.30			0.10	0.15	0.05 (13)	0.15	Remainder
5005	0.30	0.7	0.20	0.20	0.50-1.1	0.10		0.25		0.05	0.15	Remainder
* 5050	0.40	0.7	0.20	0.10	1.1-1.8	0.10		0.25		0.05	0.15	Remainder
* 5052	0.25	0.40	0.10	0.10	2.2-2.8	0.15-0.35		0.10		0.05	0.15	Remainder
5056	0.30	0.40	0.10	0.05-0.20	4.5-5.6	0.05-0.20		0.10		0.05	0.15	Remainder
* 5083	0.40	0.40	0.10	0.40-1.0	4.0-4.9	0.05-0.25		0.25	0.15	0.05	0.15	Remainder
* 5086	0.40	0.50	0.10	0.20-0.7	3.5-4.5	0.03-0.25		0.25	0.15	0.05	0.15	Remainder
* 5154	0.45 Si + Fe		0.10	0.10	3.1-3.9	0.15-0.35		0.20	0.20	0.05	0.15	Remainder
5183	0.40	0.40	0.10	0.50-1.0	4.3-5.2	0.05-0.25		0.25	0.15	0.05 (12)	0.15	Remainder
5252	0.08	0.10	0.10	0.10	2.2-2.8			0.05		0.03	0.10	Remainder
5254	0.45 Si + Fe		0.05	0.01	3.1-3.9	0.15-0.35		0.20	0.05	0.05	0.15	Remainder
5356	0.50 Si + Fe		0.10	0.05-0.20	4.5-5.5	0.05-0.20		0.10	0.06-0.20	0.05 (14)	0.15	Remainder
* 5454	0.25	0.40	0.10	0.50-1.0	2.4-3.0	0.05-0.20		0.25	0.20	0.05	0.15	Remainder
5456	0.40 Si + Fe		0.10	0.50-1.0	4.7-5.5	0.05-0.20		0.25	0.20	0.05	0.15	Remainder
5457	0.08	0.10	0.20	0.15-0.45	0.8-1.2			0.05		0.03	0.10	Remainder
5554	0.40 Si + Fe		0.10	0.50-1.0	2.4-3.0	0.05-0.20		0.25	0.05-0.20	0.05 (15)	0.15	Remainder
5556	0.40 Si + Fe		0.10	0.50-1.0	4.7-5.5	0.05-0.20		0.25	0.05-0.20	0.05 (14)	0.15	Remainder
5652	0.40 Si + Fe		0.04	0.01	2.2-2.8	0.15-0.35		0.10		0.05	0.15	Remainder
5654	0.45 Si + Fe		0.05	0.01	3.1-3.9	0.15-0.35		0.20	0.05-0.15	0.05 (14)	0.15	Remainder
5657	0.08	0.10	0.10	0.03	0.6-1.0			0.05		0.02 (16)	0.05	Remainder
6003 (3)	0.35-1.0	0.6	0.10	0.8	0.8-1.5	0.35		0.20	0.10	0.05	0.15	Remainder
6005	0.6-0.9	0.35	0.10	0.10	0.40-0.6	0.10		0.10	0.10	0.05	0.15	Remainder
A053	--	0.35	0.10		1.1-1.4	0.15-0.35		0.10		0.05	0.15	Remainder
* 6061	0.40-0.8	0.7	0.15-0.40	0.15	0.8-1.2	0.04-0.35		0.25	0.15	0.05	0.15	Remainder
* 6063	0.20-0.6	0.35	0.10	0.10	0.45-0.9	0.10		0.10	0.10	0.05	0.15	Remainder
6066	0.9-1.8	0.50	0.7-1.2	0.6-1.1	0.8-1.4	0.40		0.25	0.20	0.05	0.15	Remainder
6070	1.0-1.7	0.50	0.15-0.40	0.40-1.0	0.50-1.2	0.10		0.25	0.15	0.05	0.15	Remainder
6101 (3)	0.30-0.7	0.50	0.10	0.03	0.35-0.8	0.03		0.10		0.03 (17)	0.10	Remainder
6151	0.6-1.2	1.0	0.35	0.20	0.45-0.8	0.15-0.35		0.25	0.15	0.05	0.15	Remainder
6162	0.40-0.8	0.50	0.20	0.10	0.7-1.1	0.10		0.25	0.10	0.05	0.15	Remainder
6201	0.50-0.9	0.50	0.10	0.03	0.6-0.9	0.03		0.10		0.03 (18)	0.10	Remainder
6253 (3)	(34)	0.50	0.10		1.0-1.5	0.15-0.35		1.6-2.4		0.05	0.15	Remainder
6262	0.40-0.8	0.7	0.15-0.40	0.15	0.8-1.2	0.04-0.14		0.25	0.15	0.05 (19)	0.15	Remainder
6351	0.7-1.3	0.50	0.10	0.40-0.8	0.40-0.8			0.20	0.20	0.05	0.15	Remainder
6463	0.20-0.6	0.15	0.20	0.05	0.45-0.9					0.05	0.15	Remainder
6951	0.20-0.50	0.8	0.15-0.40	0.10	0.40-0.8			0.20		0.05	0.15	Remainder
7001	0.35	0.40	1.6-2.6	0.20	2.6-3.4	0.18-0.35		6.8-8.0	0.20	0.05	0.15	Remainder
7005	0.35	0.40	0.10	0.20-0.7	1.0-1.8	0.06-0.20		4.0-5.0	0.01-0.06	0.05 (20)	0.15	Remainder
7008 (21)	0.10	0.10	0.05	0.05	0.7-1.4	0.12-0.25		4.5-5.5	0.05	0.05	0.10	Remainder
7011 (5)	0.15	0.20	0.05	0.10-0.30	1.0-1.6	0.05-0.20		4.0-5.5	0.05	0.05	0.15	Remainder
* 7072 (7)	0.7 Si + Fe		0.10	0.10	0.10			0.8-1.3		0.05	0.15	Remainder
7075	0.40	0.50	1.2-2.0	0.30	2.1-2.9	0.18-0.35		5.1-6.1	0.20 (10)	0.05	0.15	Remainder
7079	0.30	0.40	0.40-0.8	0.10-0.30	2.9-3.7	0.10-0.25		3.8-4.8	0.10	0.05	0.15	Remainder
7178	0.40	0.50	1.6-2.4	0.30	2.4-3.1	0.18-0.35		6.3-7.3	0.20	0.05	0.15	Remainder

(1) Composition in percent maximum unless shown as a range or a minimum.

(2) For purposes of determining conformance to these limits, an observed value or a calculated value obtained from analysis is rounded off to the nearest unit in the last right-hand place of figures used in expressing the specified limit, in accordance with AN Standard Rules for Rounding Off Numerical Values (ANSI Z25.1).

Analysis is regularly made only for the elements for which specific limits are shown, except for unalloyed aluminum. If, however, the presence of other elements is suspected to be, or in the course of routine analysis is indicated to be in excess of the specified limits, further analysis is made to determine that these other elements are not in excess of the amount specified.

(3) The aluminum content for unalloyed aluminum not made by a refining process is the difference between 100.0 percent and the sum of all other metallic elements present in amounts of 0.010 percent or more each, expressed to the second decimal before determining the sum.

(4) Also contains 0.40-0.7 percent each of lead and bismuth.

(5) Electric conductor. Formerly designated EC.

(6) Cladding alloy. See Table 6.1.

(7) Foil.

(8) Vanadium 0.05 percent maximum.

(9) Also contains 0.20-0.6 percent each of lead and bismuth.

(10) Brazing alloy.

(11) Bus conductor.

(12) Vanadium plus titanium 0.02 percent maximum, boron 0.05 percent maximum; gallium 0.03 percent maximum.

(13) Zirconium plus titanium 0.25 percent maximum.

(14) Zirconium 0.08-0.20.

(15) Silicon 45 to 65 percent of magnesium content.

(16) Beryllium 0.0008 maximum for welding electrode and welding rod only.

(17) Boron 0.06 percent maximum.

(18) Vanadium 0.05-0.15; zirconium 0.10-0.25.

(19) Gallium 0.03 percent maximum; vanadium 0.05 percent maximum.

(20) Zirconium plus titanium 0.20 percent maximum.

(21) In addition to those alloys referencing footnote (16), any alloy to be used as welding electrode or welding rod shall have 0.0000 percent maximum beryllium.

*Alloys likely to be used for solar energy applications.

From: "Aluminum Standards and Data," Publication #1. The Aluminum Association, Washington, D. C.

Table II

Suggested Alloy Selections for Components

Component	Alloy
Heat Exchanger Tubing	3003, Alclad 3003, 3105 5050, 5052, 6063
"Flat Plate" Absorbers	3003, 5052 for rolled sheet or plate 6063-T5 or 6063-T6 for interlocking extruded plates
Wind Mill Blades	6063-T5 or 6063-T6 extrusions
Piping	6061-T4 or 6061-T6, 6063-T4 or 6063-T6, 3003-H112
Storage Tankage	3003, 5052, 5454, 6061
Structural Members	6061-T6, 6063-T6

Table III

Comparative characteristics of some alloys

Alloy and Temper	Resistance to corrosion: General ①	Stress-Corrosion Cracking ②	Workability (Cold) ④	Machinability ④	Brazeability ⑤	Weldability ⑤: Gas	Arc	Resistance Spot and Seam
EC-0	A	A	A	E	A	A	A	B
H12,H111	A	A	A	E	A	A	A	A
H14,H24	A	A	A	D	A	A	A	A
H16,H26	A	A	B	D	A	A	A	A
H18	A	A	B	D	A	A	A	A
1060-0	A	A	A	E	A	A	A	B
H14	A	A	A	D	A	A	A	A
1100-0	A	A	A	E	A	A	A	B
H14	A	A	A	D	A	A	A	A
3003-0	A	A	A	E	A	A	A	A
H14	A	A	B	D	A	A	A	A
3004-0	A	A	A	D	B	B	A	B
H32	A	A	B	D	B	B	A	A
5050-0	A	A	A	D	B	A	A	B
H32	A	A	A	D	B	A	A	A
H34	A	A	B	D	B	A	A	A
5052-0	A	A	A	D	C	A	A	B
H32	A	A	B	D	C	A	A	A
H34	A	A	B	C	C	A	A	A
H36	A	A	C	C	C	A	A	A
H38	A	A	C	C	C	A	A	A
5083-0	A ①	B ①	B	D	D	C	A	B
H321	A ①	B ①	C	D	D	C	A	A
5086-0	A ③	A ③	A	D	D	C	A	B
H32	A ③	A ③	B	D	D	C	A	A
5154-0	A ③	A ③	A	D	D	C	A	B
H32	A ③	A ③	B	D	D	C	A	A
5454-0	A	A	A	D	D	C	A	B
5456-0	A ③	B ③	B	D	D	C	A	B
6061-0	B	A	A	D	A	A	A	B
T4	B	B	B	C	A	A	A	A
T6	B	A	C	C	A	A	A	A
6063-T6	A	A	C	C	A	A	A	A
T831	A	A	C	C	A	A	A	A

① Ratings A through E are relative ratings in decreasing order of merit, based on exposures to sodium chloride solution by intermittent spraying or immersion. Alloys with A and B ratings can be used in industrial and seacoast atmospheres without protection. Alloys with C, D and E ratings generally should be protected at least on faying surfaces

② Stress-corrosion cracking ratings are based on service experience and on laboratory tests of specimens exposed to the 3.5% sodium chloride alternate immersion test.

- A = No known instance of failure in service or in laboratory tests
- B = No known instance of failure in service, limited failures in laboratory tests of short transverse specimens.
- C = Service failures with sustained tension stress acting in short transverse direction relative to grain structure, limited failures in laboratory tests of long transverse specimens.
- D = Limited service failures with sustained longitudinal or long transverse stress.

③ This rating may be different for material held at elevated temperature for long periods.

④ Ratings A through D for Workability (cold), and A through E for Machinability, are relative ratings in decreasing order of merit.

⑤ Ratings A through D for Weldability and Brazeability are relative ratings defined as follows:

- A = Generally weldable by all commercial procedures and methods.
- B = Weldable with special techniques or for specific applications which justify preliminary trials or testing to develop welding procedure and weld performance.
- C = Limited Weldability because of crack sensitivity or loss in resistance to corrosion and mechanical properties.
- D = No commonly used welding methods have been developed.

From: "Aluminum in Desalination Equipment," The Aluminum Association Publication #74, Washington, D. C.

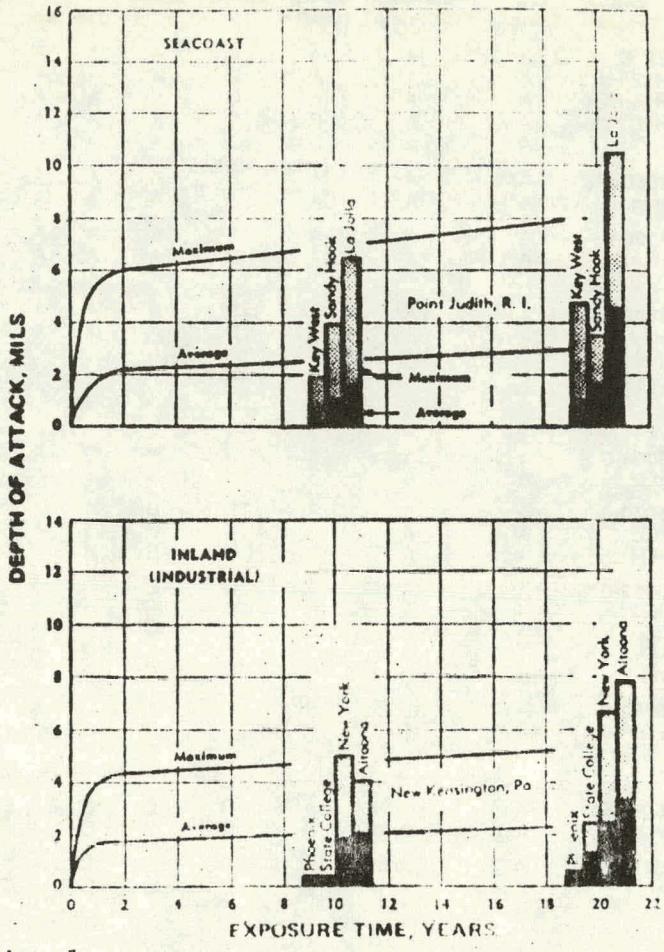


Fig. 1 Atmospheric corrosion. Measured depths of attack on 3003 at 10 and 20-year periods superimposed on curves for related alloys 1100 and 3003. From ASTM Special Technical Publication No. 175.

WEATHERING PERFORMANCE OF ALUMINUM ALLOYS SEVEN YEAR EXPOSURE TO DIFFERENT ATMOSPHERES

Location	Atmosphere Classification	Corrosion Rate (mils per year)				
		1100-H14	2024-T3	Alclad 3003-H14	5154-H34	6061-T6
Kure Beach, N.C.*	East Coast Marine	0.0122	0.0196	0.0097	0.0135	0.0134
Newark, N.J.*	Moderately Severe Industrial	0.0150	0.0222	0.0175	0.0344	0.0198
Point Reyes, Calif.*	West Coast Marine	0.0051	0.0154	0.0036	0.0042	0.0060
State College, Pa.*	Rural	0.0025	0.0027	0.0024	0.0047	0.0027
		1199-H14				
Corpus Christi, Texas**	Gulf Coast Marine	0.0009	0.0133	0.0018	0.0012	0.0014
Richmond, Va.**	Moderate Industrial	0.0109	0.0228	0.0162	0.0164	0.0145
McCook, Ill.**	Industrial	0.0233	0.0370	0.0545	0.0547	0.0667
Kure Beach, N.C.**	Rural Marine	0.0022	0.0112	0.0036	0.0030	0.0060

*Paper No. 23 Seventieth Annual Meeting of ASTM (1967), ASTM Committee B-3
**Paper No. 24 Seventieth Annual Meeting of ASTM (1967)

From: "Aluminum With Food and Chemicals," 4th Edition, The Aluminum Association, Washington, D.C. Publication #60.

☆ U.S. GOVERNMENT PRINTING OFFICE: 1980-O-677-175/109